EUROPEAN COOPERATION

ECSS

FOR SPACE STANDARDIZATION

Space engineering

Thermal design handbook - Part 13: Fluid Loops

Foreword

This Handbook is one document of the series of ECSS Documents intended to be used as supporting material for ECSS Standards in space projects and applications. ECSS is a cooperative effort of the European Space Agency, national space agencies and European industry associations for the purpose of developing and maintaining common standards.

The material in this Handbook is a collection of data gathered from many projects and technical journals which provides the reader with description and recommendation on subjects to be considered when performing the work of Thermal design.

The material for the subjects has been collated from research spanning many years, therefore a subject may have been revisited or updated by science and industry.

The material is provided as good background on the subjects of thermal design, the reader is recommended to research whether a subject has been updated further, since the publication of the material contained herein.

This handbook has been prepared by ESA TEC MT/QR division, reviewed by the ECSS Executive Secretariat and approved by the ECSS Technical Authority.

Disclaimer

ECSS does not provide any warranty whatsoever, whether expressed, implied, or statutory, including, but not limited to, any warranty of merchantability or fitness for a particular purpose or any warranty that the contents of the item are error-free. In no respect shall ECSS incur any liability for any damages, including, but not limited to, direct, indirect, special, or consequential damages arising out of, resulting from, or in any way connected to the use of this document, whether or not based upon warranty, business agreement, tort, or otherwise; whether or not injury was sustained by persons or property or otherwise; and whether or not loss was sustained from, or arose out of, the results of, the item, or any services that may be provided by ECSS.

Table of contents

Bibliography

Figures

Tables

1
Scope

Fluid loops are used to control the temperature of sensitive components in spacecraft systems in order to ensure that they can function correctly.

While there are several methods for thermal control (such as passive thermal insulations, thermoelectric devices, phase change materials, heat pipes and short-term discharge systems), fluid loops have a specific application area.

This Part 13 provides a detailed description of fluid loop systems for use in spacecraft.

The Thermal design handbook is published in 16 Parts

ECSS-E-HB-31-01 Part 1A	Thermal design handbook – Part 1: View factors
ECSS-E-HB-31-01 Part 2A	Thermal design handbook – Part 2: Holes, Grooves and Cavities
ECSS-E-HB-31-01 Part 3A	Thermal design handbook – Part 3: Spacecraft Surface Temperature
ECSS-E-HB-31-01 Part 4A	Thermal design handbook – Part 4: Conductive Heat Transfer
ECSS-E-HB-31-01 Part 5A Composite	Thermal design handbook – Part 5: Structural Materials: Metallic and Composite
ECSS-E-HB-31-01 Part 6A	Thermal design handbook – Part 6: Thermal Control Surfaces
ECSS-E-HB-31-01 Part 7A	Thermal design handbook – Part 7: Insulations
ECSS-E-HB-31-01 Part 8A	Thermal design handbook – Part 8: Heat Pipes
ECSS-E-HB-31-01 Part 9A	Thermal design handbook – Part 9: Radiators
ECSS-E-HB-31-01 Part 10A	Thermal design handbook – Part 10: Phase – Change Capacitors
ECSS-E-HB-31-01 Part 11A	Thermal design handbook – Part 11: Electrical Heating
ECSS-E-HB-31-01 Part 12A	Thermal design handbook – Part 12: Louvers
ECSS-E-HB-31-01 Part 13A	Thermal design handbook – Part 13: Fluid Loops
ECSS-E-HB-31-01 Part 14A	Thermal design handbook – Part 14: Cryogenic Cooling
ECSS-E-HB-31-01 Part 15A	Thermal design handbook – Part 15: Existing Satellites
ECSS-E-HB-31-01 Part 16A	Thermal design handbook – Part 16: Thermal Protection System

2
References

ECSS-S-ST-00-01	ECSS System - Glossary of terms
ECSS-E-HB-31-01 Part 8	Thermal design handbook – Part 8: Heat Pipes
ECSS-E-HB-31-01 Part 9	Thermal design handbook – Part 9: Radiators
ECSS-E-HB-31-01 Part 10	Thermal design handbook – Part 10: Phase-Change Capacitors
ECSS-E-HB-31-01 Part 14	Thermal design handbook – Part 14: Cryogenic Cooling
ECSS-E-HB-31-01 Part 15	Thermal design handbook – Part 15: Existing Satellites

All other references made to publications in this Part are listed, alphabetically, in the **Bibliography**.

3
Terms, definitions and symbols

3.1   Terms and definitions

For the purpose of this Standard, the terms and definitions given in ECSS-S-ST-00-01 apply.

3.2   Abbreviated terms

The following abbreviated terms are defined and used within this Standard.

A/D	analog-to-digital converter
ARS	atmosphere revitalization subsystem
ATCS	active thermal control system
BOL	beginning of life
CACSD	computer-aided control system design
CAD	computer-aided design
CAPL	capillary pumped heat transport loop
CPL	capillary pumped loop
CPU	central processing unit
D/A	digital-to-analog converter
DCR	direct condensation radiator
ECLA	experiment cooling system with liquid to air heat exchanger
EDHX	experiment dedicated heat exchanger
EOL	end of life
FCL	freon coolant loop
FL	fully developed flow
GSE	ground support equipment

HP	heat pipe
HPSTM	high power spacecraft thermal management
HTEL	combined hydrodynamical and thermal entry length
HX	heat exchanger
I	integral controllers
I/O	input/output
Mac	maximum allowable concentration
MBA	multiple berthing adaptor
MPU	microprocessor unit
NPSH	net positive suction head
OAO	orbiting astronomical observatory
P	proportional controllers
PC	phase change
PCCP	prototype capillary cold plates
PCM	phase change material
PD	proportional-derivative controllers
PI	proportional-integral controllers
PID	proportional-integral-derivative controllers
S/H	sample-and-hold
SLMS	seal leakage management subsystem
STS	space transportation system
TED	thermoelectric device
TEL	thermal entry length
TMS	thermal management system
TS	thermal storage
VCHP	variable conductance heat pipe

3.3 Symbols

A	heat transfer surface area, [m²]
A_{FL}	internal cross-sectional area of a duct. [m²]. Also called free flow area
A_{FR}	frontal area of a heat exchanger core, [m²]
A_G	gas filled part of the cross-sectional area of a duct. [m²]
A_L	liquid filled part of the cross-sectional area of a duct, [m²]
A_f	fin area, [m²]
A_k	wall cross-sectional area for longitudinal heat conduction, [m²]
A_w	Clause 9: inside wall heat transfer surface area, [m²] Clause 11: average wall area, [m²]
C	Chaps 5 and 11: capacity rate of a flow stream, [W.K⁻¹] $C = mc_p$ Clause 14: Chisholm parameter. Eq. [14-9] Clause 15: electrical capacitance, [F]
C^*	capacity rate of the in parallel stream, [W.K⁻¹] refers to assemblies of heat exchangers in parallel in one of the streams
$Cost_{Ntu}$	degradation in the heat exchanger thermal performance, $Cost_{Ntu} = 1 - (N_{tueff}/N_{tu})$
D	diameter, [m]
D_E	equivalent or hydraulic diameter of a duct of Non-Circular Cross Section. [m]. $D_E = 4A_{FL}/\Pi$.
D_{Ea}	equivalent or hydraulic diameter of a finned duct, [m]
D_M	inner diameter of a rough tube defined on a volumetric basis, [m] $D_M = (4v/\pi L)^{1/2}$
D_b	diameter of the largest cross section in an axial displacement heat transfer enhancement device. [m]
D_m	no-shear diameter in the flow through an annular duct, [m]
E	emissive power, [W.m⁻²]
E_L	specific energy lost by a pump, [J.kg⁻¹] it is defined per unit liquid mass

E_n	specific energy developed by a pump, [J.kg⁻¹] it is defined per unit liquid mass
E_s	specific energy supplied to a pump, [J.kg⁻¹] it is defined per unit liquid mass
E_v	specific suction energy of a pump, [J.kg⁻¹] it is defined per unit liquid mass
F	Clause 9: fin factor. ratio of the total convective heat transfer to that transferred through the tube walls alone, Clause 10: cooling effectiveness of a fluid
F_{Low}	fraction of channels carrying lower-than-average flow on the nonuniform side of a split counterflow heat exchanger (fleming's model)
F_r	froude number, $F_r = V^2/gD$
F_1	factor in tube banks, it accounts for variable fluid properties
F_2	factor in tube banks, it accounts for abnormal number of rows, $(N \neq 10)$
F_3	factor in tube banks, it accounts for the effect of tube yaw
F_4	factor in tube banks, it gives the row to row variation of heat transfer coefficient
Gr	Grashof number. $Gr = \dfrac{\beta g D_E^3 \rho^2 |T_w - T_b|}{\mu^2}$
Gz	Graetz number, $Gz = \pi D_E/4LPr\ Re = mc_p/kL$.
H	Clause 12: head, [m] Clause 14: liquid level in stratified flow, [m]
J_c	thermal capacitor stored energy, [J]
K	Clause 6: dean number, $K = Re\ (r/R)^{1/2}$ Clause 7: correction factor, it accounts for the fact that the cross section of the tube is not circular
L	length, [m]
L_E	equivalent length, [m]
L_{ent}	entrance length, [m]
M	Clause 7: mach number, $M = V/a$ Clauses 13 and 15: system mass, [kg]

M_{CP}	cold plate mass, [kg]
M_P	fluid driver mass, [kg]
M_{SP}	solar panel mass, [kg]
M_{wL}	(wet) plumbing mass, [kg]
M^+	mass penalty if a fluid loop, [kg] it includes the equivalent mass due to pumping power
N	Clause 6: number of rows in tube banks, the rows are counted in the flow direction Clause 11: passage count of a heat exchanger core, [m^{-2}]
N_{TD}	parameter in the Taitel-Duckler limit for stratified flow, Eq. (10.42)
N_{tu}	number of heat transfer units
N^o_{tu}	overall number of heat transfer units, refers to a liquid-coupled system of heat exchangers $$N^o_{tu} = \left(\frac{1}{N_{tu1}} + \frac{1}{N_{tu2}} \right)^{-1}$$
Nu	Nusselt number, $Nu = hD_E/k$.
Nu_T	Nusselt number for constant wall temperature
Nu_q	Nusselt number for constant heat flux through the wall
Nu_{11}	Nusselt number for the inner wall of a cylindrical annulus when the outer wall is insulated
Nu_{22}	Nusselt number for outer wall of a cylindrical annulus when the inner wall is insulated
P	power supplied to a pump, [W]
P	Peclet number, $Pe = PrRe$.
Pr	Prandtl number, $Pr = \mu c_p/k$.
Q	heat transfer rate, [W]
$Q(x)$	convective heat transfer rate in a tube, from onset of heat transfer to station x, [W]
Q_c	thermal capacitor energy storage rate, [W]
R	radius of the centerline in curved pipes, [m] Clauses 5, 11 and 13: capacity ratio, $R = C_1/C_2 \le 1$

R_E	Wicks-Dukler entrainment parameter, [m².s] Eq. (10.29)
R	Reynolds number, $Re = \rho V D_E / \mu$
S	suction specific speed of a pump at given operating conditions, $S = \dfrac{\omega(m/\rho)^{1/2}}{E_v^{3/4}}$
Sf	Stefan number, $Sf = \dfrac{h_{fg}}{c_{pL}(T_{sat} - T_w)}$
St	Stanton number, $St = Nu/PrRe = h/\rho V c_p$
T	temperature, [K]
T_R	reference temperature, [K] Clause 15: radiator temperature, [K]
T_S	source temperature, [K]
T_{av}	fluid average temperature, $T_{av} = \dfrac{\int\limits_{A_{FL}} T dA_{FL}}{A_{FL}}$
T_b	fluid bulk temperature, $T_b = \dfrac{\int\limits_{A_{FL}} uT dA_{FL}}{VA_{FL}}$
T_{bam}	arithmetic mean bulk temperature [K], $T_{bam} = (T_{bi} + T_{bo})/2$.
T_c	Clauses 5, 11, 13 and 15: cold temperature, [K] Clause 9: cooling water temperature, [K]
T_{sat}	liquid-vapor temperature, [K]
T_w	wall temperature, [K]
$T_{.5}$	fluid film temperature, [K], $T_{.5} = (T_w + T_b)/2$
T^+	dimensionless temperature, $T^+ = \rho u^* c_p / h$
U	overall thermal conductance, [W.m⁻².K⁻¹], $U = q/(T_h - T_c)$.
V	mean fluid velocity, [m.s⁻¹]
We	Weber number, $We = \rho_G V^2 D/\sigma$.
X	Lockhart-Martinelli parameter. Eq. [14-3]

Z	influence coefficient, it relates the one-surface-heated Nusselt number for the cylindrical annulus to Nusselt numbers on both surfaces when they are heated with any ration of heat fluxes.
a	Clause 7: velocity of sound, [m.s⁻¹]. Clauses 11 and 13: wall or plate thickness, [m]
a'	parting sheet thickness, [m]
b	protrusion spacing, [m] it can be measured in either axial or circumferential direction
c	mass fraction of a given species, when several species are present
c_K	pressure loss coefficient, $c_K = (p_1 - p_2)/(1/2\rho V^2)$
c_p	constant-pressure fluid specific heat, [J.kg⁻¹.K⁻¹] for gases c_p is used in distinction to c_v, the constant-volume specific heat
d	Clause 7: diameter of an orifice, wire or tube placed inside a duct, [m] Clause 11: cell height, [m] Clause 15: interplate distance of a capacitor [m]
e	roughness height, [m]
e^+	dimensionless roughness height, $e^+ = eu^*/\upsilon = (e/D)Re(f/2)^{1/2}$
f	fanning friction ractor, $f = \lambda/4$
f^*_c	fanning friction factor for the homogeneous core mixture flowing alone in the duct
f_F	fanning liquid film friction factor at the wall, annular flow with entrainment
f_{Gi}	fanning core friction factor at the interface, ideal annular flow
f^*_{Gi}	fanning core friction factor at the interface, annular flow with entrainment
f_L	fanning liquid film friction factor at the wall, ideal annular flow
f_{TP}	fanning friction factor at the wall, two-phase mixture model
g	acceleration due to gravity, [m.s⁻²] Clause 5: dimensionless heat transfer similarity function

h	convective heat transfer coefficient, [W.m^{-2}.K^{-1}]
h_c	thermal joint conductance, [W.m^{-2}.K^{-1}]
h_{fg}	heat of vaporization or condensation, [J.kg^{-1}]
h'_{fg}	heat of condensation corrected by partial subcooling effect, [J.kg^{-1}] Eq. (10.34)
j	colburn factor for heat transfer, $j = StPr^{2/3}$
k	thermal conductivity, [W.m^{-1}.K^{-1}] Clause 7: incremental pressure loss factor, it accounts for entrance effects
m	fluid mass flow rate, [kg.s^{-1}] Clauses 6 and 9: exponent, it appears in the loading factor accounting for the influence of fluid temperature on heat transfer
m_E	mass flow rate of the fluid entrained in the core, [kg.s^{-1}] annular flow with entrainment
m_F	mass flow rate of the liquid remaining in the film, [kg.s^{-1}] annular flow with entrainment
n	Clause 6: number of tubes in tube banks, also number assigned to the nth row tubes in tube banks Clause 7: number of wires per unit length of wire gauze, [m^{-1}] exponent Clauses 11 and 13: number of assembled heat exchangers Clause 12 and 15: rotating speed, [revolutions per minute]
n_s	(optimum) specific speed of a pump, [m$^{3/4}$.s$^{-3/2}$] $$n_s = \left.\frac{n(m/\rho)^{1/2}}{H^{3/4}}\right|_{opt}$$
p	pressure, [Pa]
p_{sat}	liquid-vapor pressure, [Pa]
p_t	total pressure, [Pa]
q	heat flux, [W.m^{-2}]
r	radius or radial coordinate, [m]
r_f	fouling resistance, [K.m^{-2}.W^{-1}]
s	protrusion thickness, [m] it is measured in axial direction

s_1	longitudinal pitch in tube banks, [m]
s'_1	diagonal pitch in staggered tube banks, [m]
s_t	transverse pitch in either in-line or staggered tube banks, [m]
t	Clauses 7 and 9: thickness, [m] Clause 11: temperature, [K] Clause 15. time, [s], [min], [h] or [yr]
u	local fluid velocity [m.s^{-1}]
u^*	friction velocity, [m.s-1], $u^* = (\tau_w/\rho)^{1/2}$.
u^+_c	dimensionless velocity, $u^+ = u/u^*$
u^+	dimensionless friction factor similarity function
v	volume, [m^3]
w	vapor quality
x	axial distance, [m] Clause 11: mass flow fraction
x^+	dimensionless axial distance to duct entry, $x^+ = (x/r)/PrRe = \pi/2Gz$
y	Clause 9: tube diameter per 180° fin or tape twist Clause 14: distance to the wall of the duct, [m]
z	vertical distance above arbitrary datum plane, [m]
ΔT_m	mean wall-to-fluid bulk temperature differential, [K]
Δp	pressure loss, [Pa]
Γ	radiator area density, [kg.m^{-2}]
Λ	longitudinal wall conduction parameter, $\Lambda = (k/L)A_k/C_1$
Π	wetted perimeter of a duct, [m]
Φ	Chaps 5, 7 and 11: ratio of free-flow area to total frontal area, also called porosity Clause 14: Lockhart-Martinelli pressure loss multiplier Eq. [14-2]
Ψ	upstream to downstream area ratio, refers to sudden area changes in ducts, factor in tube banks, it accounts for the effect of tube yaw on pressure loss
Ω	(optimum) specific speed of a pump, ECUACION

α		Clause 11: area density, [m².m⁻³], ratio of total heat transfer area on one side of a closed-type heat exchanger or recuperator to total exchanger volume, in the case of periodic type exchangers or regenerators α is based on the area of both sides Clauses 14 and 15: void fraction
α_1		factor in bends, it accounts for the aspect-ratio of the bend cross section
α_2		factor in bends, it accounts for the bend angle
α_3		factor in orifices, it accounts for the relative thickness of an orifice plate when $t/d < 0,8$
α_4		factor in orifices, it accounts for the relative thickness of an orifice plate when $t/d \geq 0,8$
a_5		factor in screens, it accounts for low Reynolds number in round-wire gauzes
α_6		factor in valves, it accounts for partial opening
α_s		solar absorptance
β		Clauses 5 and 11: area density, [m².m⁻³] ratio of total heat transfer area on one side of a plate-fin closed-type heat exchanger or recuperator to the volume between the plates on that side, in the case of periodic type exchangers or regenerators β is based on the area of both sides Clauses 6 and 9: coefficient of volumetric thermal expansion, [K⁻¹] Clause 7: factor in bends, it accounts for the interaction between two circular arc bends having a bend angle of 90° each Clause 15: 90° minus the angle between the line to the Sun and the normal to orbit plane
γ		Ratio of specific heats in a gas
δ		Clause 7: ratio of valve control travel from closed position to total valve control travel Clause 8: laminar sublayer thickness, [m] Chaps 14 and 15: film thickness, [m]
δm		correction to allow for differences between dimensionless temperature and dimensionless velocity in the fully turbulent core in pipe flow, see clause 13.2.
$\delta \varepsilon$		decrease in effectiveness of a heat exchanger because of longitudinal wall conduction

δ^+	dimensionless film thickness, $\delta^+ = \delta u^*/\upsilon$
ε	Clauses 5, 11 and 13: exchanger heat transfer effectiveness Clause 9: radial gap between the twisted-tape insert used for enhancing the heat transfer and the tube wall, [m] Clause 15: hemispherical total emittance Clause 15: dielectric permittivity, [F.m⁻¹]
ε_{cp}	cold plate effectiveness
ε_0	dielectric permittivity of vacuum, $\varepsilon_0 = 8{,}8542 \times 10^{-12}$ F.m⁻¹
ε_t	overall heat transfer effectiveness of an association of heat exchangers
η	heat transfer effectiveness
η_f	fin effectiveness
η_p	overall efficiency of a pump
θ	Clause 6: yaw angle, [angular degrees] Clause 7: total angle turned through by a bend, [angular degrees]
λ	friction factor
λ_B	baker parameter
μ	fluid dynamic viscosity, [Pa.s] it is also known as viscosity coefficient
ν	fluid kinematic viscosity, [m².s⁻¹]
ρ	fluid density, [kg.m⁻³]
σ	surface tension, [N.m⁻¹] Clause 15: Stefan-Boltzmann constant, $\sigma = 5{,}6697 \times 10^{-8}$ W.m⁻².K⁻⁴
τ	shearing stress, [Pa]
ϕ	Clause 11: flow maldistribution parameter, it is defined, although not in a unique fashion, in terms of the mass flow rate Clause 14: polar angle of stratified flow interface, [angular degrees]
ψ_B	baker parameter
ω	rotating speed, [radians per second]

Subscripts

F	liquid film, annular flow with entrainment	
G	Clause 7: gross value Clause 14: gas	
Gi	gas at the interface	
H	affected by hall's transformation	
High	refers to channels with higher-than average flow on the nonuniform side of a split counterflow heat exchanger (fleming's model)	
L	Clause 7: refers to length L Clause 11: refers to liquid stream in liquid-coupled heat exchanger Clause 14: liquid	
Low	refers to channels with lower-than average flow on the nonuniform side of a split counterflow heat exchanger (Fleming's model)	
M	phase-change	
N	net value	
P	evaluated at constant pumping power	
R	radiator	
S	refers to heat source	
SG	gas flowing alone in the duct	
SL	liquid flowing alone in the duct	
T	refers to total (axial plus spiral) values in spiralling flow	
TP	two phase in the mixture theory	
a	heat transfer enhanced date Clause 15: Earth Albedo.	
am	arithmetic mean value	
av	average value	
b	fluid bulk properties	
c	Clauses 5, 11, 13 and 15: cold stream	

	Clause 7: cylindrical tubes Clause 14: core, annular flow with entrainment
d	downstream tangent of a bend
e	spatial and temporal mean conditions at the tip level of the roughness elements Clause 15: space environment condition
equiv	equivalent
f	refers to fin or twisted-tape
f	hot stream
i	Clauses 5, 6 and 15: inlet conditions Clause 14: interface
im	inlet mean value
ir	infrared
lm	logarithmic mean value
m	mean value between commencement of heat transfer and station x
max	maximum value
n	refers to the nth component of an ensemble
o	outlet conditions Clause 9: heat transfer nonenhanced data
opt	optimum conditions
r	reference value for given thermal and/or geometrical characteristics of a system, it is omitted when no correction is made
s	refers to static pressure Clause 15: solar
t	refers to total pressure
tt	turbulent liquid, turbulent gas
tv	turbulent liquid, laminar gas
u	upstream tangent of a bend
vt	laminar liquid, turbulent gas
vv	laminar liquid, laminar gas

w	wall conditions
x	local conditions at section *x* of a duct
δ	conditions at the edge of the laminar sublayer
0	refers to an orifice plate of zero relative thickness
0,8	refers to an orifice plate if relative thickness t/d = 0,8
1	Clauses 5, 11 and 13: conditions for the stream with smaller capacity rate Clauses 6 and 9: inner wall conditions in a cylindrical annulus Clause 7: upstream reference conditions
2	Clauses 6 and 9: outer wall conditions in a cylindrical annulus Clause 7: downstream reference conditions Clause 11 conditions for the stream with larger capacity rate

Superscripts

-	mean value
*	entrainment effects included

4
General introduction

Fluids can be used to protect from thermal loads sensitive components of spacecraft systems.

This protection can be achieved on the basis of two completely different procedures.

1) The fluid is at rest although changing its phase, storing heat through melting (or evaporation) when the temperature increases, and restoring it through freezing (or condensation), for dissipation at a later time, when the temperature decreases. This is typical of phase change capacitors whose main features are discussed in ECSS-E-HB-31-01 Part 10.

Single phase fluids at rest are not used for thermal control purposes because of the far better qualities of solid materials, either as thermal) insulators or as thermal conductors.

2) The fluid is in motion, absorbing the heat at a relatively steady rate from the component whose temperature is controlled, transferring it to a heat sink which can be placed fairly apart from the source.

Heat transfer can be achieved either through sensible heat change or through phase change (latent heat):

2.1) Sensible heat change. A liquid or gas phase is used to transfer heat according to the equation $Q = mc_p\Delta T$. In order to increase the heat transfer rate, Q, either the mass flow rate, m, or the temperature difference, ΔT, is increased for a particular fluid. The specific heat, c_p, is more or less the same for all liquids and gases at normal conditions.

2.2) Phase change. The heat transferred is used to evaporate the working liquid according to the equation $Q = mh_{fg}$, where h_{fg} is the latent heat of vaporization. Now the heat transfer is much higher than in 2.1 for the same mass flow rate and the same type of fluid, whereas the temperature gradient along the duct is much smaller (system isothermality which allows the maintenance of isothermal heat load interfaces).

Forcing of the fluid through the duct can be performed by use either of:

2.3) A pumping device, centrifugal or positive displacement pump, normally driven by an electric motor, as in the case of both single and two phase fluid loops which are the subject of this Part.

2.4) Capillary forces, as in Heat Pipes. Such devices are discussed extensively in ECSS-E-HB-31-01 Part 8.

A capillary pumped loop (CPL) is a two-phase heat transfer system whichconsists of multiple parallel evaporators and where the pumping function is achieved through a fine pore size capillary structure. Unlike conventional) evaporators where heat is transferred through a liquid layer to the evaporating surface, in the CPL evaporator the heat is transferred directly to the vaporization surface. These devices present the same boiling, priming and capillary pressure limits associated with heat pipes (see ECSS-E-HB-31-01 Part 8, clause 5.2).

2.5) Short-term discharge of a stored fluid. This may be accomplished by use of either of (see ECSS-E-HB-31-01 Part 14, clause 5.3):

2.5.1) Sudden expansion of a gas stored in a high-pressure bottle, with the associated decrease in total temperature (Joule-Thomson process).)

2.5.2) Boiling of liquids such as water or cryogenic fluids. These liquids are selected on the basis of their high latent heats and (or) their low boiling points.

2.5.3) Sublimation of solids.

Because the large volume ratio associated with these open cycle processes, the fluid is vented out of the vehicle once it has absorbed the heat.

4.1   Fluid loops

The aim of the fluid loop, as of any other thermal control system, is to keep the temperature of a given component within the range which secures its correct functioning. To this goal, the heat flow rate evacuated should be equal to the heat rate dissipated by the component plus that coming from external sources.

According to their working mode, fluid loops may be either considered as:

1.   Thermal insulators, the aim of which is to protect the component against a thermally hostile environment, or

2.   Thermal acceptors transferring the exceeding thermal energy from the component to the thermal sink.

The coolant may circulate through a single-walled chamber enclosing the component, or through a double-walled component heat exchanger package. The single-walled jacket affords more efficient heat transfer than the heat exchanger, but the fluid can contaminate, corrode or chemically react with the materials of the component which is being thermally controlled.

Dual-loop configurations, consisting of two circulating coolant loops coupled by an interloop heat exchanger, are used very often. A dual-loop configuration offers a more precise temperature control than could a single-loop; in addition, it provides more flexibility to accommodate changes in the heat dissipating elements, spacecraft thermal loads, and coolant inlet temperature requirements.

The heat rejection depends on whether the coolant is expendable or non-expendable. An expendable coolant is rejected from the vehicle once it has accomplished its mission, while a non-expendable coolant is recirculated again after losing its thermal energy excess; in the last case the excess heat is radiated to the space via a radiator.

Single-phase fluid loops incorporating space radiators are fairly simple but massive. Two-phase systems are less massive and more flexible in the accommodation of system growth or changing heat loads, but require careful design to work properly under reduced gravity conditions (phase separation, good heat transfer, appropriate condensation rates, ...). Mass saving of two-phase systems are confined to pumps, fluid inventory and plumbing. Pipe diameters are also smaller than those corresponding to a single-phase liquid line, providing the possibility of retrofitting an existing single phase system to two-phase operation (Sadunas, Lehtinen & Parish (1985) [153].

Major disadvantages of the two-phase pumped loop system are the lack of long-life qualified pumps and potentially complex valving, metering and control algorithms (Wise (1986) [192]).

When cryogenic cooling below 70 K is required, the direct radiation to the space is hardly possible, then the fluid loop incorporates a refrigerating system (Brayton, Stirling, or Vuilleumier cycles) which

compresses the gas at ambient temperature and then expands it at a lower temperature. During the expansion, heat is added to the gas providing the required cooling. This heat is radiated to the space. Several refrigerators used onboard satellites are described in ECSS-E-HB-31-01 Part 14, clause 5.2.

4.2 Comparison between fluid loops and alternative systems

In order to define the field of application of fluid loops it should be convenient to compare them briefly with alternative insulating or refrigerating systems.

4.2.1 Passive thermal insulations

Fairly sophisticated, highly reliable, and extremely efficient passive thermal insulations are available for use in spacecraft. Data in ECSS-E-HB-31-01 Part 7 are referred to for details on the subject. Although these systems can be used in conjunction with component precooling, they cannot insulate for long times components having low thermal capacity, unless requiring prohibitively thick insulations. Among these low-thermal- capacity components, mention should be made to heavy electronic devices, such as batteries and tape recorders, which have a specific heat of the order of $c = 850$ J.kg^{-1}.K^{-1}, common to many electronic systems (Werth et al. (1966) [189]. In addition, thermal insulations are not appropriate for controlling components which operate in repeating on-off cycles, since in these cases it is required both to keep off the heat flowing outside and to evacuate the heat dissipated from inside.

In addition to being well suited to thermal protection of electronic and similar components, fluid loops afford a very precise control of the thermal energy being evacuated, and the flexibility to be adapted to a previously defined geometrical configuration.

4.2.2 Thermoelectric devices

Thermoelectric devices (TEDs), also called Peltier-effect devices, are low-voltage, high-current active thermal control modules that provide heating or cooling with the reliability associated with a purely electrical device. The relatively low performance efficiency of TEDs in conjunction with its high mass have prevented previous spacecraft application as a prime active thermal control system.

The comparison of TEDs with fluid loops within the normal range of application of these last devices makes little sense, the fluid loops being far superior. Nevertheless TEDs present several features which fluid loops cannot match. A few typical values could substantiate these assertions.

1. A typical thermoelectric module having an area of 0,03 m x 0,03 m pumps 5 W of heat through a 50 K temperature differential (Scott (1974), p. 216). Assuming that the thermally controlled area equals the thermoelectric pellet area, the heat flux would be 5,5 x 10^3 W.m^{-2}. This figure looks, however, very biased in favor of TEDs since several modules are placed a bit apart from each other on the surface to be controlled; a value of 110 W.m^{-2} is quoted as typical by Chapter & Johnsen (1973) [24]. On the other side, the laminar single-phase flow of water through a tube of cylindrical cross section, with an internal diameter of 5 x 10^{-3} m could remove 30 x 10^3 W.m^{-2} from the tube wall whose temperature is assumed to be 50 K above that of water, and this figure can be improved with turbulent single- phase flow and with two-phase flow.

2. A useful measure of the efficiency of a TED module is the "coefficient of performance", ratio of the heat pumped to the power that is supplied to operate the module. This

coefficient is of the order of unity for a typical TED (Scott (1974) [161], p. 221), whereas it could be as large as 400 for a single-phase fluid loop (see Figure 13-5 in this Part).

3. The comparison is somewhat more favorable for TED when the penalties associated with mass and volume are taken into account. Werth et al. (1966) [189] performed a trade-off analysis in which they considered the cooling, either by a moving fluid or by a thermoelectric device, of a cubical component, at uniform temperature, having a side of 0,3 m. The heat flux was of the order of 700 $W.m^{-2}$ for a surface temperature of 310 K. Mass and volume of the power system, supporting structure, bracketry, fittings, ... were neglected in both cases. The study showed that the ratio of TED controlled to fluid loop-controlled required mass was 1,5, and the ratio of required volumes 2,7.

Studies to reduce TED mass and to formulate large-scale manufacturing procedures to permit direct application of TEDs to spacecraft thermal control have been sponsored by NASA. These studies were concentrated on the development of thin film coatings that utilize vacuum deposited semiconductor materials.

TEDs on their part present the following advantages:

1. Thermoelectric devices operate on electronic principles. They require no pump, valves, piping, coolants and the fixtures associated with fluid loops.

2. Thermoelectric devices provide variable heat pumping by varying the input current. This allows for programmable internal temperatures through current modulation.

    Needless to say that the heat transfer rate can be increased in a fluid loop by increasing the fluid mass flow rate, but this requires either a variable speed pump or an electrically controlled throttle.

3. Heating or cooling can be provided by reversing the current. The fluid loop does not exhibit a similar feature.

4. A given heat transfer rate can be pumped no matter how small the source to sink temperature difference could be, whereas in single-phase fluid loops it is not feasible to reduce the source to sink temperature difference, for a given heat removal rate, by increasing the coolant mass flow rate beyond a certain value. Two-phase fluid loops do not present this limitation to the same extent.

Summarizing, under present state of development TEDs are only suited for heat conditioning small components which require very close temperature control.

4.2.3   Phase change materials (pcm)

Although PCM systems are normally used to absorb the abnormal heat dissipation peaks of an equipment which transfers somehow the heat that it dissipates to a sink, they are used sometimes as the sole heat sink for achieving the thermal control of solitary equipment. See ECSS-E-HB-31-01 Part 10.

Werth et al. (1966) [189] showed that the required mass of the PCM cell (radiator excluded) is of the order of twice the mass of the cooling jacket of the) fluid circulation cooling system evacuating the same heat flow rate. This indicates that the PCM system is competitive, on a mass basis, when it is used to protect components which are so small that the mass of the cooling jacket becomes of the order of the mass of the pump, valves and piping associated with this system.

Substantial gains in system mass, through radiator area savings can be achieved by incorporating thermal capacitors in the loop. This occurs in systems which are subject to alternant heating and

cooling regimes or when the radiator area grows to cope with α_s degradation (Lehtinen & Sadunas (1985) [114].

4.2.4 Heat pipes

Heat pipes are considered in ECSS-E-HB-31-01 Part 8.

The constant conductance heat pipe is a very powerful heat transfer device, which is basically simple although complex to manufacture and of) limited reliability.

Compared with constant conductance heat pipes, which normally do not require auxiliary power, and which are best suited for long mission on relatively simple satellites, the fluid loops presents the following advantages:

1. The heat flow rate can be controlled through the fluid flow rate, by use of appropriate temperature-controlled valves as has been already said.

2. The loop can be adapted to fairly complicated and relatively large configurations, although this advantage may be at the expense of increased power requirements. The idea of matching fluid loops and heat pipe radiators to decrease loop tubing and associated power requirements has been often set forth. However, heat pipe radiators require an additional heat exchanger to produce a temperature jump across the heat exchanger-radiator interface, resulting in larger system mass.

3. Different temperature levels, suited to each individual component, can be achieved by using regenerative heat exchangers. These are devices in which the heat exchanging surfaces come in contact successively with fluid media at different temperatures.

The noncondensable gas generated in a constant conductance heat pipe represents a problem; in a variable conductance heat pipe (VCHP), however, it is purposefully introduced (see ECSS-E-HB-31-01 Part 8, clause 7) to provide a variable blockage of the condenser region and then to varythe conductance as a function of the heat load.

As the required heat transfer rates increase and remote and (or) deployable radiators are being considered, the limits of current heat pipes are exceeded. Pump-assisted heat pipes are being considered at present.

4.2.5 Short-term discharge systems

Open cycle discharge systems are normally used to absorb short term peak thermal loads. Although these devices look simple, a fairly complex shielding system is required to avoid direct impinging of the coolant on the component. When cryogenic boiling liquids are used, this direct impinging results in very extreme local cooling effects.

In open-cycle high-pressure gas systems, high-pressure gas provides the necessary cooling. When a real gas is expanded at constant enthalpy (Joule-Thomson or throttling process) the total temperature of the gas decreases when the pressure decreases, provided that gas temperature is below a certain "inversion temperature". This effect results in cooling. Notice that under normal pressure and temperature conditions the gas behaves as a perfect gas and there is no total temperature change during throttling, thence no cooling effect would appear. Details concerning Joule-Thomson open refrigerators, as well as other discharge systems, can be found in ECSS-E-HB-31-01 Part 14, clause 5.3.

Discharge systems are uneconomic under orbital operation. In addition, the propulsive effect of the ejected fluid on the spacecraft flight trajectory should not be overlooked. For example, Nast, Barnes & Wedel (1976) [131] report the temporary upsetting of the Nimbus F spacecraft because of the venting

of cooling methane and the subsequent impingement of the exhaust plume on the spacecraft. In spite of these drawbacks, discharge systems could be useful in some cases, for instance, thermal protection during reentry of reusable space vehicles can be improved by means of expendable coolant systems (Helenbrook, Anthony & Fisher (1971) [84].

5
Analysis of a fluid loop

5.1   General

The purpose of this clause is to describe the way in which a fluid loop is analyzed and to show how the data presented in the following clauses may be used to this end.

A very simple fluid loop is considered for convenience. It consists of a circuit formed by fluid-carrying tubes which connect a heat sink to a heat source. A circulation pump moves the fluid through the loop so that heat is transported from source to sink by forced convection. Figure 5-1 is a schematic representation of the fluid loop.
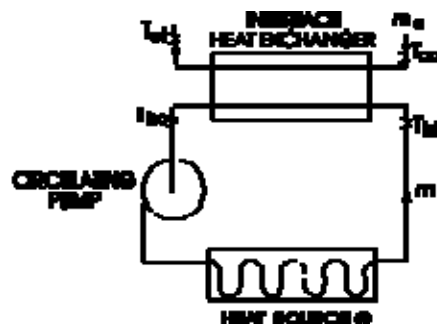
Figure 5-1: Schematic representation of the fluid loop.

The heat source could be an energy dissipating component such as electronic equipment, an experimental module involving exothermic reactions or any other heat-producing device. In some applications the heat source element is mounted on and thermally linked to a could plate, and the coolant flows through the latter, in which case the cold plate may be considered as the heat source. In the following analysis the heat source is simply identified by its heat production rate, Q, and no consideration is given to the details of the heat transfer mechanism from source to coolant fluid.

The heat sink can be a heat exchanger, in which case heat is transferred to a "cold" fluid circulating in another loop (dual loop configuration), or it may be a radiator which rejects the heat directly to deep space. In the present example transfer to a second loop through an interface heat exchanger is considered.

The procedure presented in this clause to analyze the fluid loop in Figure 5-1 may be easily generalized to other systems.

The following data are assumed to be known:

1.   General layout of the fluid loop, including heat exchanger surface geometry and dimensions.

2.   Heat flow rate to be evacuated, Q.

3.   Mass flow rate in each loop: m_h, m_c.

4.   Inlet temperature of the cold fluid, T_{ci}.

From these data, the temperatures throughout the loop and the pumping power requirements are computed. The mass flow rate through the cold fluid loop is often determined by means of some optimization procedure (see Clause 13). In the present analysis, however, only the performance of the fluid loop for a given mass flow rate is considered.

5.2   Thermal performance

Assuming, 1) thermally insulated tubes for the fluid transport between heat source and heat sink, 2) no temperature increase in the circulation pump, and 3) no temperature increase due to friction, the temperature at the entrance of the sink, T_{hi}, equals the temperature at the exit of the source, and the temperature at the exit of the sink, T_{ho}, equals the temperature at the entrance of the source (see Figure 5-1).

To calculate the temperature T_{hi}, T_{ho}, and T_{co}, the following equations for the heat flow rate may be used:

$$Q = sC_1 \left(T_{hi} - T_{ci} \right) \tag{5-1}$$

$$Q = C_h \left(T_{hi} - T_{ho} \right) \tag{5-2}$$

$$Q = C_c \left(T_{co} - T_{ci} \right) \tag{5-3}$$

where C_1 is the smallest of C_h and C_c.

Eq. [5-1] describes the heat transfer rate from hot fluid to cold fluid in the heat exchanger, in terms of the heat transfer effectiveness, ε (see Eq. [5-4] of clause 11.2.2 where a slightly different nomenclature has been used for convenience). Eqs. [5-2] and [5-3] are simply an energy balance for the hot and cold fluid, respectively. From Eqs. [5-1] to [5-3], the temperature through the loop are obtained.

$$T_{co} = T_{ci} + \frac{Q}{C_c} \tag{5-4}$$

$$T_{hi} = T_{ci} + \frac{Q}{sC_1} \tag{5-5}$$

$$T_{ho} = T_{ci} + Q \left(\frac{1}{sC_1} - \frac{1}{c_h} \right) \tag{5-6}$$

If the heat source is a could plate, there is an additional equation to describe the heat transfer process at the plate, namely

$$Q = s_{cp} c_h \left(T_S - T_{ho} \right)$$ [5-7]

where ε_{cp} is the effectiveness of the heat transfer surface at the heat source, and T_S is the temperature of the source. Eq. [5-7] determines the temperature at the source.

Summarizing, to compute the temperatures in the loop, the heat transfer effectiveness of the heat exchanger must be calculated. The following steps are needed to this end:

1. Compute heat transfer areas, free flow areas and frontal areas, for the hot side and the cold side of the exchanger. To describe a heat transfer surface the following parameters are often used:

A,	Total heat transfer area on one side.[m²].
A_{FL},	Free flow area on one side.[m²].
A_{FR},	Frontal area on one side.[m²].
D_E,	Hydraulic diameter. [m].
L,	Flow length on one side. [m].
α,	Ratio of total heat transfer area on one side of a closed-type exchanger or recuperator to total exchanger volume. [m².m⁻³]. This ratio is called "area density α".
Φ,	Ratio of free-flow area to frontal area of one side of exchanger. This ratio is called "porosity".

The following equations relate surface factors with core factors, for each side of the exchanger, and may be used to calculate heat transfer areas and free-flow areas,

$$D_E = 4L \frac{A_{FL}}{A}$$ [5-8]

$$\Phi = \frac{A_{FL}}{A_{FR}} = \frac{\alpha D_E}{4}$$ [5-9]

2. Compute fluid properties. The fluid properties are evaluated at an arithmetic mean temperature as follows,

$$T_c = \frac{T_{ci} + T_{co}}{2} \quad , \quad T_h = \frac{T_{hi} + T_{ho}}{2}$$ [5-10]

where T_{co} and T_{hi} are given by Eqs. [5-4] and [5-5] respectively, and T_{ho} may be computed from Eq. [5-6] assuming a heat transfer effectiveness $\varepsilon = 0{,}8$. This estimation has to be verified a posteriori.

See clause 6.2.4 for further details on the evaluation of the average temperature.

The following fluid properties are needed: density, ρ, specific heat, c_p, thermal conductivity, k, dynamic viscosity, μ, and Prandtl number, $Pr = \mu c_p / k$. Table 10-1 gives the values of these properties for relevant liquid coolants.

3. Compute Reynolds number. The Reynolds number is given by

$$Re = \frac{m D_E}{A_{FL} \mu}$$

[5-11]

It is computed for each side of the exchanger.

4. Compute the Nusselt number Nu and the convective heat transfer coefficient, h.

The thermal analysis developed in Clause 6 presents data to compute the Nusselt number as a function of the Reynolds number, Prandtl number and geometry (Figure 6-1 to Figure 6-38), for most basic configurations. These figures may be also used to estimate the Nusselt number in more complicated geometries.

If the heat transfer surface is one of those presented in clause 11.3, the Nusselt number may be obtained from figures given by Kays& London (1964) [102], which relate the Stanton number.

$$St = \frac{Nu}{PrRe}$$

[5-12]

to the Reynolds number, for many different heat exchanger surfaces.

Clause 9 presents data to estimate the Nusselt number, when turbulence promoters or other type of heat transfer enhancement devices are used.

The convective heat transfer coefficient, h, is given by

$$h = \frac{kNu}{D_E}$$

[5-13]

or

$$h = \frac{C}{A_{FL}} St$$

[5-14]

5. Compute the temperature effectiveness of the surface due to fins, η. The temperature effectiveness is given by Eq. [5-3] of clause 11.2.2, where fin effectiveness's, η_f, for typical fins are given in Figure 11-7 and Figure 11-8.

6. Compute the overall thermal conductance, U, for each side of the exchanger.

This coefficient is given by Eq. [5-2] and of clause 11.2.2, in terms of both the hot and the cold side of the exchanger. When fouling has to be considered, the above equation should be replaced by the equation which appears in clause 11.6.2.

7. Compute the number of heat transfer units, N_t, as defined in Eq. [5-5] of clause 11.2.2.

8. Compute the exchanger effectiveness, ε.

   The heat transfer effectiveness, ε, of the exchanger is presented in Clause 11 as a function of the number of heat transfer units, N_{tu}, capacity rate ratio, R, and flow arrangement. The results are given in graphical form, for many different arrangements, in Figure 11-9 to Figure 11-28. These figures may be also used to estimate the heat transfer effectiveness for many flow arrangements not explicitly considered in Clause 11.

In some instances, particularly for heat exchangers of very high heat transfer effectiveness, the effects discussed in clause 11.4 should be taken into account.

If the resulting effectiveness is very different from the one used in point (2) to compute the fluid properties, the steps just described should be repeated.

Once the heat transfer effectiveness is known, Eqs. [5-4] to [5-6] yield the temperature through the loop.

5.3   Power requirements

The power, P, which is supplied to the circulation pump can be expressed as

$$P = \frac{1}{\eta_p} \Delta p \frac{m}{\rho}$$

[5-15]

where η_p is the overall efficiency of the pump, Δp the pressure loss through the loop, m the fluid mass flow rate and ρ the fluid density at the location of the pump. m/ρ is then the fluid volume flow rate through the pump. Equations and graphics to evaluate the pressure loss are given in Clause 7. Values of η_p for typical spaceborne pumps can be found in Clauses 12 and 9. Generally, the pressure loss may be split into the following terms:

1. pressure loss in the supply plumbing;

2. pressure loss in the return plumbing;

3. pressure loss in the heat source, and

4. pressure loss in the heat sink.

To compute these losses, the following steps are needed.

1. Compute the Reynolds number in the supply and return plumbing,

$$Re = \frac{4}{\pi} \frac{m}{D_E \mu}$$

[5-16]

where D_E is the diameter of the tube and μ the fluid viscosity. Since the viscosity is temperature dependent the Reynolds number is different on each leg of the plumbing.

2.   Compute the friction factor λ for the straight parts of the ducts, from Figure 7-2 and Figure 7-3 in Clause 7. The friction factor is a function of the Reynolds number and should be computed for the supply and for the return plumbing.

3.   Compute pressure loss due to friction along the tube walls,

$$\Delta p = \lambda \frac{L}{D_E} \frac{1}{2} \rho V^2 \qquad\qquad [5\text{-}17]$$

4.   Compute pressure loss for each one of the bends of the circuit,

$$\Delta p = C_k \frac{1}{2} \rho V^2 \qquad\qquad [5\text{-}18]$$

where C_k can be obtained by use of Figure 7-4 to Figure 7-14 in Clause 7.

5.   Compute pressure loss in valves, manifolds, entrances, etc. by using Figure 7-15 to Figure 7-27 or the data submitted by the manufacturer of the particular component. Data for entrance effects can be found in clause 7.2.5.

6.   Compute pressure loss in heat source and heat sink. This pressure loss may be estimated from Figure 7-2 to Figure 7-30 in Clause 7. If the heat source or sink is a heat exchanger with a core-surface geometry like the ones presented in Clause 11.3, the friction factor may be obtained from figures given by Kays & London (1964) [102].

6
Thermal analysis

6.1   General

Data concerning the convective heat transfer between a fluid and the tube wall surface are presented in this clause. These data can be used, together with the heat exchanger theory presented in clause 11.2 for the analysis of heat exchangers.

The data are divided into two main parts. The first part concerns internal flows, i.e., configurations where the fluid flows inside the domain bounded by the heat transfer surface. In the second part external flows are considered, i.e., configurations where the fluid flows outside of the domain bounded by the surface.

Data for both laminar flow and turbulent flow are presented.

Concerning the heat flux distribution, two cases are considered, constant wall temperature and constant heat transfer rate per unit length. The case of constant heat transfer rate can be easily dealt with theoretically, nevertheless most experiments are performed under nearly constant wall temperature. In practical instances the constant wall temperature boundary condition is applicable in such heat exchangers as evaporators, condensers and in any heat exchanger where one fluid has a very much higher capacity rate that the other. The constant heat transfer rate boundary condition is applicable in counter flow heat exchangers, when the fluid capacity rates are similar. These two boundary conditions cover the usual extremes met in heat exchanger design.

The data for constant heat flux may be applied directly to other boundary conditions provided that the real variation of the heat transfer rate, $Q(x)$, is smooth enough or, more precisely, that the following inequality

$$\frac{dQ}{dx} << \frac{Q}{D}$$

[6-1]

is satisfied. Additional comment on this point are given in clause 9.1.4.

6.2   Analytical background

6.2.1   Heat transfer coefficient

The convective local heat transfer between the tube wall and a fluid moving relative to the wall can be calculated in term of the temperature difference, T_w-T_b, and a local heat transfer coefficient, h_x, by means of the following expression:

$$q_x = h_x \left(T_w - T_b \right)_x \qquad [6\text{-}2]$$

Usually the wall temperature, T_w, and the local heat transfer coefficient are uniform at each section, x, of the tube, while the fluid bulk temperature is given by the expression:

$$T_b = T_i + \frac{Q(x)}{mc_p} \qquad [6\text{-}3]$$

The definition of the bulk temperature in terms of the local properties is given in clause 6.2.4.

Sufficiently far from the tube entrance, the fluid velocity and temperature profiles for conditions of constant wall temperature and of constant heat rate become self-similar. The non dimensional temperature profiles are invariant with the axial distance x, and therefore the heat transfer coefficient h_x becomes independent of x.

The heat transfer up to the station x is evaluated by using the mean heat transfer coefficient h_m

$$Q(x) = h_m \Delta T_m x \pi D \qquad [6\text{-}4]$$

where h_m is defined by the following averaging process:

$$h_m \Delta T_m x = \int_0^x h_x \left(T_w - T_b \right)_x dx \qquad [6\text{-}5]$$

Three terms of the coefficient h_m may be used, according to the following three definitions of temperature difference, ΔT_m:

    1.   Inlet mean temperature difference:

$$\Delta T_{im} = \left(T_w - T_b \right)_i \qquad [6\text{-}6]$$

    2.   Arithmetic mean temperature difference:

$$\Delta T_{am} = \frac{\left(T_w - T_b \right)_i + \left(T_w - T_b \right)_o}{2} \qquad [6\text{-}7]$$

    3.   Logarithmic mean temperature difference:

$$\Delta T_{lm} = \frac{(T_w - T_b)_i + (T_w - T_b)_o}{\ln \frac{(T_w - T_b)_i}{(T_w - T_b)_o}}$$ [6-8]

6.2.2 Dimensionless groups

It is customary to introduce the following dimensionless parameters, which are defined either locally or through some averaging process.

1. Nusselt number

$$Nu = \frac{hD_E}{k}$$ [6-9]

The Nusselt number indicates what multiple of mere thermal conduction is transferred by convection. It is usually defined in terms of the equivalent or hydraulic diameter, D_E.

2. Prandtl number

$$Pr = \frac{\mu c_p}{k}$$ [6-10]

which measures the ratio of fluid viscous to thermal diffusivities.

3. Reynolds number

$$Re = \frac{\rho V D_E}{\mu}$$ [6-11]

giving the ratio of inertia to viscous forces.

Sometimes the heat transfer depends on the product $PrRe$ and the Graetz number is used to present the available data.

$$Gz = \frac{\pi}{4} \frac{D_E}{L} PrRe$$ [6-12]

From the Nusselt, Prandtl and Reynolds numbers the Stanton number is deduced.

$$St = \frac{Nu}{PrRe}$$ [6-13]

4.   Grashof number

$$Gr = \frac{\beta g D_E^3 \rho^2 |T_w - T_b|}{\mu^2}$$ [6-14]

The Grashof number expresses the ratio of buoyancy to viscous forces.

A dimensional analysis indicates that the heat transfer coefficient may be related to the fluid properties and flow parameters in the following way.

$$Nu = f\left(Pr, Re, Gr, x/D_E\right)$$ [6-15]

6.2.3   Simplifying assumptions

The following simplifying assumptions are introduced:

1.   Buoyancy can be neglected, especially during orbital flight, ever for very low fluid mass flow rates; $Gr = 0$. Nevertheless, buoyancy can be introduced intentionally, by swirling of the flow, in order to enhance the convective heat transfer (see clause 9.1.1 and Figure 9-8 to Figure 9-11).

2.   Fluid properties are evaluated at some reference temperature. The resulting values are assumed to prevail through the fluid bulk. This assumption is discussed in clause 6.2.4.

3.   The effect of surface roughness on heat transfer is neglected. Sometimes surface roughness is created intentionally to enhance the heat transfer (see clause 9.1.1 and Figure 9-1 to Figure 9-9).

4.   The fluid configuration is steady.

6.2.4   Temperature-dependence of fluid properties

The heat transfer data presented in this clause are based on the assumption that the fluid properties, which are evaluated at a reference temperature, are temperature independent. In applications where temperature differences between the fluid and the surface are large, the variations of fluid viscosity, thermal conductivity and density ought to be taken into account.

The variation of fluid properties differs substantially for gases and liquids. For gases, thermal conductivity, viscosity, and density all vary with temperature to a considerable degree. For liquids, on the other hand, the only property that is highly temperature dependent is viscosity, which varies with temperature much more than any of the gas properties.

Temperature-dependence effects at a particular flow cross section can usually be compensated for by evaluating certain or all of the properties at the fluid bulk temperature, T_b, for this cross section,

$$T_b = \frac{\int\limits_{A_{FL}} uT dA_{FL}}{V A_{FL}}$$ [6-16]

where u and T are the local velocity and local temperature, A_{FL} is the surface area of the cross section, and V the mean fluid velocity. T_b is sometimes termed the mixing-cup temperature.

In many cases the mean film temperature, the arithmetic average of T_w and T_b, is used as reference temperature.

There are cases in which the use of a reference temperature is inadequate, for example when the wall-to-bulk temperature ratio differs greatly from one. The problem is then approached by introducing into the transfer law a loading factor of the form $(T_w/T_R)^m$ or $(\mu_w/\mu_R)^m$, where T_R is the reference temperature independently of the way in which it has been defined.

It is not to be expected that the correction has the same form for gases and liquids, nor for fluids of the same phase but widely differing Prandtl numbers, nor for different transferred entities (heat or momentum), nor for laminar and turbulent flow.

For gases at wall-to-bulk temperature ratios in the range $0{,}5 < T_w/T_b < 2$, the effect on the heat transfer coefficient of radial property variations does not exceed 10 per cent (ESDU 68006 (1968) [48]). Values of the exponent m for a wider range of T_w/T_b, for several physical situations, and for both heat transfer and friction, can be found in Kays & London (1964) [102], p. 88.

In the case of liquids, the viscosity is normally a strongly decreasing function of temperature. When the wall-to-bulk temperature difference is large, the fluid velocity near the wall departs from that calculated assuming uniform viscosity. This distortion of the velocity profile changes the heat transfer coefficient. Experimental data indicate (ESDU 68006 (1968) [48]) that this effect can be accounted for by means of the following formula

$$\frac{Nu}{Nu_b} = \left(\frac{\mu_b}{\mu_w}\right)^{0{,}14} \qquad\qquad [6\text{-}17]$$

in the range $0{,}004 < \mu_b/\mu_w < 20$. This expression, extensively quoted, was suggested by Deissler for laminar flow in circular ducts. Exponents for turbulent flow, deduced after experiments by Deissler, are given in Kays & London (1964) [102], p. 90. In all these cases the reference temperature is T_b.

In many applications, temperature variations along the tube are more pronounced than those over the cross section, and a mean temperature with respect to the tube length ought to be used to evaluate fluid properties. This reference temperature is identified as T_{bm}.

The evaluation of T_{bm} is not an easy task, and the designer should exercise his judgments for avoiding fairly tedious trial-and-error procedures. T_{bm} depends on the variations of heat flux and temperature differential along the tube. Several typical cases are considered:

1. For constant heat flux, the wall-to-bulk temperature difference remains nearly constant, and since the wall temperature usually varies linearly, the mean fluid temperature is merely the arithmetic average of inflow and outflow temperatures.

$$T_{bm} = T_{bam} = \frac{T_{bi} + T_{bo}}{2} \qquad\qquad [6\text{-}18]$$

2. Constant wall temperature. The fluid temperature variation along the tube will be close to exponential, provided that the heat transfer coefficient does not vary markedly with tube length.

$$T_{bm} = T_w - \frac{T_{bo} - T_{bi}}{(4L/D_e)St}$$ [6-19]

where St is estimated beforehand.

3. When the heat transfer coefficient decreases with tube length, as occurs with laminar flow, the true mean temperature with respect to tube length is close to the fluid exit temperature, since the large heat transfer rates upstream are responsible for the comparatively sharp changes in the fluid bulk temperature near the tube entrance.

6.2.5 Laminar versus turbulent fluid flow

The characteristics of the fluid flow in a pipe depend on the Reynolds number.

The motion is laminar for sufficiently low values of the Reynolds number, becoming turbulent when some transition value is exceeded.

For fluids flowing through pipes the transition Reynolds number is normally of the order of 2400. In the range $2000 < Re < 2800$ the fluid flow is characterized by an intermittent turbulence which takes the form of alternating slugs of laminar or turbulent fluid moving down the pipe. For $Re \approx 4000$ the turbulent regime is fully developed.

The disorder associated with the turbulence improves the heat transport process at the cost of a larger energy dissipation.

Several considerations concerning laminar versus turbulent fluid flow should be made.

1. Normally laminar flow should be preferred because the power requirements are lower than in the turbulent case. Nevertheless, the low velocities required for laminar flow, together with low thermal conductivity of most fluids (particularly gases) result in low heat transfer rates per unit surface area. Thus, large surface areas are required.

2. Low velocity flow are more sensitive to control than the high velocity ones.

3. Transitional flow with the associated intermittency should be, as a general rule, avoided. In compact-heat exchanger applications, however, the Reynolds-number range of interest is usually about 500 to 15000; thus the transition region can hardly be avoided.

4. If the Reynolds number must be decreased preserving the flow rate, the inner diameter of the tube must be increased, and conversely.

6.2.6 Heat transfer to internal flows

Data on convective heat transfer to internal flows are presented in Clause 6.3 (Figure 6-1 to Figure 6-27). The data are given in terms of the Nusselt number, Nu, either local, averaged or both. The heat transfer coefficient, h, is deduced from the value of Nu, the fluid thermal conductivity, k, and the hydraulic diameter of the duct, D_E.

The sequence of figures is arranged as follows:

1. Figure 6-1 to Figure 6-12 concern laminar flow (clause 6.3.1.1), and Figure 6-14 to Figure 6-27 turbulent flow (clause 6.3.1.3). The prediction of Nusselt numbers in the transitional flow regimen ($2000 < Re < 4000$) is difficult and thus the available information is fairly limited in scope (clause 6.3.1.2). Figure 6-13, which shows a typical range of local Nusselt numbers for transitional gas flow, is intended to indicate that the Nusselt numbers are somewhere between the laminar and turbulent values.

2. Within each flow regime the first few figures apply to the region far removed from the entrance to the tube, where both a fully developed velocity profile and a fully developed temperature profile exist. This is the case of Figure 6-1 to Figure 6-5 for laminar flow, and Figure 6-14 to Figure 6-22 for turbulent flow.

3. The next group of figures in either the laminar or turbulent regime apply to the case in which the velocity profile is fully developed and remains fixed, while the temperature profile develops. In these configurations the fluid temperature upstream of some section is assumed to be uniform and equal to the wall surface temperature, there being no heat transfer in this region. Following the mentioned section heat transfer takes place. These thermal-entry-length solutions only apply rigorously when a hydrodynamic starting length is provided so that the velocity profile is fully developed before heat transfer starts, a condition rarely encountered in practice. However, when the temperature change is concentrated near the wall ($Pr \gg 1$), the temperature gradient at the wall reacts quickly to changing conditions, and these solutions are excellent approximations to the real cases.

4. Finally, Figure 6-10 to Figure 6-12 apply to the case of combined hydrodynamic and thermal entry length; that's, when both the velocity and the temperature profile are uniform at the entrance of the tube. The relevant variable for these thermal entry length solutions is the non-dimensional axial distance

$$x^+ = \frac{x/r}{PrRe} = \frac{\pi}{2Gz}$$ [6-20]

which is related to the inverse of the Graetz number, Gz.

Most of the data refer to cylindrical tubes of circular cross section. For turbulent flow these data can be applied to other cross-sectional shapes provided that the equivalent or hydraulic diameter, D_E, is used as characteristic length.

Exceptions to this rule concern the heat transfer to a fluid flowing through a cylinder of annular cross section or between two parallel plates (which is a limiting case of annulus). These are the simplest geometrical configurations allowing different heating rates from different walls of the same cross section of the duct. Only two fundamental solutions suffice to obtain the solution for any combination of heat fluxes through these walls. The mentioned fundamental solutions are: a) inner wall heated with outer insulated (subscript 11), b) outer wall heated with inner insulated (subscript 22). The heat transfer coefficients on the inner and outer tubes, h_1 and h_2, are defined as follows:

$$q_1 = h_1(T_1 - T_b) \quad , \quad q_2 = h_2(T_2 - T_b)$$ [6-21]

and the Nusselt numbers as:

$$Nu_1 = \frac{h_1 D_E}{k} \quad , \quad Nu_2 = \frac{h_2 D_E}{k} \qquad [6\text{-}22]$$

These Nusselt numbers can be calculated from the fundamental solutions for any heat flux ratio, through the relationships

$$Nu_1 = \frac{Nu_{11}}{1 - (q_2 / q_1) Z_1} \quad , \quad Nu_2 = \frac{Nu_{22}}{1 - (q_1 / q_2) Z_2} \qquad [6\text{-}23]$$

where Z_1 and Z_2 are the influence coefficients which may be evaluated from the fundamental solutions. The values of Nu_{11}, Nu_{22}, Z_1, Z_2 are presented in graphical form in Figure 6-3, Figure 6-4, Figure 6-8 and Figure 6-18 to Figure 6-21 for annuli. Similar data, for parallel plates, are given in Figure 6-6, Figure 6-7, Figure 6-12, Figure 6-16, Figure 6-17 and Figure 6-27.

Curved ducts are widely used in heat transfer equipment. In these ducts the heat transfer (and the friction) is augmented by secondary flows which appear because of the fact that the radial pressure gradient imposed by the high velocity core is not balanced by the local centripetal acceleration. The effect of the secondary flow is accounted for through an additional dimensionless parameter, the Dean number, K, which is defined as:

$$K = Re \sqrt{\frac{r}{R}} \qquad [6\text{-}24]$$

where r is the radius of the tube cross section and R the radius of the coil.

It should be said that the onset of turbulence in coiled pipes is delayed owing to the suppression of transverse motions of fluid elements by centrifugal forces. Kubair & Kuloor (1966) [111] propose the following formula to predict the critical Reynolds number for transition from laminar to turbulent flow,

$$Re = 1{,}273 \times 10^4 \left(\frac{r}{R} \right)^2 \qquad [6\text{-}25]$$

Figure 6-5, Figure 6-9 and Figure 6-22 present data on the heat transfer to fluid moving through tube coils.

6.2.7   Heat transfer to external flows

In many configurations of practical interest the heated or cooled surface is submerged in the fluid instead of bounding it.

The convective heat transfer rate between the external surface of a cylinder and a fluid moving relative to it can be calculated in terms of the temperature difference, T_w-T_b, and a mean heat transfer coefficient, h, by using the following expression:

$$Q = h\pi DL\left(T_{wm} - T_b\right) \qquad [6\text{-}26]$$

where D is a characteristic length of the cylinder cross section, L is the cylinder length, T_b is the bulk temperature corresponding to the undisturbed fluid, and T_{wm} is a mean temperature of the outer surface of the cylinder. A perimeter-mean value of T_w is normally used, although different definitions of the average value may be considered without substantially influencing the experimental data on Nusselt numbers.

A dimensional analysis indicates that the heat transfer coefficient can be related to the fluid properties, cylinder geometry and flow parameters in the following way:

$$Nu = f\left(Pr, Re, Gr, L/D, \theta\right) \qquad [6\text{-}27]$$

θ being the inclination of the cylinder axis to the incoming flow.

The influence of Grashof number can be neglected as above, whereas end effects are insignificant for L/D greater than about 3.

Figure 6-28 and Figure 6-29 (clause 6.3.1.2) give data for a constant temperature circular cylinder.

The problem is far more complicated in the case of tube banks. The convective heat transfer rate between a fluid and a tube bank constituted by n circular cylinders of length L and diameter D is given by

$$Q = n\overline{h}\,\pi DL\left(T_{wm} - T_b\right) \qquad [6\text{-}28]$$

where $\overline{h}$ is the mean heat transfer coefficient for the particular tube bank under consideration.

A dimensional analysis shows that, when free convection can be ignored, the mean Nusselt number, $\overline{Nu}$, of a tube bank is related to the flow parameters, fluid properties and geometry by the expression

$$\overline{Nu} = f\left(Re_b, Pr_b, Pr_w, s_t/D, s_l/D, N, L/D, \theta\right) \qquad [6\text{-}29]$$

where in this instance

$$\mathrm{Re}_b = \frac{\rho_b V_{\max} D}{\mu_b} \qquad [6\text{-}30]$$

and V_{max} is based on the minimum free area available for fluid flow, regardless of whether this minimum area occurs in the transverse or diagonal openings.

It is customary, ESDU 73031 (1973) [57], to base heat transfer data on a Nusselt number, Nu_r, which corresponds to the following reference conditions:

1. Constant fluid properties.

2. Number of rows in the tube bank, N = 10 with at least 6 tubes in each row.

3. Cylinder axis normal to flow, $\theta = 90°$.

4. L/D > 5.

Reference Nusselt numbers, Nu_r, vs. Reynolds number, Re_b, are shown in clause 6.3.2.2. Figure 6-31 and Figure 6-32 are for in-line tube banks, and Figure 6-33 for staggered tube banks. The fluid bulk Prandtl number, Pr_b, is assumed to be equal to one in all these three figures. Corrections for Prandtl number effects can be deduced from Figure 6-34.

Once Nu_r is known, the Mean Nusselt number, $\overline{Nu}$, is expressed in the simplified form,

$$\overline{Nu} = Nu_r F_1 F_2 F_3 \qquad\qquad [6\text{-}31]$$

where the factor F_1 takes into account the variation of the fluid properties, F_2 is a correction factor for a bank having $N \neq 10$, and F_3 corrects for the yaw angle of the bank. These three correction factors are given in Figure 6-35, Figure 6-36 and Figure 6-37, respectively.

To calculate the heat transfer for a particular row (the nth) a new factor, F_4, relating the performance of that row to the average for the 10 rows bank is used (Figure 6-38).

$$Nu_n = Nu_r F_1 F_3 F_4 \qquad\qquad [6\text{-}32]$$

Heat transfer data for other exchanger configurations can be found in Kays & London (1964) [102]. Geometrical descriptions of the many configurations tested by these authors are given in Clause 11.3.

Each group of figures giving the data for both internal and external flows is preceded by tables allowing a quick assessment of the content of each figure. The table in the next page is for internal flows. The table for external flows is placed immediately before the corresponding figures.

6.3 Thermal performance data

6.3.1 Heat transfer to internal flow

The following summarizes the data presented in the following pages.

The data are categorized according to: flow characteristics, heat flux distribution, and duct geometry.

The labels used to distinguish these categories are the following:

- Type of flow: L, laminar. T, turbulent. IT, transitional.

- Degree of flow development: FL, fully developed flow. TEL, thermal entry length. HTEL, combined hydrodynamical and thermal entry length.

- Heat flux distribution: q, constant heat transfer rate. T, constant wall temperature.

Type of flow	Flow devel.	Heat flux distribution	Geometry	Input Variables	Output	Fig.	References
L	FL	q & T	Several	Geometry	Nu_q, Nu_T	Figure 6-1	Kays & London(1964) [102]
			Straight tube of rectangular cross section	a/b	Nu_q, Nu_T	Figure 6-2	
		q	straight tube of annular cross section	r_1/r_2	Nu_{11}, Nu_{22}	Figure 6-3	
					Z_1, Z_2	Figure 6-4	
			Coil	K, Pr = 0,1, 0,2, 0,7, 1,4, 10	Nu	Figure 6-5	Mori et al. (1965) [128]
	TEL	T	Circular cylinder, parallel plates, straight tube of rectangular cross section	x^+	Nu_x, Nu_{1m}	Figure 6-6	Kays (1966) [101]
		q	Circular cylinder, parallel plates		Nu_x, Z	Figure 6-7	
			Straight tube of annular cross section	x^+, r_1/r_2= 0,1,0,5	Nu_{11}, Nu_{12}, Z_1, Z_2	Figure 6-8	
		T	Coil	x^+, r/R = 0,025,0,1	Nu_x	Figure 6-9	Kubair et al. (1966) [111]
	HTEL		Circular cylinder	x^+	Nu_x, Nu_{1m}	Figure 6-10	ESDU 68006 (1968) [48]
		q		x^+, Pr = 0,01,0,7,10	Nu_x	Figure 6-11	Heaton et al. (1964) [82]

Type of flow	Flow devel.	Heat flux distribution	Geometry	Input Variables	Output	Fig.	References
			Parallel plates		Nu_x, Nu_z	Figure 6-12	
IT	FL	T	Circular cylinder	$Re, Pr = 0,7$	Nu_x	Figure 6-13	ESDU 68006 (1968) [48]
T	FL	q		$Re, Pr = 0,7, 1,3, 10, 50, 10^2, 10^3, 10^4, 10^5$	Nu	Figure 6-14	Petukhov & Roizen (1975) [143]
		ratio Nu_q/Nu_T		$Re, Pr = 0, 0,005, 0,01, 0,02, 0,03, 0,04, 0,10, 0,718$	Nu_q/ Nu_T	Figure 6-15	Sleicher & Tribus(1957) [167]
		q	Parallel plates	$Re, Pr = 0,01, 0,03, 0,7, 3, 10, 30, 10^2, 10^3$	Nu	Figure 6-16	Kays (1966) [101]
					Z	Figure 6-17	
			Straight tube of annular cross section	$Re, Pr = 0,01,0,7,10, r_1/r_2 = 0,2$	Nu_{11}, Z_1	Figure 6-18	
					Nu_{22}, Z_2	Figure 6-19	
				$Re, Pr = 0,01,0,7,10, r_1/r_2 = 0,5$	Nu_{11}, Z_1	Figure 6-20	
					Nu_{22}, Z_2	Figure 6-21	
			Coil	$Re, r/R = 0,05,0,1$	$Nu\,Pr^{-0,4}$	Figure 6-22	Seban et al. (1963) [162]
	TEL	T	Circular cylinder	$x/D, Re = 0,5x10^5, 10^5, 2x10^5, Pr = 0,01$	Nu_x,Nu_{1m}	Figure 6-23	Kays (1966) [101]
				$x/D, Re = 0,5x10^5, 10^5, 2x10^5, Pr = 0,7$		Figure 6-24	
		q		Nu_x/Nu	Figure 6-25		
				$x/D, Pr = 0,01,0,7,10, Re = 10^5$	Figure 6-26		
			Parallel plates	$x/D_E, Pr = 0,01,0,1,10 Re = 7096,73612$	$Nu_x/Nu,Z$	Figure 6-27	

6.3.1.1 Laminar flow

SHAPE ($L/D_E > 100$)	Nu_q	Nu_T
Circle	4,364	3,66
Equilator Triangle	3,00	2,35
Square	3,63	2,89
Parallel lines	8,235	7,54
Parallel lines, one of them insulated	5,385	4,86

Figure 6-1: Nusselt numbers, *Nu*, for fully developed laminar flow through straight pipes of several cross-sectional shapes. *Nu_q* is the Nusselt number for constant heat transfer rate along the duct, and *Nu_T* that for constant wall temperature along the duct. From Kays & London (1964)
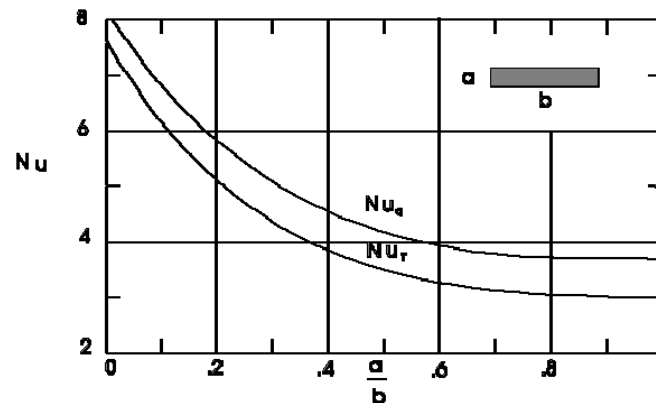
[102].

Figure 6-2: Nusselt numbers, *Nu*, vs. ratio, *a/b*, of short side to long side for fully developed laminar flow through straight pipes of rectangular cross section. From Kays & London (1964) [102].
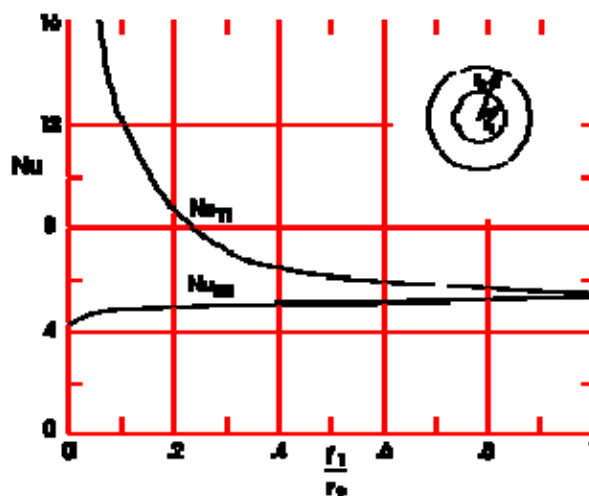
Figure 6-3: Nusselt numbers, *Nu*, vs. ratio of inner to outer diameter, *r₁/r₂*, for fully developed laminar flow in concentric- circular-tube annuli. Constant heat transfer rate. From Kays & London (1964) [102].
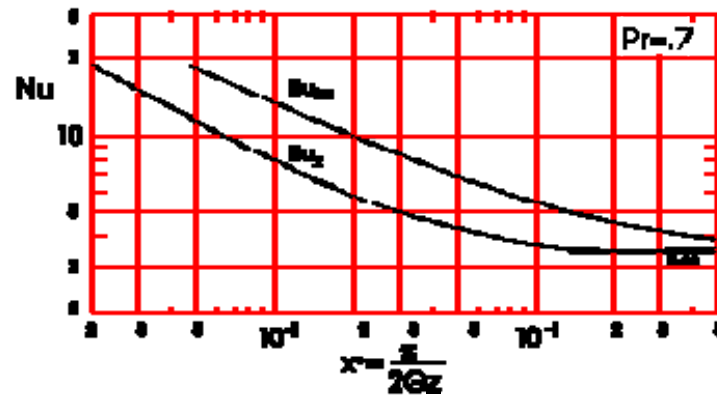
Figure 6-4: Influence of coefficients, *Z*, vs. ratio of inner to outer diameter, r_1/r_2, for fully developed laminar flow in concentric-circular-tube annuli. Constant heat transfer rate. From Kays & London (1964) [102].
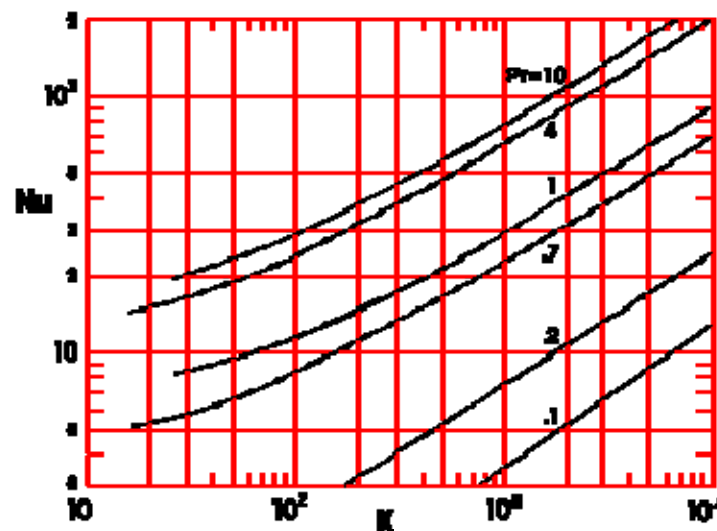
Figure 6-5: Nusselt number, *Nu*, vs. Dean number, *K*, for fully developed laminar flow in curved pipe of circular cross section. Constant heat transfer rate. Results are shown for different Prandtl numbers, *Pr*. Calculated by the compiler after Mori & Nakayama (1965) [128].
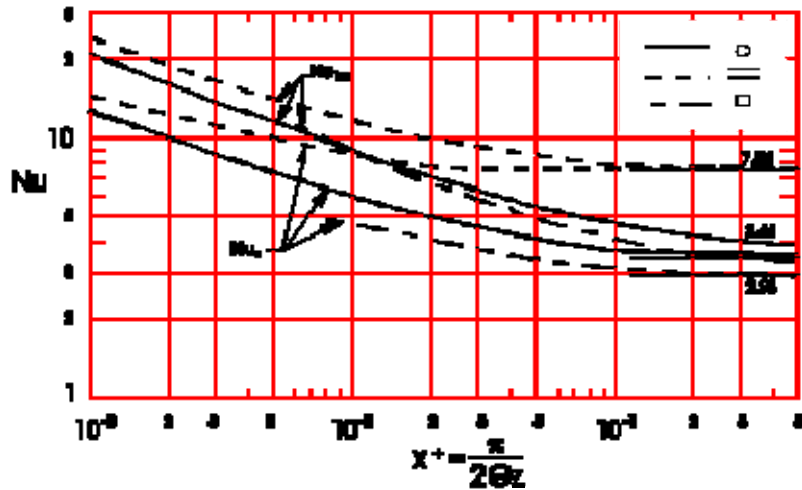
Figure 6-6: Thermal entry length Nusselt numbers, *Nu*, vs. non-dimensional axial distance, *x⁺*, for laminar flow through straight pipes. Constant wall temperature. Calculated by the compiler after Kays (1966) [101].
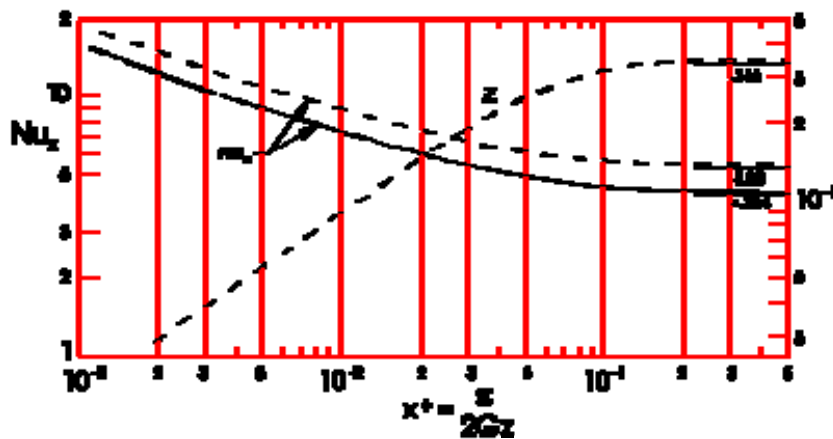
Figure 6-7: Thermal entry length Nusselt number, *Nuₓ*, vs. non-dimensional axial distance, *x⁺*, for laminar flow through straight pipes. Constant heat transfer rate. Also shown the influence coefficient, *Z*, for laminar flow between parallel plates with one side insulated. Calculated by the compiler after Kays (1966) [101].
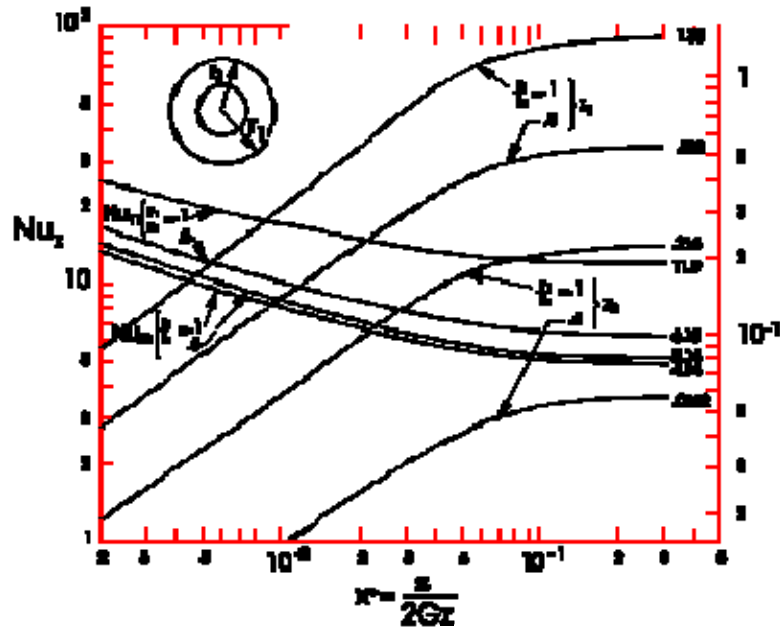
Figure 6-8: Thermal entry length Nusselt numbers, *Nu$_x$*, and influence coefficients, *Z*, vs. dimensionless axial distance, *x$^+$*, for laminar flow in concentric-circular-tube annuli. Constant heat transfer rate. Calculated by the compiler after Kays (1966) [101].
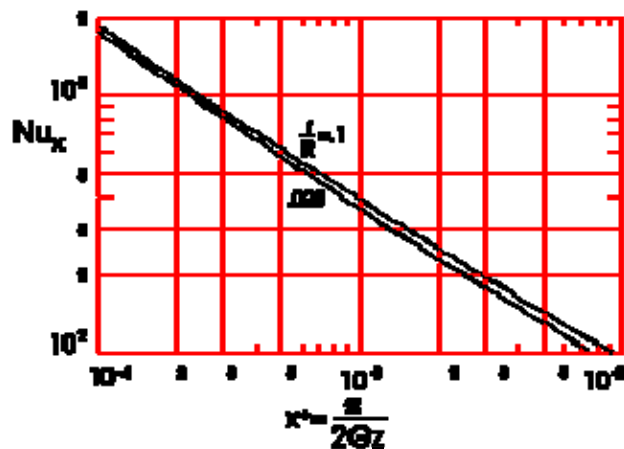
Figure 6-9: Thermal entry length Nusselt number, *Nu$_x$*, vs. non dimensional distance along the coil centerline, *x$^+$*, for laminar flow through a coil. The results are given for two values of the ratio, *r/R*, between the cross-sectional radius and the coil radius. Constant wall temperature. Calculated by the compiler after Kubair & Kuloor (1966) [111].
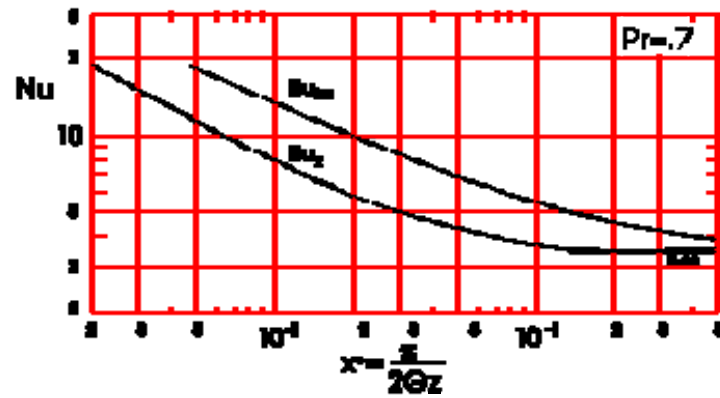
Figure 6-10: Nusselt numbers, *Nu*, vs. non-dimensional axial distance, *x⁺*, for the combined hydrodynamical and thermal entry length. Laminar flow through straight pipes of circular cross section. Constant wall temperature. *Pr* = 0.7. Replotted by the compiler after ESDU 68006 (1968) [48].
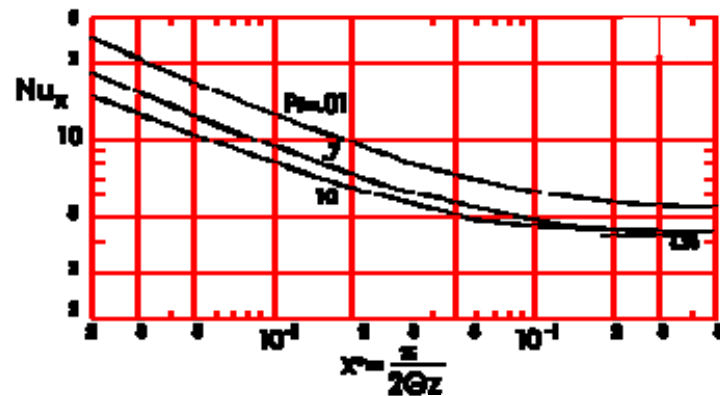
Figure 6-11: Local Nusselt number, *Nuₓ*, vs. non-dimensional axial distance, *x⁺*, for the combined hydrodynamical and thermal entry length. Laminar flow through straight pipes of circular cross section. Constant heat transfer rate. Results are shown for different Prandtl numbers, *Pr*. Calculated by the compiler after Heaton et al. (1964) [82].
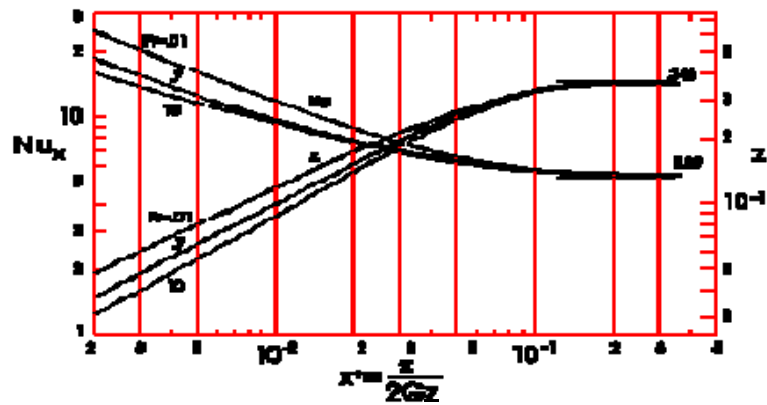
Figure 6-12: Local Nusselt number, Nu_x, and influence coefficient, Z, vs. dimensionless axial distance, x^+, for the combined hydrodynamical and thermal entry length. Laminar flow between parallel plates, one of them insulated. Constant heat transfer rate. Results are shown for different Prandtl numbers, Pr. Calculated by the compiler after Heaton et al. (1964) [82].

6.3.1.2 Transitional flow
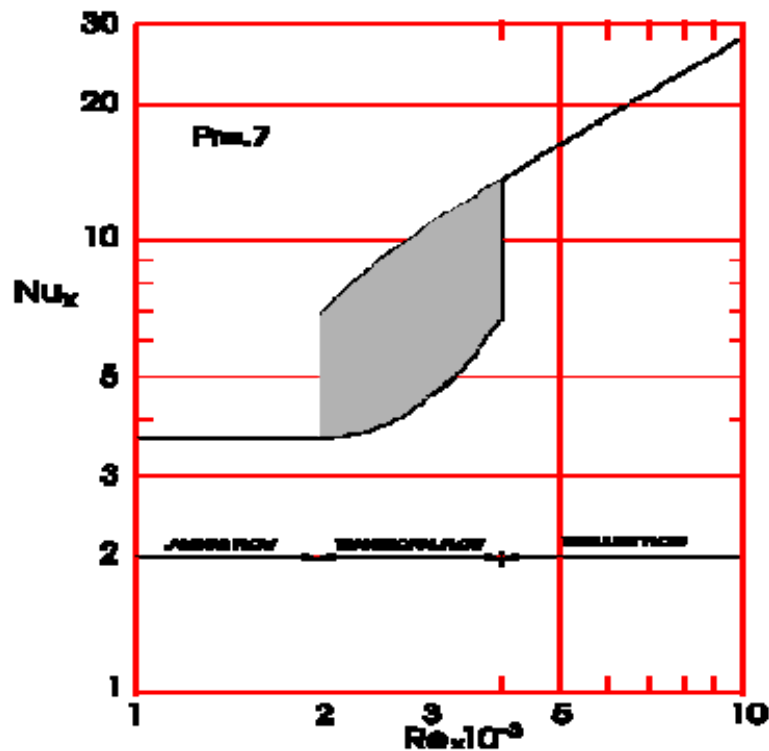
Figure 6-13: Local Nusselt number, Nu_x, vs. Reynolds number, Re, for fully developed transitional flow through cylindrical ducts of circular cross section. Constant wall temperature. Gas Flow ($Pr \approx 0.7$). From ESDU 68006 (1968) [48].

6.3.1.3   Turbulent flow
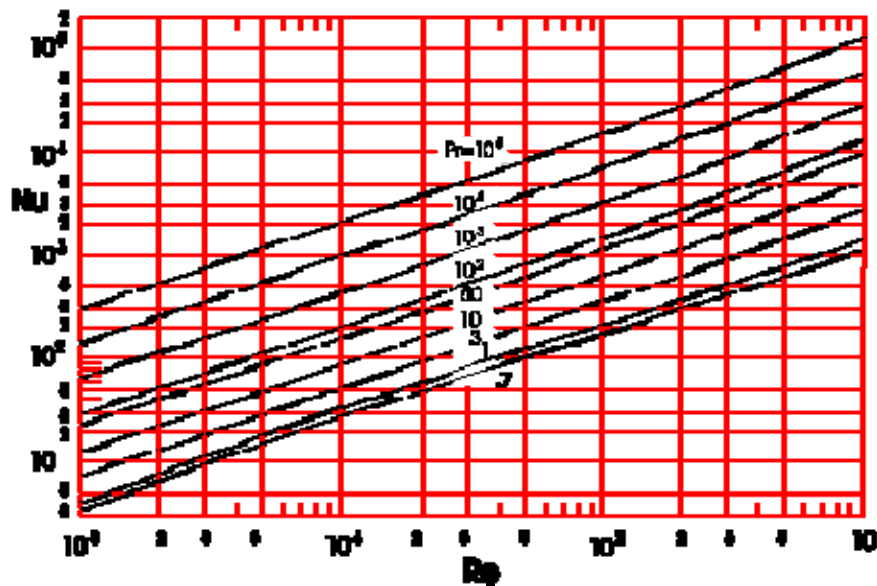
Figure 6-14: Nusselt number, *Nu*, vs. Reynolds number, *Re*, for fully developed turbulent flow through cylindrical ducts. Constant heat transfer rate. Results are shown for different Prandtl numbers, *Pr*. Calculated by the compiler after Petukhov & Roizen (1975) [143].
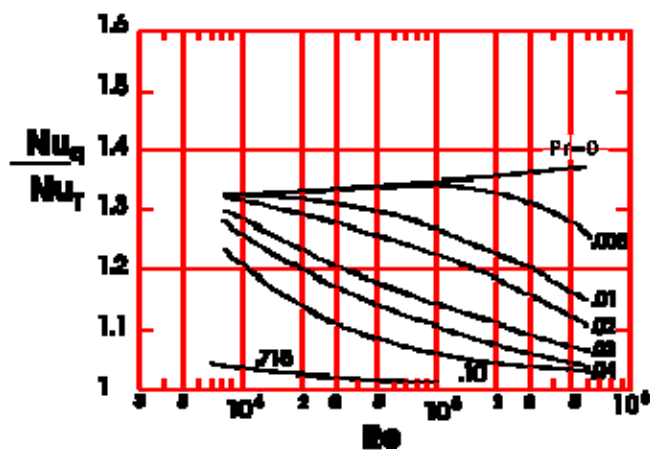
Figure 6-15: Ratio of Nusselt number at constant heat transfer rate, Nu_q, to Nusselt number at uniform wall temperature, Nu_T, vs. Reynolds number, *Re*, for fully developed turbulent flow through a straight pipe of circular cross section. Results are shown for different Prandtl numbers, *Pr*. From Sleicher & Tribus (1957) [167].
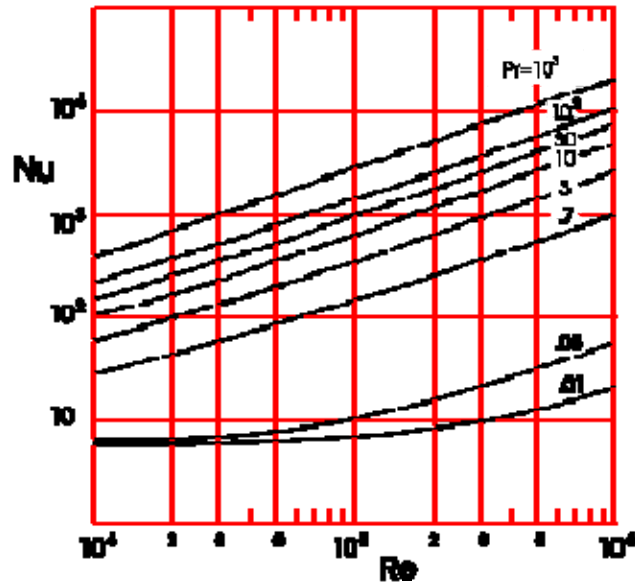
Figure 6-16: Nusselt number, *Nu*, vs. Reynolds number, *Re*, for fully developed turbulent flow between parallel plates, one of them insulated. Constant heat transfer rate. Results are shown for different Prandtl numbers, *Pr*. Calculated by the compiler after Kays (1966) [101].
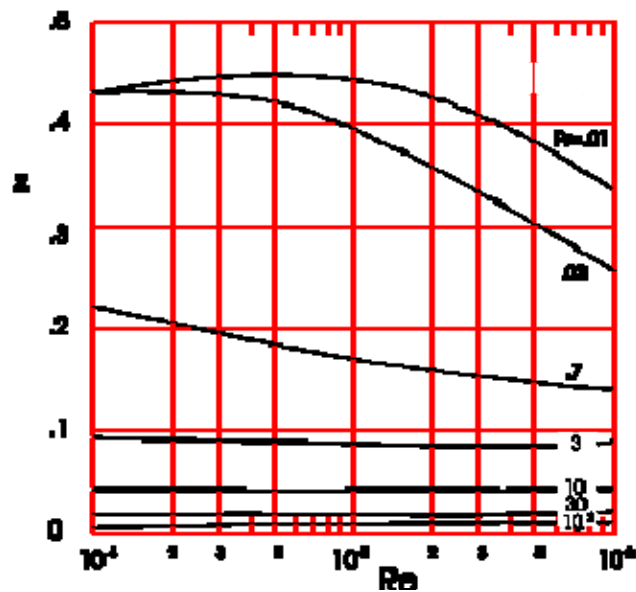
Figure 6-17: Influence coefficient, *Z*, vs. Reynolds number, *Re*, for fully developed turbulent flow between parallel plates. Constant heat transfer rate. Results are shown for different Prandtl numbers, *Pr*. Calculated by the compiler after Kays (1966) [101].
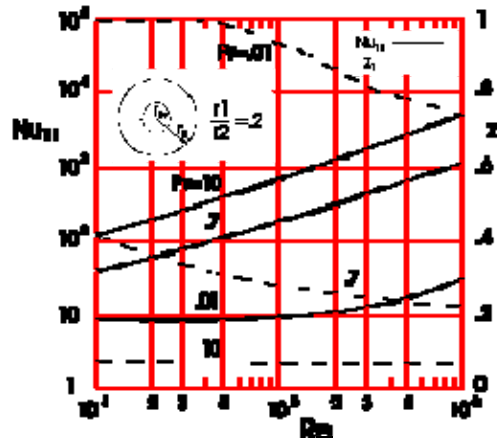
Figure 6-18: Nusselt number, Nu_{11}, and influence coefficient, Z_1, vs. Reynolds number, Re, for fully developed turbulent flow in concentric-circular-tube annuli. $r_1/r_2 = 0,2$. Constant heat transfer rate. Results are shown for different Prandtl numbers, Pr. Calculated by the compiler after Kays (1966) [101].
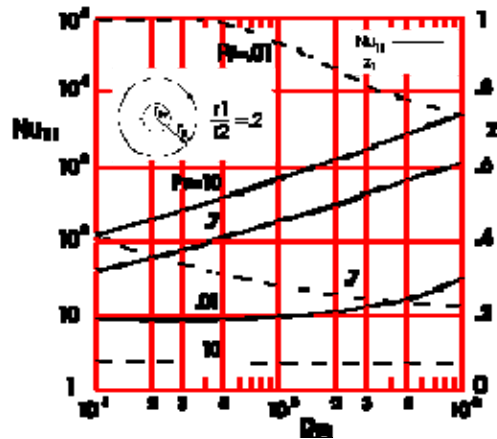
Figure 6-19: Nusselt number, Nu_{22}, and influence coefficient, Z_2, vs. Reynolds number, Re, for fully developed turbulent flow in concentric-circular-tube annuli. $r_1/r_2 = 0,2$. Constant heat transfer rate. Results are shown for different Prandtl numbers, Pr. Calculated by the compiler after Kays (1966) [101].
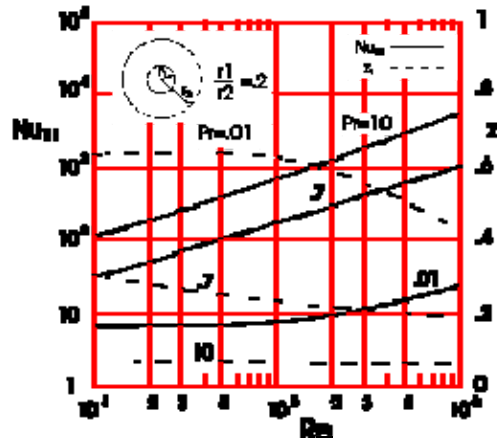
Figure 6-20: Nusselt number, Nu_{11}, and influence coefficient, Z_1, vs. Reynolds number, Re, for fully developed turbulent flow in concentric-circular-tube annuli. $r_1/r_2 = 0,5$. Constant heat transfer rate. Results are shown for different Prandtl numbers, Pr. Calculated by the compiler after Kays (1966) [101].
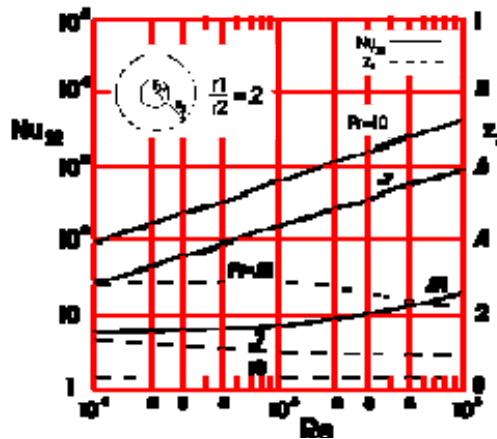
Figure 6-21: Nusselt number, Nu_{22}, and influence coefficient, Z_2, vs. Reynolds number, Re, for fully developed turbulent flow in concentric-circular-tube annuli. $r_1/r_2 = 0,5$. Constant heat transfer rate. Results are shown for different Prandtl numbers, Pr. Calculated by the compiler after Kays (1966) [101].
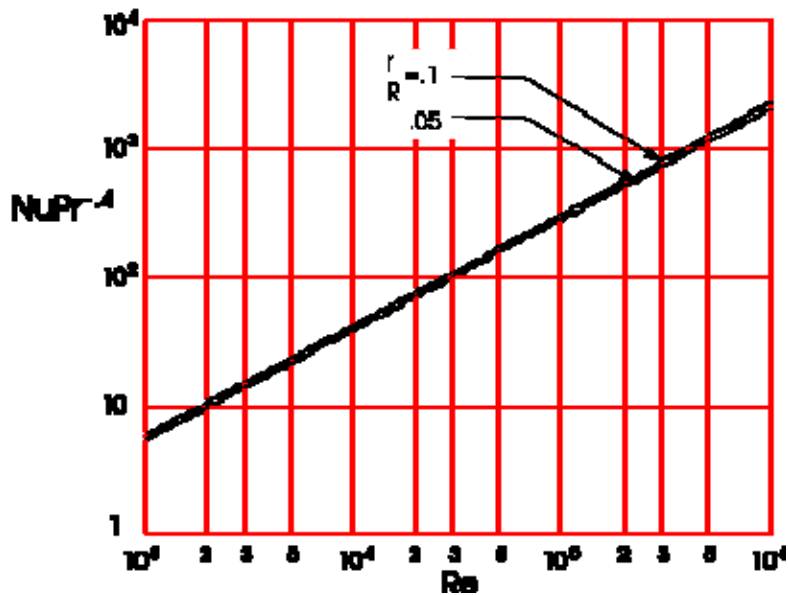
Figure 6-22: Nusselt number times Prandtl number to the minus 0.4 power, *NuPr* ⁻⁰·⁴, vs. Reynolds number, *Re*, for fully developed turbulent flow in helically coiled tubes. The results are given for two values of the ratio, *r/R*, between the cross-sectional radius and the coil radius. Constant heat transfer rate. Calculated by the compiler after an experimental correlation obtained by Seban & McLaughlin (1963) [162] from data for water.
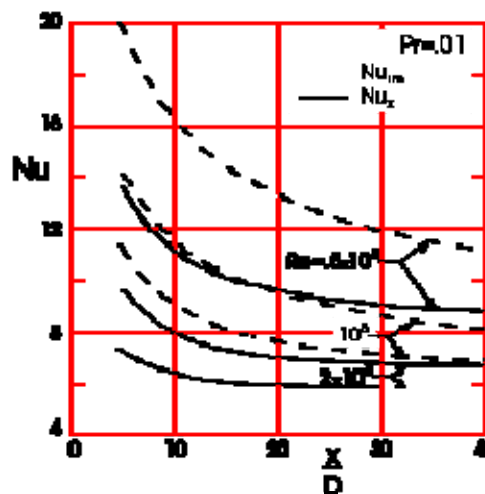
Figure 6-23: Thermal entry length Nusselt numbers, *Nu*, vs. non-dimensional axial distance, *x/D*, for fully developed turbulent flow through a straight pipe of circular cross section. Constant wall temperature. *Pr* = 0.01. Results are shown for different Reynolds numbers, *Re*. Calculated by the compiler after Kays (1966) [101].
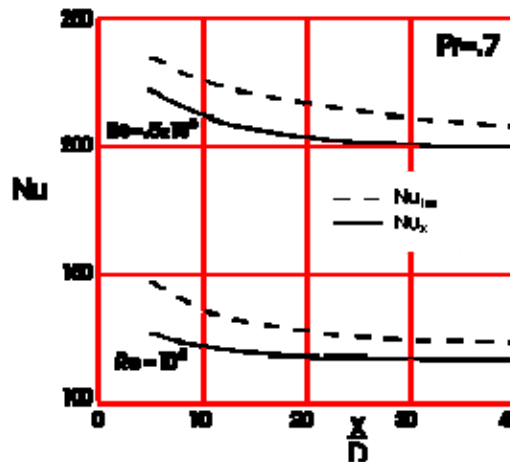
Figure 6-24: Thermal entry length Nusselt numbers, *Nu*, vs. non-dimensional axial distance, *x/D*, for fully developed turbulent flow through a straight pipe of circular cross section. Constant wall temperature. *Pr* = 0.7. Results are shown for different Reynolds numbers, *Re*. Calculated by the compiler after Kays (1966) [101].
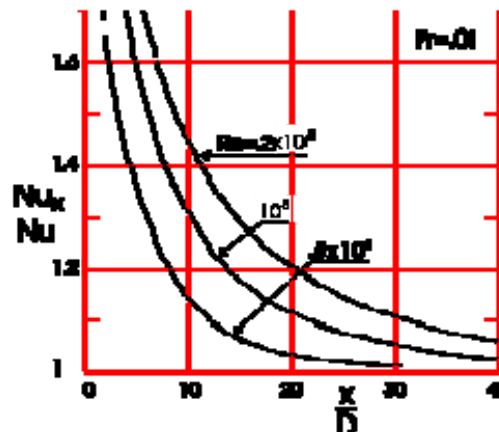
Figure 6-25: Ratio of thermal entry length Nusselt number, *Nu_x*, to Nusselt number for fully developed turbulent flow, *Nu*, vs. non-dimensional axial distance, *x/D*. Straight pipe of circular cross section. Constant heat transfer rate. *Pr* = 0.01. Results are shown for different Reynolds numbers, *Re*. Calculated by the compiler after Kays (1966) [101].
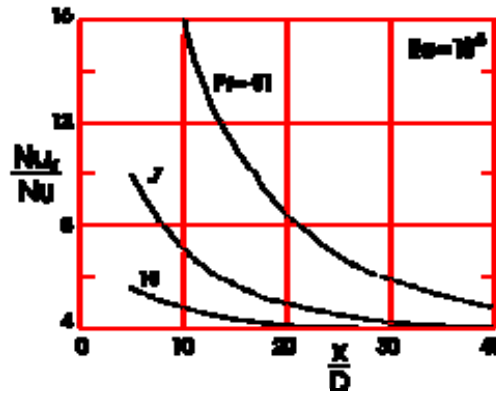
Figure 6-26: Ratio of thermal entry length Nusselt number, *Nux*, to Nusselt number for fully developed turbulent flow, *Nu*, vs. non-dimensional axial distance, *x/D*. Straight pipe of circular cross section. Constant heat transfer rate. *Re* = 10⁵. Results are shown for different Prandtl numbers, *Pr*. Calculated by the compiler after Kays (1966) [101].
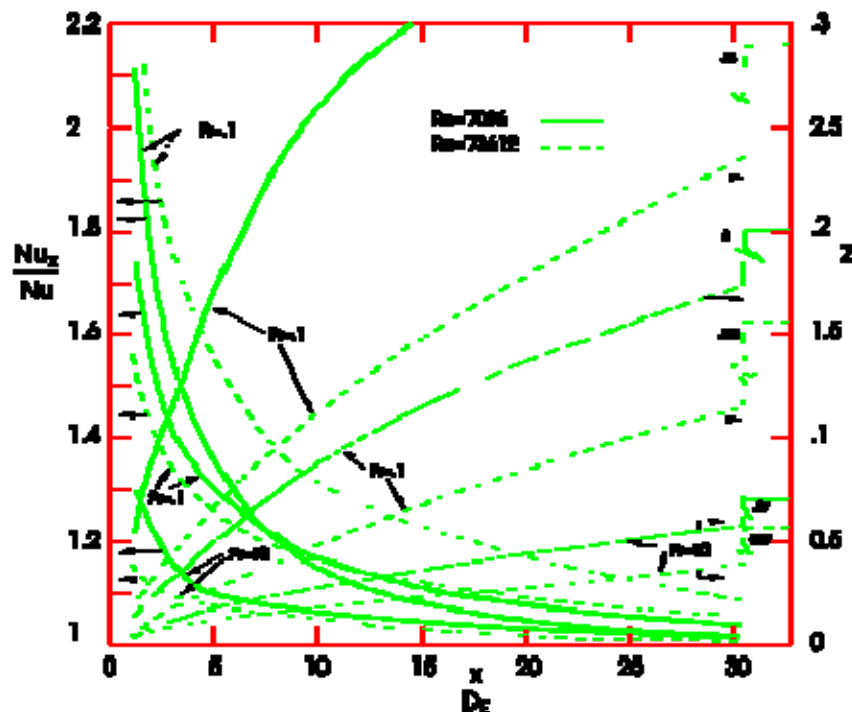
Figure 6-27: Ratio of thermal entry length Nusselt number, *Nux*, to Nusselt number for fully developed turbulent flow, *Nu*, vs. non-dimensional axial distance, *x/DE*. Parallel plates at distance 2*DE*, one of them insulated. Constant heat transfer rate. Also shown the influence coefficient, *Z*. Results are shown for three different Prandtl numbers, *Pr*, and two Reynolds numbers, *Re*. Calculated by the compiler after Kays (1966) [101].

6.3.2 Heat transfer to external flows

The table below summarizes the data presented in the following pages. All these data correspond to external flows, i.e. configurations where the fluid flows outside the domain bounded by the heat transfer surface.

Geometry	Input Variables	Output	Fig.	References
Circular Cylinder Normal to Flow. Fluid with constant property values.	Re, $Pr = 0,7,5,3,5$	Nu_b	Figure 6-28	ESDU 69004 [50], Fig. 6.
Circular Cylinder Normal to Flow. Liquids with variable fluid properties.	$0,061 < \mu_{wm}/\mu_b < 0,936$	Nu/Nu_b	Figure 6-29a	ESDU 69004 [50], Fig. 7.
Circular Cylinder Normal to Flow. Gases with variable fluid properties.	$0,20 < T_{wm}/T_b < 4,47$	Nu/Nu_b	Figure 6-29b	ESDU 69004 [50], Fig. 8.
Circular Cylinder Yawed to Flow.	$40° < \theta < 90°$	$Nu_\theta/Nu_{90°}$	Figure 6-29c	ESDU 69004 [50], Fig. 9.
In-Line Tube Bank.			Figure 6-30	ESDU 73031 [57], Fig. 5.
In-Line Tube Bank. Fluids with constant property values.	Re_b, $Pr_b = 1$	Nu_r	Figure 6-31	ESDU 73031 [57], Fig. 6.
In-Line Tube Bank. Fluid with constant property values.	Re_b, $Pr_b = 1$	Nu_r	Figure 6-32	ESDU 73031 [57], Fig. 6.
Staggered Tube Bank. Fluids with constant property values.	Re_b, $Pr_b = 1$	Nu_r	Figure 6-33	ESDU 73031 [57], Fig. 7.
In-Line or Staggered Tube Bank. Fluids with constant property values.	Pr_b	$\dfrac{Nu_r}{(Nu_r)_{Pr_b=1}}$	Figure 6-34	ESDU 73031 [57], Fig. 8.
In-Line or Staggered Tube Bank. Fluids with constant property values.	Pr_b/Pr_w	F_1	Figure 6-35	ESDU 73031 [57], Fig. 9.
In-Line or Staggered Tube Bank.	N	F_2	Figure 6-36	ESDU 73031 [57], Fig. 10.
In-Line or Staggered Tube Bank Yawed to Flow.	$20° \leq \theta \leq 90°$	F_3	Figure 6-37	ESDU 73031 [57], Fig. 11.

Geometry	Input Variables	Output	Fig.	References
In-Line or Staggered Tube Bank. Characteristics of the n-th row.	$1 \leq n \leq 20$	F_4	Figure 6-38	ESDU 73031 [57], Fig. 12.

6.3.2.1 Cylindrical bodies
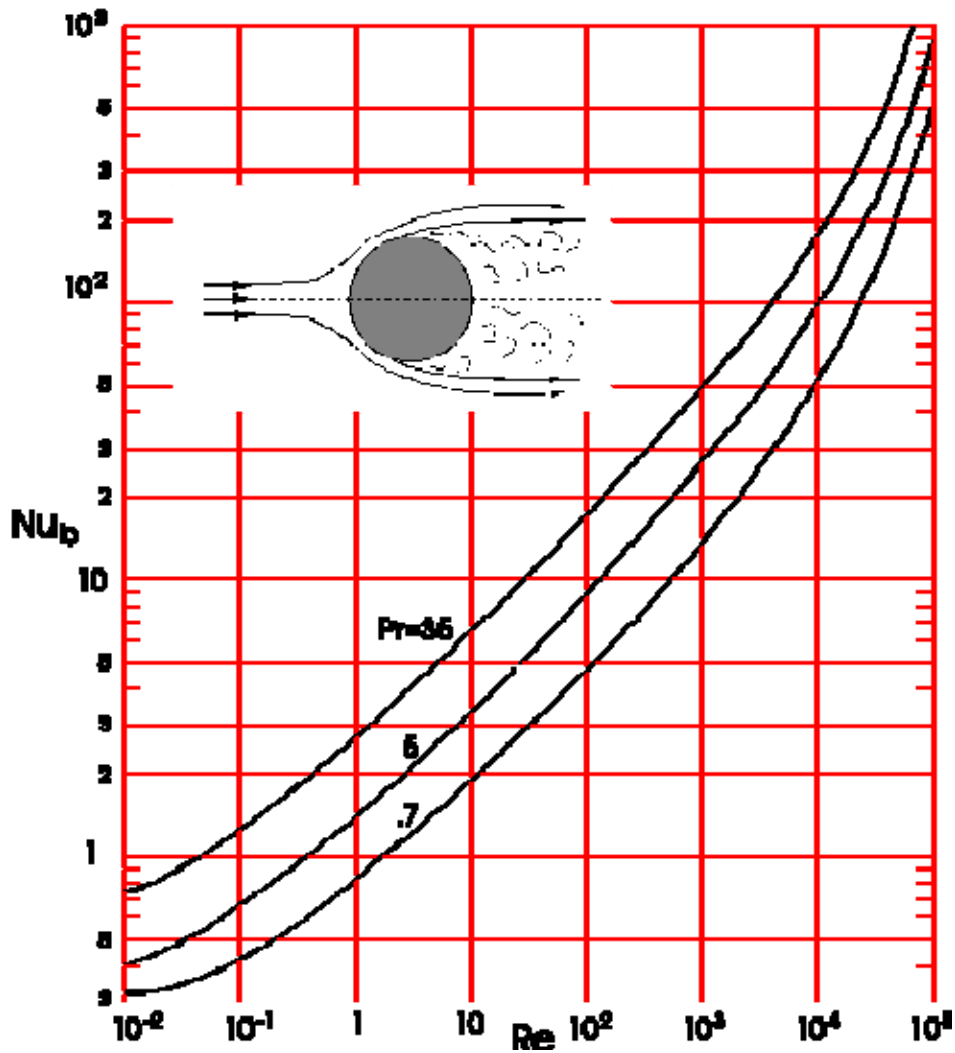
Figure 6-28: Nusselt number, *Nu*, vs. Reynolds number, *Re*. Flow of a fluid having constant physical properties over a constant temperature circular cylinder whose axis is normal to the incoming flow. From ESDU 69004 (1969) [50].
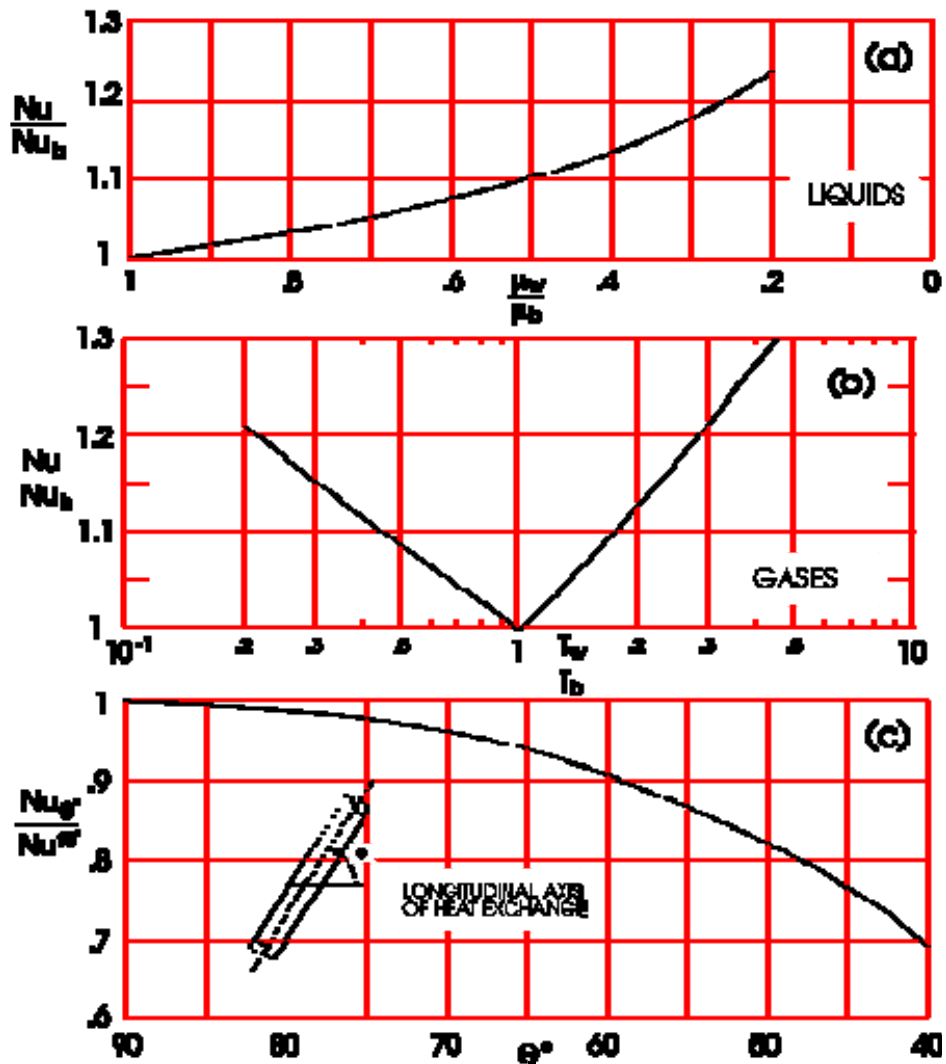
Figure 6-29: Effect of variable fluid properties, (a) and (b), and of inclination angle, (c), on the Nusselt number corresponding to the flow of a fluid over a constant temperature cylinder. Nu_b ($Nu_{90°}$) can be deduced from Figure 6-28. From ESDU 69004 (1969) [50].

6.3.2.2   Tube banks
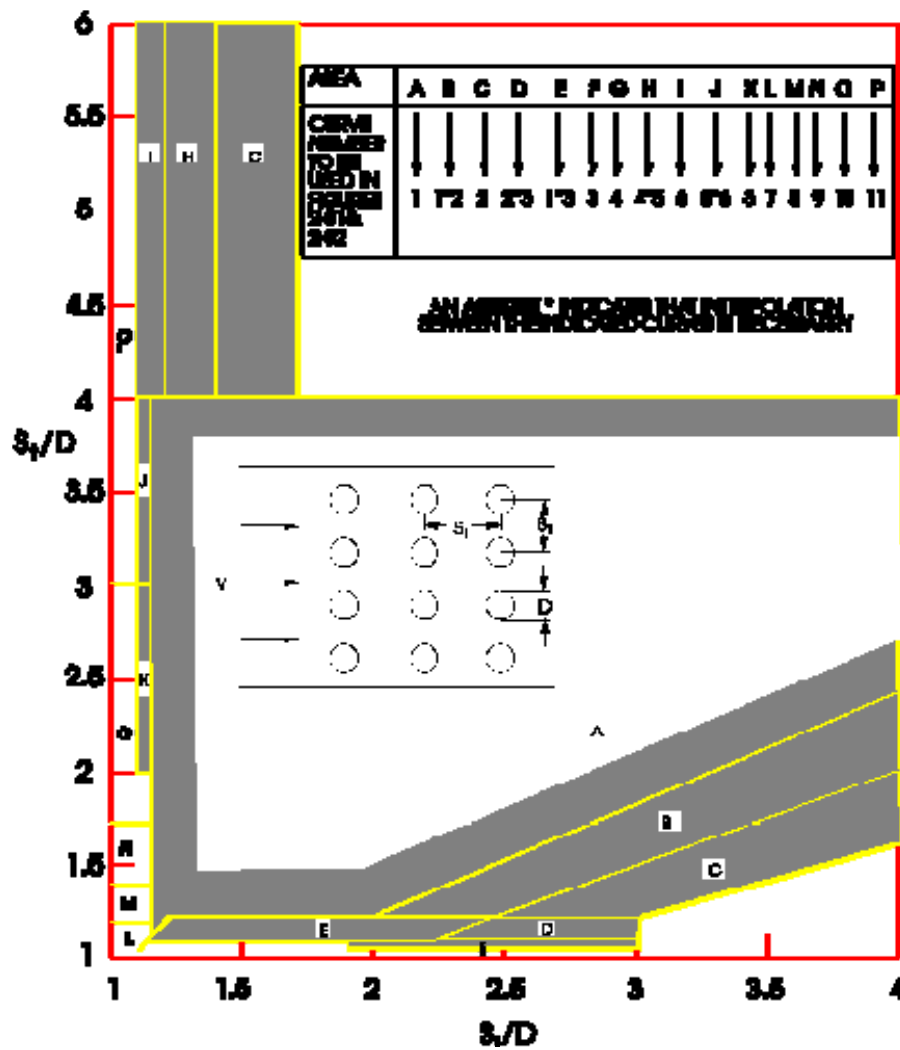
Figure 6-30: Guide for the selection of the curves given in Figure 6-31 and Figure 6-32 concerning in-line tube banks of different relative pitches. From ESDU 73031 (1973) [57].
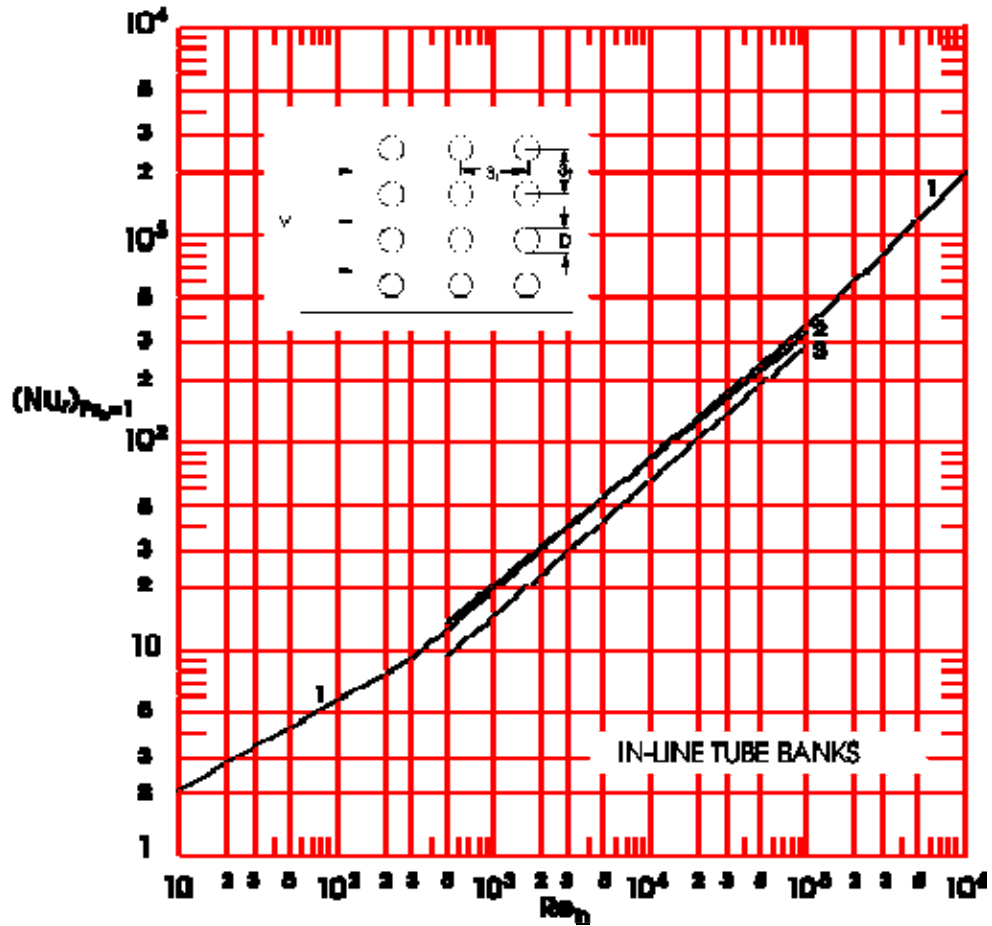
Figure 6-31: Reference Nusselt number, Nu_r, for Pr_b = 1, as a function of Reynolds number, Re. In-line tube banks. See Figure 6-30 for the meaning of the numbers which appear on the curves. From ESDU 73031 (1973) [57].
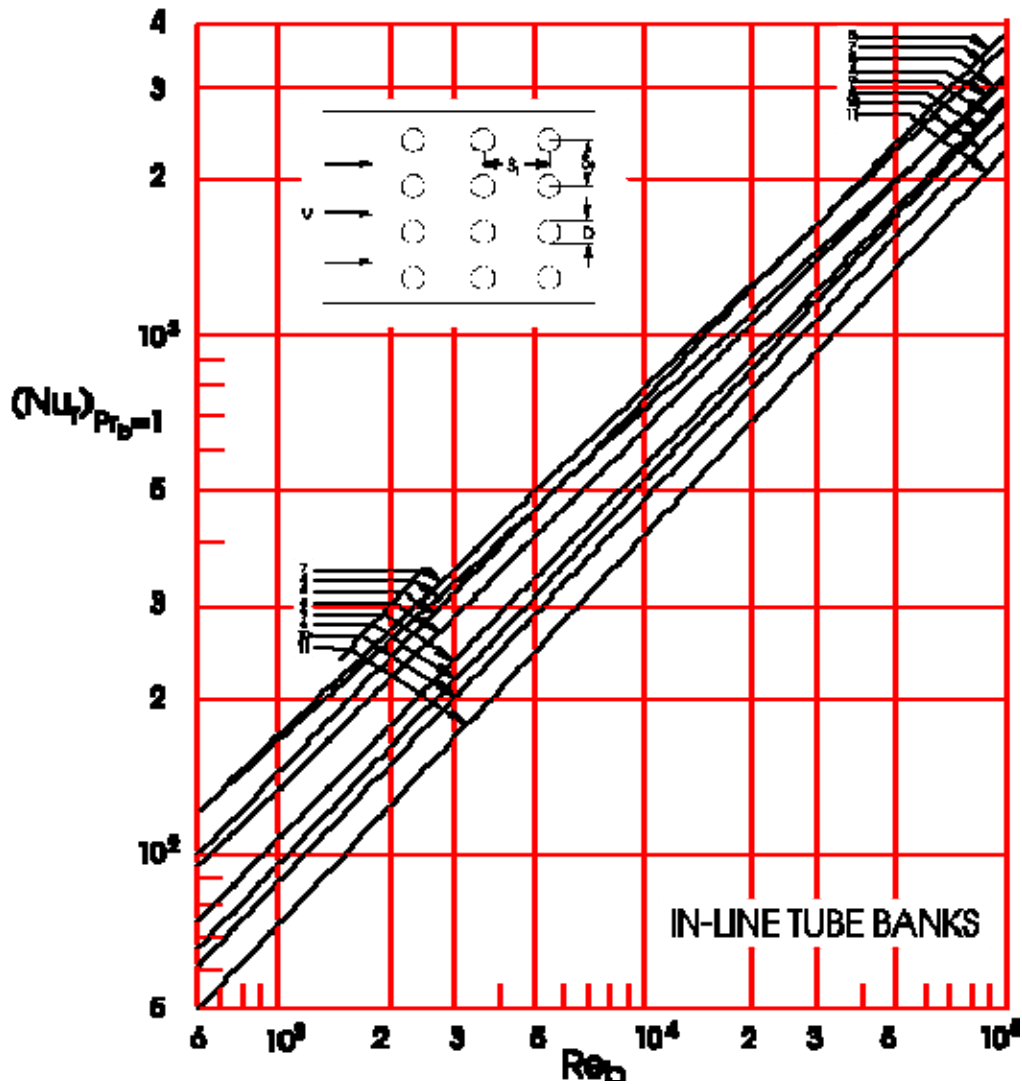
Figure 6-32: Reference Nusselt number, *Nuᵣ*, for *Prᵦ* = 1, as a function of Reynolds number. *Re*. In-line tube banks. See Figure 6-30 for the meaning of the numbers which appear on the curves. From ESDU 73031 (1973) [57].
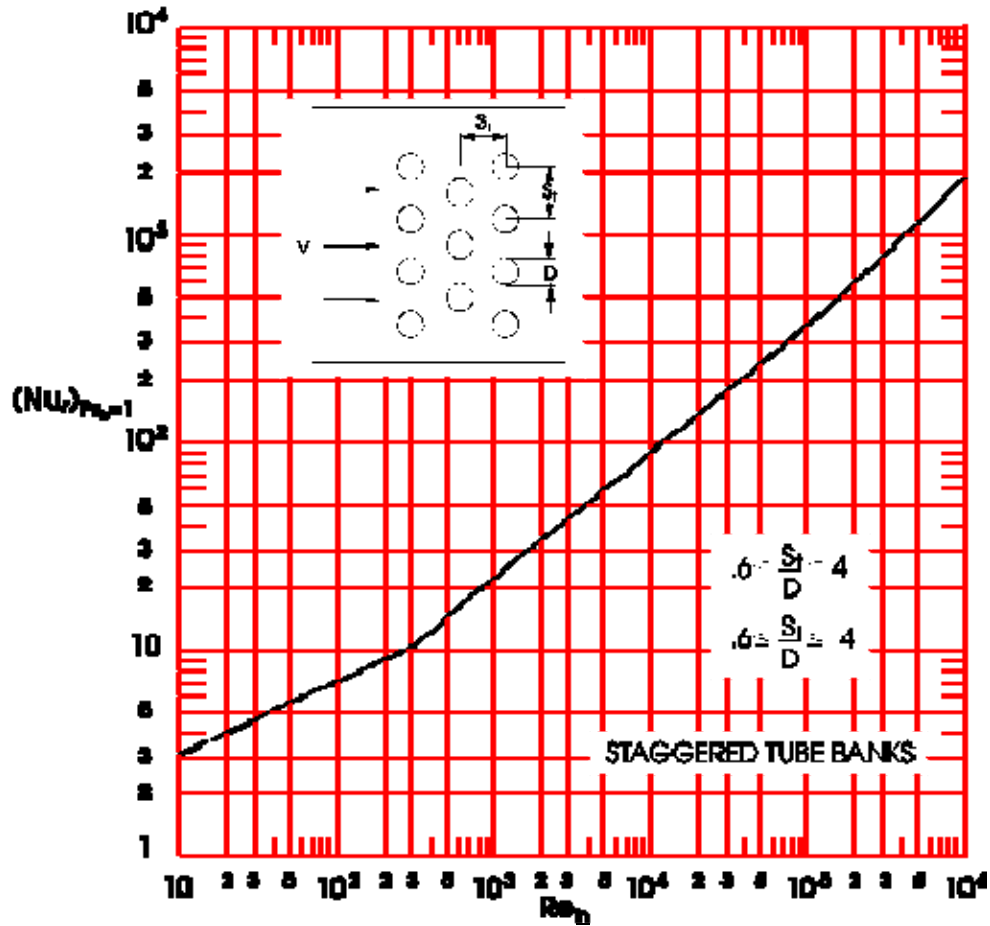
Figure 6-33: Reference Nusselt number, *Nu*ᵣ, for *Pr*ᵦ = 1, as a function of Reynolds number. *Re*. In-line tube banks. Staggered tube banks. From ESDU 73031 (1973) [57].
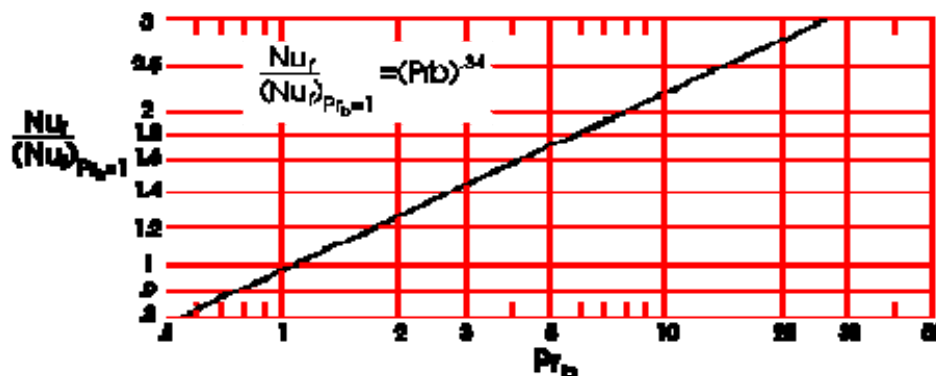
Figure 6-34: Effect of the Prandtl number, *Pr*ᵦ, on the reference Nusselt number, *Nu*ᵣ, for both in-line and staggered tube banks. From ESDU 73031 (1973) [57].
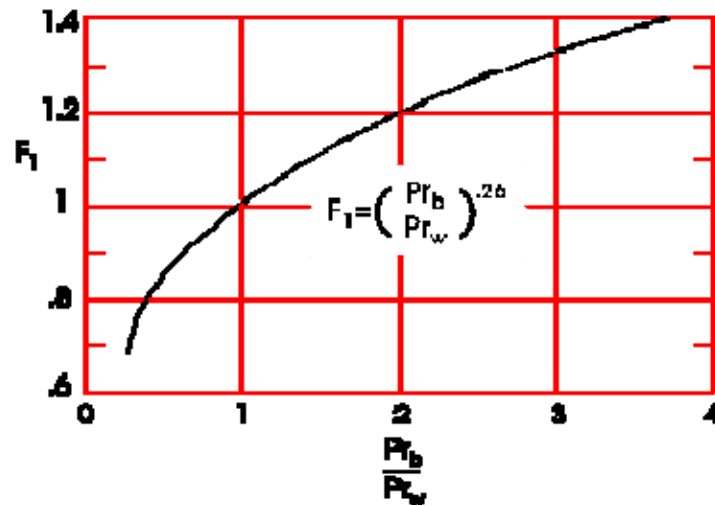
Figure 6-35: The factor F_1 to account for variable fluid properties. From ESDU 73031 (1973) [57].
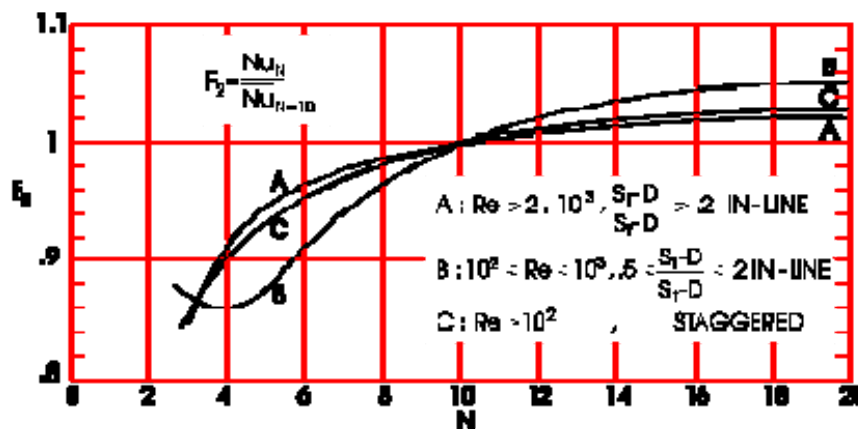
Figure 6-36: The factor F_2 accounting for abnormal number of rows vs. that number, N. From ESDU 73031 (1973) [57].
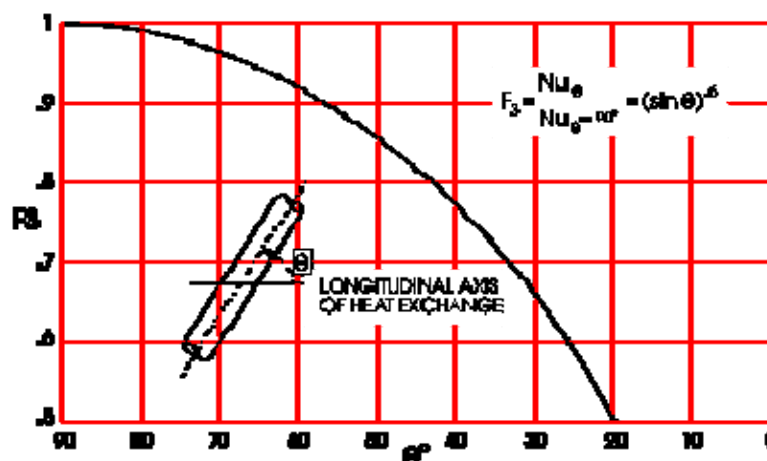
Figure 6-37: The factor F_3 accounting for the effect of yaw vs. the inclination angle, θ. From ESDU 73031 (1973) [57].
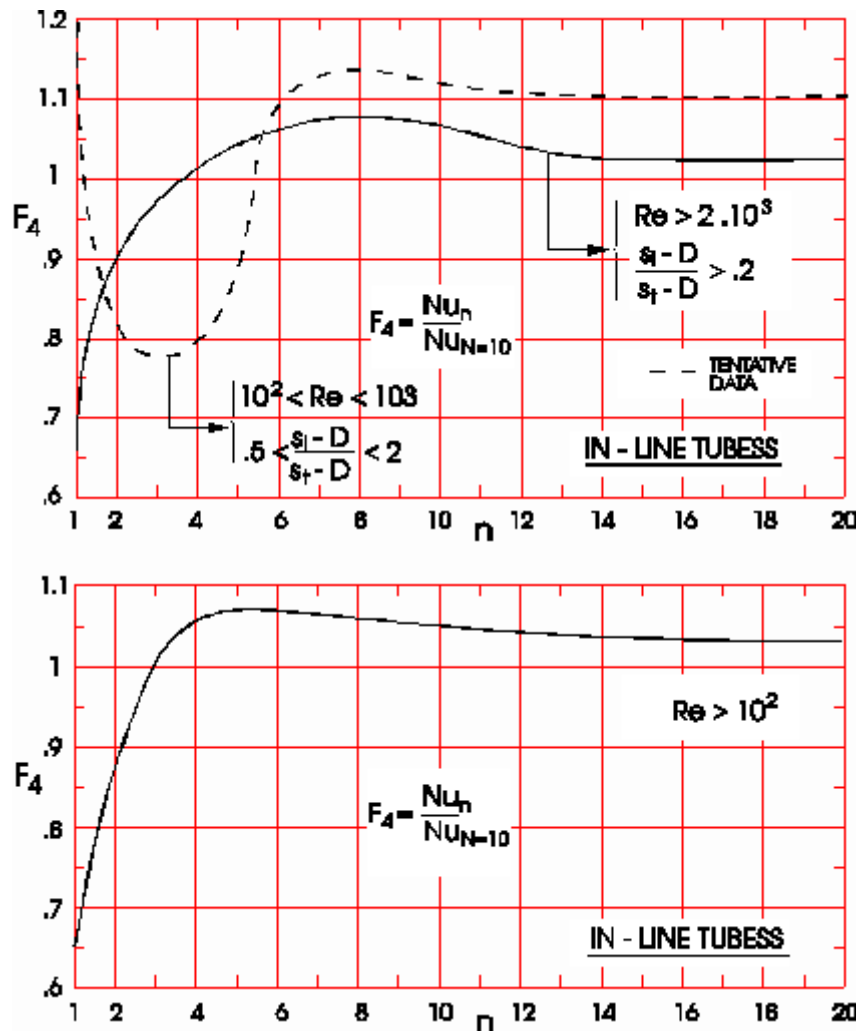
Figure 6-38: The factor *F4* for estimating the Nusselt number of the n-th row. From ESDU 73031 (1973) [57].

7
Frictional analysis

7.1 General

Once the thermal analysis of the fluid loop has been performed, the pressure drop through the loop will be estimated. The aim of this estimation is twofold:

1. To fix the pressure level of the working fluid. This level is of concern in many cases. For instance, vaporization is normally avoided when liquid coolants are used, because of the associated cooling effectiveness degradation. This is not always the case since advantage is taken of boiling (and subsequent condensation) in several heat exchanger devices to store the heat in the fluid during its transfer from heat source to heat sink. However, only fluids that remain in their liquid state throughout the loop are considered here.

2. To select the appropriate pump. The power, $\eta_p p$, required to force the fluid through the duct is deduced from the pressure drop, Δp, the mass flow rate, m, and the fluid density, ρ, by use of the following expression:

$$\eta_p p = \Delta p \frac{m}{\rho}$$ [7-1]

This clause is aimed at estimating the pressure drop, Δp, of a loop having fairly general geometric configuration, in terms of the pressure loss at each individual component and the appropriate interference factors, when they are available and relevant.

If the power requirements calculated by means of the pertinent data are too stringent, a careful look to the pipework could be required. Reductions in the mass flow rate -and, thence, in the pressure loss- would imply higher operating temperature differentials and larger heat rejecting systems.

When the mass flow rate is reduced the thermal analysis of the loop should be undertaken again.

7.2 Analytical background

7.2.1 Introduction

The flow of a real fluid through a pipe is characterized by the significance of friction forces. Associated with these forces there is a pressure drop, Δp.

A dimensional analysis indicates that, for a pipe system of given geometry running full, the pressure drop between two sections may be related to flow properties, fluid properties and geometrical characteristics of the pipe in the following way:

$$\frac{\Delta p}{\frac{1}{2}\rho V^2} = f\left(\frac{e}{D}, Re, M, \gamma, geometry\right)$$

[7-2]

In the applications which will be considered, compressibility effects - which in the above expression are measured by the Mach number, M, and the ratio of specific heats, γ - will be neglected.

7.2.2　Fully developed flow in straight pipes

The pressure drop due to friction in a cylindrical pipe of any cross section running full is accounted as

$$\Delta p = \lambda \frac{L}{D_E} \frac{1}{2} \rho V^2$$

[7-3]

Many authors, especially from the United States, use the Fanning friction factor, $f = \lambda/4$, instead of λ. We will use indiscriminately both λ and f throughout this clause and Clauses 8, 9, 10, 11 and 13.

For laminar flow the friction factor does not depend on the relative roughness of the tube wall. In particular, when the cross section of the pipe is circular:

$$\lambda = 64/Re$$

[7-4]

which is the well known Hagen-Poiseuille formula, valid for $Re < 2400$ and fully developed flow. Values of λ (of f) for fully developed laminar flow and other cross-sectional shapes can be found in Figure 7-3, in ESDU 66027 (1966) [46] and in Kays & London (1964) [102], p. 103.

In the transition between laminar and turbulent flows, the value of the direction factor is uncertain. However, it is surely bounded below and above by the extrapolation of the laminar line and the turbulent line corresponding to the relative roughness of the pipe wall, respectively.

In the case of fully developed turbulent flow the friction factor, λ, strongly depends on the relative roughness of the wall, but is fairly insensitive to the shape of the cross section. Reference is made to Schlichting (1960) [157] for details concerning the turbulent flow through pipes of non-circular cross section.

The law of friction for rough pipes depends on the size (and shape) of the roughness as compared to the thickness of the laminar sublayer of fluid close to the wall.

1.　When the roughness size is so small that all protrusions are contained within the laminar sublayer, the pipe is "hydraulically smooth". For these pipes at very large Reynolds number the following law of friction applies:

$$\frac{1}{\sqrt{\lambda}} 2,035 \log\left(Re\sqrt{\lambda}\right) - 0,91 \qquad\qquad [7\text{-}5]$$

This expression is often written as:

$$\sqrt{\frac{2}{f}} = 2,5 \ln\left(Re\sqrt{f}\right) - 0,85 \qquad\qquad [7\text{-}6]$$

which is usually known as Karman-Nikuradse friction law.

Many authors (Schlichting (1960) [157]) use the slightly different expression

$$\frac{1}{\sqrt{\lambda}} = 2 \log\left(Re\sqrt{\lambda}\right) - 0,8 \qquad\qquad [7\text{-}7]$$

known as Prandtl's universal law of friction for smooth pipes. This law has been verified by Nikuradse's experiments up to a Reynolds number of $3,4 \times 10^6$, and may be extrapolated to arbitrarily large Reynolds numbers provided that the tube is smooth.

2. In the case of rough pipes the law of friction deviates from that corresponding to smooth pipe, once the Reynolds number exceeds a definite value whose magnitude increases as the relative roughness, e/D_E, decreases. Above some even higher value of the Reynolds number the friction factor becomes constant and depends on the relative roughness only (see Figure 7-2).

    In this regime, called the "completely rough regime", all protrusions reach outside the laminar sublayer, whose thickness decreases when the Reynolds number increases.

    The law of friction for the completely rough regime was first derived by von Kármán in the form:

$$\sqrt{\frac{2}{f}} = 2,5 \ln\frac{D_E}{2e} + 4,75 \qquad\qquad [7\text{-}8]$$

In terms of the friction factor λ,

$$\frac{1}{\sqrt{\lambda}} = 2,035 \log\frac{D_E}{2e} + 1,679 \qquad\qquad [7\text{-}9]$$

A comparison with Nikuradse's experimental results shows that closer agreement can be obtained by use of the following expression (Schlichting (1960) [157]):

$$\frac{1}{\sqrt{\lambda}} = 2 \log\frac{D_E}{2e} + 1,74 \qquad\qquad [7\text{-}10]$$

3. In the intermediate region, protrusions extend partly outside the laminar sublayer.

A friction similarity law which is valid over a wide range of roughness's and Reynolds numbers has been developed by Nikuradse for sand-grain-type roughness.

$$\sqrt{\frac{2}{f}} = 2{,}5\ln\frac{D_E}{2e} + u_e^+\left(e^+\right) - 3{,}75 \qquad [7\text{-}11]$$

The roughness function, $u_e^+(e^+)$, for sand-grain-type roughness, is shown in Figure 9-1b. For large values of the dimensionless protrusion height, e^+, the roughness function tends to an asymptotic value close to $u_e^+ = 8{,}50$, yielding the previously quoted expression for the completely rough regime.

Expressions similar to that developed by Nikuradse are useful reducing the experimental work involved in the determination of f. Since the constants 2,5 and 3,75 are universal, it is only necessary to determine the function u_e^+, which normally depends on e^+ and on the type of roughness. u_e^+ for several discrete roughness's is shown in Figure 9-2b and Figure 9-3b.

For commercially rough pipes the Moody diagrams or the Colebrook-White formula can be used. Moody's diagram is based on an equivalent sand roughness, to be determined, for each commercial pipe, by use of an auxiliary equivalence chart (see Schlichting (1960) [157], pp. 528-529).

Table 7-1 gives the equivalent roughness height, e, for a number of common surfaces.

Table 7-1: Effective roughness height of a number of common surfaces.
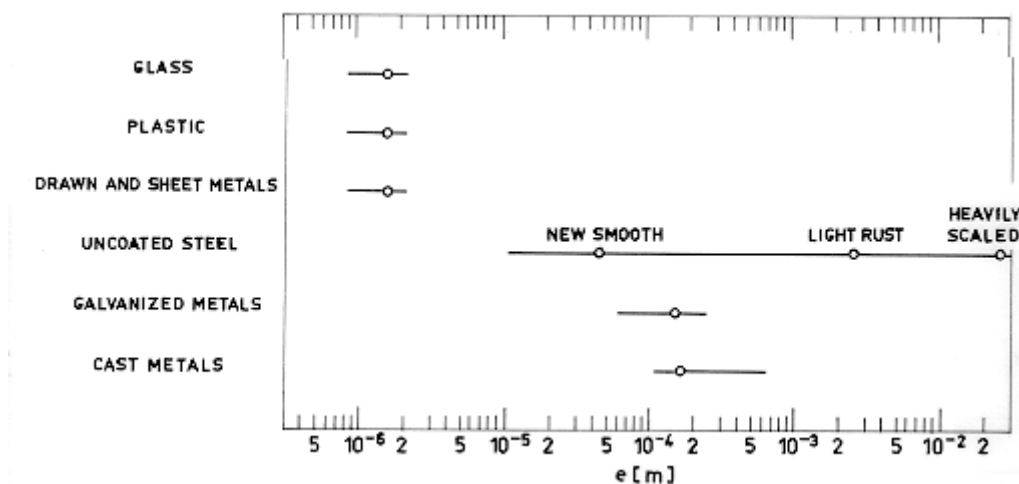
The Colebrook & White formula (Schlichting (1960) [157]) correlates the whole transition region from hydraulically smooth to completely rough flow,

$$\frac{1}{\sqrt{\lambda}} = 1{,}74 - 2\log\left(\frac{2e}{D_E} + \frac{18{,}7}{Re\sqrt{\lambda}}\right) \qquad [7\text{-}12]$$

When e $\rightarrow$ 0 this equation yields that for the hydraulically smooth regime. For $Re \rightarrow \infty$, it transforms into the equation for the completely rough regime. In the transition region it gives results which resemble those obtained by use of the Moody diagram.

In practice the surface roughness can be distributed in either a random or a systematic way, or can be concentrated at intervals along the system as occurs with welding seams in pipes or internal supports. Although these imperfections may become insignificant with careful manufacturing, and their effect on the flow is small except at very high Reynolds number, specific tests are required to determine the pressure loss induced in each particular case. Some general trends of the friction law for several roughness types can be deduced from the analysis of Figure 7-1 in order to separate the several curves, they have been plotted for different values of the equivalent roughness, *e*, otherwise their asymptotic value (λ for $Re \rightarrow \infty$) would be the same.

Figure 7-1: Friction characteristics associated with four types of roughness geometry. Notice that the equivalent roughness is different in every case. From Reynolds (1974).

Type A: Sand grains and other closely spaced elements. As the Reynolds number rises all peaks emerge at once from the laminar sublayer. Once the peaks emerged the stress is transmitted by the drag of the peaks, thence becoming independent of the Reynolds number.

Type B: Protrusions of various sizes, as produced by many manufacturing processes or by aging. The emergence is gradual and the elements progressively start to transmit stress by drag.

Type C: Isolated protrusions on an otherwise fairly smooth wall. The drag coefficient of the large elements becomes Reynolds number independent, while the friction coefficient for the surrounding wall continues to fall as the Reynolds number increases. This behavior may be expected when less than half of the surface area is occupied by the roughness elements.

Type D: Isolated depressions or grooves in an otherwise fairy smooth wall. The contribution of the depression rises slowly as the viscous layer thins. This is so because this type of roughness has little effect until the free stream turbulence penetrates into the cavity.

There are surfaces, however, which do not fit into these categories. This happens to be the case, for example, when large inserts are used to enhance the heat transfer (see clause 9.1.1).

7.2.2.1 Power-law approximations for the hydraulically smooth regime

Numerical work can be reduced by representing the friction factor by a power-law approximation

$$f = C_1 + C_2 Re^{-n} \qquad [7\text{-}13]$$

with C_1, C_2 and n so chosen as to fit the above logarithmic formulae.

The following expressions have been borrowed from Reynolds (1974) [149].

Table 7-2: Constants for Power Law Approximation. Hydraulically Smooth Regime.

C_1	C_2	n	Re Range	Accuracy	Comments
0	0,079	0,25	$<10^5$	2% of the experimental values	Blasius friction formula. As accurate as the logarithmic formula
0	0,046	0,20	10^5 - 10^6	Not given	
0,0014	0,125	0,32	$< 10^7$	3% of the log formula for $Re < 10^6$. 7% of the log formula for $Re < 10^7$	

7.2.3 Temperature-dependence of fluid properties

The friction data presented in this clause correspond to isothermal conditions.

The simplest approach to account for property variation is to evaluate all fluid properties at the reference temperature (see clause 6.2.4) and to introduce a temperature ratio correction factor of the form $(T_w/T_R)^n$ or $(\mu_w/\mu_R)^n$.

The correction is inherently small for turbulent flow, whereas the available experimental evidence suggests that it is much larger in the laminar flow case.

Table 7-3 below presents relevant data for fully developed flow in cylindrical tubes of circular cross section.

Table 7-3: Loading Factors Accounting for Temperature-Dependence of Diabatic Friction

Type of Flow	Fluid	Loading Factor λ/λ_b	n		Comment
			Fluid Heating	Fluid Cooling	
Laminar Fully Developed Tubes of Circular Cross Section	Gas	$(T_w/T_b)^n$	0,45	0,30	In the range $1/3 < T_w/T_b < 3$
	Liquid	$(\mu_w/\mu_b)^n$	0,58	0,50	More experimental confirmation is required
Turbulent	Gas	$(T_w/T_b)^n$	-0,10	0	In the range $1/3 < T_w/T_b < 3$
Fully Developed	Liquid Pr = 10	$(\mu_w/\mu_b)^n$	0,03	0,05	
Tubes of Circular	Liquid Pr = 10^2		-0,04	0,01	
Cross Section	Liquid Pr = 10^3		-0,12	-0,02	

NOTE   From Kays & London (1964) [101]

7.2.4   Several definitions of pressure loss coefficient

The total pressure, p_t, in a given section of a duct is defined as

$$p_t = p + \frac{1}{2}\rho V^2 + \rho g z \qquad [7\text{-}14]$$

1.   A coefficient of total pressure loss between two stations 1 and 2 along a pipe is defined as follows:

$$c_{K_t} = \frac{p_{t1} - p_{t2}}{\frac{1}{2}\rho V^2} \qquad [7\text{-}15]$$

When the cross-sectional areas 1 and 2 are different, the loss coefficient may be expressed in terms of the value of the dynamic pressure, $\rho V^2/2$, at either section. Care should be

exercised to ensure that the correct reference dynamic pressure is used when interpreting the pressure loss coefficient data.

ALL THE DATA PRESENTED HERE, WITH THE ONLY EXCEPTION OF THE SUDDEN CONTRACTION, ARE BASED ON THE CONDITIONS EXISTING UPSTREAM OF THE COMPONENT INVOLVED.

2. In real flows the total pressure varies over the cross section, while the static pressure is uniform provided that the streamlines are almost parallel. Thence, in practice, it is often simpler to define the mean static pressure, rather than the mean total pressure at a section.

Since the contribution of the geometrical head term, ρgz, depends on the orientation of the pipework, the quoted data correspond to static pressure differences between two points in the same horizontal plane. The contribution of ρgz, when significant, is accounted for independently.

The static pressure loss coefficient between two stations 1 and 2 along the pipe is defined as follows:

$$c_{K_s} = \frac{p_1 - p_2}{\frac{1}{2}\rho V^2}$$
[7-16]

Notice that when the cross-sectional area increases in the direction of the flow the static pressure can increase, in which case the pressure loss is negative.

In the case of incompressible flow through constant cross section ducts the total pressure loss, c_{Kt}, equals the static pressure loss, c_{Ks}. In that case the subscripts t or s have been omitted.

3. The pressure loss due to a component, let say a sudden area change or a bend, can be considered to be made up of two terms. One is the pressure loss that would have existed in the absence of the component -i.e. that pressure loss corresponding to fully developed flows in lengths equal to the straight portions upstream and downstream of the component- and the other is the pressure loss directly attributable to the component.

The gross pressure loss, Δp_G, is defined as:

$$\Delta p_G = p_1 - p_2 - \left(\Delta p_{x_1} + \Delta p_{x_2} \right)$$
[7-17]

where Δp_{x1} and Δp_{x2} are the static pressure losses due to friction for fully developed flows in lengths of straight pipe equal to x_1 and x_2 respectively.

The net pressure loss, Δp_N, is defined as:

$$\Delta p_N = \Delta p_G - \Delta p_L$$
[7-18]

where the static pressure loss due to friction for fully developed flow through the length, L, of the component has been subtracted.

The usefulness of these definitions is that, provided the static pressure loss is referred to stations 1 and 2 in the regions of fully-developed flow, the corresponding coefficients are independent of x_1 and x_2.

The use of the gross static pressure loss should be preferred to that of the net static pressure loss because:

1. Components with unequal entry and exit areas can be dealt with conveniently.

2. The definition of L is often arbitrary as occurs in the case of very localized singularities such as: sudden area changes, orifices, valves, ...

For simple mitre bends L is equal to zero, so that there is no difference between gross and net pressure losses.

ALL THE DATA PRESENTED ARE BASED ON THE GROSS PRESSURE LOSS

7.2.5 Entrance effects

The fully-developed flow does not take place just from the tube entrance, rather and "entrance length" is required for the velocity profiles to relax from the initial practically uniform distribution to the parabolic distribution which is characteristic of laminar flows.

The entrance length, L_{ent}, can be deduced from the following approximate formula (Nekrasov (1969) [132]).

$$L_{ent}/D = 0,029 Re \qquad \text{[7-19]}$$

The pressure loss in the entrance length is greater than in subsequent sections because of the larger velocity gradients at the duct wall associated with the near uniform velocity profiles.

The friction factor corresponding to laminar flow through a cylindrical tube of circular cross section, whose length, L, is commensurable with the entrance length is given (Nekrasov (1969) [132]) by:

$$\lambda = 1,165\frac{D}{L} + \frac{64}{Re} \qquad \text{[7-20]}$$

Notice that an additive term, D/L, incorrectly neglected by Nekrasov (who gives 0,165D/L instead of 1,165D/L) appears in this expression. This term accounts for the change in dynamic pressure, $\rho V^2/2$, between the entrance and the given section.

The above value ($k = 1,165$) was deduced analytically by Schiller. Experimentally obtained values are somewhat larger (see, for example, Lundgren, Sparrow & Starr (1964) [121]). The analytical value obtained by these authors ($k = 4/3$) is very close to that resulting from Schiller's experiments.

Values of k for several cross-sectional shapes can be found in Lundgren et al. (1964) [121], who applied their theory to circular, elliptical, rectangular, isosceles triangular and annular ducts. The case of circular-segment cross sections has been considered by Sparrow & Haji Sheikh (1966) [169].

The inlet length in turbulent flow is considerably shorter that in laminar flow. According to experiments performed by Nikuradse (quoted by Schlichting (1960) [157]) the fully-developed velocity profile exists after an inlet length of 25 to 40 diameters.

7.2.6 Interferences and networks

The pressure loss coefficients of the different components can be deduced from Figure 7-2 to Figure 7-30 or from the data submitted by the manufacturer of the component, when these data are available.

All these coefficients will be referred to the nominal cross section of the loop by using the equation of mass preservation.

The interaction between consecutive components of the loop can only be taken into account in special cases. When data are available for particular interactions, the components concerned should be considered as single entities.

The pressure loss coefficient of elements placed in series can be added, once they are referred to the nominal cross section.

When n elements are in parallel an equivalent pressure loss coefficient is calculated on the basis of the following two facts:

(a) The mass flow approaching any junction or branch must equal the mass flow leaving them.

(b) The overall pressure loss through several routes in parallel is the same for all of them.

From these considerations the following alternative expressions of the equivalent pressure loss coefficient can be deduced:

(a) For laminar flows, where the pressure loss is proportional to the mean velocity:

$$\frac{1}{c_{K_{equiv}}} = \sum_{i=1}^{n} \frac{1}{c_{K_i}}$$

[7-21]

(b) For turbulent flows, where the pressure loss-mean velocity relationship is quadratic:

$$\frac{1}{\sqrt{c_{K_{equiv}}}} = \sum_{i=1}^{n} \frac{1}{\sqrt{c_{K_i}}}$$

[7-22]

The pressure loss, Δp, in the loop is related to the total coefficient of pressure loss, c_K, by means of the equation

$$\Delta p = c_K \frac{1}{2} \rho V^2$$

[7-23]

where V is the mean flow velocity in the nominal cross section.

7.2.7   Flow chart

The flow chart is intended to guide in the selection of the appropriate pressure loss data. This guidance is achieved by means of a series of questions concerning the parameters involved. The figures quoted in the several boxes are those enclosed in Clause 7.3.

In addition to the pressure loss data which are collected in clause 7.3, the following sources of data are worthy of being mentioned.

Two updated data items on pressure losses in curved ducts have been issued by ESDU. The item ESDU 77008 (1977) [58] deals with single bends, whereas ESDU 77009 (1977) [59] gives interaction factors for two bends in series.

Flow-friction design data for many heat exchanger configurations can be found in Kays & London (1964) [102]. The geometries of the configurations considered by these authors are described in clause 11.3 of this Part.

Additional information on pressure loss data for branching flows through planar three-leg junctions is given in ESDU 73022 (1973) [55]. Data for Y-junctions, angled junctions, general dividing junctions, and tapered-leg junctions are presented in the mentioned data item. Similar information, but now for confluent flows, is given in ESDU 73023 (1973) [56].

Finally, the book by Idel'cik (1969) [97] should be mentioned. This book presents data on straight pipes (for both fully developed flow and entrance effects), area changes, bends, dividing and combining flows, orifices, valves and other configurations of technical interest.

Flow chart for the Selection of Pressure Loss Data

START

Sudden constriction
c_{K_t} from Fig 3-19

What's change ?

Variable cross section duct

What's element ?

Constant cross section duct

What's geometry ?

Straight pipe λ_c from Fig 3-2 K from Fig 3-3
$c_K = K \lambda_c \frac{L}{D}$

Sudden enlargement

Bends

Is interference significant $(L_d < 50D)$?

No → Single bends

SEE NEXT PAGE

Uniform
c_{K_t} from Fig 3-15

What's velocity profile ?

Singularities in a constant cross-section duct

Yes

Data only available for two bends in series

Non-uniform. Choose velocity profile from Fig 3-16

Branching T and +
c_K from Fig 3-30

What's singularity type ?

Valve
c_{K_r} from Fig 3-26
α_6 from Fig 3-27
$c_K = \alpha_6 \ c_{K_r}$

What's bends type ?

c_{K_t} from Fig 3-17
c_{K_s} from Fig 3-18

Circular arc

Mitre bend

Turbulent cross-flow over tube banks

In line
c_K from Fig 3-28

Staggered
c_K from Fig 3-29

Constrictions:
- orifice plate
- perforated plate
- cylindrical tube orifice
- flowmeter orifice plate

Round-wire gauzes
c_{K_r} from Fig 3-24
α_5 from Fig 3-25

$c_K = \alpha_5 \ c_{K_r}$

β from Fig 3-13

β from Fig 3-14

$c_K = \beta (c_{K_1} + c_{K_2})$

Fig 3-23 could be used to estimate the upper and lower bounds of c_K

Relative plate thickness ?

$t/d < .8$
c_{K_0} from Fig 3-20
α_3 from Fig 3-21

$t/d \geq .8$
$c_{K.8}$ from Fig 3-20
α_4 from Fig 3-22

$c_K = \alpha_3 \ c_{K_0}$

$c_K = \alpha_4 \ c_{K.8}$

7.3 Pressure loss data

7.3.1 Straight pipes
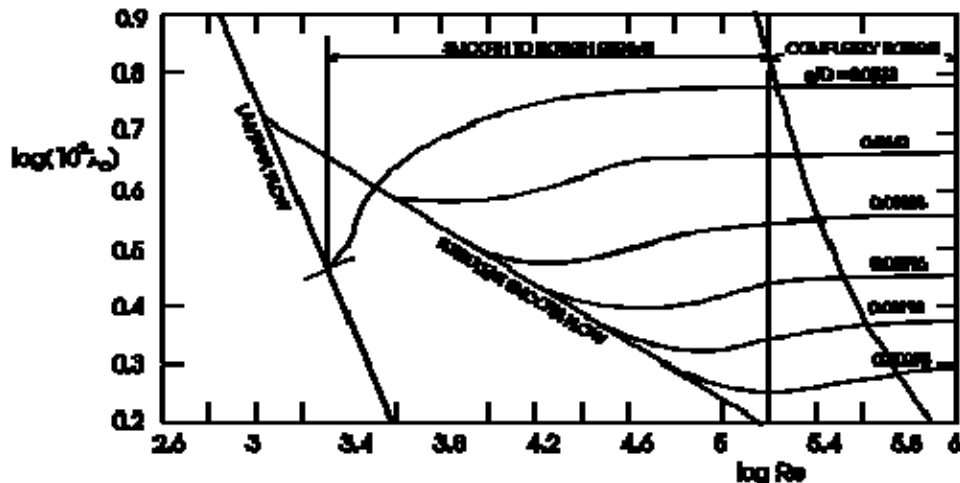
Figure 7-2: Friction factor, λ_c, as a function of Reynolds number, Re, for different values of the relative roughness, e/D: Cylindrical tubes of circular cross section. From Idel'cik (1969) [97].
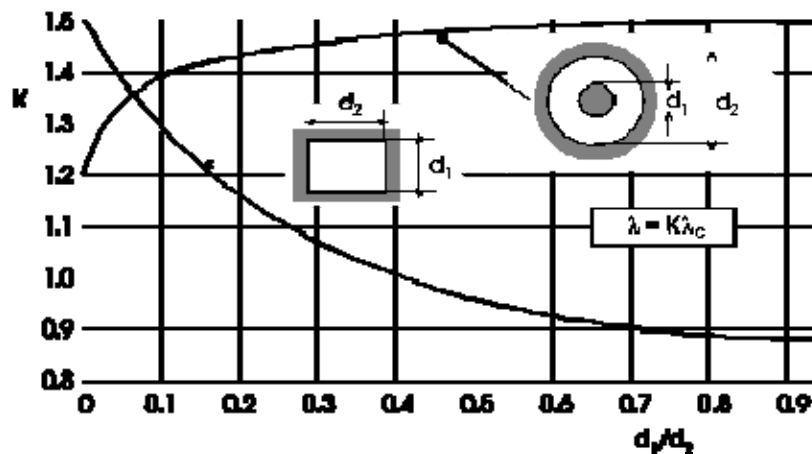
Figure 7-3: Correction factor, K, to be used when the cross section of the duct is not circular. Laminar flow. $K = 1$ for turbulent flow through hydraulically smooth ducts. From ESDU 66027 (1966) [46].

7.3.2 Bends
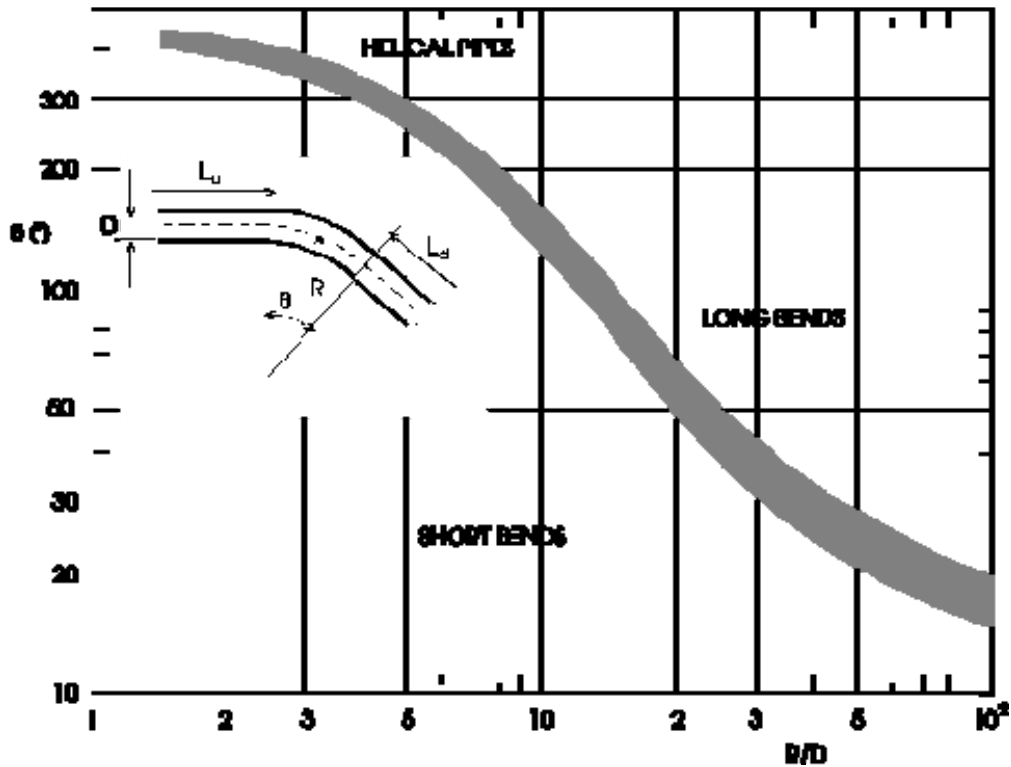
Figure 7-4: Boundary between short and long circular arc bends. From ESDU 67040 (1967) [47].
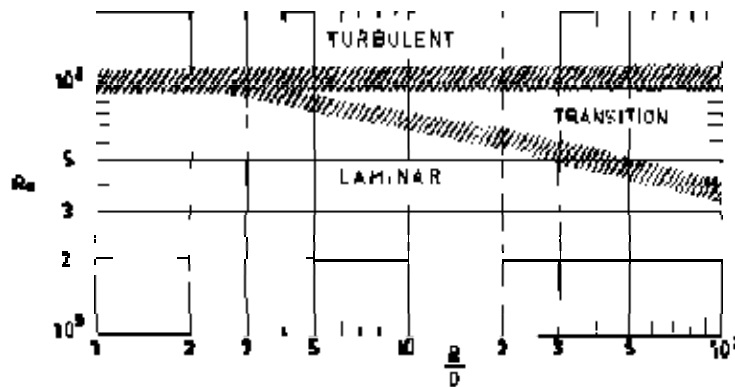
Figure 7-5: Boundaries between laminar, transitional and turbulent flows in long circular arc bends. From ESDU 67040 (1967) [47].
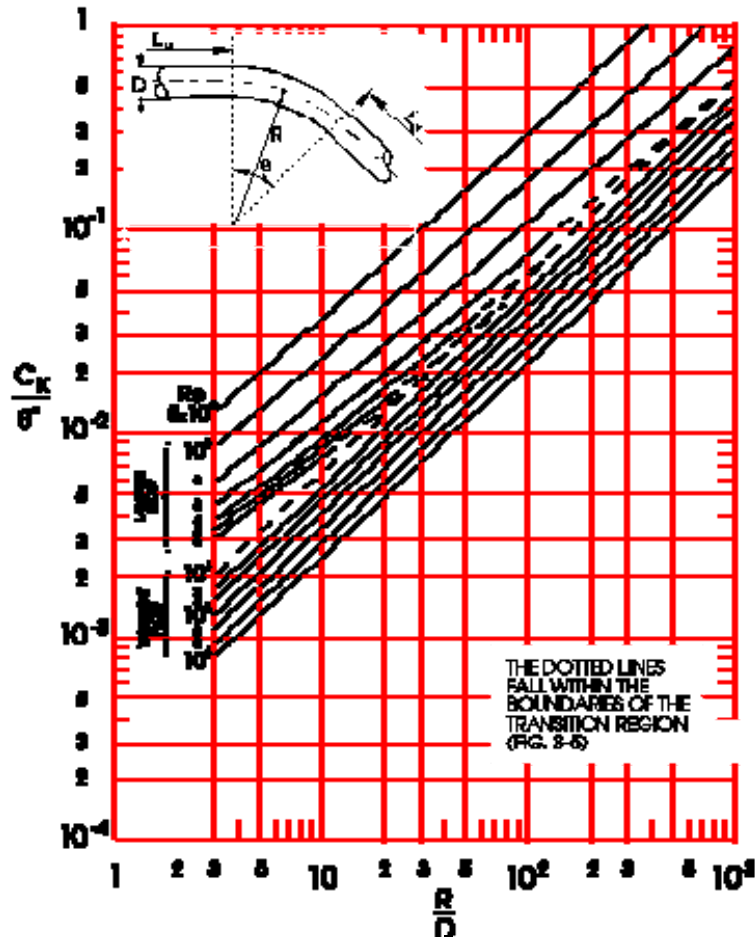
Figure 7-6: Pressure loss coefficient per unit bend angle, c_K/θ, as a function of the dimensionless radius of curvature of bend centerline, R/D, for different values of Reynolds number, Re. Either circular or square cross section. From ESDU 67040 (1967) [47].
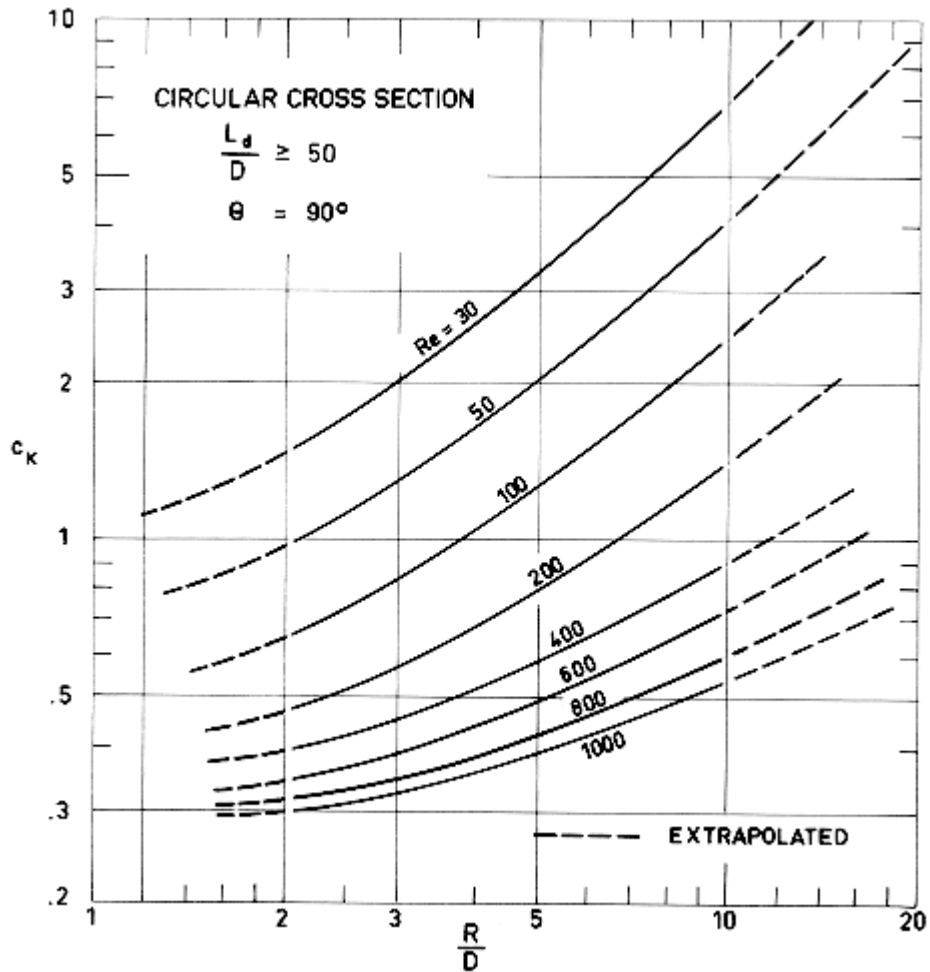
Figure 7-7: Pressure loss coefficient, c_K, as a function of the dimensionless radius of bend centerline, R/D, for different values of Reynolds number, Re. Laminar flow through short circular arc bends. From ESDU 67040 (1967) [47].
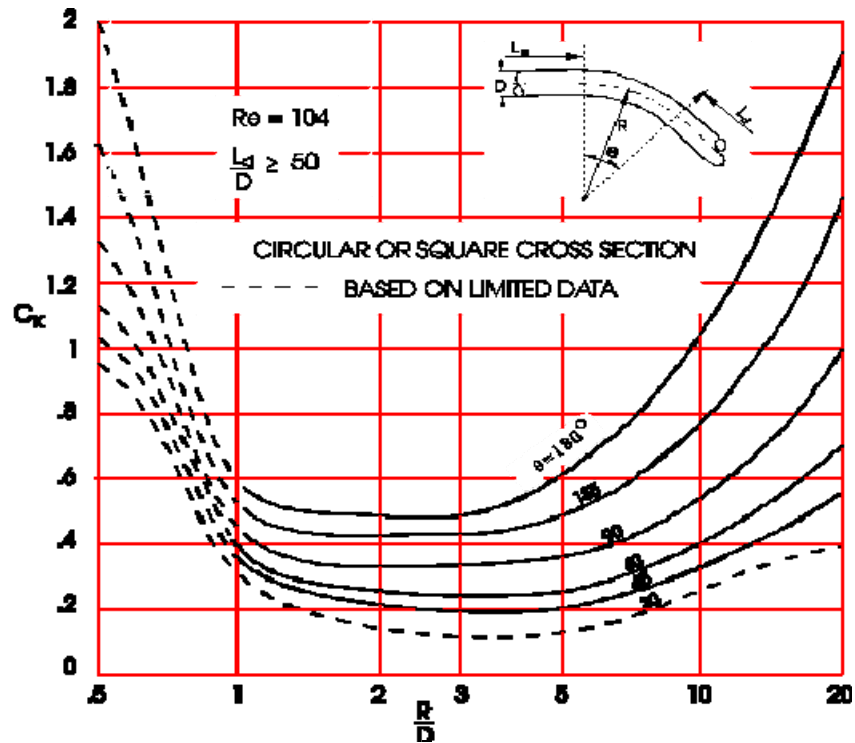
Figure 7-8: Pressure loss coefficient, *c*_K, as a function of the dimensionless radius of bend centerline, *R/D*, for different values of bend angle, *θ*. Turbulent flow through short circular arc bends. Either circular or square cross section. From ESDU 67040 (1967) [47].
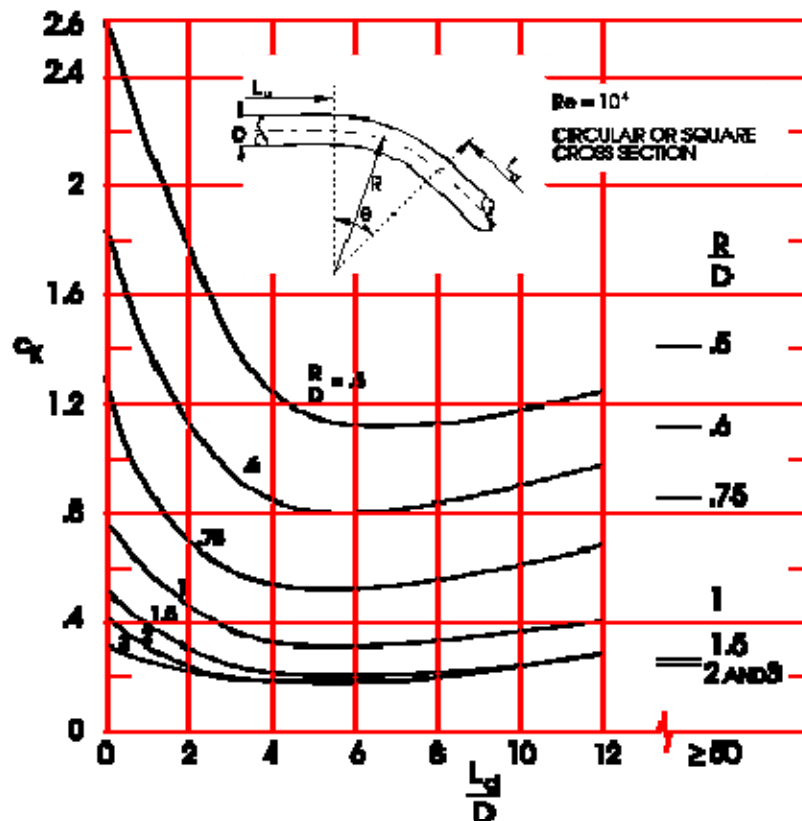
Figure 7-9: Pressure loss coefficient, c_K, for short circular arc bends, having a short downstream tangent of length, L_d, as a function of L_d/D, for different values of the dimensionless radius of bend centerline, R/D. Turbulent flow. Either circular or square cross section. From ESDU 67040 (1967) [47].
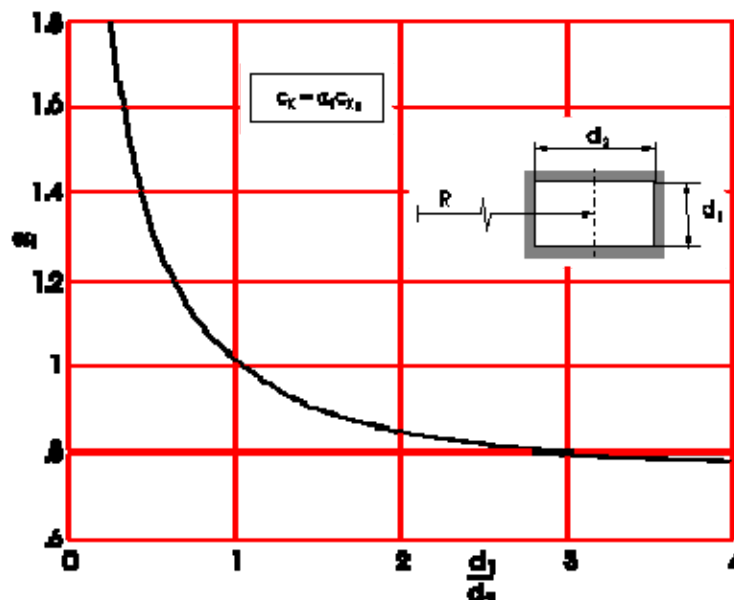
Figure 7-10: The factor α_1 to account for the aspect-ratio of the bend cross section. From ESDU 67040 (1967) [47].
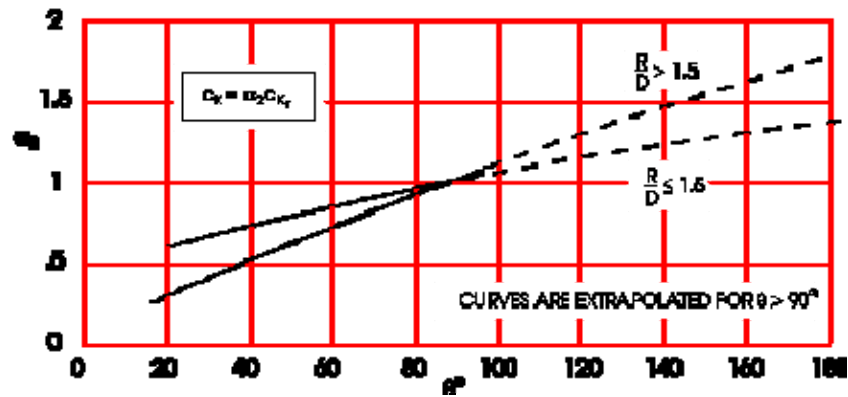
Figure 7-11: The factor α_2 to account for the bend angle. From ESDU 67040 (1967) [47].
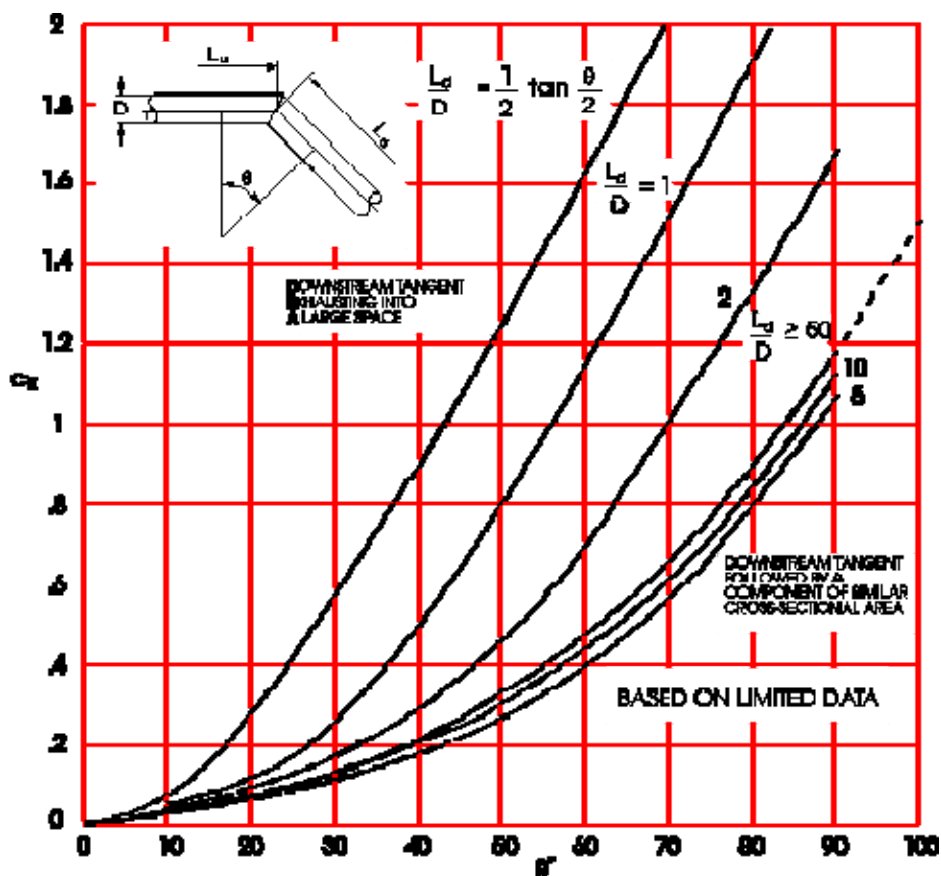
Figure 7-12: Pressure loss coefficient, c_K, for single mitre bends, as a function of bend angle, θ, for different values of the dimensionless length, L_d/D, of the downstream tube. Turbulent flow. Either circular or square cross section. From ESDU 67040 (1967) [47].
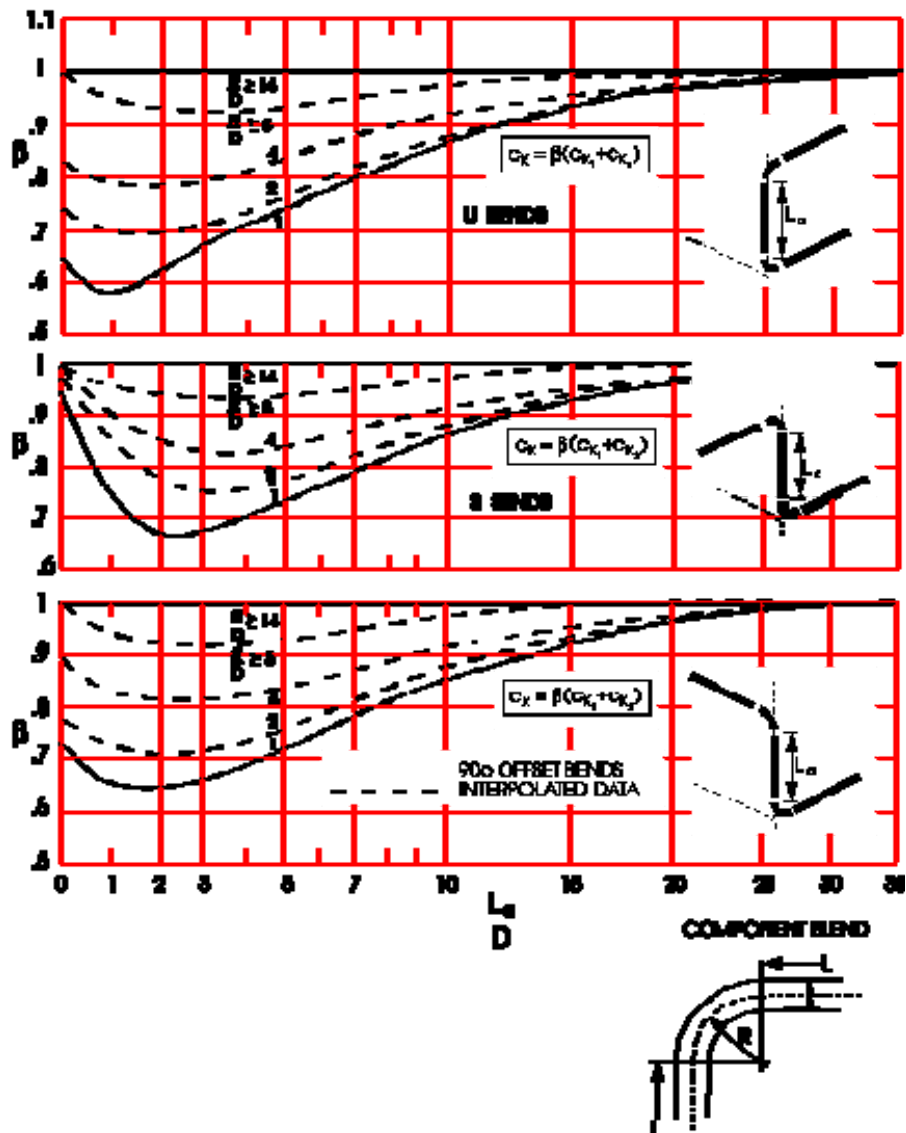
Figure 7-13: Factor *β*, which account for the interaction between two 90° -circular arc bends-, as a function of the dimensionless distance between both bends, *La/D*. From ESDU 68035 (1968) [49].
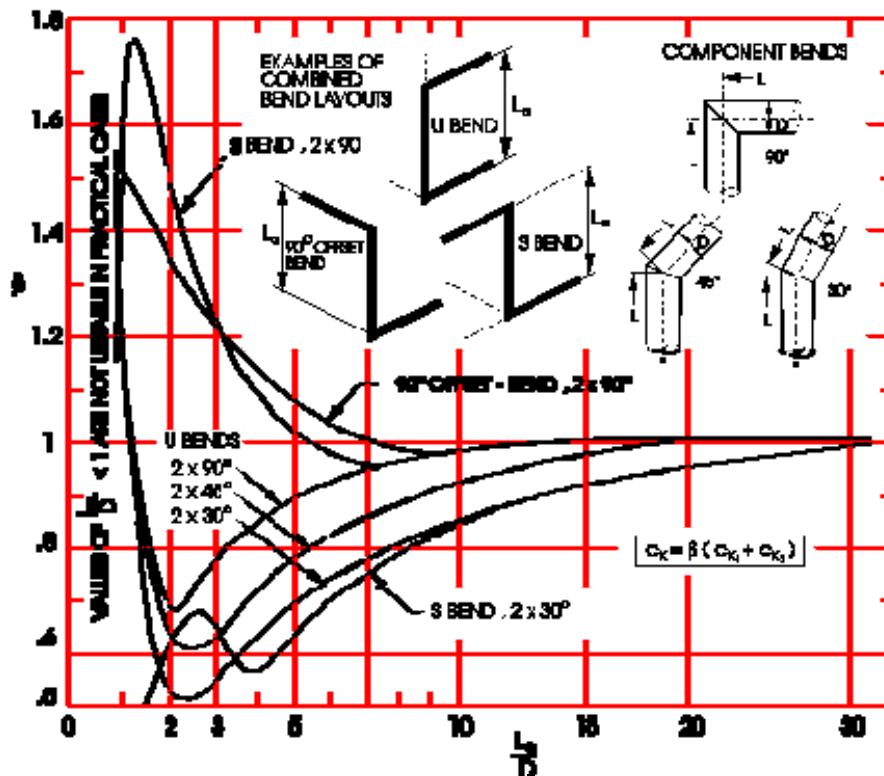
Figure 7-14: Factor β, which account for the interaction between two mitre bends, as a function of the dimensionless distance between both bends, L_a/D. From ESDU 68035 (1968) [49].

7.3.3 Sudden changes of area
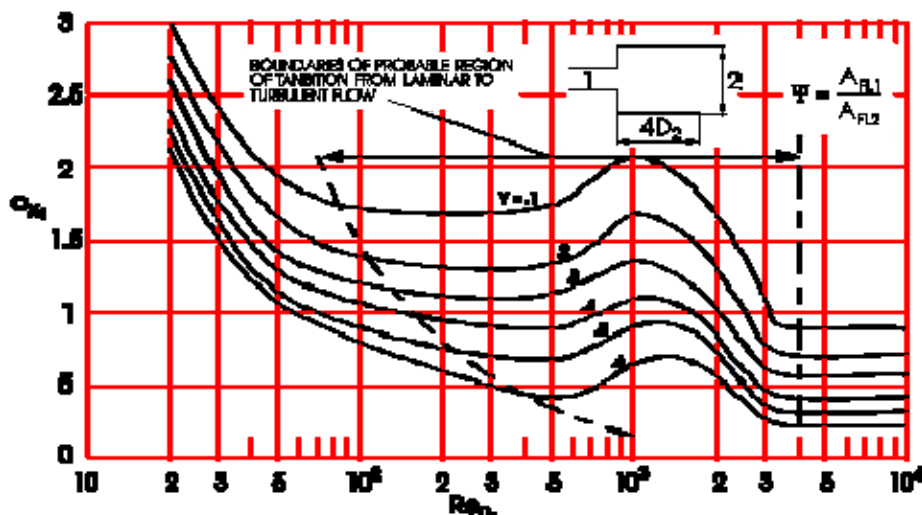
Figure 7-15: Total-pressure loss coefficient, c_{Kt}, as a function of Reynolds number, Re_{D1}, for different values of the area ratio, ψ. Enlargement with a duct downstream $4D_2$ long. Uniform incoming flow at low Reynolds number. From ESDU 72011 (1972) [54].
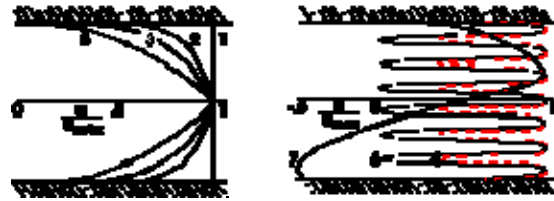
Curve	U_{max}/U	Typical of:	Curve	$-U_{max}/U$	Typical of:
1	1,0	Uniform flow	4	1,4	Exit from grid, high porosity
2	1,24	Fully-developed turbulent flow	6	2,0	Exit from grid, low porosity
3	1,44		7	2,9	Exit from sharp-radius bend, radius ratio < 1,5, and exit from plane diffuser 8-15° half-angle
5	1,87	Exit from conical diffuser 2° half-angle			
		Exit from conical diffuser 4° half-angle			

Figure 7-16: Different velocity profiles upstream of a sudden enlargement. From ESDU 72011 (1972) [54].
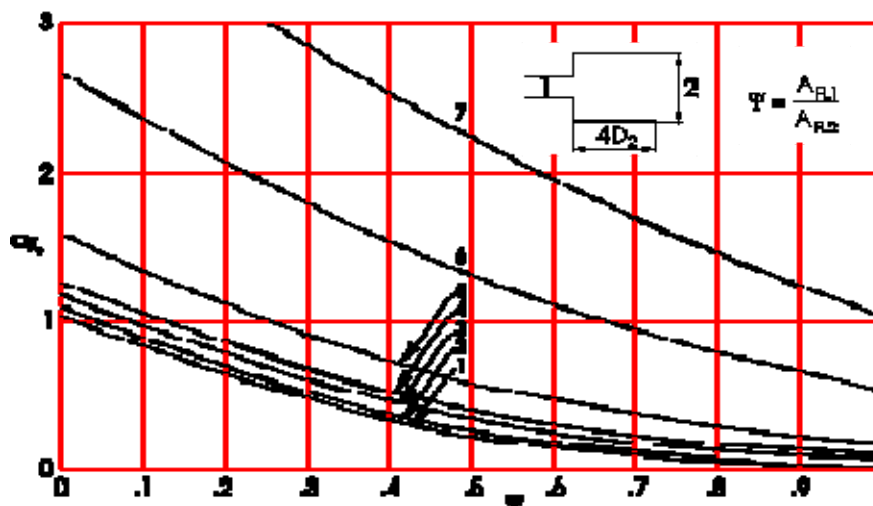
Figure 7-17: Total-pressure loss coefficient, c_{Kt}, as a function of area ratio, ψ. Enlargement with a duct downstream $4D_2$ long. Numbers on curves indicate the velocity profile in Figure 7-22 for which the curve applies. From ESDU 72011 (1972) [54].
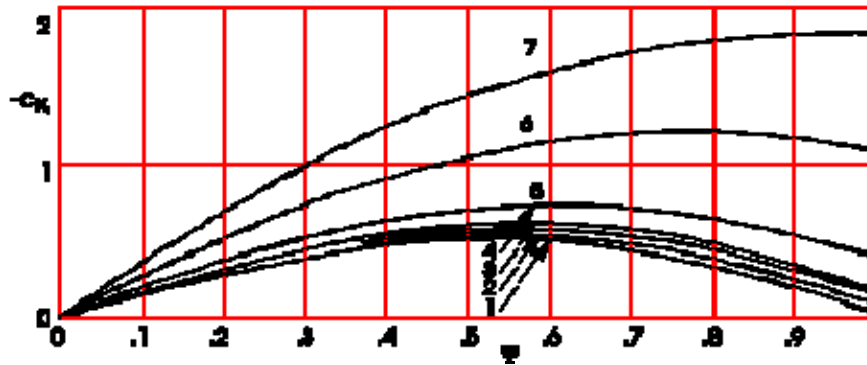
Figure 7-18: Static-pressure loss coefficient, -c_{Ks}, as a function of area ratio, ψ. Enlargement with a duct downstream $4D_2$ long. Numbers on curves indicate the velocity profile in Figure 7-22 for which the curve applies. From ESDU (1972) [54].
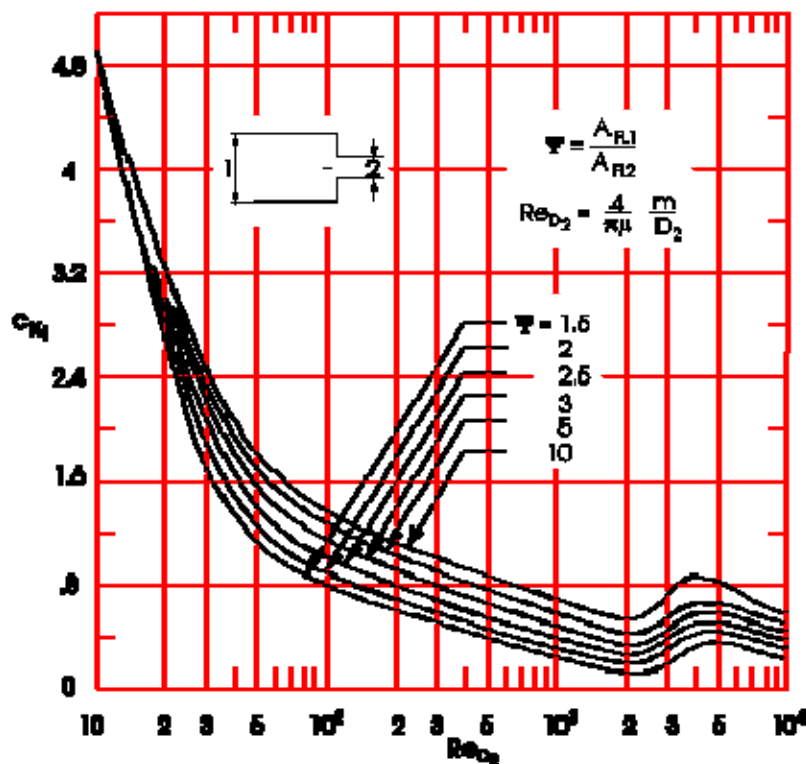
Figure 7-19: Total-pressure loss coefficient, c_{Kt}, as a function of Reynolds number, Re_{D2}, for different values of the area ratio, ψ. The pressure loss coefficient is expressed in terms of the dynamic pressure at clause 6. From Idel'cik (1969) [97].

7.3.4   Orifices and diaphragms
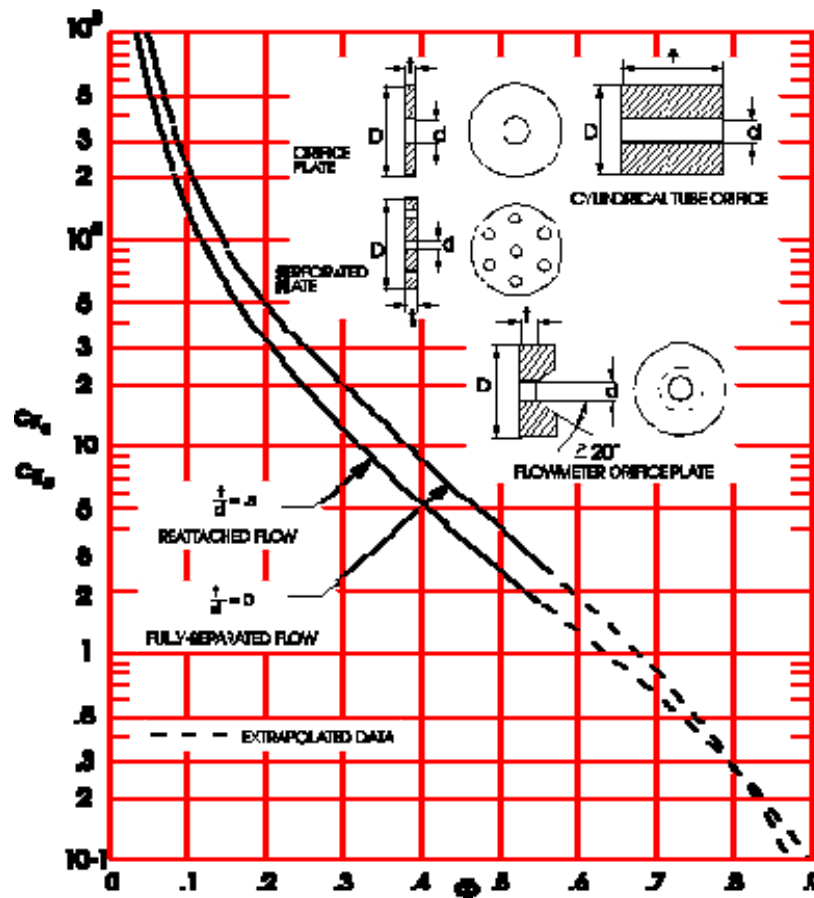
Figure 7-20: Reference values of the pressure loss coefficient, c_K, as a function of the ratio, ϕ, of the area available for fluid flow to the total area of the duct cross section. Perforated plates and orifices. From ESDU 72010 (1972) [53].
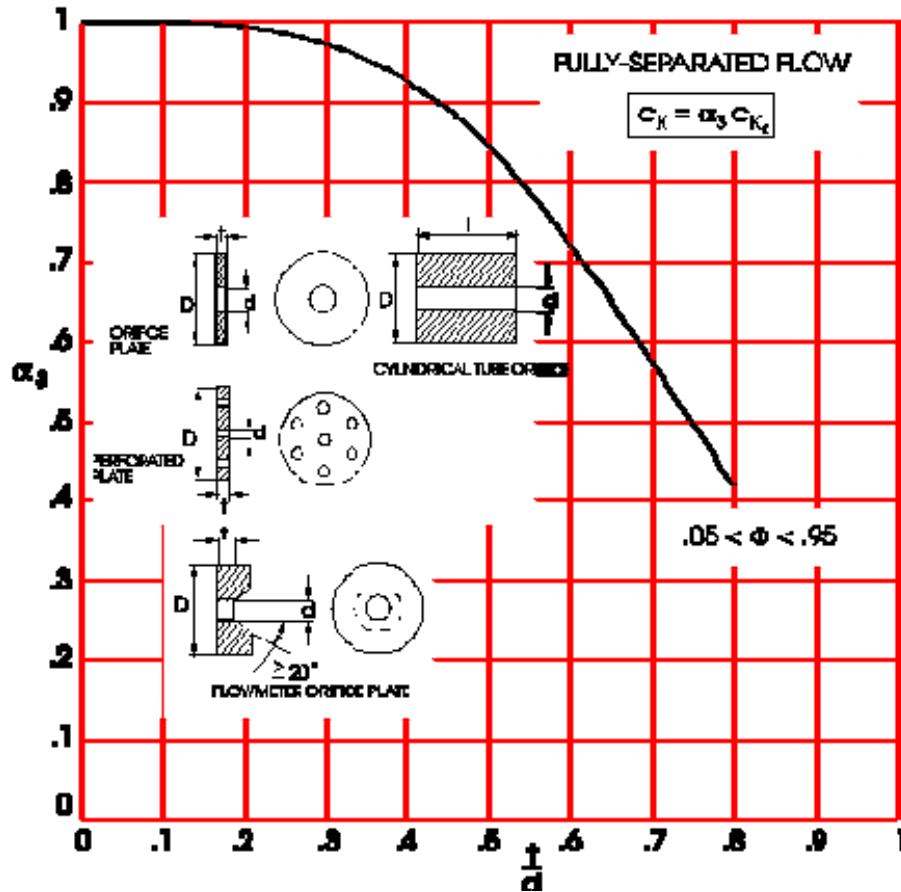
Figure 7-21: The factor α_3 to account for the effect of plate thickness when $t/d < 0,8$. c_{Ko} is given in Figure 7-19. From ESDU 72010 (1972) [53].
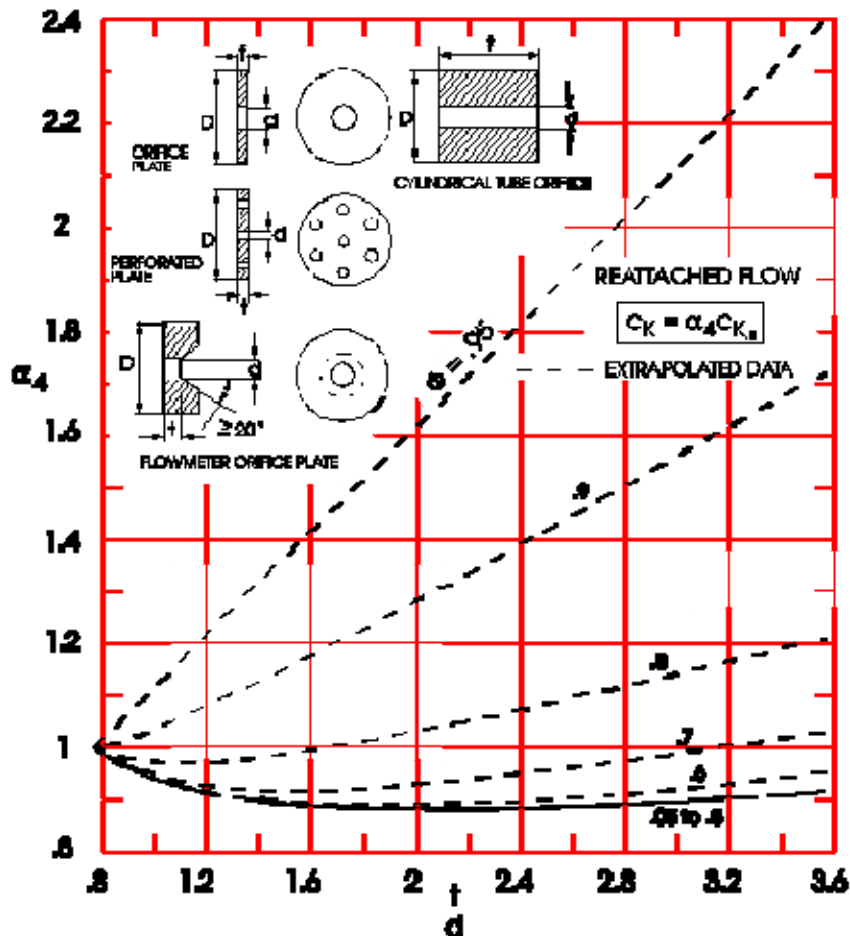
Figure 7-22: The factor α_4 to account for the effect of plate thickness when $t/d \geq 0,8$. $c_{K0,8}$ is given in Figure 7-19. From ESDU 72010 (1972) [53].
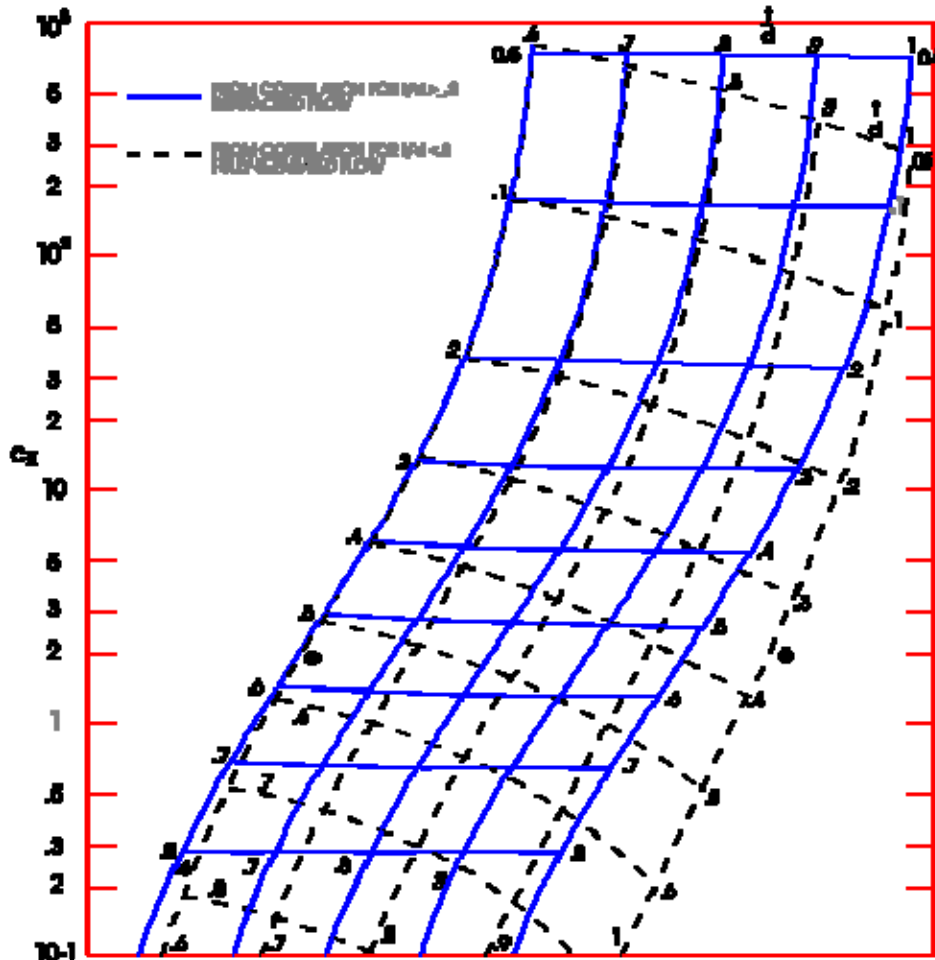
Figure 7-23: Comparison between the pressure loss coefficients, *cK*, in the intermediate region calculated by assuming either of the two extreme cases, fully-separated or reattached orifice flow. From ESDU 72010 (1972) [53].

7.3.5   Screens
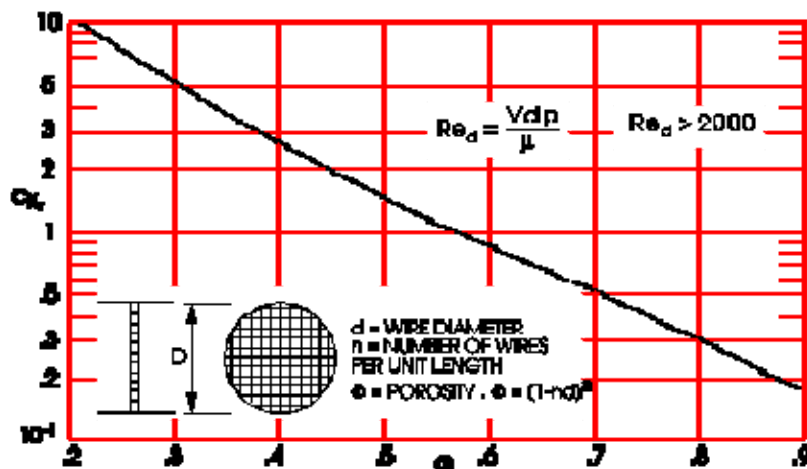
Figure 7-24: Reference pressure loss coefficient, *cKr*, as a function of porosity, ϕ. Round-wire gauzes. From ESDU 72009 (1972) [52].
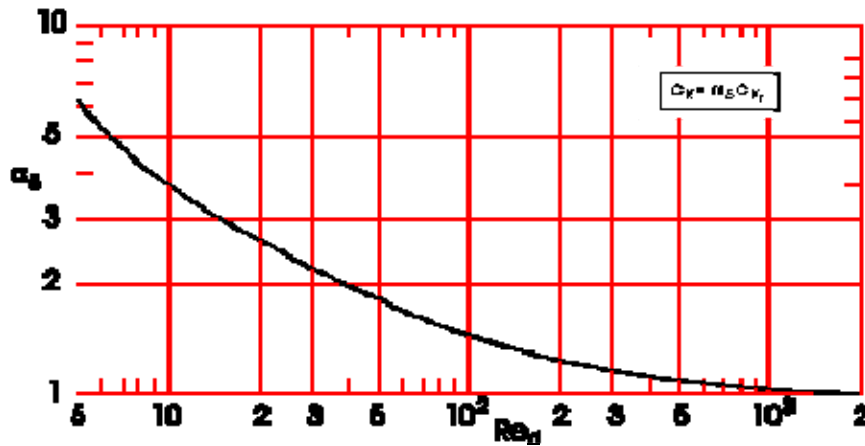
Figure 7-25: Factor α_s to account for low Reynolds number effects in round-wire gauzes. Reynolds number based on the wire diameter. From ESDU 72009 (1972) [52].

7.3.6   Valves
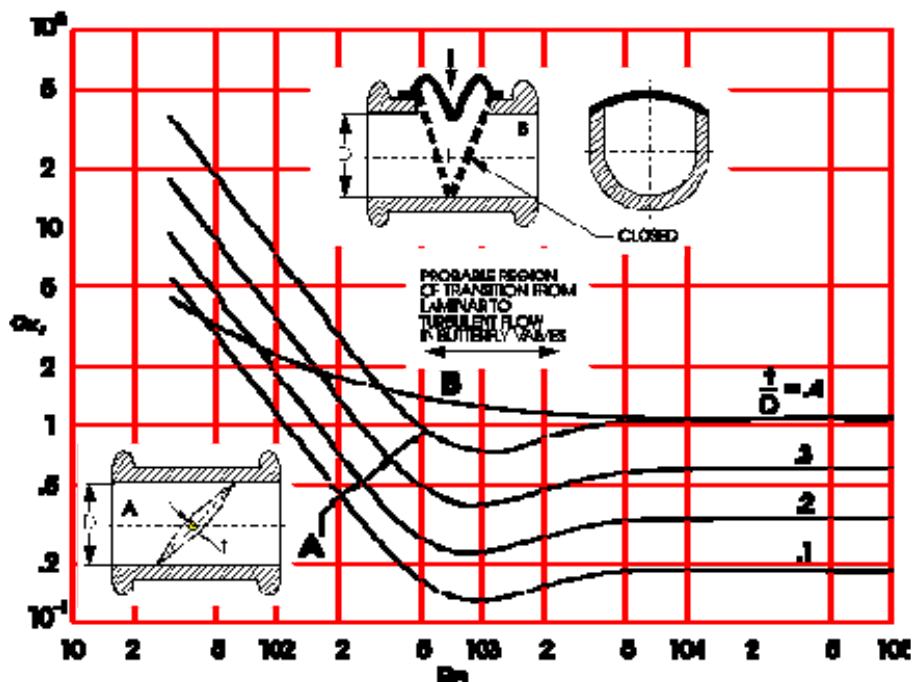
Figure 7-26: Reference pressure loss coefficient, c_{Kr}, as a function of Reynolds number, Re, for diaphragm and butterfly valves fully open. Prepared by the compiler after ESDU 69022 (1969) [51].
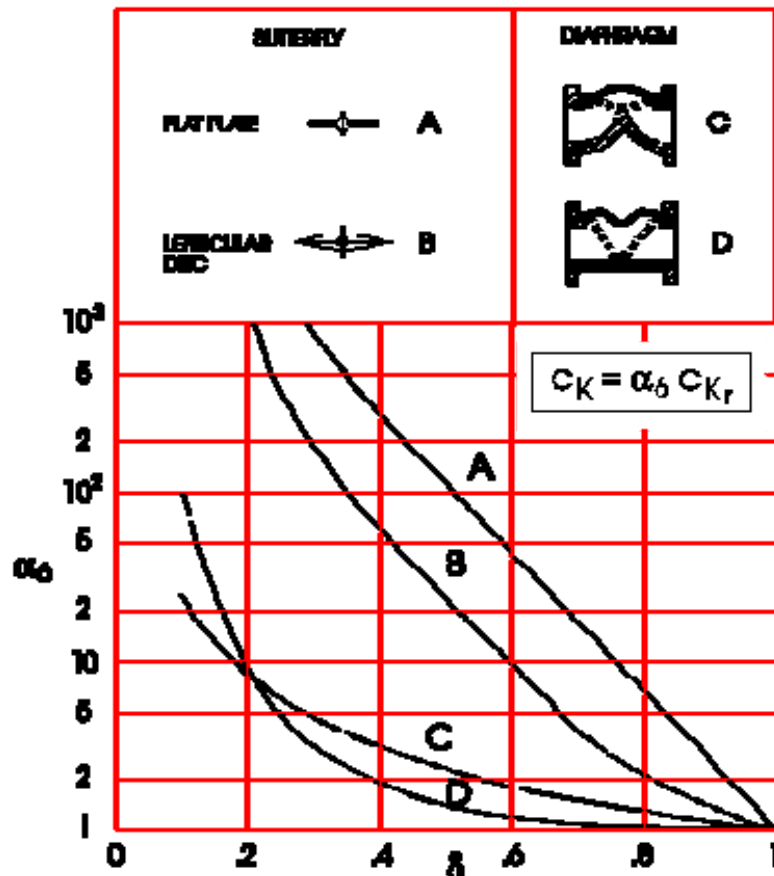
Figure 7-27: Factor α_δ, which accounts for the partial opening of the valve, as a function of the degree of valve opening, δ. δ is defined as the ratio of valve control travel from closed position to total valve control travel. From ESDU 69022 (1969) [51].

7.3.7   Tube banks

$$c_K = \psi A (Re)^m N + 2 \frac{T_o - T_i}{T_i}$$

[7-24]

N: number of transversal rows.

1. When $s_t \leq s_l$, then $A = ab$

    where a is given in Figure 7-28a, b is given in Figure 7-28b and $(Re)^m$, for $(s_t-d)/(s_l-d) = 1$ is given in Figure 7-28c

2. When $s_t > s_l$, then $A = bc$

    where c is given in Figure 7-28a, b is given in Figure 7-28b and $(Re)^m$ is given in Figure 7-28c
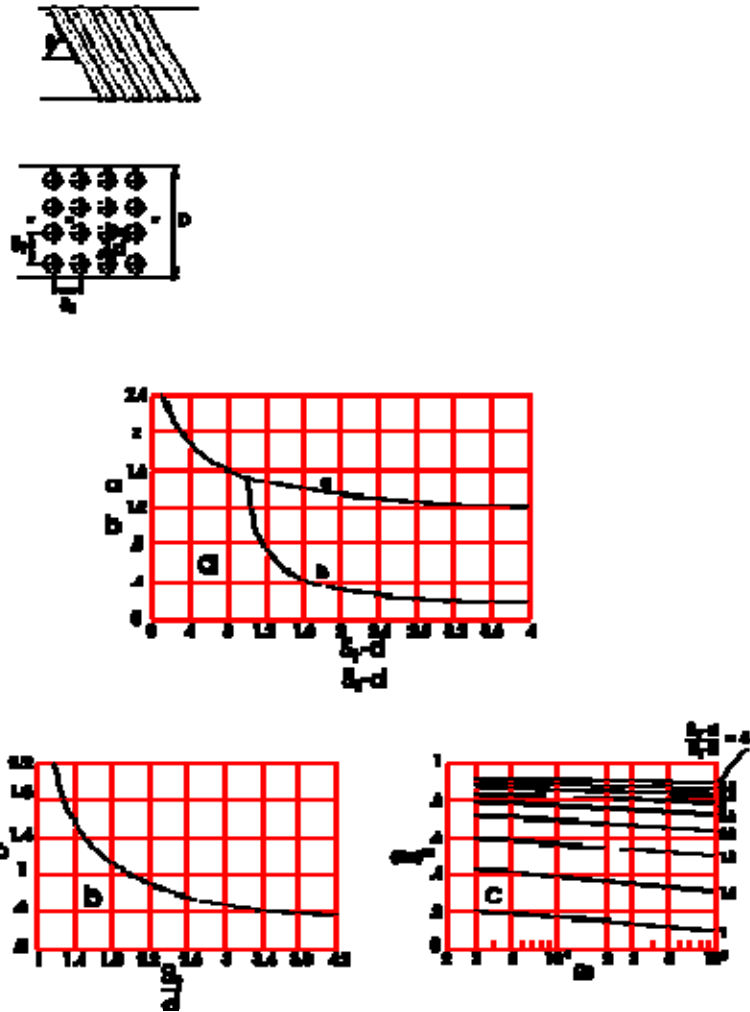
Figure 7-28: Graphics for estimating the pressure loss coefficient, c_K, for in-line tube banks of several relative pitches, s_l, s_t, and yaw angles, θ. The influence of the heat exchange on the pressure loss is taken into account through the tube bank inlet and exit temperatures, T_i and T_o, respectively. From Idel'cik [97].

$$c_K = \psi A (Re)^{-0,27} (N+1) + \frac{T_o - T_i}{T_i}$$

[7-25]

N: number of transversal rows.

1. When $s_t/d < 2$ and $0,14 \leq (s_t-d)/(s'_l-d) < 1,7$, then $A = ab + 3,2$

   where a is given in Figure 7-29a, b is given in Figure 7-29b and $(Re)^{-0,27}$, is given in Figure 7-29c

2. When $s_t/d \geq 2$ and $0,14 \leq (s_t-d)/(s'_l-d) \leq 1,7$, then $A = 3,2$

3. When $s_t/d \geq 1$ and $1,7 \leq (s_t-d)/(s'_l-d) \leq 5,2$, then $A = c$

   where c is given in Figure 7-29a
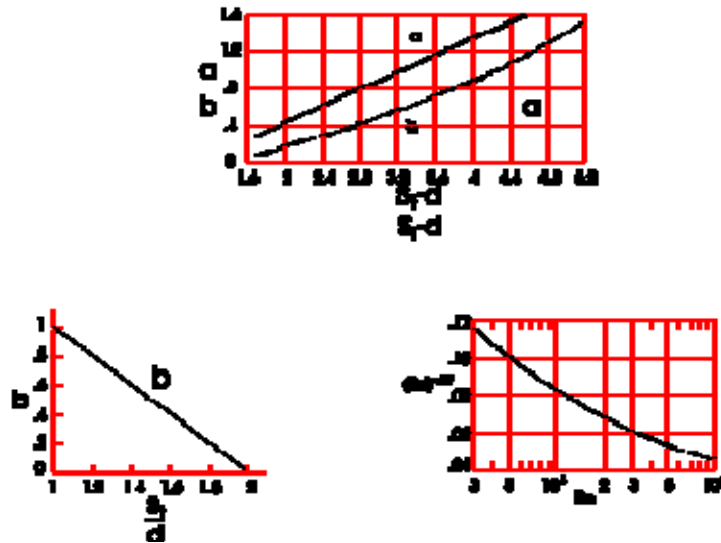
Figure 7-29: Graphics for estimating the pressure loss coefficient, *cK*, for staggered tube banks of several relative pitches, *sl*, *st*, and yaw angles, *θ*. The influence of the heat exchange on the pressure loss is taken into account through the tube bank inlet and exit temperatures, *Ti* and *To*, respectively. From Idel'cik (1969) [97].

7.3.8 Branching of tubes

SKETCH **All cross sections have the same diameter, D**	CURBE NUMBER			
	CONFLUENCE $c_{k_{32}} = \dfrac{\Delta p_{32}}{\frac{1}{2}\rho V_2^2}$	**BRANCHING** $c_{k_{13}} = \dfrac{\Delta p_{13}}{\frac{1}{2}\rho V_1^2}$	**CONFLUENCE** $c_{k_{12}} = \dfrac{\Delta p_{12}}{\frac{1}{2}\rho V_2^2}$	**BRANCHING** $c_{k_{12}} = \dfrac{\Delta p_{12}}{\frac{1}{2}\rho V_1^2}$
	1	**1′**	**2**	**2′**
	$r/D = 0{,}1$ **3** $r/D = 0{,}2$ **4**		$r/D = 0{,}1$ **5** $r/D = 0{,}2$ **6**	
	$m_4/m_3 = 2$ **7** $m_4/m_3 = 1$ **8** $m_4/m_3 = 0{,}5$ **9**		**10**	
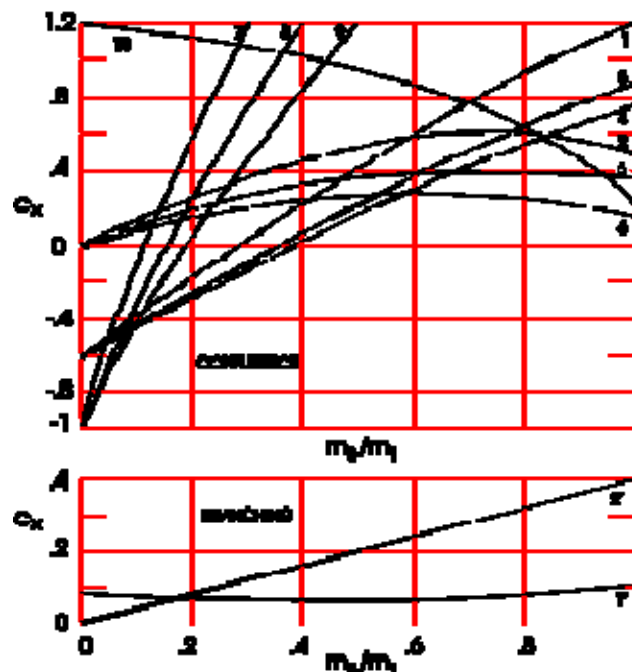
Figure 7-30: Pressure loss coefficient, c_K, as a function of the ratio of lateral to total mass flow rates in branching tubes. The mixed confluence-branching case is not considered. From Idel'cik (1969) [97].

8
Combined thermal and frictional analysis

8.1   General

The aim of this clause is to provide information relating heat transfer and fluid friction in turbulent flow through smooth pipes.

The interplay between heat transfer and fluid friction comes from two different causes:

1.   The transport of any fluid entity in a turbulent flow depends on the mean and fluctuating velocity fields. Thus the analysis of a turbulent transfer process requires some understanding of momentum transfer and the associated velocity variation, as will be shown in this clause.

2.   In many instances, there is a dependence of the velocity field on the heat transfer. The temperature variations associated with rapid heat transfer (or with very high velocities) give rise to changes in the molecular transport properties of the fluid, with the consequent modifications in the structure of the fluid layers close to the wall where molecular transport still dominates. This point has been already discussed in clause 6.2.4 and clause 7.2.3.

It has been mentioned above that this clause exclusively concerns flow through smooth pipes. Data on convective heat transfer and fluid friction in rough pipes are given in clause 9.2.

8.2   Analogies between momentum and heat transfer

It can be deduced from the first consideration in clause 8.1 that analogies relating rates of heat transfer to momentum transfer exist. These analogies could be useful to the engineer when data on turbulent heat transfer are not available whereas data on fluid friction are.

From the many analogies existing in the literature only those most commonly used will be introduced here. Reference is made to the book by A.J. Reynolds (Reynolds (1974) [149]) for both an account of the motivation and justification of these analogies and for a survey of those exhibiting simple mathematical formulations.

8.2.1   The Reynolds analogy

In 1874 Osborne Reynolds postulated that the laws governing turbulent transfer of momentum and heat were the same.

Turbulent transfer is induced by the random fluctuations in velocity which are superimposed to the mean flow. Because of these fluctuations small lumps of fluid move backwards and forwards across

the stream. This movement must involve the transfer of momentum (or heat) when there is a transverse velocity (or temperature) gradient.

If the fluid particles move on the average from a region where the mean velocity is V and the bulk temperature is T_b, to the wall surface where the mean velocity is zero and the temperature is T_w, the Reynolds analogy would imply,

$$\frac{Rate\ of\ heat\ transfer}{Rate\ of\ momentum\ transfer} = \frac{q}{\tau_w} = \frac{c_p(T_w - T_b)}{V} \qquad [8\text{-}1]$$

where q is the heat flow rate per unit wall surface area and τ_w is the wall friction.

An expression for the heat transfer coefficient, $h = q/(T_w - T_b)$, or for the Stanton number, $St = q/\rho V c_p(T_w - T_b)$, may be obtained from Eq. [8-1]

$$h = \tau_w \frac{c_p}{V} \qquad [8\text{-}2]$$

$$St = \frac{f}{2} \qquad [8\text{-}3]$$

where $f = 2\tau_w/\rho V^2$ is the Fanning friction factor ($f = \lambda/4$).

In order to check the validity of the Reynolds analogy, experimental values of the dimensionless parameter $2St/f$ (which according to Eq. [8-3] should be equal to unity) have been plotted in Figure 8-1 as a function of Reynolds number, Re, for different values of the Prandtl number, Pr. The experimental curves have been deduced by combination of data for St from Eagle & Ferguson, and frictional data for f from Stanton and Pannell (both quoted by Goldstein (1950) [73]). The experiments by Eagle & Ferguson extended over a range of values of Pr from 3 to 10, and a range of Reynolds numbers from 5 x 10^3 to 2 x 10^5. The following empirical correlation has been used to plot these curves:

$$\frac{2St}{f} = \frac{1}{\alpha + (Pr-1)\beta - (Pr-1)^2 \gamma} \qquad [8\text{-}4]$$

where α, β and γ are given as functions of Re, in Table 65, p. 659, by Goldstein. The curve for $Pr = 1$ has been obtained by use of the correlation (4) outside its range of proven validity ($3 \leq Pr \leq 10$).
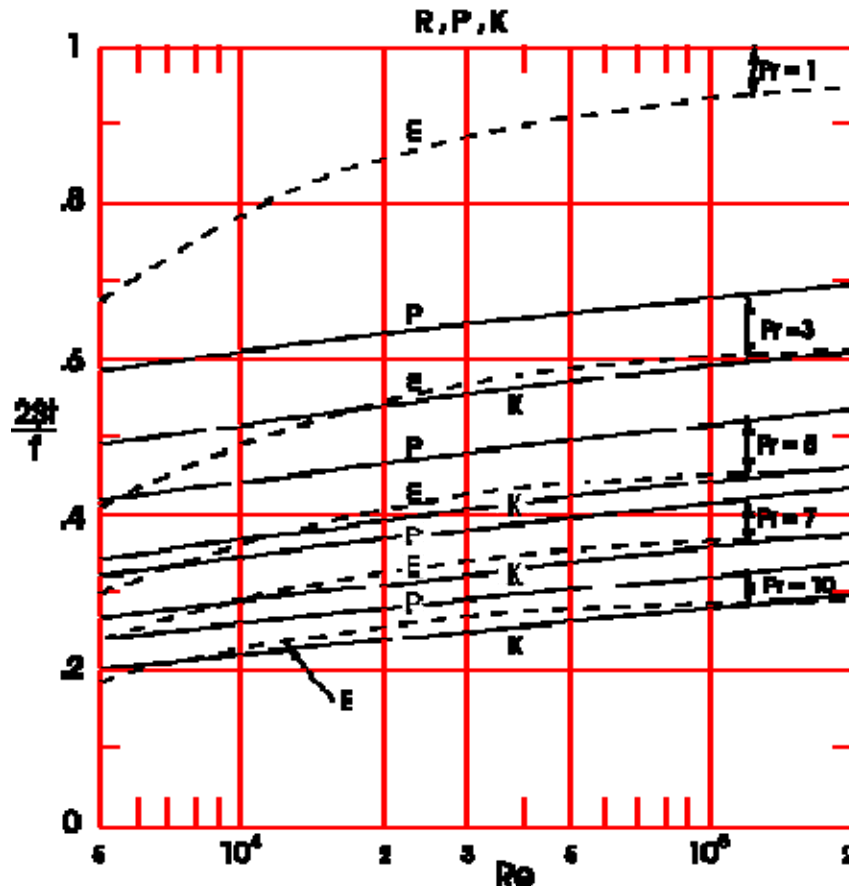
Figure 8-1: The ratio 2*St*/*f*, for turbulent flow in constant wall temperature cylindrical tubes, as calculated by use of several expressions, vs. the Reynolds number, *Re*. E: Correlation of experimental results. From Goldstein (1950) [73]. R: Reynolds Analogy. P: Prandtl Analogy. K: von Kármán Analogy. Calculated by the compiler.

It can be deduced from Figure 8-1 that the Reynolds analogy fails under two circumstances:

1. For fluids for which *Pr* substantially differs from unity. This so because of the existence of a layer near the wall (the laminar sublayer) where the transfer of heat and momentum by thermal conductivity and viscosity are of importance. These laminar transfer processes are strictly similar when *Pr* = 1. For common gases, however, *Pr* = 0,7 and Reynolds analogy can be applied.

2. When *Re* is not large, Eq. [8-3] cannot be applied when the flow is laminar. Its use for transitional flows has not been validated by the experiments either. Nevertheless, it has been indicated (Reynolds (1974) [149], p. 244) that the analogy gives fairly accurate results in several instances of laminar pipe flow. Let us consider, for example, the fully developed laminar flow through straight pipes of circular cross section. For constant heat transfer rate *Nu* = 4,364 (see clause 7.2.1, Figure 6-1), whereas *f* = λ/4 = 16/*Re* (see clause 7.2.2). In terms of *St* and *f*

$$\frac{2St}{f} = \frac{6}{11Pr}$$

[8-5]

The analogy being most accurate for common gases ($Pr \approx 0,7$).

8.2.2 The Prandtl analogy

According to Prandtl, the Reynolds analogy is strictly valid only for the central core of fully developed turbulent flow, outside the laminar sublayer.

In that case, Eq. [8-1] becomes

$$\frac{q}{\tau_w} = \frac{c_p(T_\delta - T_b)}{V - u_\delta}$$

[8-6]

where subscript δ refers to conditions at the edge of the laminar sublayer.

In the laminar sublayer. whose thickness is δ, where the temperature and velocity profiles are linear functions of the distance to the wall,

$$\frac{k(T_w - T_\delta)}{q} = \frac{\mu u_\delta}{\tau_w} = \delta$$

[8-7]

Elimination of T_δ between [8-5] and [8-6] yields:

$$St = \frac{f/2}{1 + (Pr - 1)(u_\delta / V)}$$

[8-8]

which reduces to Eq. [8-3] when $Pr = 1$. Eq. [8-7] takes partly into account the velocity distribution across the tube through the ratio u_δ/V.

In order to apply Eq. [8-7] to particular cases it is necessary to make a suitable assumption about the ratio of the velocity, at the outer edge of the laminar sublayer to the velocity far from the wall. In the case of turbulent flow in a smooth pipe (Schlichting (1960) [157]),

$$\frac{u_\delta}{V} = 5\sqrt{\frac{f}{2}}$$

[8-9]

with this approximation Pradntl's equation becomes

$$St = \frac{f/2}{1 + 5\sqrt{f/2}(Pr - 1)}$$

[8-10]

Curves labeled P in Figure 8-1 have been deduced from Eq. [8-8] with the values of $f(Re)$ tabulated by Goldstein(1950) [73]. Alternative expressions of f for smooth tubes could be also used (see clause 7.2.2 and Table 7-2 of clause 7.2.2.1). It can be seen that the analytical results are now in better agreement with the experimental data than they were when the Reynolds analogy was used.

8.2.3   The Von Karman analogy

Von Kármán improved further the Prandtl analogy by introducing an intermediate buffer layer in which molecular and turbulent diffusion were active. He maintained the same boundaries for the several layers of the velocity and temperature variations, and assumed that the coefficients for turbulent transport of heat and momentum were the same.

The resulting expression for the Stanton number is

$$St = \frac{f/2}{1 + 5\sqrt{f/2}\{Pr - 1 + \ln[1 + (5/6)(Pr - 1)]\}}$$ [8-11]

The reader interested in the details leading to this result could consult the books by Goldstein (1950) [73], Hinze (1959) [89] or Schlichting (1960) [157], among others.

Curves deduced from Eq. [8-9], with the values of $f(Re)$ tabulated by Goldstein (1950) [73], are represented in Figure 8-1. It can be seen that the agreement between these curves and the experimental ones is excellent except for the lower part of the Reynolds number range.

8.2.4   Other analogies

Many other attempts have been made to relate heat transfer to fluid friction in turbulent pipe flows. Nevertheless, since the algebra of the more advanced models becomes very complicated, only two examples which will be used in other clauses of this Part will be presented here. A short survey of analogies can be found in Knudsen & Katz (1958) [107], pp. 417-455 and in Reynolds (1974) [149] pp. 272-73.

1.   Martinelli retained von Kármán's distribution for turbulent transport coefficients of heat and momentum, but he allowed these coefficients to be different in the viscous core, assuming instead the same linear distribution for the rate of heat transfer across the tube as exists for the shear.

    A detailed description of this analogy can be found in Knudsen & Katz (1958) [107].

2.   Colburn analogy. This simple and very useful analogy, which is entirely based on empirical data, is written as:

$$\frac{f}{2} = j$$ [8-12]

    f being the fanning friction factor and j the Colburn factor for heat transfer $j = StPr^{2/3}$. See Knudsen & Katz (1958) [107] for details on this analogy.

9
Heat transfer enhancement

9.1 General

The performance of conventional heat exchangers can be substantially improved -and equipment size reduced- by a number of augmentative techniques. Existing systems can often be upgraded by using an augmentative method, while in the spaceborne heat exchangers an augmentative scheme may be mandatory in order for the system to function properly and meet the size (and/or power) limitations imposed. This may be particularly true for systems transferring heat between a liquid -which is normally an effective heat carrier- and a gas -which is not so effective.

An introduction to the literature on the subject has been given by Bergles (1969) [8]. References to more recent studies can be found in Bergles (1973) [7].

Table 9-1, from Bergles (1973) [7], classifies both techniques and modes of heat transfer. The techniques are grouped according to passive methods, which require no external power, and active schemes, which require external power. A final category, compound augmentation techniques, encloses those situations where two or more of these basic techniques are utilized simultaneously.

A X in Table 9-1 means that the technique has been used, according to the literature, to enhance the heat transfer mode.

Table 9-1: Heat Transfer Enhancement Techniques

Technique	Mode of Heat Transfer	Single-Phase Free Convection	Single-Phase Forced Convection	Pool Boiling	Flow Boiling	Condensation
PASSIVE						
Treated Surfaces				X	X	X
Rough Surfaces		X	X		X	
Extended Surfaces		X	X	X	X	X
Displaced Enhan. Devices			X		X	
Swirl Flow Devices			X		X	
Surfaces Tension Devices			X	X		
Additives for Liquids			X	X	X	

Mode of Heat Transfer / Technique	Single-Phase Free Convection	Single-Phase Forced Convection	Pool Boiling	Flow Boiling	Condensation
Additives for Gases		X			
ACTIVE					
Mechanical Aids		X	X		
Surfaces Vibration	X	X	X	X	X
Fluid Vibration	X	X	X		X
Electrostatic Fields	X	X	X		X
Injection or Suction		X	X		X
COMPOUND		X			

NOTE   From Bergles (1973) [7]

This clause presents data concerning the singles-phase forced convection mode of heat transfer (second row in table below). Techniques involving complicated or massive devices, such as surface vibration or electrostatic fields, whose reliable and sage use in space is open to question, have not been considered.

9.1.1   Basic augmentation mechanisms

The most usual passive techniques for improving single phase forced convection are based on one, or more, of the following mechanisms: 1) Turbulence promotion; 2) Extension of the heat transfer surface, and 3) Swirling of the flow.

1.   Turbulence promotion. Transport processes are more effective under turbulent than under laminar conditions. Nevertheless, the rate of heat transfer to a surface, no matter the turbulence of the flow, is controlled by a purely molecular property of the fluid, its thermal conductivity. This is so because of the laminar sublayer which appears close to the surface.

     The resistance to heat transfer of the laminar sublayer is proportional to its thickness, thence any reduction of the thickness will result in an increase in the heat transfer.

     One means of reducing the thickness of the laminar sublayer consists in increasing the level of turbulence of the flowing stream. This can be achieved by use of turbulence promoters, either attached to or detached from the heat transfer surface.

2.   Extension of the heat transfer surface. It is clear that, even in the absence of turbulence promotion, the heat transfer coefficient referred to the nominal area increases by the addition of fins.

     In order to get the desired increase in the heat transfer coefficient, especially when liquid heat carriers are used, good thermal contact between the fin and the tube wall is crucial.

3. Swirling of the flow. Swirling improves the heat transfer due to increased velocity near the tube wall, and to a centrifugal convection effect which is present when the direction of heat flow is from larger to smaller radii.

Swirling can be easily induced by means of twisted metallic strips inserted in the flow duct.

In many cases the augmentation achieved with a given technique may be attributed to various of the mentioned mechanisms, rendering it difficult the absolute classification of the technique. For example, spiral fins could simultaneously profit from the three basic mechanisms.

Although several active techniques aim at "scraping away" or "sucking off" the laminar sublayer, the augmenting effect is obtained in many other systems by means of periodic flow oscillations superposed to the steady flow.

The effect of low frequency pulsations, which probably have the most potential for practical application, can be easily understood on the basis of a quasi-steady approach. At very low frequencies one can assume that the instantaneous heat transfer rate is equal to that corresponding to the steady flow at the instantaneous velocity. The following conclusions result:

1. Slow frequency oscillations do not influence the fully developed laminar flow (provided that no transition is induced) since the steady flow heat transfer rate, h, is velocity independent.

2. When the oscillations are superposed to a turbulent flow a decrease in the oscillation is so large that reverse flow appears during part of the cycle.

3. When the oscillations are superposed to a turbulent flow a decrease in the heat transfer results, unless the amplitude of the oscillation is so large that reverse flow appears during part of the cycle. The reason is that, being the heat transfer rate proportional to a power of the velocity close to 0,5, the gain achieved by increasing the instantaneous velocity in a given amount is less than the loss resulting from decreasing it in the same amount.

Fluid oscillations may be generated either vibrating the duct, pulsating the mass flow rate, or acoustically disturbing the fluid flow.

The first procedure, although used to cool small components submerged in a coolant bath, is difficult to apply and, as a general rule, leads to mechanical failure of the equipment in a short time. Modulation of the mass flow rate can be induced by means of a piston-type pump. Acoustic fields applied to air flows are generally impractical because of the required sound intensities well above human tolerance. With liquids there is considerable difficulty in disturbing systems of not too small sizes.

9.1.2   Criterion for the evaluation of the several techniques

To establish a generally applicable selection criterion for augmentative techniques is difficult. Even if cost considerations, and reliability and safety factors are disregarded -which should not- the problem arises that the augmentative technique increases -at constant velocity- both the heat transfer and the friction.

It appears that among the many available ways to relate heat transfer and friction for evaluation purposes, the most favorable one consists in representing the ratio of augmented, h_a, to non-augmented, h_o, convective heat transfer coefficient for constant power, P. Therefore, this ratio has been used in all cases throughout the present item.

The comparison on the basis of equal pumping power is natural when one aims ate upgrading the heat transfer capability of an existing heat exchanger or when, as happens to be the case in spacecraft, the available power is limited.

When $(h_a/h_o)_P$ is larger than unity, the heat transfer rate for a constant temperature difference, T_w-T_b, can be increased, or for the same heat flux, q, the temperature difference can be decreased, at no extra pumping power consumption. Even when $(h_a/h_o)_P < 1$, a gain in the performance of the loop could result, since the decreased mass flow rate reduces the pressure loss in the remainder of the system, reducing the required overall pumping rate. In order to ease the estimation of this reduction by the user, data on both heat transfer and wall friction under augmentative conditions are presented by means of empirical correlations.

Regarding active techniques, P will still be the pumping power but the required external power should be taken into account in the evaluation of the technique.

9.1.3   Index of the compiled data.

The data which are presented in clause 9.2 are indexed in the Table shown below. Two points should be taken into account in connection with the classification of the several techniques.

1.   Some difficulty could arise when identifying a given system either as surface roughness or as extended surface. Inserts for which no particular care has been exercised to optimize solid heat transfer to the heated surface have been classed either surface roughness -when they contact the surface- or extended surfaces -when they do not. Twisted tapes which do contact the surface are the single exception to this rule. Nevertheless, no matter how conductive this contact might be, these tapes swirl the flow and are grouped in a separate class.

2.   Another difficulty appears when trying to distinguish between machined roughness and other small internal protrusions. Provided that these protrusions are parallel to the tube axis or slightly spiralled, they do not increase the level of turbulence and are classed as fins, otherwise they would be included under surface roughness.

9.1.4   Validity of the empirical correlations

The validity of the empirical correlations given in clause 9.2 rests upon the fulfillment of several conditions, which are listed side by side with the correlation. These conditions are based either on the particular experiment devised to obtain the correlation, on the theoretical background on which it is based, or on both. Sometimes theoretical and experimental conditions conflict.

The user interested in applying the correlations under slightly different conditions should take into account the following considerations.

1.   Length to diameter ratio, L/D, required to achieve fully developed conditions.

In most cases the value L/D listed under Conditions is that of the experimental set up. The correlation can be used for other values of L/D provided that they are larger than both the thermal and frictional entrance lengths. See clause 6.3.1 Figure 6-6 to Figure 6-12), clause 6.3.1 (Figure 6-23 to Figure 6-27) and clause 7.2.5 for estimates of these lengths.

2.   Temperature dependence of the fluid properties.

The convective local heat transfer coefficient, h_x, is calculated in terms of the local temperature difference, $(T_w-T_b)_x$, as is indicated in clause 6.2.1.

The fluid properties are evaluated at the bulk temperature, T_{bx}, of the tube section, x, as defined in clause 6.2.4.

$$T_b = \frac{\int_{A_{FL}} uTdA_{FL}}{VA_{FL}} \qquad [9\text{-}1]$$

In several instances the fluid properties are evaluated at the average temperature, T_{avx}, of the section, x.

$$T_{av} = \frac{\int_{A_{FL}} TdA_{FL}}{A_{FL}} \qquad [9\text{-}2]$$

The difference between both temperatures is insignificant, particularly for turbulent flows, and when the variation of T along the tube is small (Reynolds (1974) [149], pp. 174-175).

Both procedures are, however, inadequate when large wall to fluid temperature differentials exist. In these instances a "loading factor", of the form $(T_b/T_w)^m$ or $(\mu_b/\mu_w)^m$, must be introduced (see clause 6.2.4 and clause 7.2.3).

In many practical instances the heat transfer coefficient is deduced by use of an averaging experiment. This happens to be the case, for example, when the heat transfer is related to the power required to hold constant the temperature of a highly conductive tube. Since the bulk temperature do change along the duct, the average value of the heat transfer coefficient are based on an average bulk temperature.

3. 3) Heat flux distribution.

The case of constant heat flux is fairly easily dealt with theoretically, nevertheless most experiments are performed under nearly constant temperature differentials. Normally, a heat transfer coefficient based on the local temperature differential will be lower for a constant wall temperature than for constant flux, since the large differentials upstream leave the temperature near the wall higher than it would be for a constant differential.

The Table 9-2 below indicates that for turbulent flow, the difference in the heat transfer coefficient is virtually negligible, compared with other sources of uncertainty, except at very small Prandtl numbers.

Table 9-2: Ratio of heat transfer coefficients for constant wall temperature, Nu_T, and constant heat flux, Nu_q, for turbulent pipe flow. From Reynolds (1974) [149].

PrRe	10^6	10^5	10^4	10^3	10^2	10
Nu_T/Nu_q	0,96	0,95	0,90	0,83	0,75	0,73

For laminar flows the effect is larger as can be seen in Figure 6-1, clause 6.3.1.1. However Nu_T/Nu_q is larger than 0,8 in most cases.

Index of Compiled Data Single-Phase Forced Convection								
Technique	Main Operating Mode	Description	Duct	Fluid	Enclosed Data			Fig.
					$(h_a/h_o)_p$	λ or f	Nu or St	
PASSIVE								
Rough Surface	Inducing Transition to Turbulence	Commercial Roughness	Tube					
		Sand-Grain Roughness		Water	X	X	X	Figure 9-1
		Machined Roughness						
		Small Ring-Type Inserts		Several	X	X	X	Figure 9-3
		Large Ring-Type Inserts						
		Wire-Coil Roughness						
		Mesh Inserts						
		Protuberances or Groves	Annulus	Water	X	X	X	Figure 9-6
Extended Surfaces	Increasing Transfer Area	Straight Internal Fins	Tube	Air				
				Water	X	X	X	Figure 9-9
		Low-Spiral Internal Fins			X	X	X	Figure 9-10
		High-Spiral Internal Fins			X	X	X	Figure 9-11
		Externally Finned Tubes	Annulus					
Displaced Enhancement Devices	Inducing Transition to Turbulence	Ring and Discs	Tube					
		Discs		Water				
		Streamlined Bodies			X			Figure 9-12
		Rings	Annulus					
Swirl Flow Devices	Increasing Fluid Path Length	Twisted-Tape Inserts	Tube	Liquid	X	X	X	Figure 9-13
				Air	X	X	X	Figure 9-14
				Water	X	X	X	Figure 9-16

					X	X	X	Figure 9-17
		Brush-Type Inserts						
		Propeller-Type Inserts						
		Inlet Vortex Generators						
ACTIVE								
Surface Scrapers	Removing the laminar Sublayer	Rotating Blade	Wall in Channel					
Fluid Vibration	Increasing Local Convection	Acoustic Vibrations	Tube					
		Mechanically-Induced Vibrations						

9.2   Single-phase forced convection data

SAND-GRAIN-TYPE ROUGHNESS
TURBULENT FLOW IN TUBES
WATER
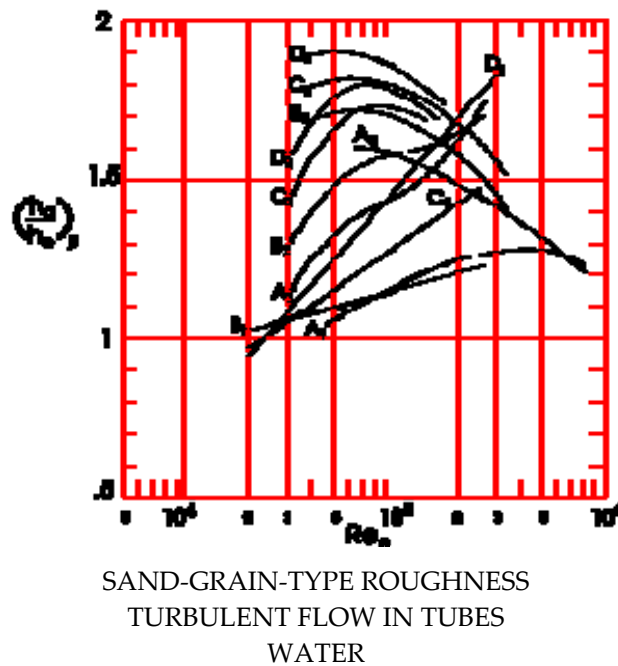
Figure 9-1: Constant power heat transfer ratio, $(h_a-h_o)_P$, vs. Reynolds number based on non-augmentative conditions, Re_o. From Bergles (1969) [8].

Explanation

Key	A₁	B₁	C₁	D₁	A₂	B₂	C₂	D₂	A₃	B₃	C₃	D₃
Investigator	Dipprey & Sabersky (1963) [35]											
D x 10³ [m]	10											
L/D (Diabatic)	38											
(e/D) x 10⁴ᵃ	24				138				488			
T_i [K]	416,5[b]	338	312,5	300	416,5[b]	338	312,5	300	416,5[b]	338	312,5	300
(T_w - T_b) [K] [c]	0											
Pr	1,20	2,79	4,38	5,94	1,20	2,79	4,38	5,94	1,20	2,79	4,38	5,94
Re_a	$1,4 \times 10^4$ - $5,2 \times 10^5$											
Heating/Cooling	H											

[a] The roughness is defined by means of the hydraulic equivalent sand grand size. This size is determined by comparing the friction factor of the present pipes with that predicted by the von Kármán-Nikuradse law for the completely rough refine (see 7.2.2).

[b] The water is pumped by nitrogen gas pressure. The pressure level is not quoted in the source.

[c] The empirical correlations deduce from these experimental data are based on the constant fluid properties assumption. Tests at three different values of the heat flux were performed for each of the nominal combinations of Reynolds numbers and Prandtl number. To obtain the reported isothermal heat transfer, devoided of the effects of radial temperature gradients, the data from each test were first adjusted to correspond to the nominal local Reynolds and Prandtl number conditions. The adjusted heat transfer coefficients were plotted against wall to fluid temperature difference. An extrapolation of the straight line best approximating the three points provided the zero temperature difference value. This value is taken to represent the isothermal heat transfer.

The three rough tubes used for the experiments were produced by electroplating nickel over mandrels coated with closely graded sand grains. The mandrels were subsequently dissolved with chemicals, leaving a pure nickel shell which served as the test tube. The smooth reference tube was also produced by the same method using a smooth mandrel.

Empirical Correlations	Conditions	Comments
DISPREY & SABERSKY (1963) [35] $$\sqrt{\frac{2}{f}} = 2,5\ln\left(\frac{D}{2e}\right) + u_e^+\left(e^+\right) - 3,75$$ or its equivalent $$\frac{1}{\sqrt{\lambda}} = 2,035\log\left(\frac{D}{2e}\right) +$$ $$+ 0,354 u_e^+\left(e^+\right) - 1,323$$	Straight tube of circular cross section. Fluid properties evaluated at T_b. Re based on D_M. $Re > 2 \times 10^3$, $L/D > 25$ - 40. Statistically uniform roughness pattern, geometrically similar from tube to tube with only one scale factor.	$u_e^+(e^+)$ for Nikuradse sand grain roughness is given in Figure 9-2b When $e^+ > 67$, $u_e^+ = 8,48$, thence the von Kármán-Nikuradse law of friction for the completely rough regime results. (See 7.2.2).
$$St_c = \frac{f/2}{1 + \sqrt{f/2}\left[g\left(e^+, Pr\right) - 8,48\right]}$$	Straight tube of circular cross section. Fluid properties evaluated at T_b, and assumed to be constant. Re based on D_M. $Re > 2 \times 10^3$, $e^+ > 67$, $L/D > 25$ - 40. Statistically uniform roughness pattern, geometrically similar from tube to tube with only one scale factor. Constant heat flux at the wall. The expression for St is based on the following four additional assumptions: 1) Closed to the wall the velocity distribution depends exclusively on the local conditions (law of the wall). 2) The law of the wall applies to the temperature defect profile, T_w-T, as well as to the velocity profile, u. 3) The Reynolds analogy is valid in the fully turbulent core. 4) Velocity and temperature reach their cross-sectional mean values at the same distance from the wall.	It is assumed that the time-mean flow in and about the cavities of depth e constituting the rough wall is induced by a pattern of standing vortices with axes normal to the mean velocity. Thence the function g is expressed as: $$g \equiv St_e^{-1} = \frac{\rho c_p u_e \left(T_w - T_e\right)}{q}$$ The analysis of the experiments leads to: $g = 5,19(e^+)^{0,2}Pr^{0,44}$ The proven range of validity of this expression is: $e^+ > 65$, $1,2 < Pr < 6$.
OWEN & THOMSON(1963) [138] $$St_c = \frac{f/2}{1 + \sqrt{f/2}\left[g\left(e^+, Pr\right) + 17,8\sqrt{f/2}\right]}$$	Same as above	The time-mean flow is induced by horseshoe vortices which wrap themselves around the individual excrescences and trail downstream. The main difference with the above model appears in the velocity near the

		edge of the roughness elements which here is assumed to be small compared to u^*. $g \equiv (St_e)^{-1} = 0,52(e^+)^{0,45}Pr^{0,8}$ under the conditions $e^+ > 67,\ 0,7 < Pr < 7,5$.

Comments concerning the data presented in Figure 9-1a.

The gain obtained by roughening increases with the roughness and with the Prandtl number.

For each value of e and Pr there is a value of Re which optimizes the ratio $(h_a-h_o)_P$. These optimum conditions occur in the transition region rather than in the completely rough region.
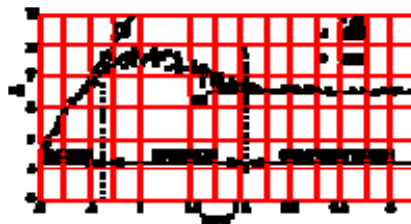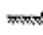
Figure 9-2: Roughness function $u_e^+(e^+)$ for Nikuradse's sand roughness. (1) Hydraulically smooth. (2) $u_e^+ = 8,48$, completely rough. From Schlichting (1960) [157].
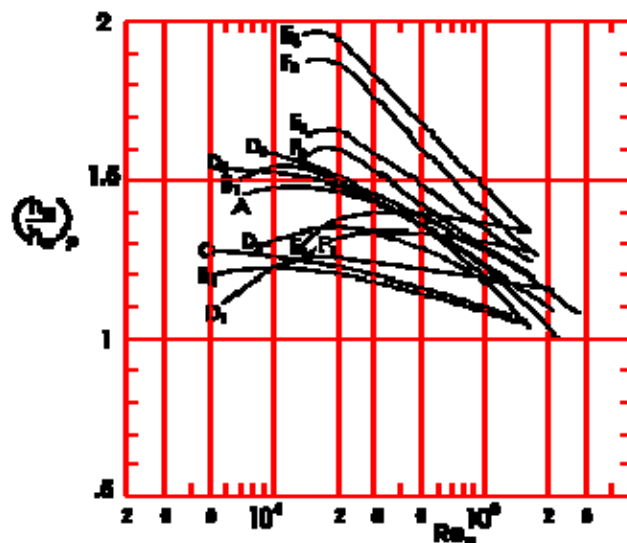
SMALL-RING TYPE INSERTS
TURBULENT FLOW IN TUBES
SEVERAL FLUIDS

Figure 9-3: Constant power heat transfer ratio, $(h_a-h_o)_P$, vs. Reynolds number based on non-augmentative conditions, Re_o. Curves A to D are from Bergles (1969) [8], curves E and F have been calculated by the compiler after Webb, Eckert & Goldstein (1971) [186].

Explanation

Key	A	B₁	B₂	C	D₁	D₂	D₃	D₄	E₁	E₂	E₃	F₁	F₂	F₃
Investigator	Nunner (1956) [134]								Webb, Eckert & Goldstein (1971) [186]					
$D \times 10^3$ [m]	50								36,8					
L/D (Diabatic)	20								41					
Roughness [a] Shape														
$(e/D) \times 10^4$	400				800				200					
s/e	1,25	2		7,5	2				0,52					
b/e	20,4	20,4		81,7	2	5,1	10,2	20,4	10			20		
T_i [K]	300-320													
$(T_w - T_b)$ [K]	20-80													
Fluid	Air								Air	Water	1-Butanol	Air	Water	1-Butanol
Pr	0,71								0,71	5,10	21,7	0,71	5,10	21,7
Re_o[d]	$5 \times 10^2 - 7 \times 10^4$								$6 \times 10^3 - 10^5$					
Heating/Cooling	H								H					

[a] These configurations, useful for laboratory studies, are difficult to adapt to commercial practice.

[b]

[c] Not given. In the liquid tests, the power input was selected to give $Pr/Pr_w \sim 1,1$.

[d] Nunner defines the Reynolds number on the basis of D_M, and of Webb, Eckert & Goldstein on the basis of D.

Empirical Correlations	Conditions	Comments
WEBB, ECLERT & GOLDSTEIN (1971) [186] $$\sqrt{\frac{2}{f}} = 2,5\ln\left(\frac{D}{2e}\right) + u_e^+(e^+, b/e) - 3,75$$ or its equivalent $$\frac{1}{\sqrt{\lambda}} = 2,035\log\left(\frac{D}{2e}\right) + \\ + 0,354u_e^+(e^+, b/e) - 1,323$$	Straight tube of circular cross section. Fluid properties evaluated at T_b. Re based on D. $Re > 2 \times 10^3$ Repeated-rib roughness.	$u_{e^+}(e^+, b/e)$ for repeated-rib roughness is given in Figure 9-4b. When e^+ 30, $u_{e^+} = 0,95(b/e)^{0,53}$. The following correlation has been used by the compiler for data reduction $$u_e^+ = (b/e)^{0,53}\left[\begin{array}{c} 0,95 + (10b/D)^{-0,05e^+} \\ \exp(-0,0343e^+) \end{array}\right]$$ $$\text{for } e/D \geq 0.1$$
$$St_b = \frac{f/2}{1 + \sqrt{f/2}\left[g(e^+, b/e, Pr) - u_e^+(e, b/e)\right]}$$	Straight tube of circular cross section. Fluid properties evaluated at T_b, and assumed to be constant. Re based on D. $Re > 2 \times 10^3$, $L/D > 25 - 40$. Repeated-rib roughness. Heat transfer coefficient in terms of the tube area. The expression for St is based on the following additional assumptions: 1) Closed to the wall the velocity distribution depends exclusively on the local conditions (law of the wall). 2) The law of the wall applies to the temperature defect profile, T_w-T, as well as to the velocity profile, u. 3) The Reynolds analogy is valid in the fully turbulent core. 4) Velocity and temperature reach their cross-sectional mean values at the same distance from the wall.	The analysis of the experiments leads to: $g = 4,50(e^+)^{0,28}Pr^{0,57}$ the effect of b/e being insignificant. The proven range of validity of this expression is: $e^+ > 25$, $0,71 < Pr < 38$ The following expression can be used to account for the effect of radial temperature gradients. $$\frac{St}{St_b} = \left(\frac{Pr_b}{Pr_w}\right)^m$$ $m = 0,15$ for smooth tubes $m = 0,25$ for rough tubes.

GOMELAURI (1974) [74] $Nu = 0,021Re^{0,8}Pr^{0,43}(Pr_b/Pr_w)0,25\varepsilon_r$ $\varepsilon_r = 1,04Pr^{0,04}\exp[0,85\psi(b/e)]$	Straight tube of circular, annular or rectangular cross section. Fluid properties evaluated at T_{bam}. Nu and Re based on D_E., $10^4 < Re < 5 \times 10^5$, $0.7 < Pr < 250$.	$\psi(b/e)=[(b/e)_{opt}/(b/e)]$ when $b/e \geq (b/e)_{opt}$ $\psi(b/e)=[(b/e)/(b/e)_{opt}]$ when $b/e \leq (b/e)_{opt}$ $(b/e)_{opt}$ = 12 to 14

An empirical correlation for St has been also given by Nunner (1956) [134]. Although this correlation fits the data for ring inserts at $Pr = 0,7$, it deviates for other types of roughness and higher Prandtl numbers. See criticisms by Bergles (1969) [8], Webb et al. (1971) [186] and Gomelauri (1974) [74].

Comments concerning the data presented in Figure 9-3a.
Isothermal friction data have been used in the computations leading to $(h_a-h_o)_P$ for the curves from Webb et al.
The optimum value of b/e is about 10-20 for the cases considered. The existence of this optimum is related to the flow pattern near the wall (Figure 9-4c). Separation occurs at the rib, and reattachment 6-8 rib heights downstream from the separation. The local heat transfer is maximum in the reattachment zone. Reattachment does not occur for $b/e < 8$. Nevertheless, because of the recirculation, the local heat transfer in the separated flow region is larger than that corresponding to an attached boundary layer.
The gain achieved by roughening increases with the Prandtl number.
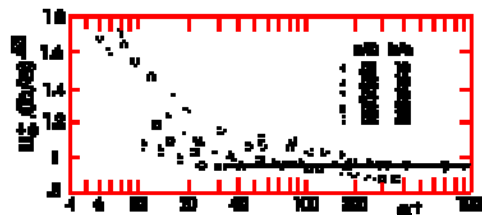
Figure 9-4: Roughness function ue⁺(e⁺,b/e) for repeated-rib roughness. From Webb et al. (1971) [186].

Figure 9-5: Flow pattern near the wall for different values of b/e.

DISCRETE ROUGHNESS
TURBULENT FLOW IN ANNULI
AIR OR WATER
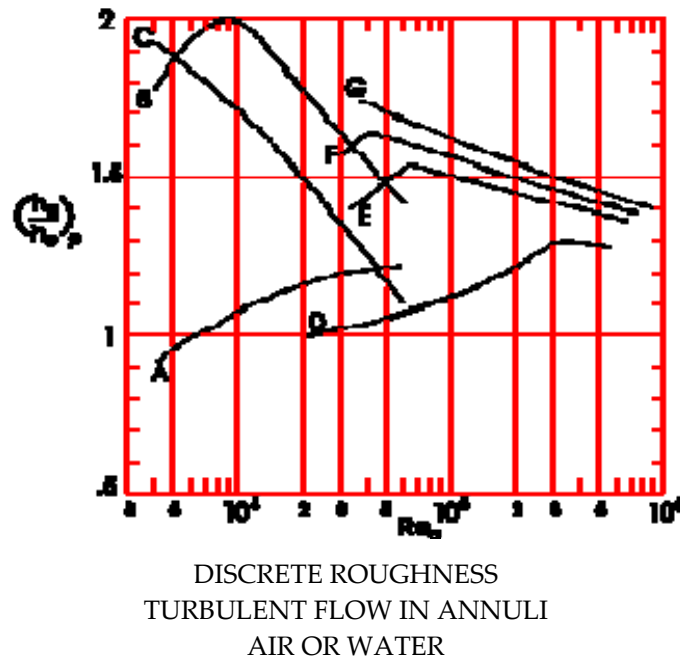
Figure 9-6: Constant power heat transfer ratio, $(h_a-h_o)_P$, vs. Reynolds number based on non-augmentative conditions, Re_o. Curves A, B, C are from Bergles (1969) [8], curves D to G have been calculated by the compiler after Sheriff & Gumley (1966) [166].

Explanation

Key	A	B	C	D	E	F	G
Investigator	Kemeny & Cyphers (1961) [103]			Sheriff & Gumley (1966) [166]			
D_1 x 10^3 [m]	12,7			26,2			
D_2 x 10^3 [m] [a]	17,5			79,5			
$L/(D_2-D_1)$ (Diabatic)	82			48			
Roughness Shape [b]	⌣	⌢	●		●		
$[e/(D_2-D_1)]$ x 10^4 [c]	276	244	281	23,8	95,2	135,7	190,5
s/e	2			1			
b/e	10			10			
T_i [K]	300-320			≈ 310			
(T_w-T_b) [K]	≈ 10			≈ 50			
Fluid	Water			Air			
Pr	5,5			0,71			
Re_a	4 x 10^3 - 8 x 10^4			10^4 - 2 x 10^5			
Heating/Cooling [d]	H			H			

a   Sheriff & Gumley base the effective diameter and heat transfer area on an annulus with the inner surface taken as the cylinder enveloping the roughness peaks. The diameter given here corresponds to the base surface of the roughness elements.

b   Helical element whose cross section is sketched.

c   Roughness elements added to the inner tube. The outer tube remains smooth.

d   Heat is transferred from the inner tube. The outer tube is adiabatic.

Empirical Correlations	Conditions	Comments
SHERIFF & GUMLEY (1966) [166] $$\sqrt{\frac{2}{f_H}} = 2,5\ln\frac{D_H}{2e} + u_e^+\left(e^+, b/e\right) - 3,75$$ or its equivalent $$\frac{1}{\sqrt{\lambda_H}} = 2,035\log\frac{D_H}{2e} + 0,354 u_e^+\left(e^+, b/e\right) - 1,323$$ subscript H refers to the Hall transform passage. The transformation is described in the next.	Straight tube of circular cross section. Fluid properties evaluated at T_b Re_H based on D_H. $Re_H > 2$ x 10^3, $L/D_H > 25 - 40$ Wire coil roughness. Friction factor based on the cylindrical surface enveloping the roughness peaks.	$u_e^+(e^+, b/e)$ for wire coil roughness, and $b/e = 10$, is given in Figure 9-7b. The following correlation has been used by the compiler for data reduction $u_e^+ = 4,9 - 3,6/e^+$ for $e^+ > 1$. The value of u_e+ for the fully rough regime is somewhat larger than that quoted in the source, which is 4,65. This is due to the fact that the data points for e=0,01 in., which look defective, have been excluded.
$$\frac{f_H}{2St_H} - 1 = \sqrt{\frac{f_H}{2}}\left[\begin{array}{c}g\left(e^+, b/e, Pr\right) - \\ -u_e^+\left(e^+, b/e + \delta m\right)\end{array}\right]$$	Straight tube of circular cross section. Fluid properties evaluated at Tb, and assumed to be constant. Re_H based on D_H. $Re_H > 2$ x 10^3, $L/D_H > 25 - 40$ Wire coil roughness. Constant heat flux at the wall. Heat transfer coefficient based on the cylindrical surface enveloping the roughness peaks. The expression for St is based on the following four additional assumptions: 1) Close to the wall the velocity distribution depends exclusively on the local conditions (law of the wall). 2) The law of the wall applies to the temperature defect profile, T_w-T, as well as to the velocity profile, u. 3) In the fully turbulent core the dimensionless temperature profile, T^+-T^+_{max} and the dimensionless velocity profile, u^+_{max}-u^+, are	The analysis of the experiments leads to: $g = 5,387(35+\mid e^+-35\mid)^{0,198}$ The proven range of validity of this expression is: $e^+ > 10$, $b/e = 10$, $Pr = 0,71$ The value of δm depends on the velocity and temperature distributions, which in turn depend on the ratio of the eddy diffusivities, $\varepsilon_M/\varepsilon_H$. Values of δm are to be found from the measured velocity and temperature profiles. A mean value $\delta m = -1,8$ is quoted in the source.

Empirical Correlations	Conditions	Comments
	similar. 4) The same profiles referred to their respective mean values, are slightly different because of the averaging procedure used to calculate T_b. The difference (temperature minus velocity is expressed as δm.	

Comments concerning the data presented in Figure 9-6a.

Although grooves are cheaper to produce and are less subject to erosion damage than protrusions, they have little effect until the free stream turbulence penetrates into the cavity.

Attached protrusions are less effective than integrally machined protrusions because of the thermal resistance between wire and wall. This resistance plays a more important role the higher the over-all heat flux becomes. At the lowest Reynolds numbers, however, the slightly greater height of the wire results in an improved heat transfer over the integral protrusion.

The influence of the roughness can be seen in curves D to G. The gain obtained by roughening increases with the roughness. For each value of e there is a value of Re which optimizes the ratio $(h_a-h_o)_P$. This optimum value is associated to the minimum exhibited by g at $e^+ = 35$.

The tube used for comparison by Sheriff & Gumley (1966) [166] is not smooth. By use of the Moody diagram for commercially rough pipes (Slichting (1960) [157]) an equivalent sand roughness of $e/D_H = 4,2 \times 10^{-4}$ results from friction data in the relevant Reynolds numbers range. Heat transfer data for this tube can be correlated by means of the following formula:

$Nu = 0,0125 Re^{0,845} Pr^{0,4}$, (Pr = 0,71)

The Re-exponent (larger than 0,8) and the constant factor (smaller than 0,023) support the evidence of roughness.

Both Kemeny & Cyphers and Sheriff and Gumley used a pitch to height ratio b/e = 10. .Data from Brauer, quoted by Bergles (1969) [8], indicate that the optimum b/e for the annular geometry appears to the about 3, which is lower than the value, 10, quoted for tubes of circular cross section.
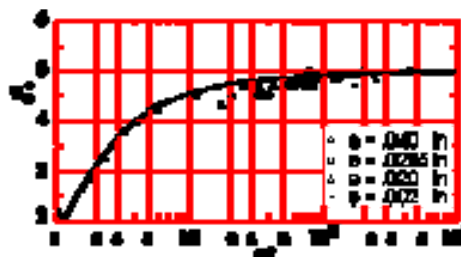
Figure 9-7: Roughness function, $u_e^+(e^+,b/e)$, for wire coil roughness. Plotted by the compiler after Sheriff & Gumley (1966) [166].

Hall's transformation of heat transfer data for annular ducts

This transformation (Hall (1962) [78]) reduces the data for annular passages with only the core tube heated and roughened to those for circular cross section tubes having the same relative roughness.

The velocity and temperature distributions across the annular passage are assumed to be known.

1. From the velocity distribution the radius of maximum velocity is determined. This radius defines a cylindrical surface at which there is no shear stress. This is not strictly true for turbulent flow, as shown by Hanjalic & Launder (1972) [80], who used a channel with parallel plates, one of them roughened, or by Rehme (1975) [148], using concentric annuli with smooth walls. This feature, however, is disregarded here.

2. By applying a force balance on the region of the annular passage between the inner radius, $D_1/2$, and the radius of no shear, $D_m/2$, the friction factor on the rough surface, f_H, is related to the experimental pressure loss, dp/dx, to the kinetic energy of the flow through the passage (per unit volume), $(\rho V^2)_H/2$, and to the hydraulic diameter of the "transformed passage", $D_H = (D_m^2 - D_1^2)/D_1$.

$$\frac{dp}{dx} = \frac{1}{2}\left(\rho V^2\right)_H \frac{4 f_H}{D_H} = \frac{1}{2}\rho V^2 \frac{4 f}{D_E} \qquad [9\text{-}3]$$

This equation relates also the average friction factor, f, for the whole of the annular passage to the friction factor, f_H, for the transformed passage.

3. The assumption is made that the resulting friction factor-Reynolds number relation is the same as that which would exist for a circular tube having diameter D_H and identical relative roughness.

4. The temperature distribution across the passage is adjusted so that the no-shear surface becomes adiabatic too (Figure 9-8c). The transformation is based on the following features:
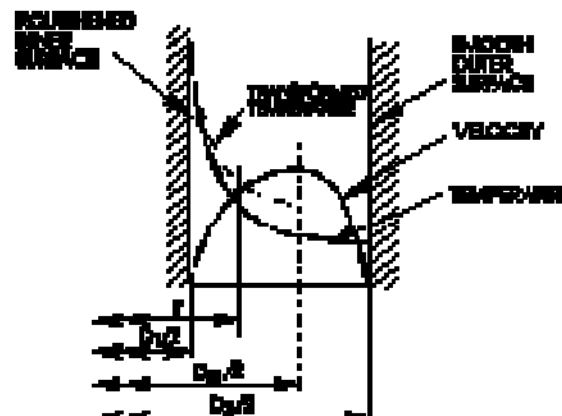
Figure 9-8: Velocity and Temperature distributions across the annulus.

(a) The local value of the coefficient of thermal diffusivity is assumed to be unaffected by the condition of no heat flux at D_m.

(b) The heat flux at the roughened surface in the transformed system is assumed to be the same as in the experimental system.

Application of a thermal balance on the region of the annular passage between the inner radius, $D_1/2$, and a given radius, r, for both the experimental and the transformed system yields, after some manipulation, the following ratio of transformed to experimental radial temperature gradients:

$$\frac{(\partial T/\partial r)_H}{\partial T/\partial r} = \frac{m(D_1, D_2)}{m(D_1, D_m)}\frac{m(r, D_m)}{m(r, D_2)}$$

$$with\ m(a,b) = 2\pi\int_a^b \rho u r\, dr$$

[9-4]

For gases, since the Hall transformation does not change the pressure field, $\rho \approx T^{-1}$. For liquids ρ disappears altogether from the equation.

Equation above is Hintegrated to yield $T_H(r)$. The integration constant may be chosen so that either the wall temperature or the fluid bulk temperature becomes invariant under the transformation. Although the second option looks inconvenient from the computational point of view, it simplifies the transformation of the data since the fluid properties are then invariant under the transformation.

(c)   c. The heat transfer coefficients are in the inverse ratio to the values of the wall to bulk temperature differences. The ratio of transformed to experimental Stanton numbers is then:

$$\frac{St_H}{St} = \frac{T_w - T_b}{(T_w - T_b)_H}\frac{\rho V}{(\rho V)_H}$$

[9-5]

5.   According to Sheriff & Gumley (1966) [166] the velocity profiles are given by means of a "logarithmic law", valid in the logarithmic layer near the rough wall, and a "velocity defect law", valid up to D_m. The experiments indicate that the defect law is universal, within the roughness range considered ($e/D_E \le 0.02$), as happens to be the case for tubes of circular cross section. Thence, D_m is independent of both Re and e/D_E, and its value can be deduced from a single experiment. In this particular case $(D_m-D_1)/(D_2-D_1) = 0,476$. This value is very close to that which would be obtained if the flow were laminar, which results to be 0,454. This stricking coincidence has been already noted for smooth annuli (Knudsen & Katz (1958) [107]).

The value of D_m for laminar flow is given by:

$$D_m = \frac{D_2^2 - D_1^2}{2\ln(D_2/D_1)}$$

[9-6]

The following table gives ratios of transformed to experimental values of several variables as deduced from one of the experiments by Sheriff & Gumley [166]. All these ratios, except h_H/h, can be assumed to be equal to unity. Values of h_H/h for different Re and e are given by the authors in their Table 6. Although a slight Reynolds number dependence can be noted, the quoted values deviate from 1,08 by less than $\pm 2\%$.

ψ	ψ_H/ψ
T_b	1,013
h	1,080
ρV	1,006
ρV^2	1,028
$\rho V/\mu$	1,013
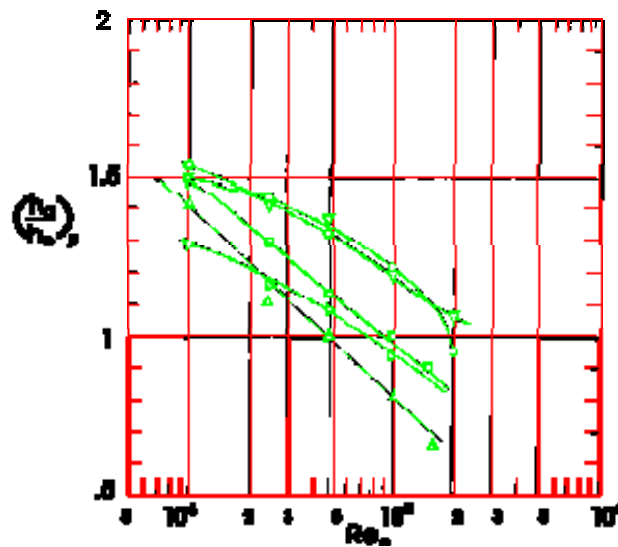
STRAIGHT INTERNAL FINS
TURBULENT FLOW IN TUBES
WATER

Figure 9-9: Constant power heat transfer ratio, $(h_a/h_o)_P$, vs. Reynolds number based on non-augmentative conditions, Re_o. From Carnavos (1974) [19].

Explanation

Key	○	□	△	▽	▷
Investigator	Carnavos (1974) [19]				
Shape					
Number of Fins	0 [a]	6	10	12	14	20
$D \times 10^3$ [m]	26,0	11,5	14,2	11,6	18,0	25,3
$D_E \times 10^3$ [m]	26,0	7,87	8,53	6,99	10,8	14,3

Key		○	□	△	▽	▷
e/D	0	0,148	0,111	0,094	0,099	0,073
b/D_E	0	0,494	0,348	0,312	0,287	0,213
A_{FL}x10^3 [m²]	0,529	0,099	0,143	0,100	0,237	0,478
L/D [b]	94	211	171	210	135	96
Nominal Wt. Area [m²]	0,1995	0,0884	0,1088	0,0889	0,1381	0,1944
Unfinned Wt. Area [m²]	0,1995	0,0684	0,0645	0,055	0,0872	0,1118
Finned Wt. Area [m²]	0	0,0604	0,0986	0,0856	0,1318	0,2140
Total Wt. Area/Nom. Wt. Area	1,00	1,46	1,50	1,58	1,59	1,68

[a]   Smooth tube tested for comparison.

[b]   *L* = 2,435 m.

Empirical Correlations	Conditions	Comments
CARNAVOS (1974) [19] $f_a = 0,406 Re^{-0,39}(b/D_{Ea})^{0,16}$	Fluid properties evaluated at T_b. f_a and Re based on D_{Ea}. $5 \times 10^3 < Re < 7,5 \times 10^4$ $e/D_{Ea} < 0,21$ $0,21 < b/D_{Ea} < 0,50$ $L/D \approx 100$ Checked with water.	For the experiments reported by Carnavos (1974) [19] the standard deviation is ± 10,8 %. No details are given in the source on the apparatus and procedure used in these experiments.
$Nu_{ab} = 0,212 Re^{0,6} Pr^{1/3}(b/D_{Ea})^{0,34}$ $Nu_a/Nu_b = (\mu_b/\mu_w)^{0,14}$	Fluid properties evaluated at T_b. Nu_a based on D_{Ea} and total wetted area. Re based on D_{Ea}. $5 \times 10^3 < Re < \times 10^5$ $e/D_{Ea} < 0,21$ $0,21 < b/D_{Ea} < 0,50$ $L/D \approx 100$ Checked with water.	For the experiments reported by Carnavos (1974) [19] the standard deviation is ± 10%. No data on the temperature level prevailing in the experiments is given in the source. The factor $(\mu_b/\mu_w)^{0,14}$, accounting for the temperature dependent viscosity is valid in the range $0,004 < \mu_b/\mu_w < 20$. (See clause 6.2.4)

Comments concerning the data presented in Figure 9-9.

The performance of straight finned tubes approaches that of a smooth tube as the Reynolds number increases.

In the low Reynolds number range (Re ≈ 10^4) straight finned tubes give lower performance than spiral finned tubes, compare data in Figure 9-9 with those in Figure 9-10 and Figure 9-11.

In the higher Reynolds number range (Re ≈10^5) the performance of straight finned tubes is nearly

equal to that of spiral finned tubes.

For eaual total wetted areas the improvement achieved by the use of internal fins increases with the ratio of the average distance between fins, b, to the hydraulic diameter, D_E. This is what might be expected upon inspection of the empirical correlations which reveal that the Nusselt number increases more rapidly with b/D_{Ea} than does the friction factor.

Much work should be done to draw genera conclusions concerning the optimum fin configuration and number of fins. Attempts have been made by several authors (Hu & Chang (1973) [92]), Masliyah & Nandakumar (1976) [123]) to optimize internally finned tubes for heat transfer. Their theoretical approaches, however, which deal only with fully developed (both frictional and thermal) laminar flow and constant heat flux along the wall, are fairly limited in scope.

LOW-SPIRAL INTERNAL FINS
TURBULENT FLOW IN TUBES
WATER
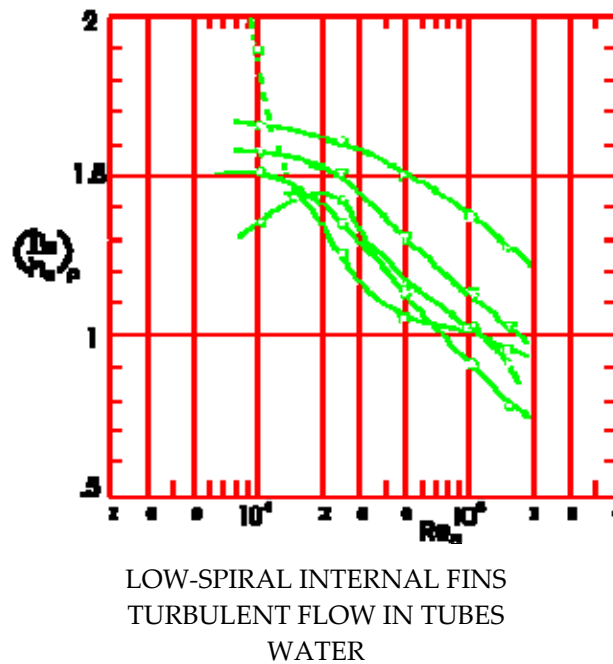
Figure 9-10: Constant power heat transfer ratio, $(h_a/h_o)_P$, vs. Reynolds number based on non-augmentative conditions, Re_o. From Carnavos (1974) [19].

Explanation

Key		○	□	△	▽	▷
Investigator			Carnavos (1974) [19]			
Shape	○	○	○	○	○	○
Number of Fins	0 [a]	30	30	32	32	50
$Dx10^3$ [m]	26,0	20,0	25,7	14,7	24,8	31,5
$D_{EX}10^3$ [m]	26,0	13,6	15,7	8,76	14,1	21,4

Key		○	□	△	▽	▷
e/D	0	0,037	0,037	0,047	0,042	0,026
b/D_E	0	0,123	0,129	0,116	0,120	0,072
y	0	3,81	2,97	10,4	3,46	3,12
$A_{FL} \times 10^3$ [m²]	0,529	0,299	0,517	0,161	0,479	0,761
L/D [b]	94	122	95	166	98	77
Nominal Wt. Area [m²]	0,1995	0,1531	0,1965	0,1127	0,1899	0,2413
Unfinned Wt. Area [m²]	0,1995	0,0794	0,1224	0,0471	0,0874	0,0841
Finned Wt. Area [m²]	0	0,1556	0,2211	0,1330	0,2648	0,2880
Total Wt. Area/Nom. Wt. Area	1,00	1,54	1,75	1,598	1,855	1,54

[a]   Smooth tube tested for comparison.

[b]   *L* = 2,435 m.

Empirical Correlations	Conditions	Comments
CARNAVOS (1974) [19] $f_a = 0,535 Re^{-0,39} y^{-0,2}$	Fluid properties evaluated at T_b. f_a and Re based on D_{Ea}. $5 \times 10^3 < Re < 7,5 \times 10^4$ $e/D_{Ea} < 0,34$ $0,07 < b/D_{Ea} < 0,52$ $3 < y < 17$ $L/D \approx 100$ Checked with water.	For the experiments reported by Carnavos (1974) [19] the standard deviation is ± 12,3 %. No details are given in the source on the apparatus and procedure used in these experiments.
$Nu_a = 0,306 Re^{0,63} Pr^{1/3} (b/D_{Ea})^{0,21} y^{-0,27}$ $Nu_a/Nu_b = (\mu_b/\mu_w)^{0,14}$	Fluid properties evaluated at T_b. Nu_a based on D_{Ea} and total wetted area. Re based on D_{Ea}. $5 \times 10^3 < Re < \times 10^5$ $e/D_{Ea} < 0,34$ $0,07 < b/D_{Ea} < 0,52$ $3 < y < 17$ $L/D \approx 100$ Checked with water.	For the experiments reported by Carnavos (1974) [19] the standard deviation is ± 12,8%. No data on the temperature level prevailing in the experiments is given in the source. The factor $(\mu_b/\mu_w)^{0,14}$, accounting for the temperature dependent viscosity is valid in the range $0,004 < \mu_b/\mu_w < 20$. (See clause 6.2.4)

Comments concerning the data presented in Figure 9-10.

Spirally finned tubes provide convective heat transfer augmentation by extension of the heat transfer surface and by induction of spiral flow. Hence, these tubes give a slightly higher performance than straight fin tubes. This could also be expected upon inspection of the empirical correlations which reveal that the Nusselt number increases more rapidly with spiralling than does the friction factor. By comparison with data for straight finned tubes (Figure 9-9), it is deduced that the heat transfer augmentation due to spiralling motion is larger at low Reynolds numbers (Re $\approx 10^4$).

The top performer tube has 50 triangular fins with twist y = 3,12. It is difficult, however, to draw general conclusions on the optimum configuration from these data because of the wide variety of geometries tested. Additional work should be done with trapezoidal and triangular shaped fins to better understand their influence on performance.

One of the tubes (square) exhibits a sudden decrease in heat transfer for a Reynolds number very nearly coincident with that corresponding to an increase in friction factor. The reason for this drastic performance change is by no means obvious.
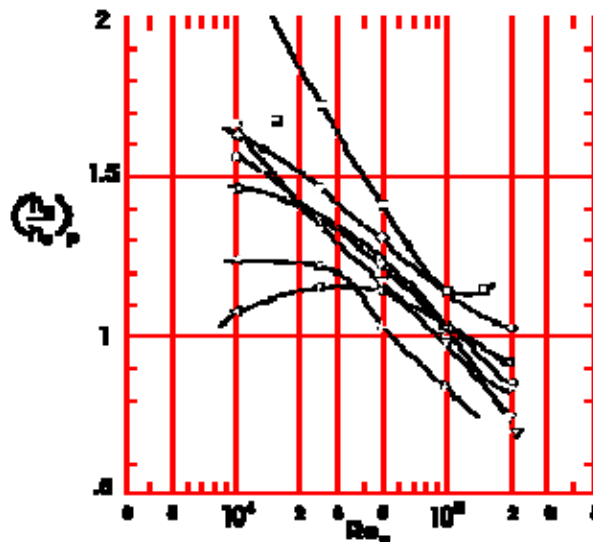
HIGH-SPIRAL INTERNAL FINS
TURBULENT FLOW IN TUBES
WATER

Figure 9-11: Constant power heat transfer ratio, $(h_a/h_o)_P$, vs. Reynolds number based on non-augmentative conditions, Re_o. From Carnavos (1974) [19].

Explanation

Key	○	□	△	▽	▷	◁	◇
Investigator	Carnavos (1974) [19]						
Shape							
Number of Fins	0 [a]	6	8	16	16	16	16	16
$D \times 10^3$ [m]	26,0	11,8	30,4	10,7	14,0	17,2	20,4	25,4
$D_E \times 10^3$ [m]	26,0	7,54	17,93	4,47	6,60	8,59	11,30	14,96
e/D	0	0,158	0,149	0,144	0,119	0,105	0,097	0,088
b/D_E	0	0,516	0,433	0,244	0,265	0,240	0,270	0,243
y	0	7,26	3,34	16,66	10,00	6,48	4,98	3,00
$A_{FL} \times 10^3$ [m²]	0,529	0,100	0,675	0,077	0,139	0,218	0,310	0,474
L/D [b]	94	206	80	228	174	142	119	96
Nominal Wt. Area [m²]	0,1995	0,0905	0,2327	0,0817	0,1070	0,1314	0,1562	0,1944
Unfinned Wt. Area [m²]	0,1995	0,0684	0,1518	0,0465	0,0580	0,0748	0,0969	0,1115
Finned Wt. Area [m²]	0	0,0598	0,2267	0,1282	0,1568	0,1750	0,1782	0,2081
Total Wt. Area/Nom. Wt. Area	1,00	1,417	1,626	2,139	2,00	1,90	1,76	1,64

[a] Smooth tube tested for comparison.

[b] $L = 2,435$ m.

Empirical Correlations	Conditions	Comments
CARNAVOS (1974) [19] $f_a = 0{,}535\,Re^{-0{,}39}y^{-0{,}2}$	Fluid properties evaluated at T_b. f_a and Re based on D_{Ea}. $5 \times 10^3 < Re < 7{,}5 \times 10^4$ $e/D_{Ea} < 0{,}34$ $0{,}07 < b/D_{Ea} < 0{,}52$ $3 < y < 17$ $L/D \approx 100$ Checked with water.	For the experiments reported by Carnavos (1974) [19] the standard deviation is $\pm 12{,}3$ %. No details are given in the source on the apparatus and procedure used in these experiments.
$Nu_a = 0{,}306\,Re^{0{,}63}Pr^{1/3}(b/D_{Ea})^{0{,}21}y^{-0{,}27}$ $Nu_a/Nu_b = (\mu_b/\mu_w)^{0{,}14}$	Fluid properties evaluated at T_b. Nu_a based on D_{Ea} and total wetted area. Re based on D_{Ea}. $5 \times 10^3 < Re < \times 10^5$ $e/D_{Ea} < 0{,}34$ $0{,}07 < b/D_{Ea} < 0{,}52$ $3 < y < 17$ $L/D \approx 100$ Checked with water.	For the experiments reported by Carnavos (1974) [19] the standard deviation is $\pm 12{,}8$%. No data on the temperature level prevailing in the experiments is given in the source. The factor $(\mu_b/\mu_w)^{0{,}14}$, accounting for the temperature dependent viscosity is valid in the range $0{,}004 < \mu_b/\mu_w < 20$. (See clause 6.2.4)

Comments concerning the data presented in Figure 9-11.

Spirally finned tubes provide convective heat transfer augmentation by extension of the heat transfer surface and by induction of spiral flow. Hence, these tubes give a slightly higher performance than straight fin tubes. This could also be expected upon inspection of the empirical correlations which reveal that the Nusselt number increases more rapidly with spiralling than does the friction factor. By comparison with data for straight finned tubes (Figure 9-9), it is deduced that the heat transfer augmentation due to spiralling motion is larger at low Reynolds numbers (Re $\approx 10^4$).

The top performer tube has 8 trapezoidal fins with twist $y = 3{,}34$. It is difficult, however, to draw general conclusions on the optimum configuration from these data because of the wide variety of geometries tested. Additional work should be done with trapezoidal and triangular shaped fins to better understand their influence on performance.

One of the tubes (square) exhibits a sudden decrease in heat transfer for a Reynolds number very nearly coincident with that corresponding to an increase in friction factor. The reason for this drastic performance change is by no means obvious.

A value $(h_a/h_o)_P = 2{,}19$ for Re $\approx 10^4$, which is not enclosed in Figure 9-11, is also given in the source in connection with this tube.
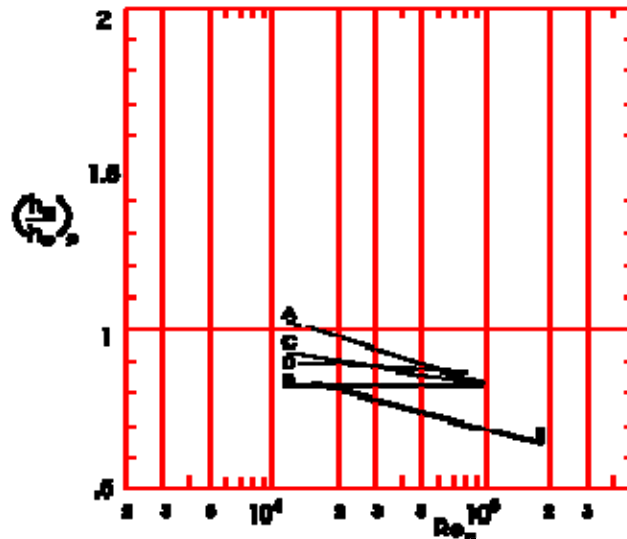
STREAMLINED AXIAL BODIES
TURBULENT FLOW IN TUBES
WATER

Figure 9-12: Constant power heat transfer ratio, $(h_a/h_o)_P$, vs. Reynolds number based on non-augmentative conditions, Re_o. From Bergles (1969) [8].

Explanation

Key	A	B	C	D	E
Investigator	Evans & Churchill (1963) [61]				
D x 10^3 [m]	25,53				
L/D (Diabatic)	64				
D_b x 10^3 [m] [a]	15,88			19,05	22,23
D_b/D	0,622			0,746	0,871
L_b/D [a]	4	8	12		
D_T x 10^3 [m] [a]	3,17				
T_i [K]	300				
$(T_w - T_b)$ [K]	10 - 50 [b]				
Re_a	5 x 10^3 - 5 x 10^4				
Heating/Cooling	H				

NOTE   The streamlined bodies are composed of a cone and a hemisphere, machined from nylon. They are fitted on a central rod through a hole drilled in the axis of the body. The bodies are held in place by small screws, and centered by means of three aluminium pins, installed at the section of maximum diameter and just touching the tube wall.

b Estimated by the compiler from reported values of the heat transfer coefficient and power spent in heating electrically the wall.
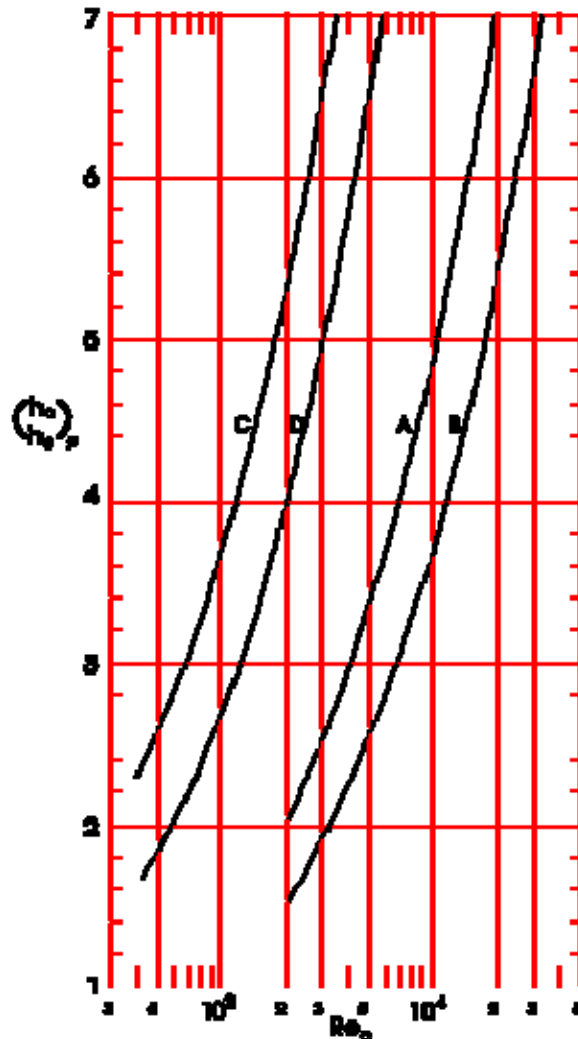
TWISTED-TAPE INSERTS
LAMINAR FLOW IN TUBES
LIQUIDS

Figure 9-13: Constant power heat transfer ratio, $(h_a/h_o)_P$, vs. Reynolds number based on non-augmentative conditions, Re_o. Calculated by the compiler after Hong & Bergles (1976) [91].

Explanation

Key	A	B	C	D
Investigator	Hong & Bergles (1976) [91]			
Liquid	Water		Ethylene	Glycol
D x 10³ [m]	10,2			
L/D (Diabatic)	120			
y	2,45	5,08	2,45	5,08
t x 10³ [m]	0,46			
Tape fit [a]	5			
m x 10³ [kg.s⁻¹]	5,5-9,5		1,8-33	
q x 10⁻³ [W.m⁻²]	0,5-38,5		5,2-27,6	
Pr	3,0-7,0		84-192	
Re$_a$	83-2460		13-390	
Heating/Cooling	H			

[a] The tape fits are categorized by means of numbers as follows:

NOTE   1. Special care taken to increase the thermal joint conductance.

2. Tight tape fit. No measurable gap between the tape and the tube wall.

3. Snug tape fit. Gap of less than 0,25 x 10⁻³ m.

4. Loose tape fit. Gap estimated to be greater than 0,25 x 10⁻³ m.

5. Special care taken to reduce the thermal joint conductance. In the present case the tapes were covered at both edges 2,5 x 10⁻³ wide strips of black No. 33 Scotch electrical tape, and backed in a furnace at 530 K for about one minute.

Empirical Correlations	Conditions	Comments
HONG & BERGLES (1976) [91] $$\lambda_a = \left(\frac{\pi + 2 - 2\frac{t}{d}}{\pi - 4\frac{t}{d}} \right)^2 \frac{63,06}{Re_a} + 1,463\frac{D}{L}$$ with this expression for λ_a: $$\Delta P = \lambda_a \frac{L}{D}\frac{1}{2}\rho V^2$$	Straight tube of semicircular cross section. Diameter, D. Fluid properties evaluated at T_b. Re based on D. Re < 2,4 x 10³ Sparrow & Haji-Sheikh (1966) [169].	Data for tubes with twisted tape inserts from Hong & Bergles (1976) [91] correlate with the analytical results of Sparrow & Haji-Sheikh (1966) [169] for circular tubes with a diametral dividing wall. The additive term accounting for en trance effects should be taken into account for Re≈ 10³. The reductions in pressure drop because of heating were, in these experiments, too small to be accurately assessed.
$$\lambda_o = \frac{64}{Re_o} + 1,333\frac{D}{L}$$ Hagen-Poiseuille formula	Straight tube of circular cross section. Fluid properties evaluated at T_b. Re based on D. Re < 2,4 x 10³	See clause 7.2.5. The entrance length coefficient, K = 1,333, is from Sparrow & Haji-Sheikh (1966) [169].
$$Nu_a = 5,172\sqrt{1 + 5,484 \times 10^{-3} Pr^{0,7}\left(\frac{Re_a}{5} \right)^{5/4}}$$	Fluid properties evaluated at T_b. Constant wall temperature. Nu and Re based on D. 10 < Re < 2 x 10³ 3 < Pr < 200 2,5 < y < 5 L/D = 120	A linear variation in bulk temperature from the inlet to the exit of the heated length is assumed. When $y \to \infty$, $Nu_a \to 5,172$. This value corresponds to a straight circular tube with a diametral adiabatic dividing wall.
Nu_o= 3,656	Straight tube of circular cross section. Fluid properties evaluated at T_b. Constant wall temperature. Nu based on D. GrPr < 10⁻¹ for Re > 1 (see comments) L/D > 0,125PrRe. Knudsen & Katz (1958).	The limitation imposed on GrPr should be fulfilled to keep the buoyancy effects at a negligible level. More precise data regarding this limitation can be found in ESDU 69004 (1969) [50].

Empirical Correlations	Conditions	Comments
Comments concerning the data presented in Figure 9-13. The increase in pressure drop with tape-generated swirl flow is less than the increase in heat transfer coefficient. Provided that buoyancy effects can be neglected, a situation which is of the greatest interest for space application, the maximum increase in the heat transfer coefficient is of the order of ten times the empty tube constant property value, while the corresponding pressure drop is of the order of three times the empty tube pressure drop. This is in contrast to turbulent flow, where comparable increases in heat transfer coefficient result in pressure drops which are several orders of magnitude larger that the empty tube values. Since the Nusselt number for the empty tube flow is independent of Reynolds number, the usual coupling between augmented and empty tubes does not appear here. Hence, Nu_a/Nu_o vs. Re_a is the same for a constraint of fixed flow rate, pressure drop or pumping power. For consistency with other data in this item it is, however, convenient to plot h_a/h_o as a function of the Reynolds number, Re_o, based on non-augmentative conditions. To related both augmentative and non-augmentative Reynolds numbers, the required of equal pumping power is written down as: $(\lambda Re^3 \Pi)_o = (\lambda Re^3 \Pi)_a$. Incorporating friction factors and Reynolds numbers, all of them based on the inner tube diameter, and the perimeter ratio, $\Pi_a/\Pi_o = (\pi + 2-2t/D)/\pi$, the above expression yields: $Re_o = 2,186 Re_a$.		

TWISTED-TAPE INSERTS
TURBULENT FLOW IN SMOOTH TUBES
AIR
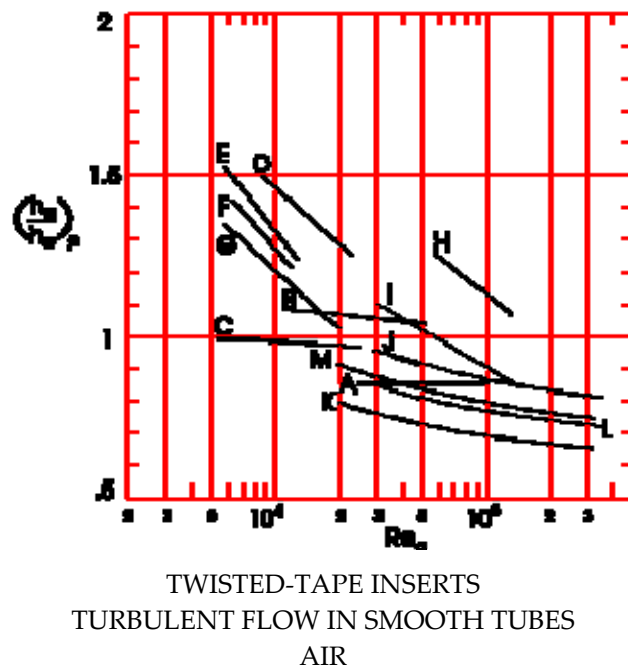
Figure 9-14: Constant power heat transfer ratio, $(h_a/h_o)_P$, vs. Reynolds number based on non-augmentative conditions, Re_o. Curves A to I are from Bergles (1969) [8], curves J to M have been calculated by the compiler after Thorsen & Landis (1968) [178].

Explanation

Key	A	B	C	D	E	F	G	H	I	J	K	L	M
Investigator	Colburn & King (1931) [27]			Evans & Sarjant (1951) [61]				Smithberg et al. (1964) [168]		Thorsen & Landis (1968) [178]			
D x 10³ [m]	66,67			63,5				35,1		25,35		25,37	
L/D (Diabatic)	13,7			33,6				29		36			
y	0,57 [a]	1,14 [a]	2,67	2,80	3,60	4,80	5,60	1,81	11	1,58	4,00	1,58	4,00
t x 10³ [m]	[b]			2,38				0,56		[b]			
Tape fit [c]	4			4				3		3			
T_i [K]	≈ 590	390-170	380-660	<755				300		300		<519	
│ T_w-T_b│	≈ 160	60-270	220-280	105-125				<50		<350		200	
T_w/T_b	0,67-0,73	0,55-0,84	0,52-0,82	0,790				1,2		1,9		0,6	
Re_a	1,9 x 10³ - 5,6 x 10³			3,3 x 10³ - 1,5 x 10⁴ [d]				1,5x10⁴-9x10⁴		5x10³-10⁵			
Heating/Cooling	C			C				H		H		C	

[a]   The tape is wrapped around a small-diameter axial rod.

[b]   Not given, it is presumably negligible compared to D.
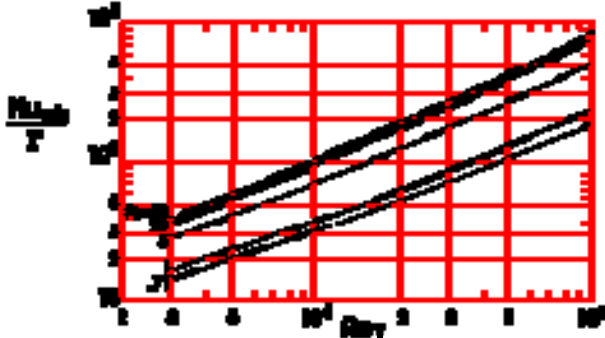
[c]   The numbers categorize the tape fit as follows.

3.   Snug tape fit. Gap of less than

4.   Loose tape fit. Gap estimated to be greater than 9,25 x 10⁻³ m.

[d]   Based on D.

Empirical Correlations	Conditions	Comments
THORSEN & LANDIS (1968) [178] $f_{ab}/f = \Gamma$ $\sqrt{\dfrac{2}{f}} = 2,5\ln\left(Re_T\sqrt{f}\right) - 0,85$ or its equivalent $\dfrac{1}{\sqrt{\lambda}} = 2,035\log\left(Re_T\sqrt{\lambda}\right) - 0,91$ $\Gamma = 1,126 + 0,0094K$	Fluid properties evaluated at T_b. f_{ab} and f based on Re_T and D_E. $5\times10^3 < Re < 10^5$ $1,58 < y < 4$ $K > 10 \ m^{-1}$ $L/D = 36$	Re_T based on the average total velocity and D_E. Re based on average axial velocity and D_E. $Re_T/Re = (2/3)([1+(\pi/2y)^2]^{3/2}-1)/(\pi/2y)^2$ For $Re_T > 10^4$, $f = 0,046Re_T^{-0,2}$. K is the flow path curvature near the wall. $KD/2 = (\pi/2y)^2/[1+(\pi/2y)^2]$
$\dfrac{f}{f_{ab}} = \left(\dfrac{T_w}{T_b}\right)^{-0,1}$	Same as above. $0,6 < T_w/T_b < 1,9$	
$Nu_{ab} = F(Re_T, Pr, \Gamma)$ Corresponds to isothermal flow through the spiral channel.	The validity of the analytical expression relating Nu_{ab} to Re_T, Pr and Γ has been experimentally checked for air (Pr ≈ 0,71) under the above stated conditions. The analysis requires that heat flux and shear stress at the wall vary in the same way.	Nu_{ab}/Γ vs. Re_T, for several values of Pr, is given in Figure 9-15b. Nu_{ab}/Γ is practically independent of Γ. The error incurred in neglecting this dependency is of the order of 0,6% for Pr = 0,71, and increases with Pr. For Pr = 50 that error is of the order of 9,5%. Thorsen & Landis (1968) [178] suggest the use of the Dittus-Boelter formula, modified as: The computations leading to Figure 9-15b do not validate this alternative, particularly regarding the Pr dependence, except when Pr ≈ 1.
Heating $\dfrac{Nu_a}{Nu_{ab}} = \left(\dfrac{T_w}{T_b}\right)^{-0,32}\left[1 + \dfrac{\pi}{2y}\dfrac{\sqrt{2(D_H/D)\beta(T_w-T_b)}}{4}\right]$ Gives the radial convection effect.	Fluid properties evaluated at T_{bam} except β, evaluated at Nu and Re based on D_E. $5\times10^3 < Re < 10^5$ $1 < T_w/T_b < 1,9$ Constant heat flux at the wall. h based on A_w.	For gases $\beta = T_f - 1$. $A_w = \left(\pi D - 2t\sqrt{1+(\pi/2y)^2}\right)L$ A term, Q_f, accounting for the conduction heat transfer through the tape must be added for evaluating the total energy transferred to or from the fluid. This term is given by: $DL(T_w - T_b)/Q_f = sD/\left(2k_f t\sqrt{1+(\pi/2y)^2}\right) + 1/\eta h$ where ε is the radial gap between strip and wall, and η the fin effectiveness.

Empirical Correlations	Conditions	Comments
Cooling $$\frac{Nu_a}{Nu_{ab}} = 1{,}07 \left(\frac{T_w}{T_b}\right)^{-0{,}1} \left[1 - \frac{\pi}{2y}\frac{\sqrt{2(D_H/D)\beta(T_b - T_w)}}{4}\right]$$ Gives the radial convection effect.	Same as above except $0{,}6 < T_w/T_b < 1$ T_b is defined as indicated under Comments.	In the experiments whose data are being correlated, cooling was achieved by counter flowing water through an outer concentric tube. T_b is defined by combination of the arithmetic mean water temperature, T_c, and the logarithmic mean fluid to water temperature difference. $$T_b = \frac{T_{ci} + T_{co}}{2} + \frac{(T_{bi} - T_{co}) - (T_{bo} - T_{ci})}{\ln\frac{(T_{bi} - T_{co})}{(T_{bo} - T_{ci})}}$$
LOPINA & BERGLES (1969) [120] See Table of Figure 9-16.		The validity of this correlation, set forth for water and moderate temperature differences, has been checked for helium and for nitrogen by Bolla et al. (1973) [15] in the range $10^4 < Re < 3 \times 10^5$. The effect on Nu_a of the radial thermal gradient is accounted for by the factor $(T_w/T_b)^{-0{,}575}$. Although these authors do not report the temperature ratio, T_w/T_b, they quote a value of the thermal flux of 45×10^4 W.m^{-2}, more than three times larger than the highest value quoted by Thorsen & Landis (1968).

Comments concerning the data presented in Figure 9-14a.

Only Thorsen & Landis (1968) [178] report the appropriate diabatic friction factor data.

The cooling data are slightly lower than the heating data. Some improvement is expected in any case due to the increased velocity because of the swirl induced by the tape.

The tightest twist ratio is not necessarily the best. A twist y = 2,5 is quoted as optimum for air.

Figure 9-15: Isothermal Nusselt number, Nu$_{ab}$. divided by the ratio of friction factors, Γ, vs. the Reynolds number, Re$_T$, for different values of the Prandtl number, Pr. Calculated by the compiler after Thorsen & Landis (1968) [178].

TWISTED-TAPE INSERTS
TURBULENT FLOW IN SMOOTH TUBES
WATER

Figure 9-16: Constant power heat transfer ratio, $(h_e/h_o)_P$, vs. Reynolds number based on non-augmentative conditions, Re_o. From Bergles (1969) [8].

Explanation

Key	A	B	C	D		E	F	G	H	I	J
Investigator	Greene (1960) [76]			Ibragimov et al. (1961) [96]		Smithberg & Landis (1964) [168]		Lopina & Bergles (1969) [120]			
D x 10³ [m]	22,6			12,0		35,1		4,91			
L/D (Diabatic)				57		29		69-76			
(e/D) x 10⁴				≈ 1		<3		0,57 (tube) 0,61 (tape)			
y	0,28	0,56	1,12	2,10	4,56	1,81	11	2,48	3,15	5,26	9,20
t x 10³ [m]				1		0,56		0,343			
Tape fit [a]				2		3		1			
T_i [K]						288		283-366			
(T_w-T_b) [K]						<50		6-78			
p x 10⁻³ [Pa]								210-690			
Re_a				10⁴-5x10⁴		8x10³-6x10⁴		8x10³-1,3x10⁵			
Heating/Cooling	H			H		H		H			

[a] The tape fits are categorized by means of numbers as follows:

NOTE   1. Special care taken to increase the thermal joint conductance; f.e., by redrawing of the tube over the twisted tape.

2. Tight tape fit. No measurable gap between the tape and the tube wall.

3. Snug tape fit. Gap of less than $0,25 \times 10^{-3}$ m.

4. Loose tape fit. Gap estimated to be greater than $0,25 \times 10^{-3}$ m.

5. Special care taken to reduce the thermal joint conductance; f.e., insulating the tape by paint.

Empirical Correlations	Conditions	Comments
LOPINA & BERGLES (1969) [120] $$f_{ab}/f_{ob} = 2,75y^{-0,406}$$	Fluid properties evaluated at T_b. f_a based on D_{Ea}. f_o and Re_o based on D. $9 \times 10^3 < Re < 1,2 \times 10^5$ $e/D < 3 \times 10^4$ $1,8 < y < 11$ Checked with both water and air.	For smooth tube in the range $5 \times 10^3 <$ $Re < 10^5$, $f_o = 0,046 Re_o^{-0,2}$ (see Table 7-2). For a wider Reynolds number range see clause 7.2.2, where $\lambda = 4f$. For the friction factor to become constant $L/D > 0,623 Re^{1/4}$.
$$f_a/f_{ab} = (\mu_w/\mu_b)^{0,35}(D_{Ea}/D)$$	Fluid properties evaluated at T_{bam} f_a based on D_{Ea}. Re based on D. $9 \times 10^3 < Re < 1,2 \times 10^5$ $e/D < 3 \times 10^4$ $2,48 < y < 9,20$ Checked with water at $T_b < 360$ K	The differences between isothermal and heated friction factors are less than for the empty tube. This is so because the tape is nearly adiabatic and, thence, the reduction in the liquid viscosity because of the increased temperature is much smaller near the tape than near the tube wall. This effect is accounted for by the factor D_{ea}/D in the exponent.
$$Nu_a = Nu_{sc} + Nu_{cc} + Nu_f$$	Liquid or gases under moderate transverse temperature gradients.	
$$Nu_{sc} = 0,023 Re^{0,8} Pr^n$$ Dittus-Boelter formula. Corresponds to flow through the spiral channel.	Straight tubes of circular cross section. Fluid properties evaluated at T_{bam}. Nu and Re based on D. $Re > 10^4$. $0,7 > Pr > 100$ $n = 0.4$ for heating, $n = 0,3$ for cooling. $L/D > 60$ Knudsen & Katz (1968) [107] The fact that n is slightly different for heating than for cooling is disregarded here. $n = 0,4$ in any case.	Nu_{sc} is predicted from conventional straight tube correlations, accounting for the increased velocity near tube wall caused by the tape insertion and spiralling flow path. For this the Reynolds number must be defined as: $Re = \alpha V D_E/\nu$, where $\alpha^2 = 1 + (\pi/2y)^2$. The constant factor, 0,023, can be modified as follows: 0,0237 for $Re < 1,5 \times 10^4$, and 0,025 for $Re < 1,5 \times 10^4$.
$$Nu_{cc} = 0,114(GrPr)^{1/3}$$ Fishenden-Saujnders formula Gives the centrifugal convection effect when the heat flows toward the tube axis.	Horizontal heated plate, width L, facing upward. Fluid properties evaluated at $T_{0,5}$, Gr based on L. $2 \times 10^7 < GrPr < 3 \times 10^{10}$. McAdams (1954) [125]. A factor 0,14 instead of 0,114 is quoted in	The Grashof number, Gr, is based on the centrifugal acceleration. $Gr/Re^2 = 2(\pi/2y)^2(D_{Ea}/D)\beta(T_w - T_b)$. THIS TERM WILLNOT BE PRESENT WHEN COOLING.

Empirical Correlations	Conditions	Comments
	this, as well as in other sources.	
$Nu_f = (F-1)(Nu_{sc}+Nu_{cc})$ Gives the heat transfer by the tape acting as a fin.	The table below gives values of F in typical instances.	This term is determined by the designer for each particular system of interest.
KLACZAK (1973) [106] $Nu_a = 1,46Re^{0,44}Pr^{0,36}y^{-0,33}$	Fluid properties evaluated at T_{bm}. Nu and Re based on D. $1,7x10^3 < Re < 2x10^4$ $2,5 < Pr < 9$ $1,63 < y < 3,79$ L/D = 35 .	

Comments concerning the data presented in Figure 9-16.

The curves exhibit rather wide scatter. For similar valuesof tape twist differences are due to variation in the fin effect and centrifugal convection effect.

The tightest twist ratio is not necessarily the best. Extremely tight twist ratios (low values of y), such as those in Greene (1960) [76], have been accomplished by wrapping the strip around a small diameter rod.

All the references, except Lopina & Bergles (1969) [120], only present isothermal friction factors.

An attempt has been made to include in the figure data from the extensive tests by Kreith & Margolis (1958). The results for water, although showing the correct trend regarding the variation with the Reynolds number, lead to far too large values of $(h_a/h_o)_P$, which at $Re = 5x10^4$ are of the order of 2,5 for y = 2,58 and 1,7 for y = 5. These results seem to be affected by experimental errors (see Smithberg & Landis (1964) [168]).

Typical values of the Fin Effect Multiplier, F

Fit [a]	Fluid	F	Reference
1	Water	1,137 for $Re < 3x10^4$ 1,10 for $Re > 3x10^4$	Lopina & Bergles (1969) [120]
3	Water	1,10	Smithberg & Landis (1961) [168]
5	He, N	1,00	Bolla et al. (1973) [15]

[a]   The tape fits are categorized by means of numbers as follows:

NOTE   1. Special care taken to increase the thermal joint conductance; f.e., by redrawing of the tube over the twisted tape.

3. Snug tape fit. Gap of less than $0,25 x 10^{-3}$.

5. Special care taken to reduce the thermal joint conductance; f.e., insulating the tape by paint.
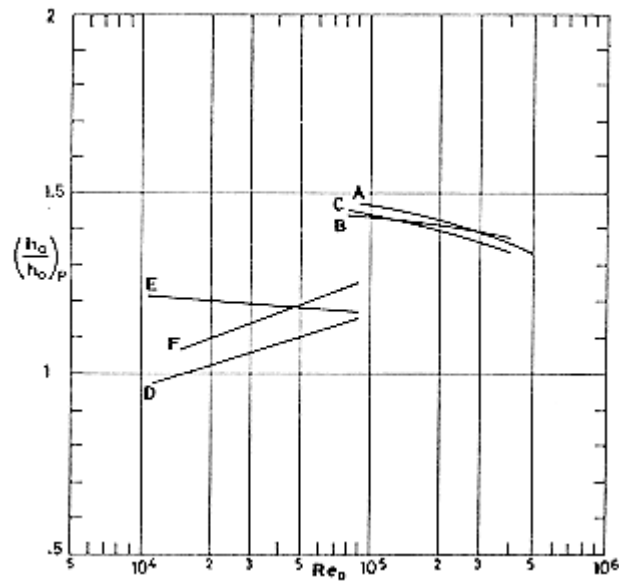
TWISTED-TAPE INSERTS
TURBULENT FLOW IN ROUGH TUBES
WATER

Figure 9-17: Constant power heat transfer ratio, $(h_a/h_o)_P$, vs. Reynolds number based on non-augmentative conditions, Re_o. Curves A, B, C from Bergles (1969) [8], curves D, E, F from Bergles, Lee & Mikic (1969) [9].

Explanation

Key	A	B	C	D	E	F
Investigator	Gambill, Bundy & Wansbrough (1961) [69]			Bergles, Lee & Mikic (1969) [9]		
$D \times 10^3$ [m]	6,32			6,35	6,30	6,35
L/D (Diabatic)	45			54-79	59-85	54-79
$(e/D) \times 10^4$	0,84 (tube) [a] 0,24 (tape)			12 (tube)	1,21 (tube) 0,605 (tape)	12 (tube) 0,60 (tape)
y	2,30	5,00	8,00	No Tape	2,42	2,55
$t \times 10^3$ [m]	0,381				0,472	
Tape fit [b]	2				1	
T_i [K]	290-300			283-366		
(T_w-T_b) [K]	≈ 80 [c]			6-78		
$p \times 10^{-3}$ [Pa]	250-3500			210-690		
Re_a	$5 \times 10^3 - 4,3 \times 10^5$			$3 \times 10^3 - 8 \times 10^4$		
Heating/Cooling	H			H		

[a]   This value is exceedingly low. From the swirl flow friction data by Gambill et al. (1961) [69] in their Fig. 10, equivalent sand roughnesses of the order of $e/D = 20 \times 10^{-4}$ result. Lopina & Bergles (1969) [120], in their Fig. 04, ascribe to these tubes the value $e/D = 17 \times 10^{-4}$.

[b]   The numbers categorize the tape fit as follows:

NOTE   1. Special care taken to increase the thermal joint conductance; f.e., by redrawing of the tube over the twisted tape.

2. Tight tape fit. No measurable gap between the tape and the tube wall.

[c]   Estimated from $T_w - T_b = (D/L)[(T_{bo}-T_{bi})/4St]$.

Empirical Correlations	Conditions	Comments
BERGLES, LEE & MIKIC (1969) [9] $f_{ab}/f_{ob} = 2{,}75y^{-0{,}406}$	Fluid properties evaluated at T_b. f_a based on D_{Ea}. f_o and Re_o based on D. $3 \times 10^3 < Re < 8 \times 10^4$ $e/D < 12 \times 10^{-4}$ $2{,}55 < y < 6{,}16$ $L/D = 60\text{-}80$ The compensation of viscosity-variation effects has been checked with water at $T_b < 360$ K	Expressions to calculate the isothermal empty tube friction factors for either smooth or rough tubes are given in clause 7.2.2.
$f_a/f_{ab} = (\mu_w/\mu_b)^{0{,}35}(D_{Ea}/D)$		The differences between isothermal and heated friction factors are less than for the empty tube. This is so because the tape is nearly adiabatic and, thence, the reduction in the liquid viscosity because of the increased temperature is much smaller near the tape than near the tube wall. This effect is accounted for by the factor D_{Ea}/D in the exponent.
$Nu_a = Nu_{sc} + Nu_{cc} + Nu_f$	Liquid or gases under moderate transverse temperature gradients.	
$Nu_{sc} = 0{,}0088Re^{0{,}915}Pr^{0{,}4}$ Corresponds to flow through the spiral channel.	Fluid properties evaluated at T_{bam} Nu and Re based on DE. $3 \times 10^3 < Re < 8 \times 10^4$ $e/D < 12 \times 10^{-4}$ $2{,}55 < y < 6{,}16$ $L/D = 60\text{-}80$	Nu_{sc} is predicted from conventional straight tube correlations, accounting for the increased velocity near tube wall caused by the tape insertion and spiralling flow path. For this the Reynolds number must be defined as: $Re = \alpha VD_E/\nu$, where $\alpha^2 = 1 + (\pi/2y)^2$. For the effect of roughness and Prandtl number on both the constant factor and Re-exponent see ECSS-E-HB-31-01 Part 3.

Empirical Correlations	Conditions	Comments
$Nu_{cc} = 0{,}114(GrPr)^{1/3}$ Fishenden-Saujnders formula Gives the centrifugal convection effect when the heat flows toward the tube axis.	Horizontal heated plate, width L, facing upward. Fluid properties evaluated at $T_{0,5}$, Gr based on L. $2 \times 10^7 < GrPr < 3 \times 10^{10}$. McAdams (1954) [125]. A factor 0,14 instead of 0,114 is quoted in this, as well as in other sources.	The Grashof number, Gr, is based on the centrifugal acceleration. $Gr/Re^2 = 2(\pi/2y)^2(D_{Ea}/D)\beta(T_w - T_b)$. THIS TERM WILL NOT BE PRESENT WHEN COOLING.
$Nu_f = (F-1)(Nu_{sc} + Nu_{cc})$ Gives the heat transfer by the tape acting as a fin.	Representative values of F are given in the Table of Figure 9-16.	This term is determined by the designer for each particular system of interest.
Comments concerning the data presented in Figure 9-17. Data on smooth swirl tubes and on rough (no swirl) tubeshave been included for comparison purposes. The improvement obtained by inserting twisted tapes in rough tubes strongly depends on Re_o or the pumping power level. At low values of Re_o the clear choice would be a smooth swirl tube; but at higher values of Re_o the rough tubes outperform the smooth swirl tubes. For these values of Re_o the rough-swirl tube is clearly the top performer.		

10
Working fluids

10.1 General

This clause is intended as an aid in the selection of coolant fluids.

Coolant fluids for satellite temperatures can be gaseous or liquids. Molten metals are used at higher temperatures.

The selection of the coolant is made on the basis of the thermal and power requirements for achieving a given cooling duty. In the case of non-expandable coolants the basic variables are: density, specific heat, thermal conductivity and viscosity, as well as temperature limits which should be compatible with the desired application. The most important factors to be taken into account when selecting expandable coolants are: specific heat and useful temperature range.

The above mentioned requirements, however, do not give the complete picture of the problem. Many fluids fulfilling the appropriate thermal and frictional requirements can be aggressive to metallic or elastomeric materials. Several coolants are toxic and their use are ruled out when manned operations are envisaged; several others are flammable, ...

Additional requirements can be defined in particular cases. For instance, good lubricity is desirable to perform hydraulic functions as well as cooling; dielectric properties become important when single-walled jackets are used and the fluid is in contact with electrical equipment. Concern with vapor pressure, storage temperature, safety and handling appears in the detailed design of the system.

According to the above considerations, this clause is divided into two distinct clauses.

The first part deals with the selection of the fluids which meet the cooling and pumping power requirements. This selection is based on the fluid thermal and frictional properties. A drastically simplified cooling loop is assumed in order to substantiate the comparison between the fluids. Eight fluid coolants are considered by way of example, four of them being liquids and the other four gases under normal operating conditions. The method used for ranking these coolants can be applied to other fluids provided that their relevant physical properties are known. From the worked cases the conclusion is drawn that liquids are far superior to gases, although the useful temperature range of liquids is restrained by boiling, high vapor pressure and thermal degradation.

In the second part of the clause, the physical and environmental properties of thirty liquid coolants are compiled. The clause ends with a clause giving thermal properties of dry air in the temperature range 270 K to 310 K, at a pressure of 10^5 Pa.

10.2 Cooling effectiveness of a fluid

The cooling effectiveness of a fluid is measured by the ratio, F, of the heat transfer rate, Q, to the mechanical power, $\Delta p(m/\rho)$, required to drive the fluid through the loop, f the heat transfer rate

$$F = \frac{Q}{\Delta p \dfrac{m}{\rho}}$$

[10-1]

A preliminary estimate of the fluid coolant merit should be based on simplified fluid loops. In our particular case the loop is constituted by a cylindrical smooth tube, of circular cross section, inner diameter D, length L_E, and diabatic length L ($L \leq L_E$). More complex loops can be reduced to this simple "equivalent" configuration once the pressure losses through them, for given flow conditions, have been evaluated.

The merit of several gaseous and liquid coolants are compared on the basis of the ratio F, for both laminar and turbulent flow, in Figure 6-1. The calculations have been made for particular, yet representative, values of the heat flux q ($q = Q/\pi DL$), inner diameter of the tube, D, and diabatic length, L.
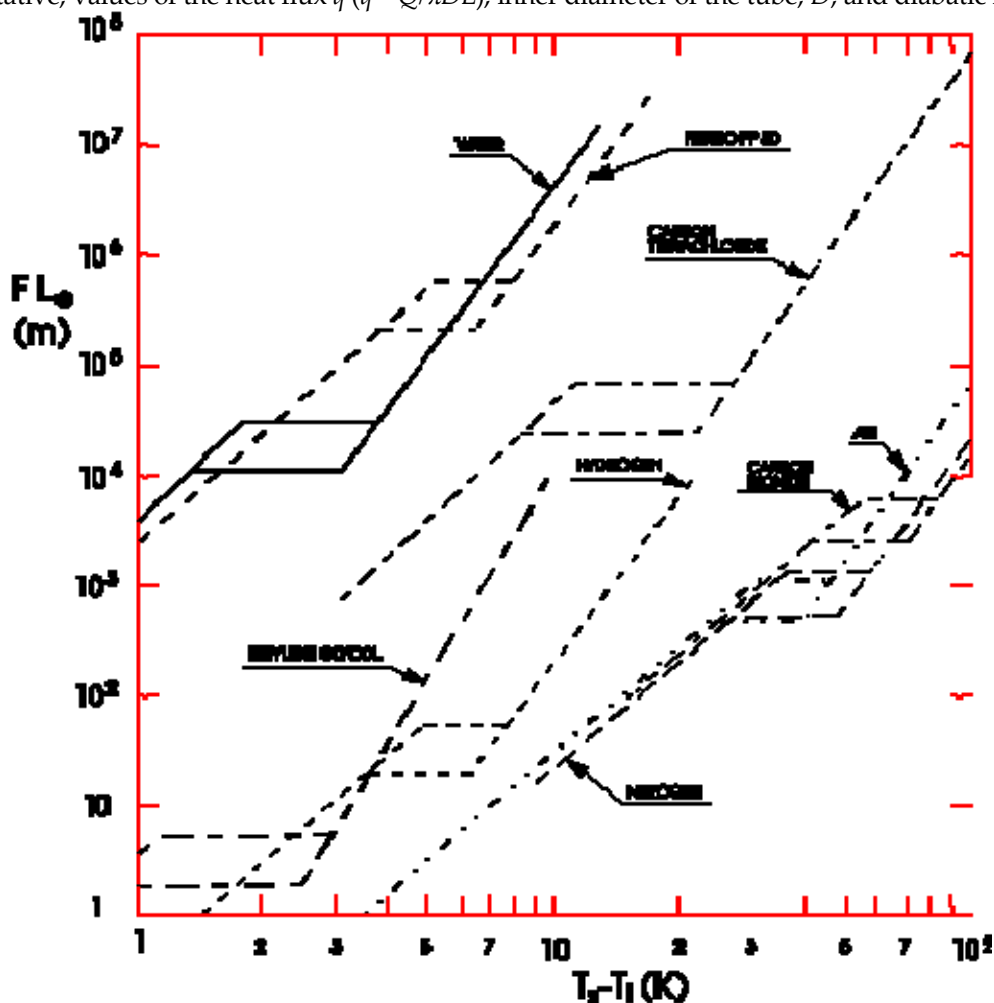
Figure 10-1: Product of cooling effectiveness, F, of several fluids times the equivalent length of the loop, L_E, as functions of the difference between the heat source and the inlet temperature, T_S - T_i, for the following reference values: Inner diameter of the duct, $D = 10^{-2}$ m. Diabatic length of the duct, $L = 1$ m. Heat flux, $q = 250$ W.m^{-2} for Air, Carbon Dioxide, Carbon Tetrachloride, Hydrogen and Nitrogen, $q = 1000$ W.m^{-2} for Ethylene Glycol, Flutec PP50 and Water. Calculated by the compiler.

It can be deduced from Figure 10-1 that liquid are superior to gases. Gases, however, can be used over a much wider temperature range since common liquid are restrained by freezing and/or high viscosities at low temperatures, and by boiling, high vapor pressure or thermal degradation at high temperatures. It is also seen that the ranking of the coolants considered is relatively unaffected by laminar or turbulent flow conditions.

Details concerning the calculations are briefly presented in the following clauses.

10.2.1 Simplified fluid loop configuration

The fluid is pumped through the circular-cylinder tube of length L_E and diameter D. The mass flow rate, m, as well as the heat transfer rate, Q, and the inlet fluid temperature, T_i, are assumed to be constant.

Some regulating device is required to enforce in practical cases these constraints. Here it is assumed that a heat exchanger placed between the pump and the tube inlet controls the inlet temperature, T_i, without changing the fluid mass flow rate, m.

The layout of the simplified configuration is sketched in Figure 10-2. The controller picks the wall temperature and controls the mass flow rate through the heat exchanger.
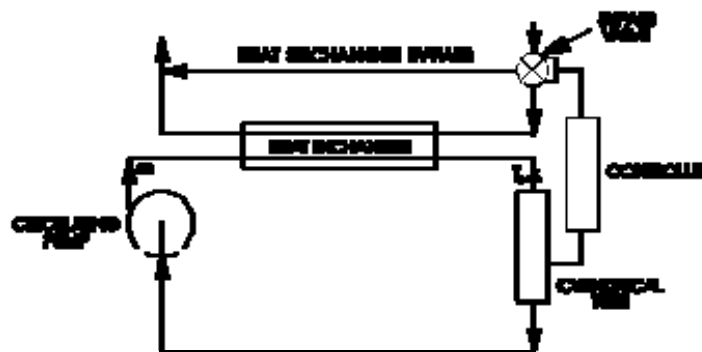
Figure 10-2: Schematic representation of the fluid loop considered for estimating the fluid cooling effectiveness.

10.2.2 Thermal performance of the simplified loop

Assuming that the fluid is heated or cooled over the diabatic length, L, the heat flow rate, Q, will be given by

$$q = h_{am}\Delta T_{am}L\pi D = mc_p\left(T_{bo} - T_i\right)$$ [10-2]

see clause 6.2.1.

The source temperature, T_s, is assumed to be equalto the wall temperature, T_w, of the diabatic cylindrical tube. This could be the case when this tube is the fluid duct of a cold plate on which the heat source is mounted.

Taking into account the definitions of the Nusselt, Prandtl and Reynolds numbers given in clause 6.2.2, Q becomes

$$Q = \frac{Nu\dfrac{k}{D}}{1 + 2\dfrac{Nu}{PrRe}\dfrac{L}{D}} \pi DL(T_S - T_i)$$ [10-3]

The Nusselt number is estimated with the aid of the following correlations:

— Fully Developed Laminar Flow ($Re < 2400$, $Gz < 9$), $Nu = 3{,}66$. See Figure 6-1.

— Thermal Entry Length Laminar Flow ($Re < 2400$, $Gz \geq 9$), $Nu = 1{,}75Gz^{1/3}$. See ESDU 68006 (1968) [48], p. 10, or alternatively, Figure 6-6 of this Part.

— Fully Developed Turbulent Flow ($Re > 4000$), $Nu = 0{,}023(Re^2 Pr)^{0,4}$. See clause 9.2, Dittus-Boelter formula.

In the transitional region both the laminar and turbulent values should be calculated. These values will correspond to the lower and upper limits of the Nusselt number.

10.2.3   Power requirements of the simplified loop

The pressure loss due to friction in the cylindrical pipe is:

$$\Delta p = \lambda \frac{L_E}{D}\frac{1}{2}\rho V^2$$ [10-4]

see clause 7.2.2. In this equation λ is given by:

— Fully Developed Laminar Flow ($Re < 2400$), $\lambda = 64/Re$. See clause 7.2.2, Hagen-Poiseuille formula.

— Fully Developed Turbulent Flow ($Re > 4000$), $\lambda = 0{,}316Re^{-0,25}$. See Table 7-2, Blasius formula.

Again the transitional friction factor, λ, is supposed to be bounded by the values obtained by extrapolation of the laminar and turbulent formulae.

10.2.4   Several examples

Values of the cooling effectiveness, F, of several fluids were plotted as functions of the temperature difference, $T_S - T_i$, in Figure 10-1. The computations were made for reference values of the heat flux, q, the inner diameter of the tube, D, and the diabatic length, L.

The same computations have been replotted for four different fluids, namely: Air, Ethylene Glycol, Flutec PP50 and Water in four separate figures (heavy lines in Figure 10-4 to Figure 10-7).

In order to estimate how sensitive the plotted values of FL_E are to changes in the assumed values of q and D a simple graphical method can be used. This method is introduced by resorting to Figure 10-3.
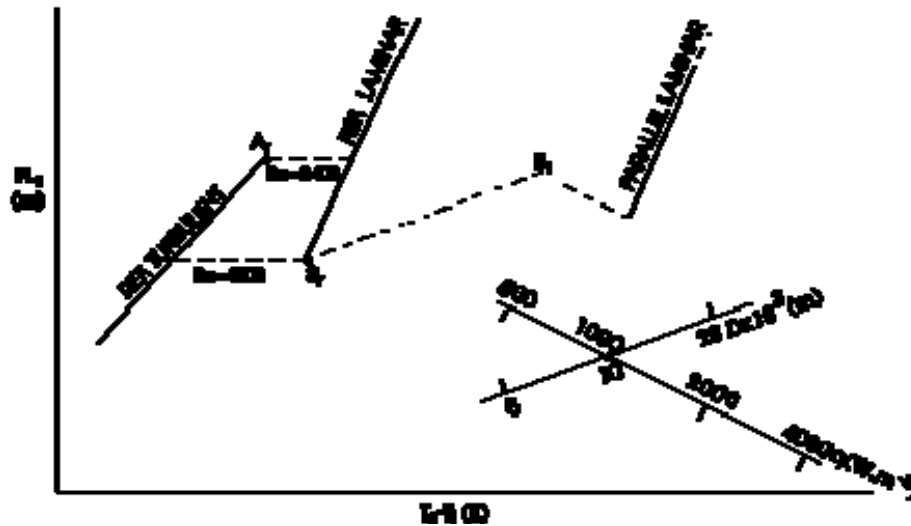
Figure 10-3: Graphical method allowing for values of heat flux, *q*, and inner diameter of the duct, *D*, different from those used in Figure 10-1.

In order to move from point B_r to point B:

1. A segment will be drawn from B_r, parallel to D axis, whose length corresponds to the new value of the duct diameter measured in the appropriate scale.

2. From the resulting point, B_1, a segment parallel to q axis and of the appropriate length will be drawn, giving the point B.

    Both q and D scales are logarithmic.

Point A_r will be moved in the same manner for pinpointing A, although different oblique coordinates q and D must be used as shown in Figure 10-4 to Figure 10-7.
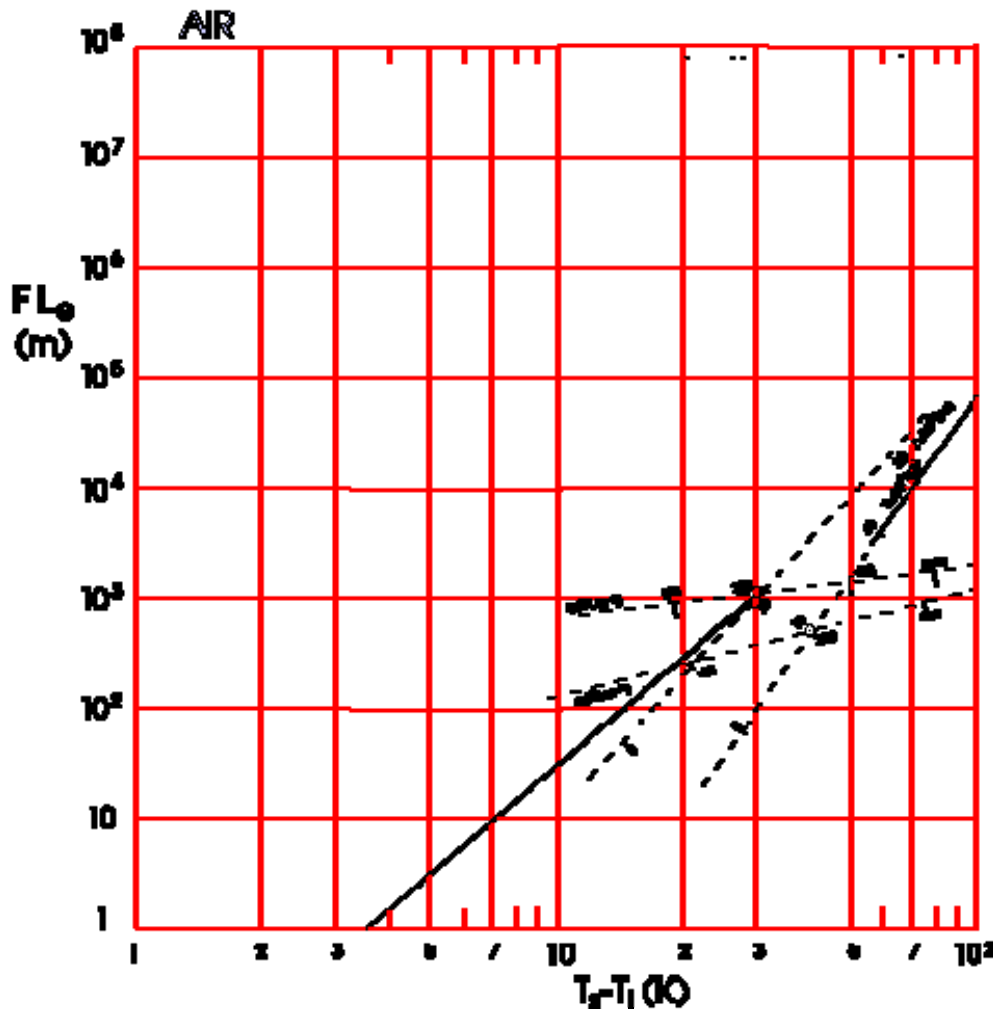
Figure 10-4: Graphic for estimating the product of the fluid cooling effectiveness, F, times the equivalent length of the loop, L_E, as a function of the difference between the heat source and the inlet fluid temperature, $T_S - T_i$. Fluid: Air. Reference values: $D = 10^{-2}$ m, $L = 1$ m, $q = 250$ W.m^{-2}. Values FL_E for different D and q, yet $L = 1$, can be calculated graphically as is indicated in the text. Prepared by the compiler.
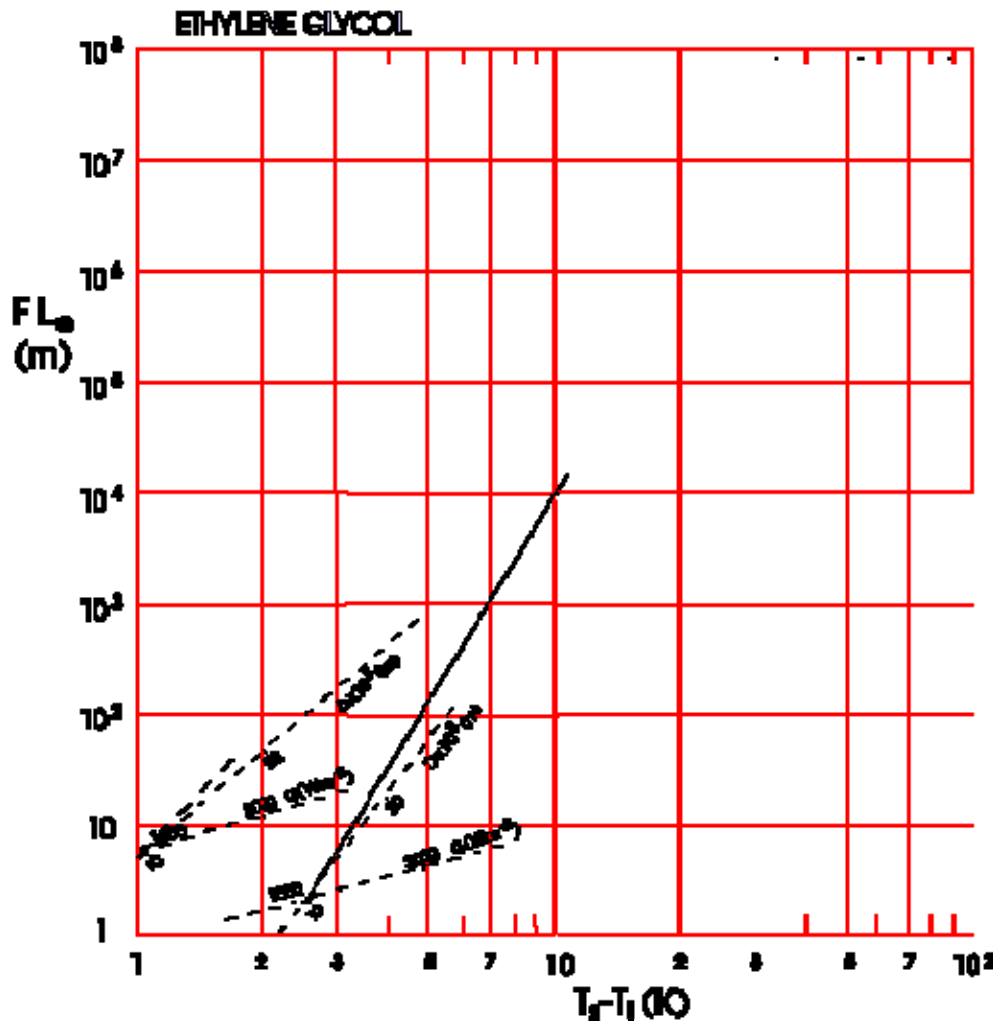
Figure 10-5: Graphic for estimating the product of the fluid cooling effectiveness, F, times the equivalent length of the loop, L_E, as a function of the difference between the heat source and the inlet fluid temperature, $T_S - T_i$. Fluid: Ethylene Glycol. Reference values: $D = 10^{-2}$ m, $L = 1$ m, $q = 1000$ W.m^{-2}. Values FL_E for different D and q, yet $L = 1$, can be calculated graphically as is indicated in the text. Prepared by the compiler.
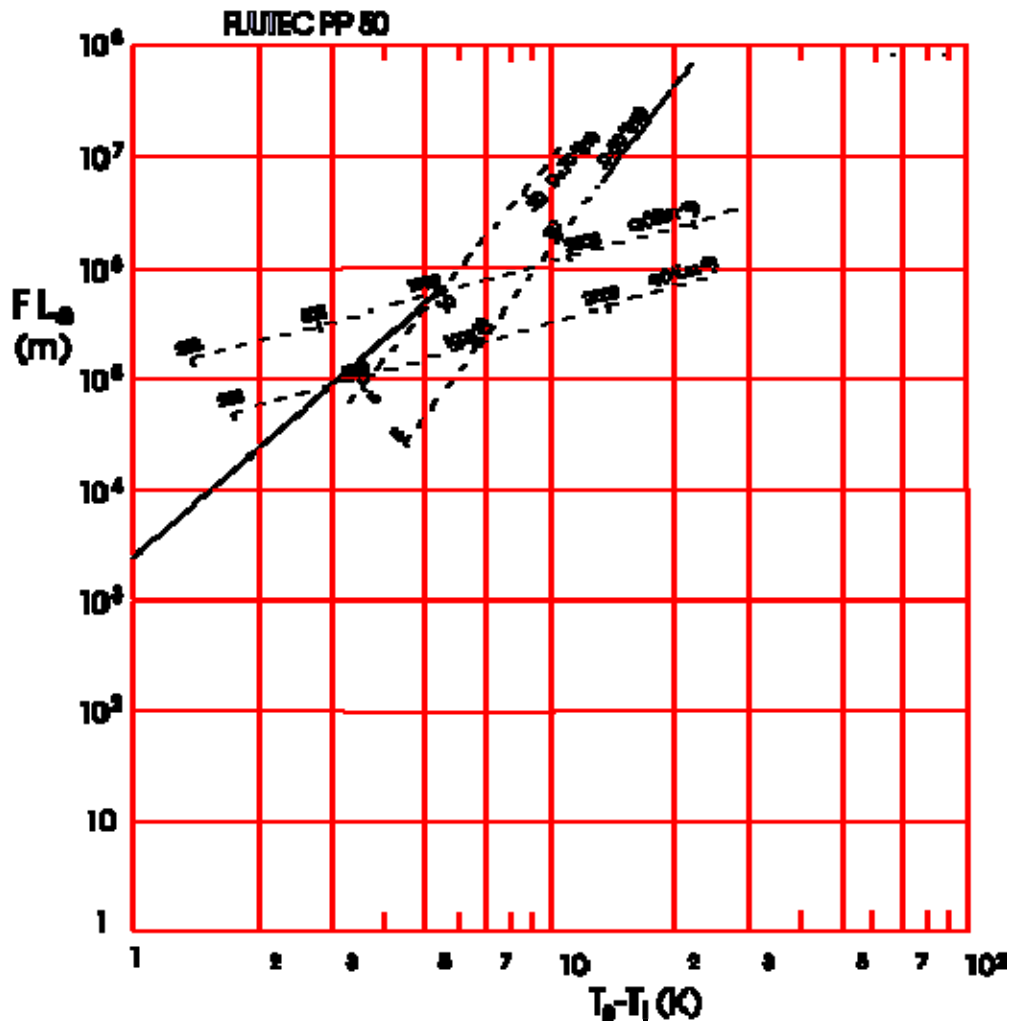
Figure 10-6: Graphic for estimating the product of the fluid cooling effectiveness, F, times the equivalent length of the loop, L_E, as a function of the difference between the heat source and the inlet fluid temperature, T_S - T_i. Fluid: Flutec PP50. Reference values: $D = 10^{-2}$ m, $L = 1$ m, $q = 1000$ W.m^{-2}. Values FL_E for different D and q, yet $L = 1$, can be calculated graphically as is indicated in the text. Prepared by the compiler.
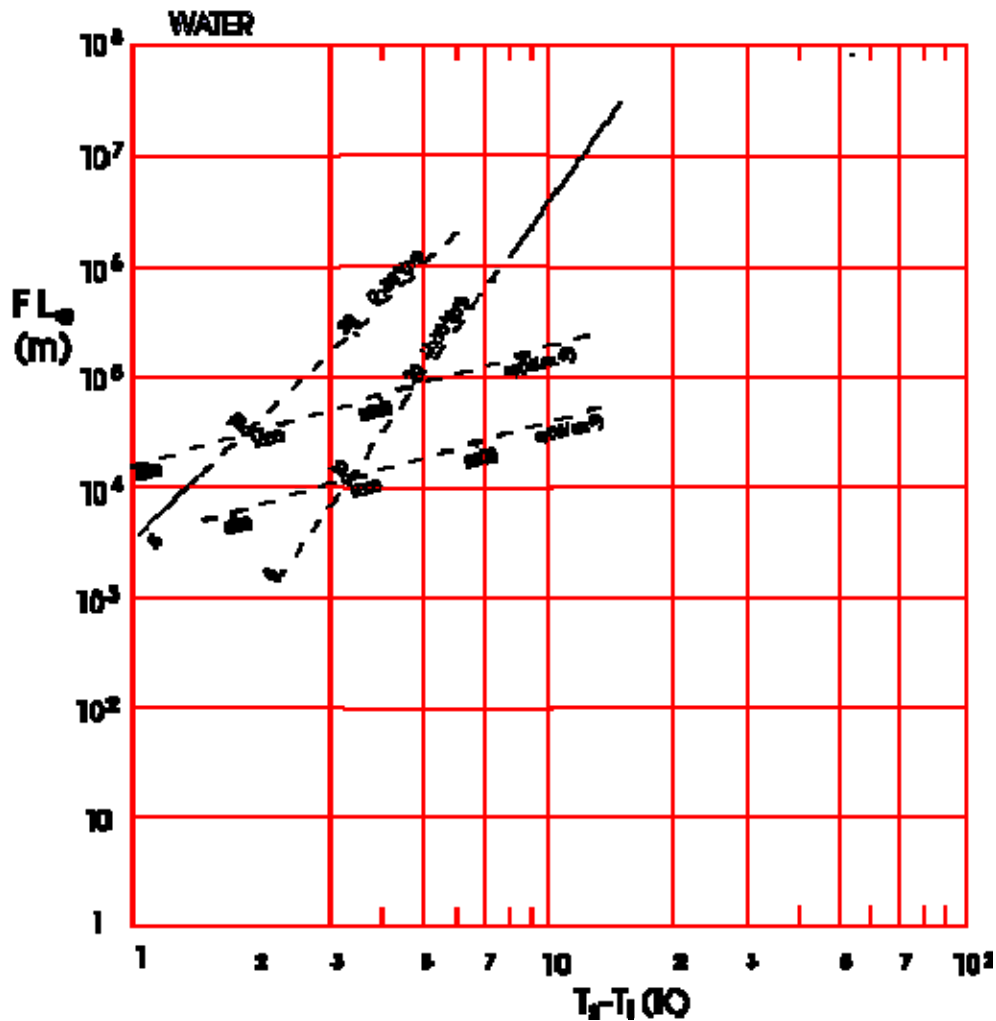
Figure 10-7: Graphic for estimating the product of the fluid cooling effectiveness, F, times the equivalent length of the loop, L_E, as a function of the difference between the heat source and the inlet fluid temperature, T_s - T_i. Fluid: Water. Reference values: $D = 10^{-2}$ m, $L = 1$ m, $q = 1000$ W.m^{-2}. Values FL_E for different D and q, yet $L = 1$, can be calculated graphically as is indicated in the text. Prepared by the compiler.

In order to draw the new laminar flow (or turbulent flow) curve relating the cooling effectiveness per unit equivalent duct length, F, with the temperature difference, T_s - T_i, for the chosen values of the heat flux, q, and the inner diameter of the duct, D, a straight line is draw from B parallel to that drawn for B_r.

This graphical method is only approximate. The reference curves are not strictly straight lines nor should be translated in parallell. however the error resulting from the use of these oversimplifications has been of the order of 5% in all the cases which have been considered.

10.3 Properties of liquid coolants

Relevant properties of thirty selected liquid coolants have been compiled in this clause.

The data are arranged as follows: Basic physical properties to be used in the preliminary selection of the coolant have been assembled in Table 10-1. These properties are: operating temperature limits,

flammability data, density, specific heat, thermal conductivity and dynamic viscosity. When the available data cannot be presented in the small space allotted to them in the Table, additional figures and tables are used. As a general rule the additional figures precede the additional tables, but are placed after the opening Table 10-1 and Table 10-2.

Environmental properties such as, odor, toxicity and materials compatibility,together with some reference to previous applications of the several coolants are presented in Table 10-2, plus the additional Table 10-4 to Table 10-9.

Table 10-1: Physical Properties of Typical Liquid Coolants

LIQUID	CHEMICAL FORMULA	FREEZING POINT [K]	BOILING POINT at 10^5 Pa [K]	FLASH POINT [K]	VAPOR PRESSURE p_{sat} [Pa]	DENSITY ρ [kg.m^{-3}]	SPECIFIC HEAT c_p [J.kg^{-1}.K^{-1}]	TERMAL CONDUC. k [W.m^{-1}K^{-1}]	DYNAMIC VISCOSITY μ [Pa.s]
Water	H_2O	273	373	None	Figure 10-8	Figure 10-9	Figure 10-10	Figure 10-11	Figure 10-12
Carbon Tetrachloride	CCl_4	250[a]	350[a]	None[b]	Figure 10-13	Figure 10-14	Figure 10-15	Figure 10-16	Figure 10-17
Coolanol 15[c]		177	422	350	Figure 10-18	Figure 10-19	Figure 10-20	Figure 10-21	Figure 10-22
Coolanol 25[c,d]		189	372	436					
Coolanol 35[c]		189	483	450					
Coolanol 45[c,e]		208		461					
DC 200	Dimethyl Siloxane Polymer	Table 10-3				Table 10-3			Figure 10-23
Ethylene Glycol	$C_2H_6O_2$	Figure 10-24	470[f]		Figure 10-25	Figure 10-26	Figure 10-27	Figure 10-28	Figure 10-29
Glycol / Water									
Flutec PP2[g]		223[h,i]	349[i]		Figure 10-30	Figure 10-31		Figure 10-33	Figure 10-34
Flutec PP9[g]		193[j]	433[i]				1080[j]		
Flutec PP50[g]	C_5F_{12}	133[j]	302[j]				Figure 10-32		
Freon 11[k]	$CFCl_3$	162	297	None	Figure 10-35	Figure 10-36	Figure 10-37	Figure 10-38	Figure 10-39
Freon 12[k]	CF_2Cl_2	115	243	None					
Freon 13[k]	CF_3Cl	92	192						
Freon 21[k]	$CHFCl_2$	138	282	None					
Freon 22[k]	CHF_2Cl	113	232						
Freon 113[k]	$C_2F_3Cl_3$	238	321						

LIQUID	CHEMICAL FORMULA	FREEZING POINT [K]	BOILING POINT at 10^5 Pa [K]	FLASH POINT [K]	VAPOR PRESSURE p_{sat} [Pa]	DENSITY ρ [kg.m^{-3}]	SPECIFIC HEAT c_P [J.kg^{-1}.K^{-1}]	TERMAL CONDUC. k [W.m^{-1}K^{-1}]	DYNAMIC VISCOSITY μ [Pa.s]
Freon 114[k]	$C_2F_4Cl_2$	179	277	None					
Freon 142[k]	$C_2H_3F_2Cl$	142[a]	263[a]						
Freon E1[k]	$(C_2F_3O)C_3HF_8$	119	314	None	Figure 10-40	Figure 10-41	Figure 10-42	Figure 10-43	Figure 10-44
Freon E2[k]	$(C_2F_3O)_2C_3HF_8$	150	377						
Freon E3[k]	$(C_2F_3O)_3C_3HF_8$	166	425						
Freon E4[k]	$(C_2F_3O)_4C_3HF_8$	179	467						
Freon E5[k]	$(C_2F_3O)_5C_3HF_8$	189	497						
FC 75[l]		160	372	None	Figure 10-45	Figure 10-46	Figure 10-47	Figure 10-48	Figure 10-49
Methanol/Water 60/40		231[j]	355[j]	294[m]		900[j]	3430[j]	Figure 10-50	Figure 10-51
Methanol/Water 80/20		170[m]	343[m]	287[m]		850[m]	2880[m]		
Monsanto [c] OS 59		208	644	461	Figure 10-52	Figure 10-53	Figure 10-54	Figure 10-55	Figure 10-56
Oronite [n] Flo-Cool 100		200	422	383	5066	891	1985	0,0986	$2,5 \times 10^3$

NOTE   All data in this table, unless otherwise stated, are from Filippi & Guerra (1977).

[a]   From Vargaftik (1975) [183].

[b]   From Weat (1966) [185].

[c]   Sislicate ester manufactured by Monsanto Chemical Co.

[d]   Also known as FFP-103 and Monsanto OS 139.

[e]   Also known as OS 45

[f]   From Raznjevic (1970) [147].

g   Manufactured by Imperial Smelting Co. Ltd.

h   Melting point.

I   From Dunn & Reay (1976) [40].

j   From Kissner (1973) [105]. Properties are given at 298 K.

k   Freon is a registered trademark of E.I. DuPont de Nemours & Co., Inc.

l   FC 75 is a fluorochemical.

m   From Ignations & Mitchell (1974) [98]. The temperatures corresponding to thermodynamic and transport properties are not reported. The apparent rage seems to be from 283 K to 298 K.

n   Oronite is a silicate ester manufactured by Oronite Chemical Co. Properties ae given at 298 K except vapor pressure and specific heat which are given at 422 K and 298 K respectively.

Table 10-2: Environmental Properties of Typical Liquid Coolants

LIQUID	ODOR	TOXICITY (Mac)[a]	MATERIALS COMPATIBILITY		APPLICATIONS
			Metals	Elastomers	
Water	None	Non toxic	Corrosive to Al alloys	No swell	Skylab, Shuttle
Carbon Tetrachloride	Noxius [b]	(315 mg.m^{-3}) [b]	Corrosive to Cu alloys [c]	Unusable [c]	
Coolanol 15	Slight	Toxic at T > 422 K	Table 10-4	Moderate swell [d]	Gemini Space Capsule
Coolanol 25		Low toxicity (1000 ppm) [d]			
Coolanol 35				Compatible with Buna N [d]	Test fluid
Coolanol 45					
DC 200	None [e]	Non toxic [e]	Chemically inert [e]		Liquid dielectric and coolant
Ethylene Glycol		(27,7 mg.m^{-3}) [f]	Compatible with Aluminium [g]		High vicosity. [g] Normally mixed with water
Glycol / Water 60/40	Slight	114 mg.m^{-3}	Corrosive	No swell	Antifreeze [h] mixture. Apollo
Flutec PP2					
Flutec PP9		Breathing vapor should be avoided	Extremely good		Coolant for computer and electronic equipment, can be used as hydraulic and dielectric fluid [h]
Flutec PP50					
Freon 11		Table 10-5	Compatible with steel, cast iron, brass, copper, tin, lead, aluminium and other structural metallic materials	Table 10-6	
Freon 12					
Freon 13					
Freon 21	Very Noxius				Skylab, Shuttle [g]

LIQUID	ODOR	TOXICITY (Mac)[a]	MATERIALS COMPATIBILITY		APPLICATIONS
			Metals	Elastomers	
Freon 22			under normal conditions of use. Mg alloys and Al alloys containing more than 2% Mg are not recommended for use in systems containing Freon were water may be present. Zinc is not recommended for use with Freon 113 [d]		
Freon 113					
Freon 114					
Freon 142					
Freon E1	None	Extremely low. Toxic at 533 K [d]		Slight swell	
Freon E2	None			Table 10-7	Heat transfer medium, dielectric coolant
Freon E3	None			Table 10-8 [i]	
Freon E4					
Freon E5					
FC 75		Low toxicity (1000 ppm) [d]		Table 10-7	Coolant for electronic equipment [h]
Methanol/Water 60/40	Noxius	26 mg.m^{-3}	Corrosive	No swell	
Methanol/Water 80/20					
Monsanto OS 59		(1000 ppm) [d]			
Oronite Flo-Cool 100				Table 10-9	

NOTE   All data in this table, unless otherwise stated, are from Ignationis & Mitchell (1974) [98].

[a]   Maximum allowable concentration

[b]   From Weast (1966) [185]. The value under Toxicity corresponds to the "Industrial Limit" which is normally ten times that allowed in Spacecraft for 90 d.

[c]   From Rabald (1968) [146].

[d]   From Filippi & Guerra (1977) [64].

[e]   From DOW CORNING (1963, 1972) [37] & [38].

[f]   From Rittenhouse & Singletary (1969). This value correspond to "Spacecraft 1 h Emergency" which is normally five times that allowed in spacecraft for 90 d.

[g]   From Kissner (1973) [105].

[h]   From Scott (1974) [161].

[I]   Also includes compatibility with plastics and wire coatings.
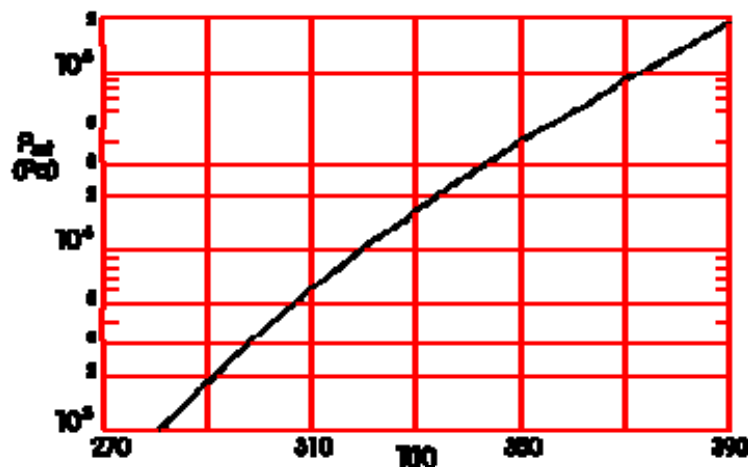
Figure 10-8: Vapor pressure, p_{sat}, of Water vs. temperature, *T*. From Vargaftik (1975) [183].
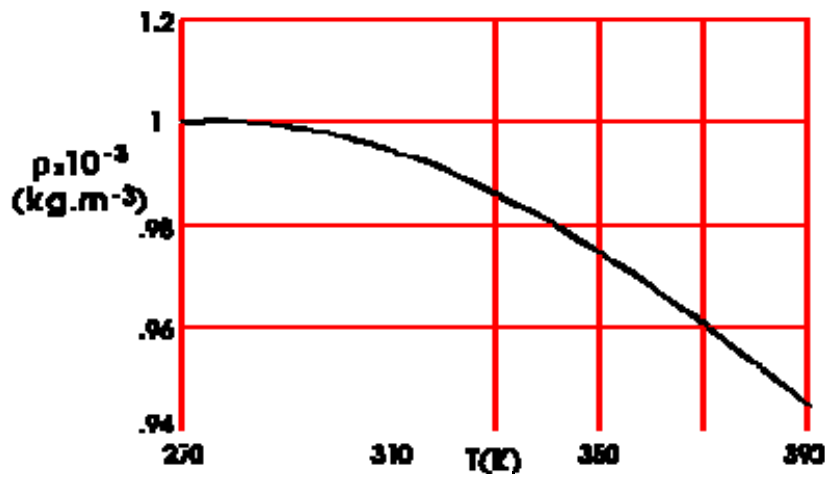
Figure 10-9: Density, ρ, of Water vs. temperature, *T*. From Vargaftik (1975) [183].
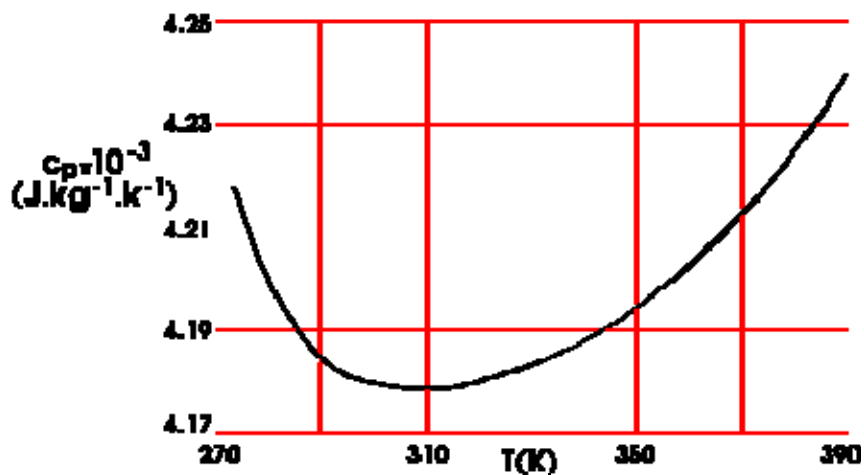
Figure 10-10: Specific heat, c_p, of Water vs. temperature, *T*. From Vargaftik (1975) [183].
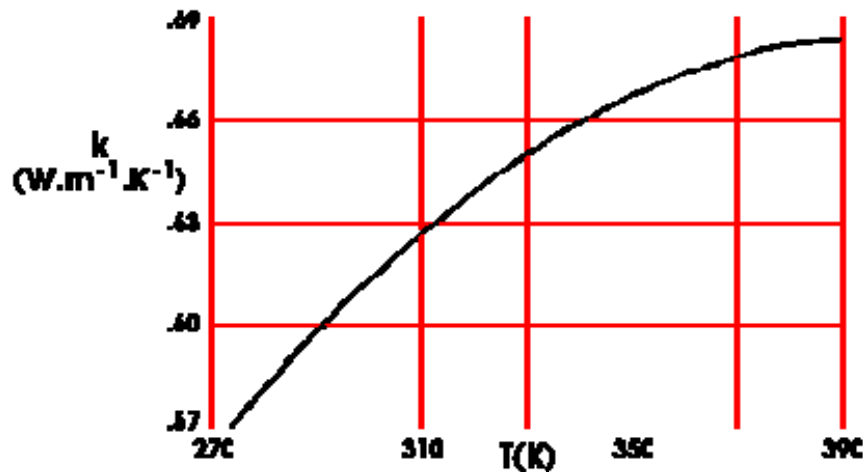
Figure 10-11: Thermal conductivity, *k*, of Water vs. temperature, *T*. From Vargaftik (1975) [183].
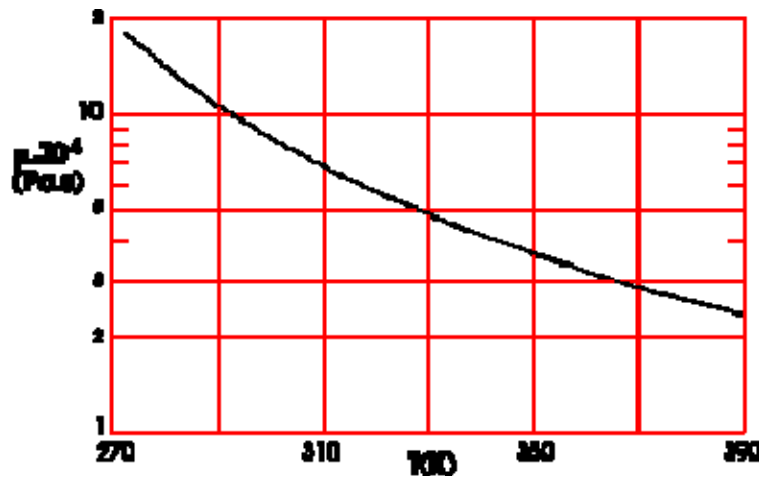
Figure 10-12: Dynamic viscosity, *μ*, of Water vs. temperature, *T*. From Vargaftik (1975) [183].
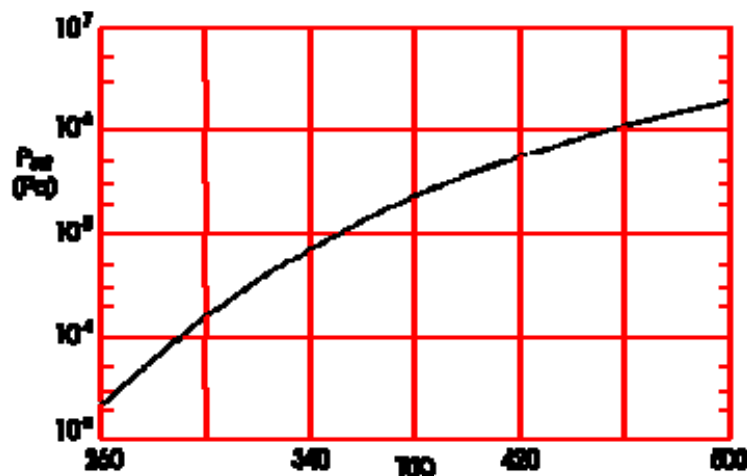
Figure 10-13: Vapor pressure, p_{sat}, of Carbon Tetrachloride vs. temperature, *T*. From Vargaftik (1975) [183].
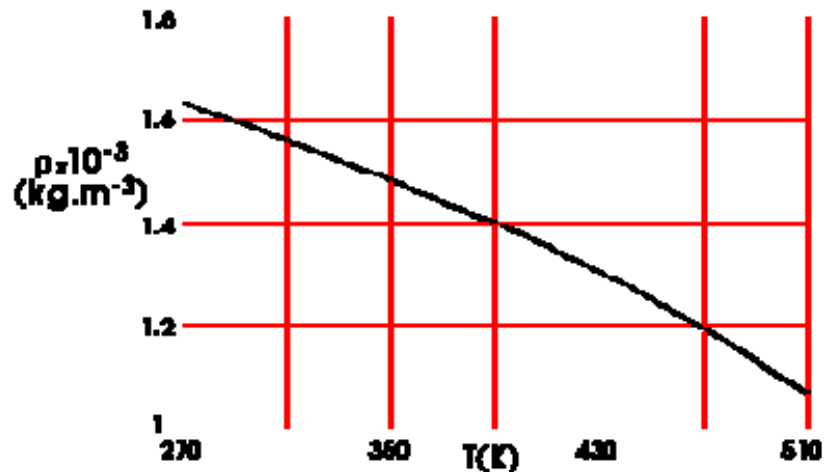
Figure 10-14: Density, ρ, of Carbon Tetrachloride vs. temperature, T. From Vargaftik (1975) [183].
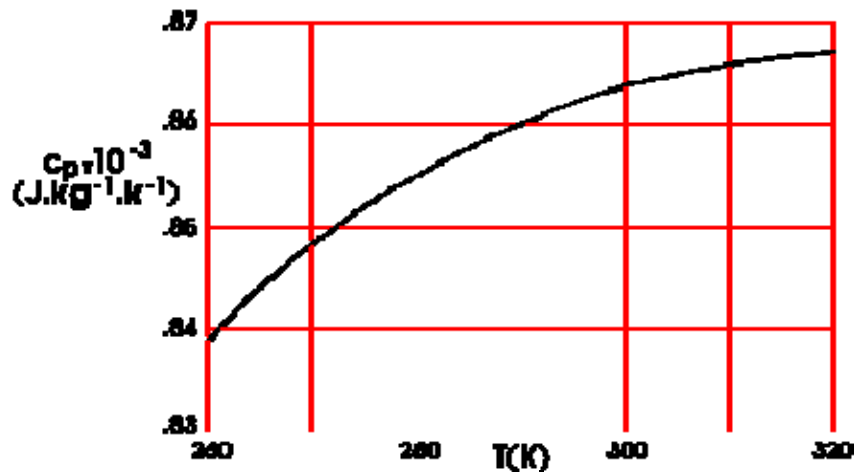
Figure 10-15: Specific heat, c_p, of Carbon Tetrachloride vs. temperature, T. From Vargaftik (1975) [183].
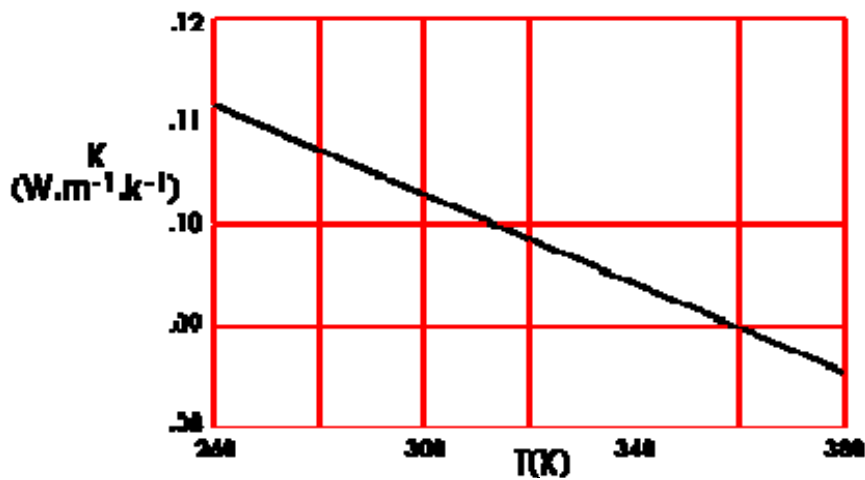
Figure 10-16: Thermal conductivity, k, of Carbon Tetrachloride vs. temperature, T. From Vargaftik (1975) [183].
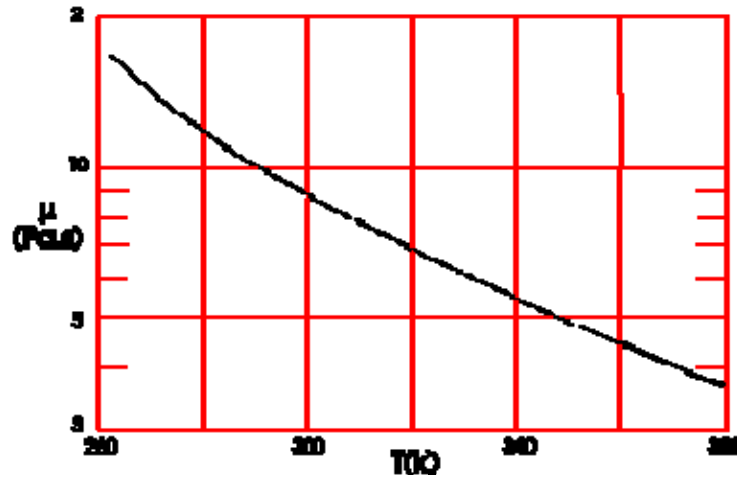
Figure 10-17: Dynamic viscosity, μ, of Carbon Tetrachloride vs. temperature, T. From Vargaftik (1975) [183].
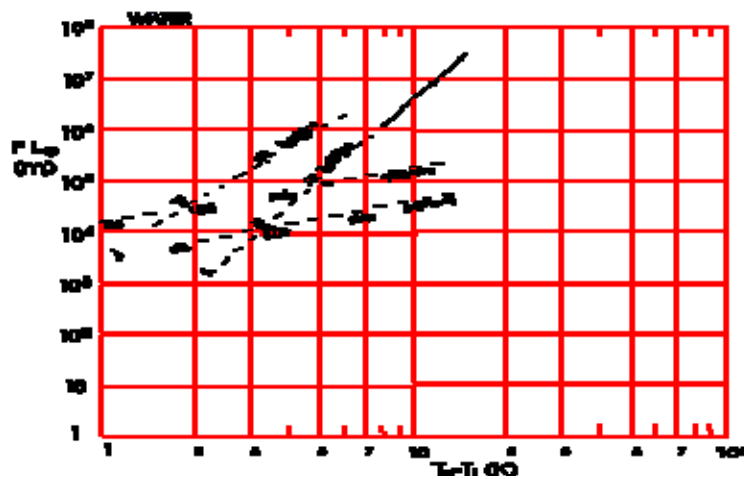
Figure 10-18: Vapor pressure, p_{sat}, of Coolanol 15, 25, 35 and 45 vs. temperature, T. From Filippi & Guerra (1977) [64].
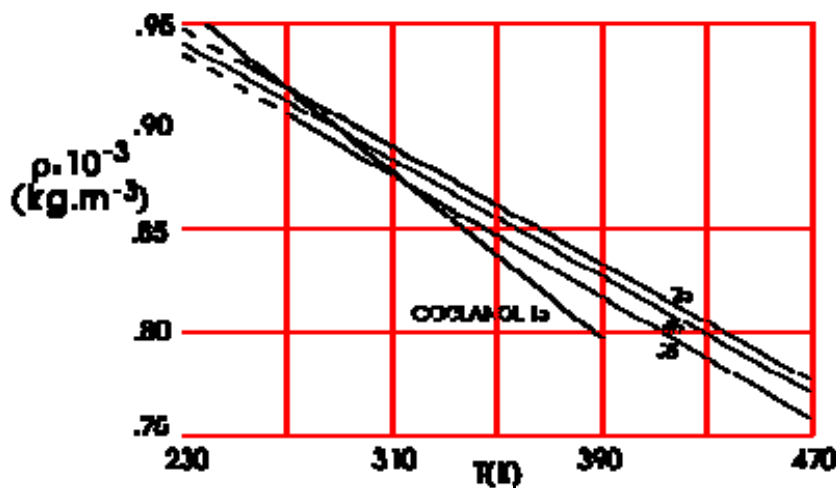
Figure 10-19: Density, ρ, of Coolanol 15, 25, 35 and 45 vs. temperature, T. From Filippi & Guerra (1977) [64].
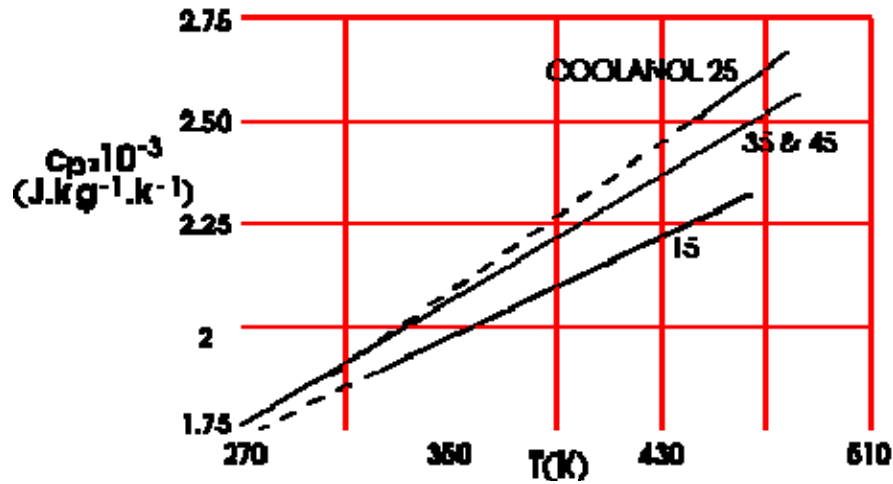
Figure 10-20: Specific heat, c_p, of Coolanol 15, 25, 35 and 45 vs. temperature, T. From Filippi & Guerra (1977) [64].
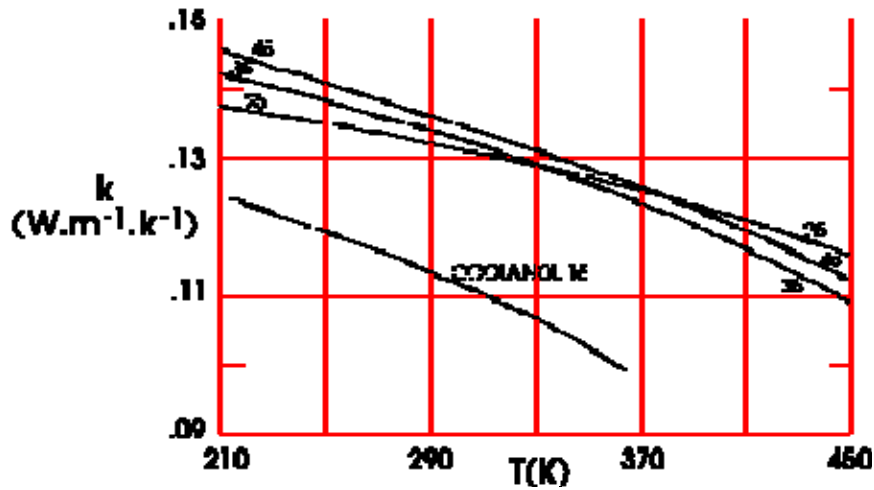
Figure 10-21: Thermal conductivity, k, of Coolanol 15, 25, 35 and 45 vs. temperature, T. From Filippi & Guerra (1977) [64].
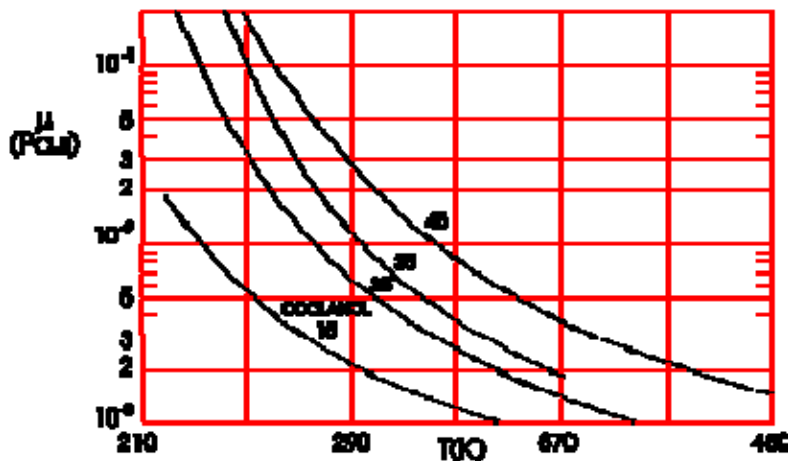
Figure 10-22: Dynamic viscosity, μ, of Coolanol 15, 25, 35 and 45 vs. temperature, T. From Filippi & Guerra (1977) [64].
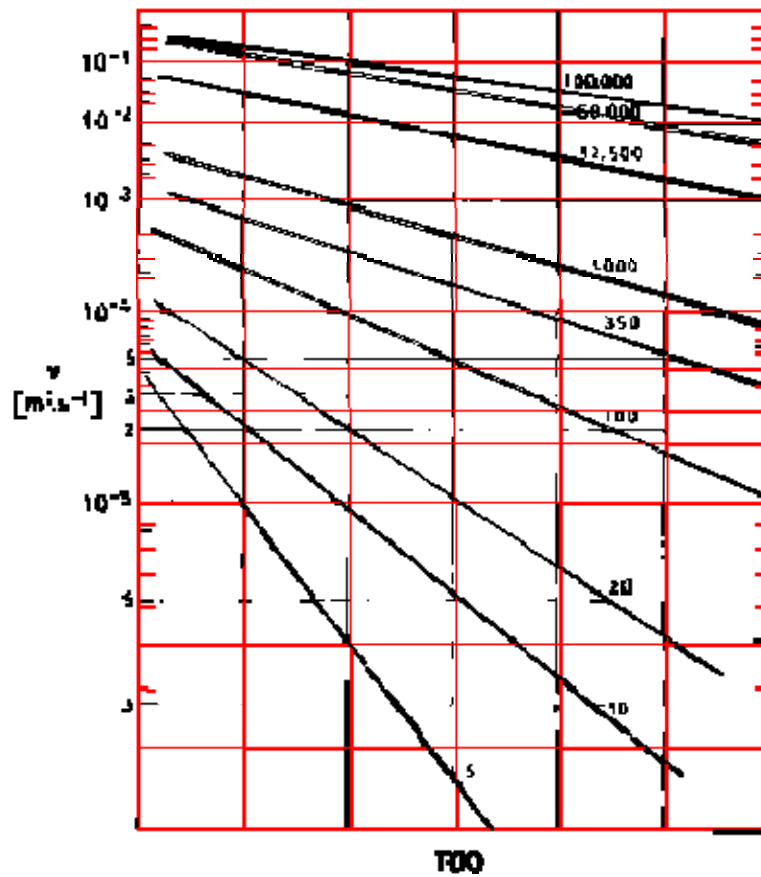
Figure 10-23: Kinematic viscosity, *ν*, of DC 200 vs. temperature *T*. Numbers on curves indicate the standard viscosity in cs. From DOW CORNING (1972) [38].
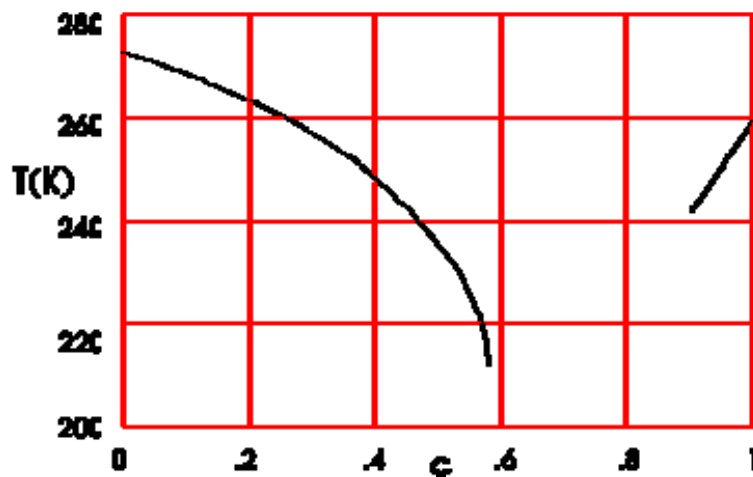
Figure 10-24: Freezing point, *T*, of Water/Glycol Solutions vs. Glycol mass fraction, *s*. From Filippi & Guerra (1977) [64].
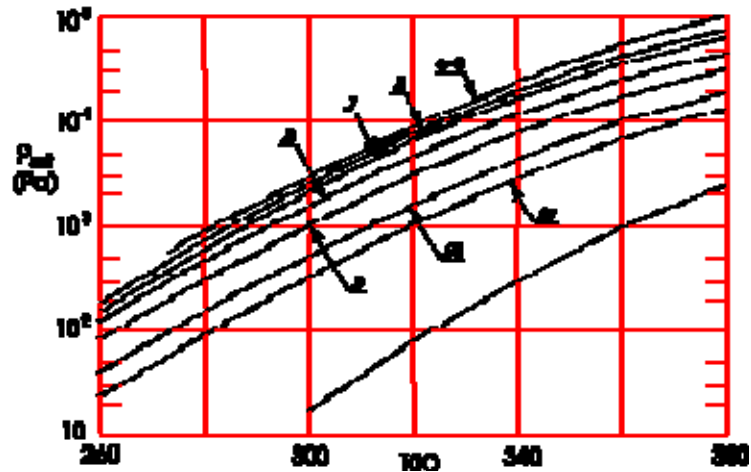
Figure 10-25: Vapor pressure, p_{sat}, of Water/Glycol Solutions vs. temperature, T. Numbers on curves indicate Glycol mass fraction, c. From Filippi & Guerra (1977) [64].
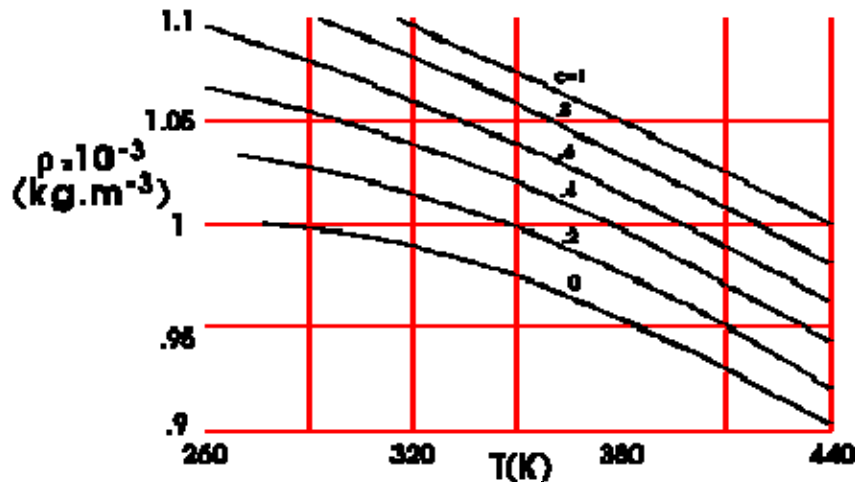
Figure 10-26: Density, ρ, of Water/Glycol Solutions vs. temperature, T. Numbers on curves indicate Glycol mass fraction, c. From Filippi & Guerra (1977) [64].
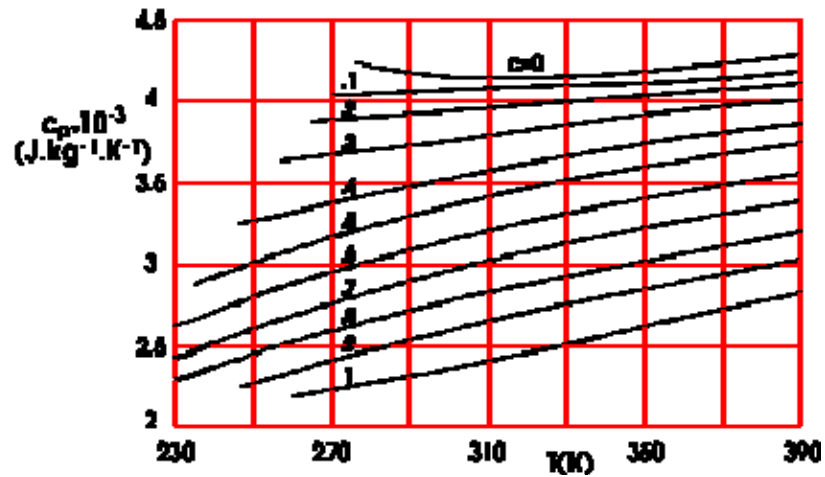
Figure 10-27: Specific heat, c_p, of Water/Glycol Solutions vs. temperature, T. Numbers on curves indicate Glycol mass fraction, c. From Filippi & Guerra (1977) [64].
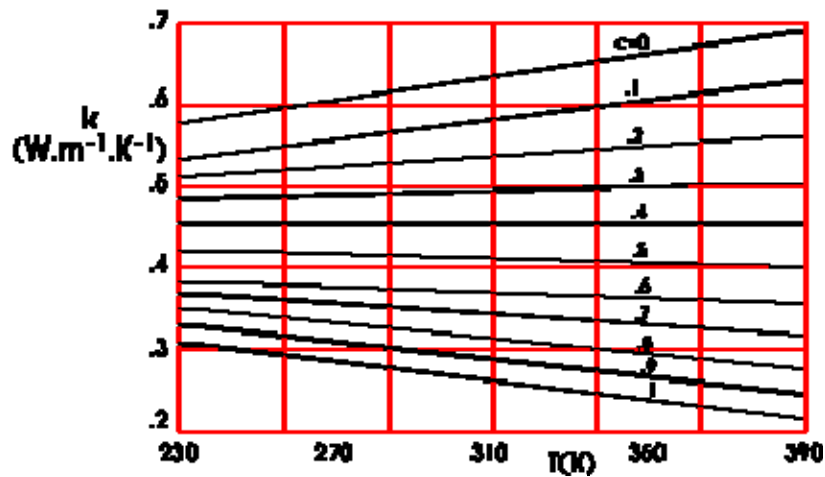
Figure 10-28: Thermal conductivity, k, of Water/Glycol Solutions vs. temperature, T. Numbers on curves indicate Glycol mass fraction, c. From Filippi & Guerra (1977) [64].
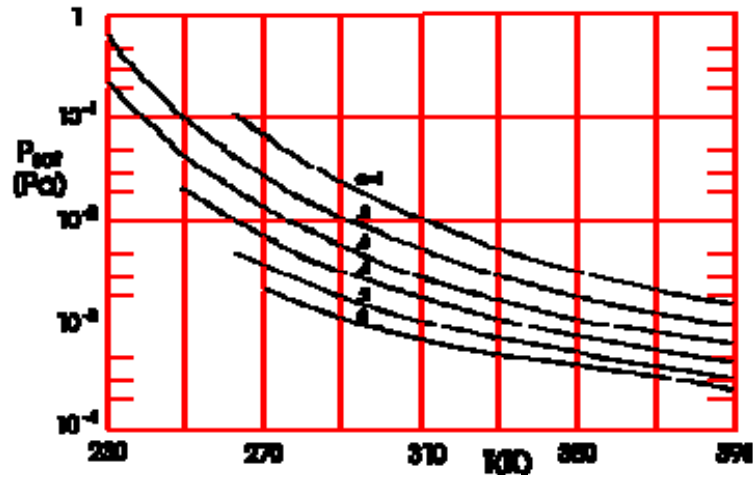
Figure 10-29: Dynamic viscosity, *μ*, of Water/Glycol Solutions vs. temperature, *T*. Numbers on curves indicate Glycol mass fraction, *c*. From Filippi & Guerra (1977) [64].
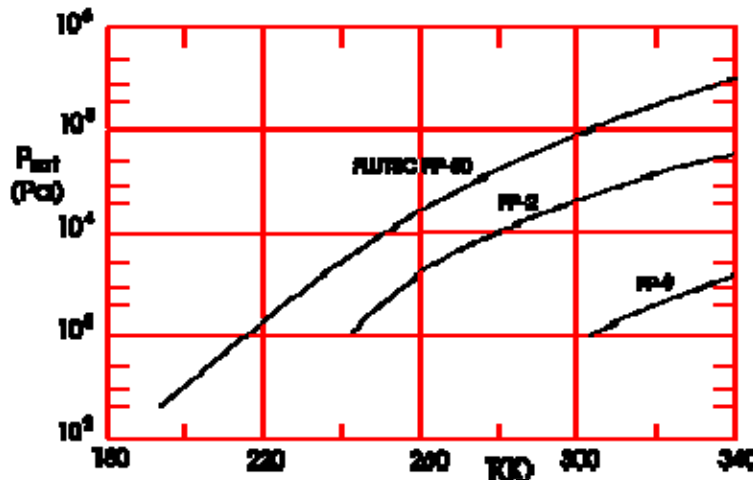
Figure 10-30: Vapor pressure, *p_{sat}*, of Flutec PP-2, PP-9 and PP-50 vs. temperature, *T*. Data are from Dunn & Reay (1976) [40] except those corresponding to Flutec PP-50 which are from Wyn-Roberts (1974) [193].
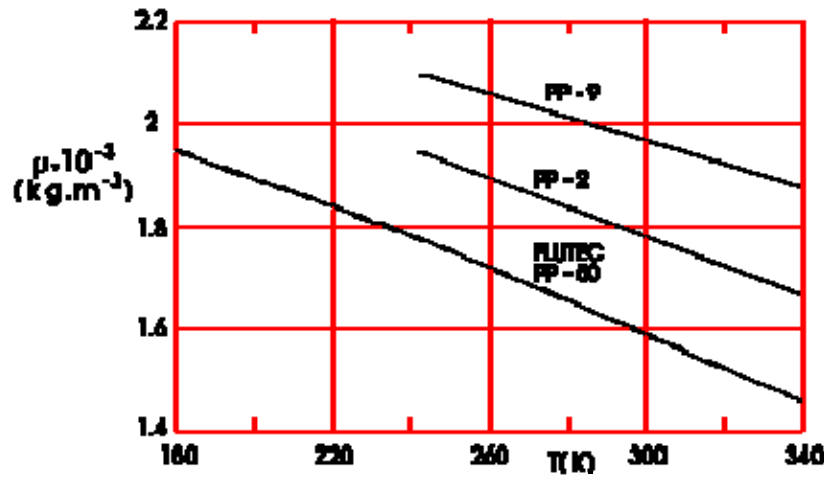
Figure 10-31: Density, ρ, of Flutec PP-2, PP-9 and PP-50 vs. temperature, T. Data are from Dunn & Reay (1976) [40] except those corresponding to Flutec PP-50 which are from Wyn-Roberts (1974) [193].
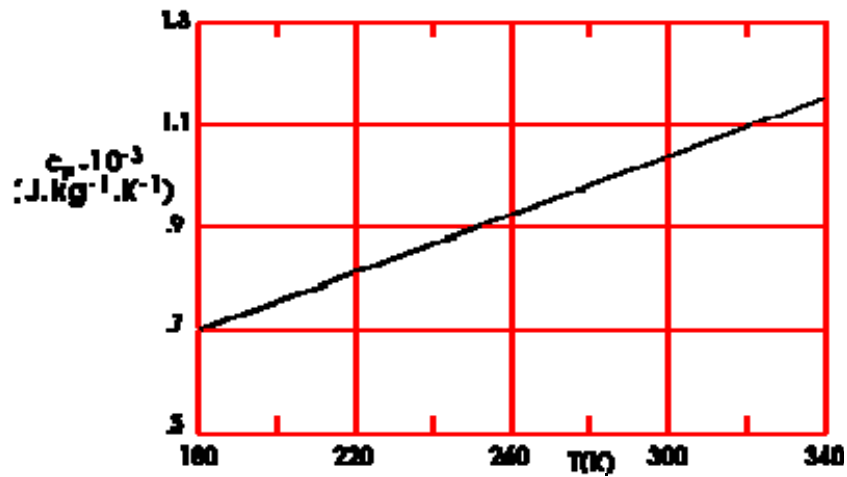
Figure 10-32: Specific heat, c_p, of Flutec PP-50 vs. temperature, T. From Wyn-Roberts (1974) [193].
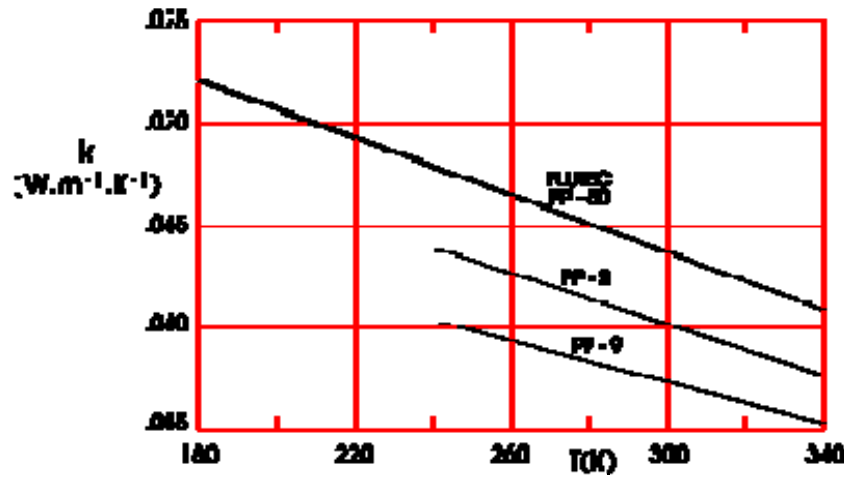
Figure 10-33: Thermal conductivity, *k*, of Flutec PP-2, PP-9 and PP-50 vs. temperature, *T*. Data are from Dunn & Reay (1976) [40] except those corresponding to Flutec PP-50 which are from Wyn-Roberts (1974) [193].
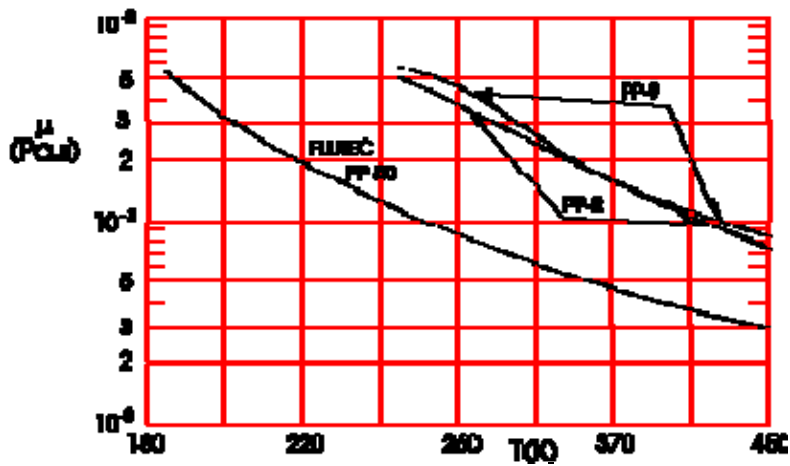
Figure 10-34: Dynamic viscosity, μ, of Flutec PP-2, PP-9 and PP-50 vs. temperature, *T*. Data are from Dunn & Reay (1976) [40] except those corresponding to Flutec PP-50 which are from Wyn-Roberts (1974) [193].
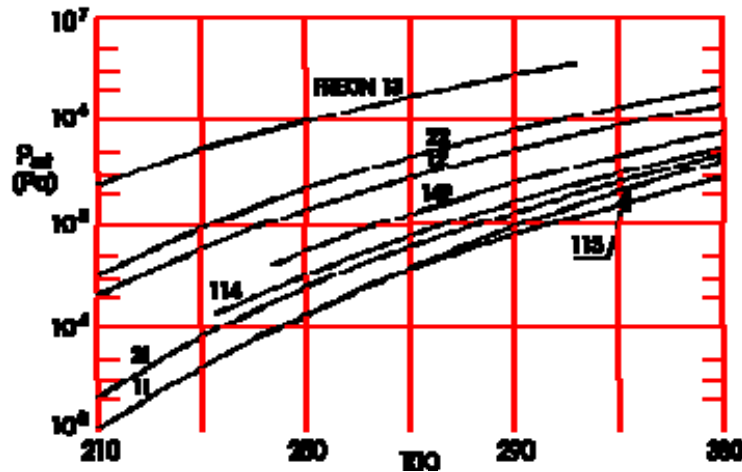
Figure 10-35: Vapor pressure, p_{sat}, of Freon 11, 12, 13, 21, 22, 113, 114 and 142 vs. temperature, T. From Vargaftik (1975) [183].
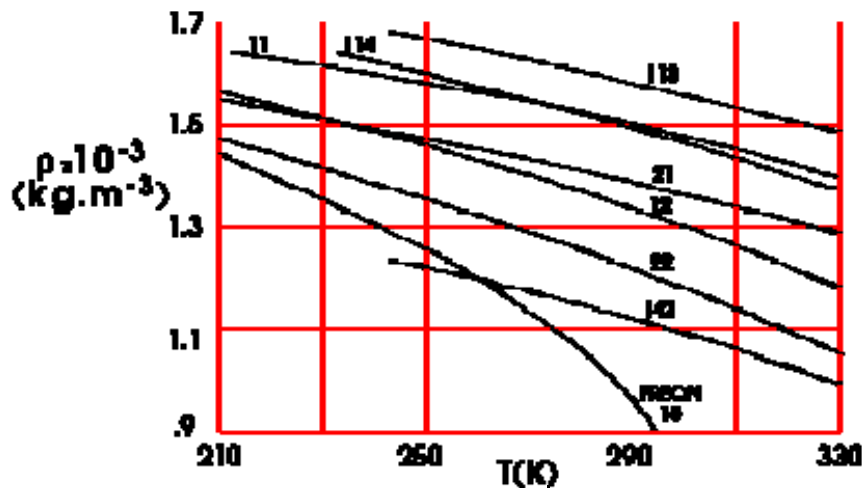
Figure 10-36: Density, ρ, of Freon 11, 12, 13, 21, 22, 113, 114 and 142 vs. temperature, T. From Vargaftik (1975) [183].
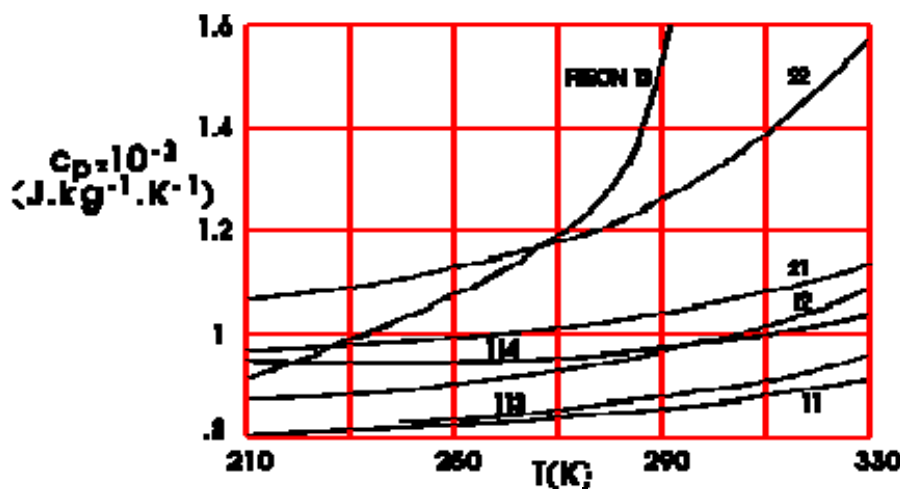
Figure 10-37: Specific heat, c_p, of Freon 11, 12, 13, 21, 22, 113, 114 and 142 vs. temperature, T. From Filippi & Guerra (1977) [64].
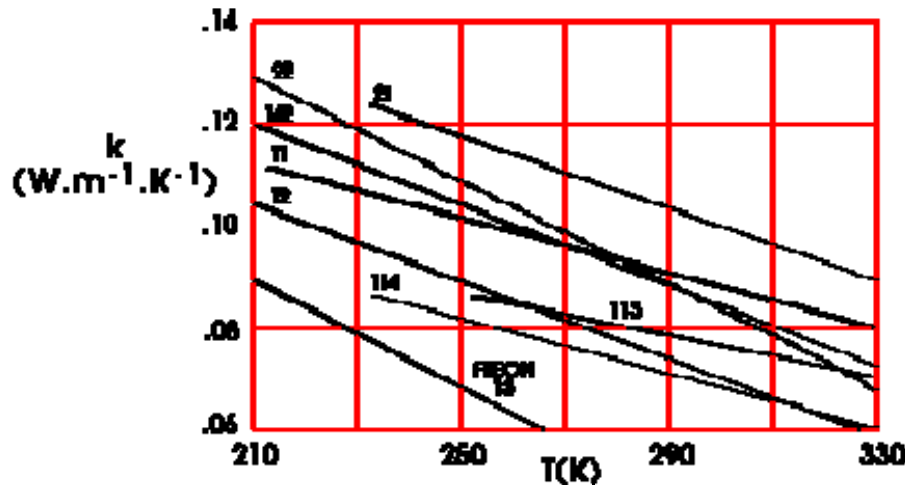
Figure 10-38: Thermal conductivity, *k*, of Freon 11, 12, 13, 21, 22, 113, 114 and 142 vs. temperature, *T*. From Vargaftik (1975) [183].
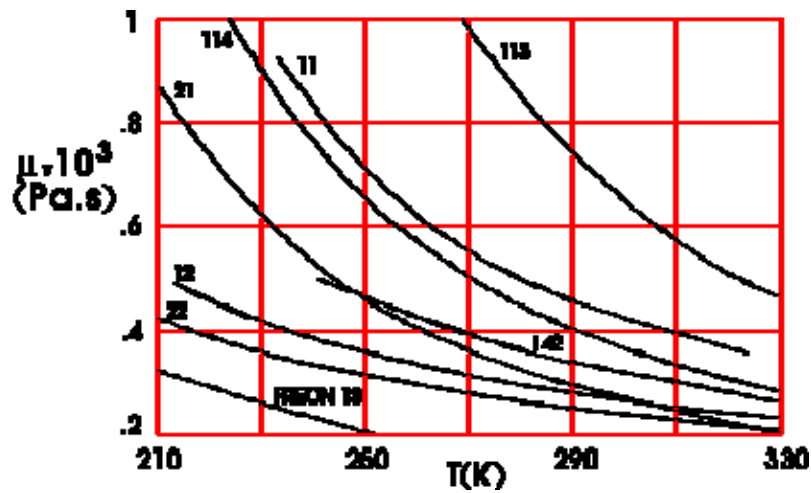
Figure 10-39: Dynamic viscosity, *μ*, of Freon 11, 12, 13, 21, 22, 113, 114 and 142 vs. temperature, *T*. Data are from Vargaftik (1975) [183] except those corresponding to Freon 13 which are from Filippi & Guerra (1977) [64].
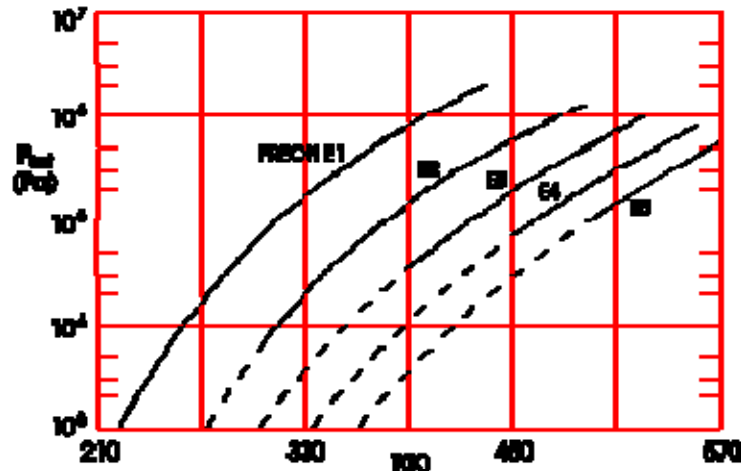
Figure 10-40: Vapor pressure, p_{sat}, of Freon E1, E2, E3, E4 and E5 vs. temperature, T. From Filippi & Guerra (1977) [64].
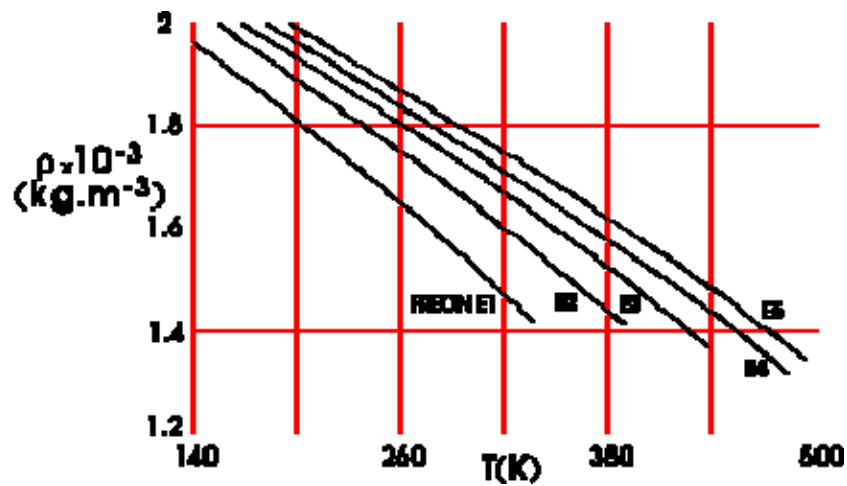
Figure 10-41: Density, ρ, of Freon E1, E2, E3, E4 and E5 vs. temperature, T. From Filippi & Guerra (1977) [64].
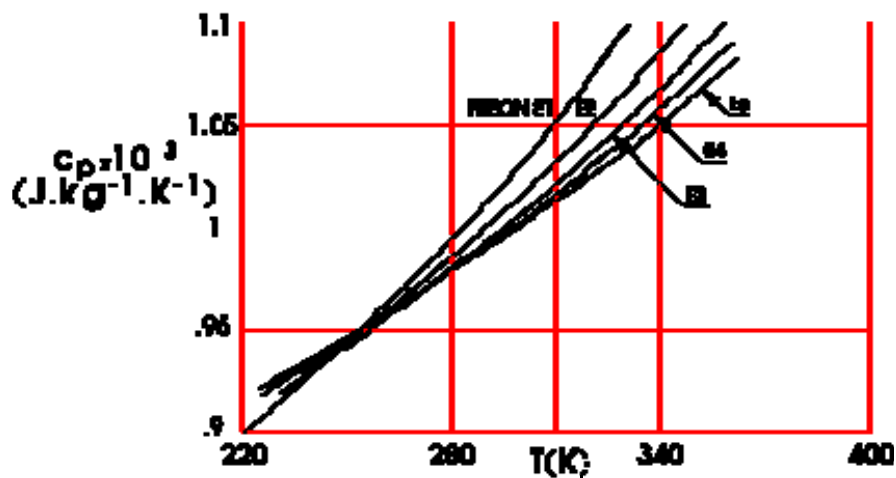
Figure 10-42: Specific heat, c_p, of Freon E1, E2, E3, E4 and E5 vs. temperature, T. From Filippi & Guerra (1977) [64].
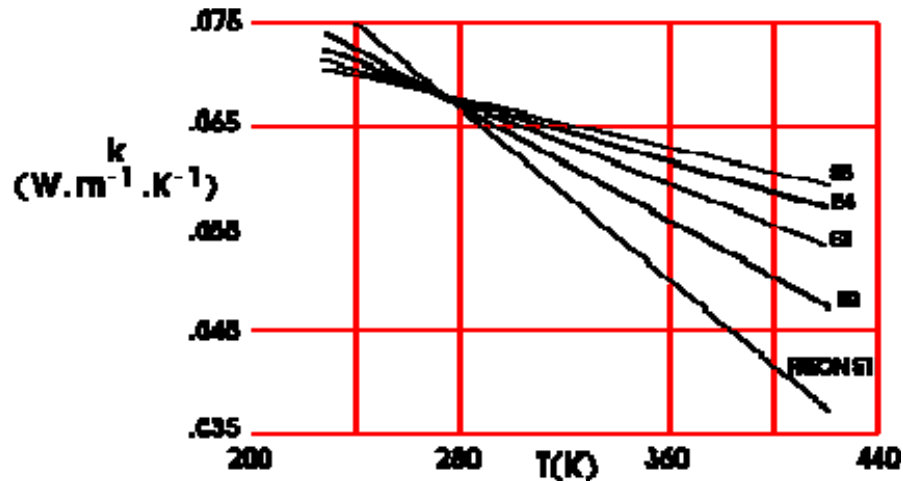
Figure 10-43: Thermal conductivity, *k*, of Freon E1, E2, E3, E4 and E5 vs. temperature, *T*. From Filippi & Guerra (1977) [64].
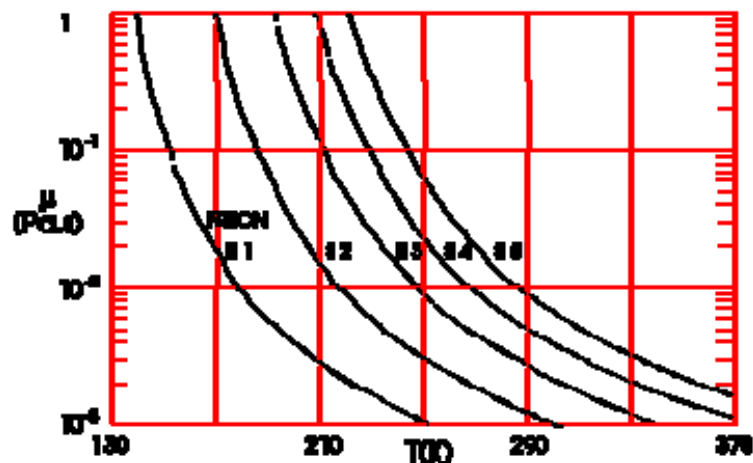
Figure 10-44: Dynamic viscosity, *μ*, of Freon E1, E2, E3, E4 and E5 vs. temperature, *T*. From Filippi & Guerra (1977) [64].
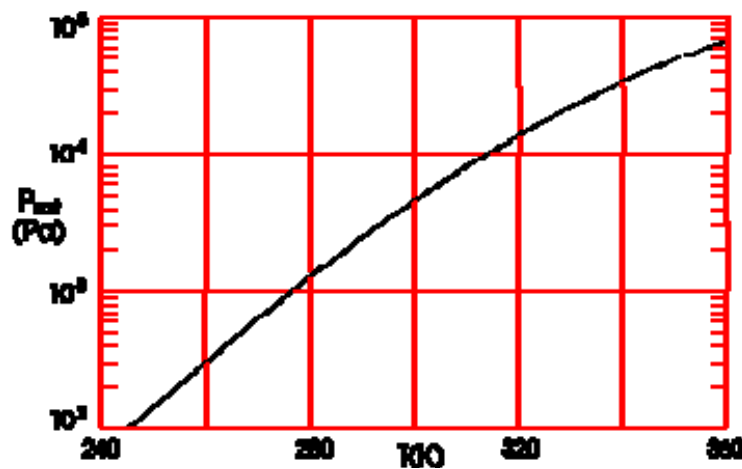
Figure 10-45: Vapor pressure, *p*$_{sat}$, of FC 75 vs. temperature, *T*. From Filippi & Guerra (1977) [64].
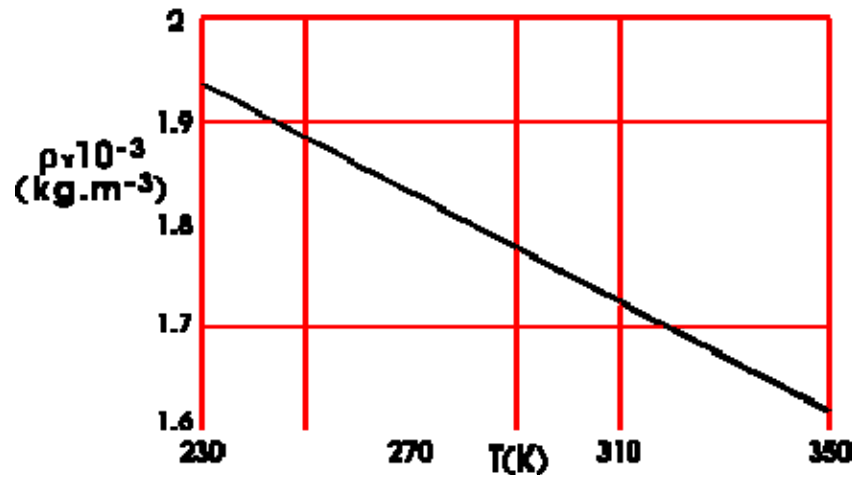
Figure 10-46: Density, ρ, of FC 75 vs. temperature, T. From Filippi & Guerra (1977) [64].
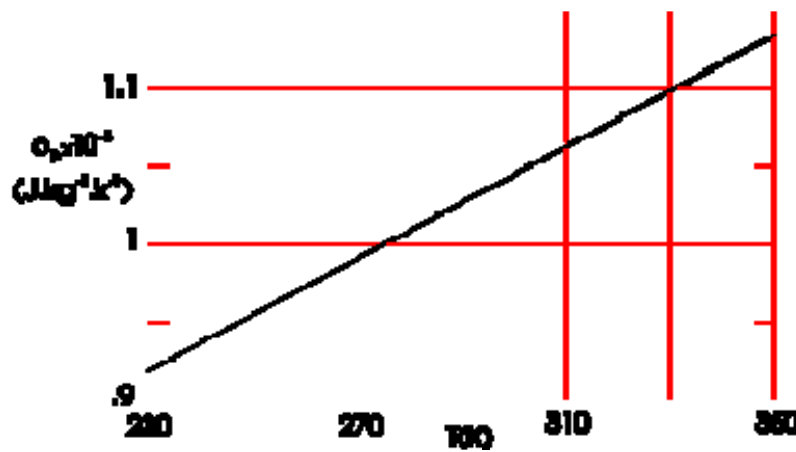
Figure 10-47: Specific heat, c_p, of FC 75 vs. temperature, T. From Filippi & Guerra (1977) [64].
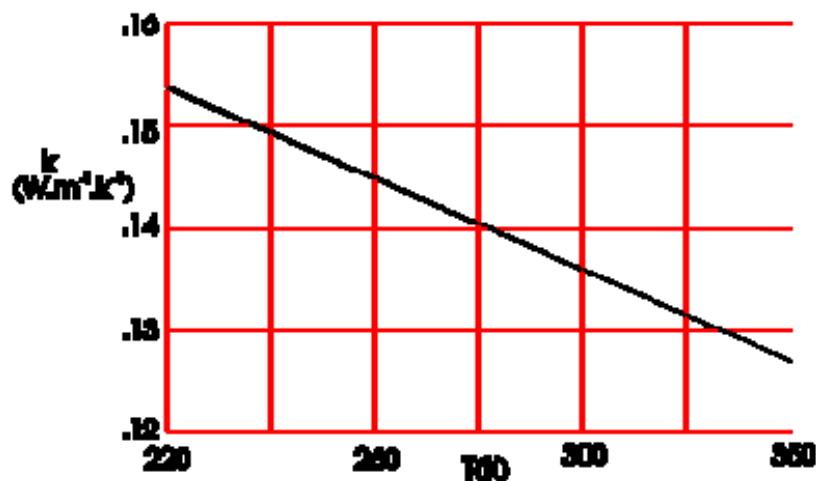
Figure 10-48: Thermal conductivity, k, of FC 75 vs. temperature, T. From Filippi & Guerra (1977) [64].
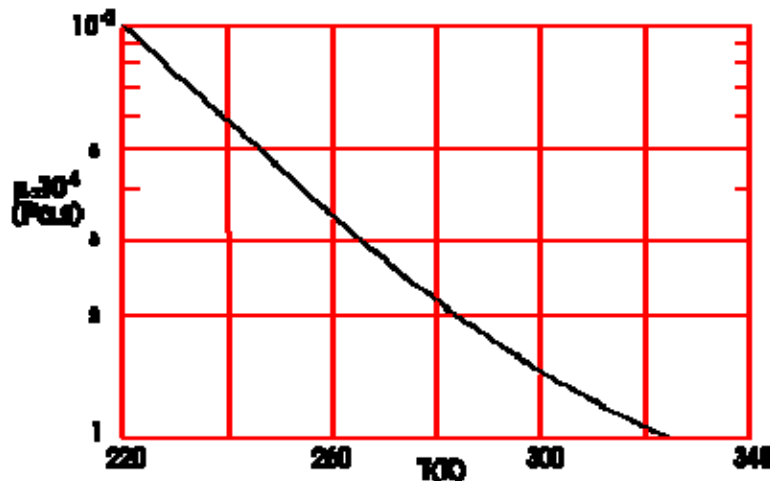
Figure 10-49: Dynamic viscosity, μ, of FC 75 vs. temperature, T. From Filippi & Guerra (1977) [64].
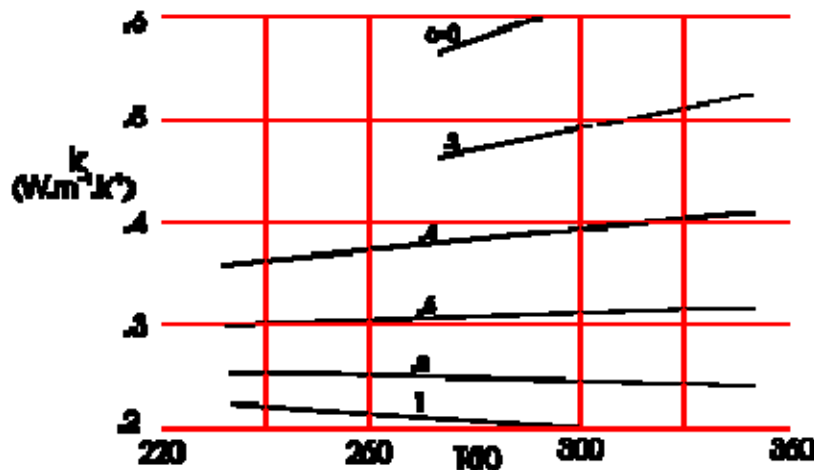
Figure 10-50: Thermal conductivity, k, of Methanol/Water Solutions vs. temperature, T. Numbers on curves indicate Methanol mass fraction, c. From Vargaftik (1975) [183].
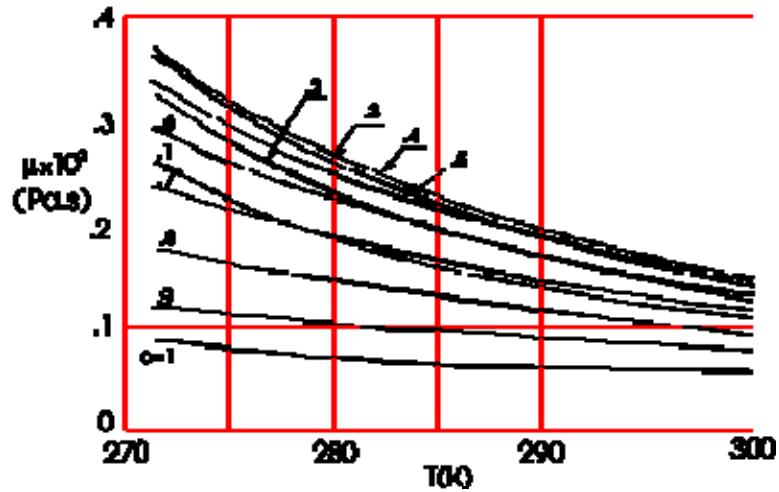
Figure 10-51: Dynamic viscosity, μ, of Methanol/Water Solutions vs. temperature, T. Numbers on curves indicate Methanol mass fraction, c. From Vargaftik (1975) [183].
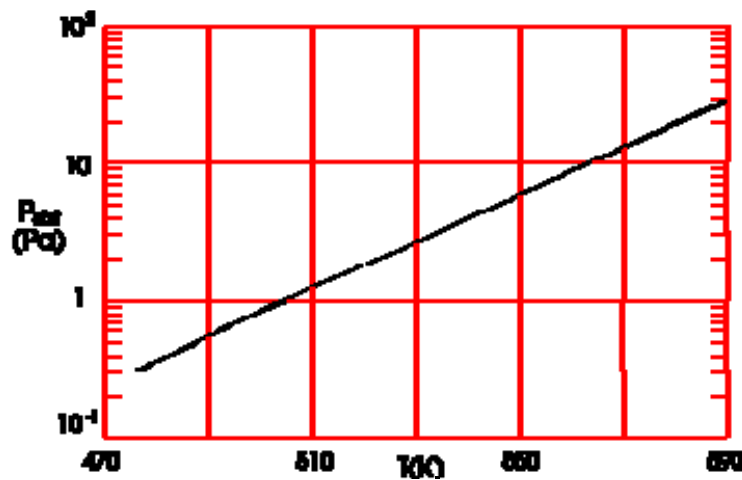
Figure 10-52: Vapor pressure, p_{sat}, of Monsanto OS 59 vs. temperature, T. From Filippi & Guerra (1977) [64].
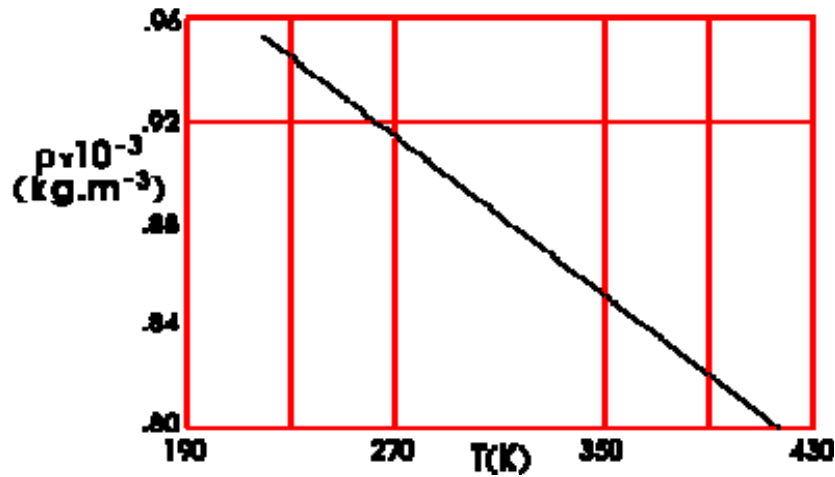
Figure 10-53: Density, ρ, of Monsanto OS 59 vs. temperature, T. From Filippi & Guerra (1977) [64].
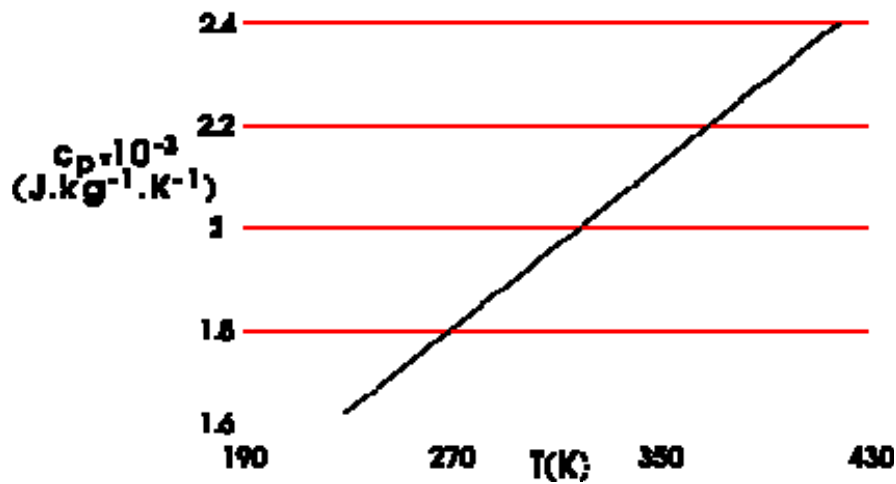
Figure 10-54: Specific heat, c_p, of Monsanto OS 59 vs. temperature, T. From Filippi & Guerra (1977) [64].
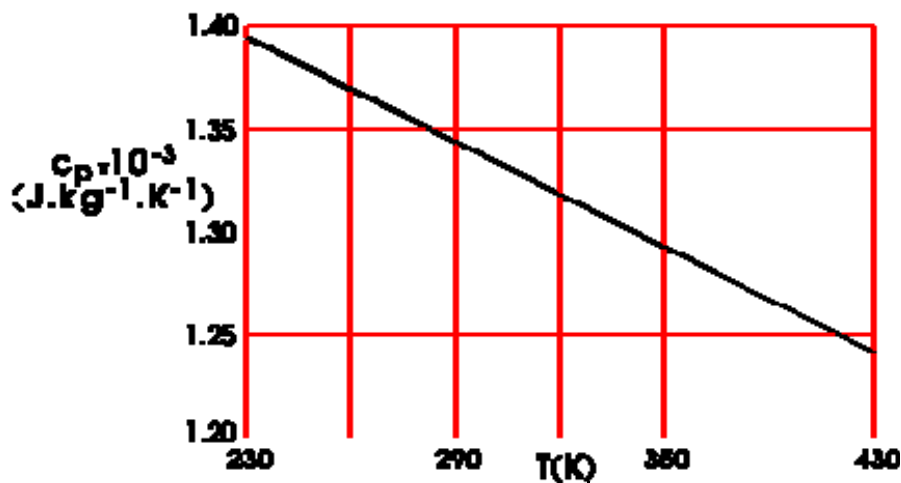
Figure 10-55: Thermal conductivity, k, of Monsanto OS 59 vs. temperature, T. From Filippi & Guerra (1977) [64].
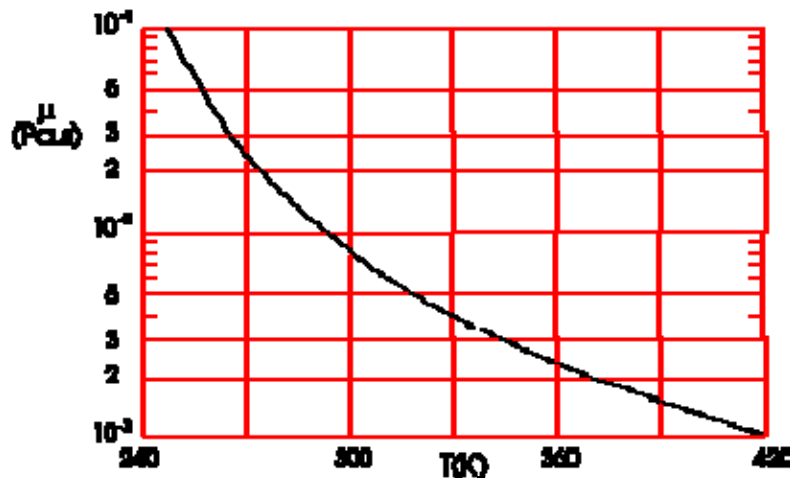
Figure 10-56: Dynamic viscosity, μ, of Monsanto OS 59 vs. temperature, T. From Filippi & Guerra (1977) [64].

Table 10-3: Properties of Dow Corning 200 Fluids (Dimethyl Siloxane Polymers)

Kinematic[a] Viscosity at 298 K, $v \times 10^6$ [$m^2 \cdot s^{-1}$]	Freezing Point [K]	Boiling Point [K]	Flash Point [K]	Density at 298 K, ρ [$kg \cdot m^{-3}$]	Specific Heat, c_P [$J \cdot kg^{-1} \cdot K^{-1}$]			Thermal Conductivity at 298 K, k [$W \cdot m^{-1} \cdot K^{-1}$]
					313 K	373 K	473 K	
0,65	205	373[c]	272	759				0,100
1	187	425[c]	311	816				
1,50	197	465[c]	336	851				0,105
2	189	343-373[d]	352	870				0,109
5	208	393-433[d]	408	917				0,117
10	173		436	931				0,134
20	189[b]		505	946	1457	1478	1516	0,142
50	203[b]		558	957				0,151
100	208[b]		588					0,155
200				967				
350					1403	1444	1478	0,159
500	223[b]			968				
1,000			594					
12,500	227[b]			972				
30,000	230[b]							
60,000	232[b]			973				
100,000	240[b]			974				

a   Numerals in this column of the table correspond to standard viscosity grades in cs (1 cs = 10^{-6} $m^2.s^{-1}$). These numerals are used to identify the various liquids in the Dow Corning 200 series.

b   Pour point (ASTM D 97-39, Sec. 5-7). Due to supercooling effects this test method yields values below the temperatures at which these fluids solidify when held at a given temperature for longer items.

c   At 10^5 Pa.

d   At 67 Pa.

NOTE   From Dow Corning (1963,1972) [37] & [38].

Table 10-4: Corrosion and Oxidation Text Data for Coolanol Liquids

Liquid		Coolanol 15		Coolanol 25		Coolanol 35		Coolanol 45	
Test [a]		A [b]	B [c]	A	B	A	B	A	B
Metal Weight Change [g.m-2]									
	Aluminium	+0,4		+0,1	+0,5	-0,2	+0,1	-0,1	+0,1
	Magnesium	+0,1		+0,2		-0,2		-0,1	
	Copper	+0,6		0	-24.	-0,2	-0,3	+0,5	0
	Silver				+0,3		0		0
	Steel	+0,4		+0,2	+0,2	-0,1	-0,2	+0,2	0
	Cadmium Plated Steel	+0,8		0		-0,1		+0,1	
Acidity [g of KOH per kg]									
	Initial			0,11	0,11	0,03	0,03	0,01	0,14
	Final			0,06	1,00	0,03	3,00	0,01	0,81
Kinematic Viscosity at 328 K									
$v \times 10^6$ [m².s-1]	Initial			3,19	3,12	4,46	4,21	8,44	8,51
	Final			3,27	5,71	4,54	8,39	8,63	9,05
	Increase [percent]			1,9	83,0	1,8	99,0	2,3	5,8
Total Fluid Weight Loss [percent]				1,8	13,5	2,8	13,0	<1	<10

[a]   Test were made as indicated in the following Table (A and B refer to code in Table 10-4).

Code	Exposure Time [h]	Temperature [K]	Air Flow Rate [m³.s-1]	Specification
A	168	394	1,389	MIL-H-5606
B	72	478		MIL-H-8446

[b]   Coolanol 15 is thermally stable at 394 K, and may be used in typical circulating systems. However, in this test, when exposed to a purge of air at this temperature, it can vaporize, oxidize and perhaps gel.

[c]   Coolanol 15 is not recommended for continuous use at 478 K.

NOTE   From Filippi & Guerra (1977) [64].

Table 10-5: Toxicity of Several Freon Liquids

Liquid	Maximum Concentration	Group	Toxicity Rate [a]
			Definition
Freon 11		5a	6. Gases or vapors which in concentrations up to at least about 20% by volume and durations of exposure at the order of 2 h do not appear to produce injury.
Freon 12	500 mg.m^{-3}	6	
Freon 13		6	5a. Gases or vapors much less toxic than Group 4 but more toxic than Group 6.
Freon 21	420 mg.m^{-3}	4 & 5	
Freon 22		5a	4 & 5. Much less toxic than Group 4 but somewhat more toxic than Group 5.
Freon 113		4 & 5	4. Gases or vapors which in concentrations of the order of 2 to 2,5% and durations of exposure of the order of 2 h are lethal or produce serious injury.
Freon 114	500 mg.m^{-3}	6	

[a]   The criterion for evaluating the toxicity is that employed by Underwriters Laboratories of Chicago. According to this criterion the fluids are divided into 6 categories ranging from Group 1 (most toxic fluids) to Group 6 (least toxic fluids). The characterization of the groups involved is given in the above table under Definition.

NOTE   From Filippi & Guerra (1977) [64].

Table 10-6: Swelling of Elastomers in Several Freon Liquids [a]

Liquid / Elastomer	Freon 11	Freon 12	Freon 13	Freon 21	Freon 22	Freon 113	Freon 114	Freon 142
Buna N (butadiene-acrylo-nitrile)	6	2	1	48	26	1	0	3
Buna S (GR - S) (butadiene-styrene)	21	3	7	49	4	9	2	4
Butyl (GR - I)	41	6	0	24	1	21	2	3
Hypalon 40 [b] (chlorosulphonatedpolyethylene)	3	1	1	24	3	1	1	4
Natural Rubber	23	6	1	34	6	17	2	5
Neoprene GN [b]	17	0	0	28	2	3	0	3
Neoprene W	9	-1	3	11	0	1	0	0
Polyvinyl Alcohol	0	-8	-1	9	6	-1	-2	-3
Thiokol FA (polysulfide)	2	1	0	28	4	1	0	1
Viton A (PV$_n$F) [b]	4	10	3	26	37	-	-	25
Viton B (PV$_n$F) [b]	6	9	4	22	28	7	9	29
Silicone Rubber	38	-	-	-	20	34	-	-
Urethane Rubber	20	5	-	-	28	7	-	-

[a]   Numbers in the Table indicate percent increase in length at room temperature.

[b]   Manufactured by E.I. DuPont de Nemours & Co., Inc.

NOTE   From Filippi & Guerra (1977) [64].

Table 10-7: Compatibility of Freon E2 and FC-75 with Elastomers [a]

Elastomers	Liquid	Swelling Change [Percent]	Tensile Strength, σ x 10^{-4} [Pa]		
			Before exposure	After exposure	Change [Percent]
Buna N	Freon E2	+2,3	11,92	13,17	+10,5
	FC - 75	+0,7		12,19	+2,6
Viton A [b]	Freon E2	-0,3	10,48	9,72	-7,3
	FC - 75	-0,7		9,84	-6,1

[a]   Numbers in the Table indicate swelling and tensile strength changes after 100 h exposure.

[b]   Manufactured by E.I. DuPont de Nemours & Co., Inc.

NOTE   From Filippi & Guerra (1977) [64].

Table 10-8: Compatibility of Freon E3 with Elastomers, Plastics and Wire Coatings [a]

Elastomers	Test [b]		Plastics	Test [b]		Wire Coatings	Test [b]	
	327 K	425 K		327 K	425 K		377 K	425 K
Adiprene C (Urethane Rubber)	1	5	Alathom 7050 [c] (Polyethylene Resin)	1	5	Acrylex (Acrylic)		6
Adiprene L (Urethane Rubber)	1	3	Alathom 9140 [c] (Polyethylene Resin)	1	1	Alkanex (Terephthalate Polyester)		6
Buna N	1	5	Delrin (Acetal Resin)	1	3			
Buna S	1	4	Ethyl Cellulose	2	5	Anavar (Isocyanate-Modified Polyvinyl Formal)		6
Buthyl	2	2	G - 10 - 3675 (Epoxy Resin)	1	3			
Hypalon 40 [c] (Chlorosulfon.Polyethyl.)	2	5	Kralastic [d] (ABS Polymer)	1	5	Ensolex (Acrylic)		6
Natural Rubber	1	2	Lexan [e] (Polycarbonate Resin)	1	2	Epoxy		6
Neoprene W	1	2	Lucite [c] (Acrylic Resin)	1	1	Formvar [f] (Polyvinyl Formal)	7	8
Nordel (Hydrocarbon Rubber)	1	3	Polyvinyl Alcohol	2	3	Nylclad (Nylon-Coated	7	8
NSR - X5602 (Nitrile	1	5	Polyvinyl Chloride	1	4			

Elastomers	Test [b]		Plastics	Test [b]		Wire Coatings	Test [b]	
	327 K	425 K		327 K	425 K		377 K	425 K
Silicone Rubber)			(Unplasticized)			Polyvinyl Formal)		
Silastic 50 (Silicone Rubber)	1	2	Styron 457 (Polystyrene)	1	5	Plain Enamel (Oleoresinous)	7	8
Thiokol FA(Polysulfide)	1	5	Teflon [c] (Tetrafluoroethylene)	1	2			
Viton A [b] (Fluoroelastomer)	1	2	Zitel 101 (Nylon Resin)	1	3			

1	Suitable for use	5	Material disintegrates or dissolves in the liquid	7	Very slight crazing, stress cracking, bucling and/or temporary softening of material		
2	Probably suitable for use						
3	Probably not suitable for use	6	No crazing, stress cracking, buckling and/or temporary softening of material	8	Severe crazing, stress cracking, buckling and/or temporary softening of material		
4	Not suitable for use						

NOTE   From Filippi & Guerra (1977) [64].

[a]   Numerals in this Table indicate test ratings according to the score in the second table.

[b]   Test were performed at quoted temperatures for 100 h.

[c]   Manufactured by E.I. DuPont de Nemours & Co., Inc.

[d]   Acrylonitrite Butadiene Styrene. Manufactured by United States Rubber Co., Naugatuck Chemical Div.

[e]   Manufactured by General Electric Company, Chemical Materials Dept.

[f]   Manufactured by Shawinigan Resins Corp.

Table 10-9: Compatibility of Oronite Flo-Cool 100 with Elastomers

Elastomer	Swelling Change [Percent]	Weight Change [Percent]	Tensile strength, σ x 10⁻⁴ [Pa]			Compression Set [Percent]	Cross Sectional Area Change [Percent]
			Before exposure	After exposure	Change [Percent]		
Buna - N	-0,2 [a]		11,92	9,95 [a]	-16,5	9,7 [b]	
Buthyl Rubber B 318 - 7	+5,3	+31.	10,31	8,16	-20,8	19,8	10.
Ethylene - Propylene E 515 - 8	+0,4	+27,9	11,40	12,04	+5,6		8.
Fluorosilicone L 308 - 8		+3,7	5,12	5,88	+14,8	12,6	2,9
Fluorosilicone L 608 - 6		+4,6	8,25	5,86	-29.	6,2	2.
LCS Fluorocarbon(per MIL - R - 83248)		+0,02	12,84	12,82	-0,02	10,6	0,1
Neoprene C 294 - 6		-1,2	16,28	9,60	-41,1	12,7	0
Neoprene C 526 - 7		+1.	18,37	7,32	-60,2	8,1	0,5
Silicone 5418 - 6	+13,2	+117,4	5,44	3,53	-35,1		45,7
Silicone 5604 - 7	+26,4	+65,6	6,76	6,06	-10,3		27.
Viton - A	+1,1 [a]		10,48	9,98 [a]	-4,8	63,6 [c]	

NOTE   All data in this Table, unless otherwise stated, have been obtained after 30 d exposure.

From Filippi & Guerra (1977) [64].

[a]   After 7 d exposure.

[b]   After 14 d exposure.

[c]   After 19 d exposure.

10.4 Properties of dry air
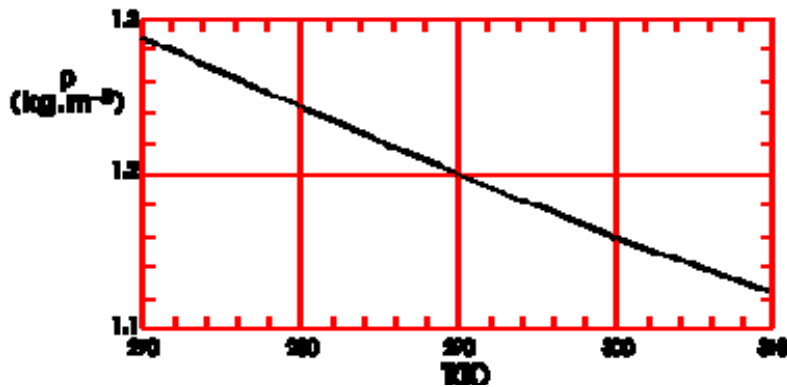
Figure 10-57: Density, ρ, of Air at a pressure of 10^5 Pa vs. temperature, T. From Vargaftik (1975) [183].
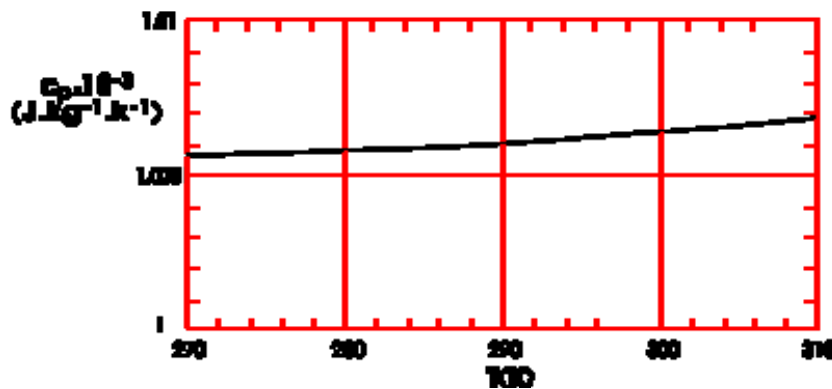
Figure 10-58: Specific heat, c_p, of Air vs. temperature, T. From Vargaftik (1975) [183].
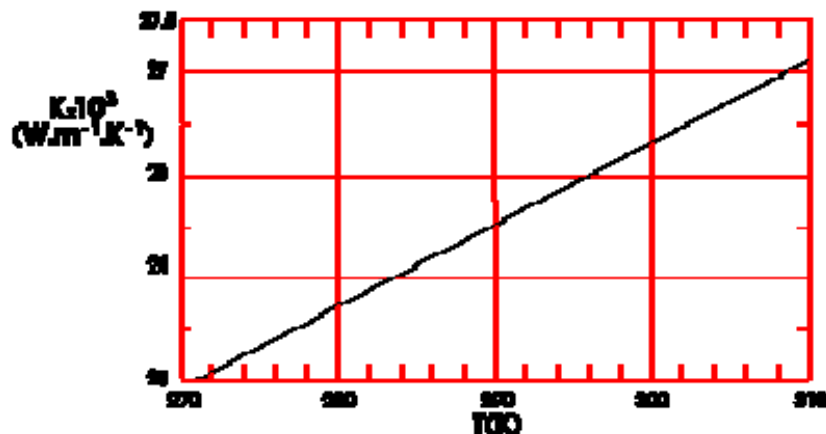
Figure 10-59: Thermal conductivity, k, of Air vs. temperature, T. From Vargaftik (1975) [183].
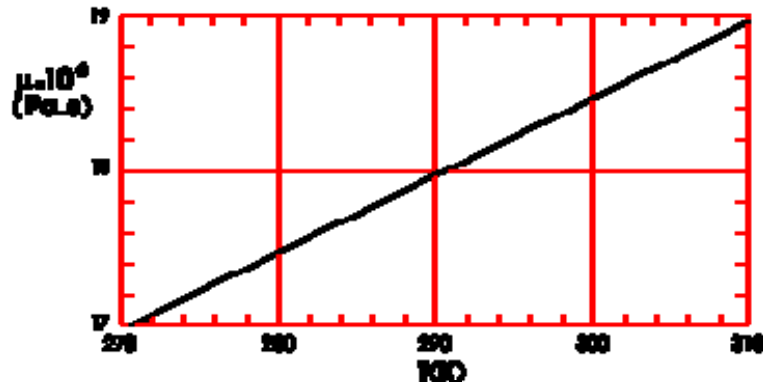
Figure 10-60: Dynamic viscosity, *μ*, of Air vs. temperature, *T*. From Vargaftik (1975) [183].

11
Heat exchangers

11.1 General

Heat exchangers are devices whose primary purpose is the transfer of energy between two fluids. Among the different types of heat exchangers, regenerators and recuperators are those most commonly used in the aerospace industry.

Periodic-Flow Type Exchangers or Regenerators are exchangers in which the hot and cold fluids flow alternatively through the same matrix surface with as little physical mixing between the two streams as possible. The amount of energy transfer depends on the properties of the fluid streams, as well as on the geometry and thermal properties of the matrix surface. Two types of regenerators are shown in Figure 11-1.
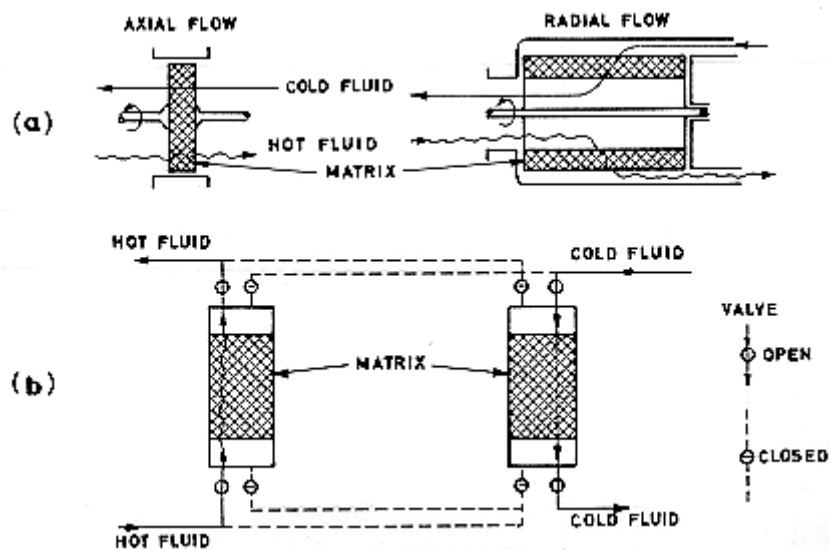
Figure 11-1: Typical regenerators. a) Rotary type. b) Valved type. From Kays & London (1964) [102].

Closed-Type Exchangers or Recuperators are exchangers in which hot and cold fluid are separated by a tube wall or some kind of surface. Energy exchange is thus accomplished from one fluid to a surface by convection, through the wall or plate by conduction and then by convection from the surface to the second fluid (Figure 11-2).
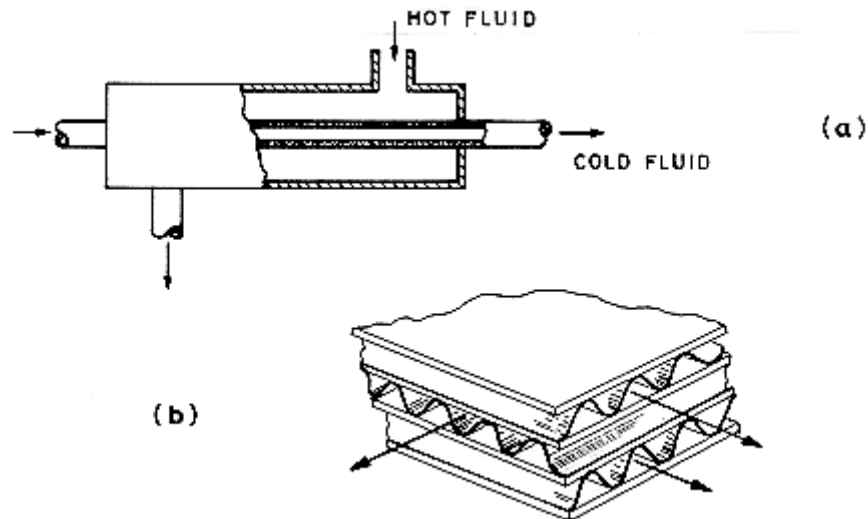
Figure 11-2: Typical recuperators. a) Counterflow heat exchanger. b) Crossflow heat exchanger. From Welty, Wicks & Wilson (1969) [188].

Recuperators are of primary importance in practice and therefore, the present review is mainly concerned with the study of this type of exchangers.

Recuperators are usually classified according to their configuration and the number of passes made by each stream as it traverses the heat exchangers. Single-pass heat exchangers are those in which the fluid flows through the exchanger only once. Depending on the relative directions of the two streams the single-pass heat exchangers are divided in parallel flow, counter-flow and crossflow heat exchangers. A multipass heat exchanger is one in which the fluid flows through the exchanger more than once. Multipassing allows a large variety of arrangements.

For most heat transfer surfaces used in heat exchangers, the heat transfer rate per unit of surface area increases with the fluid flow velocity, and this rate varies as something less than the first power of the velocity. The friction power expenditure also increases with fluid-flow velocity, but in this case the exponent of the velocity dependence varies between two and three.

Pumping power limitations generally force the designer of the heat exchanger to use low velocities; therefore the heat transfer rate tends to be low, and large heat transfer surfaces are required. To accomplish as much heat transfer in as little space as possible, it is necessary to construct exchangers with large surface area densities (surface area density is the ratio of total heat transfer area to total exchanger volume). Exchangers with large surface area densities are known as compact heat exchangers.

Several typical compact heat transfer surface arrangements are shown in Figure 11-3. It is observed that an effective way to increase surface area density is to use fins in one or both fluid sides of the surface as is shown in Figure 11-3b. To accomplish large area density on both fluid sides of the surface, the plate-fin arrangement shown in Figure 11-3d may be used. In this arrangement the exchanger is built up as a sandwich of flat plates bonded to interconnecting fins. The two fluids are carried between alternate pairs of plates and can be arranged in either counter-flow or crossflow, which provides an added degree of flexibility. The strip-fin surfaces shown in Figure 11-3e exhibit very high heat transfer rates because of the short flow length associated to each fin, thus preventing the thickening of the viscous layer.
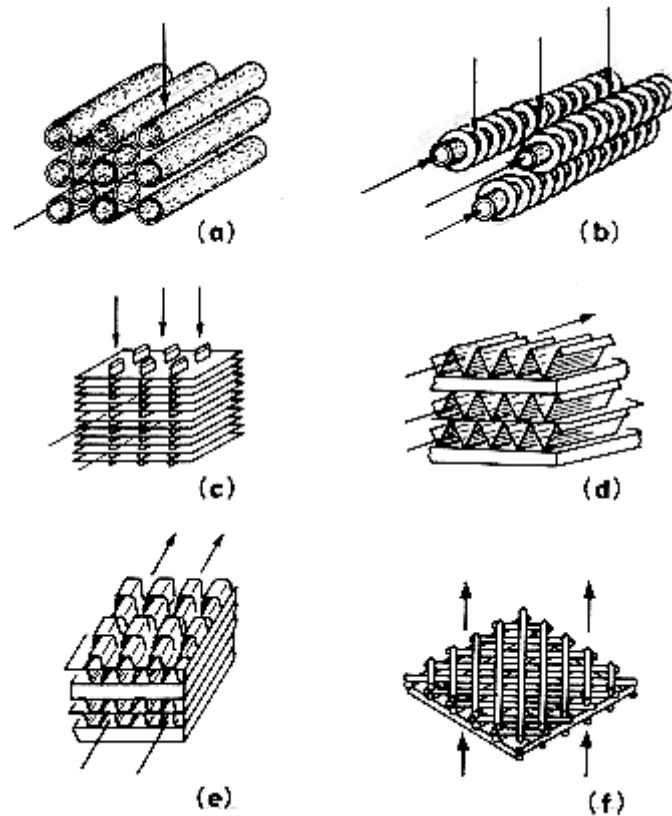
Figure 11-3: Some typical examples of compact heat exchanger surfaces. From Kays & London (1964) [102]. a) Circular tube bundle. b) Finned-circular-tube surface. c) Finned-tube surface, flat tubes, continuous fins. d) Plate-fin arrangement. e) Strip-fin surface. f) Regenerator compact matrix.

Other procedures to enhance heat transfer are discussed in Clause 9.

To accomplish as much energy transfer in as little space as possible, it is desirable to utilise multiple passes of one or both fluids. A multipassing configuration, which is commonly used for commercial and general process applications, is the shell-and-tube exchanger shown in Figure 11-4. In this particular case, the shell fluid goes through two shell passes and the tube fluid flows through six tube passes. Good mixing of the shell-side fluid is accomplished with the baffles shown, which prevent the formation of stagnant regions.
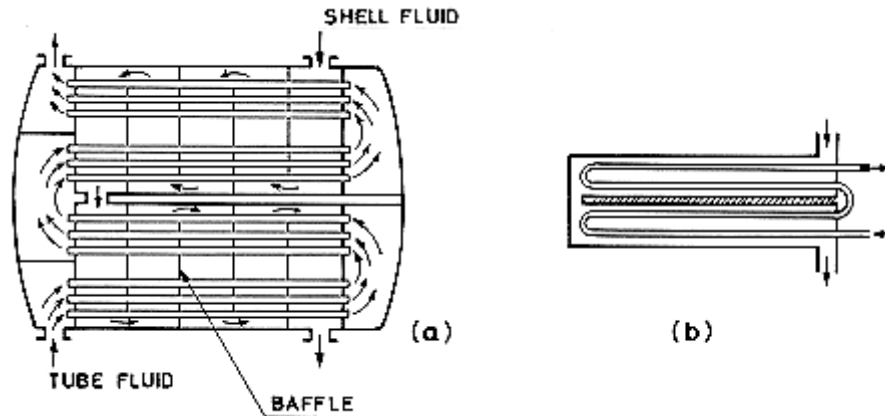
Figure 11-4: a) Shell-and-tube exchanger with two shell passes and four tube passes. b) Schematic representation of the exchanger which will be used in clause 11.2.3.

Sometimes several exchangers are connected together in series, in parallel or in series-parallel, to achieve heat-transfer rate. Another useful arrangement is the liquid-coupled indirect heat exchanger, which consists essentially of two recuperators coupled with a pumped heat transfer medium as shown in Figure 11-5. With this arrangement the circulating transfers thermal energy from the hot fluid to the cold fluid. The coupling liquid capacity rate (mass flow times specific heat), which is an independent variable, can be chosen to optimise system performance.
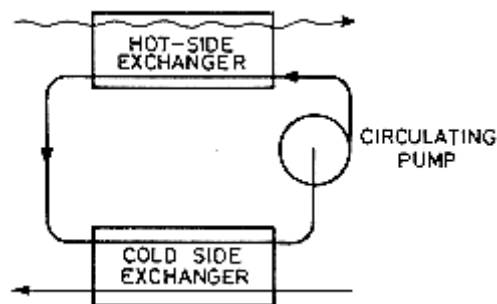
Figure 11-5: Liquid-coupled indirect-transfer type of heat exchanger. From Kays & London (1964) [102].

11.2　Basic analysis

11.2.1　Introduction

The purpose of this clause is to summarise exchanger heat transfer performance theory. The designer uses this theory, in conjunction with the basic data reported in Clauses 6 to 9, to approximately size the heat exchanger for a specified heat transfer rate and pressure drop.

The problem of optimising the heat exchanger design in a fluid loop, is a complex problem in which many qualitative judgements are introduced. Although no attempt is made to outline hear an

optimisation analysis, the present theory provides basic relationships that may be used in optimizing the design on the basis of any criterion previously selected (see Clause 13).

The equations which appear in the following clauses concern closed-type exchangers or recuperators of either the conventional direct-transfer type or of the liquid-coupled indirect-transfer type. The methodology used can, however, be extended with only minor changes to periodic-flow type exchangers or regenerators.

11.2.2 Analytical background

The heat flux, q, per unit transfer area at a certain section in the exchanger is expressed in terms of an overall thermal conductance, U, as follows:

$$q = U(T_h - T_c)$$ [11-1]

U includes the convective and conductive mechanisms which are responsible for the heat transfer from the hot to the cold fluid. The reciprocal of U is an overall thermal resistance which presents the following series components:

1. A hot-side film-convection component, which includes the temperature ineffectiveness of the extended surface or fin area on this side.

2. A wall-conduction component.

3. A cold-side film-convection component, which includes the temperature ineffectiveness of the extended surface or fin area on this side.

According to this idea U can be expressed either as:

$$\frac{1}{U_h} = \frac{1}{\eta_h h_h} + \frac{a}{(A_w / A_h)k} + \frac{1}{(A_c / A_h)\eta_c h_c}$$ [11-2]

when U is based on a unit of hot-side total area (including the extended area), or as:

$$\frac{1}{U_c} = \frac{1}{\eta_c h_c} + \frac{a}{(A_w / A_c)k} + \frac{1}{(A_h / A_c)\eta_h h_c}$$ [11-3]

when it is based on a unit of cold-side total area. Obviously $U_h A_h = U_c A_c$.

In these equations:

A_w is the average wall area. If no extended surfaces are used then $A_w \cong (A_h + A_c)/2$.

a is the wall thickness.

k is the wall thermal conductivity. Values of k for several common materials are given in Figure 11-6.
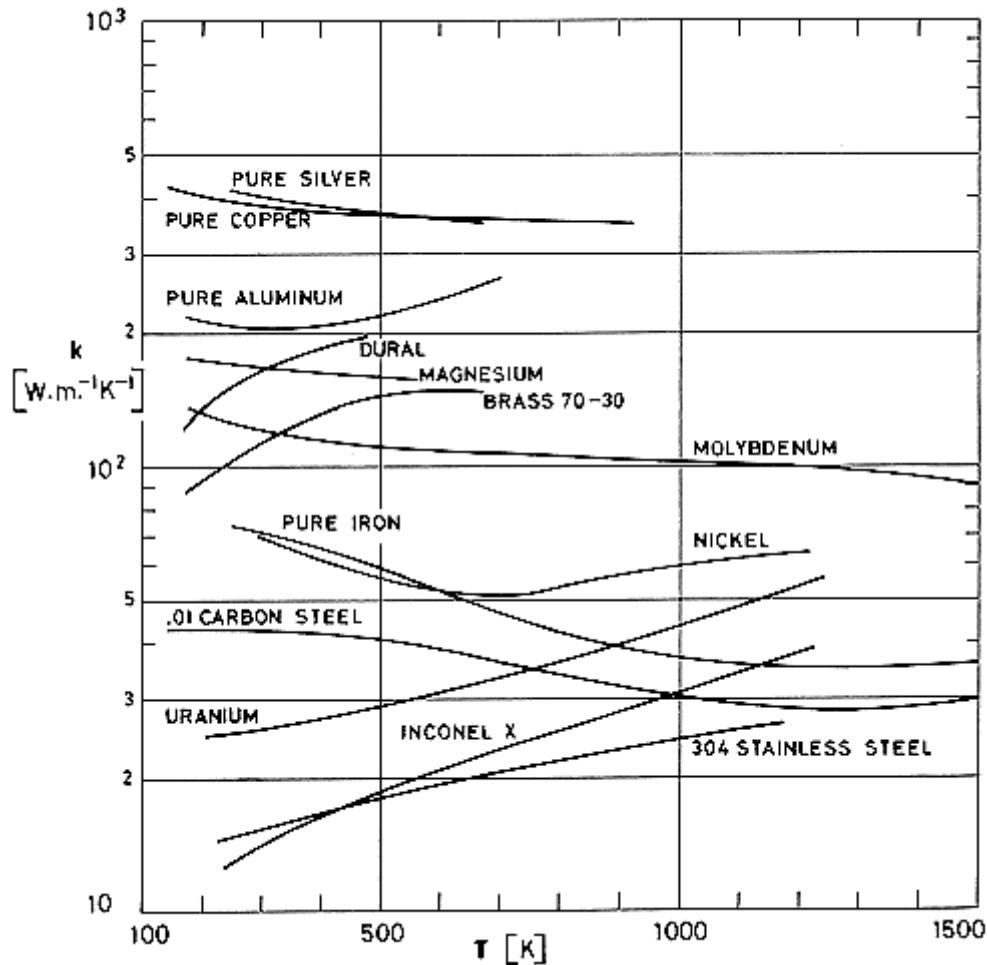
Figure 11-6: Thermal conductivity, *k*, of several metals vs. temperature, *T*. From Kays & London (1964) [102].

η_h and η_c denote the temperature effectiveness of the total area A_h and A_c, respectively due to the presence of fins. The temperature along the fin is not equal to that existing at the surface, thus reducing the effectiveness of the surface. In the absence of extended surfaces η is unity, otherwise it is a weighted average of the 100% effectiveness of the surface and the effectiveness of the fin surface.

$$\eta = 1 - \frac{A_f}{A}\left(1 - \eta_f\right)$$

[11-4]

The parameter η_f is the fin effectiveness defined as the ratio of the amount of heat actually evacuated through the fin to that which would be evacuated if the fin surface were held at the temperature of the fin base. Values of η_f versus the dimensionless film length are given in Figure 11-7 and Figure 11-8. When the fin extends from wall to wall, the effective length, *L*,is taken as half the spacing between walls.
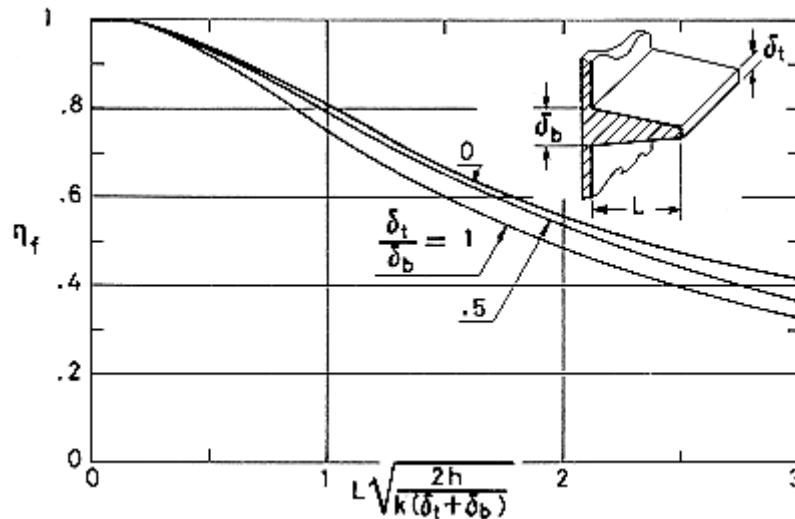
Figure 11-7: Heat transfer effectiveness, η_f, of trapezoidal fins, vs. dimensionless fin length, $L[2h/k(\delta_t+\delta_b)]^{1/2}$. Calculated by the compiler after Jakob (1958) [99].
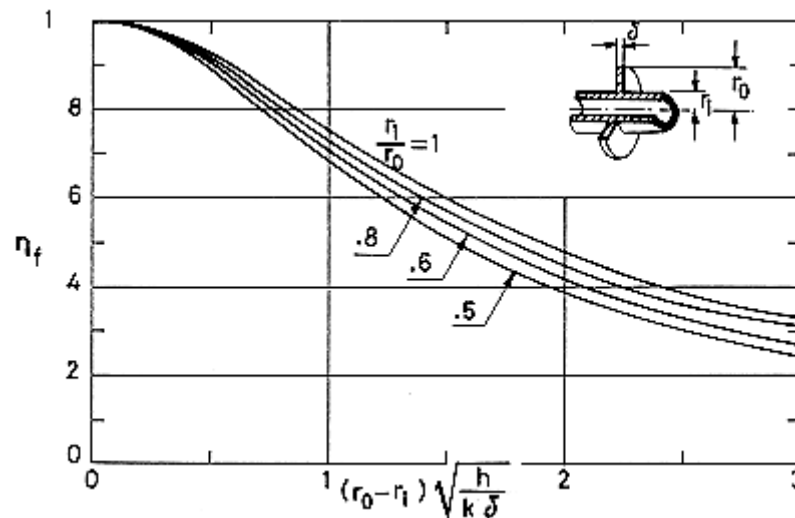
Figure 11-8: Heat transfer effectiveness, η_f, of circular fins, vs. dimensionless fin length, $(r_o-r_i)(h/k\delta)^{1/2}$. Calculated by the compiler after Jakob (1958) [99].

h_h, h_c are convective heat transfer coefficients. Clause 6 presents data to compute their values for most practical configurations.

The heat transfer rate equation (Eq. [11-1]) is combined with an energy equation equating the loss of enthalpy of the hot fluid to the gain of enthalpy of the cold fluid, so as to relate the different variables of the exchanger. To obtain the solution to this equation in a convenient form, it is useful to introduce the following non-dimensional variables:

1. The capacity rate ratio, R,

$$R = \frac{C_1}{C_2}$$

[11-5]

where C_i (i = 1,2) is the mass flow rate times specific heat for the stream i. Subscript 1 will be always assigned to the stream with lower C.

2. The heat transfer effectiveness, ε,

$$\varepsilon = \frac{Q}{Q_{max}} = \frac{T_{1i} - T_{10}}{T_{1i} - T_{2i}} = \frac{T_{2i} - T_{20}}{R(T_{2i} - T_{1i})} \qquad [11\text{-}6]$$

ε is the ratio of the actual heat transfer rate to the thermodynamically-limited maximum rate, obtained only in a counterflow exchanger of infinite transfer area. Thus, ε is the exchanger thermodynamic effectiveness.

3. The number of exchanger heat transfer unit, N_{tu},

$$N_{tu} = A\overline{U} / C_1 = \int_{o}^{A} U dA / C_1 \qquad [11\text{-}7]$$

where A is the transfer area used in the definition of U. N_{tu} is a non-dimensional expression of the "heat transfer size" of the exchanger. For small N_{tu}, the exchanger effectiveness is low. When N_{tu} increases, the effectiveness, ε, approaches asymptotically the limit imposed by flow arrangement and thermodynamic considerations.

In general the solution to the energy equation yields

$$\varepsilon = t\left(N_{tu}, R, \text{flow arrangement}\right) \qquad [11\text{-}8]$$

11.2.3 Exchanger performance

This clause presents data to solve Eq. [11-8] for several flow arrangements used in practice. These data are intended as illustrative cases. The user should resort to additional references when the particular arrangement of its interest is not included here.

Most of the figures which appear in the following pages relate ε to N_{tu}. As a general rule ε increases with N_{tu} for a given capacity rate ratio. The data presented, however, show the asymptotic character of this increase and, thence, the design engineer is confronted with the costs of attaining a large N_{tu} in terms of capitalisation, size, mass and power requirements. Since this clause deals only with the thermal aspect of the problem, no data on which the estimate of these costs could be based are reported here.

Figure 11-9 shows the ε-N_{tu} relationship for a counterflow configuration. The effectiveness, ε, approaches unity for large values of N_{tu}, no matter the value of the capacity rate ratio, R. Note that the smaller the capacity rate ratio, the higher the effectiveness for a given N_{tu}.
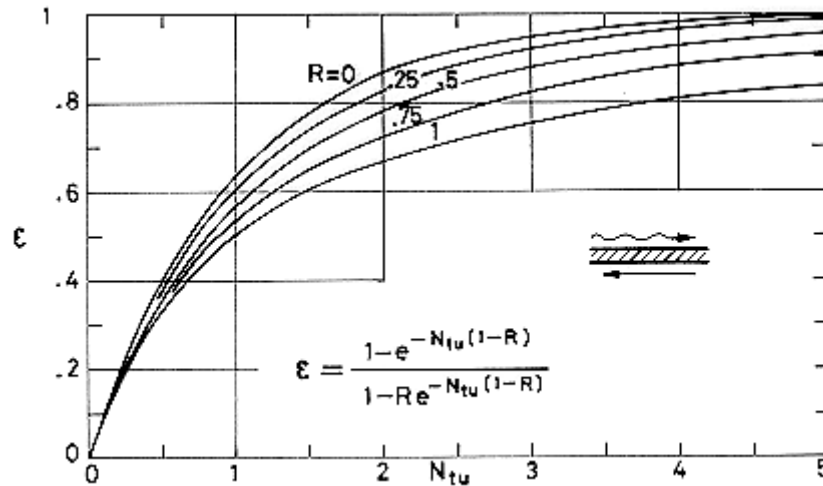
Figure 11-9: Heat transfer effectiveness, ε, vs. number of heat transfer units, N_{tu}, in a counterflow exchanger. From Kays & London (1964) [102].

The parallel flow case is considered in Figure 11-10. Now the asymptotic value for effectiveness is less than unity, except for $R = 0$. Obviously the maximum effectiveness is reached when the exit temperatures of both flow streams become identical. For $R = 1$, the maximum achievable effectiveness in parallel flow is only 0,5.
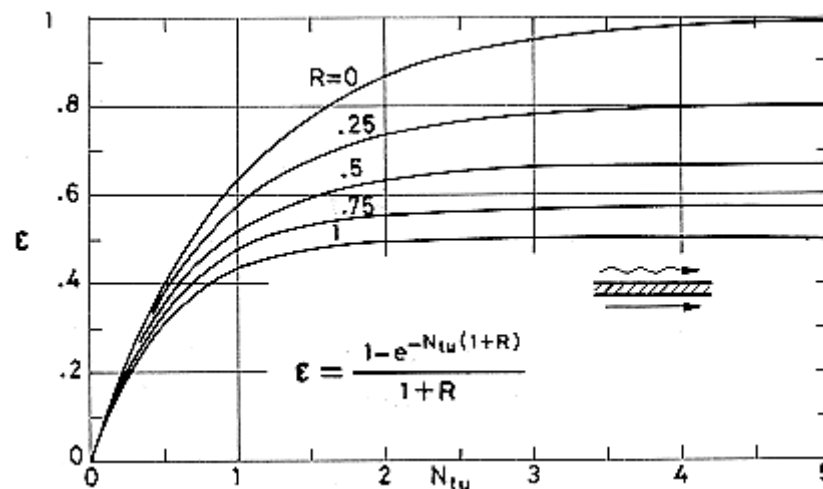
Figure 11-10: Heat transfer effectiveness, ε, vs. number of heat transfer units, N_{tu}, in a parallel flow exchanger. From Kays & London (1964) [102].

Figure 11-11 and Figure 11-12 are for crossflow arrangements. Now the results depend on whether or not cross mixing is allowed. In the case considered in Figure 11-11 it is assumed that each one of the two fluid streams has been broken up into a large number of separate flow tubes with no cross mixing. The resulting effectiveness is based on the mixed-mean temperatures of the outlet fluids, i.e., the temperature which the fluid, passing the cross-sectional exit area of any tube per unit time, would have if collected and perfectly mixed with those fluids leaving the other tubes in the same time interval.
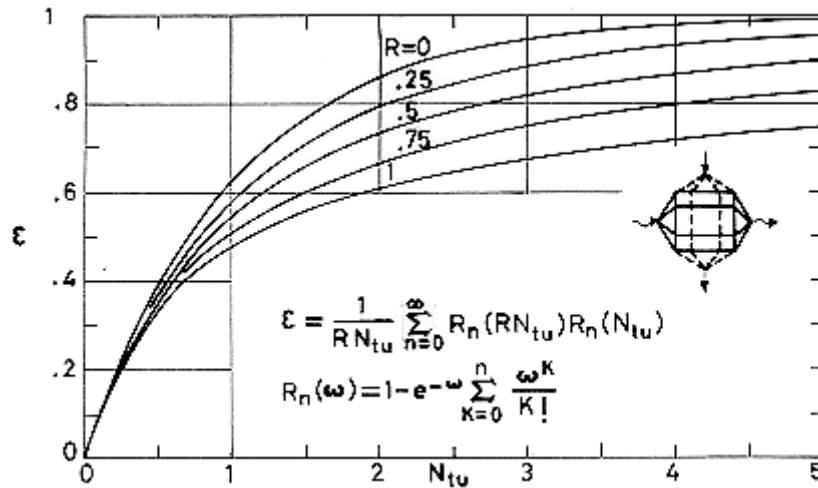
Figure 11-11: Heat transfer effectiveness, ε, vs. number of heat transfer units, N_{tu}, in a crossflow exchanger with fluids unmixed. Calculated by the compiler after Mason (1954) [124].
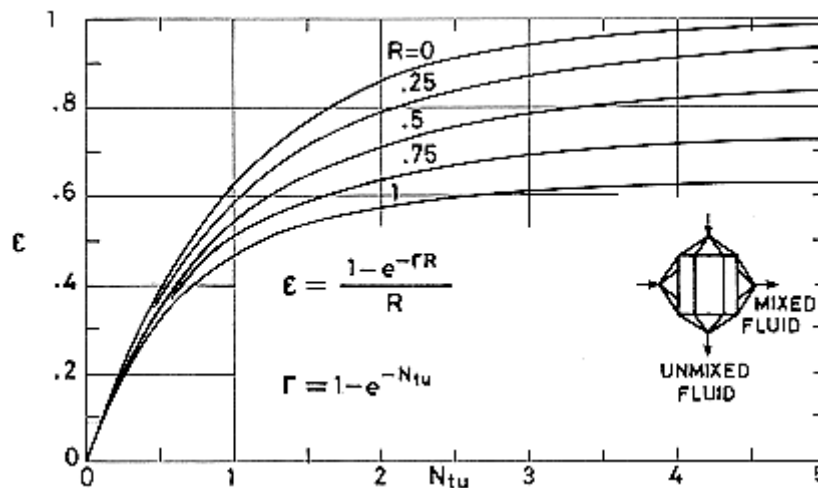
Figure 11-12: Heat transfer effectiveness, ε, vs. number of heat transfer units, N_{tu}, in a crossflow exchanger with one fluid mixed. From Kays & London (1964) [102].

In Figure 11-12 it is assumed that one stream is perfectly cross mixed, so that its temperature is uniform on sections normal to flow direction.

The case when both fluids are mixed can be found in Kays & London (1964) [102].

It is to be noted that for the limiting value $R = 0$, the results in all the cases mentioned are the same, indicating that the flow arrangement is irrelevant when one capacity rate is much larger than the other.

It is usual to characterise the different crossflow arrangements by means of sketches similar to those shown below.

BOTH FLUIDS UNMIXED   FLUID A MIXED FLUID B UNMIXED   BOTH FLUIDS MIXED
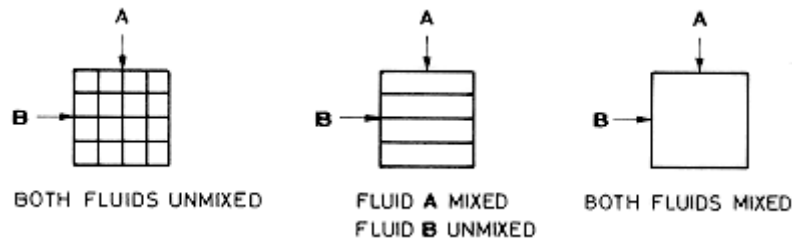
Multipass crossflow exchangers are extensively used in the aerospace industry. Nearly all of the exchangers using the so called compact heat exchanger surfaces are of this type.

Stevens, Fernández & Woolf (1957) [170] have analysed these exchangers for one, two and three passes, with either countercurrent or current flow.

Ten different arrangements are possible for both two-pass and three-pass exchangers. Analytical expressions relating the heat transfer effectiveness, ε, to the (total) number of heat transfer units, N_{tu}, can be found in five of the ten cases. Data for the cases that require numerical computation are presented by the abovementioned authors. These data are given in the form of correction factor, which are the ratio of the exchanger effectiveness to the effectiveness of a pure counter or parallel flow exchanger for the same values of R and N_{tu}.

Figure 11-13 gives the effectiveness, ε, versus the number of heat transfer units, N_{tu}, for one, two and three-pass counter-crossflow exchangers, when fluid A is unmixed throughout and fluid B mixed throughout, and with passes connected in reverse order. Streams with the same capacity rate have been assumed. Reverse order means that the mixed fluid surrounds a tube after the other in a certain order when flowing through one of the passes, and it surrounds other sections of the same tubes in the reverse order when flowing through the next pass.
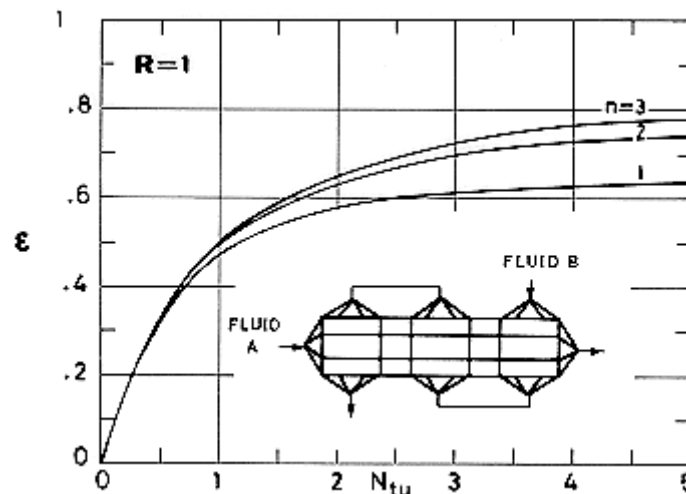
Figure 11-13: Heat transfer effectiveness, ε, vs. number of heat transfer units, N_{tu}, for the case of n-pass counter-crossflow exchangers, when fluid A is unmixed throughout and fluid B mixed throughout, and with passes connected in reverse order. Calculated by the compiler after Stevens, Fernandez & Woolf (1957) [170].

Figure 11-14 gives similar data but now the passes are connected in identical order.
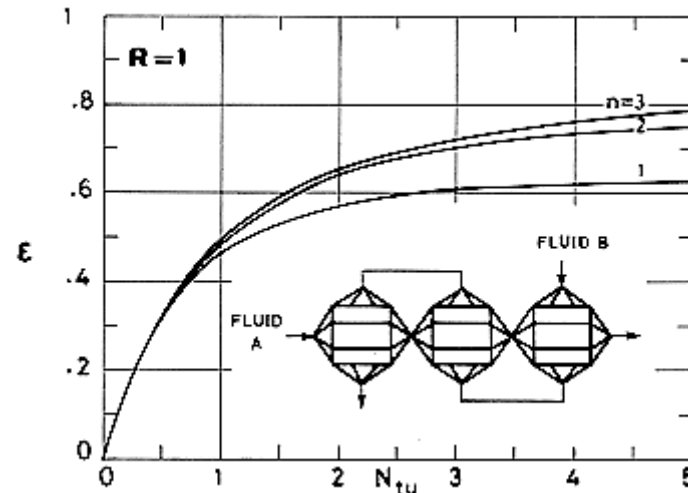
Figure 11-14: Heat transfer effectiveness, ε, vs. number of heat transfer units, N_{tu}, for the case of n-pass counter-crossflow exchangers, when fluid A is unmixed throughout and fluid B mixed throughout, and with passes connected in identical order. Calculated by the compiler after Stevens, Fernandez & Woolf (1957) [170].

Additional results can be found in Kays & London (1964) [102]. These data are for counter-crossflow exchangers, with one to four passes, in the following three particular cases.

1.   Both fluids mixed between passes, but unmixed in each pass.

2.   One of the fluids mixed between passes, unmixed in each pass. The other fluid unmixed throughout. Inverted order.

3.   Both fluids unmixed throughout, both inverted order.

Comparison of data in Figure 11-13 and Figure 11-14 with those in Figure 11-9 demonstrates that the larger the number of passes, the more nearly the performance approaches pure counterflow performance, but a large number of passes is often not warranted. Trade-off studies performed by Trusch & Nason (1975) [180], in connection with compact heat exchangers for the Space Shuttle, indicated that, although there is a significant reduction in exchanger mass when the number of passes increases from 2 to 4, the decrease in mass when the number of passes is further increased to 6 is negligible.

Figure 11-15 to Figure 11-20 give the exchanger effectiveness for parallel counterflow configurations when one of the fluids is mixed. This is the case of the shell-and-tube heat exchanger, which is one of the most common configurations for general process applications. Simple versions of these exchangers have been used in Spacecraft (Ebersole (1970) [41]). Nevertheless, light-weight compact exchangers are of the counter-crossflow type, as has been said already, and this is so because of reasons which will be made apparent very soon.
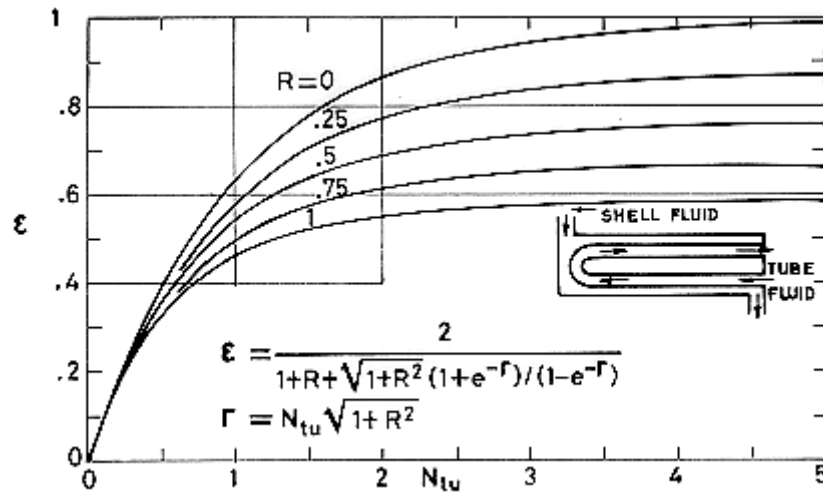
Figure 11-15: Heat transfer effectiveness, ε, vs. number of heat transfer units, N_{tu}, in a multipass exchanger with 1 shell pass and 2 or more tube passes. From Kays & London (1964) [102].
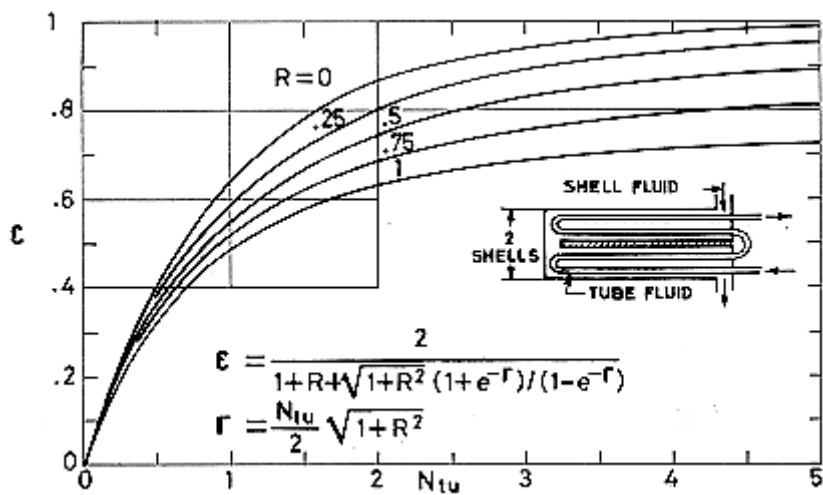
Figure 11-16: Heat transfer effectiveness, ε, vs. number of heat transfer units, N_{tu}, in a multipass exchanger with 2 shell passes and 4, 8, 12, …. tube passes. From Kays & London (1964) [102].
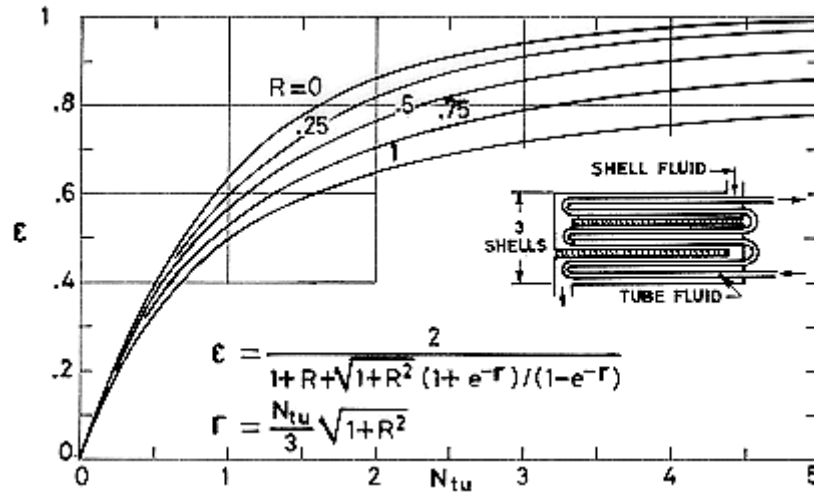
Figure 11-17: Heat transfer effectiveness, ε, vs. number of heat transfer units, N_{tu}, in a multipass exchanger with 3 shell passes and 6, 12, 18, ... tube passes. From Kays & London (1964) [102].
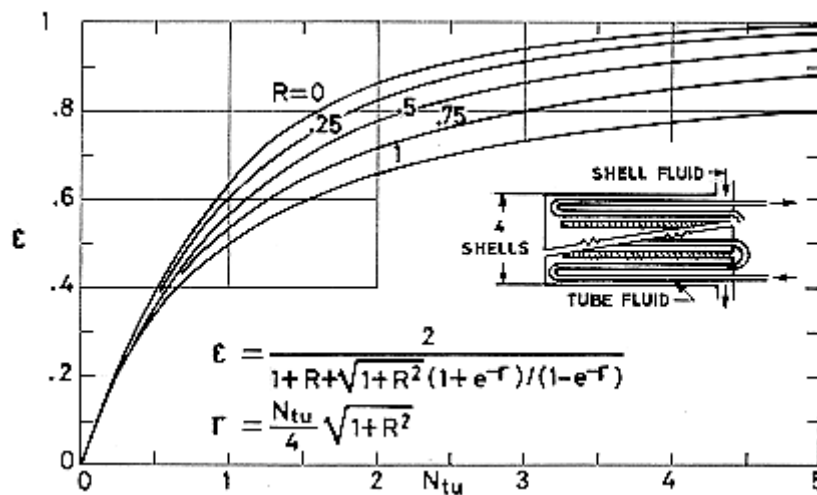
Figure 11-18: Heat transfer effectiveness, ε, vs. number of heat transfer units, N_{tu}, in a multipass exchanger with 4 shell passes and 8, 16, 24, ... tube passes. From Kays & London (1964) [102].
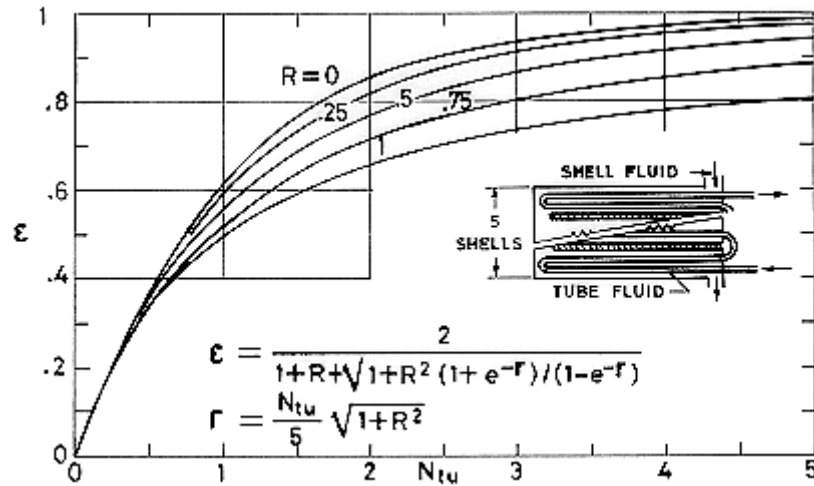
Figure 11-19: Heat transfer effectiveness, ε, vs. number of heat transfer units, N_{tu}, in a multipass exchanger with 5 shell passes and 10, 15, 20, ... tube passes. From Kays & London (1964) [102].
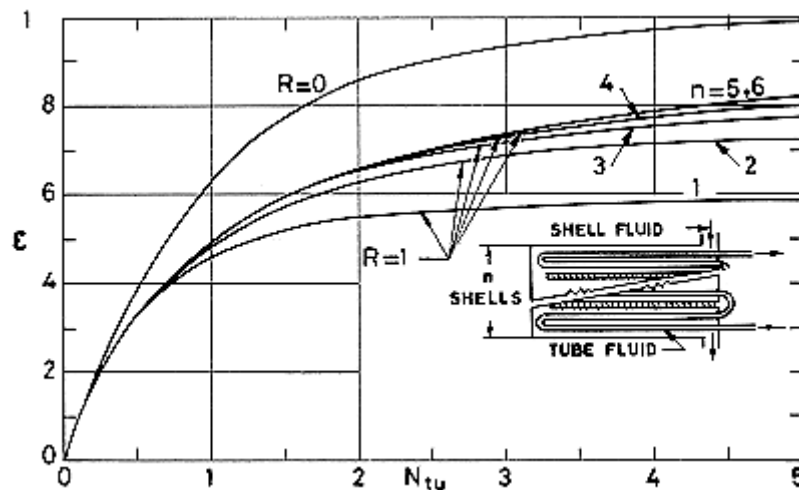
Figure 11-20: Heat transfer effectiveness, ε, vs. number of heat transfer units, N_{tu}, for different number of shell passes, in a multipass exchanger with $R = 1$. The case $R = 0$ is also shown for comparison. Calculated by the compiler after Kays & London (1964) [102].

The mathematical expression in Figure 11-15 is for one shell pass and two tube passes. Numerical results for four, six, eight, ... tube passes are very close to those shown in the figure.

Figure 11-16 to Figure 11-18 present the effect of multipassing the basic parallel counterflow arrangement.

Some of the results from the previous figures are summarised in Figure 11-20. Leaving aside the case $R = 0$, whose effectiveness, ε, does not depend on the number, n, of shell passes, one can deduce, from considerations of the cases $R = 1$, that little is gained by increasing the number of shell passes over four or five.

A comparison among the data presented up to the moment indicates that, for a given N_{tu}, the largest effectiveness is achieved with pure counterflow configurations (Figure 11-9), whereas the smallest

effectiveness corresponds to parallel flow configurations (Figure 11-10). Crossflow-fluids unmixed-configurations (Figure 11-11) yield results slightly below the pure counterflow case. Allowing one of the fluids to be mixed lowers a bit the performance of the cross flow (Figure 11-12), but these performances can be increased by multipassing as in the counter-crossflow configurations considered in Figure 11-13 and Figure 11-14. On the other side, parallel counterflow arrangements of the shell-and-tube type (Figure 11-20) yield performances substantially above those for the parallel flow but still below those for crossflow.

Another way toward the pure counterflow performance is the liquid-coupled indirect heat exchanger. The coupling-liquid capacity rate is an independent variable in such system, and this additional freedom can be used to maximise the overall effectiveness for given heat transfer areas, given hot and cold fluid capacities, and given overall thermal conductances.

Figure 11-21 to Figure 11-24 analyse the performance of a liquid-coupled indirect heat exchanger. Subscripts 1 and 2 refer, respectively,to properties of the exchanger with smaller and larger flow stream capacity-rate. Subscript L refers to properties of the liquid coupling stream.
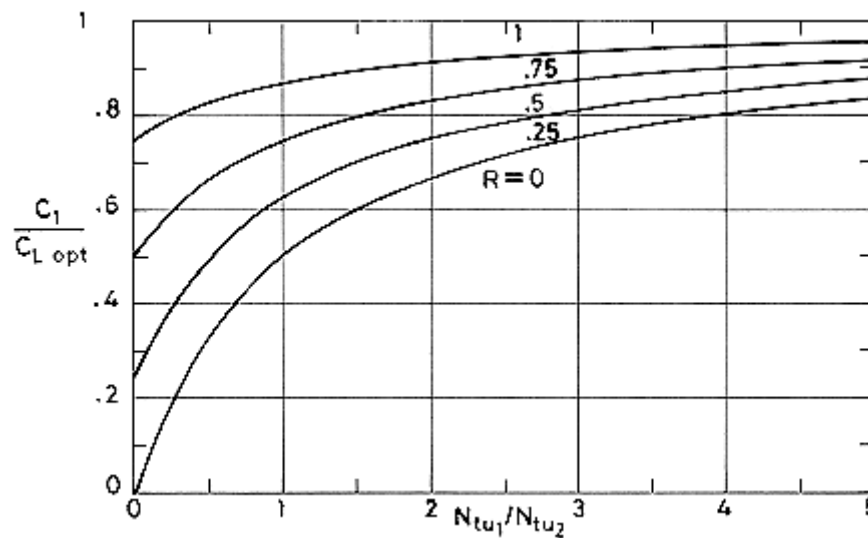
Figure 11-21: Optimum liquid flow capacity rate, C_1/C_{Lopt}, to maximize the heat transfer effectiveness vs. ratio of the number of heat transfer units $N_{tu}1/N_{tu}2$, of exchanger 1 to exchanger 2. Calculated by the compiler after Holmberg (1975) [90].
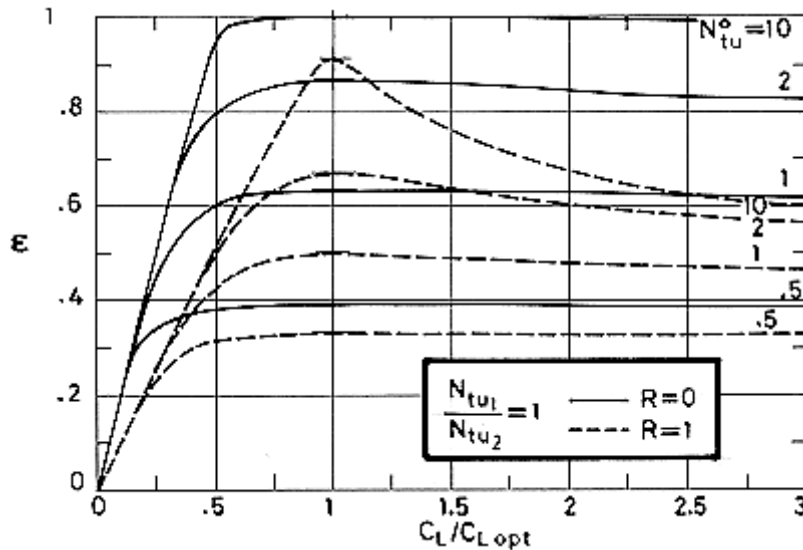
Figure 11-22: Heat transfer effectiveness, ε, vs. liquid flow capacity rate, C_L/C_{Lopt}, for different values of the overall number of heat transfer units, N^o_{tu}. $N_{tu}1/N_{tu}2 = 1$. Calculated by the compiler after Holmberg (1975) [90].
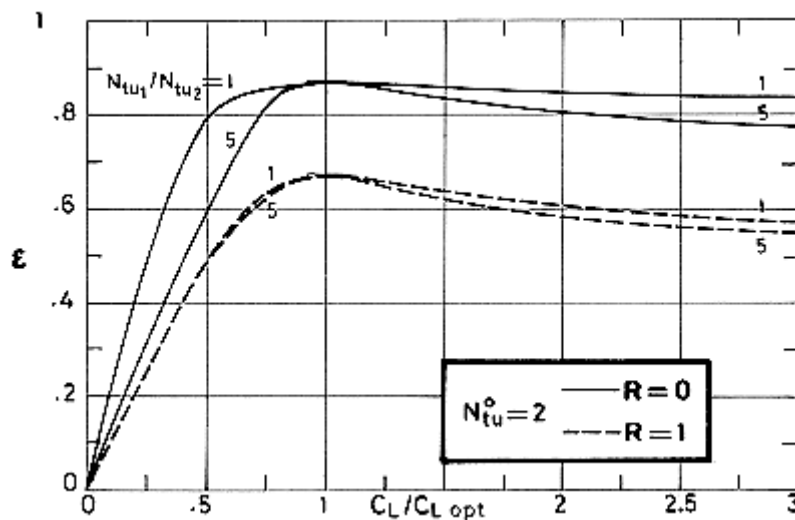
Figure 11-23: Heat transfer effectiveness, ε, vs. liquid flow rate, C_L/C_{Lopt}, for different values of the ratio between the number of heat transfer units of exchanger 1 to exchanger 2, $N_{tu}1/N_{tu}2$. $N^o_{tu} = 2$. Calculated by the compiler after Holmberg (1975) [90].
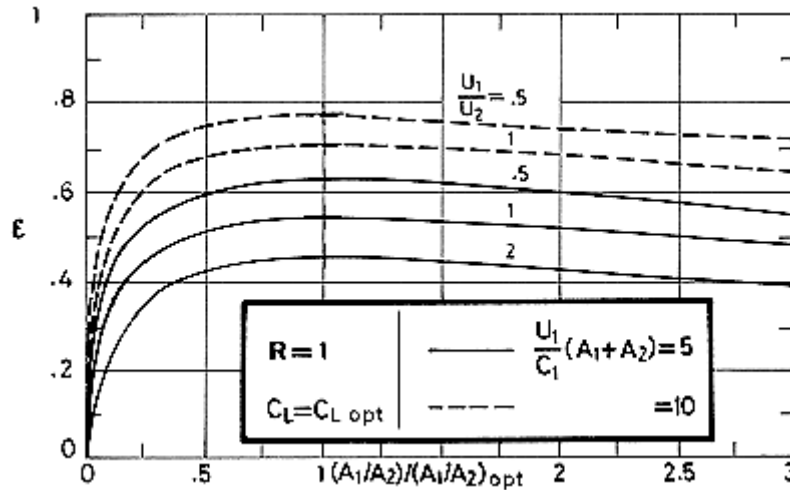
Figure 11-24: Overall heat transfer effectiveness, ε, vs. area ratio between exchanger 1 and 2, $(A_1/A_2)/(A_1/A_2)_{opt}$, for the case of optimum liquid flow capacity rate and $R = 1$. Calculated by the compiler after Holmberg (1975) [90].

The optimum liquid flow capacity rate, C_1/C_{Loptt}, is given in Figure 11-21 versus the ratio N_{tu1}/N_{tu2}, for different values of the ratio, R, of cold fluid to hot fluid capacity rates. Optimisation is performed by choosing the coupling-liquid flow capacity rate, C_L, so that the overall effectiveness is maximised for given N_{tu} values of both exchangers.

The relationship between the optimum value of the overall effectiveness and the overall number of heat transfer units for the liquid-coupled system, N^o_{tu}, is the same as that for pure counterflow (Holmber (1975) [90]). Thence, Figure 11-9 can be used to calculate the overall effectiveness in the case of optimum coupling-liquid flow capacity rate, once N^o_{tu} is deduced from

$$N^o_{tu} = \left(\frac{1}{N_{tu_1}} + \frac{1}{N_{tu_2}} \right)^{-1}$$

[11-9]

Non-optimum performance can be discussed by means of Figure 11-22 and Figure 11-23. The overall effectiveness, ε, is represented in these figures versus C_L/C_{Lopt} for some values of the parameters R, N^o_{tu} and N_{tu1}/N_{tu2}. It can be seen that the achievement of optimum performance becomes critical only for large values of N^o_{tu1} and that it becomes less crucial when R goes to zero.

One could further optimise the area ratio A_1/A_2 for given total heat transfer area, $A_1 + A_2$, assuming that the coupling liquid capacity rate is optimum. It is shown (Holmberg (1975) [90]) that

$$\left(\frac{A_1}{A_2} \right)_{opt} = \sqrt{\frac{U_2}{U_1}}$$

[11-10]

where U_1 and U_2 are the overall thermal conductances for both streams.

Figure 11-24 shows how a non-optimum distribution of total heat transfer area affects the overall effectiveness. One can deduce from this figure that the optimum is very flat for all realistic values of the parameters.

Heat exchangers can be combined to achieve a given heat transfer duty. One resorts to these combinations either because existing exchangers are used, or because the optimum configuration is impractical due to manufacturing limitations.

The exchangers can be combined in series, parallel, or series-parallel. They are often of non-identical type (or size), and a multiplicity of associations are possible. Typical associations of exchangers are shown below.

OVERALL PARALLEL FLOW

OVERALL COUNTER FLOW

PARALLEL IN ONE STREAM
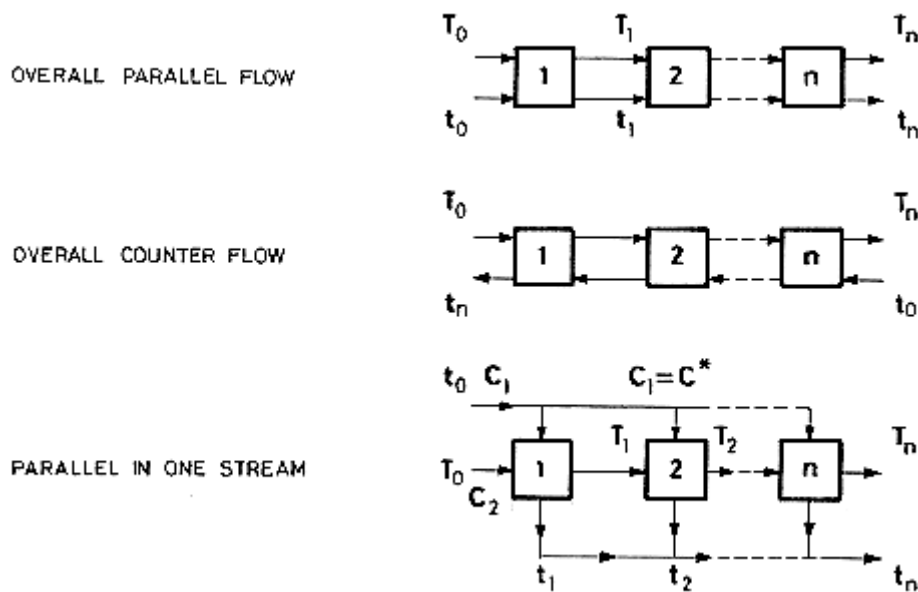
The results given in Figure 11-25 to Figure 11-28, which have been borrowed from Domingos (1969) [36], are based on the following assumptions:
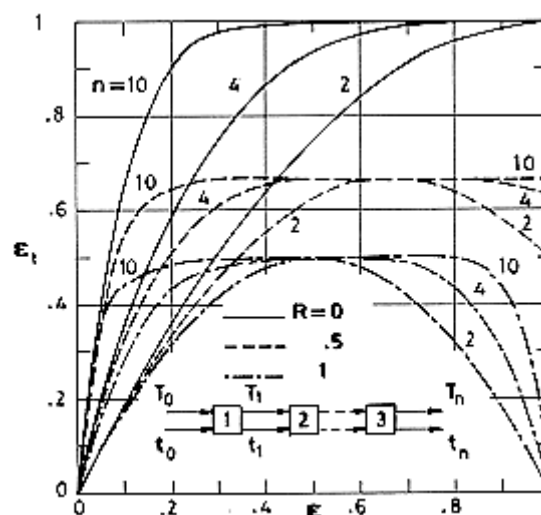
Figure 11-25: Overall heat transfer effectiveness, ε_t, of an assembly of n identical exchangers in parallel, vs. effectiveness, ε, of a single exchanger. Calculated by the compiler after Domingos (1969) [36].
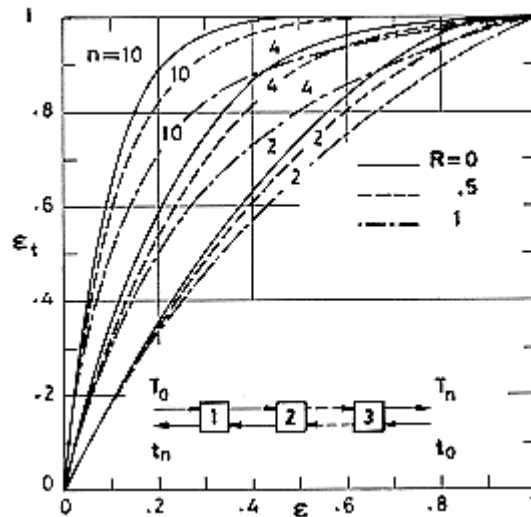
Figure 11-26: Overall heat transfer effectiveness, ε_t, of an assembly of n identical exchangers in counterflow, vs. effectiveness, ε, of a single exchanger. Calculated by the compiler after Domingos (1969) [36].
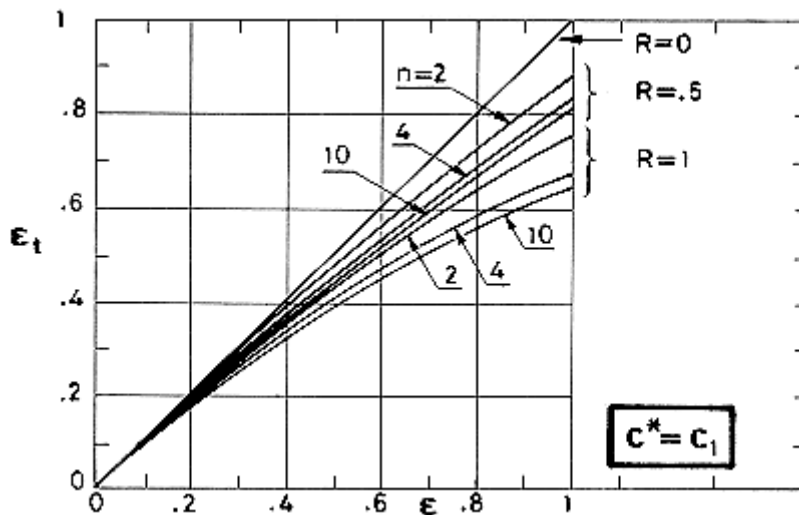
Figure 11-27: Overall heat transfer effectiveness, ε_t, of an assembly of n identical exchangers in parallel in the stream of lower capacity rate, vs. effectiveness, ε, of a single exchanger. Calculated by the compiler after Domingos (1969) [36].
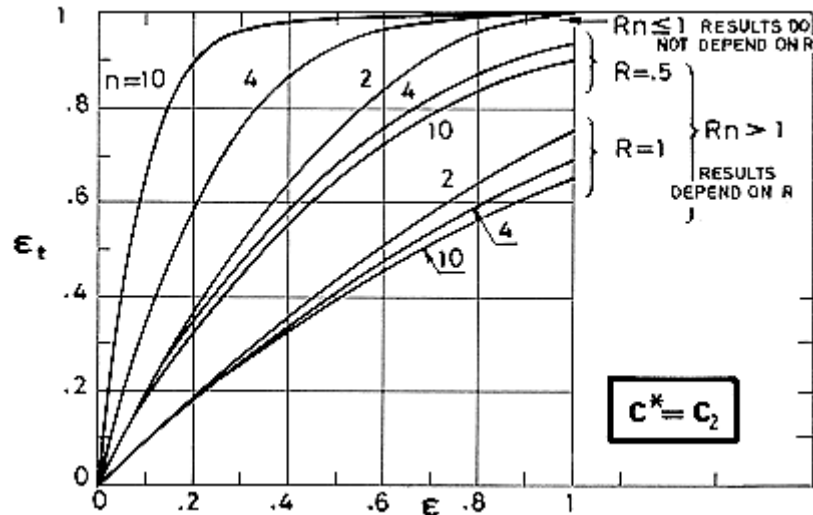
Figure 11-28: Overall heat transfer effectiveness, ε_t, of an assembly of n identical exchangers in parallel in the stream of higher capacity rate, vs. effectiveness, ε, of a single exchanger. Calculated by the compiler after Domingos (1969) [36].

1. The overall thermal conductance, U, is a constant for each exchanger.

2. Fluid capacity rate ratio, R, is constant.

3. Each fluid is completely mixed at the inlet and outlet of each exchanger.

4. In the cases considered in Figure 11-25 to Figure 11-28 all the exchangers are identical.

Analytical expressions for non-identical exchangers can be found in Domingos (1970) [36] where, in addition to the assemblies sketched above, mixed assemblies are considered. In such assemblies some elements are in overall counterflow and some others in overall parallel flow.

Data in Figure 11-25 to Figure 11-28 relate the overall effectiveness, ε_t, of the association to those of the components, ε, irrespective of the type of exchangers involved.
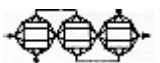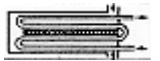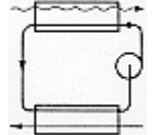
Figure 11-25 shows the drawbacks associated to assembling in parallel an even number of exchangers. The maximum achievable effectiveness of the association equals that for a parallel flow exchanger (Figure 11-10). To increase the effectiveness of the individual component would give quite defective results; the overall effectiveness would decrease! As a limiting case, notice that when two fluids with the same capacity rate ($R = 1$), flow through two identical counterflow exchangers, with effectiveness $\varepsilon = 1$, associated in parallel, the exit conditions for the second exchanger are exactly equal to those prevailing at the entrance of the first one.
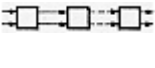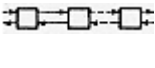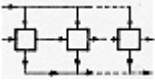
The situation for counterflow assemblies is quite different (Figure 11-26). The overall effectiveness of the assembly is greater than that for each individual component, and the gain increases with the number of components.

Figure 11-27 and Figure 11-28 give data for assemblies in parallel in one of the streams. In these assemblies one of the streams is equally divided between n exchangers, each with the same effectiveness. In Figure 11-27 the stream of lower capacity rate is the one divided, whereas in Figure 11-28 the stream of higher capacity rate is the one flowing in parallel.

One can deduce from these figures that, when an assembly in parallel in one of the stream is used, the stream with larger capacity should be that subdivided between the exchangers. But the advantages of this configuration can be fully exploited when the number o exchangers, n, is, at most, equal to $1/R$.

The Table below summarizes the data on exchanger performance which are presented in the following pages.

Arrangement	Description	Sketch	Input Variables	Output	Fig.	References
Basic arrangements	Counterflow		N_{tu} R=0 0,25 0,50 0,75 1	ε	Figure 11-9	Kays & London (1964) [102]
	Parallel flow				Figure 11-10	
Crossflow Exchangers	Fluids unmixed				Figure 11-11	Mason (1954) [124]
	One fluid mixed				Figure 11-12	Kays & London (1964) [102]
Counter cross-flow Exchangers. One fluid unmixed	Reverse order		N_{tu} R =1 n = 1 2 3		Figure 11-13	Stevens, Fernández & Woolf (1957) [170]
	Identical order				Figure 11-14	
Parallel counterflow exchangers. One fluid unmixed (Shell-and-tube exchangers)	One shell pass		N_{tu} R = 0 0,25 0,50 0,75 1		Figure 11-15	Kays & London (1964) [102]
	Two shell passes				Figure 11-16	
	Three shell passes				Figure 11-17	
	Four shell passes				Figure 11-18	
	Five shell passes				Figure 11-19	
	One to six shell passes		N_{tu}, R = 1 n = 1,2,3,4,5,6		Figure 11-20	
Indirect Transfer Heat exchangers	Liquid-coupled heat exchangers		N_{tu1}/N_{tu2} R = 0,0,25,0,50,0,75,1	C_1/C_{Lopt}	Figure 11-21	Holmberg (1975) [90]
			C_L/C_{Lopt}, N_{tu} = 0,5,1,2,10 $N_{tu1}/N_{tu2} = 1$, R = 0,1	ε	Figure 11-22	

Arrangement	Description	Sketch	Input Variables	Output	Fig.	References
			C_L/C_{Lopt}, N^o_{tu} = 2 N_{tu1}/N_{tu2} = 1,5, R = 0,1		Figure 11-23	
			$(A_1/A_2)/(A_1/A_2)_{opt}$+$U_1/U_2$= 0,5,1,2 R=1,$C_L=C_{Lopt}$ +$U_1(A_1+A_2)/C_1$=5,10		Figure 11-24	
Assembly of identical heat exchangers	Parallel assembly		ε R = 0 0,5 1 n = 2 4 10	ε_t	Figure 11-25	Domingos (1969) [36]
	Counterflow assembly				Figure 11-26	
	In parallel in the stream of lower capacity rate				Figure 11-27	
	In parallel in the stream of higher capacity rate				Figure 11-28	

11.3 Exchanging surface geometries

The purpose of this clause is the geometrical description of the compact heat transfer surfaces for which thermal and frictional data are given in Kays & London (1964) [102], Clause 14.

Besides the sketch, designation and dimensions of the surfaces, all of them reproduced in this clause, the following data are enclosed in the original source.

1. Core geometry data which require some elaboration such as: hydraulic diameter, D_E; free flow area ratio, $\Phi = A_{FL}/A_{FR}$; area densities α or β, whichever significant, and so forth.

2. Fin material used for the tests. This could be significant because of the reasons indicated in clause 11.5.3.

3. Heat transfer and flow friction data.

Heat transfer data are presented in terms of the Colburn factor, $j = StPr^{2/3}$. Actually the tests were made heating air either by means of a steady state steam-to-air system or by means of a transient, heated wall, procedure.

Friction data are given in terms of the Fanning friction factor, f.

The abscise are in both cases the Reynolds number, *Re*. To define *Re* the mean velocity is based on the minimum free flow area. In the case of matrix surfaces the free flow area is deduced from the porosity, ϕ, and the frontal area of the exchanger, A_{FR}. The characteristic length for calculating *Re* is the hydraulic diameter of the core.

The Reynolds number, *Re*, varies approximately in the range $200 \leq Re \leq 10^4$.

The following Table presents several symbols used by Kays & London (1964) [102] in connection with the above data. The equivalence to the symbols used in this Part is also indicated.

Kays & London (1964) [102]	this Part	Definition
G	ρV	Flow stream mass velocity
N_{Pr}	Pr	Prandtl number
N_R	Re	Reynolds number ($N_R = 4r_h G/\mu$)
N_{St}	St	Staunton number ($N_{St} = h/G_{cp}$)
$N_{St}N_{Pr}^{2/3}$	j	Colburn factor
f	f	Fanning friction factor
p	Φ	Porosity
$4r_h$	D_E	Hydraulic diameter
α	α	Area density. (Heat transfer area/Total volume)
β	β	Area density. (Heat transfer area/volume between plates)
σ	A_{FL}	Free flow area

11.3.1   Tubular surfaces
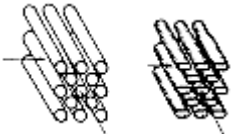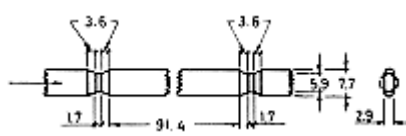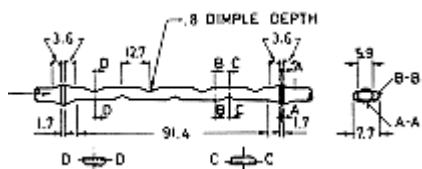
Sketch	Fundamental Types of surfaces	Table
	Flow inside circular and flattened circular tubes	Table 11-1
	Flow normal to banks of bare tubes	Table 11-2

Table 11-1: Flow Inside Circular and Flattened Circular Tubes

Sketch	Surface Designation [a]	Dimensions	For heat transfer and friction data see the following tables and figures in Kays & London (1964) [102]	
			Table	Fig.
	ST-1	See Sketch (Dimensions are given in mm)	10-1	10-1
	FT-1		10-1	10-2
	FTD-1		10-1	10-3

[a] Designation is the same as in Kays & London (1964) [102]. ST indicates flow inside straight tubes, while FT refers to flattened tubes and FTD to flattened and dimpled tubes.

Table 11-2: Flow Normal to Banks of Bare Tubes

Sketch	Surface Designation [a]	Dimensions [b] [m]			For Heat Transfer and Friction data see the following tables and figures in Kays & London (1964) [102]	
		$a \times 10^3$	$b \times 10^3$	$c \times 10^3$	Table	Fig.
	S1,50-1,25(s)	6,4	9,5	7,9	10-2	10-4
	S1-50-1,25	9,5	14,3	11,9		10-5
	S1,25-1,25		11,9	11,9		10-6
	S1,50-1,00		14,3	9,5		10-7
	S1,50-1,50		14,3	14,3		10-8
	S2,00-1,00		19,1	9,5		10-9
	S2,50-0,75		23,8	7,2		10-10
	I1,50-1,25(s)	6,4	9,5	7,9	10-2	10-12
	I1,50-1,25	9,5	14,3	11,9		10-13
	I1,25-1,25		11,9			10-14
	FT-2	See Sketch (Dimensions are given in mm)			10-2	10-17
	FTD-2				10-2	10-18

[a] Designation is the same as in Kays & London (1964) [102]. The capitals S or I indicate whether the circular tubes are staggered or in line. The numerals which follow give respectively the transverse and the longitudinal pitch ratios. FT refers to flattened tubes and FTD to flattened and dimpled tubes.

[b] Additional details on surface geometry are given in Kays & London (1964) [102], Table 11-2.
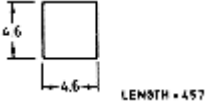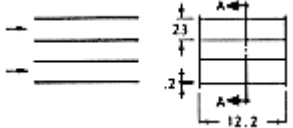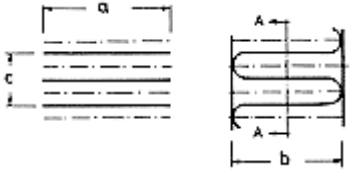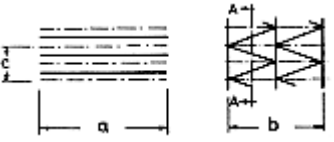
11.3.2 Plate-fin surfaces

Sketch	Fundamental Types of surfaces	Table
	Plate-Fin surfaces, plain fins	Table 11-3
	Plate-Fin surfaces, louvered fins	Table 11-4
	Plate-Fin surfaces, strip fins	Table 11-4
	Plate-Fin surfaces, wavy fins	Table 11-6
	Plate-Fin Surfaces, perforated fins	Table 11-7
	Plate-Fin Surfaces, pin fins	Table 11-8

Table 11-3: Plate-Fin surfaces, plain fins

Sketch	Surface Designation [a]	Dimensions [b] [m]				For Heat Transfer and Friction data see the following tables and figures in Kays & London (1964) [102]	
		$a \times 10^3$	$b \times 10^3$	$c \times 10^3$	$d \times 10^3$	Table	Fig.
	2,0	305	19,1	13,6	10,2	10-3	10-19
	3,01			9,5	5,7		10-20
	3,97			6,4	4,8		10-21
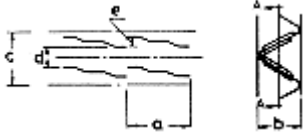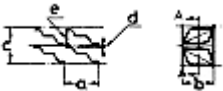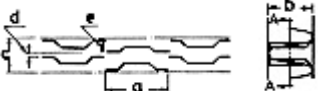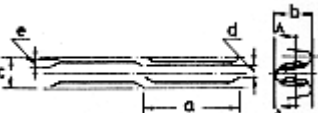
Table 11-3: Plate-Fin surfaces, plain fins (continued)

Sketch	Surface Designation [a]	Dimensions [b] [m]			For Heat Transfer and Friction data see the following tables and figures in Kays & London (1964) [102]	
		a x 10³	b x 10³	c x 10³	Table	Fig.
	4,00	See Sketch (Dimensions are given in mm)			10-3	10-22
	6,2				10-3	10-24
	1,11(a)				10-3	10-27
	5,3	63,5	11,9	9,6	10-3	10-23
	11,1		6,4	4,6		10-26
	14,77		8,4	3,4		10-28
	19,86	65,6	6,4	2,6		10-30
	9,03	302	20,9	5,6	10-3	10-25
	15,08	174	10,6	3,4		10-29
	10,27 T	63,5	13,8	4,9	10-3	10-31
	11,94 T	127	6,3	4,3		10-32
	12,00 T	63,5	6,4	4,2		10-33
	46,45 T	66,8	2,5	1,1		10-37
	16,96 T	127	6,5	3	10-3	10-34
	25,97 T	63,5	5,2	2		10-35
	30,33 T		8,8	1,7		10-36

[a]   Designation is the same as in Kays & London (1964) [102]. The numerals indicate fin density in fins per inch.
[b]   Additional details on surface geometry are given in Kays & London (1964) [102], Table 13-3.
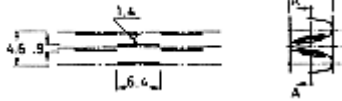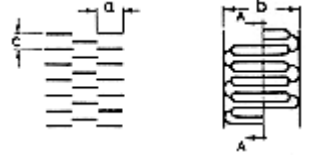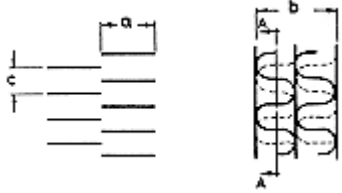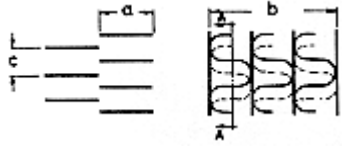
Table 11-4: Plate-Fin surfaces, louvered fins

Sketch	Surface Designation [a]	Dimensions [b] [m]					For Heat Transfer and Friction data see the following tables and figures in Kays & London (1964) [102]	
		$a \times 10^3$	$b \times 10^3$	$c \times 10^3$	$d \times 10^3$	$e \times 10^3$	Table	Fig.
	3/8-6,06	9,5	6,4	8,4	2,8	1,4	10-4	10-28
	1/2-6,06	12,7						10-40
	3/8-7,8	9,5	6,4	5,8	1,5	1,4		10-42
	3/16-11,1	4,8	6,4	4,6	0,9	1,4		10-44
	1/4-11,1	6,4						10-45
	3/8-11,1	9,5						10-47
	1/2-11,1	12,7						10-49
	3/8(a)-6,06	9,5	6,4	8,4	0,9	3,3	10-4	10-39
	1/2(a)-6,06	12,7						10-41
	3/8(a)-8,7	9,5	6,4	5,8	0,9	2		10-43
	1/4(b)-11,1	6,5	6,4	4,6	0,9	1,4	10-4	10-46
	3/8(b)-11,1	9,5	6,4	4,6	0,9	1,4	10-4	10-48
	3/4-11,1	19,1	6,4	4,6	1,3	1	10-4	10-50
	3/4(b)-11,1	10,1	6,4	4,6	1,3	1	10-4	10-51

[a] Designation is the same as in Kays & London (1964) [102]. The first numerals indicate fin length, a, in inches, the second indicate fin density in fins per inch.

[b] Additional details on surface geometry are given in Kays & London (1964) [102], Table 13-3.

Table 11-5: Plate-Fin surfaces, strip fins

Sketch	Surface Designation [a]	Dimensions [b] [m]			For Heat Transfer and Friction data see the following tables and figures in Kays & London (1964) [102]	
		a x 10³	b x 10³	c x 10³	Table	Fig.
	1/4(S)-11,1	See Sketch (Dimensions are given in mm)			10-5	10-52
	3/32-12,22	2,4	12,3	2,1	10-5	10-53
	1/8-5,2	3,2	10,5	1,7	10-5	10-54
	1/8-13,95		9,5	1,8		10-55
	1/2-11,94(D)	12,7	6	2,1	10-5	10-56
	1/4-15,4(D)	6,4	5,2	1,7		10-57
	1/6-12,18(D)	4,2	9	2,1		10-58
	1/7-15,75(D)	3,6	7,7	1,6		10-59
	1/8-20,06(D)	3,2	5,1	1,3		10-60
	1/8-19,82(D)		5,2	1,3		10-61
	1/8-16,12(D)		5,2	1,6		10-62
	1/8-16,00(D)		6,5	1,6		10-63
	1/8-16,12(T)	3,2	8	1,6	10-5	10-64

[a]   Designation is the same as in Kays & London (1964) [102]. The first numerals indicate fin length, a, in inches, the second indicate fin density in fins per inch.

[b]   Additional details on surface geometry are given in Kays & London (1964) [102], Table 13-3.
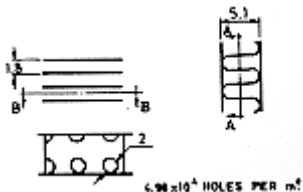
Table 11-6: Plate-Fin surfaces, wavy fins

Sketch	Surface Designation [a]	Dimensions [b] [m]				For Heat Transfer and Friction data see the following tables and figures in Kays & London (1964) [102]	
		ax10³	bx10³	cx10³	dx10³	Table	Fig.
	11,44-3/8 W	9,5	10,5	2,2	2	10-6	10-65
	11,5-3/8 W		9,5	2,2	2		10-66
	17,8-3/8 W		10,5	1,4	2		10-67

[a] Designation is the same as in Kays & London (1964) [102]. The first number indicates fin density in fins per inch and the second fin wavelength, a, in inches. W is for wave-fin surfaces.

[b] Additional details on surface geometry are given in Kays & London (1964) [102], Table 13-3.

Table 11-7: Plate-Fin surfaces, perforated fins

Sketch	Surface Designation [a]	Dimensions [b] [m]	For Heat Transfer and Friction data see the following tables and figures in Kays & London (1964) [102]	
			Table	Fig.
	13,95 (P)	See Sketch (Dimensions are given in mm)	10-7	10-74

[a] Designation is the same as in Kays & London (1964) [102]. The first numerals indicate fin density in fins per inch. P is for perforated.

[b] Additional details on surface geometry are given in Kays & London (1964) [102], Table 13-3.

Table 11-8: Plate-Fin surfaces, pin fins

Sketch	Surface Designation [a]	Dimensions [b] [m]	For Heat Transfer and Friction data see the following tables and figures in Kays & London (1964) [102]	
			Table	Fig.
	AP-1	See Sketch (Dimensions are given in mm)	10-7	10-68
	AP-2		10-7	10-69
	PF-3		10-7	10-70
	PF-4(F)		10-7	10-71
	PF-9(F)		10-7	10-72
	PF-10(F)		10-7	10-73

[a]   Designation is the same as in Kays & London (1964) [102]. This designation is not descriptive of the surface.

[b]   Additional details on surface geometry are given in Kays & London (1964) [102], Table 13-3.

11.3.3 Finned tubes
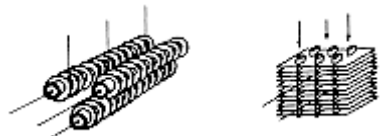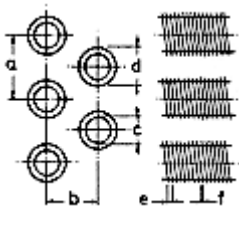
Sketch	Fundamental Types of surfaces	Table
	Finned tubes, circular tubes, circular fins	Table 11-9
	Finned tubes, circular tubes, continuous fins	Table 11-10
	Finned tubes, flat tubes, continuous fins	Table 11-11
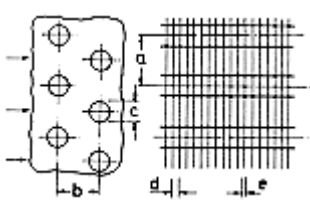
Table 11-9: Finned tubes, circular tubes, circular fins

Sketch	Surface Designation [a]	Dimensions b [m]						For Heat Transfer and Friction data see the following tables and figures in Kays & London (1964) [102]	
		ax10³	bx10³	cx10³	dx10³	ex10³	fx10³	Table	Fig.
	CF-7,34	24,8	20,3	9,7	23,4	3,5	0,5	10-8	10-75
	CF-8,72					2,9			10-76
	CF-8,72(C)			10,7	21,9	2,9			10-77
	CF-11,46			9,7	23,4	2,2	0,4		10-78
	CF-7,0-5/8J	31,3	34,3	16,4	28,5	3,6	0,3		10-79
	CF-8,7-5/8J-A	31,3	34,3	16,4	28,5	2,9	0,3		10-80
	CF-8,7-5/8J-B	46,9							
	CF-9,05-3/4J-A	39,5	44,5	19,7	37,2	2,8	0,3		10-81
	CF-9,05-3/4J-B	50,3							
	CF-9,05-3/4J-C	69,2							
	CF-9,05-3/4J-D	69,2	20,3						
	CF-9,05-3/4J-E	50,3	34,9						
	CF-8,8-1,0J-A	49,8	52,4	26	44,1	2,9	0,3		10-82
	CF-8,8-1,0J-B	78,2							

a   Designation is the same as in Kays & London (1964) [102]. CF refers to circular fins. The first numerals refer to the number of fins per inch, the second refer to the nominal outside diameter of the tube, d, in inches.

b   Additional details on surface geometry are given in Kays & London (1964) [102], Table 13-4.
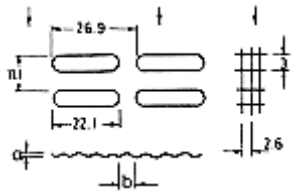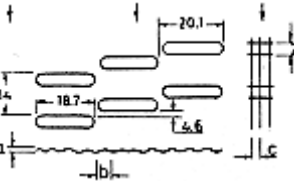
Table 11-10: Finned tubes, circular tubes, continuous fins

Sketch	Surface Designation [a]	Dimensions [b] [m]					For Heat Transfer and Friction data see the following tables and figures in Kays & London (1964) [102]	
		$a \times 10^3$	$b \times 10^3$	$c \times 10^3$	$d \times 10^3$	$e \times 10^3$	Table	Fig.
	8,0-3/8T	25,4	22	10,2	3,2	0,3		10-83
	7,75-5/8T	38,1	44,5	17,2	3,3	0,4		10-84

[a] Designation is the same as in Kays & London (1964) [102]. The first numerals refer to the number of fins per inch, the second refer to the nominal outside diameter of the tube, c, in inches.

[b] Additional details on surface geometry are given in Kays & London (1964) [102], Table 13-4.

Table 11-11: Finned tubes, flat tubes, continuous fins

Sketch	Surface Designation [a]	Dimensions [b] [m]				For Heat Transfer and Friction data see the following tables and figures in Kays & London (1964) [102]	
		$a \times 10^3$	$b \times 10^3$	$c \times 10^3$		Table	Fig.
	9,68-0,87	0	∞	Other dimensions are given, in mm, in the sketch		10-8	10-85
	9,68-0,87-R	0,6	6,4				10-87
	9,1-0,737-S	0	∞	2,8	Other dimensions are given, in mm, in the sketch	10-8	10-86
	9,29-0,737-SR	0,6	6,4	2,7			10-88
	11,32-0,737-SR			2,2			10-89
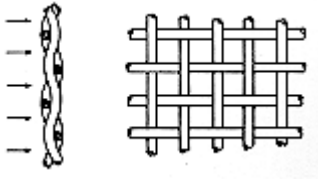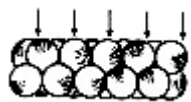
[a] Designation is the same as in Kays & London (1964) [102]. The first numerals refer to the number of fins per inch, the second refer to the tube dimension in the flow direction. S indicates staggered arrangement.

[b] Additional details on surface geometry are given in Kays & London (1964) [102], Table 13-4.

11.3.4   Matrix surfaces

Table 11-12: Crossed-Rod, woven-screen and sphere matrices

Sketch	Matrix Surface Designation [a]	Surface Description [b]		For Heat Transfer and Friction data see the following tables and figures in Kays & London (1964) [102]	
		Porosity	Transverse Pitch, s_t	Table	Fig.
	Crossed-Rod, Inline Stacking	0,832	4,675	10-9	10-90
		0,766	3,356		
		0,675	2,417		
		0,602	1,974		
		0,500	1,571		
	Crossed-Rod, Staggered Stacking	0,832	4,675	10-9	10-91
		0,766	3,356		
		0,675	2,417		
		0,602	1,974		
		0,500	1,571		
	Crossed-Rod, Random Stacking	0,832	4,675	10-9	10-92
		0,817	4,292		
		0,766	3,356		
		0,725	2,856		
		0,675	2,417		
		0,602	1,974		
		0,500	1,571		

Sketch	Matrix Surface Designation [a]	Surface Description [b]		For Heat Transfer and Friction data see the following tables and figures in Kays & London (1964) [102]	
		Porosity	Transverse Pitch, s_t	Table	Fig.
	Woven-screen	0,832			7-8 7-9
		0,817			
		0,766			
		0,725			
		0,675			
		0,602			
	Sphere matrix	0,37 to 0,39		10-10	7-10

[a]   Designation is the same as in Kays & London (1964) [102].

[b]   Additional details on crossed-rod matrix geometry are given in Kays & London (1964) [102], Table 13-5.

11.4   Deviations from basic analysis

11.4.1   Introduction

The exchanger theory presented in Clause 11.2 is based on several idealisations. It is assumed, for example, that thermal conduction in the flow direction can be neglected, and that the fluid flow does not detach from the heat exchanger surfaces and is evenly distributed among the several flow passages.

The conditions for the validity of these idealisations are usually met. Nevertheless, we can confront configurations where one or another of the simplifying assumptions fails.

As an example of situation where the axial heat conduction along the exchanger core can hardly be neglected, let us consider the heat exchangers used in typical cryogenic refrigeration cycles. These exchangers are characterised by its very high effectiveness and limited pressure drop, and these requirements are fulfilled by using large heat transfer surfaces and short flow passages, thence axial heat conduction becomes significant.

Simplifying assumptions concerning the fluid flow pattern cannot be easily introduced in all cases. For example, the flow in the shell side of shell-and-tube heat exchangers is so complicated that some allowance for the departure of actual flow from that assumed in the theoretical predictions should be taken into account. This departure from the ideal flow patterns is usually called maldistribution.

Flow maldistribution appears in exchangers with parallel channels as an imbalance of the fluid mass flow rate among the passages. This imbalance is mainly due to tolerances in manufacturing, pressure drop in the manifolds, and deposition of impurities on the exchanging surfaces. The extent of the problem increases rapidly as the desired efficiency is raised, and is also more severe with increasing the number of heat transfer units. Although the magnitude of the deviations from the nominal performances will vary with the care used in designing and fabricating the heat exchanger, there are some upper limits to the manufacturing accuracy which cannot be exceeded at a reasonable cost, thus some technique should be devised to compensate the imbalance whenever it is significant.

11.4.2   Longitudinal heat conduction

Is has been assumed up to now that there is no heat conduction in the flow direction, either through the fluid or through the solid wall.

The effect of axial heat conduction through the fluid is usually neglected in conventional heat exchanger design, since the thermal conductivity of fluids is small (liquid metals excepted). The order of magnitude of the longitudinal fluid conduction compared with longitudinal fluid convection equals the inverse of the Peclet number, $Pe = PrRe$, so that the effect of longitudinal conduction can be ignored in comparison with longitudinal convection effects for Peclet numbers exceeding 100. The analysis by Schmidt & Zeldin (1970) [159] could be used to estimate the heat transfer rate in the entrance region of ducts taking into account the effect of longitudinal conduction.

Well-conduction effects may be important in heat exchangers designed for high effectiveness ($\varepsilon > 0,9$). The effect of wall conduction is to reduce the temperature gradient along the fluid, thus decreasing the heat exchanger effectiveness.

A rough estimate of the effect of heat conduction through the wall may be obtained by equating the ratio between the decrease in effectiveness due to wall conduction, and the effectiveness in absence of wall conduction, to the ratio between heat conducted through the wall and heat convected by the flow.

$$\frac{\delta\varepsilon}{\varepsilon} = \frac{(k/L)A_k}{C_1} = \Lambda \qquad [11\text{-}11]$$

where k is the wall thermal conductivity, L the flow length of the duct, and A_k the cross-sectional area of the wall for longitudinal conduction. Λ is the conduction parameter, defined as shown. For high effectiveness exchangers ($\varepsilon \cong 1$), the exchanger ineffectiveness, $1 - \varepsilon$, is approximately equal to Λ.

To obtain a better estimate of the effect of wall conduction it is necessary to solve the differential equations describing the heat exchanger process with the appropriate boundary conditions. Kroeger (1967) [110] carried out such an analysis, for the case of a counterflow exchanger, both for balanced flow, $R = 1$, and for unbalanced flow $R < 1$, under the basic assumption of constant material properties. Figure 11-29 to Figure 11-31 show the ineffectiveness, $1 - \varepsilon$, as a function of the overall number of heat transfer units,

$$\frac{1}{N_{tu}} = \frac{1}{N_{tu_1}} + \frac{1}{N_{tu_2}} \qquad [11\text{-}12]$$

for three different values of R.
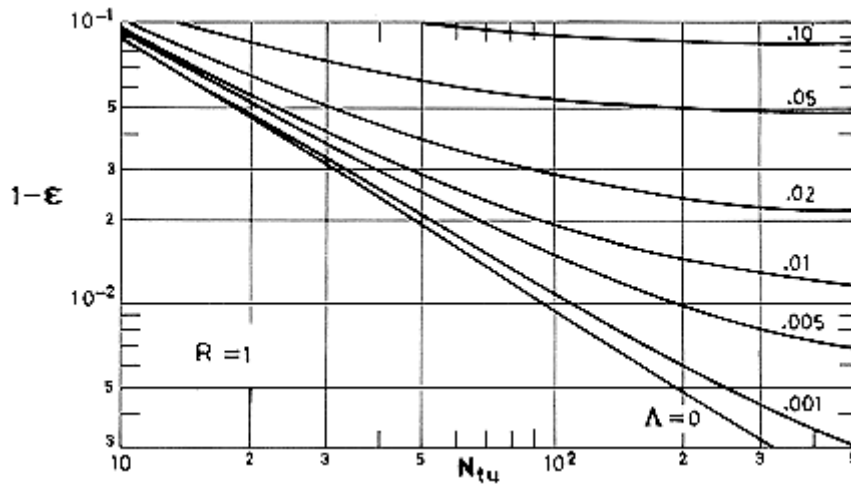
Figure 11-29: Heat exchanger ineffectiveness, 1–ε, vs. number of heat transfer units, N_{tu}, for a counterflow heat exchanger. Results are shown for $R = 1$ and different values of the wall conduction parameter, Λ. From Kroeger (1967) [110].
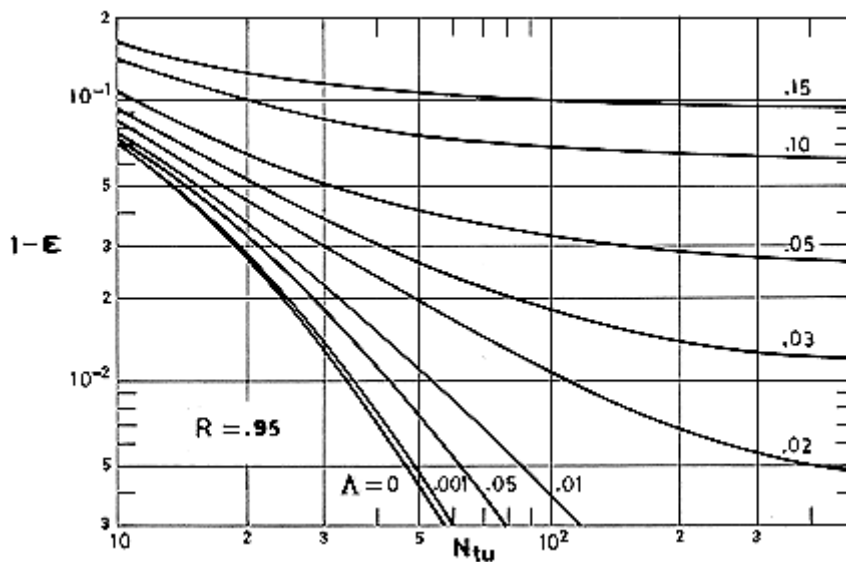
Figure 11-30: Heat exchanger ineffectiveness, 1–ε, vs. number of heat transfer units, N_{tu}, for a counterflow heat exchanger. Results are shown for $R = 0,95$ and different values of the wall conduction parameter, Λ. From Kroeger (1967) [110].
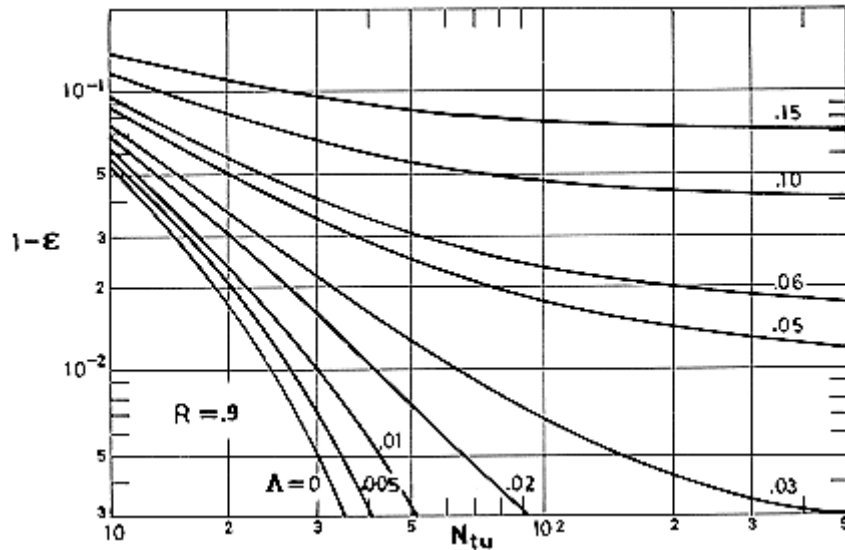
Figure 11-31: Heat exchanger ineffectiveness, 1–ε, vs. number of heat transfer units, N_{tu}, for a counterflow heat exchanger. Results are shown for R = 0,90 and different values of the wall conduction parameter, Λ. From Kroeger (1967) [110].

Typical values of N_{tu} range widely. For the Spacelab Freon to Water Interloop Heat Exchanger (see clause 11.7) N_{tu} varies from about 5 to about 20, depending on the operating conditions (Owen, Sessions & Walker (1976) [139], pp. 54-55). On the other side, Cowans (1974) [28] describes a counterflow heat exchanger, for a cryogenic life-support system, which was designed to operate at a value of N_{tu} as large as 200.

Figure 11-32 gives the ineffectiveness, 1 - ε, as a function of the conduction parameter, Λ, for N_{tu} = 50 and several values of the capacity-rate ratio, R.
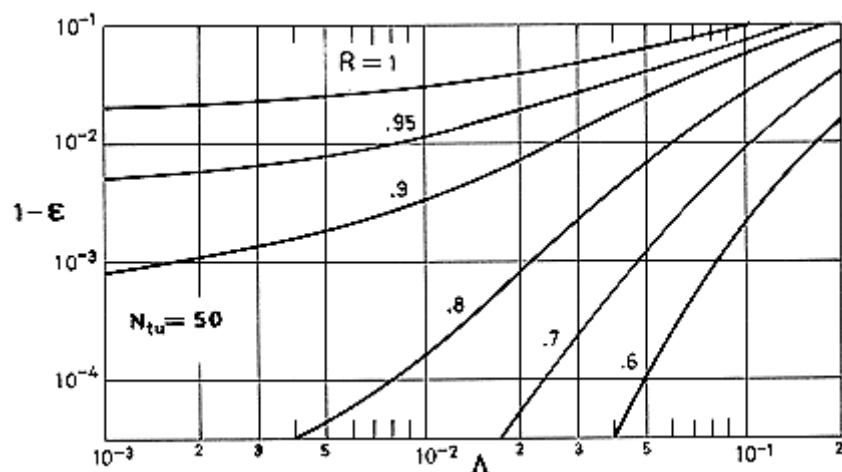
Figure 11-32: Heat exchanger ineffectiveness, 1-ε, vs. dimensionless wall conduction, Λ, for a counterflow heat exchanger. Results are shown for N_{tu} = 50 and different values of the capacity-rate ratio, R. Calculated by the compiler after Kroeger (1967) [110].

Curves labelled Λ = 0 in these figures relate the ineffectiveness, 1 - ε, to the number of heat transfer units, N_{tu}, when wall conduction effects are absent, thence the increase in ineffectiveness for a given

non-zero value of Λ can be estimated from the figures. It is seen that the wall conduction effects increase with the number of heat transfer units. For large values of N_{tu} the ineffectiveness approaches an asymptotic minimum which, according to Kroeger (1967) [110], is given by:

$$\lim_{N_{tu} \to \infty} (1 - \varepsilon) = \frac{\Lambda}{1 + 2\Lambda} \quad , \quad for \ R = 1 \qquad [11\text{-}13]$$

or

$$\lim_{N_{tu} \to \infty} (1 - \varepsilon) = \frac{1 - R}{\dfrac{R + 1}{3R - 1} e^{\frac{1-R}{\Lambda R}} - R} \quad , \quad for \ R < 1 \qquad [11\text{-}14]$$

It should be indicated that while the expression for $R = 1$ is "exact", within the validity of the assumptions used throughout the analysis, the expression for $R < 1$ involves further assumptions.

The results presented in Figure 11-29 to Figure 11-32 also indicate that the capacity rate ratio, R, has a strong influence on the ineffectiveness, the most severe deterioration arising when both fluids have the same flow capacity rate ($R = 1$).

11.4.3 Flow maldistribution

Flow maldistribution appears when the fluid flow is not uniformly distributed over the heat transfer surface or, still worse, when portions of the stream bypass the surface entirely.

The problem of predicting performance as a function of flow maldistribution cannot be completely solved because of the infinite number of ways the flow can distribute in a heat exchanger. The purpose of this clause is then to discuss the several ways in which maldistribution can take place; to predict performance degradation in some very simple cases; to indicate some cures to performance degradation, and to introduce the relevant literature on the subject. No attempt is made here to relate flow maldistribution to manufacturing tolerances, poor header design or in service degradation of the exchanging surfaces, rather the level of maldistribution is defined by means of appropriate parameters and the effect of these parameters on the performance is assessed. Manufacture and in service degradation will be considered in Clause 11.5. The effect of header design on flow distribution has been discussed by Cichelly & Boucher (1956) [26] and by Freas & Ozisik (1965) [67], among others.

11.4.3.1 Simple analyses

In order to introduce the subject let us discuss several simple examples where performance degradation can be estimated without difficulty.

First we will consider the case of surface bypassing. The fluid velocity and, hence, the heat transfer coefficient, h, are decreased by departure of a portion of the total outside stream from the available area through the active surface. Thus the bypass stream reaches the exchanger outlet uncooled (for unheated) in the worst conceivable case, and only there mixes with the active stream. The resulting outlet temperature will be:

$$T_o = \phi T_i + (1 - \phi) T_o^1 = T_o^1 + \phi (T_i - T_0^1) \qquad [11\text{-}15]$$

where ϕ is the mass fraction bypassed, and T_o^1 is the outlet temperature of the active stream, whose mass fraction is $1 - \phi$. If the desired heat duty is to be accomplished, the active-outlet to inlet temperature difference is increased according to:

$$T_o^1 - T_i = \frac{1+\phi}{1-\phi}\left(T_o - T_i\right)$$
[11-16]

This form of maldistribution appears in the shell side of shell-and-tube heat exchangers, and will be discussed with some detail in clause 11.4.3.2.

Flow maldistribution is not so drastic in the case of parallel channels although performance degradation can be more important if high efficiencies are required.

To illustrate the effect of flow maldistribution on the performance of heat exchangers formed by parallel channels, we will consider the following simple example, borrowed from Weimer & Hartzog (1973) [187]. Let us start with the problem of countercurrent flow between two fluid streams with the same capacity rate ratio ($C_h = C_c = C$). Then, for a perfectly balanced exchanger (see clause 11.2.2),

$$Q = C\left(T_{hi} - T_{ho}\right) = C\left(T_{co} - T_{ci}\right) = A\overline{U}\Delta T$$
[11-17]

and

$$N_{tu} = \frac{A\overline{U}}{C}$$
[11-18]

If the two fluids are not divided evenly among the several parallel sections of the exchanger, then for one of these sections, n, with the inlet temperatures fixed,

$$Q_n = C_{h,n}\left(T_{hi} - T_{ho,n}\right) = C_{c,n}\left(T_{co,n} - T_{ci}\right) = \left(A\overline{U}\right)_n T_{lm,n}$$
[11-19]

where the logarithmic mean temperature difference (see clause 6.2.1) is used since the hot fluid to cold fluid temperature difference is no longer constant, along the passages because of the flow imbalance ($C_{h,n} \neq C_{c,n}$).

$$\Delta T_{lm,n} = \frac{T_{hi} - T_{co,n} - \left(T_{ho,n} - T_{ci}\right)}{\ln \dfrac{T_{hi} - T_{co,n}}{T_{ho,n} - T_{ci}}}$$
[11-20]

Combination of the above equations yields:

$$\ln \frac{1 + \dfrac{1}{N_{tu}} - \dfrac{Q_n}{Q}\dfrac{C}{C_{c,n}}}{1 + \dfrac{1}{N_{tu}} - \dfrac{Q_n}{Q}\dfrac{C}{C_{h,n}}} = N_{tu}\frac{\left(A\overline{U}\right)_n}{AU}\left(\frac{C}{C_{h,n}} - \frac{C}{C_{c,n}}\right) \qquad [11\text{-}21]$$

Illustrative results are given in Figure 11-33 and Figure 11-34. To calculate the data shown in these figures the heat exchanger is assumed to be divided into two equal parts, each having surface A_n = $A/2$, $\overline{U}_n = \overline{U}$ and $C_{c,n} = C/2$, but having the hot fluid maldistributed such that in one of the Exchangers $C_{h,1} = C(1 + \phi)/2$, whereas in the other $C_{h,2} = C(1 - \phi)/2$, ϕ being the maldistribution parameter. It is also assumed that the fluid specific heat is independent of temperature.
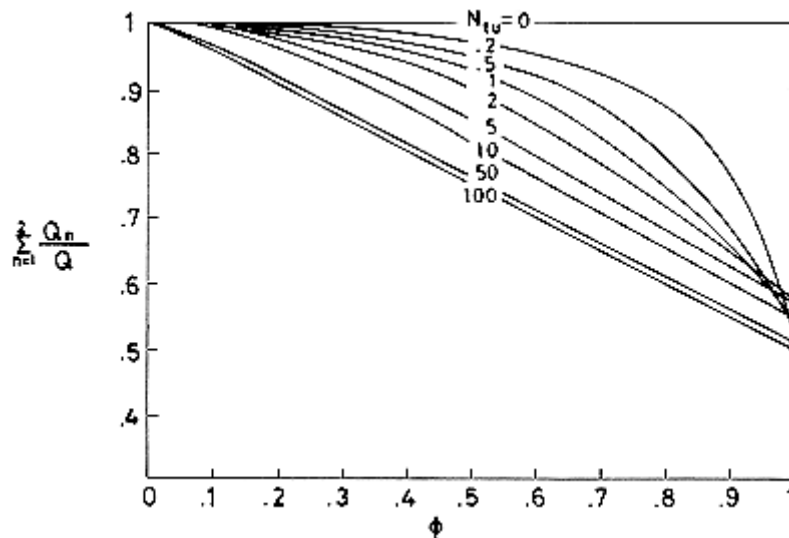
Figure 11-33: Relative capacity, $\Sigma Q_n/Q$, of a simple two fluid heat exchanger vs. the maldistribution parameter, ϕ, for several values of the nominal number of heat transfer units, N_{tu}. From Weimer & Hartzon (1973) [187].
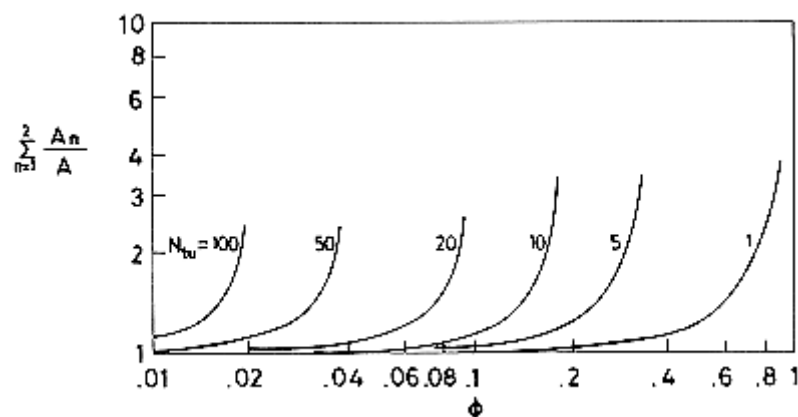
Figure 11-34: Relative surface requirements, $\Sigma A_n/A$, of a simple two fluid exchanger for fixed total duty vs. the maldistribution parameter, ϕ. Results are shown for several values of the nominal number of heat transfer units, N_{tu}. From Weimer & Hartzog (1973) [187].

Figure 11-33 shows the reduction in duty of the heat exchanger as a function of the maldistribution parameter, ϕ, for several values of N_{tu}.

It can be seen that the effect of a given degree of maldistribution is strongly affected by the nominal number of heat transfer units in the exchanger. It should be said, however, that large values of ϕ are highly unrealistic; for a countercurrent plate-fin exchanger, maldistribution parameters of 0,1 are normally tolerated.

Figure 11-34 indicates how much surface should be added to the exchanger to achieve the same heat transfer duty for a maldistributed case as for a perfectly distributed case.

Notice that for each design value of N_{tu} there is a limiting degree of maldistribution beyond which no further increase in exchanger surface can restore the original duty.

A slightly more general approach to performance prediction in terms of maldistribution has been taken up by Fleming (1967) [65], who considered a split counterflow heat exchanger, Figure 11-35. One side of this heat exchanger, the "uniform" side, has flow distributed uniformly among all its channels. The other side, the "nonuniform" side, which carries the same total flow rate as the uniform side, is divided into two parts, the first one carries a lower-than-average flow in each channel uniformly distribution among the fraction F_{Low} of the total channels, whereas the second part carries a higher-than-average flow in each channel uniformly distributed among the fraction $1 - F_{Low}$ of the total channels.
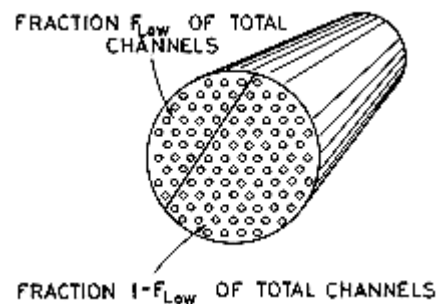
Figure 11-35: Flow distribution model for the non-uniform side. From Fleming (1967) [65].

The first problem considered by Fleming corresponds to the case of paired channels. Paired channels means that each channel with hot fluid is in thermal contact with a single channel with cold fluid for the whole length of the exchanger. A purely counterflow shell-and-tube exchanger or a plate-fin exchanger almost fits into this category, although the channels are not paired strictly on a on-to-one basis, but rather, each channel may exchange heat with more than one channel on the other side.

Representative results are given in Figure 11-36. Data on Figure 11-36a have been computed for a nominal number of heat transfer units $N_{tu} = 10$, and those in Figure 11-36b for $N_{tu} = 100$.
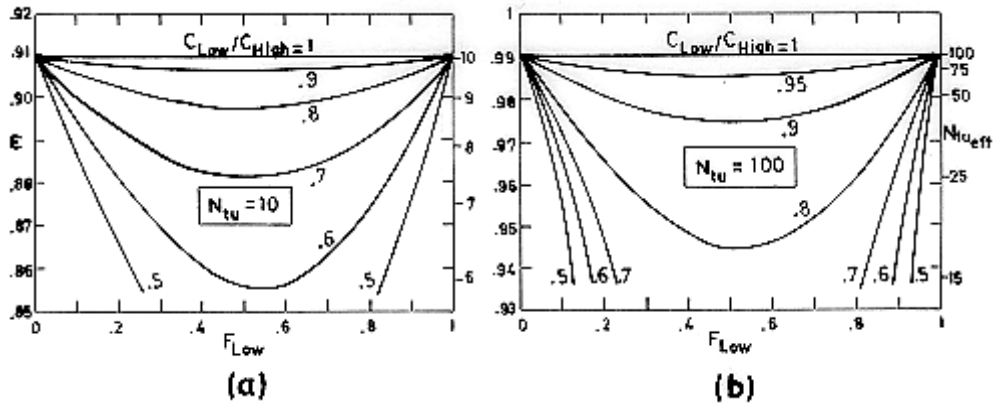
Figure 11-36: Overall effectiveness, ε, and effective number of heat transfer units, $N_{tu\,eff}$, vs. the fraction, F_{Low}, of channels which carry lower-than-average flow on the nonuniform side of a "paired channels" heat exchanger. Results are shown for different values of the ratio of the capacity rate, C_{Low}, of a single channel with lower-than-average flow to the capacity rate, C_{High}, of a single channel with higher-than-average flow. (a) is for a nominal number of heat transfer units N_{tu} = 10 and (b) for N_{tu} = 100. From Fleming (1967) [65].

It can be deduced from Figure 11-36 that the effect of flow maldistribution increases with increasing the nominal number of heat transfer units and can be very severe for high N_{tu} values, thence a strong emphasis should be placed on good header design and on channel uniformity. As a demonstration of the effect of flow maldistribution, suppose an exchanger designed with N_{tu} = 100 for an overall effectiveness of 0,99. If, however, half the tubes on one side each carries 0,8 of the flow carried by each tube of the other half (F_{Low} = 0,5, C_{Low}/C_{High} = 0,8 in Figure 11-36b) the actual overall effectiveness will be only ε = 0,944 and the effective number of heat transfer units, $N_{tu\,eff} \cong$ 16,5.

The situation is much more favourable if it is assumed that the uniform flow side is completely and continuously mixed throughout the heat exchanger. An example of exchanger which comes close to this case would be the purely counterflow shell-and-tube exchanger, if the tube side is considered to be the nonuniform side. As a consequence of the complete mixing assumption the fluid temperature in the uniform side is uniform at any cross section.

Results from calculations performed by Fleming (1967) [65] are given in Figure 11-37. It can be seen that even for large non uniformities (C_{Low}/C_{High} = 0,5) there is little effect on the exchanger thermal performance, and that this effect is more pronounced for smaller values of N_{tu}.
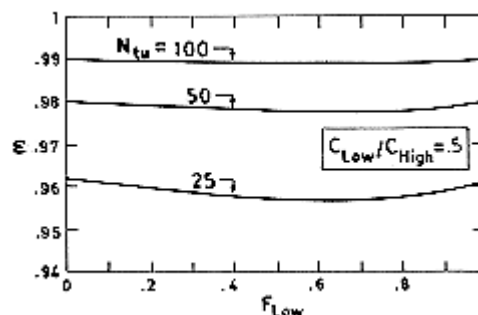
Figure 11-37: Overall effectiveness, ε, vs. the fraction, F_{Low}, of channels which carry lower-than-average flow on the nonuniform side of a heat exchanger with uniform

side mixed. Results are shown for different values of the nominal number of heat transfer units N_{tu}, and of the ratio C_{Low}/C_{High}. From Fleming (1967) [65].

Complete mixing at any cross section is an ideal limit which cannot be realised in any real heat exchanger. A step in the direction of continuous mixing would be the collecting and mixing of one or both streams at intervals along the exchanger length. This case has been also considered by Fleming (1967). In order to move beyond the considerations presented above, it is necessary to particularise the study to configurations of actual heat exchangers and to develop mathematical models for simulating actual exchanger performance. Results for helical coil-wound exchangers and for plate-fin exchangers, both two-fluid and four-fluid exchangers, have been given by Weimer & Hartzog (1973) [187].

11.4.3.2 Maldistribution compensating techniques in shell-and-tube heat exchangers

The ideal flow distribution in the shell side of a baffled exchanger is shown schematically in Figure 11-38.
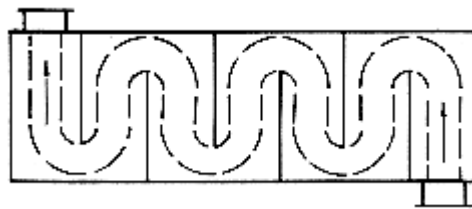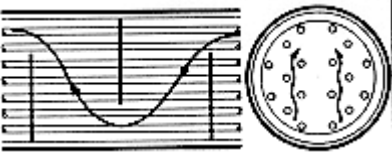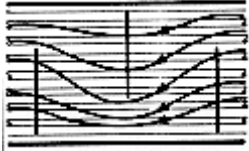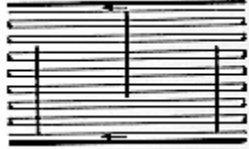
Figure 11-38: Ideal flow distribution in the shell side of shell-and-tube heat exchangers.

The actual situation is far from ideal, however, unless especial provisions are taken to minimise the adverse effects. The several fluid pathways which appear in practical cases are shown in Table 11-13. Although the performance degradation associated with each fluid pathway can be estimated (see a critical survey of the available design methods by Taborek (1974) [171]) engineering practices for reducing maldistribution in the sell side of shell-and-tube exchangers are well known. These practices are summarised in Table 11-14.

Table 11-13: Fluid Paths in the Shell Side of Shell-and-Tube Exchangers [a]
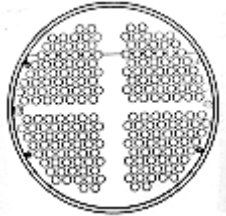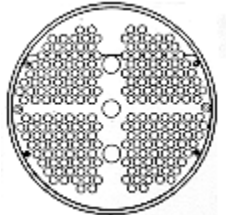
Stream	Definition	Sketch	Source of Maldistribution	Comments
B	True crossflow stream			Basis for comparison of both heat transfer and pressure drop.
A	Flow through the gap between the tube and the baffle tube hole, which is induced by the pressure differential on the two sides of the baffle		Standard baffle tube holes are drilled $0{,}79 \times 10^{-3}$ m (1/32") over the tube outer diameter for unsup-ported tube lengths below 0,914 m. For larger lengths or for pulsating conditions tube holes may be drilled smaller than standard (TEMA (1968) [176]).	Fully effective for heat transfer. Decreases the overall pressure drop.
C	Flow bypassing the bundle		Bundle-to-shell clearance. Blocking devices are be used when these clearances are larger than approximately one tube layout pitch.	Partially effective for heat transfer as the fluid contacts the heat transfer-ring surfaces on one side of the tubular field only
D	Flow through open passages in tube layout partitions when they are in the direction of the main crossflow stream		Open passages in tube layout partitions. Use of blocking devices is recommended.	More effective for heat transfer than C-stream.

Stream	Definition	Sketch	Source of Maldistribution	Comments
E	Leakage flow between baffle and shell.		Shell-to-baffle clearance. For heat exchangers of general purpose applications this clearance is equal to $2,54 \times 10^{-3}$ m for nominal shell inside diameters in the range 0,152 m to 0,330 m (TEMA (1968) [176]).	Very ineffective for heat transfer. It greatly distorts the temperature profiles.

a   Arranged by the compiler after Taborek (1974) [171]. Capital letters labeling the different pathways are those used by Taborek.

Table 11-14: Engineering Practices for Reducing Maldistribution in the Shell Side of Shell-and-Tube Exchangers [a]

Configuration and correction practice	Sketch	Comments
Basic configuration. Conventional 4 pass layout. No baffles are used. The fluid in the tube side flows perpendicularly to the plane of the figure. In two of the bundles the fluid flow toward the observer, and in the other two from the observer toward the figure, thus the fluid in the tube side traverses four times the heat exchanger before leaving it.		The flow in the shell side is essentially parallel to the tubes, and because of the open space and the frictional resistance of the tubes, the actual velocity in the vicinity of the tubes is considerably less than the velocity through the open spaces. Calculations of the heat transfer coefficient based on the mean velocity through the shell side will be in error.
Addition of segmented baffles. A baffle cut of approximately 20% is provided as indicated in the sketch.		Even assuming that clearances between inside diameter of the shell and baffle diameter are kept to a minimum and that other bypass paths are minimized, mere addition of segmental baffles does not guarantee agreement between theoretical prediction and actual performance. The flow is partly parallel and partly normal to the tubes and, in addition, bypass lanes still exist.

Configuration and correction practice	Sketch	Comments
Addition of tie rods and concentric spacers may be so chosen as to block the bypass area between the outermost tubes and the inside of the shell.		Tie rods and concentric spacers are used to hold baffles in position against mechanical forces during bundle assembly or removal, and against fluid forces during operation.
Insertion of rods or dummy tubes.		The aim of these rods is to block the bypass are in tube layout partitions. The number and size of the dummy tubes vary with the size of the tube bundle and the width of the pass lane. It is considered good practice to use a dummy tube at every fifth row.

a   Arranged by the compiler after Gilmour (1965) [72].

11.4.3.3 Maldistribution compensating techniques in parallel counterflow heat exchangers

A way to solve the imbalance problem in parallel counterflow heat exchangers has been suggested by Cowans (1974) [28]. The device, which can only be used with gases, is based on the effects of maldistribution upon the fluid temperature profiles along the heat exchangers, Figure 11-39.
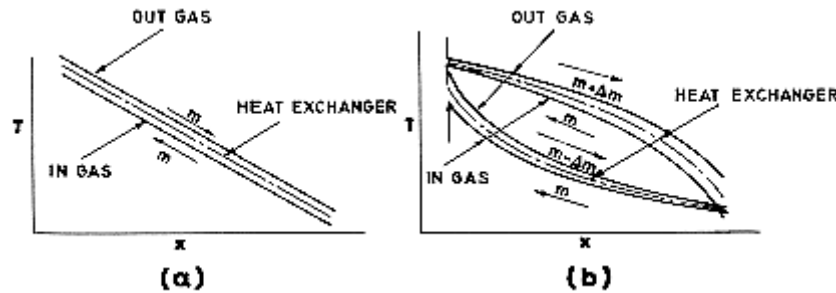
Figure 11-39: Schematic of the temperature distribution along the heat exchanger. (a) Balanced case. (b) Imbalanced case. From Cowans (1974) [28].

Figure 11-39a shows the temperature profile for a balanced heat exchanger. The resulting curves are parallel-straight lines. Figure 11-39b, in its turn, corresponds to a case of flow imbalance. It is realised from these figures that when the mass flow rate of the hot flow becomes higher-than-average the temperature profiles shift up, particularly in the middle of the heat exchanger, and that they will shift down when the mass flow rate of the hot flow becomes below average. This shift in temperature induces a shift in pressure drop.

For laminar flow,

$$\frac{dp}{dx} \sim \frac{\mu}{\rho}$$

[11-22]

since $dp/dx \sim \mu m/\rho$ (see clause 7.2.2).

For turbulent flow, on the other hand,

$$\frac{dp}{dx} \sim \frac{\mu^{0,2}}{\rho}$$

[11-23]

since $dp/dx \sim \lambda m^2/\rho$ and $\lambda \sim Re^{-0,2 \text{ to } 0,25}$ (see clause 7.2.2 and Table 7-2 in clause 7.2.2.1). In addition, for most gases $\mu \sim T^{0,6 \text{ to } 0,8}$ and $\rho \sim T^{-1}$. Thus, dp/dx increases when the temperature increases for both laminar and turbulent flow of gases.

The shift in temperature does not mitigate the flow imbalance in a typical heat exchanger since both sides of the exchanger are affected in the same manner because the temperature profiles are quite similar. Cowans (1974) [28] conceived the idea of shaping the two sides of the heat exchanger passages differently (Figure 11-40) so that the temperature shift in the middle of the exchanger strongly affects the pressure drop of the hot flow only. According to Cowans the power of this feedback is quite substantial. He reports that the performance of a high-efficiency ($\varepsilon > 0,9925$) balanced-flow

countercurrent heat exchanger designed for operation at $N_{tu} = 200$, was so degraded by flow imbalance that the actual effectiveness of the prototype was $\varepsilon = 0,95$ and $N_{tu} \cong 20$. After improvement of design and manufacturing techniques the performance improved to $\varepsilon = 0,97$, $N_{tu} = 33$. No further improvements in manufacturing techniques could be attained. After the feedback compensation technique was conceived another unit was designed and built identical to the last unit but with the passages tapered from $0,7 \times 10^{-3}$ m to $0,3 \times 10^{-3}$ m in one dimension, as indicated in Figure 11-40. All other parameters remained unchanged. The efficiency of the modified unit improved to $\varepsilon = 0,994$ giving $N_{tu} = 167$.
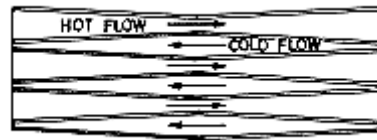
Figure 11-40: Flow imbalance compensating technique for gas to gas heat exchangers. From Cowans (1974) [28].

This feedback compensation technique cannot be used with liquids since in this case ρ is practically temperature independent whereas μ decreases when the temperature increases. Thence, an increase in temperature produces a decrease in pressure drop and conversely.

No information has been found on flow imbalance compensating techniques for liquid to liquid heat exchangers.

11.5 Manufacturing defects

11.5.1 Introduction

The advantage which present heat exchangers employing high area density surfaces can be fully exploited when manufacturing tolerances are kept under close control. Nevertheless, there are some upper limits to the achievable accuracy. For instance, it is difficult to fabricate heat transfer surfaces to a dimensional tolerance better than ± 5%. This figure would be typical of very good practice.

The aim of this clause is to relate manufacturing imperfections to performance degradation in real heat exchangers. In several instances analytical models exist which provide useful guidance in the definition of the manufacturing tolerances. In other cases. however, one must resort to the testing of representative configurations. The influence of manifold irregularities is difficult to assess since any effect due to this factor can be hidden in the overall design by increasing the total pressure loss through the exchanger core. According to Cowans (1974) [28], a ± 5% variation in the pressure loss for a given mass flow rate due to this cause could be considered excellent practice.

11.5.2 Variations of the flow passages

A theoretical analysis of the performance degradation in laminar flow regenerators (clause 11.1) because of small variations in spacing between corrugations was made by London (1970) [118]. The non uniformities considered are either of the "plate-spacing type", Figure 11-41a, or of the "fin-spacing type", Figure 11-41b. The geometrical characteristics of the surfaces are summarised in Table 11-15.
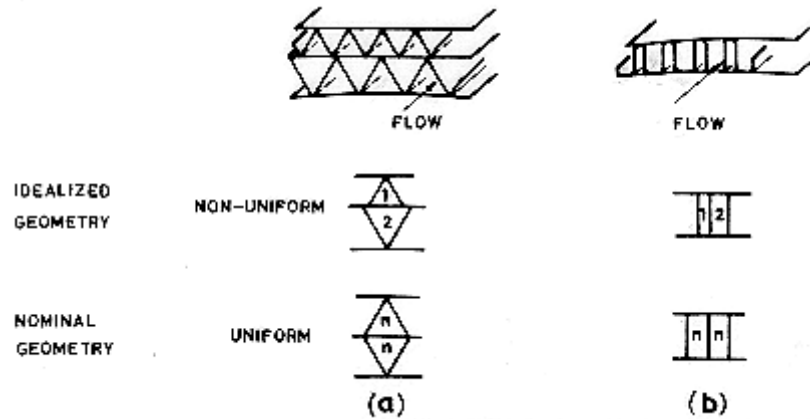
Figure 11-41: Plate spacing, (a), and fin spacing (b), type flow passage non-uniformities. From London (1970) [118].

Table 11-15: Nominal Dimensions for Numerical Results

Glass-ceramic isosceles triangular passage geometry	Stainless steel deppfold configuration
Cell base c x 10³ [m] :0,643	Passage width c x 10³ [m] :0,360
Cell height d x 10³ [m] :0,457	Passage height b x 10³ [m] :2,88
Cell height-to-width ratio :0,710	Passage aspect ratio b/c :8,00
Apex angle [angular degrees] :109,2	Foil thickness a x 10⁶ [m] :53,3
Passage count Nx10⁻⁶ [Passages.m⁻²] :3,4	Fraction of foil surface coverage[c], y :0,125
Porosity [a] ϕ :0,650	Passage count N x 10⁻⁶ [Passages.m⁻²] :0,809
Area density [b] α [m².m⁻³] :7900	Porosity [a] ϕ :0,840
Flow area per passage A_FL x 10⁶ [m²] :0,190	Area density [b] α [m².m⁻³] :5250
Hydraulic diameter D_E x 10³ [m] :0,330	Flow area per passage A_FL x 10⁶ [m²] :1,037
	Hydraulic diameter D_E x 10³ [m] :0,640

[a] Porosity, ϕ, is the ratio of flow are to frontal area of matrix core.

[b] Area density, α, is the ratio of heat transfer surface area (two sides) to core volume.

[c] Fraction of foiled surface coverage, y, is the fraction of foil stock surface that covers itself for the deepfold surface. For exactly rectangular folding: $y = (c+2a)/(2c+b+2a)$.

NOTE   From London (1970) [118].

The assumptions on which the analysis is based are listed in Table 11-16. The approach can be applied to other geometrical configurations, other types of non-uniformities and other flow conditions.

Table 11-16: Basic assumptions for the theoretical analysis

1. Heat transfer coefficient and friction factor are constant with passage flow length.

2. The flow is assumed to be laminar (the passage Reynolds number, Re, is less than 500). Although in the case of triangular passage geometry, the cells are isosceles triangles of apex 109 deg, data for equilateral triangles are used in the analysis.

3. End losses are small enough relative to tube friction so that their influence is negligible.

4. Fluid properties, μ, ρ and Pr are the same for all passages and can be treated as constant.

5. To deal with flow passage cross section non-uniformities, the following assumptions are made.

5.1. Wall temperature increases linearly along each passage reaching a common maximum value at the exit.

5.2. The fluid bulk temperature at the passage entrance is the same in any case.

5.3. Wall to fluid temperature difference remains constant along the tube.

As a consequence of these assumptions the following simple relations between passage heat transfer effectiveness, ε, and passage number of heat transfer units, N_{tu}, holds:

$$\varepsilon_n = \frac{N_{tu,n}}{1 + N_{tu,n}} \quad , \quad n = 1,2$$

where ε and N_{tu} are defined as follows:

$$\varepsilon = \frac{T_{bo} - T_{bi}}{T_{wo} - T_{bi}}$$

$$N_{tu} = \frac{h \pi D_E L}{m c_p} = \frac{Q}{m c_p (T_w - T_b)}$$

N_{tueff} for the combination 1-2 passage system can be expressed as

$$N_{tu_{eff}} = \frac{\varepsilon_{av}}{1 - \varepsilon_{av}}$$

where ε_{av} represents the weighted average of the mixed flow outlet stream temperatures,

$$\varepsilon_{av} = \frac{m_1 \varepsilon_1 + m_2 \varepsilon_2}{m_1 + m_2}$$

5.4. The mass flow rates m_1 and m_2 through passages 1 and 2 respectively, are distributed so as to ensure that the pressure drop is the same for both passages.

NOTE   Arranged by the compiler after London (1970) [118].

The results are presented in Figure 11-42 as a heat transfer performance penalty and a pressure loss reduction (a gain) relative to the behaviour of the exchanger with uniform geometry, versus the geometrical non-uniformity, which is measured in terms of the relative change of a characteristic length of the passage cross section.
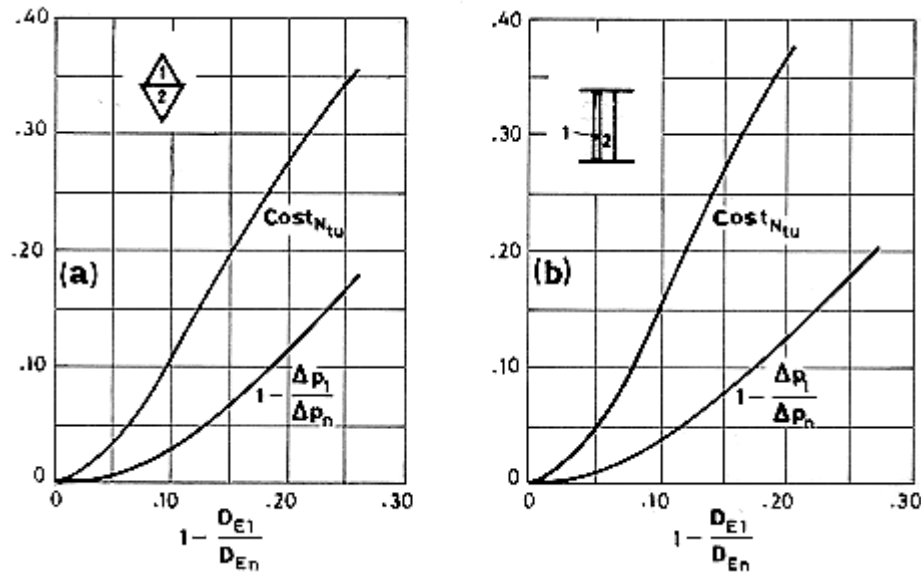
Figure 11-42: Degradation in the heat exchanger thermal performance, measured by *Cost_Ntu*, and relative gain in pressure loss, 1-($\Delta p_1/\Delta p_n$), as functions of the deviation in channel size, 1-(D_{E1}/D_{En}). Results in (a) apply to any cylindrical passage provided that the non-uniformities are geometrically similar. Results in (b) are for non-uniformities of the fin-spacing type. From London (1970) [118].

The degradation in the heat exchanger thermal performances is expressed by means of the cost fraction

$$Cost_{N_{tu}} = 1 - \frac{N_{tu_{eff}}}{N_{tu}}$$
[11-24]

N_{tu} corresponding to the nominal configuration.

Manufacturing tolerances can be tentatively specified on the bases of these results. It is not yet clear what statistical methodology should be used to relate manufactured cores, with a distributed range of sizes, to the equivalent two-size-passage model used in the analysis. As a tentative proposal, based on Figure 11-42a and b, the following manufacturing tolerance targets are recommended.

1. Geometries where the distortions tend to preserve geometrical similarity with the nominal configuration

$$\left(1 - \left(\frac{D_E}{D_{E_n}}\right)^2\right)_{av} = \pm 20 \ percent$$
[11-25]

and 95 percent of the passages within ± 40 percent. This corresponds to 1 - (D_{E1}/D_{En}) = 0,10 in Figure 11-42a.

2. Deepfold plate-fin surfaces for fin-spacing non uniformities

$$\left(1 - \frac{c}{c_n}\right)_{av} = \pm 10 \; percent \qquad [11\text{-}26]$$

and 95 percent of the passages within ± 20 percent.

11.5.3 Fin leading edge imperfections

This effect is particularly noteworthy when strip-fin surfaces, as those shown in Figure 11-3e, are used in compact heat exchangers. Fins of this type are generally constructed by a machine-cutting process that inevitably leaves a slightly bent and scarfed fin edge, whose geometrical characteristics depend upon the fin material and upon the cutting tool. Since a few microns of scarfing can have a considerable effect on the friction performance of the surfaces, it is difficult to either dimensionally describe this effect or to exactly reproduce the test surfaces.

A soft material, such as aluminium, may be expected to yield fin edges which are somewhat different that those obtained from a hard material, such as stainless steel. Thence, some experimental uncertainty should be accounted for when performance data obtained with aluminium test surfaces are applied to surfaces of stainless steel construction. In these situations, some conservatism in design is advisable (Kays & London (1964) [102]).

11.5.4 Brazing

Brazing is used in compact exchanger surfaces for structural stability purposes and for insuring adequate thermal contact between fin and base plate.

The influence of brazing on the heat transfer characteristics is small. Brazing results in coverage of surface with consequent reduction of the total heat transfer area. This is detrimental in the case of regenerators where brazing is used only for structural purposes.

On the other hand, the influence of brazing on flow friction is quite significant because of the roughness it introduces. This roughness is of two types: 1) a fine grained surface roughness and 2) that produced by the flow of excess braze material during the fusion process which partially blocks the flow passages. The influence of brazing roughness decreases as the core becomes less compact, because then both the dimensionless roughness, e/D_E, and the blocking of the flow passages are reduced.

The influence of brazing on the performances of compact heat exchangers has been studied experimentally by Shah & London (1970) [164]. Although these authors tested three different heat transfer surfaces, only two of them will be considered here because their geometries are very similar and because their performances were measured by used of the same experimental method.

The configurations chosen for the test are offset rectangular plate-fin surfaces of the plate-fin strip-fin variety. The general features of the fins are depicted in Figure 11-43, whereas Table 11-17 provides a comparison of the tested surfaces.
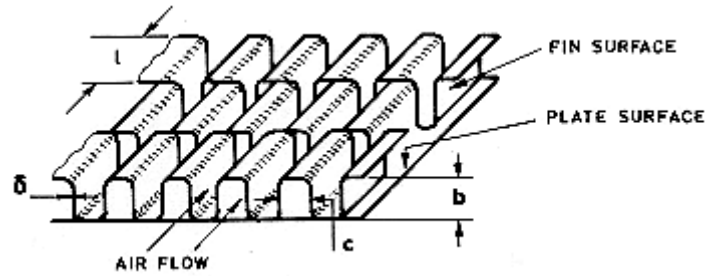
Figure 11-43: Fin center of offset rectangular plat-fin surface. From Shah & London (1970) [164].

Table 11-17: Characteristics of Offset Rectangular Plate-Fin Surfaces

Core Number [a]	501	501 MOD
Plate spacing, $b \times 10^3$ [m]	0,673	0,665
Fin pitch, $c \times 10^3$ [m]	0,688	0,711
Fin offset length, $l \times 10^3$ [m]	1,27	1,27
Plate thickness, $a \times 10^3$ [m]	0,154	0,025
Fin thickness, $\delta \times 10^3$ [m]	0,025	0,025
Porosity [b], ϕ	0,744	0,896
Area density [c], α [m².m⁻³]	4610	6240
Area density [d], β [m².m⁻³]	5650	6483
Hydraulic diameter, $D_E \times 10^3$ [m]	0,645	0,574
Dimensionless core length in flow direction, L/D_E	101,2	113,2
Dimensionless fin offset length, l/D_E	1,97	2,21
Aspect ratio, $\alpha^* = (b-\delta)/(c-\delta)$	0,977	0,933
Brazed construction	yes	no

[a] Author's designation.

[b] Porosity is the ratio of free flow air on one side of the heat exchanger core to frontal area of that side.

[c] Area density a is the ratio of total heat transfer area of one side of the heat exchanger to total exchanger volume.

[d] Area density b is the ratio of total heat transfer area on one side of a plate-fin heat exchanger to the volume between the plates on that side.

NOTE   From Shah & London (1970) [164].

Both surfaces were built into cores for the heat transfer testing with a 82,5 x 10^{-3} by 82,5 x 10^{-3} m test cross section and a 65,3 x 10^{-3} m air flow length. In Core 501, the fins were separated by plates of 0,152 x 10^{-3} m thickness and the core was brazed. In Core 501 MOD the fins and the plates both were 0,025 x 10^{-3} m thick and were stacked alternatively without brazing. Material for the plates and fins for both cores was stainless steel (AISI 347 type).

The values of Φ, α, β and D_E in Table 11-17 are calculated on the basis of some geometrical idealisation of the cells constituting the core. Figure 11-44 shows the models used to derive these properties.
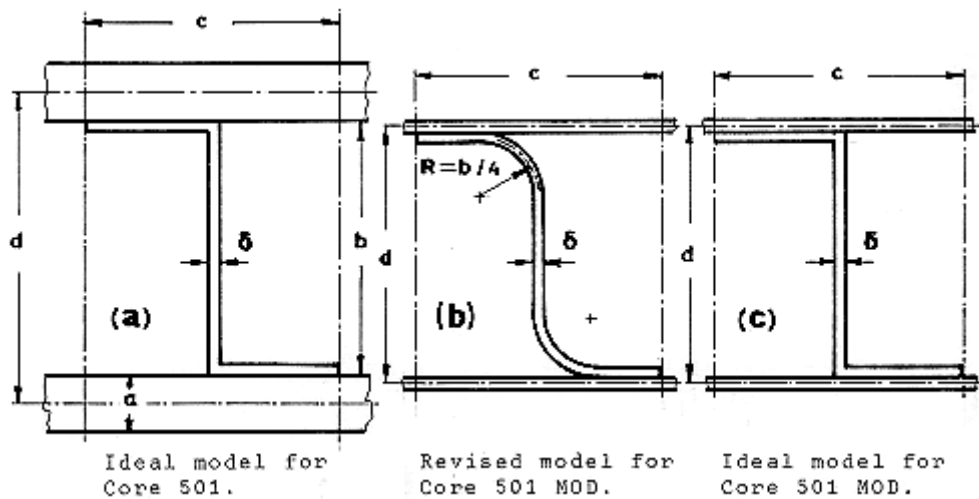
Figure 11-44: Assumed core geometries. From Shah & London (1970) [164].

Model (b) represents fairly realistically the unbrazed surface, which did not exhibit as complete mechanical contact between fins and plate as could be wrongly deduced from model (c). The values of the relevant parameters as deduced from models (b) and (c) are compared in Table 11-18. It can be seen that model (b) yields the higher area density, and consequently the lower D_E, by about 14 percent.

Table 11-18: Core 501 MOD Geometries Derived from Different Models

	Table 11-17	Rectangular Model Figure 11-44c	Modified Model Figure 11-44b
Cell height, d x 10^3 [m]	0,691	SAME	
Cell width, c x 10^3 [m]	0,711		
Plate thickness, a x 10^3 [m]	0,025		
Fin thickness, δ x 10^3 [m]	0,025		
Porosity, Φ	0,896 [a]	0,893	0,902
Area density, α [m².m⁻³]	6240	5381	6240
Hydraulic diameter, D_E x 10^3 [m]	0,575	0,667	0,574

[a]   Porosity determined gravimetrically.

NOTE   From Shah & Londono (1970) [164].

Heat transfer tests were made by the single-blow transient testing technique. A summary of the theory underlying this technique, a description of an experimental facility, and comments on the applicability of the test results can be found in Pucci, Howard & Piersall (1967) [145]. Pressure loss was measured by the conventional steady-flow procedure.

The dimensionless heat transfer and fluid friction characteristics are presented in Figure 11-45 as functions of the Reynolds number, Re, based on the hydraulic diameter, D_E. Heat transfer data are presented in terms of the Colburn factor, j (see Eq. [11-12] in clause 8.2.4). Fluid friction data are given in terms of the Fanning friction factor, f (see clause 7.2.2). Estimates of the experimental uncertainty are as follows: $j \pm 13$ %, $f \pm 3$ % and $Re \pm 2$ %.

It can be seen from Figure 11-45 that both surfaces exhibit quite closely the same heat transfer characteristics. At low Reynolds number the gross blockage due to brazing would reduce j slightly. At high Reynolds number, however, brazing roughness induces an earlier transition to turbulence improving the heat transfer. The different slope of the two curves could be also due to a 10 percent difference in $1/D_E$, as indicated in Table 11-17.
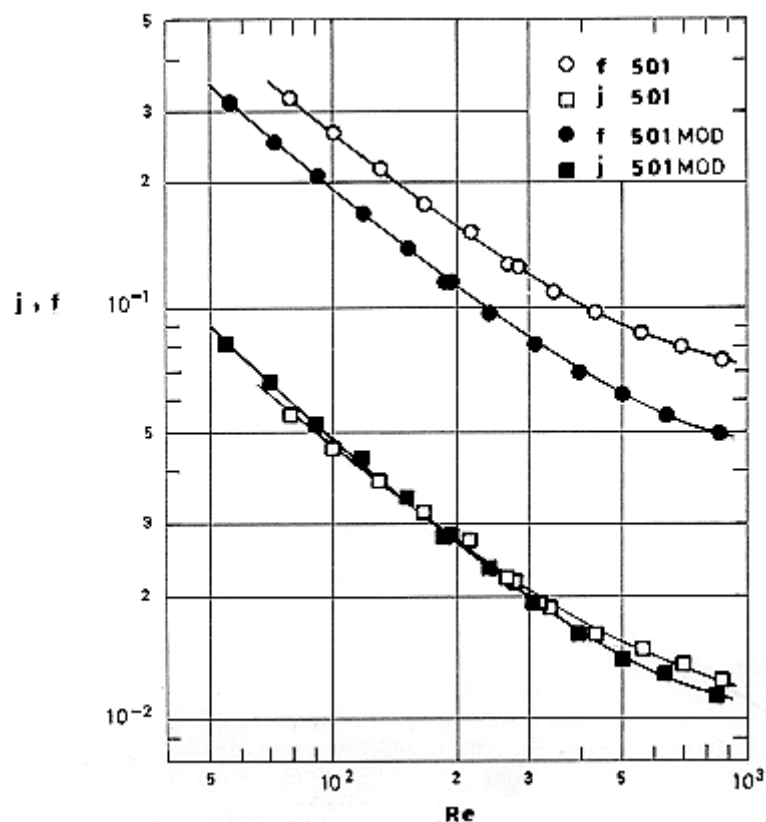
Figure 11-45: Heat transfer, j, and friction, f, characteristics as functions of Reynolds number, Re, for surfaces 501 and 501 MOD. From Shah & London (1970) [164].

The frictional characteristics are, on the other hand, strongly influenced by brazing. The surface with the greatest relative roughness (Core 501) has 35-50 percent higher friction factor relative to the smooth surface (501 MOD).

Figure 11-46 shows the flow area goodness factor, measured by the ratio j/f, as a function of the Reynolds number, Re.
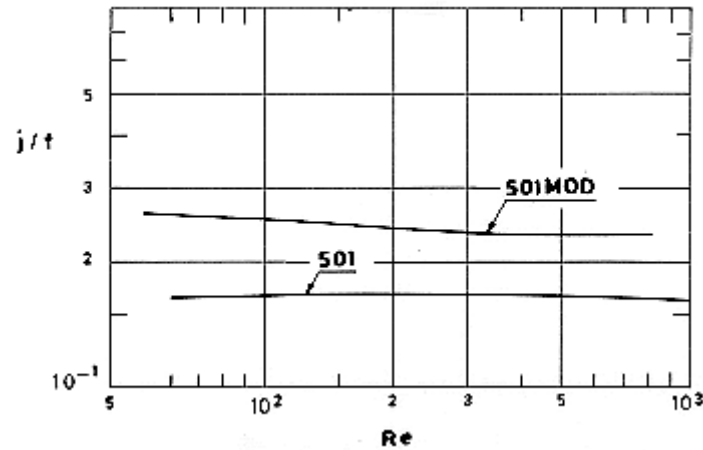
Figure 11-46: Flow area goodness factor, *j/f*, as a function of Reynolds number, *Re*, for surfaces 501 and 501 MOD. From Shah & London (1970) [164].

11.6 In service degradation

11.6.1 Introduction

Performance degradation of real heat exchangers could be due to incompatibility of the working fluid with the material surfaces and to impurity deposits. Data on material compatibility of typical liquid coolants with both metals and elastomers are given in clause 10.3, Table 10-2 to Table 10-9. The effect of impurity deposits can vary enormously. If the stream is pure and the time between overhauls short, the effect can be nil. Because of the relatively short orbital time of present manned spacecraft, which are the only satellites in which the use of relatively sophisticated fluid loops is envisaged, the effect of impurity deposits is negligible. Nevertheless, the problem will become more acute in the future with the advent of reusable space vehicles.

11.6.2 Fouling

The term fouling is used in the literature to describe any undesirable deposit on heat exchanger surfaces which increases resistance to heat transfer. There are a great variety of fouling forms (polymerisation, chemical reaction deposits, crystallisation, sedimentation, corrosion, etc.). This fact, prevents a systematic treatment of the problem.

In general, the effect of fouling is described in terms of a fouling resistance, r_f (often referred to as fouling factor), which is added to the inverse thermal conductance (see Eqs. [11-2] in clause 11.2.2).

The expression for U_h, thus becomes

$$U_h = \left[\frac{1}{\eta_h h_h} + \frac{a}{(A_w/A_h)k} + \frac{1}{(A_c/A_h)\eta_c h_c} + r_f + \frac{A_h}{A_c} r_{f_c} \right]^{-1} \qquad \text{[11-27]}$$

where the value of r_f in each particular case can be found in some experience-based table. The most comprehensive source of fouling data has been compiled by the US Tubular Exchanger Manufacturers Association (TEMA Standards). Some useful values are given in Table 11-19.

Table 11-19: Fouling Resistance of Several Common Materials [a]

Material	r_f x 10^4 [K.m^2.W^{-1}]
Gases and Vapors	
Steam	0,88
Refrigerant Vapors	3,5
Compressed Air	3,5
Industrial Organic Heat Transfer Media	1,8
Liquids	
Distilled Water	0,88
Refrigerant Liquids	1,8
Hydraulic Fluids	1,8
Industrial Organic Heat Transfer Media	1,8
Molten Heat Transfer Salts	0,88

[a] From TEMA Standars (1968) [176].

While the fouling process is obviously a time function, a constant value of the fouling resistance is generally used for design. This if then interpreted as a value to be reached in some reasonable time at which the user of the equipment is willing to clean it. However, the fact that during short times the equipment is clean and, therefore, will operate under frequently drastically different conditions is rarely examined. Designing with a large fouling resistance, which is thought to be reached after a certain time, often leads to a more rapid deterioration of the exchanger (Taborek, Aoki, Ritter, Palen & Knudsen (1972a) [173]).

In practice, large fouling resistances occur often as a consequence of poor design. To avoid this, care should be taken to prevent stagnant regions, by-passes, flow maldistributions, inadequate location of baffles and rods, etc. (Gilmour (1965) [72]).

For many typical heat transfer processes, an improvement in the ability to predict the heat transfer coefficient will be useless, unless accompanied by a correspondingly increased understanding of fouling.

Yet, the efforts presently devoted to fouling are almost negligible. According to Taborek et al. (1972a) [172], the main reasons for this state of affairs are:

1.   Fouling is ill-suited for university-based investigations.

2.   It is difficult to control the relevant parameters in a laboratory.

3.   A continuous supply of flow, always under the same conditions, is required.

4.   Long time is needed to obtain meaningful data.

5.   There are many different types of fouling.

6.   Fouling is influenced by many different factors.

Predictive methods for fouling behaviour are scarce. A good review of the models proposed in the past has been recently completed by Taborek et al. (1972b) [173].

The different forms of fouling, and the effect of the different parameters for each fouling process are discussed in the following tables, especial emphasis is placed on those processes relevant in thermal control technology. Table 11-20 describes the various fouling mechanisms. The effects on fouling of different physical parameters are summarised in Table 11-21.

Table 11-20: Fouling Mechanisms [a]

Mechanism	Description
Crystallization of inverse solubility salts.[b]	• One of the most common causes of fouling. • Crystallization fouling exhibits different behavior depending on whether the solution contains a single salt or a mixture of salts. 1. When the solution contains purely (or primarily) a single salt, the crystalline formations show freat adherence to the surface and between themselves. Because of this strong bond, the removal mechanism is ineffective or negligible, so that fouling is insensitive to flow velocity and thickness of the deposit layer. Thence: • Fouling-time curve is growing function with no asymptotic value. • Generally, an induction period exists during which no fouling deposit occurs, until suddenly fouling starts and keeps growing thereafter. The induction period is a function of surface material and roughness. 2. When the solution is a mixture of salts, crystalline clusters build up in irregular patterns, forming cavities between them which permit deposition of suspended particles, thus decreasing the crystalline cohesion. In this case the removal mechanism is a function of the flow velocity, and of the thickness of the deposit layer. Thence: • Fouling-time curve approaches an asymptotic value. • The variety of crystalline forms, makes fouling initiation less sensitive to the size and distribution of nucleation cavities.
Sedimentation	• Occurs in many practical cases under normal gravity conditions. • Some of the sedimented particles can act as catalysts or enter into complex reactions. • There are many types of fouling by sedimentation and therefore it is difficult to state conclusions. • Very sensitive, in general, to flow velocity.
Chemical Reaction and Polymerization	• In many cases combined with crystallization. • A critical variable is the surface temperature, since the reaction rate will be very sensitive to changes in surface tempearture. • Normally the fouling-time curves approach an asymptotic value, indicating the existence of flow velocity-dependent removal mechanisms.
Organic Material	• Common to untreated water.

Mechanism	Description
Growth	• In most cases combined with crystallization or sedimentation fouling, it can, however, exist as the predominant form. • Existing studies are largely confined to specification of proper treatment material.
Corrosion	• Due to two different mechanism. 1. Creation of a crusty, heat resistance producing layer, such as rust. 2. Roughening of the surface, invariably connected with corrosion, will produce nucleation sites for cyrstallization and sedimenetation. • Systematic studies on this form of fouling are rare since it is often difficult to separate corrosion fouling from other fouling processes.

[a]   Arranged by the compiler after Tabored, Aoki, Ritter, Palen & Knudsen (1972a) [172]

[b]   Inverse solubility salts are those exhibiting decreasing saturation concentration beyond a certain temperature. As a consequence deposits start to form when such solutions contact heated surfaces. Water could contain many salts of the inverse solubility type, especially $CaCO_3$ and $CaSO_4$.

Table 11-21: Effects of Different Physical Parameters on Fouling [a]

Parameter	Effect
Flow velocity	Very strong effect on most fouling processes
Wall surface temperature	Affects many fouling processes particularly crystallization and chemical reaction
Fluid bulk temperature	Affects reaction and crystallization rates
Material	Important effect on fouling initiation. Possible catalytic action and corrosion
Surface finish	Important effect on fouling initiation. Roughness, size and density of cavities will affect crystalline nucleation, sedimentation and adherence tendency of deposits.
Equipment design, geometry and flow pattern	Considerable differences exist depending on flow patterns, velocity and wall temperature distribution, turbulence level, etc.

[a]   Arranged by the compiler after Taborek, Aoki, Ritter, Palen & Knudsen (1972a) [172].

11.7 Existing systems

FREON TO WATER INTERCHANGER

1. Developer: Hamilton Standard, Division of United Aircraft Corporation (now United Technologies Corporation), Bradley Field Road, Windsor Locks, Conn. 06096.

2. Function: Transfers heat from Space Shuttle Atmosphere Revitalisation Subsystem (ARS) water loop to the Freon Coolant Loop (FCL). Normally heat is transferred from one of the two redundant water loops to both Freon loops. In an abort situation, only one of the two Freon loops may be operational.

3. Sketch:
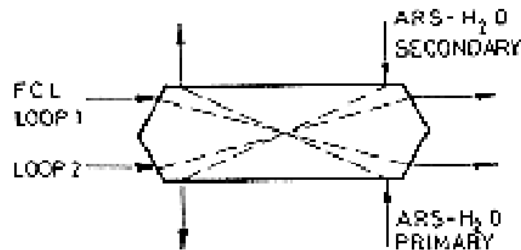
4. Description: Plate-fin configuration, Counterflow arrangement except for the "tent top" area at both ends of the core.

	Fins			Part. Sheets	Area Density α [m².m⁻³]	Core Size			Dry Mass [kg]
	Height $h \times 10^3$ [m]	Thickness $a \times 10^3$ [m]	Fins per meter [m⁻¹]	Thickness, $a' \times 10^3$ [m]		Hot Flow Length, L_h [m]	Clod Flow Length, L_c [m]	No Flow Length, L_{nf} [m]	
ARS Water	0,51	0,051	1260	0,127	6300	0,102	0,610	0,048	15,01
FCL Freon 21	0,51	0,051	1260		6300				

Material: Fins, parting sheets, headers, bosses, etc. - Stainless steel.

5.   Performances:

	Heat transfer rate [W]	Temperatures		Fluid Mass Flow rate, m [kg.s⁻¹]	Effectiveness ε	Pressure drop Δp x 10⁻³ [Pa]
		T_i [K]	T_o [K]			
ARS Water	14140	321,5 [a]	280,5	0,058-0,129	0,93 [b]	20,7 for m = 0,120 kg.s⁻¹
FCL Freon 21		277,5	318 [a]	0,567 (2 loops)		18,6 for m = 0,567 kg.s⁻¹

[a]   Data from Hamilton Standard, CEI No. MC 250-0001-0040. Item No. 7.7. Post-landing conditions.

[b]   From the previously quoted temperatures.
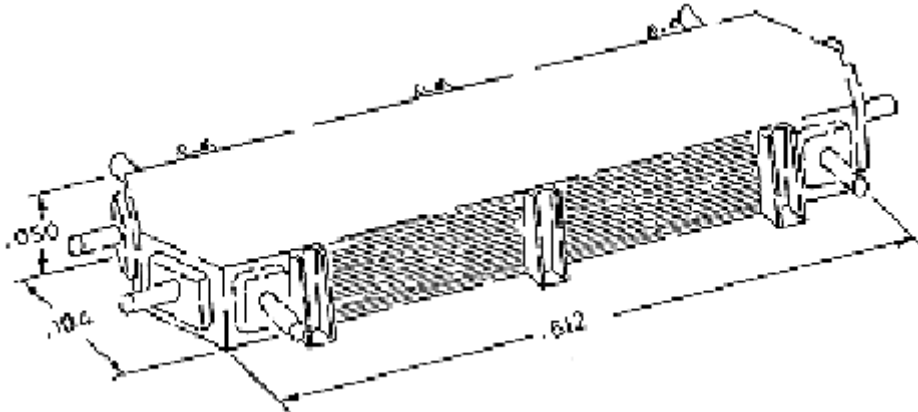
6.   References: The data are from Trusch & Nason (1975) [180], unless otherwise stated.

GSE HEAT EXCHANGER

1.   Developer: Hamilton Standard, Division of United Aircraft Corporation (now United Technologies Corporation), Bradley Field Road, Windsor Locks, Conn. 06096.

2.   Function: Rejects heat from the Space Shuttle Freon Coolant Loop (FCL) to the Ground Support Equipment (GSE) coolant loops, during prelaunch and ground checkout mission modes. Normally heat is transferred from one of the two redundant GSE loops to both FCL loops.

3.   Sketch:
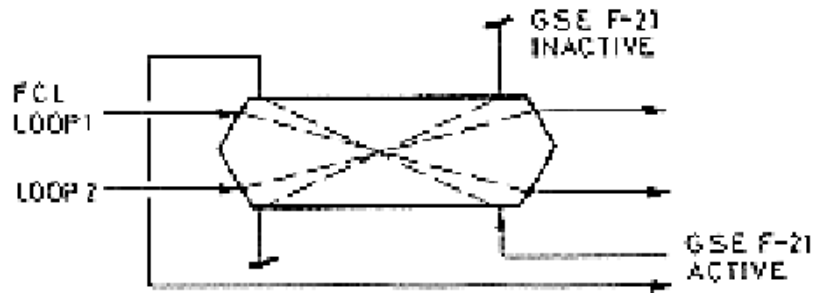
4. Description: Plate-fin configuration. Counterflow arrangement except for the "tent top" area at both ends of the core. The FCL loop flow uses the way of minimum pressure drop to minimise in flight Freon pumping power, whereas the GSE loop uses the way-side ports, which lead to higher pressure drop, even though the mass flow rate is greater than that for the FCL. This is no because pumping power of the GSE is of less concern.

	Fins			Part. Sheets	Area Density α [m².m⁻³]	Core Size			Dry Mass [kg]
	Height $hx10^3$ [m]	Thickness $ax10^3$ [m]	Fins per meter [m⁻¹]	Thickness, $a'x10^3$ [m]		Hot Flow Length, L_h [m]	Clod Flow Length, L_c [m]	No Flow Length, L_{nf} [m]	
FCL Freon 21	0,51	0,051	1260	0,127	6300	0,063	0,198	0,086	6,58
GSE Freon 21	0,51	0,051	1260		6300				

Material: Fins, parting sheets, headers, basses, etc. - Stainless steel.

5. Performances:

	Heat transfer rate [W]	Temperatures		Fluid Mass Flow rate, m [kg.s⁻¹]	Effectiveness ε	Pressure drop Δp x 10⁻³ [Pa]
		T_i [K]	T_o [K]			
FCL Freon 21	31,194	355,5 [a]	275	0,693 (2 loops)	88 [b]	12,1 for m = 0,693 kg.s⁻¹
GSE Freon 21		264	286 [a]	1,260		103,4 for m = 1,260 kg.s⁻¹

a   Data from Hamilton Standard, CEI No. MC 250-0001-0025. Item No. 7.5. The heat exchanger described in this
     document from HS, which resulted from a pre-contract award study, slightly differs from that described here.
     Nevertheless, input and output temperatures are presumably the same for both heat exchangers. The quoted
     temperatures correspond to prelaunch conditions.

b   From the previously quoted temperatures.
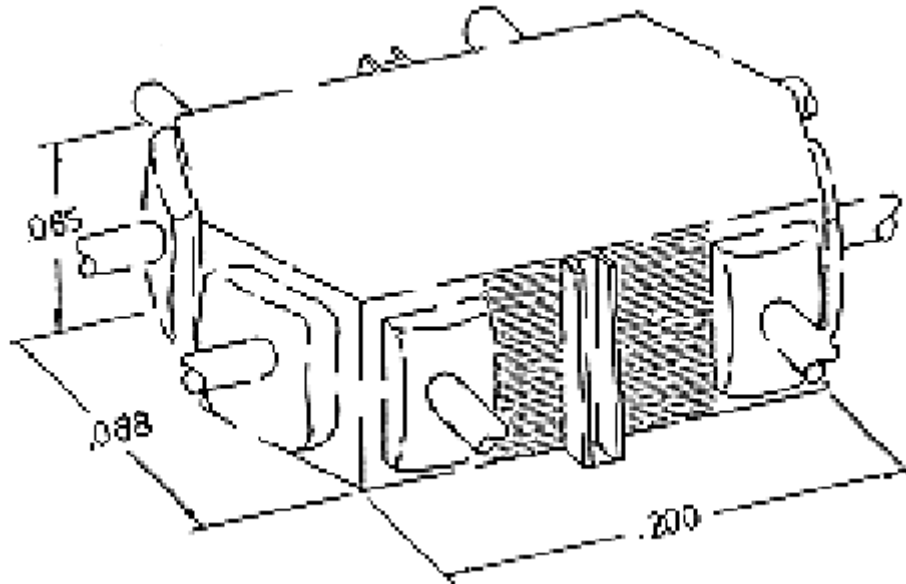
6.   References: The data are from Trusch & Nason (1975) [180], unless otherwise stated.

AVIONICS HEAT EXCHANGER

1.   Developer: Hamilton Standard, Division of United Aircraft Corporation (now United
      Technologies Corporation), Bradley Field Road, Windsor Locks, Conn. 06096.

2.   Function: Cools re circulated air in three closed compartments of the Space Shuttle which
      contain air-cooled electronic equipment. It is a component of the Atmosphere
      Revitalisation Subsystem.

3.   Sketch:
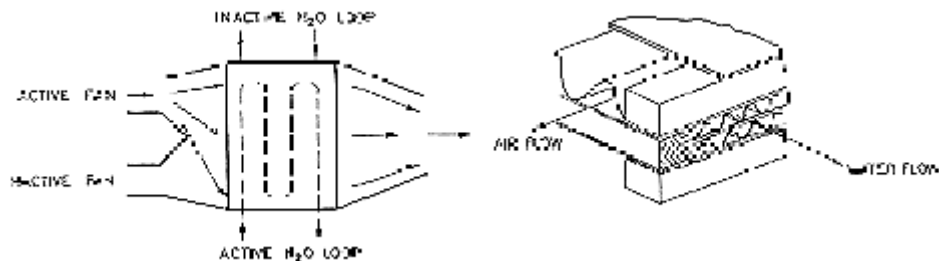
4.   Description: Plate-fin configuration. The core is composed of alternate layers of air,
      primary coolant, and secondary coolant fins separated by parting sheets.

      Air is circulated by one of two redundant fans which are mounted directly to the split
      inlet header. Air cooling is provided by one of two redundant water coolant loops, both
      of which pass through the unit in a four-pass counter crossflow manner.

	Fins			Part. Sheets	Area Density α [m².m⁻³]	Core Size			Dry Mass [kg]
	Height $h \times 10^3$ [m]	Thickness $a \times 10^3$ [m]	Fins per meter [m⁻¹]	Thickness, $a' \times 10^3$ [m]		Hot Flow Length, L_h [m]	Clod Flow Length, L_c [m]	No Flow Length, L_{nf} [m]	
ARS Air	5,08	0,051	945	0,102	2350	0,066	0,284	0,122	6,31
ARS Water	1,27	0,051	1102		3900				

Material: Fins, parting sheets, headers, basses, etc. - Stainless steel.

5. Performances:

	Heat transfer rate [W]	Temperatures		Fluid Mass Flow rate, m [kg.s⁻¹]	Effectiveness ε	Pressure drop $\Delta p \times 10^{-3}$ [Pa]
		T_i [K]	T_o [K]			
ARS Air	1541	331,5 [a]	311	0,110	0,65 [b]	0,164 for m = 0,110 kg.s⁻¹
ARS Water		300	313,5 [a]	0,040		9,997 for m = 0,044 kg.s⁻¹

[a] Data deduced from the values of ε, m and c_p for Air and Water. See Eq. [11-16] in clause 11.2.2 With R = 0,664.

[b] Additional data on the predicted performance of this heat exchanger are plotted below.
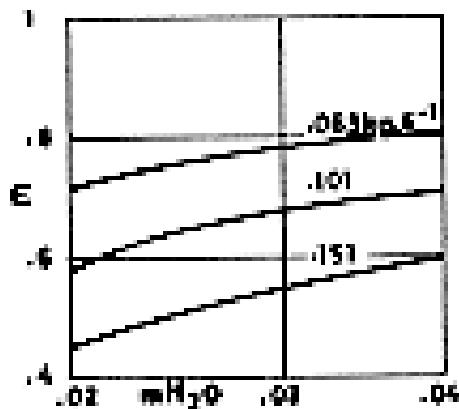
Effectiveness, ε, of the Avionics Heat Eschanger vs. water mass flow rate, m_{H2O}, for several values of air mass flow rate.
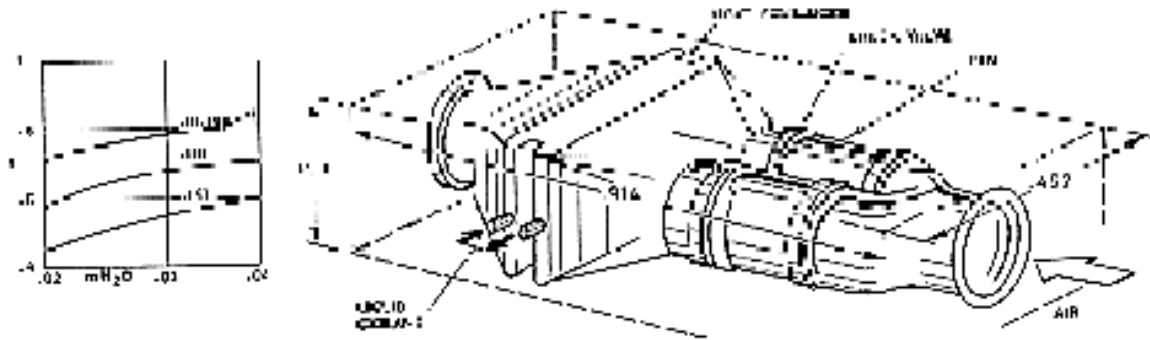
6. References: The data are from Trusch & Nason (1975) [180], unless otherwise stated. The last sketch is from Hamilton Standard, CEI No: MC621-0008-0002. Item No. 2,30.

FREON TO WATER INTERLOOP HEAT EXCHANGER

1. Developer: Microtecnica, Via Madama Cristina 147 - Casella postale 210/Ferr., 10100 Torino (Italy).

2. Function: Transfers heat from a Freon loop, cooling the pallet-mounted equipment, to the Spacelab water loop.

    A heat exchanger based on an identical core is also provided for additional equipment cooling. This heat exchanger is called Experiment Dedicated Heat Exchanger (EDHX).

3. Sketch:
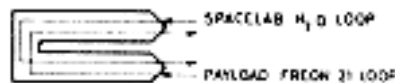
4. Description: Plate-fin configuration. Counterflow arrangement once folded. The strip-fin-plate-fin surface designed 1/8-19,82(D) is described in Table 11-5, clause 11.3.1.

	Fins			Part. Sheets	Area Density α [m².m⁻³]	Core Size			Dry Mass [kg]
	Height $hx10^3$ [m]	Thickness $ax10^3$ [m]	Fins per meter [m⁻¹]	Thickness, $a'x10^3$ [m]		Hot Flow Length, L_h [m]	Clod Flow Length, L_c [m]	No Flow Length, L_{nf} [m]	
Payload Freon 21	5,21	0,102	780	0,152	2231				10,2 [a]
Spacelab Water	5,21	0,102	780		2231				

[a] Data from Bellomo (1975) [6].

    Material: Fins-nickel. Parting sheets, core strips, brakets, headings and bosses - Stainless Steel (Bellomo (1975) [6]).

5. Performances: Data corresponding to two typical cases are presented.

	Heat transfer rate [W]	Temperatures		Fluid Mass Flow rate, m [kg.s^{-1}]	Effectiveness ε	Pressure drop [a] Δp x 10^{-3} [Pa]
		T$_i$ [K]	T$_o$ [K]			
Payload Freon 21	4000	341	280	0,063	0,999	0,98 for m = 0,063 kg.s^{-1}
Spacelab Water		280	295,5	0,063		1,88 for m = 0,063 kg.s^{-1}

	Heat transfer rate [W]	Temperatures		Fluid Mass Flow rate, m [kg.s^{-1}]	Effectiveness ε	Pressure drop [a] Δp x 10^{-3} [Pa]
		T$_i$ [K]	T$_o$ [K]			
Payload Freon 21	4000	296,5	286,5	0,378	0,938	8,31 for m = 0,378 kg.s^{-1}
Spacelab Water		280	295,5	0,063		1,88 for m = 0,063 kg.s^{-1}

[a]   Data from Bellomo (1975) [6].
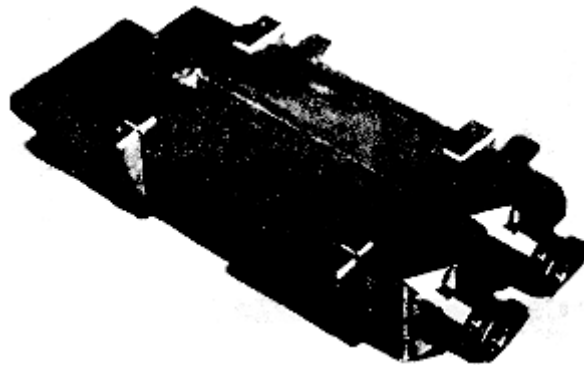
6. References: The data are from Owen, Sessions & Walker (1976) [139], unless otherwise stated.

COLD PLATE

1. Developer: Microtecnica, Via Madama Cristina 147 - Casella postale 210/Ferr., 10100 Torino (Italy).

2. Function: Cooling of avionics equipment onboard Spacelab.

3. Sketch:

4.   Description: Three different types have been developed. Their dimensions are:

   (a)   0,762 m x 0,508 m x 5,08 x 10⁻³ m.

   (b)   0,381 m x 0,508 m x 5,08 x 10⁻³ m.

   (c)   0,305 m x 0,508 m x 5,08 x 10⁻³ m.

   Material: Stainless steel.

5.   Performances: When water is used as coolant liquid.

   Overall thermal conductance, U = 3500 W.m⁻².K⁻¹.

   Mass flow rate, m = 0,063 kg.s⁻¹.

   Pressure drop, Δp = 689 Pa.

   When Freon 21 is used as coolant liquid.

   Overall thermal conductance, U = 2000 W.m⁻².K⁻¹.

   Mass flow rate, m = 0,38 kg.s⁻¹.

   Pressure drop, Δp = 8620 Pa.

   The photograph below shows the fins internal disposition and the inner part of the bosses.

6.   References: The data are from Microtecnica (1977) [126]. Some information concerning cold plate design data can be found in Baum (1969) [5].

12
Pumps

12.1 General

A pump is a machine which imparts energy to a fluid, in most cases a liquid. Compressors, fans, and blowers impart energy to gases rather than to liquids.

The net amount of energy, E_n, transferred to the unit liquid mass equals the ratio of the pressure rise imparted to the liquid, Δp, to the liquid density, ρ.

Most manufacturers still use the head, H, to measure the pressure rise to density ratio, $\Delta p/\rho$. The dimension of head is length, the physical meaning of the concept being potential energy of the unit liquid weight at an elevation H (gravity potential). Since the introduction of gravity is highly artificial we will avoid, as far as possible, the use of the term head throughout this clause.

The pressure rise enables the liquid to overcome hydraulic resistances (see Clause 7).

A pump consumes more power than it gives off. The ratio of the specific energy (energy per unit liquid mass) developed by the pump, E_n, to the energy per unit liquid mass supplied to it, E_s, is the overall efficience, η_p. In order to relate the present notation with that used in clause 7.1, it is indicated that $E_n = \eta_p E_s = \eta_p P/m$.
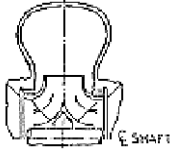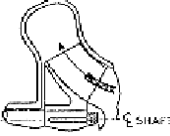
The (negative) difference $E_L = E_n - E_s$ is the energy lost by the pump per unit liquid mass flowing through it. The energy loss accounts for three types of losses:

1. Hydraulic losses due to liquid friction and turbulence,

2. volume losses due to the fact that some of the fluid leaks back through internal passages forced by the pressure rise produced by the pump, and

3. mechanical losses because of friction in bearings, packings, etc.

Spaceborne pumps seem to vary enormously in design and principle of action. Nevertheless, they can all be divided into two main types: rotodynamic pumps and displacement pumps.

1. A rotodynamic pump imparts energy to a liquid through the work done by a rapidly rotating vaned impeller. Examples of rotodynamic pumps are radial-flow centrifugal pumps, mixed-flow pumps and axial-flow pumps or propellers. Relevant rotodynamic pumps are classified in Table 12-1.
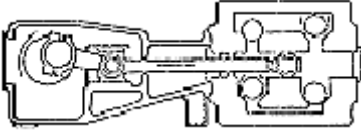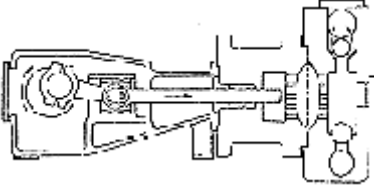
Table 12-1: Rotodynamic Pumps

Class	Sketch of a Typical Model
Radial flow	
Mixed flow	
Axial flow or propeller	

NOTE   From Hydraulic Institute (1975) [95].
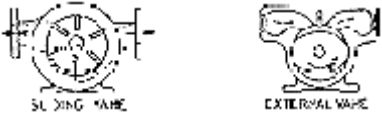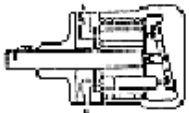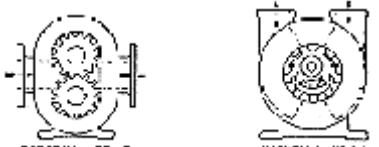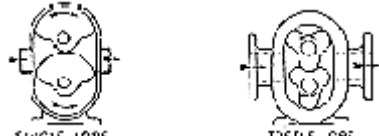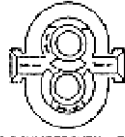
2.   Displacement pumps, which include reciprocating and rotary pumps, impart energy by a positive displacement action. Reciprocating pumps are shown in Table 12-2, and rotary pumps in Table 12-3.

Table 12-2: Displacement Pumps. Reciprocating

Class	Sketch of a Typical Model
Piston	
Diaphragm	

NOTE   From Hydraulic Institute (1975) [95].

Table 12-3: Displacement Pumps. Rotary

Class	Sketches of Typical Models
Vane	
Piston	
Flexible member	
Gear	
Lobe	
Circumferential piston	
Screw	

NOTE   From Hydraulic Institute (1975) [95].

Several features of typical pumps, which should be kept in mind in the selection of a pump for a given duty, are listed in Table 12-4.

Table 12-4: Main Features of Typical Pumps

Rotodynamic Pumps	Positive Displacement Pumps
Very efficient when operating at speeds from 1200 to 3600 rpm, within the range of usual alternating current electric motors.	They operate at very low rotating speed (220 to 500 rpm).
Cannot be run efficiently at low speeds to pump small quantities.	Efficiencies, although can be high, are below those for rotodynamic pumps.

Rotodynamic Pumps	**Positive Displacement Pumps**
Overall efficiency usually ranges from 0,7 to 0,85.	
Not easily regulated. Regulation by throttling is simple but wasteful. Regulation by running speed adjustment maintains more or less the efficiency but requires auxiliary equipment which is expensive, complicated and unreliable. The use of multiple winding motors and invertors to control motor speed through voltage and frequency control deserves consideration.	Efficiency decreases when wear increases leakage.
	The discharge characteristic is a pulsating one. A smoother discharge is obtained in double or treble acting units. Rotary pumps exhibit greater uniformity of deliver than reciprocating pumps.
	The delivery is substantially constant, regardless of the pressure rise developed.
Cannot deliver at high pressure unless a large and heavy type is used. The pressure risk increases with increasing the peripheral speed.	Can be used with very viscous liquids. This is particularly true in the case of rotary pumps. The pressure rise drops with increasing viscosity.
Cannot handle viscous liquids.	Self priming and capable of coping with high suction lifts.
Not self priming. This can be overcome in various ways, see the radial flow rotodynamic pump in Table 12-1.	Relief or bypass valves are to be used. Unable to operate against a closed discharge. Even a slight decrease in delivery may cause a substantial pressure rise.
No relief valves are to be used. Even complete throttling does not present any danger to the pump or loop as not further pressure rise develops.	Able to handle large proportions of vapor. Enough liquid should be present to provide a liquid sealing film for the clearances. Suitable for pumping hot liquids.
Limited by cavitation and power.	Limited by pressure and power.
Leak through the shaft seal. Submerged pumps can be used to prevent this drawback.	Problems of leakage are minimized particularly with diaphragm pumps.
Smaller in size than other types for equal capacity.	Much bigger than rotodynamic because of low rotating speed.
Low cost. Rugged, reliable in operation.	Complicated construction. Inlet and outlet valves should be used (not in the case of rotary pumps). Very sensitive to wear because comparatively large surface areas move in close contact. Diaphragm pumps do not present friction, but diaphragm materials are of limited use at elevated temperatures.

NOTE   Arranged by the compiler after: Nekrasov (1969) [132], London (1974) [118], Pollak & Cruger (1974) [144], Scobie (1974) [160], Settles et al. (1977) [163].

12.2 Specified speed

The characteristics of a pump are given by means of an experimentally generated curve which relates the power imported to the liquid, $\eta_p P$, with the volume flow rate, m/ρ, for constant rotating speed. The volume flow rate, which is usually known as pump capacity, is denoted by Q in most textbooks. Nevertheless, we will depart from this practice since Q represents the heat transfer rate in this Part.

Typical dimensional characteristic curves of a centrifugal pump are shown in Figure 12-1.
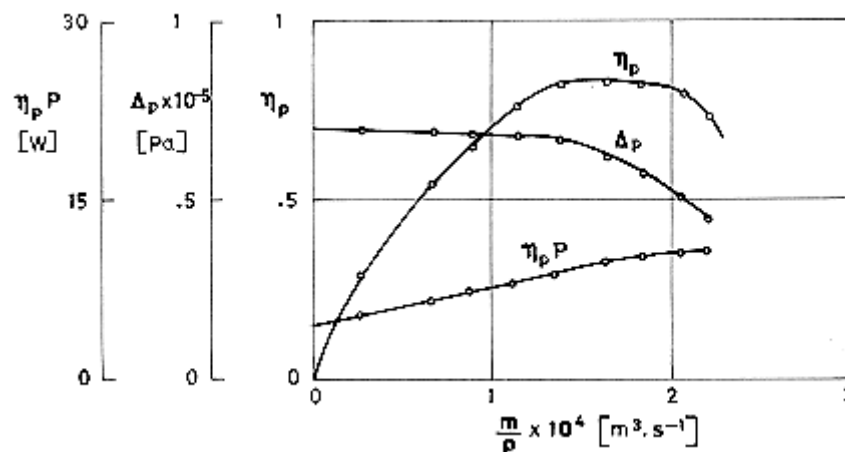
Figure 12-1: Typical characteristic curves of a centrifugal pump for a given rotating speed.

It can be deduced from Figure 12-1 that an optimum operating point (point of maximum efficiency) exists at a certain rotating speed-flow rate combination. The numerical values which several dimensionless variables reach at optimum conditions provide a quantitative basis for the classification of all pumps. It has been found, for example, that machines exhibiting similar design features have approximately the same specific speed, n_s. This dimensional parameter is defined as:

$$n_s = \left.\frac{n(m/\rho)^{1/2}}{H^{3/4}}\right|_{opt} \tag{12-1}$$

where n means revolutions per minute (or sixty times a characteristic frequency of the impeller), and H is the head in m. Subscript "opt" indicates that n, m/ρ and H are the values at the optimum point.

Formulae relating efficiency to specific speed are available for rotodynamic pumps. For example, Nekrasov (1969) [132] takes into account the leakage, the friction between impeller shroud and fluid, and the mechanical friction in packing and bearings. Nevertheless, he is unable to offer an analytical expression for the total hydraulic losses inside the pump, since these losses depend on a number of factors whose effects are poorly known. On the other hand, expressions similar to those just mentioned have been critiqued on the grounds that, although based on best standard practice, they need revision in the light of modern technological developments (Settles et al. (1977) [163]).

The use of specific speed, n_s, defined as in Eq. [12-1], presents two main inconveniences. The first one derives from the fact that the head, H, appears in the definition of n_s. In addition, n_s is not a dimensionless number and thence, comparison of machines originating in different countries, or even of products from different manufacturers, becomes difficult because of the wide variety of practical

units in use. This is why modern authors (see for example Csanady (1964) [29]) use a dimensionless number, Ω, proportional to n_s and defined as:

$$\Omega = \frac{\omega(m/\rho)^{1/2}}{(\Delta p/\rho)^{3/4}}\bigg|_{opt} \qquad [12\text{-}2]$$

where ω is measured in radians per second, m/ρ in $m^3.s^{-1}$, and $\Delta p/\rho$ in $m^2.s^{-2}$. Notice that Ω depends on the working liquid through its density, ρ. Table 12-5 could be helpful in reducing data from various sources to a common non-dimensional basis.

Table 12-5: Conversion Factors in the Deduction of Ω from n_s

When n_s is given by	Divide by
rpm(cfs)$^{1/2}$(ft)$^{-3/4}$	129
rpm(gpm)$^{1/2}$(ft)$^{-3/4}$ [a]	2730
rpm(hp)$^{1/2}$(ft)$^{-5/4}$[b]	42
rpm(metric hp)$^{1/2}$(m)$^{-5/4}$ [b]	187
rpm($m^3.s^{-1}$)$^{1/2}$(m)$^{-3/4}$	53

[a]   gpm = US gallons per minute.

[b]   Working fluid is water.

NOTE   From Csanady (1964) [29].

Rotodynamic pumps may be classified according to their Ω values as follows (Nekrasov (1969) [132]):

1.   Low-speed radial-flow: $\Omega \leq 0{,}40$; $D_2/D_1 = 2{,}2\text{-}3{,}5$,

2.   Normal-speed radial-flow: $\Omega = 0{,}40\text{-}0{,}80$; $D_2/D_1 = 2{,}2\text{-}1{,}8$,

3.   High-speed radial-flow: $\Omega = 0{,}80\text{-}1{,}60$; $D_2/D_1 = 1{,}8\text{-}1{,}3$,

4.   Mixed-flow: $\Omega = 1{,}60\text{-}3{,}20$; $D_2/D_1 = 1{,}3\text{-}1{,}1$,

5.   Axial-flow or propeller: $\Omega \leq 3{,}20\text{-}6{,}40$; $D_2/D_1 = 1$.

The impeller shapes corresponding to the five types listed above are shown in Figure 12-2. The changes in shape are necessary to accommodate the relatively higher flow rates at large Ω, and to cope with the relatively high pressure rises at small Ω. A lower bound of Ω for an "efficient" rotodynamic pump could be fixed near $\Omega = 0{,}18$ (Csanady (1964) [29]).
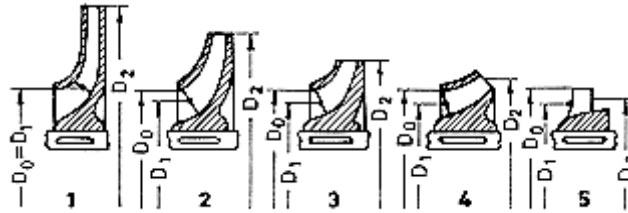
Figure 12-2: Rotodynamic pump impellers. From Nekrasov (1969) [132].

It should be said that different authors quote slightly different limiting values of Ω for the several classes of pumps. A correlation of rotor design and specific speed similar to that shown in Figure 12-2 is given in Csanady (1964) [29].

In order to select the machine(s) suitable for a given duty (given rotating speed, capacity, pressure rise, and working fluid), Ω is calculated. Then, the rotodynamic machine best suited to that duty can be selected from Figure 12-2.

12.3 Net suction energy

In many cases the working liquid contains varying quantities of vapour, and cavitation may appear. This results in an intermittent stream, a characteristic noise, and reductions in the pump capacity, pressure rise and efficiency.

Cavitation appears when the difference between the absolute liquid pressure and the vapour pressure of the liquid at the operating temperature becomes negative, but event at (small) positive values of this difference cavitation can be triggered by the presence of dissolved gases which are released at reduced pressure or increased temperature.

In order to avoid cavitation the absolute pressure in the suction loop must exceed a certain threshold value. To define this value the net positive suction head (NPSH) is traditionally used. NPSH is the absolute total head of the pump inlet above the fluid vapour pressure (measured in consistent units) at the working temperature.

The concept of "head" disappears when the net suction energy per unit mass, E_v, is introduced:

$$E_v = \frac{p_i - p_{sat}}{\rho} + \frac{V_i^2}{2}$$

[12-3]

where p_i and V_i are pressure and velocity at the inlet section of the pump, p_{sat} is the liquid vapour pressure, and ρ the (constant) liquid density.

Leaving aside viscosity effects, the performance law of a family of geometrically similar pumps with incipient cavitation will depend on two independent dimensionless parameters. The first one could be the, so called, flow coefficient, $(m/\rho)/\omega D^3$, where D is the rotor diameter. The other parameter will be based on the net suction energy, E_v. Although several combinations are possible, the most convenient choice is the suction specific speed S of Wislicenus, which is defined as:

$$S = \frac{\omega (m/\rho)^{1/2}}{E_v^{3/4}}$$

[12-4]

The performance law then becomes,

$$\eta_p = f\left(\frac{m/\rho}{\omega D^3}; S\right)$$

[12-5]

Most present-day pumps are designed for the avoidance of cavitation. With this purpose, a maximum value S = 2,88 is widely used for conventionally-designed machines over the whole specific speed range (Scobie (1974) [160]). This would narrow the choice of the pump, since

$$\Omega \leq 2{,}88\left(\frac{E_v}{\Delta p/\rho}\right)^{3/4}\bigg|_{opt}$$

[12-6]

When limitation (6) is untenable other cures to cavitation can be found. Some of them are:

1. Placing the pump into the system at a position where it deals with fluids at moderately low temperatures.

2. Increasing the working pressure.

3. Installing a booster pump at the entrance of the suction line, and

4. Mounting an axial wheel immediately before the impeller to increase pressure and impart whirl to the fluid. This results in a reduction of the relative (to the vane) velocity and improves operating conditions of the impeller. Notice that, although the auxiliary runner can prevent cavitation from developing at the impeller, cavitation can develop on the auxiliary runner itself unless its rotational speed is less than that of the impeller.

12.4 Requirements for spaceborne pumps

The following requirements are normally imposed to pumps for spaceborne fluid loops:

1. Low mass.

2. High overall efficiency.

3. Low mass to output-power ratio.

4. Hermetically sealed.

5. Quiet in operation and exhibiting high operational reliability.

6. Able to accept mission vibration and shock loads.

7. Compatible with onboard electrical services.

8. Made from materials suitable for use in the aerospace environment.

9. Able to handle typical liquid coolants (see Table 10-1).

More detailed environmental, safety, reliability and compactness requirements are defined for each particular spacecraft. In addition, self priming under reduced gravity may be required in several instances.

Concerning the required performances, two general categories of spaceborne liquid pumps will be considered here:

1. Class A. Pumps used in large manned spacecraft, such as the Space Shuttle. Typical rates and pressure rises for these pumps are (Owen et al. (1976) [139]):

   Capacity, m/ρ, from $0,5 \times 10^{-4}$ $m^3.s^{-1}$ to 2×10^{-4} $m^3.s^{-1}$.

   Pressure rise, Δp, from $0,5 \times 10^5$ Pa to 10^5 Pa.

   From these values it is deduced that the output power, $\eta_p P = \Delta p m/\rho$, is in the range from 2,5 W to 20 W.

2. Class B. Small pumps for unmanned satellites (Ebersole (1970) [41]), astronaut cooling (Carson (1972)) or similar duties.

   Capacity, m/ρ, from 10^{-5} m^3,s^{-1} to $0,5 \times 10^{-4}$ m^3,s^{-1}.

   Pressure rise, Δp, from 10^5 Pa to 2×10^5 Pa.

   The power imparted to the liquid is in this case of the order of 1 W.

12.5 Commercially available pumps

The applicability of commercially available pumps to spaceborne fluid loops has been discussed several times (Carson (1972) [20], Wyn-Roberts (1973) [194], Berner & Schleicher (1976) [13].

Carson (1972) [20] describes the development of a diaphragm pump whose aim is providing body cooling for an astronaut performing extravehicular work. The characteristics of this pump are given in Table 12-6. Early attempts to use a commercially available centrifugal pump with the purpose of astronaut cooling proved to be unsuccessful mainly because of too low an overall efficiency for the required power.

Table 12-6: Characteristics of Several Commercially Available Pumps

Type	Pump	Size			Mass	Capacity	Pressure	Electrical Input			Comments
		Ht. [m]	Wd. [m]	Lg. [m]	[kg]	$(m/\rho)x10^4$ [$m^3.s^{-1}$]	rise $\Delta p x10^{-5}$ [Pa]	W	V	Ph/Hz	
Rotodynamic. Radial Flow	Cadet [a] "Mini"	0,123	0,128	0,216	4,0	Figure 12-3		~40	220-250	1/50	Domestic central heating pumps. Working pressure: 6 x 10^5 Pa. Maximum operating temperature: 383 K.
	Cadet [a] "S"	0,124	0,128	0,216	4,3			~70			
	Euramo [b] MX32-E	0,180	0,095	0,175	3,5	Figure 12-4		25	220	1/50	Domestic central heating pumps. Working pressure: 6 x 10^5 Pa. Temperature range: 280 K to 383 K
	Euramo [b] XA15-R	0,180	0,130	0,173	5,1			15			
	[c]	0,076	0,050			Figure 12-5					Submersible pump transferring liquid nitrogen and for use in closed-cycle cooling systems. Temperature range: 77 K to 300 K
	Eastern- [d] Iwaki MD-15T	0,102	0,082	0,216	2,5	Figure 12-6		37	115	1/50-60	Magnet driving impeller is fully encapsulated in polypropylene, supported by a TFE bearing and rotating on a stationary ceramic spindle. Material: Glass filled polypropylene.
	Eastern- [d] Iwaki MDR-30T	0,127	0,089	0,267	3,4						
	AC-3C-MD [d]	0,108	0,102	0,206	2,9	Figure 12-7		175	115	1/50-60	Low cost pump for chemicals. Magnetic driven impeller. Plastic components are glass filled polypropylene. Pump hermetically sealed.

Type	Pump	Size			Mass	Capacity	Pressure	Electrical Input			Comments
		Ht. [m]	Wd. [m]	Lg. [m]	[kg]	$(m/\rho)x10^4$ $[m^3.s^{-1}]$	rise $\Delta p x10^{-5}$ [Pa]	W	V	Ph/Hz	
											Not fully enclosed motor.
Displacement Reciprocating Diaphragm	[e]	0,086	0,056	0,101	0,61	0,30 [f]	0,36 [f]	9,7	16,8±0,8	DC	Developed by NASA for astronaut cooling. Diaphragm: Dacron fabric with butyl rubber coating. Inlet temperature: 289,15 K.
Displacement Rotary. Flexible Vane	413-7-1285 [d]				0,63	Figure 12-8		37	12	DC	Vanes: Delrin or Teflon. Rotors and Shaft: 304SS. Bodies: Phenolic or Epoxy. O rings: Buna N, Viton or Ethylene Propylene. For hard-to-handle chemicals. Temperature range: 230 K to 390 K.

[a]   Sealed Motor Construction Co. Ltd. Bristol Road, Bridgwater. Somerset, England. Telephone 4366.

[b]   Le Matériel Téléphonique, Division Electro-Hydraulique, 46,47 Quai Alphonse Le Gallo-BP402, 92102 Boulogne Billancourt, CEDEX, France.

[c]   From Engel & Walter (1974) [43]

[d]   Gelber Pump Co. 5806 North Lincoln Avenue, Chicago, Illinois 50659, USA.

[e]   From Carson (1972) [20].

[f]   Optimum operating point.
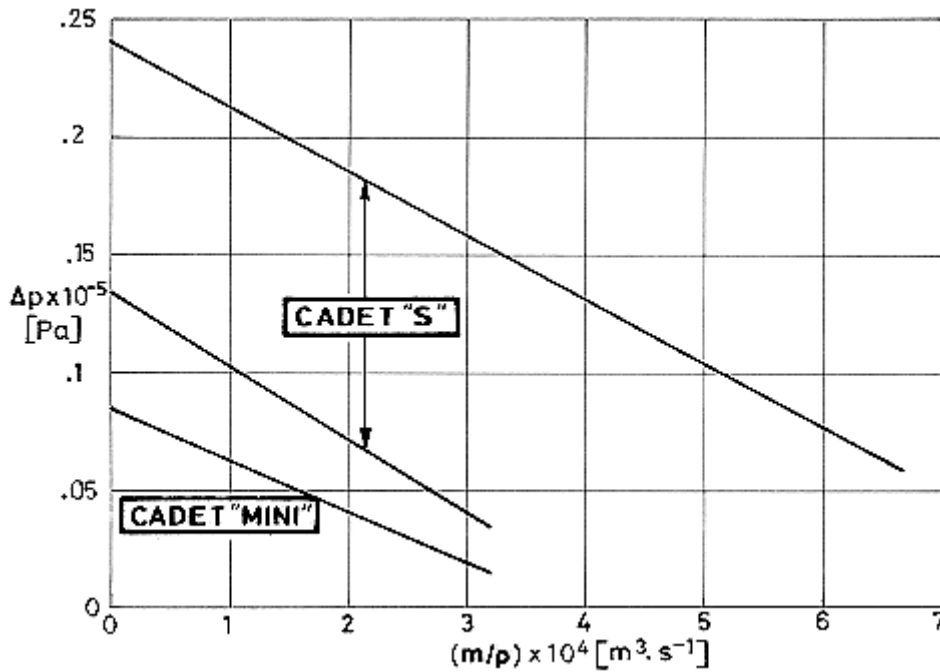
Figure 12-3: Characteristic curves of SEALED MOTOR CONSTRUCTION Centrifugal Pumps Cadet "Mini" and Cadet "S" pumping water. From Wyn-Roberts (1973) [194].
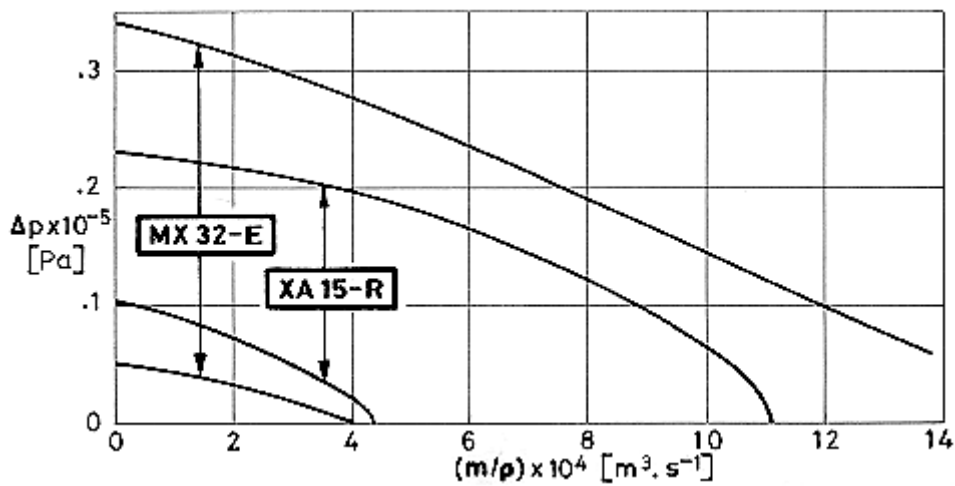
Figure 12-4: Characteristic curves of EURAMO Centrifugal Pumps Cadet MX 32-E and XA 15-R pumping water. From EURAMO-POMPES SALMSON (1977) [60].
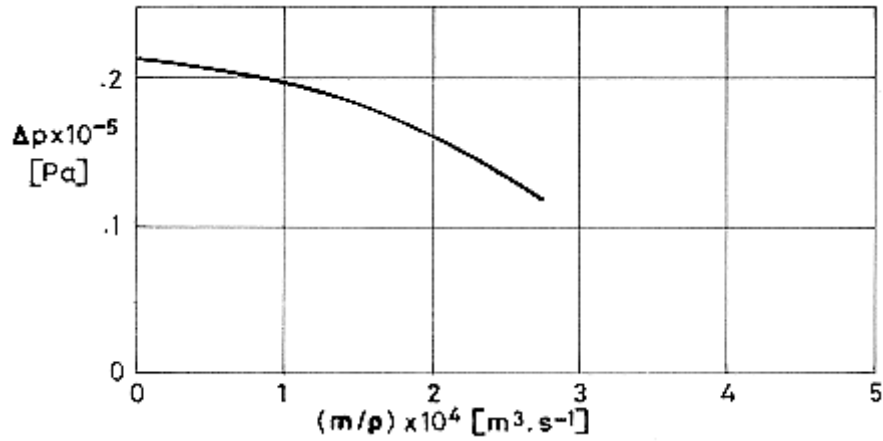
Figure 12-5: Characteristic curve of the Centrifugal Pump devised by Engel & Walter Cadet "Mini" and Cadet "S" pumping water. From Wyn-Roberts (1973) [194].
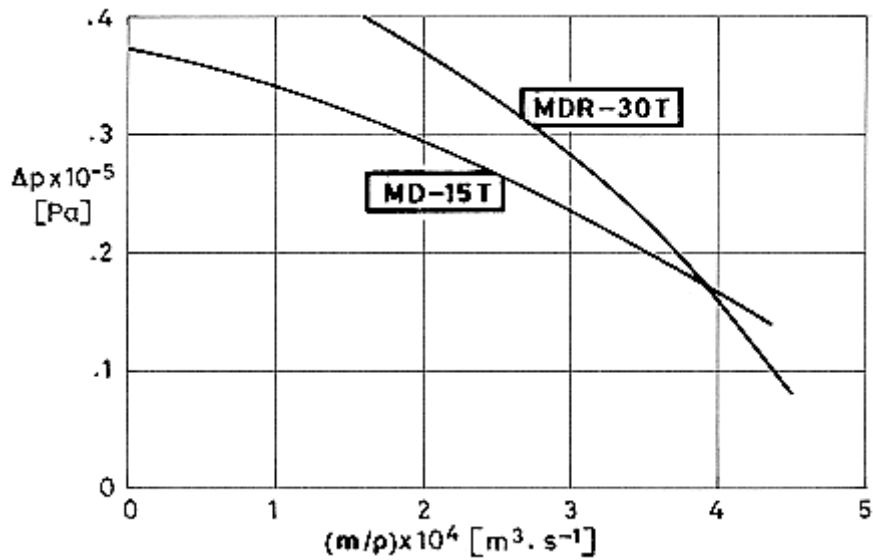
Figure 12-6: Characteristic curves of Eastern-Iwaki Centrifugal Pumps MD-15T and MDR-30T pumping water. From GELBER (1976) [71].
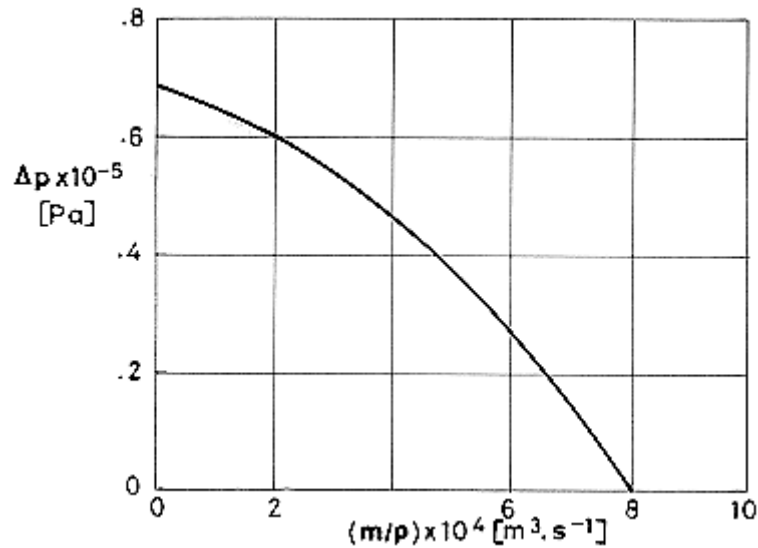
Figure 12-7: Characteristic curve of Centrifugal Pump AC-3C-MD pumping water. From GELBER (1976) [71].
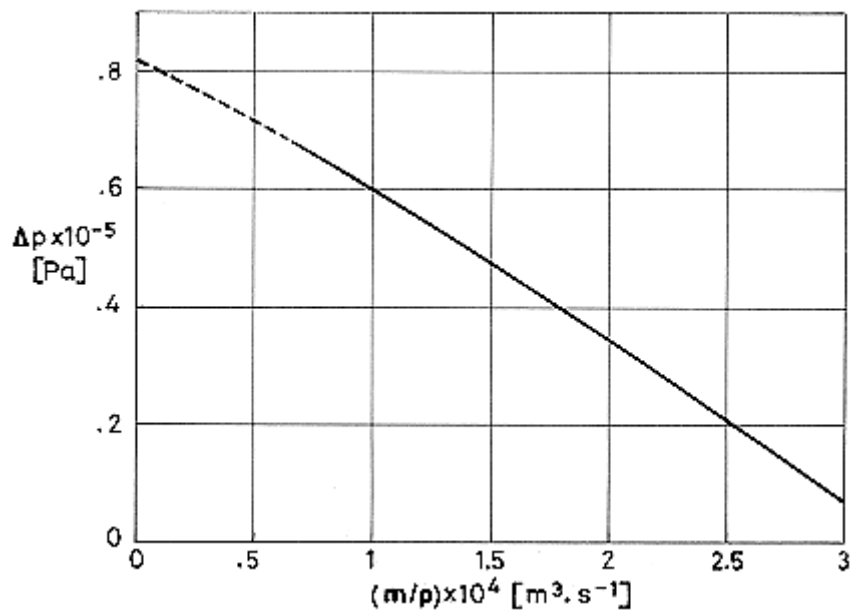
Figure 12-8: Characteristic curve of Positive Displacement Rotary Pump 413-7-1285 pumping water. From GELBER (1976) [71].

Wyn-Roberts (1973) [194] surveyed the products from 20 European manufacturers. The imposed requirements were 4), 5) and 8) in Clause 12.4. The selected pumps are too large for the typical performances mentioned above, with the exception of two pumps manufactured by Sealed Motor Construction Co., whose characteristics are summarised in Table 12-6 below.

From the survey made by Berner & Schleicher (1976) [13] two pumps by Pompes Salmson are singled out. The characteristics of these pumps are also given in Table 12-6.

Special purpose pumps have been described in several instances. A centrifugal pump for transferring liquid nitrogen has been developed by Engel & Walter (1974) [43]. Data on this pump are also included in Table 12-6.

12.6 European pump manufacturers

According to Wyn-Roberts (1973) [194] the following European firms offer pumps which look promising for spacecraft application. The two manufacturers mentioned in connection with Table 12-6 have been not included in this list.

- Bertin,

  Allée Gabriel Voisin,

  B.P. 3,

  78-Plaisir,

  France.

- Hermetic Pumpen GmbH,

  7803 Gundelflingen b Freiburg,

  Gewerbestrasse 20,

  Germany.

- Novametic Pumpen GmbH,

  Mühlenkamp 59,

  Hamburg 39 2000,

  Germany.

- Watson-Marlow Ltd.,

  Falmouth TR11 4RU,

  Cornwall,

  England.

13
System optimization

13.1   General

The engineer engaged in the design of a fluid loop to meet some specified requirements, under a certain set of constraints, is faced with an optimization problem. He should decide which, among a set of different alternatives should be preferred on the basis of some optimization criteria. The purpose of this clause is to discuss these optimization procedures, and to introduce the types of trade-off analyses which could be used by the designer. It should be pointed out, however, that it is difficult to give general rules, and that in practice each case should be analyzed by itself, considering the requirements, constraints and optimization criteria of that particular case. Often, the designer does not address the question of which of all possible solutions is the best according to the optimization criterion chosen, but instead selects some of the parameters and characteristics of the loop based on experience, availability and other engineering criteria, and performs an optimization analysis of one or two parameters left unspecified.

Due to the above mentioned characteristics of the problem, no attempt will be made toward a formal description of system optimization, rather, a fairly general approach devised by Barker, Stephens & Taylor (1967) [3] will be used to indicate how a basic analysis can be performed. In addition, two more particular, yet illustrative, examples will be shown.

One important parameter which is used in most of these studies is the mass needed to meet a certain pumping power requirement. This equivalent mass is obtained through the use of a pumping power penalty factor which can be taken between 0,5 k.W-1 (Barker et al. (1967) [3] and 0,2 kg.W-1 (Trusch (1974) [179]. It should be mentioned that, as can be deduced from Table 12-6, several conventional pumps show mass to power ratios no far above 0,2 kg.W^{-1}

13.2   Basic analysis

The design of a liquid coolant system to transfer heat from the environmental control and life support system of a satellite to a space radiator in the satellite has been discussed by Barker, Stephens & Taylor (1967) [3]. The procedure used is to sub-optimize individual components of the system on the basis of power requirement and mass, at various coolant flow rates. The mass due to pumping power is determined through a power penalty factor which is taken as 0,5 kg.W^{-1}. For each flow rate used, the minimum total mass penalties (sum of mass of the individual components and equivalent mass due to pumping power) are computed and added together to yield the minimum total system mass penalties. From these results the lowest minimum total system mass is calculated, thus obtaining the optimum coolant flow rate.

The thermal control system consists of an interface heat exchanger, a bypass valve, a controller, a space radiator and supply and return plumbing, Figure 13-1. Heat is supplied to the system through the heat exchanger from a fluid loop with water as working fluid. The coolant in the thermal control

system is Freon 21, which receives the heat through the exchanger and transports it to the space radiator. The aim of the bypass valve and valve controller, which are located upstream of the radiator, is to maintain the temperature downstream of this radiator at 274,5 K in order to preclude freezing of water vapour on the exterior surface of plumbing.
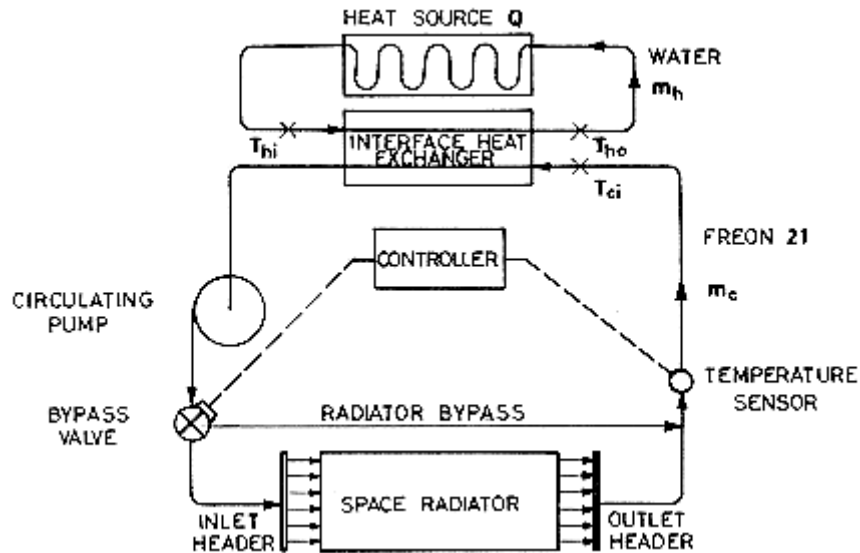
Figure 13-1: Schematic representation of the fluid loop considered by Barker, Stephens & Taylor (1967) [3].

The main characteristics of the system are: heat load, $Q = 15 \times 10^3$ W; water inlet temperature, $T_{hi} = 316,5$ K; water outlet temperature, $T_{ho} = 277,5$ K and Freon 21 inlet temperature, $T_{ci} = 274,5$ K. The heat exchanger is of counterflow, plate-fin surface configuration, and is made from stainless steel. The fin height is $h = 2,53 \times 10^{-3}$ m, fin thickness, $a = 0,1 \times 10^{-3}$ m with 787 fins per meter, all these data on both sides. Parting sheet thickness is $a' = 0,25 \times 10^{-3}$ m.

The sub-optimization procedure is outlined in the following clause.

13.2.1 Interface heat exchanger

The procedure consists in finding the best heat exchanger envelope at a given coolant flow rate, to minimize the total mass penalty. It is observed that for each coolant flow rate, the water flow rate and outlet Freon 21 temperature can be computed since the heat load is known. Essentially, the following steps are performed iteratively.

1. total penalty is initially estimated and later specified on step 14 during subsequent iterations.

2. Heat exchanger effectiveness, ε, is obtained from the imposed design conditions; fluid specific heats, flow rates and temperatures (see Eq. [11-8] in clause 11.2.2).

3. The number of heat transfer units, N_{tu}, is computed from the effectiveness, ε, and the capacity rate ratio, R, for the assumed flow arrangement (see clause 11.2.3).

4. Pressure drops are initially estimated and later specified from step 14 during subsequent iterations.

5. $A \overline{U}$ is computed from the N_{tu} value and C_1 (see Eq. [11-7] in clause 11.2.2).

6.   Reynolds numbers are initially estimated and later corrected from the results of step 11 during subsequent iterations.

7.   The heat transfer coefficient, *h*, and Fanning friction factor, *f*, are computed from the data for the specified exchanger core (see Clause 11.3 and Kays & London (1964) [102] or the appropriate data for the particular core).

8.   The overall surface effectiveness, η, and overall heat transfer coefficient, *U*, are computed (see clause 11.2.2).

9.   The heat transfer area, *A*, is computed from the overall heat transfer coefficient, *U*, and the product $A \, \overline{U}$ computed in step 5.

10.   Frontal area of the exchanger, A_{FR}, hydraulic diameters, D_E, and flow lengths, *L*, are deduced from core geometries and heat transfer area (see Clause 11.3 or the appropriate data for the particular core).

11.   Pressure losses are computed from Reynolds numbers, lengths, flow rates and friction factors (see steps 6, 7 and 10).

12.   Pressures losses from steps 11 are compared with previous pressure losses from step 4 and the procedure continues at step 6 or 13. The process is finished when the error in pressure loss remains within specified bounds.

13.   The heat exchanger volume, frontal areas, and envelope dimensions are computed.

14.   The total mass penalty is computed and compared with its previous value. This total mass penalty includes core, headers and shell, fluid and the equivalent mass due to pumping power (headers and shell weight account for 30 % of core weight). The procedure is either terminated or continued at step 4 depending on the comparison. New pressure losses are estimated if it appears that the mass penalty can be further reduced.

As a result of this procedure the optimum shape of the heat exchanger is obtained for different Freon 21 flow rates. As the flow rate increases, the required power increases but the heat exchanger mass decreases. In the case considered by Barker et al. (1967) [3] the sum of heat exchanger mass and mass due to pumping reached its minimum value at a Freon 21 flow rate of 0,63 kg.s^{-1}.

The envelopes for these optimum heat exchangers are long and slender, thence the actual design of such units would involve folding the heat exchanger into a more convenient package. This folding would undoubtedly result in some degradation of the heat transfer and pressure drop characteristics. These degradations would ideally be traded-off against the benefits of the more convenient package.

13.2.2   Supply and return plumbing

These circuits are optimized by determining the tube diameter and wall thickness combination yielding a minimum value for the sum of the mass of fluid, plumbing and equivalent mass due to pumping power, for a given coolant flow rate. Plumbing mass includes one set of tubes, fittings and a redundant set of manifolds. To calculate the pumping power, the pressure loss in valves, manifolds, fittings, ... is accounted for by doubling the pressure loss based on straight tube length and bends. Equations are used to express these masses as functions of tube diameter and wall thickness, and these parameters are changed over a range of standard values until the optimum combination is found. The result of this procedure shows that the minimum total penalty increases with increasing mass flow rate.

13.2.3   Radiator

The radiator is optimized through a procedure similar to the one used for plumbing. In this case, for each flow rate there are 3 parameters to be defined, number of tubes, tube diameter and wall thickens, and they are determined by minimizing the sum of fluid mass, tubing mass and equivalent mass due to pumping power. The wall thickness was taken as $2,5 \times 10^{-3}$ m. On the other hand, it was found from heat transfer considerations that turbulent flow should be preferred, so that a Reynolds number of 10^4 was used. This fact provides a relationship between tube diameter and number of tubes for each flow rate, and therefore the tube diameter is the only variable which has to be optimized.

The results of these suboptimization procedures are shown in Figure 13-2, where it may be observed that the total system penalty is minimized in the vicinity of 0,38 kg.s^{-1} Freon 21 flow rate. This minimum is largely due to the rapid increase in heat exchanger penalty at reduced flow rate, whereas both the radiator, and supply and return plumbing penalties decrease with decreasing mass flow rate. The increase in heat exchanger penalty is due to the greater heat exchanger transfer areas required at these flow rates.
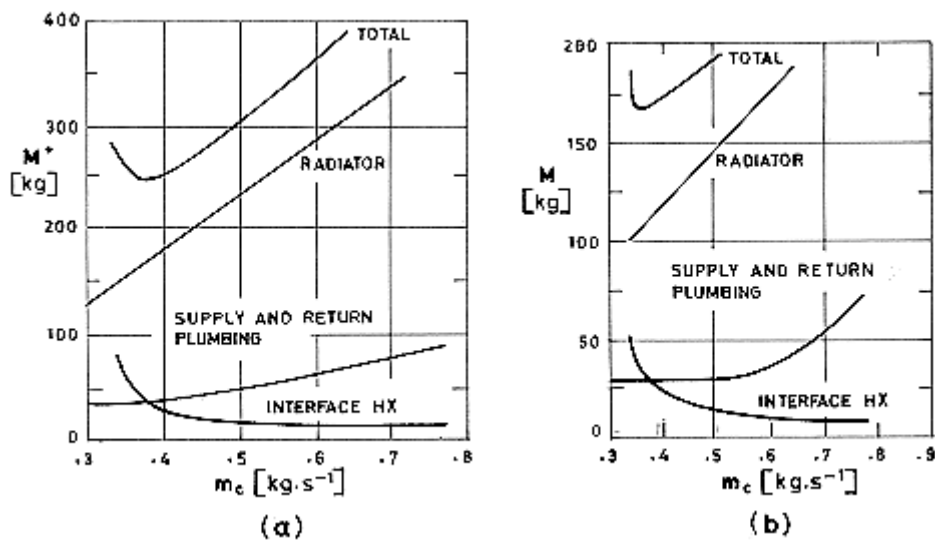
Figure 13-2: Results of the liquid coolant system optimization analysis. a) gives the mass penalty, M^+, of the system components vs. Freon 21 mass flow rate, m_c. The mass penalty includes the equivalent mass due to pumping power. b) gives the system mass, M, vs. Freon 21 mass flow rate, m_c. From Baker, Stephens & Taylor (1967) [3].

Therefore through the procedure just described not only the optimum mass flow rate is derived, but also the optimum heat exchanger shape, tube diameter and wall thickness of supply and return plumbing, and the number of tubes and tube diameter of the radiator.

13.3   Special examples

The example in Clause 13.2 was intended to illustrate how an optimization study should be undertaken in a very general case. No constraints other than heat load and operating temperatures were introduced a priori in the process of calculating the coolant flow rate giving minimum system mass, and in the process of devising the optimum fluid loop system.

There are problems, however, where the optimization procedure is not so clear-cut, and where some trade-off between alternative optimization criteria should be made. Furthermore, in several instances a subsystem is integrated into an already existing system, and the possibilities of optimizing the subsystem are severely curtailed by the constraints imposed by the integration.

The following two examples will illustrate how the design engineer faces these problems.

13.3.1 Constraints based on source temperature

There are situations where the source temperature, T_s, appears in the optimization problem, either because it is specified or because it is to be optimized, for a given heat load, Q. This introduces a new feature in the problem.

Berner & Schleicher (1976) [13] have analyzed a fluid loop with a given liquid to liquid heat exchanger; the so called Experiment Dedicated Heat Exchanger (EDHX), which has been developed for use in Spacelab. The mentioned fluid loop is sketched in Figure 13-3. Details concerning a heat exchanger similar to the EDHX can be found in clause 11.7. The heat source, which is the setup used for performing scientific experiments onboard Spacelab, is mounted on a cold plate (see clause 11.7), thence the source temperature is assumed to be the wall temperature of the flow passages through the cold plate.
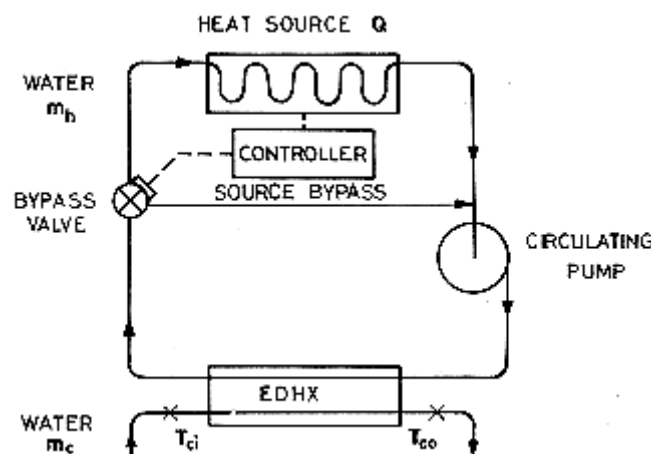
Figure 13-3: Schematic representation of the fluid loop with EDHX. From Berner & Schleicher (1976) [13].

In order to control the source temperature a percentage of the coolant flow is bypassed around the source.

An attempt is made to optimize the hot fluid mass flow rate so that the mass of the supply and return plumbing plus the equivalent mass due to pumping power is minimized under the following set of assumptions and specifications.

    1. Concerning the working fluids.

         o Hot and cold fluids are water

         o Mass flow rate of cold fluid, 0,0631 kg.s^{-1}

         o Percentage of hot fluid mass flow rate bypassed around source for temperature control purposes, 50 %

2.   Concerning operating temperatures.

   o   Inlet temperature of cold fluid at EDHX, T_{ci} = 293 K

   o   Outlet temperature of cold fluid at EDHX, $T_{co} \leq$ 313 K

3.   concerning supply and return plumbing.

   o   Length of forward and return legs of the loop, 2,5 m each

   o   Number of 90° bends in each leg, 5

   o   Ratio of bend radius to tube radius, R/r = 6

   o   Material of plumbing, stainless steel

   o   The pressure drop in valves, manifolds, etc., is accounted for by doubling the pressure drop based on tube length and bends

4.   Concerning pumping.

   o   Pump efficiency, η_p = 0,1

   o   Power penalty factor, 0,5 kg.W^{-1}

For each mass flow rate, m_h, the sum of the masses of tubes and fluid, plus the equivalent mass due to pumping power is calculated for different values of the inner diameter of the tubes. The resulting values, which are practically independent of the heat load, Q, indicate that, for a given diameter, the total mass decreases as the flow rate decreases. however, for a given heat load, Q, the source temperature, T_s, increases as the mass flow rate, m_h, decreases. In those situations in which the source temperature is fixed there is a particular tube diameter optimizing the system mass, otherwise a trade-off between low source temperature and low system mass is required.

Figure 13-4 shows an example of this type of trade-off analysis. The data shown in this figure are for Q = 10^3 W. Other values of Q, in the range 0,5 x 10^3 W to 4 x 10^3 W, have been considered by Berner & Schleicher (1976) [13] resulting in fairly large changes of the values of T_s and only small changes in the mass penalty, M^+. It may be noticed from Figure 13-4 that at a certain low constant value of M^+ a minimum value of T_s is obtained for an intermediate tube diameter. Likewise, for source temperatures above some threshold value a minimum value of M^+ could be obtained by varying the diameter. When both source temperature and system mass should be optimized there is no criterion on which this optimization could be based and a compromise between low T_s and low M^+ is necessary. Sometimes the pumping power required by the "optimum" system is so low that it is doubtful that a 0,1 pumping efficiency may be reached. To illustrate this, the interrupted line in Figure 13-4 has been drawn through the points on each of the candidate systems for which the pumping power requirement, $\eta_p P$, equals 0,5 W. It can be deduced from Figure 13-4 that, for constant pumping power, the mass penalty must increase if the source temperature is to be decreased, but there are values of the inner diameter of the tube above which relatively modest decreases in source temperature imply large mass penalties. Thus, at least in the case considered in Figure 13-4, an inner diameter of 10^{-2} m could represent a good compromise.
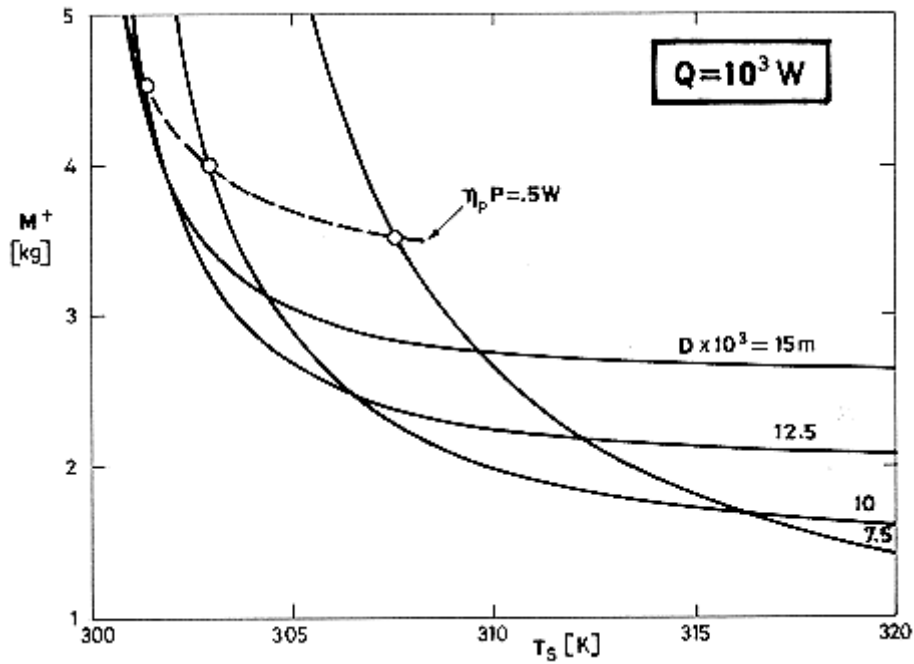
Figure 13-4: Mass penalty, M^+, of the supply and return plumbing system vs. source temperature, T_S. M^+ includes mass of tubes and fluid plus the equivalent mass due to pumping. Heat load, $Q = 10^3$ W. From Berner & Schleicher (1976) [13].

Figure 13-5 shows the relationship between the source temperature, T_S, and the coolant mass flow rate, m_h, for several values of the heat load, Q. The power requirements are in the range 0,5 to 1 W. Thus, even if a relatively low pumping efficiency is assumed, the power supplied to the pump would be a few watts only.
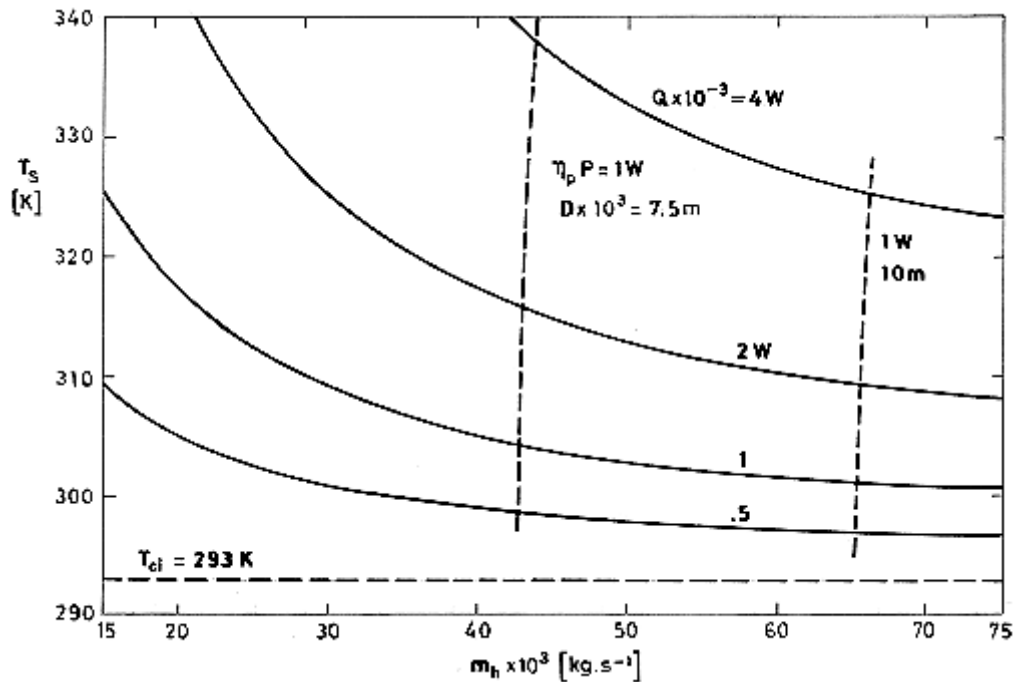
Figure 13-5: Source temperature, T_s, vs. coolant mass flow rate, m_h, for different values of the heat transfer rate, Q. The interrupted lines are drawn through the points for which the power requirements, for a given D_i, equals 1 W. From Berner & Schleicher (1976) [13].

An important conclusion drawn from Figure 13-5 is that it is not possible to reduce the difference between source and sink temperatures, for a given heat load by increasing the coolant mass flow rate beyond a certain value, and that this difference can be relatively high. Figure 13-5 shows that, for instance, when $Q = 10^3$ W the source temperature cannot be decreased below 300 K. Therefore, if lower source temperatures are specified, some refrigeration equipment, not necessarily based on a convective heat transfer mechanism, should be incorporated. Berner & Schleicher (1976) [13] present an optimization analysis of a system in which a heat pump has been incorporated to further decrease the source temperature. The aim of this heat pump is to extract thermal energy from the fluid returning toward the heat source and to give it off to the fluid flowing from source to sink.. Although a system incorporating a heat pump could operate even in the case of negative source to sink temperature differences, the power requirement of the heat pump is much larger than that of the circulation pump. Thus, the mass of a fluid loop system with heat pump strongly depends on the value of the pumping power penalty factor.

13.3.2   Constraints imposed by the integration

Sometimes the integration of the system onboard the satellite imposes constraints which must be taken into account in the optimisation process. In several cases the selected optimum configuration does not meet all the imposed requirements and some sort of trade-off should be made.

A cooling system with liquid -Flutec 9950- to air heat exchanger (ECLA) has been studied by Berner, Schleicher, Oesch, Nyfeler & Steinhauser (1977) [14] for use in Spacelab. The basic ECLA system is sketched in Figure 13-6. The heat source, which is the setup used for performing certain scientific experiments is mounted on a cold plate (see clause 11.7), and its temperature is controlled by removing heat which is then transferred to the Avionics Air Loop of the Spacelab. A set of liquid to air

cross-flow heat exchangers, combined in series, constitutes the thermal link between coolant loop and air loop.
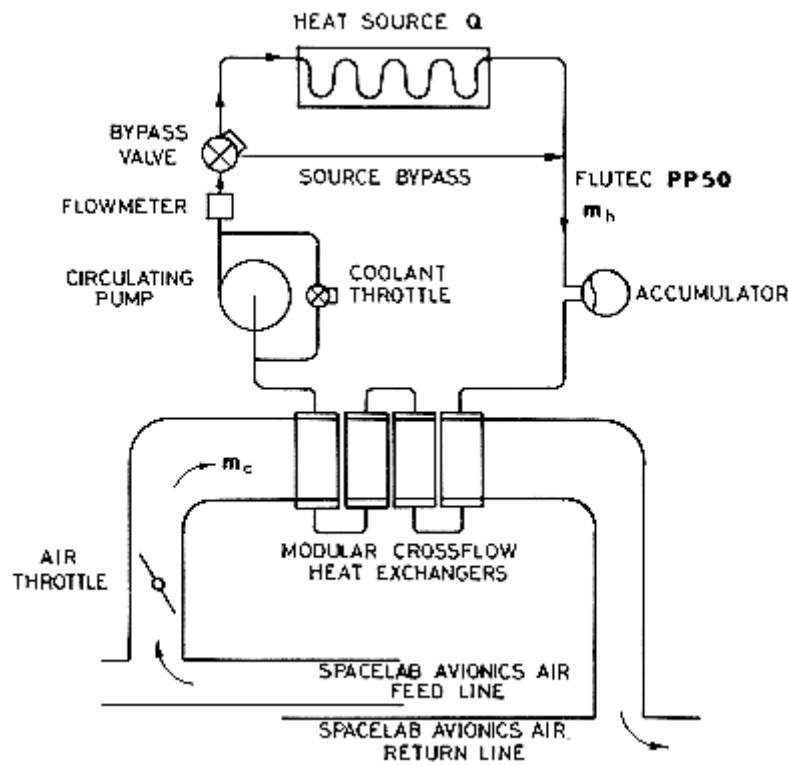
Figure 13-6: Schematic representation of basic ECLA system. The aim of the accumulator, which is not mentioned in the text, is to accommodate changes in coolant density with temperature. The coolant throttle is used for adjusting the coolant mass flow rate, m_h. From Berner & Schleicher (1976) [13].

In order to control the source temperature, T_s, part of the coolant flow is bypassed around the heat source. This is achieved by means of a flow proportioning valve monitored through the difference between measured and desired source temperature. In this way the source temperature, T_s, is limited from above and from below for a given heat load, Q. The upper limit of T_s is set by the danger of instability in the control loop. This instability appears because the derivative of T_s with respect to coolant mass flow rate through the heat source becomes very large at low flow rates. The lower limit for T_s is reached with no bypass. Sometimes the desired T_s cannot be reached within the operating limits of the valve, then the air mass flow rate can be changed by a throttle in the air duct of the ECLA system. To extend the operating range to lower values of the source to sink temperature differences a heat pump is incorporated in the fluid loop. The performance of the ECLA system with heat pump has been considered by Berner et al. (1977) [14], but it will not be discussed here.

The requirements specified for ECLA are:

1.   Heat loads, Q, from 100 W to $1,5 \times 10^3$ W.

2.   Source temperature, T_s, adjustable between 283 K and 353 K with a margin of ±5 K.

Integration of ECLA in the Spacelab Avionics Air Loop introduces other requirements:

1.   The maximum allowed air mass flow rate is $m_c = 0,0908$ kg.s^{-1}.

2.   Inlet air temperature, T_{ci}, ranges from 293 K to 297 K.

3. Pressure drop of the air between the position where it is withdrawn from the forward line of the Avionics Air Loop and given back to the return line should not exceed 250 Pa (1 inch of water), otherwise a fan must be incorporated in the air duct through ECLA.

4. Air velocities above 6 m.s^{-1} are undesirable from the stand point of noise generation.

Other engineering criteria which should be taken into account are the following: the heat exchanger is of the crossflow type similar to those used in the "radiator" of motor cars. In order to reach acceptable performances a multipass arrangement is used. This can be best implemented with a series arrangement of several modules. Each module has a fixed cold flow length. The size of the system is such that it can be accommodated in the Spacelab module racks.

The aim of the optimization is the achievement of a minimum heat exchanger mass for a selected operating condition (basically, for given Q and $T_s - T_{ci}$). The data used in the present case are the following:

Heat load, $Q = 0,5 \times 10^3$ W

Air mass flow rate, $m_c = 0,0303$ kg.s^{-1} and $0,0817$ kg.s^{-1}

Air inlet temperature, $T_{ci} = 295$ K

Coolant mass flow rate, $m_h = 0,067$ kg.s^{-1}

Percentage of hot fluid mass flow rate bypassed around source for temperature control purposes, 10 %

Product of total heat transfer area and overall thermal conductance of the cold plate $(UA)_s = 500$ W.K^{-1}

The air free flow area at the inlet of the first heat exchanger module, A_{FL}, is obviously an important parameter for optimization. In addition, since the cold flow length of the modules is the same regardless of the module size, the optimization of the heat exchanger is based on A_{FL} and on the number, n, of modules.

From a number of detail designs of heat exchanger modules, with square inlet air flow cross sections (of different sizes) a dependence between the mass, M, of the module (including the liquid in it) and the air free flow area, A_{FL}, as been found, namely:

$M = 97\, A_{FL} + 0,26$

where M is in kg and A_{FL} in m^2. This relation is used in the mass optimization of the exchanger.

The numerical results for two different cases are summarized in Table 13-1.

Table 13-1: Optimization of the Liquid to Air Heat Exchanger
Case 1) $m_c = 0,0303$ kg.s^{-1}, $T_s - T_{ci} = 20$ K

No. of Modules	A_{FL} [m²]	M [kg]	nM [kg]	Cold Flow Length [m]	Volume, [a] v x 10³ [m³]	For $m_c = 0,0908$ kg.s^{-1} [b] Air velocity [m.s⁻¹]	Air pressure drop, Δp x 10⁻³ [Pa]
2	0,01740	1,948	3,896	0,150	4,26	5,6	0,050
3	0,00892	1,125	3,376	0,225	3,63	10,9	0,051
4	0,00553	0,796	3,186	0,300	3,47	17,6	0,052
5	0,00395	0,643	3,216	0,375	3,52	24,7	0,053

Table 13-2: Optimization of the Liquid to Air Heat Exchanger
Case 2) $m_c = 0,0817$ kg.s^{-1}, $T_S - T_{ci} = 10$ K

No. of Modules	A_{FL} [m²]	M [kg]	nM [kg]	Cold Flow Length [m]	Volume, [a] v x 10³ [m³]	For $m_c = 0,0908$ kg.s^{-1} [b] Air velocity [m.s^{-1}]	Air pressure drop, Δp x 10^{-3} [Pa]
2	0,02070	2,268	4,536	0,150	4,96	4,7	0,055
3	0,01075	1,303	3,909	0,225	4,21	9,1	0,057
4	0,00688	0,927	3,709	0,300	3,98	14,2	0,059
5	0,00495	0,740	3,701	0,375	3,97	19,7	0,061
6	0,00370	0,619	3,713	0,450	4,13	26,4	0,061

[a]   Volume of the cube circumscribing the heat exchanger.

[b]   Maximum allowable air mass flow rate.

NOTE   From Berner, Schleicher, Oesch, Nyfeler & Steinhauser (1977) [14].

It is apparent from these results that a heat exchanger with an $A_{FL} = 0,005$ m² would have a nearly minimum mass and occupy about the smallest volume, thus it may be considered an optimum result.

The air velocity in the cross section of area A_{FL} and the air pressure drop through the heat exchanger have been calculated also on the bases of maximum allowable air mass flow rate. The aim of these calculations is to test the fulfillment of requirements 5) and 6) above. It is seen that requirement 6) may not be fulfilled when the optimum exchanger is used. Thence this optimum configuration is ruled out and a value $A_{FL} = 0,0225$ m² has been chosen. With this value of A_{FL} the above operating conditions can be satisfied with $n = 2$ modules. Larger values of n will be probably required when Q is increased and/or T_S is decreased before setting up a heat pump with its large power consumption.

14
Two-phase flow

14.1 General

Gas-liquid flow in a duct is a very complex phenomenon because an interface between two fluids, one of them compressible, is present.

Different flow patterns exist depending on the conditions. The definition of these flow patterns and of their boundaries have been much debated. The reader should be addressed to basic texts on the field, such as Govier & Aziz (1972) [75], Hetsroni (1982) [85], among others.

Figure 14-1 shows a flow-pattern map for vertical upward flow of air and water, which has been prepared after Hewitt (1982) [86]. A similar map also for air and water but in horizontal flow is given in Figure 14-2.
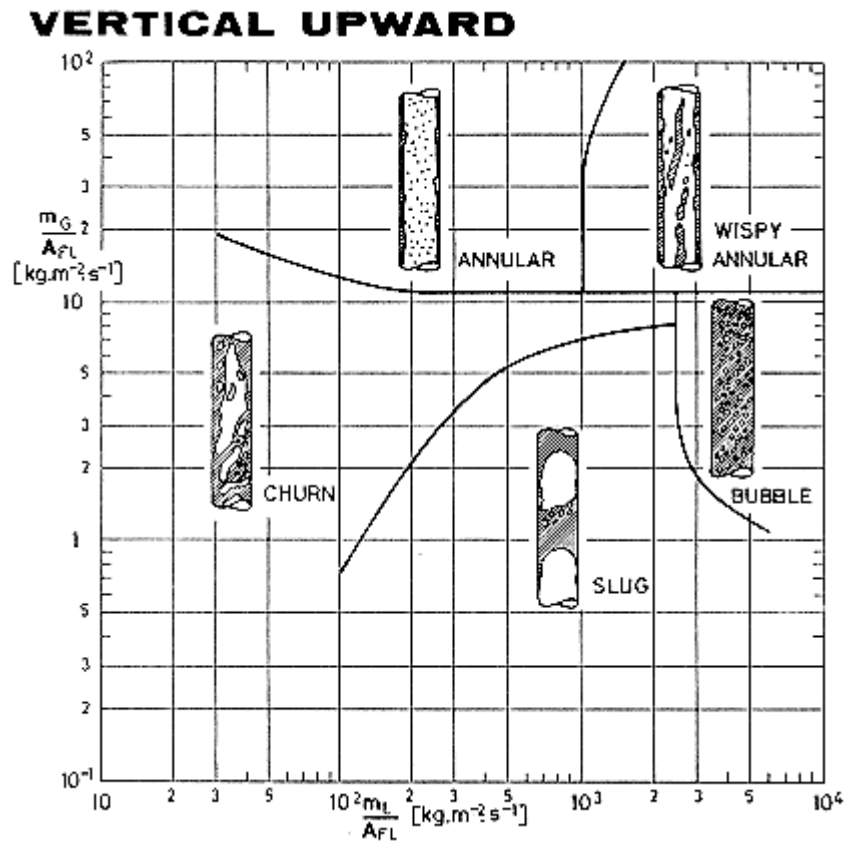
VERTICAL UPWARD

Figure 14-1: Flow-pattern map for vertical upward air-water flow. Prepared by the compiler after Hewitt (1982) [86]. m_G and m_L are the gas and liquid mass flow rates, respectively. A_{FL} is the internal cross-sectional area of the duct.
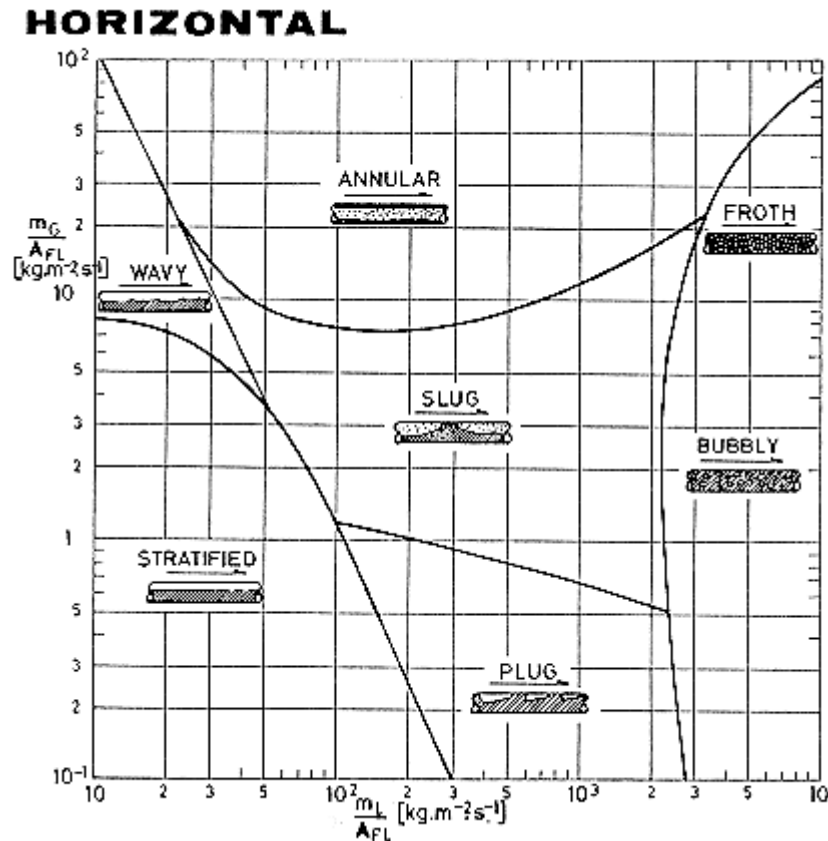
HORIZONTAL

Figure 14-2: Baker flow-pattern map for horizontal air-water flow. From Hewitt (1982) [86]. m_G and m_L are the gas and liquid mass flow rates, respectively. A_{FL} is the internal cross-sectional area of the duct.

This type of maps has been criticized very often on the grounds that so different transition processes hardly can be controlled by the same parameters. Thus, different investigators use different maps, with different boundaries, intermediate patterns and even different nomenclatures.

Data covering a wider range of fluid properties are also available. For example, in the case of horizontal flow, and following Baker, the physical properties of the fluids are taken into account through the following two parameters

$$\lambda_B = \left(\frac{\rho_G}{1,205} \frac{\rho_L}{10^3} \right)^{1/2} \quad , \quad \psi_B = \frac{0,0728}{\sigma} \left[\frac{\mu_L}{0,001002} \left(\frac{10^3}{\rho_L} \right)^2 \right]^{1/3} \qquad [14\text{-}1]$$

where the numerical values correspond to air and water under standard conditions (10^5 Pa, 293 K).

The flow-pattern map is then given in terms of $m_G/\lambda_B A_{FL}$ vs. $m_L \psi_B / A_{FL}$. Obviously, λ_B and ψ_B are equal to unity for standard air-water flow.

Information on the flow patterns in reduced gravity is scarce. Comparison of Figure 14-1 and Figure 14-2 indicate that

    1.   Gravity effects are important.

    2.   The annular flow pattern remains in the same position in both maps: low (but not too low) liquid velocity and large gas velocity.

14.2 Pressure loss

14.2.1 Lockhart-martinelli correlation

The flow pattern under reduced gravity is uncertain. The pressure loss would depend on this flow pattern, but the available experience indicates that this dependence is not large.

For horizontal flows through small diameter ducts (few centimeters in diameter), without phase change or significant acceleration, the Lockhart-Martinelli correlation (Lockhart & Martinelli (1949) [116]) has been widely used during the last thirty years. It is simple to use, it does not depend on the details of the flow pattern and it is often used to calculate both the void fraction and frictional pressure loss even when other effects are not negligible. This procedure leads to progressively increasing errors as the frictional component of pressure loss decreases in proportion to the other terms (acceleration or phase change). Clearly, separate correlations should be used for each flow pattern, as has been suggested by many investigators, but when data from these partially-valid correlations are compared to those from Lockhart-Martinelli the agreement, although poor, could suffice for many engineering purposes.

In the Lockhart-Martinelli correlation the frictional pressure loss of the two phase flow, $\Delta p/L$, is related to either $(\Delta p/L)_{SL}$ or $(\Delta p/L)_{SG}$ through pressure loss multipliers which are defined as follows:

$$\Phi_L^2 = \frac{\Delta p/L}{(\Delta p/L)_{SL}} \quad , \quad \Phi_L^2 = \frac{\Delta p/L}{(\Delta p/L)_{SG}} \qquad [14\text{-}2]$$

where $(\Delta p/L)_{SL}$ is the pressure loss that would occur if the flow rate of liquid were flowing alone in the duct,

$(\Delta p/L)_{SG}$ is the pressure loss that would occur if the flow rate of gas were flowing alone in the duct.

The pressure gradient, dp/dx, is very often used for the pressure loss, $\Delta p/L$. $\Delta p/L = -dp/dx$.

It is assumed that $(\Delta p/L)_{SL}$ and $(\Delta p/L)_{SG}$ are known.

In order to avoid having the unknown two-phase pressure loss in both correlating parameters it is convenient to introduce a new variable (the Lockhart-Martinelli parameter),

$$X^2 = \frac{(\Delta p/L)_{SL}}{(\Delta p/L)_{SG}} = \frac{\Phi_G^2}{\Phi_L^2} \qquad [14\text{-}3]$$

X^2 gives a measure of the degree to which the two-phase mixture behaves as the liquid rather than as the gas.

Let us introduce a Reynolds number, Re, to calculate X in the different cases

$$Re = \frac{mD}{A_{FL}\mu_G} \qquad [14\text{-}4]$$

m is the total mass flow rate, [kg.s^{-1}].

D is the diameter of the duct, or the equivalent diameter if the cross section of the duct is not circular, [m].

A_{FL} is the internal cross sectional area of the duct, [m²].

μ_G is the dynamic viscosity of the gas phase, [Pa.s].

In terms of the Reynolds number, Re, and the vapor quality, w, which is defined as

$$w = \frac{m_G}{m}$$ [14-5]

the Reynolds numbers of each phase become, respectively,

$$Re_L = (1-w)\frac{\mu_G}{\mu_L} Re \quad , \quad Re_G = wRe$$ [14-6]

In terms of the friction factors, f_{SG} and f_{SG}, the Lockhart-Martinelli parameter can be written out as (see clause 7.2 for the relation between $\Delta p/L$ and $f = \lambda/4$)

$$X^2 = \frac{\rho_G}{\rho_L}\left(\frac{1-w}{w}\right)^2 \frac{f_{SG}(Re_G)}{f_{SL}(Re_L)}$$ [14-7]

where ρ is the density, [kg.m⁻³], and f_s the friction factor of each phase if it were flowing alone in the duct.

Using for the friction factor vs. Re_L and Re_G either the Hagen-Poiseuille (clause 7.2) or the Blasius formula (clause 7.2.2.1), X can be expressed as follows:

$$X = E\left(\frac{\rho_G}{\rho_L}\right)^{1/2}\left(\frac{\mu_L}{\mu_G}\right)^{n_1} \frac{(1-w)^{n_2}}{w^{n_3}}$$ [14-8]

E is a constant factor, and n_1, n_2, n_3 are constant exponents.

According to Lockhart-Martinelli, Φ_L and Φ_G are functions of X only although there is a slight difference which depends on the nature, laminar or turbulent, of the two separate phase-alone flows. The transition liquid and gas Reynolds numbers are $Re = 1000$, smaller than that for single-phase flow, clause 7.2 (see Govier & Aziz (1972) [75], p. 534). The factor E and the exponents n_1, n_2 and n_3 of Eq. [14-8] also depend on the nature of single-phase flow and are given in the following Table.

LIQUID	GAS	SUBSCRIPT	E	n_1	n_2	n_3
Turbulent	Turbulent	tt	1	1/8	7/8	7/8
Laminar	Turbulent	vt	$19,2/Re^{3/8}$	1/2	1/2	7/8
Turbulent	Laminar	tv	$Re^{3/8}/14,2$	1/8	7/8	1/2
Laminar	Laminar	vv	1	1/2	1/2	1/2

Chisholm (1967) [25] suggested a simple and accurate analytic representation of the multipliers (Figure 14-3).
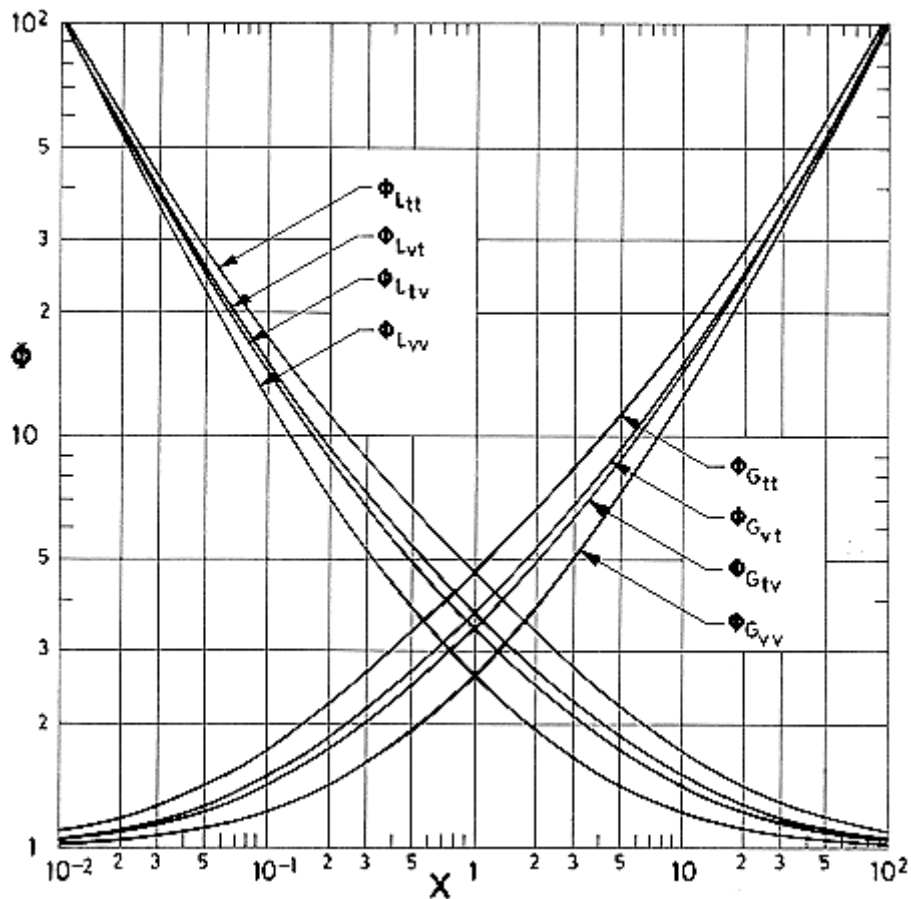
Figure 14-3: Lockhart - Martinelli correlation for pressure loss multipliers. The figure has been drawn by use of Chisholm analytical representation. See text.

$$\Phi_L^2 = 1 + \frac{C}{X} + \frac{1}{X^2} \quad , \quad \Phi_G^2 = 1 + CX + X^2 \qquad [14\text{-}9]$$

where C depends on the nature of the phase-alone flow as follows

Subscript	tt	vt	tv	vv
C	20	12	10	5

Other representation of Φ_L and Φ_G is (Wallis (1969) [184], p. 50)

$$\Phi_L^2 = \left(1 + X^{-2/n}\right)^n \quad , \quad \Phi_G^2 = \left(1 + X^{2/n}\right)^n \qquad [14\text{-}10]$$

where n also depends on the nature of the phase-alone flow

Subscript	tt	vt	tv	vv
n	4	3,5	2,75 for $X < 5$	3,5 for $X > 5$

A comparison of Eqs. [14-9] and [14-10] with experimental data is given in Figure 14-4.
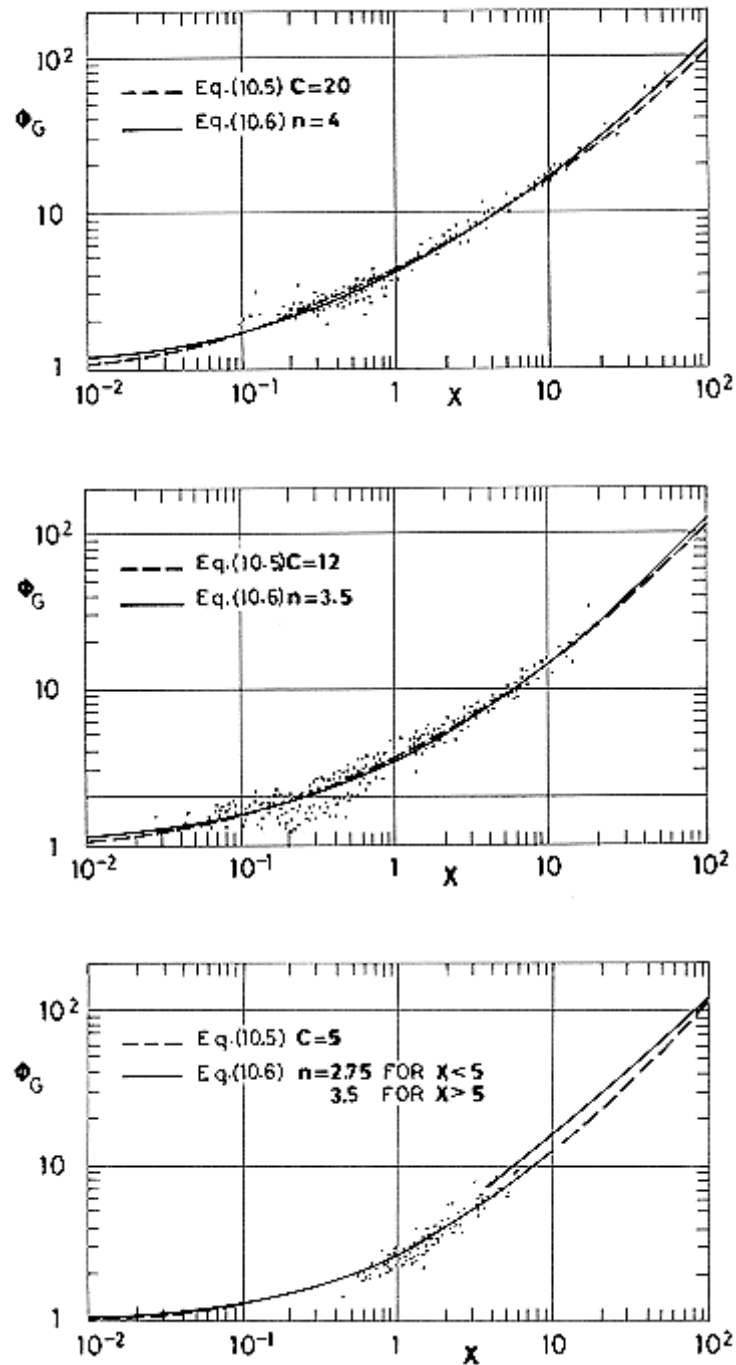
Figure 14-4: Gas phase pressure loss multiplier, Φ_G, vs. Lockhart - Martinelli parameter, X, as deduced from Eqs. [14-9] and [14-10] and from experimental data. a) tt case; b) vt case; c) vv case. Experimental points are from Wallis (1969) [184].

The void fraction, α, represents the fraction of an element of volume which is occupied at an instant by the gas phase (or the lighter phase in a stratified flow). $1 - \alpha$ is the liquid fraction.

The Lockhart-Martinelli correlation also gives the void fraction, α, in terms of X (Figure 14-5). The curve can be fairly represented by the equation (Wallis (1969) [184], p. 51)

$$\alpha = \left(1 + X^{0,8}\right)^{-0,378} \qquad [14\text{-}11]$$
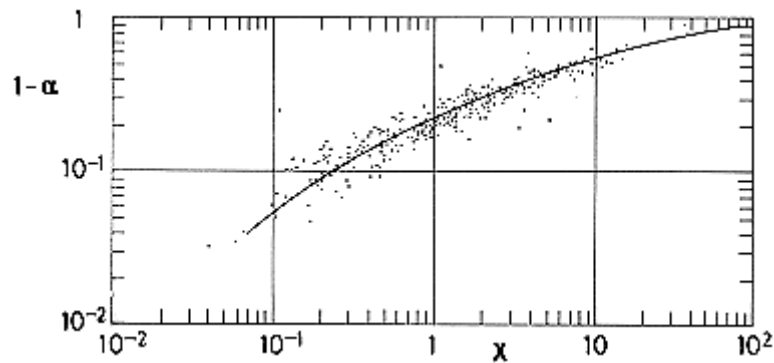
Figure 14-5: Liquid fraction, 1-α, vs. Lockhart - Martinelli parameters, X. From Wallis (1969) [184].

14.2.2 Improvements upon martinelli correlation

Equations [14-9] are general for all types of flow and can be easily adapted to specific data by correlating the factor C.

The last two terms of the right hand side of Eqs. [14-9] correspond to the theory for the limiting cases of approaching all gas or all liquid flows respectively. The factor C has been found to be a function of flow regime, vapor and liquid Reynolds numbers, density ratio, geometry, and surface tension.

Martinelli & Nelson (1948) [122] noted that the Lockhart-Martinelli correlation does not become asymptotic to the correct value as the critical pressure, p_c, is approached. C should decrease with increasing pressure and theoretically become zero at the critical pressure.

Originally, it was intended to multiply the factor C by (1 - p/p_c). However, as pointed out by Palen (1976) [140], limited data for condensing n-pentane at $p/p_c \approx$ 0,5 indicate that the correction cannot be extended to all fluids.

Based on Martinelli's results, HTRI (Yang & Palen (1977) [195] developed a generalized curve-fit relation valid when both phases are turbulent:

$$\Phi_{L_{tt}}^2 = \left[1 + \frac{3\left(1 - p/p_c\right)}{X_{tt}^{0,55}} + \frac{1}{X_{tt}^{1,11}} \right]^{1,75}$$

[14-12]

where p is the local pressure and p_c the local average critical pressure of the gas phase.

Equation [14-12], which was developed from data obtained in horizontal duct flow, can be used for flow regimes other than turbulent-turbulent due to overall data scatter.

The Lockhart-Martinelli correlation also fails to take adequate account of the influence of flow quality, w. It tends to predict too low Φ_L at high quality and too high at low quality flows, Figure 14-6.
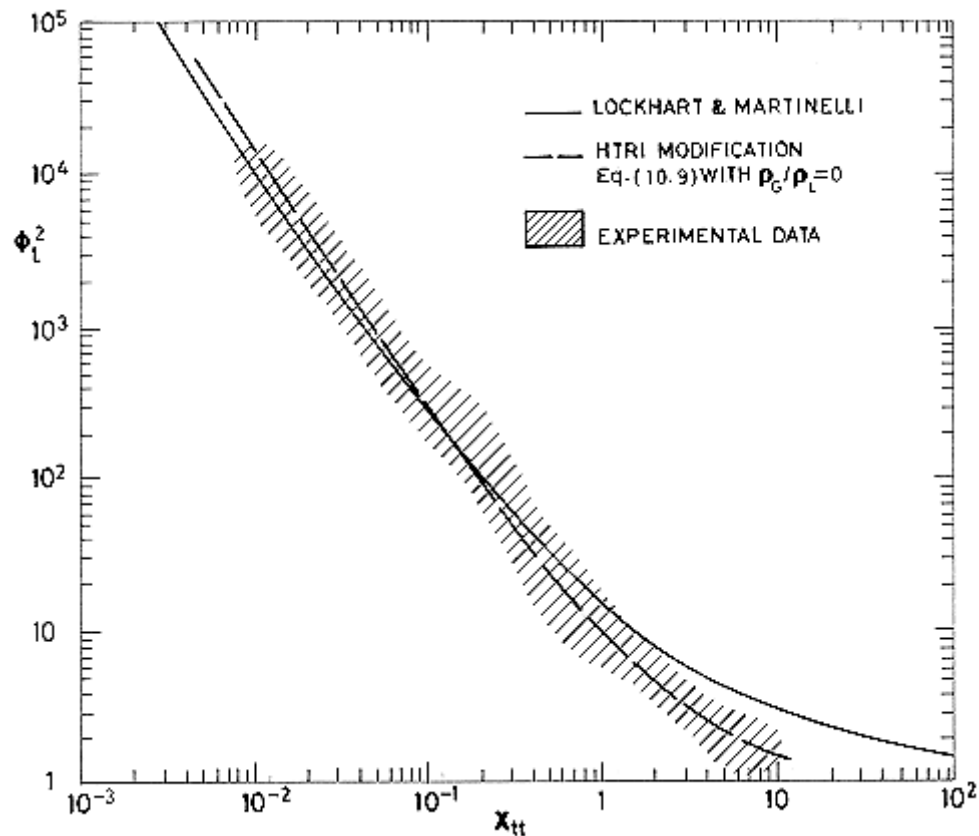
Figure 14-6: Comparison of Lockhart - Martinelli with available experimental data. Points with *C* as per Eq. [14-13], with $\rho_G/\rho_L = 0$ are also shown. From Yang & Palen (1977) [195].

Yang & Palen (1977) [195] suggested the following simple expression for *C* in the turbulent-turbulent case for shear-controlled flow regimes

$$C = 2{,}75 \left(1 + \frac{2}{X_{tt}^{0,5}}\right)\left(1 - \frac{\rho_G}{\rho_L}\right)^{1,5} \qquad \text{[14-13]}$$

This expression gives as good a fit to experimental data as many of the more complicated forms and is recommended for condensation pressure drop.

Continuing attempts have been made to improve the correlations for frictional pressure loss, see a fairly recent account in Hewitt (1982) [86].

14.3 Annular flow

Annular flow is the most ubiquitous of the flow regimes. It consists of a homogeneous mixture of gas and droplets (the gas core) surrounded by a liquid layer near the wall (the liquid film). If the core contains a significant number of entrained droplets, the flow is described as annular mist, which can be regarded as a transition between ideal annular flow and fully dispersed drop flow pattern. In general, the phases may not be in equilibrium with respect to temperature and concentrations. In

many cases, however, the interface heat and mass transfer rates are very high because of the large interfacial area and high turbulence, thence the phases reach an equilibrium during their passage through the duct.

Annular flow is the predominant flow pattern in evaporators, natural gas pipelines, steam heating systems and, in general, reduced gravity flows in ducts.

14.3.1   Ideal annular flow model

Let us assume steady motion through a duct of circular cross section when no liquid is entrained in the gas core.

14.3.1.1   Mass preservation equation for either phase

As the pressure and temperature do not change within a section of the duct, the density of the gas core does not change within that section, therefore the mass preservation equation for each phase is

$$\frac{dm_G}{dx} = \frac{dm_L}{dx} = 0 \qquad [14\text{-}14]$$

m being the mass flow rates.

Central gas core and outer liquid film are shown in Figure 14-7.
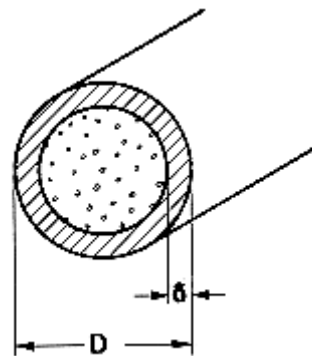
Figure 14-7: The annular flow configuration.

14.3.1.2   Axial momentum equation for either phase

1.   The momentum equation for the liquid film can be expressed as:

$$\frac{dp}{dx} = -\frac{1}{r}\frac{d(r\tau)}{dr} \qquad [14\text{-}15]$$

where τ is the shear stress in the liquid. It is assumed in the above equation that δ is constant so that acceleration terms are zero. Gravity effects are also neglected.

If we integrate once the above equation with the boundary condition $\tau = \tau_i$ at $r = (D - 2\delta)/2$, being τ_i the shear stress at the interface, we obtain

$$\tau = \tau_i \frac{D - 2\delta}{D - 2y} - \frac{dp}{dx} \frac{(D - y - \delta)(\delta - y)}{D - 2y} \qquad \text{[14-16]}$$

Here y is the distance measured from the wall of the duct: $y = (D/2) - r$. At the wall, $y = 0$, we have,

$$\tau_w = \tau_i \frac{D - 2\delta}{D} - \frac{dp}{dx} \frac{(D - \delta)\delta}{D} \qquad \text{[14-17]}$$

2. In the gas core the differential momentum equation can be written exactly as before if we neglect the inertia term compared with the pressure term. This is justified when changes in pressure and temperature are small compared with the prevail- ing pressure and temperature levels, respectively.

    Integrating once with the boundary condition $\tau = 0$ at $r = 0$ we get,

$$\tau = -\frac{dp}{dx} \frac{r}{2} \qquad \text{[14-18]}$$

which at the interface, $r = (D - 2\delta)/2$, becomes

$$\tau_i = -\frac{dp}{dx} \frac{D - 2\delta}{4} \qquad \text{[14-19]}$$

Combination of Eqs. [14-17] and [14-19] relates the wall shear stress, τ_w, to the pressure loss per unit length of the duct, $-dp/dx$.

$$\tau_w = -\frac{dp}{dx} \frac{D}{4} \qquad \text{[14-20]}$$

14.3.1.3 Pressure loss vs. friction factors fl and fgi

In order to calculate τ_w and τ_i, we introduce the friction factors for the liquid at the wall, f_L, and for the gas at the interface, f_{Gi}, as follows:

1. For the liquid at the wall:

$$\tau_w = \frac{1}{2} \rho_L V_L^2 f_L \qquad \text{[14-21]}$$

V_L being the liquid mass-average velocity,

$$V_L = \frac{m_L}{\rho_L \pi \delta (D - \delta)} \qquad [14\text{-}22]$$

and $f_L = f_L (Re_L)$, Re_L being the Reynolds number for the liquid,

$$Re_L = \frac{4m_L}{\pi D \mu_L} \qquad [14\text{-}23]$$

With the above expression of τ_w, Eq. [14-20] becomes:

$$\frac{dp}{dx} = -\frac{2m_L^2 f_L}{\rho_L \pi^2 D \delta^2 (D - \delta)^2} \qquad [14\text{-}24]$$

2. For the gas at the interface:

$$\tau_i = \frac{1}{2} \rho_G V_G^2 f_{Gi} \qquad [14\text{-}25]$$

where V_G is the gas mass-average velocity,

$$V_G = \frac{4m_G}{\rho_G \pi (D - 2\delta)^2} \qquad [14\text{-}26]$$

Recalling Eq. [14-19],

$$\frac{dp}{dx} = -\frac{32m_G^2 f_{Gi}}{\rho_G \pi^2 (D - 2\delta)^5} \qquad [14\text{-}27]$$

14.3.1.4   Laws of friction for fl and fgi

Equations [14-24] and [14-27] give two relations between the pressure loss, $-dp/dx$, the friction factor at the wall, f_L, the friction factor at the interface, f_{Gi}, and δ/D. Therefore we would need two additional relations to close the problem.

1. If the liquid were flowing alone in the duct, the pressure loss would be given by (clause 7.2 with $\Delta p/L = -(dp/dx)_{SL}$, $\lambda = 4f_{SG}$, $D_E = D$, $\rho = \rho_L$, $V = 4m_L/\rho_L \pi D^2$).

$$\left(\frac{dp}{dx}\right)_{SL} = -\frac{32m_L^2 f_{SL}}{\rho_L \pi^2 D^5} \qquad [14\text{-}28]$$

where f_{SG} is a function of the Reynolds number $Re_{SG} = -4m_L/\pi D\mu_L$). Since $Re_{SG} = Re_L$, as defined in clause 14.3.1.3, the friction factor at the wall will be the same as thatif the liquid were flowing alone at the same flow rate, $f_L = f_{SG}$. The value of f_L vs. Re_L will be given by

$$f_L = \frac{16}{Re_L} \qquad [14\text{-}29]$$

for laminar flow (Hagen-Poiseuille, clause 7.2.2),

$$f_L = 0{,}079 Re_L^{-0{,}25} \qquad [14\text{-}30]$$

for turbulent flow (Blasius, see Table 7-2)

For the transition regime, f_L has been numericallycalculated by Hewitt (1982) [86], see Figure 14-8
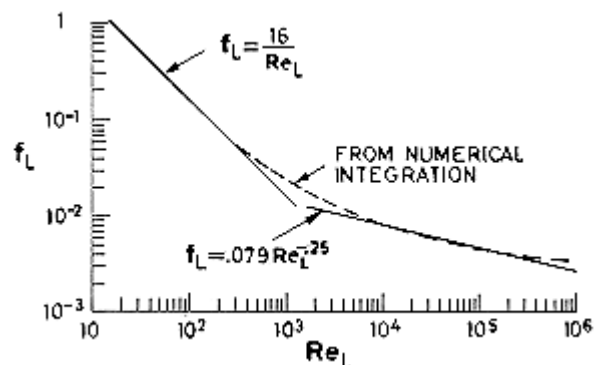
Figure 14-8: Liquid film friction factor, f_L, as a function of liquid film Reynolds number, Re_L, for annular two-phase flow in cylindrical ducts of circular cross-section. From Hewitt (1982) [86]. The full lines correspond, respectively, to Hagen-Poiseuille formula and to Blasius formula. f_L is equal to the friction factor f_{sL} which corresponds to the single phase flow along the duct at the same Reynolds number except for an intermediate Re_L.

2.   The most widely used method for calculating f_{Gi} consists in assuming that the interface affects the core flow as a rough duct wall should, and to seek an empirical relationship between f_{Gi} and the dimensionless film thickness, δ/D. Whalley & Hewitt (1978), quoted by Hewitt (1982) [86], suggest the expression

$$\frac{f_{Gi}}{f_{SG}} = 1 + 24 \left(\frac{\rho_L}{\rho_G} \right)^{1/3} \frac{\delta}{D}$$
[14-31]

where f_{SG} is the friction factor for the gas if it were flowing alone in the duct.

14.3.1.5 Expressions in terms of martinelli parameters

The pressure losses in the liquid and gas phase, given respectively by Eqs. [14-24] and [14-27] should be equal. Thus,

$$\frac{f_{Gi}}{f_L} = \frac{\rho_G m_L^2}{\rho_L m_G^2} \left(\frac{D}{4\delta} \right)^2 \frac{\left(1 - 2\dfrac{\delta}{D} \right)^5}{\left(1 - \dfrac{\delta}{D} \right)^2}$$
[14-32]

Since $f_L = f_{SL}$, Eq. [14-32] furnishes an alternative expression of f_{Gi}/f_{SG} in terms of the Lockhart-Martinelli parameter, X (Eq. [14-3]), clause 14.2.1)

$$\frac{f_{Gi}}{f_{SG}} = \frac{\rho_G m_L^2 f_{SL}}{\rho_L m_G^2 f_{SG}} \left(\frac{D}{4\delta} \right)^2 \frac{\left(1 - 2\dfrac{\delta}{D} \right)^5}{\left(1 - \dfrac{\delta}{D} \right)^2} = X^2 \left(\frac{D}{4\delta} \right)^2 \frac{\left(1 - 2\dfrac{\delta}{D} \right)^5}{\left(1 - \dfrac{\delta}{D} \right)^2}$$
[14-33]

where X^2 is known for given m_L, m_G, D and the densities of pure liquid, ρ_L, and pure gas, ρ_G.

Elimination of f_{Gi}/f_{SG} from Eqs. [14-31] and [14-33] gives the equation

$$X^2 = \left[1 + 24 \left(\frac{\rho_L}{\rho_G} \right)^{1/3} \frac{\delta}{D} \right] \left(\frac{4\delta}{D} \right)^2 \frac{\left(1 - \dfrac{\delta}{D} \right)^2}{\left(1 - 2\dfrac{\delta}{D} \right)^5}$$
[14-34]

which relates δ/D with ρ_L/ρ_G and X. δ/D in its turn is related to the (volumetric) liquid fraction, $1 - \alpha$, through the purely geometric expression

$$1 - \alpha = \frac{4\delta}{D} \left(1 - \frac{\delta}{D} \right)$$
[14-35]

Finally, the Martinelli pressure gradient multiplier, $\Phi_L{}^2$, (Eq. [14-2], clause 14.2.1) can be deduced from Eqs. [14-24] with $f_L = f_{SL}$, and [14-28],which yield an expression only dependent on δ/D

$$\Phi_L^2 = \left(\frac{D}{4\delta}\right)^2 \frac{1}{\left(1-\dfrac{\delta}{D}\right)^2}$$

[14-36]

Φ_L, $\Phi_G = X\Phi_L$, δ/D and $1 - \alpha$ vs. X are shown in Figure 14-9
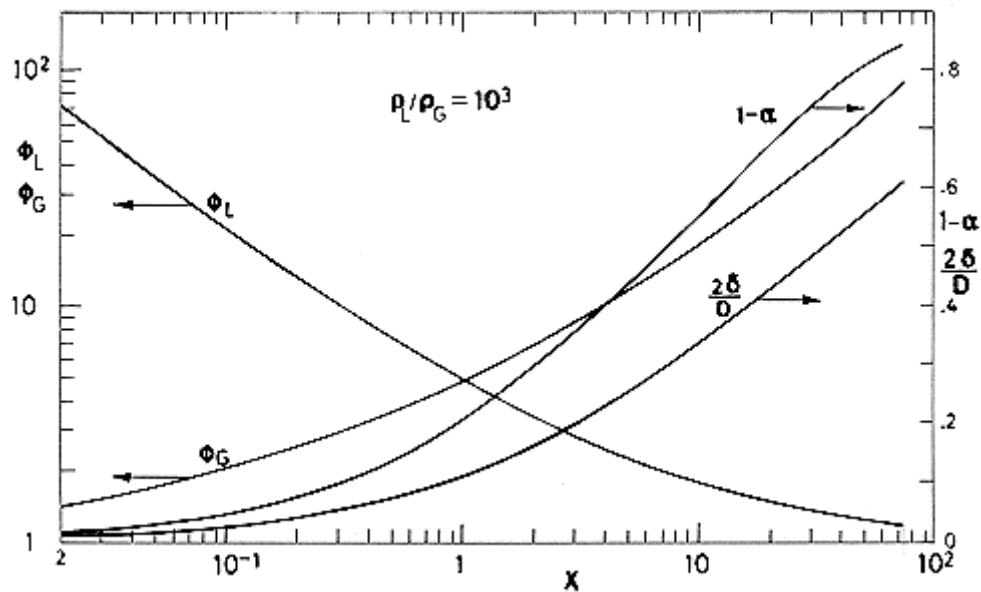
Figure 14-9: Pressure gradient multipliers, Φ_L and Φ_G, dimensionless film thickness, δ/D, and liquid fraction, 1-α, according to Eqs. [14-34], [14-35] and [14-36], with ρ_L/ρ_G = 1000. Calculated by the compiler.

A comparison between theoretical and experimental values of $1 - \alpha$ and Φ_G vs. X can be seen respectively, in Figure 14-10 and Figure 14-11.
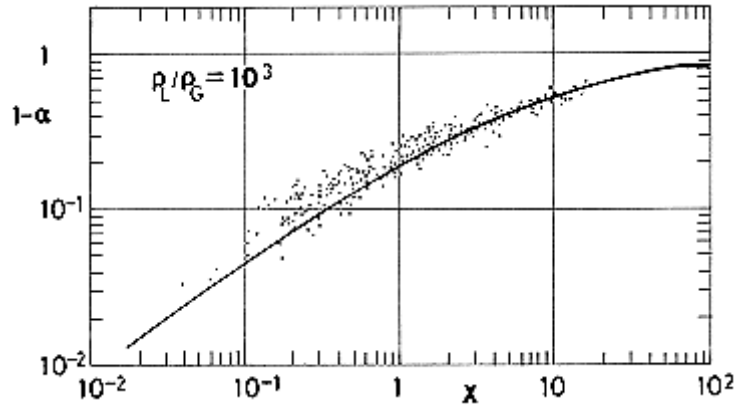
Figure 14-10: Comparison of the liquid fraction, 1-α, vs. Lockhart - Martinelli parameter, X, as deduced from Eqs. [14-34] and [14-35], with ρ_L/ρ_G = 1000, with experimental data from Wallis (1969) [184].
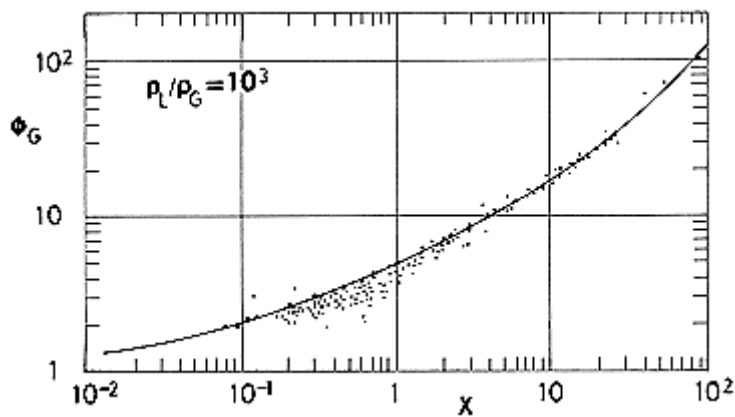
Figure 14-11: Comparison of the gas pressure gradient multiplier, $\Phi_G = x\Phi_L$, vs. Lockhart - Martinelli parameter, X, as deduced from Eqs. [14-34] and [14-36], with ρ_L/ρ_G = 1000, with experimental data from Wallis (1969) [184]. tt case.

14.3.1.6 Summary

It is convenient to summarize here, for further reference, the steps pursued to estimate the pressure drop in the IDEAL annular flow along a horizontal cylindrical duct.

The momentum balance in either phase gives the shear stresses at the wall, τ_w, and at the interface, τ_i.

$$\tau_w = -\frac{dp}{dx}\frac{D}{4}$$
[14-37]

$$\tau_i = -\frac{dp}{dx}\frac{D-2\delta}{4}$$
[14-38]

where the value of dp/dx is the same in both cases.

The shear stresses τ_w and τ_i are related to the friction factors f_L and f_{Gi}, respectively

$$\tau_w = \frac{1}{2}\rho_L V_L^2 f_L \qquad\qquad [14\text{-}39]$$

being V_L the mean liquid velocity, $V_L = m_L/\rho_L\pi\delta(D-\delta)$.

$$\tau_i = \frac{1}{2}\rho_G V_G^2 f_{Gi} \qquad\qquad [14\text{-}40]$$

with the mean gas velocity $V_G = 4m_G/\rho_G\pi(D-2\delta)^2$.

In terms of f_L and f_{Gi} the pressure gradient along the duct becomes

$$\frac{dp}{dx} = -\frac{2m_L^2 f_L}{\rho_L\pi^2 D\delta^2(D-\delta)^2} \qquad\qquad [14\text{-}41]$$

$$\frac{dp}{dx} = -\frac{32m_G^2 f_{Gi}}{\rho_G\pi^2(D-2\delta)^5} \qquad\qquad [14\text{-}42]$$

The friction factors f_G and f_{Gi} are related to those corresponding to either phase flowing alone with the same mass flow rate through the duct. The last mentioned friction factors, f_{SG} and f_{SG}, are known functions of the respective Reynolds numbers, Re_L and Re_G.

$$\frac{f_L}{f_{SL}} = 1 \quad , \quad \frac{f_{Gi}}{f_{SG}} = 1 + 24\left(\frac{\rho_L}{\rho_G}\right)^{1/3}\frac{\delta}{D} \qquad\qquad [14\text{-}43]$$

Since the same combinations of friction factors appear in the Lockhart-Martinelli formulation, we could express X^2, Φ_L^2 and $\Phi_G^2 = X^2\Phi_L^2$ as functions of δ/D exclusively.

$$X^2 = \left[1 + 24\left(\frac{\rho_L}{\rho_G}\right)^{1/3}\frac{\delta}{D}\right]\left(\frac{4\delta}{D}\right)^2\frac{\left(1-\dfrac{\delta}{D}\right)^2}{\left(1-2\dfrac{\delta}{D}\right)^5} \qquad\qquad [14\text{-}44]$$

$$\Phi_L^2 = \left(\frac{D}{4\delta}\right)^2\frac{1}{\left(1-\dfrac{\delta}{D}\right)^2} \qquad\qquad [14\text{-}45]$$

14.3.1.7 Worked example

Measurements performed with an air-water flow at 293 K in a horizontal duct of diameter 2,5 x 10^-2 m at mass flow rates m_L = 0,15 kg.s^-1 and m_G = 8,5 x 10^-3 kg.s^-1 showed that, when the exit pressure is 10^5 Pa, the pressure 5 m upstream is found to be 1,11 x 10^5 Pa. Compare these data with the predictions of 1) pure annular flow, and 2) Lockhart-Martinelli correlation.

The density and viscosity of air and water at 293 K are, respectively:

ρ_G = 1,21 kg.m^-3,

ρ_L = 998 kg.m^-3,

μ_G = 1,85 x 10^-5 Pa.s^-1,

μ_L = 1,003 x 10^-3 Pa.s^-1.

The Reynolds numbers are:

$$Re_L = \frac{4m_L}{\pi D \mu_L} = 7620$$

$$Re_G = \frac{4m_G}{\pi D \mu_G} = 23400$$

[14-46]

Therefore, the regimes are turbulent in both phases.

Using Blasius formula (clause 14.3.1.4) we have:

f_{SG} = 0,079 x (7620)^-0,25 = 0,0085,

f_{SG} = 0,079 x (23400)^-0,25 = 0,0064.

The Lockhart-Martinelli parameter, X, is (Eq. [14-3], clause 14.2.1)

$$X^2 = \frac{(\Delta p / L)_{SL}}{(\Delta p / L)_{SG}} = \frac{\rho_G}{\rho_L}\left(\frac{m_L}{m_G}\right)^2 \frac{f_{SL}}{f_{SG}} = 0,50$$

[14-47]

1. Pure annular flow model.

   Using Eq. [14-34] with X^2 = 0,50 we obtain δ/D = 0,044.

   Equation [14-36] with δ/D = 0,044 yields Φ_L^2 = 35,3.

   The pressure loss if the liquid were flowing alone through the duct would be given by Eq. [14-28]

$$-\left(\frac{dp}{dx}\right)_{SL} = \frac{32m_L^2 f_{SL}}{\rho_L \pi^2 D^5} = 63,6 \, Pa.m^{-1}$$

[14-48]

   and the pressure loss for the two phase flow,

$$-\frac{dp}{dx} = -\Phi_L^2\left(\frac{dp}{dx}\right)_{SL} = 2250\,Pa.m^{-1} \qquad\qquad [14\text{-}49]$$

2. Lockhart-Martinelli correlation.

    If the Lockhart-Martinelli correlation were used in the Chisholm form, Eq. [14-9], with C = 20

    $\Phi_L^2 = 31,2$,

    and α deduced from Eq. [14-11] would be:

    $\alpha = 0,081$,

    whereas that deduced for pure annular flow, Eq. [14-35] with $\delta/D = 0,044$ as above, would be:

    $\alpha = 0,083$.

The results from the annular flow model are compared to those from Lockhart-Martinelli correlation in the following Table.

	Annular model	**L-M correlation**
Φ_L^2	35,3	31,2
α	0,083	0,081
dp/dx [Pa.m^{-1}]	-2250	-1980

The measured pressure loss, 2200 Pa.m^{-1}, fairly agrees with that predicted by means of the annular model. The much simpler Lockhart-Martinelli correlation gives a not so good result.

14.3.2   Annular flow with entrainment model

When the core gas velocity is low, its effect on the film is negligible. However, with increasing relative velocity a destabilizing effect is noted. At the beginning small ripples travelling in the direction of the film appear. Higher core velocities lead to an increase in the amplitude of the ripples and soon three-dimensional disturbances are generated. When the core velocity is sufficiently high, drag forces on the tops of the roll waves pull-off droplets of liquid toward the gas core.

The data of many workers confirm that, except at low liquid rates, a significant portion of the liquid may be carried as droplets in the gas core. The flow in the liquid film initially increases with liquid flow rate, but eventually levels out at a value largely dependent on the gas flow rate. At the highest gas and liquid flow rates approximately 90 percent of the liquid is carried in entrained droplets.

14.3.2.1   Mass preservation equation for either phase

The mass flow rates of gas, m_G, and liquid, m_L, remain constant along the duct, as in clause 14.3.1.2. Now m_L consists of the mass flow rate of liquid entrained in the gas core, m_E, plus that in the liquid film, m_F. The mass preservation equations are:

$$\frac{dm_G}{dx} = \frac{d(m_E + m_F)}{dx} = 0 \qquad\qquad [14\text{-}50]$$

14.3.2.2 Axial momentum equation for either phase

If we assume that inertia terms are negligible compared with the pressure terms and if the amount of liquid entrained in the core does not change along the duct, because mass transfer due to entrainment by the core and to deposition of droplets in the film cancel to each other (hydrodynamic equilibrium hypothesis), the momentum equation for the liquid in the film reduces to Eq. [14-20], whereas that for the gas core reduces to Eq. [14-19]. The problem is now to calculate the shear stress at the wall, τ_w, and the shear stress at the interface, now called τ^*, to distinguish it from that without entrainment, τ.

14.3.2.3 Pressure loss vs. friction factors ff and fgi

Here we will follow as closely as feasible the approach of clause 14.3.1.3.

1. 1) For the liquid at the wall.

    The shear stress at the wall is calculated as in the case of no-entrainment, taking into account that the mass flow rate of liquid flowing in the film is now m_L - m_E. That is:

$$\tau_w = \frac{1}{2}\rho_L V_F^2 f_F \qquad\qquad [14\text{-}51]$$

V_F being the liquid film mass-average velocity,

$$V_F = \frac{m_L - m_E}{\rho_L \pi \delta (D - \delta)} \qquad\qquad [14\text{-}52]$$

and f_F the friction factor at the wall. $f_F = f_F(Re_F)$, Re_F being the Reynolds number for the mass flow rate of liquid in the film,

$$Re_F = \frac{4(m_L - m_E)}{\pi D \mu_L} \qquad\qquad [14\text{-}53]$$

With the above expression of τ_w, Eq. [14-20] becomes:

$$\frac{dp}{dx} = -\frac{2(m_L - m_E)^2 f_F}{\rho_L \pi^2 D \delta^2 (D - \delta)^2} \qquad\qquad [14\text{-}54]$$

The friction factor at the wall, f_F, is the same as that if the liquid in the film were flowing alone at the mass flow rate m_L - m_E.

2. For the gas core at the interface.

Equation [14-19] relating $-dp/dx$ to τ_i remains valid by writing τ^* in place of τ_i.

In order to relate τ^* with the interfacial friction factor with entrainment, $f_{Gi}{}^*$, we need a mean core density, ρ_c, and a characteristic velocity at the interface, be it the mean core velocity, V_G, or the tangential velocity jump at the interface.

Following Wallis (1969) [184], p. 363, we will envisage the core as a homogeneous mixture with a mean density, ρ_c, which can be written as

$$\rho_c = \frac{m_G + m_E}{m_G / \rho_G + m_E / \rho_L} \sim \rho_G \frac{m_G + m_E}{m_G} \qquad \text{[14-55]}$$

since $m_E/\rho_L \ll m_G/\rho_G$.

The mean velocities of droplets and gas are assumed to be the same, that is, there is no slip between them. Then this mean velocity, V_G, is given in clause 14.3.1.3. V_G is uniform throughout the core.

The shear stress at the interface, τ^*, should be made dimensionless with the mean density, ρ_c, and the interfacial velocity jump which, in principle, differs from V_G.

When the film thickness is small, the shear stress within the film is nearly constant and then the interface velocity at the liquid side results to be twice the average liquid velocity, V_F. This is justified, at least for laminar flow in the film, because a constant shear stress in the film implies a linear velocity profile.

With the above assumptions, the interfacial shear stress will be,

$$\tau_i^* = \frac{1}{2}\rho_c V_G^2 \left(1 - \frac{2V_F}{V_G}\right)^2 f_{Gi}^* \cong \frac{1}{2}\rho_c V_G^2 f_{Gi}^* \qquad \text{[14-56]}$$

where $f_{Gi}{}^*$ is the interfacial friction factor with entrainment. $2V_F/V_G$ is, in most cases, small. Recalling Eq. [14-19], but with τ_i^* instead of τ_i, we get

$$\frac{dp}{dx} = -\frac{32 m_G^2}{\rho_G \pi^2 (D - 2\delta)^5} \frac{m_G + m_E}{m_G} f_{Gi}^* \qquad \text{[14-57]}$$

14.3.2.4 Laws of friction for ff and fgi*

1. The friction factor at the wall, f_F, can be obtained using either Poiseuille formula, Blasius formula, or Figure 14-8. We only will replace Re_L by Re_F.

2. For the friction factor at the interface Wallis assumes that the expression

$$\frac{f_{Gi}^*}{f_c^*} = 1 + 24\left(\frac{\rho_L}{\rho_G}\right)^{1/3}\frac{\delta}{D} \qquad \text{[14-58]}$$

analogous to Eq. [14-31], holds. Here $f_c{}^*$ is the friction factor if the homogeneous core mixture were flowing alone in the duct with the same viscosity of the gas, μ_G; that is, $f_c{}^*$ is the same function of the Reynolds number $Re_c = 4(m_G + m_E)/\pi D \mu_G$, as those given by Poiseuille, Blasius formulae or in Figure 14-8, changing in any case Re_L by Re_c.

14.3.2.5   Expressions in terms of martinelli parameters

The pressure losses in the liquid and gas phase, given respectively by Eqs. [14-54] and [14-57] should be equal. Thus,

$$\frac{f_{Gi}^*}{f_F} = \frac{\rho_G}{\rho_L}\left(\frac{m_L - m_E}{m_G}\right)^2 \left(\frac{m_G}{m_G + m_E}\right)\left(\frac{D}{4\delta}\right)^2 \frac{\left(1 - 2\dfrac{\delta}{D}\right)^5}{\left(1 - \dfrac{\delta}{D}\right)^2} \qquad [14\text{-}59]$$

which is akin to Eq. [14-32] for the ideal annular flow case.

Introducing the Lockhart-Martinelli parameter, X, again deduced from the only-liquid to only-gas pressure loss ratio,

$$X^2 = \frac{\rho_G}{\rho_L}\left(\frac{m_L}{m_G}\right)^2 \frac{f_{SL}}{f_{SG}} \qquad [14\text{-}60]$$

Eq. [14-59] becomes:

$$\frac{f_{Gi}^*}{f_c^*} = X^2 \left(\frac{f_{SG}}{f_c^*}\right)\left(\frac{f_F}{f_{SL}}\right)\left(\frac{m_L - m_E}{m_L}\right)^2$$

$$\left(\frac{m_G}{m_G + m_E}\right)\left(\frac{D}{4\delta}\right)^2 \frac{\left(1 - 2\dfrac{\delta}{D}\right)^5}{\left(1 - \dfrac{\delta}{D}\right)^2} \qquad [14\text{-}61]$$

Note that the friction factors f_{SG} and f_{SG} which appear in the Lockhart-Martinelli formulation correspond respectively to the mass flow rates m_L and m_G of the whole liquid and whole gas flowing in the duct. f_F, in its turn, corresponds to the mass flow rate, $m_L - m_E$, of the liquid in the film, and $f_c{}^*$ to the mass flow rate, $m_G + m_E$, of the fluid in the core.

Elimination of $f_{Gi}{}^*/f_c{}^*$ from Eqs. [14-58] and [14-61] results in the following equation

$$X^2 \left(\frac{f_{SG}}{f_c^*}\right)\left(\frac{f_F}{f_{SL}}\right)\left(\frac{m_L - m_E}{m_L}\right)^2 \left(\frac{m_G}{m_G + m_E}\right) = F\left(\frac{\delta}{D}\right) \qquad [14\text{-}62]$$

where

$$F\left(\frac{\delta}{D}\right) = \left(\frac{4\delta}{D}\right)^2 \left[1 + 24\left(\frac{\rho_L}{\rho_G}\right)^{1/3}\frac{\delta}{D}\right]\frac{\left(1-\frac{\delta}{D}\right)^2}{\left(1-2\frac{\delta}{D}\right)^5}$$ [14-63]

is precisely the function which appears in the right hand side of Eq. [14-34]. In Eq. [14-62] m_L and m_G as well as ρ_L and ρ_G are known and then f_{SG}, f_{SG} and X can be deduced. If the mass flow rate of the liquid entrained in the gas core, m_E, were also known we could obtain f_c^* (which depends on $m_G * m_E$), and f_F (depending on $m_L - m_E$). In that case, Eq. [14-62] would give the value of δ/D.

$F(\delta/D)$ vs. δ/D for different values of ρ_L/ρ_G is given in Figure 14-12. Note that changes of ρ_L/ρ_G in the range $700 < \rho_L/\rho_G < 1100$ do not affect the values of $F(\delta/D)$.
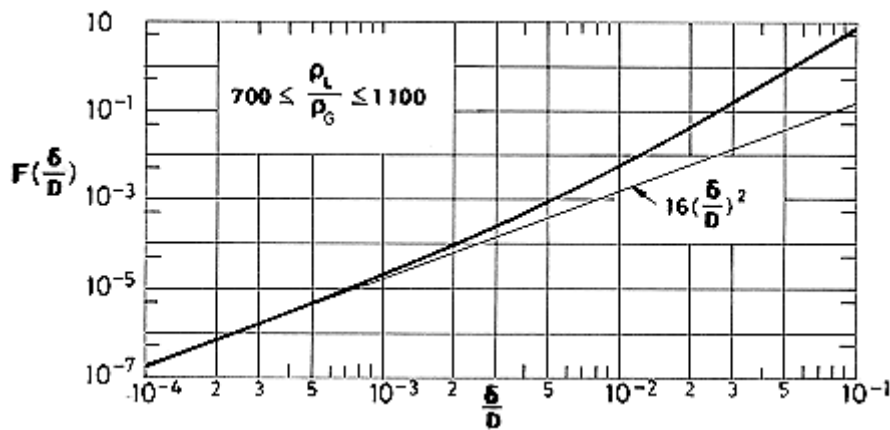
Figure 14-12: The function $F(\delta/D)$ which appears in Eq. [14-62]. The effect of the liquid-gas density ratio is negligible for the range of values given in the figure. Compare the values given in this curve with those given by $2\delta/D$ vs. X in Figure 14-9.

An additional relation between the mass flow rate, m_E, of the liquid entrained in the gas core and the liquid film thickness, δ/D, is required at this point. Figure 14-13, which refers to air-water mixtures, relates the Martinelli parameter, X, with an entrainment parameter, R_E, defined as
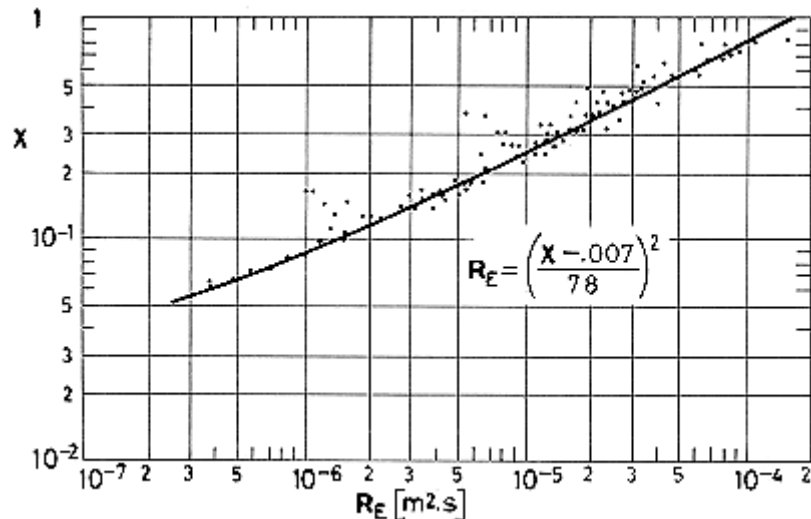
Figure 14-13: Martinelli parameter, X, vs. entrainment parameter, R_E, as deduced from air-water flow experiments. From Wicks & Duckler (1960) [190]. Note that R_E is not dimensionless.

$$R_E = \left(\frac{\rho_G}{\rho_L}\right)\left(\frac{m_L}{m_G}\right)\frac{We\,m_E}{-(dp/dx)_{SG}}$$

[14-64]

In this equation R_E has dimensions [m^2.s]. The dimensionless critical Weber number, $We = \rho_G(V_G - V_L)^2 D/\sigma$, where V_G and V_L are entering air and water velocities, depends on how the liquid is introduced in the duct. The value $We = 16$ is taken when the liquid is introduced abruptly, as with a tee entry, and the value $We = 22$ when the liquid is introduced smoothly as in an annular entrance device.

Once m_E is known, we obtain δ/D from Eq. [14-62], dp/dx from Eq. [14-54], and $(dp/dx)_{SL}$ from Eq. [14-28]. The liquid pressure gradient multiplier, Φ_L, becomes:

$$\Phi_L^2 = \left(\frac{m_L - m_E}{m_L}\right)^2\left(\frac{f_F}{f_{SL}}\right)\left(\frac{D}{4\delta}\right)^2\frac{1}{\left(1-\dfrac{\delta}{D}\right)^2}$$

[14-65]

Compare this equation with Eq. [14-36].

14.3.2.6 Additional data on entrainment

Information on entrainment for annular flow in ducts is scarce. The mechanism of entrainment is not well understood and the experimental difficulties are large.

Figure 14-14 shows a collection of data, by Hutchinson & Whalley (1973) [93] for vertical annular flow in ducts of air-water and air-alcohol systems. The diameters of the ducts are in the range 9,5 x 10^{-3} m to 31,8 x 10^{-3}.
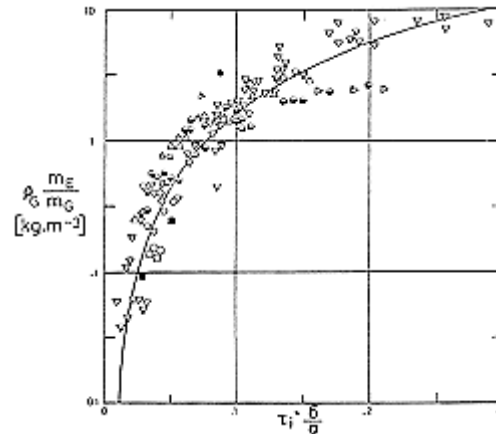
Figure 14-14: Concentration of entrained droplets in the gas core, $\phi_G m_E/m_G$, vs. dimensionless number $\tau_i^* \delta/\sigma$. Replotted by the compiler after Hutchinson & Whalley (1973) [93]. Different symbols are used to indicate experiments by different authors.

The entrainment mechanism suggested by the above authors is based on the interaction between the shear stress at the interface, τ_i^*, and the surface tension forces. The liquid film thickness, δ, is the characteristic length which appears in the expression of the capillary pressure, $2\sigma/\delta$. Thus the rate of entrainment could be characterised in terms of the dimensionless number $\tau_i^* \delta/\sigma$.

Ordinates in Figure 14-14 are concentrations, C, of droplets in the gas core which are defined as:

$$C = \frac{m_E}{\dfrac{m_E}{\rho_L} + \dfrac{m_G}{\rho_G}} \cong \rho_G \frac{m_E}{m_G} \qquad [14\text{-}66]$$

These concentrations appear under equilibrium conditions, i.e., when the rate of entrainment of droplets from the liquid film is equal to the rate of deposition of droplets into the film. The equilibrium requires long distances along the duct ($L/D > 150$) and not too large pressure gradients ($p/\Delta p/L > 20$ m). Hutchinson and Whalley disregarded data points which do not fulfil these limitations.

Also shown in Figure 14-14 are data points taken from Table 14-1, clause 14.3.2.8. Those among them which fulfil the abovementioned low pressure gradient limitation fall close to the continuous curve and all are within experimental scattering.

The data given in Figure 14-14 could be useful for purposes of clarifying the entrainment process, but can hardly be used for the calculation of the pressure loss, since they relate three a priori unknown variables, namely m_E/m_G, dp/dx (through τ_i^*) and δ.

14.3.2.7   Summary

We will summarise here the approach used for the estimation of the pressure drop along a horizontal cylindrical duct when ENTRAINMENT EFFECTS are taken into account. This clause is parallel to clause 14.3.1.6 for the IDEAL annular flow.

It is assumed that the film thickness, δ, does not change along the duct (hydrodynamic equilibrium hypothesis).

The momentum balance in the liquid film and in the core (which now consists of gas and entrained droplets) gives the shear stresses at the wall, τ_w, and at the interface, τ_i^*.

$$\tau_w = -\frac{dp}{dx}\frac{D}{4} \qquad\qquad [14\text{-}67]$$

$$\tau_i^* = -\frac{dp}{dx}\frac{D-2\delta}{4} \qquad\qquad [14\text{-}68]$$

where τ_i^* is used instead of τ_i to indicate that entrainment effects are taken into account.

The shear stresses are related to the friction factors f_F and f_{Gi}^*, respectively:

$$\tau_w = \frac{1}{2}\rho_L V_F^2 f_F \qquad\qquad [14\text{-}69]$$

where V_F is the mean liquid film velocity $V_F = (m_L - m_E)/\rho_L \pi \delta (D - \delta)$, m_L is the liquid total mass flow rate and m_E that of the liquid entrained in the core. On the other hand,

$$\tau_i^* = \frac{1}{2}\rho_c V_G^2 f_{Gi}^* \qquad\qquad [14\text{-}70]$$

with the mean core velocity

$$V_G = \frac{4m_G}{\rho_G \pi (D-2\delta)^2} \qquad\qquad [14\text{-}71]$$

The mean velocities of entrained droplets and gas in the core are assumed to be equal (no-slip assumption). In addition ρ_c is a mean core density ($\rho_c m_G = \rho_G(m_G + m_E)$).

In terms of f_F and f_{Gi}^* the pressure gradient along the duct becomes

$$\frac{dp}{dx} = -\frac{2(m_L - m_E)^2 f_F}{\rho_L \pi^2 D \delta^2 (D-\delta)^2} \qquad\qquad [14\text{-}72]$$

$$\frac{dp}{dx} = -\frac{32m_G^2}{\rho_G \pi^2 (D-2\delta)^5}\frac{m_G + m_E}{m_G} f_{Gi}^* \qquad\qquad [14\text{-}73]$$

Now we introduce the friction factor f_c^* which is that friction factor corresponding to the homogeneous core mixture, density ρ_c, flowing alone in the duct with the gas viscosity μ_G. f_c^* is related in the usual way with $Re_c = 4(m_G + m_E)/\pi D \mu_G$.

We now recall the friction factors f_{SG} and f_{SG} which appear in the Lockhart-Martinelli formulation concerning the no-entrainment case. The equation relating the Martinelli parameter, X, to the film thickness, δ/D, is now

$$X^2\left(\frac{f_{SG}}{f_c^*}\right)\left(\frac{f_F}{f_{SL}}\right)\left(\frac{m_L - m_E}{m_L}\right)^2\left(\frac{m_G}{m_G + m_E}\right) = F\left(\frac{\delta}{D}\right)$$ [14-74]

where $F(\delta/D)$ is a known function of δ/D.

Although X^2 in Eq. [14-62] is known, since it depends on m_L, m_G, ρ_L and ρ_G, neither the factor multiplying X^2 (which depends on $m_G + m_E$, and on $m_L - m_E$) nor δ/D are known.

Experimental data on entrainment, such as Figure 14-13, will provide a relation between X and m_E to close the system.

14.3.2.8 Worked example

In order to substantiate the procedure for the solution of annular flow problems with entrainment, let us consider the following example:

A liquid mass flow rate $m_L = 0,0656$ kg.s^{-1} and a gas mass flow rate $m_G = 0,0266$ kg.s^{-1} are flowing along a duct of 0,0254 m in diameter. We aim at calculating the pressure gradient along the duct and the liquid entrained in the gas core. The inlet pressure is 10^5 Pa and the temperature 293 K.

The density and viscosity of air and water at $p = 10^5$ Pa, $T = 293$ K are, respectively:

$\rho_G = 1,21$ kg.m^{-3},

$\rho_L = 998$ kg.m^{-3},

$\mu_G = 1,85 \times 10^5$ Pa.s,

$\mu_L = 1,003 \times 10^{-3}$ Pa.s.

The Reynolds numbers of the phases flowing alone are,

$$Re_G = \frac{4m_G}{\pi D \mu_G} = 72000$$ [14-75]

$$Re_L = \frac{4m_L}{\pi D \mu_L} = 3280$$ [14-76]

therefore, the regimes are turbulent in both phases.

Using Blasius formula (clause 14.3.1.4) we have:

$f_{SG} = 0,079 \times (72\ 000)^{-0,25} = 0,0048$

$f_{SG} = 0,079 \times (3\ 280)^{-0,25} = 0,0104$

The Lockhart-Martinelli parameter, X, is (clause 14.3.2.5),

$$X^2 = \frac{\rho_G}{\rho_L}\left(\frac{m_L}{m_G}\right)^2 \frac{f_{SL}}{f_{SG}} = 0,160 \quad , \quad X = 0,126 \qquad [14\text{-}77]$$

With $X = 0,126$ and Figure 14-13, the entrainment parameter, R_E, results to be

$R_E = 2,2 \times 10^{-6}$ m².s .

According to Eq. [14-28], the pressure loss for the liquid flowing alone is,

$$-\left(\frac{dp}{dx}\right)_{SL} = \frac{32 m_L^2 f_{SL}}{\rho_L \pi^2 D^5} = 13,8 \, Pa.m^{-1} \qquad [14\text{-}78]$$

and the pressure loss for the gas flowing alone,

$$-\left(\frac{dp}{dx}\right)_{SG} = -\frac{1}{X^2}\left(\frac{dp}{dx}\right)_{SL} = 863 \, Pa.m^{-1} \qquad [14\text{-}79]$$

The mass flow rate entrained in the gas core is, Eq. [14-64]:

$$m_E = -R_E\left(\frac{\rho_L}{\rho_G}\right)\frac{m_L}{m_G}\left(\frac{dp}{dx}\right)_{SG}\frac{1}{We} = \frac{0,635}{We} kg.s^{-1} \qquad [14\text{-}80]$$

Taking $We = 22$, we have

$m_E = 0,0289$ kg.s⁻¹.

The Reynolds number for the liquid film is

$$Re_F = \frac{4(m_L - m_E)}{\pi D \mu_L} = 1850 \qquad [14\text{-}81]$$

The flow corresponds to the intermediate regime (see Figure 14-8 and then

$f_F = 0,0178$.

The core Reynolds number is,

$$Re_C = \frac{4(m_G + m_E)}{\pi D \mu_G} = 150000 \qquad [14\text{-}82]$$

and the corresponding friction factor f_c*,

$f_c* = 0,079 \times (150000)^{-0,25} = 0,00401$.

Now, we deduce $F(\delta/D)$ from Eq. [14-62]

$$F\left(\frac{\delta}{D}\right) = X^2 \left(\frac{f_{SG}}{f_c^*}\right)\left(\frac{f_F}{f_{SL}}\right)\left(\frac{m_L - m_E}{m_L}\right)^2 \frac{m_G}{m_G + m_E} = \qquad\qquad [14\text{-}83]$$
$$= 0,00492$$

With this value of $F(\delta/D)$ and Figure 14-12 we obtain

$$\frac{\delta}{D} = 0,00917 \qquad\qquad [14\text{-}84]$$

Once δ/D is known, Eq. [14-65] furnishes

$\Phi_{L^2} = 402$.

From this value of the liquid pressure loss multiplier, Φ_{L^2}, and from $(dp/dx)_{SL}$ we deduce

$$-\frac{dp}{dx} = -\left(\frac{dp}{dx}\right)_{SL} \Phi_L^2 = 5550 \, Pa.m^{-1} \qquad\qquad [14\text{-}85]$$

The results of similar problems are summarised in Table 14-1. The values of ρ_L, ρ_G, μ_L, μ_G, D and We are the same as in the above example.

Table 14-1: Typical Pressure Losses in Air-Water Annular Flow with Entrainment
(D = 25,4 x 10^{-3} m, p = 10^5 Pa, T = 293 K).

m_L x 10^3 [kg.s^{-1}]	65,6	65,6	65,6	65,6	131	131	131	131	131
m_G x 10^3 [kg.s^{-1}]	30,7	26,6	19,9	16,0	62,7	55,3	48,4	42,8	36,4
Re_G x 10^{-3}	83,2	72,1	53,9	43,4	170	149	131	115	98,6
Re_L x 10^{-3}	3,28	3,28	3,28	3,28	6,54	6,54	6,54	6,54	6,54
f_{SG} x 10^3	4,7	4,8	5,1	5,5	3,9	4,0	4,2	4,3	4,5
f_{SL} x 10^3	10,4	10,4	10,4	10,4	8,8	8,8	8,8	8,8	8,8
X	0,111	0,126	0,162	0,197	0,109	0,121	0,137	0,153	0,175
$(\Delta p/L)_{SG}$x10^{-3} [Pa.m^{-1}]	1,11	0,864	0,520	0,355	3,87	3,11	2,46	1,99	1,50
R_E x 10^6 [m^2.s]	1,79	2,34	3,99	5,94	1,72	2,17	2,78	3,48	4,68
m_E x 10^3 [kg.s^{-1}]	35,0	30,7	23,6	19,3	119	107	94,0	84,9	73,1
Re_F x 10^{-3}	1,53	1,74	2,10	2,31	0,566	1,20	1,80	2,30	2,89
Re_c x 10^{-3}	178	155	117	95,7	494	439	388	345	296
f_F x 10^3	20,0	17,8	15,6	14,0	33,0	22,1	17,0	14,8	13,0
f_c* x 10^3	3,85	3,97	4,26	4,50	2,97	3,06	3,16	3,25	3,38
δ/D x 10^3	7,88	9,07	11,7	13,9	2,40	4,16	5,60	7,00	8,70
Φ_L^2	428	374	279	222	298	308	289	268	242
$(\Delta p/L)$x10^{-3} [Pa.m^{-1}]	5,90	5,13	3,82	3,66	13,7	14,1	13,4	12,5	11,1

14.3.2.9 The ideal annular and the annular with entrainment models

A comparison of Eqs. [14-34] and [14-62] indicates that the ideal annular model is valid provided that

$$\left(\frac{f_{SG}}{f_c^*}\right)\left(\frac{f_F}{f_{SL}}\right)\left(\frac{m_L - m_E}{m_L}\right)^2 \frac{m_G}{m_G + m_E} = 1 \qquad [14\text{-}86]$$

This expression depends on the gas and liquid mass flow rates, m_G and m_L, on the entrained liquid flow rate, m_E, and on the following Reynolds numbers.

1.   Reynolds number of the whole gas flowing in the duct,

$$Re_G = \frac{4m_G}{\pi D \mu_G} \qquad [14\text{-}87]$$

2.   Reynolds number of the fluid in the core, in terms of the duct diameter,

$$Re_C = \frac{4(m_G + m_E)}{\pi D \mu_G} \qquad [14\text{-}88]$$

    Note that in any case $Re_c \geq Re_G$.

3.   Reynolds number of the liquid in the film, in terms of the duct diameter,

$$Re_F = \frac{4(m_L - m_E)}{\pi D \mu_L} \qquad [14\text{-}89]$$

4.   Reynolds number of the whole liquid flowing in the duct,

$$Re_L = \frac{4m_L}{\pi D \mu_L} \qquad [14\text{-}90]$$

Again $Re_L \geq Re_F$.

Even if we leave aside transitional configurations, 9 versions of Eq. [14-86] will result depending on the laminar or turbulent characteristics of the four flows. The possible combinations are arranged in the following matrix. v and t are as in clause 14.2.1.

$$
\begin{vmatrix} 1 & 3 \\ 2 & 4 \end{vmatrix} \quad
\begin{vmatrix} v & v \\ v & v \end{vmatrix} \quad
\begin{vmatrix} v & v \\ v & t \end{vmatrix} \quad
\begin{vmatrix} v & t \\ v & v \end{vmatrix} \quad
\begin{vmatrix} v & t \\ v & t \end{vmatrix}
$$

$$
\begin{vmatrix} v & v \\ t & v \end{vmatrix} \quad
\begin{vmatrix} v & v \\ t & t \end{vmatrix} \quad
\begin{vmatrix} v & t \\ t & v \end{vmatrix} \quad
\begin{vmatrix} v & t \\ t & t \end{vmatrix}
$$

$$
\begin{vmatrix} t & v \\ v & v \end{vmatrix} \quad
\begin{vmatrix} t & v \\ v & t \end{vmatrix} \quad
\begin{vmatrix} t & t \\ v & v \end{vmatrix} \quad
\begin{vmatrix} t & t \\ v & t \end{vmatrix}
$$

$$
\begin{vmatrix} t & v \\ t & v \end{vmatrix} \quad
\begin{vmatrix} t & v \\ t & t \end{vmatrix} \quad
\begin{vmatrix} t & t \\ t & v \end{vmatrix} \quad
\begin{vmatrix} t & t \\ t & t \end{vmatrix}
$$

The shadowed row and column denote impossible configurations since 2 cannot be v when 1 is t and 3 cannot be t when 4 is v.

The two simplest cases appear when the four flows are either laminar or turbulent.

When the four flows are laminar Eq. [14-86] becomes

$$
\frac{m_E}{m_L} << 1 \tag{14-91}
$$

When the four flows are turbulent

$$
\frac{\left(1 - \dfrac{m_E}{m_L}\right)^{7/4}}{\left(1 - \dfrac{m_E}{m_G}\right)^{3/4}} \cong 1 \tag{14-92}
$$

which can be approximately expressed as

$$
\left| \frac{7}{4}\frac{m_E}{m_L} - \frac{3}{4}\frac{m_E}{m_G} \right| << 1 \tag{14-93}
$$

Similar expressions result when the gas-only and core flows are both laminar or both turbulent and, in addition, the liquid only and liquid film are both laminar or both turbulent.

In the five remaining cases D, and either μ_G or μ_L (or both) cannot be eliminated from Eq. [14-86].

The main limitation of a discussion of this type is the lack of data for calculating m_E, such as those presented in Figure 14-13, which only refers to air-water flows. In practice mechanical devices are used to throw the core droplets toward the film in the periphery.

14.4 Condensation in ducts

The flow in ducts out of evaporators would be dominated by condensation. Normal gravity enhances condensation because body forces help drive the condensed liquid. Thence, condensation in ducts under reduced gravity is much less efficient than that inside horizontal ducts under normal gravity.

The flow patterns in either case differ substantially, Figure 14-15.
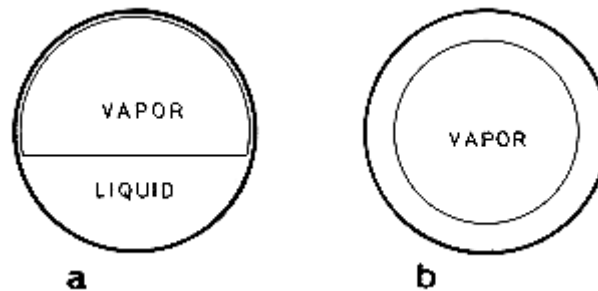
Figure 14-15: Flow geometry when gravity is dominant (a) or negligible (b). The void fraction (vapor fractional area in the figure) is the same in both cases.

A comparison of condensing flows inside ducts under normal and under reduced gravity conditions has been attempted by Keshock & Sadeghipour (1983). The basic difference between the two cases results from the stratified condensate layer which appears when gravity is dominant (Figure 14-15a) and which is almost inactive in the heat transfer process, whereas the thin condensate film formed in the duct is very effective. When gravity effects are negligible (Figure 14-15b) the annular flow pattern prevails and the much thicker layer is less effective than the thin condensate which appeared in Figure 14-15a

14.4.1 Condensing flow model

In this clause a simple unified model of condensing flow inside a duct is introduced. Later on this model will be particularised to the two extreme cases which have been sketched in Figure 14-15.

The main simplifying assumptions of the model are:

1. The duct is horizontal.

2. The static pressure is uniform in each cross section.

3. The liquid flow is assumed to be uniform in each cross section accounting for the effect of film thickening.

4. The vapour flow is also uniform in each cross section.

    Regarding the particularisation to the stratified flow case two additional features of the model should be mentioned.

5. Liquid film thickening implies an axial component of hydrostatic pressure. This effect is accounted for in a way which resembles that in open channel hydraulics although here the vapour pressure could change along the duct (Rufer & Kezios (1966) [151]).

6. The condensate formed in the film flows down the duct wall and joins the bulk liquid flowing along the bottom of the duct. Vapour contacts the wall where the condensate leaves it.

An additional simplifying assumption must be introduced in connection with the fluid thermodynamic and transport properties.

7. The wall temperature, T_w, is kept constant. On the other hand, the pressure loss is very small compared to the saturation pressure level. Then the fluid saturation pressure and temperature are assumed to be constant along the duct for calculating fluid thermodynamic and transport properties.

Figure 14-16 summarises the flow geometry. Although particularised to the stratified flow case, it is sufficiently general for the present purposes.
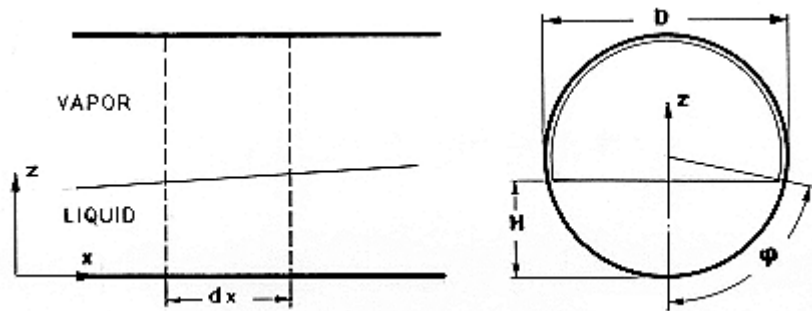
Figure 14-16: Geometry used in the model of stratified flow condensation.

The conservation equations in the control volume, which encloses liquid, L, and vapour, G, are:

Mass preservation equation

$$\frac{d}{dx}(m_L + m_G) = 0 \tag{14-94}$$

Momentum balance equation

$$\frac{d}{dx}\left(\rho_L A_L V_L^2 + \rho_G A_G V_G^2\right) = -\frac{dp}{dx} A_{FL} -$$
$$- \rho_L g \frac{d}{dx}\int_{A_L}(H-z)\frac{dA_L}{dz}\,dz - \Pi_{L}\tau_{wL} - \Pi_{G}\tau_{wG} \tag{14-95}$$

where the left hand side gives the change in momentum. The first term in the right hand side is the resultant of the static pressure on the fluid (liquid and vapour) per unit axial length of the control volume. A_{FL} is the internal cross-sectional area of the duct. The second term is the resultant of hydrostatic pressures acting on planes x and x+dx which enclose different liquid areas. This term disappears in the annular flow case. The last two terms are the wall friction of the liquid and vapour, respectively, per unit axial length, here τ_w are average shear stresses at the wall. Π_L and Π_G are the corresponding wetted perimeters.

Thermal energy equation

$$h_m(T_{sat} - T_w)A = -h'_{fg}\frac{dm_G}{dx} \tag{14-96}$$

This equation merely indicates that the heat transfer to the wall, the area of which is $A = \pi D$ per unit length, equals the enthalpy change from saturated vapour to condensate. h_m is an average heat transfer coefficient. T_{sat} is the saturated vapour temperature, T_w the wall temperature, and h'_{fg} the corrected value of the heat of condensation.

The film temperature is nonuniform and slightly below saturation temperature because of partial subcooling of the liquid, then

$$h'_{fg} = h_{fg} + 0{,}68 c_{pL}(T_{sat} - T_w) \qquad \text{[14-97]}$$

where c_{pL} is the liquid specific heat.

14.4.1.2 Static pressure loss

We will relate the static pressure loss to a friction factor via a mixture approximation correlation, which is strictly valid when acceleration terms can be neglected.

Dukler, Wicks & Cleveland (1964) [39] suggested different approximations of the two phase flow by the single phase flow of a liquid of average properties running full in the duct of diameter D. In any case the pressure loss is related to the friction factor by Eq. [14-28], clause 14.3.1.4.

$$\frac{dp}{dx} = -\frac{32m^2 f_{TP}}{\rho_{TP}\pi^2 D^5} \qquad \text{[14-98]}$$

where f_{TP} is a function of the mixture Reynolds number of the Poiseuille or Blasius type, see clause 14.3.1.4, and the subscript TP indicates two phase. The two phase flow is considered as laminar when Re_{TP} is less than 2400 and turbulent otherwise (as it occurs in the single phase flow, clause 7.2.2). The mixture Reynolds number, Re_{TP}, is defined as:

$$Re_{TP} = \frac{4m}{\pi D \mu_{TP}} = \frac{\mu_G}{\mu_{TP}} Re \qquad \text{[14-99]}$$

whereas ρ_{TP}, μ_{TP} are defined as

$$\rho_{TP} = (1 - \alpha)\rho_L + \alpha\rho_G \qquad \text{[14-100]}$$

$$\mu_{TP} = (1 - \alpha)\mu_L + \alpha\mu_G \qquad \text{[14-101]}$$

α being the cross-sectional void fraction.

The equations for the calculation of ρ_{TP} and μ_{TP} are those of SPECIAL CASE I of Dukler, Wicks & Cleveland (1964) [39]. They correspond to the no-slip restriction, $V_L/V_G = 1$. This restriction is very difficult to appraise but it gives the correct behaviour in the two extreme cases, liquid only and vapour only.

Note that, in general, Re_{TP} as well as f_{TP} will depend on α.

14.4.1.3 Friction terms

In order to evaluate the friction terms in the right hand side of Eq. [14-95] we will introduce the usual friction factors at the wall for the liquid and vapour.

$$\tau_{wL} = \frac{1}{2}\rho_L V_L^2 f_L \quad , \quad \tau_{wG} = \frac{1}{2}\rho_G V_G^2 f_G \qquad [14\text{-}102]$$

where f_L and f_G will depend on Re_L and Re_G respectively.

The average liquid and gas velocities are:

$$v_L = \frac{m_L}{\rho_L A_L} = \frac{1-w}{1-\alpha}\frac{m}{\rho_L A_{FL}}$$

$$v_G = \frac{m_g}{\rho_G A_G} = \frac{w}{\alpha}\frac{m}{\rho_G A_{FL}} \qquad [14\text{-}103]$$

w being the vapour quality.

The Reynolds numbers based on the respective hydraulic diameters, $D_{EL} = 4A_L/\Pi_L$ and $D_{EG} = 4A_G/\Pi_G$, can be written as

$$Re_L = (1-w)\frac{\mu_G}{\mu_L}\frac{\Pi}{\Pi_L}Re \quad , \quad Re_G = w\frac{\Pi}{\Pi_G}Re \qquad [14\text{-}104]$$

Finally, the expressions of the wall friction per unit duct length are, respectively:

$$\Pi_{L^{\tau}wL} = \Pi_L \frac{1}{2}\left(\frac{1-w}{1-\alpha}\right)^2 \frac{m^2 f_L}{\rho_L A_{FL}^2}$$

$$\Pi_{G^{\tau}wG} = \Pi_G \frac{1}{2}\left(\frac{w}{\alpha}\right)^2 \frac{m^2 f_G}{\rho_G A_{FL}^2} \qquad [14\text{-}105]$$

Now Re, and then f, will depend both on the geometry of the cross sectional liquid-vapour configuration, through Π_L/Π or Π_G/Π, and on the vapour quality, w. It is convenient to express f_L and f_G as:

$$f_L\left(\frac{\Pi_L}{\Pi},w\right) = f_L\left(\frac{\Pi_L}{\Pi},0\right)(1-w)^{L_L}$$

$$f_G\left(\frac{\Pi_G}{\Pi},w\right) = f_G\left(\frac{\Pi_G}{\Pi},1\right)w^{L_G} \qquad [14\text{-}106]$$

where $L = -1$ when the corresponding flow is laminar or $L = -0,25$ when it is turbulent.

14.4.1.4 Momentum equation

Bringing Eqs. [14-98]-[14-106] to Eq. [14-95] we reach:
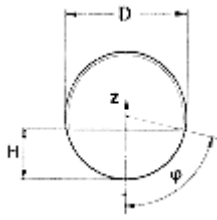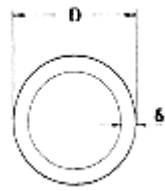
$$
D \frac{d}{dx} \left[\frac{(1-w)^2}{1-\alpha} + \frac{\rho_L}{\rho_G} \frac{w^2}{\alpha} + \frac{1}{Fr A_{FL} D} \int_{A_L} (H-z) \frac{dA_L}{dz} \, dz \right] =
$$

$$
= 2 \frac{\rho_L}{\rho_{TP}} f_{TP} - 2 \frac{\Pi_L}{\Pi} \frac{(1-w)^{2+L_L}}{(1-\alpha)^2} f_L \left(\frac{\Pi_L}{\Pi}, 0 \right) -
$$

$$
- 2 \frac{\rho_L}{\rho_G} \frac{\Pi_G}{\Pi} \frac{w^{2+L_G}}{\alpha^2} f_G \left(\frac{\Pi_G}{\Pi}, 1 \right)
$$

[14-107]

where *Fr* is a Froude number defined as:

$$
Fr = \frac{m^2}{\rho_L^2 A_{FL}^2 D g}
$$

[14-108]

Several terms, which depend on the particular model under consideration, are given in Table 14-2.

Table 14-2: Geometry and Flow-Dependent Terms in Eqs. [14-107] and [14-109]

TYPE OF FLOW	STRATIFIED	ANNULAR
Configuration		
α	$\dfrac{\pi - \varphi}{\pi} + \dfrac{\sin 2\varphi}{2\pi}$	$\left(1 - \dfrac{2\delta}{D}\right)^2$
Π_L/Π	φ/π	1
Π_G/Π	$1-\varphi/\pi$	0
$f_L\left(\dfrac{\Pi_L}{\Pi}, 0\right)$	$16 \dfrac{\mu_L}{\mu_G} \dfrac{1}{Re} \dfrac{\varphi}{\pi}$	$16 \dfrac{\mu_L}{\mu_G} \dfrac{1}{Re}$

TYPE OF FLOW	STRATIFIED	ANNULAR
	$0,079\left(\dfrac{\mu_L}{\mu_G}\dfrac{1}{Re}\dfrac{\varphi}{\pi}\right)^{0,25}$	$0,079\left(\dfrac{\mu_L}{\mu_G}\dfrac{1}{Re}\right)^{0,25}$
$f_G\left(\dfrac{\Pi_G}{\Pi},1\right)$	$16\dfrac{1}{Re}\left(1-\dfrac{\varphi}{\pi}\right)$	0
	$0,079\left(\dfrac{1}{Re}\left(1-\dfrac{\varphi}{\pi}\right)\right)^{0,25}$	0
L_L	-1	-1
	-0,25	-0,25
L_G	-1	--
	-0,25	--
$\dfrac{1}{FrA_{FL}D}\displaystyle\int_{A_L}(H-z)\dfrac{dA_L}{dz}\,dz$	$\dfrac{1}{2\pi Fr}\left[\dfrac{2}{3}\sin^3\varphi-\cos\varphi\left(\varphi-\dfrac{\sin 2\varphi}{2}\right)\right]$	0
$\dfrac{4Nu}{PrReSf}\dfrac{\mu_L}{\mu_G}$	$\dfrac{4}{\pi}\left[\dfrac{2}{3Fr}\left(1-\dfrac{\rho_G}{\rho_L}\right)\left(\dfrac{\mu_L}{\mu_G}\right)^2\dfrac{1}{Pr^3Re^2Sf^3}\right]^{1/4}\cdot$ $\cdot\left[\dfrac{4}{3}\displaystyle\int_0^{\pi-\varphi}\sin^{1/3}\omega\,d\omega\right]^{3/4}$	$(1-w)\dfrac{4Nu}{PrRe_L Sf}$ (since $Re_L=(1-w)\dfrac{\mu_G}{\mu_L}Re$)
Comments on Nu	h_m has been expressed by means of Nusselt's result for the outside of horizontal tubes (Ruffer & Keizos (1966) [151], Butterworth (1981) [17], p. 295).	Nu = Nu$_{SL}$/(1-α) $Nu_{SL}=PrRe_L\dfrac{1}{T^+(\delta^+)}\sqrt{\dfrac{f_L}{2}}$, Eq. [14-129]

14.4.1.5 Dimensionless energy equation

Equation [14-96] in dimensionless form becomes:

$$D\frac{dw}{dx}=-\frac{4Nu}{PrReSf}\frac{\mu_L}{\mu_G} \qquad [14\text{-}109]$$

where *Nu* is the Nusselt number:

$$Nu = \frac{h_m D}{k_L}$$
[14-110]

Pr the liquid Prandtl number:

$$Pr = \frac{c_{pL}\mu_L}{k_L}$$
[14-111]

Re is the Reynolds number as in clause 14.2.1 (based on the gas viscosity) with $A_{FL} = \pi D^2/4$:

$$Re = \frac{4m}{\pi D \mu_G}$$
[14-112]

and *Sf* the Stefan number:

$$Sf = \frac{h'_{fg}}{c_{pL}(T_{sat} - T_w)}$$
[14-113]

Among these four dimensionless groups only the Nusselt number, *Nu*, depends on the geometry and on the model used. See Table 14-2.

14.4.2 Variation of the vapor quality along the duct in the stratified model

Elimination of the geometric variable *x* from Eqs. [14-107] and [14-109] yields a first order differential equation relating α to *w*. This differential equation, with the boundary condition

$w = 1$, $\alpha = 1$

has been numerically integrated in typical cases. Numerical values for the computations are given in Table 14-3 and Table 14-4 and the results are summarised in Figure 14-17.

Table 14-3: Condensation in Ducts. Typical Fluid Properties.
Assumed values: T_{sat} = 300 K, T_{sat} - T_w = 10 K

Fluid	(ρ_G/ρ_L) x 10^3	μ_L/μ_G	*Pr*	*Sf*
Freon 11	5,30	43,6	4,60	21,7
Freon 12	30,1	20,6	3,54	15,0
Freon 22	39,4	14,4	3,47	15,1
Water	0,03	93,7	5,81	59,1

Table 14-4: Condensation in Ducts. Parameters Depending on *m* and *D*.
Assumed values: mh_{fg} = 1,5 x 10³ W, *D* = 16,1 x 10⁻³ m. Stratified case

Fluid	m x 10³ [kg.s-1]	Fr x 10³	Re x 10⁻³	$\dfrac{4Nu/a(\varphi)}{PrReSf}\dfrac{\mu_L}{\mu_G}\times10^3$	N_{TD} [b]
Freon 11	8,29	4,93	60,7	3,68	0,309
Freon 12	10,2	10,1	67,6	3,19	0,352
Freon 22	8,29	7,51	40,7	3,74	0,713
Water	0,615	0,058	5,34	21,9	3,62

[a] $a(\varphi)=\left[\dfrac{4}{3}\int_0^{\pi-\varphi}\sin^{1/3}\omega d\omega\right]^{3/4}$, $a(0)=2,53$.

[b] N_{TD} is the Taitel & Dukler dimensionless group which will appear in clause 14.4.3.
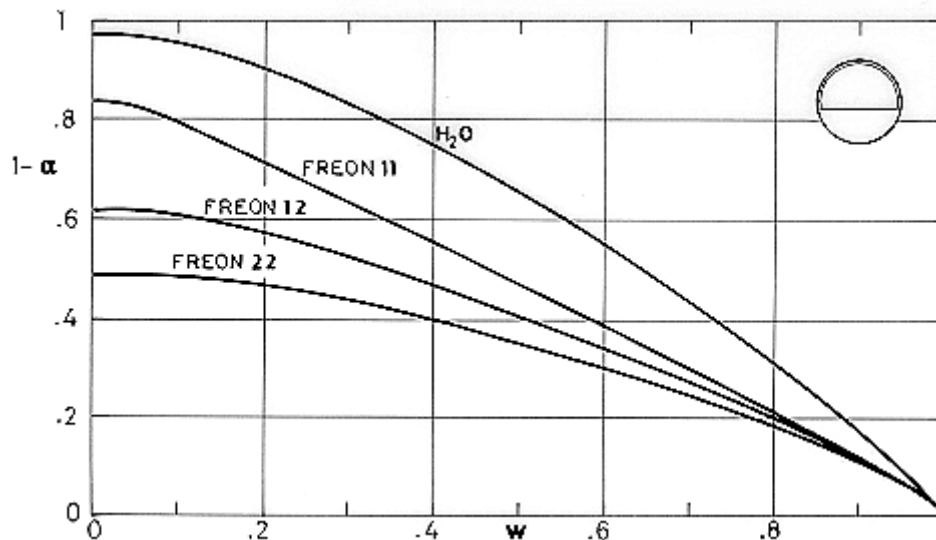
Figure 14-17: Liquid fraction, 1-α, vs. vapor quality, w. For stratified condensing flow of several liquid along horizontal ducts. Calculated by the compiler.

The model is no longer valid in the neighbourhood of $w = 0$ where the void fraction, α, does not vanish. Arriving at this situation implies large pressure variations which conflict with simplifying assumption 7 in clause 14.4.1. The effect is purely local and has not been investigated further.

Once a relation between α and w has been obtained, integration of Eq. [14-109] with

$x = 0, w = 1$

gives the evolution of the vapour quality, w, along the duct. Results are given in Figure 14-18.
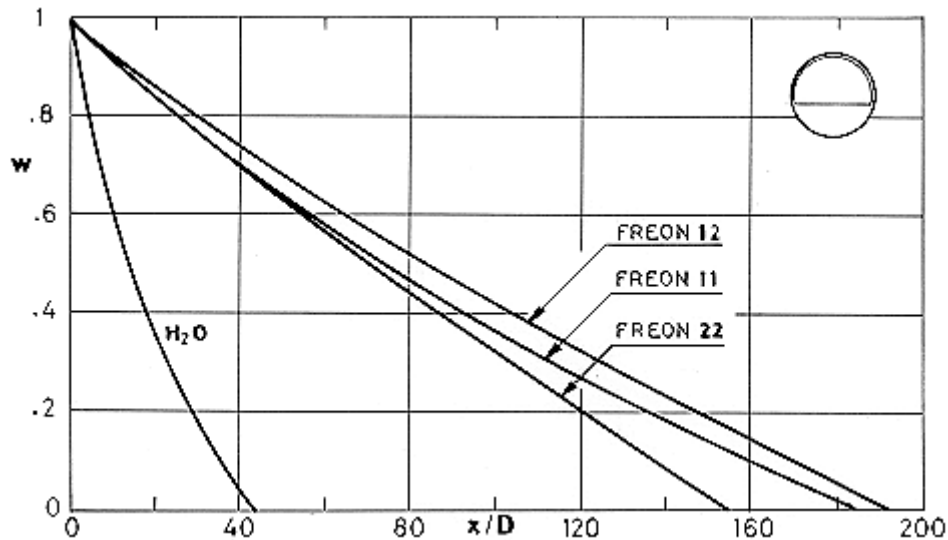
Figure 14-18: Vapor quality, *w*, vs. dimensionless distance along the duct, *x/D*, for stratified condensing flow for several liquids along horizontal ducts. Calculated by the compiler.

14.4.3 Limits of validity of the stratified model

The above stratified flow model is based on the assumption that the liquid-vapour interface is stable. This means that in any cross section m_G/A_{FL} vs. m_L/A_{FL} must be enclosed in that domain of a figure such as Figure 14-2, clause 14.1, which corresponds to stratified flow.

The limits of the stratified flow region have been expressed in analytical form by Taitel & Dukler (1976) [174]. The expressions given by these authors are more convenient for the present purposes than a flow pattern map.

The interface stability requires, in our variables,

$$\frac{w^2(1-w)}{\alpha^2(1-\alpha)} > N_{TD} \qquad \text{[14-114]}$$

where

$$N_{TD} = 400 \frac{\rho_G}{\rho_L}\left(1 - \frac{\rho_G}{\rho_L}\right)\frac{\mu_L}{\mu_G}\frac{1}{ReFr} \qquad \text{[14-115]}$$

is a dimensionless group already tabulated in Table 14-4, clause 14.4.2, for several typical cases.

Curves of constant values of the parameter $w^2(1 - w)/\alpha^2(1 - \alpha)$ in the w vs. $(1 - \alpha)$ plane have been represented in Figure 14-18.
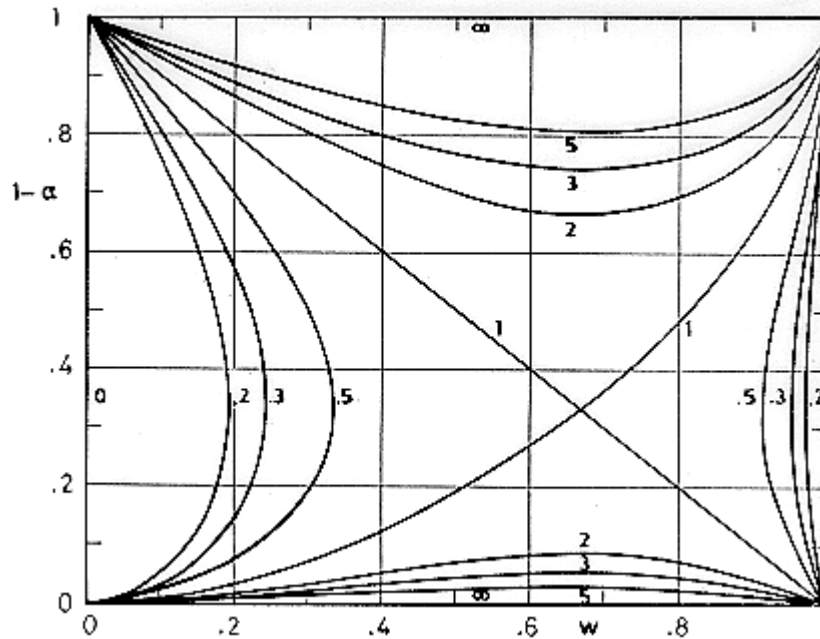
Figure 14-19: The Taitel and Dukler limit for stratified flow in the w vs. $(1-\alpha)$ plane. Numbers on the curves represent constant values of the parameter $w^2(1-w)/\alpha^2(1-\alpha)$ which appears in the left hand side of Eq. [14-114].

14.4.4 Annular flow model

Now we will introduce a similar approach for condensation with annular flow. The mathematical formulation is quite parallel to that in the previous clauses. Now the geometrical parameter is the film thickness, δ.

The conservation equations are now:

Mass preservation equation

$$\frac{d}{dx}\left(m_L + m_G\right) = 0 \qquad \text{[14-116]}$$

Momentum balance equation

$$\frac{d}{dx}\left(\rho_L A_L V_L^2 + \rho_G A_G V_G^2\right) = -\frac{dp}{dx}A_{FL} - D\tau_{wL} \qquad \text{[14-117]}$$

The physical meaning of the different terms in Eq. [14-117] is the following:

The left hand side is the change in momentum. The first term in the right hand side is the static pressure term, and the last the friction term.

The thermal energy equation is again Eq. [14-96] although the heat transfer mechanism is different here.

The average heat transfer coefficient h_m can be expressed as (Butterworth (1981) [17])

$$h_m = h_{SL} \Phi_L \qquad [14\text{-}118]$$

where h_{SL} is the heat transfer coefficient which would exist if the flow rate of liquid were flowing alone through the tube. Φ_L is the Lockhart-Martinelli pressure loss multiplier (clauses 14.3.1 and 14.3.1.5).

Written in dimensionless form Eq. [14-117] becomes:

$$
\begin{aligned}
D \frac{d}{dx}&\left[\frac{(1-w)^2}{1-\alpha} + \frac{\rho_L}{\rho_G}\frac{w^2}{\alpha} \right] = \\
&= 2\frac{\rho_L}{\rho_{TP}} f_{TP} - 2\frac{\Pi_L}{\Pi}\frac{(1-w)^{2+L_L}}{(1-\alpha)^2} f_L\left(\frac{\Pi_L}{\Pi}, 0 \right) - \\
&\quad - 2\frac{\rho_L}{\rho_G}\frac{\Pi_G}{\Pi}\frac{w^{2+L_G}}{\alpha^2} f_G\left(\frac{\Pi_G}{\Pi}, 1 \right)
\end{aligned}
\qquad [14\text{-}119]
$$

Equation [14-109] is still valid as thermal energy equation in dimensionless form, although in the annular flow case (recall Eqs. [14-35] and [14-118],

$$Nu = \frac{Nu_{SL}}{1-\alpha} \qquad [14\text{-}120]$$

where Nu_{SG} is the Nusselt number if the liquid mass flow rate were flowing alone through the tube.

This simple expression behaves correctly at both ends of the process. When $\delta/D \ll 1$ the definition of the liquid Nusselt number in terms of the hydraulic diameter of the liquid annulus would be:

$$Nu_{SL} = \frac{h_m 4\delta}{k_L} \qquad [14\text{-}121]$$

then

$$Nu = \frac{Nu_{SL}}{4\delta/D} \qquad [14\text{-}122]$$

which agrees with the previous expression of Nu when $\delta/D \ll 1$.

The agreement at the other end is obvious, when $\alpha \to 0$, $Nu \to Nu_{SG}$.

14.4.4.1 Heat transfer coefficient in annular flow

Different correlations are available for calculating the heat transfer coefficient h_m inside horizontal or slightly inclined tubes in the annular flow regime. It would be interesting to compare them before selecting the most appropriate for our purpose.

1) Duct average heat transfer coefficient, h_m,

Boyko & Kruzhilin (1967) [16] on the basis of their extensive data with $1,2 \times 10^6$ Pa to 9×10^6 Pa steam over a liquid Reynolds number range of 6×10^3 to 3×10^5 suggest the following correlation for the average Nusselt number, $\overline{Nu}$

$$\overline{Nu} = \frac{0,024}{(1-w)^{0,8}} Pr^{0,43} Re_L^{0,8} \left(\frac{1 + \sqrt{\rho_l / \rho_G}}{2} \right)$$

[14-123]

This correlation is also recommended for other than steam-water systems in the same (liquid) Prandtl number range (0,9 to 3).

2) Correlations for h_{SL}.

These correlations are justified on the basis of Eqs. [14-118] and [14-120] and have been used widely in liquid flow heat transfer calculations.

2,1) Kosky & Staub (1971) [108] give the local Nusselt number in the liquid -alone case in terms of the friction velocity

$$u^* = \sqrt{\tau_w / \rho}$$

[14-124]

and in terms of the dimensionless temperature function $T^+(\delta^+)$. Taking into account Eq. [14-3] the friction velocity, u^*, becomes:

$$u^* = \sqrt{\frac{D}{4\rho_L} \left(-\frac{dp}{dx} \right)}$$

[14-125]

whereas the dimensionless temperature, $T^+(\delta^+)$, is defined as:

$$T^+\left(\delta^+\right) = \frac{\rho_L u^* c_{pL}}{h_m}$$

[14-126]

$\delta^+ = \delta u^* / \nu$ is a dimensionless film thickness.

This correlation is based on the Martinelli analogy between turbulent momentum and heat transfer, which has been quoted in clause 8.2.4.

$T^+(\delta^+)$ is given by the following sequence of equations:

$$T^+\left(\delta^+\right) = \begin{cases} \delta^+ Pr \quad , & for\ \delta^+ \leq 5 \\ 5\left\{ Pr + \ln\left[1 + Pr\left(\frac{\delta^+}{5} - 1 \right) \right] \right\} \quad , & for\ 30 \geq \delta^+ > 5 \\ 5\left\{ Pr + \ln[1 + 5Pr] + 0,495 \ln\frac{\delta^+}{30} \right\} \quad , & for\ \delta^+ > 30 \end{cases}$$

[14-127]

and the dimensionless film thickness, δ^+, is given by

$$\delta^+ = \begin{cases} \sqrt{\dfrac{Re_L}{2}} & , \quad for\ Re_L < 1000 \\ 0,0504\,Re_L^{7/8} & , \quad for\ Re_L > 1000 \end{cases}$$

[14-128]

The liquid-alone local Nusselt number, $Nu_{SG}(x)$, can be written as

$$Nu_{SL}(x) = PrRe_L \frac{1}{T^+(\delta^+)} \sqrt{\frac{f_L}{2}}$$

[14-129]

where the liquid-alone friction factor is (clause 14.3.1.4)

$$f_L = \begin{cases} \dfrac{16}{Re_L} & , \quad for\ Re_L < 1000 \\ 0,079\,Re_L^{-0,25} & , \quad for\ 1000 < Re_L < 10^5 \end{cases}$$

[14-130]

2,2) Correlation introduced in clause 6.

When the liquid film motion is laminar ($Re_L < 1000$)

Nu_{SL} = 3,66, see Figure 6-1, clause 6.3.1.1.

The thermal entry length, i.e. the distance required to reach the fully developed value, Nu_{SL} = 3,66, is of the order of 50 diameters and, thence, it has been neglected (see Figure 6-6, clause 6.3.1.1).

The Nusselt numbers calculated on the basis of values given in Table 14-4, clause 14.4.2, which correspond to the stratified case, are nearly two orders of magnitude larger than those which appear in the annular laminar flow case.

When the liquid film motion is turbulent ($Re_L > 1000$) it is advisable to write down the right hand side of Eq. [14-109] in terms of $Re_L = (1 - w)(\mu_G/\mu_L)Re$, since $Nu_{SL}/PrRe_L$ is given in Figure 6-14, clause 6.3.1.1. This figure has been drawn by use of the following mathematical formulae (Petukhov & Roizen (1975) [143]):

$$\frac{Nu_{SL}(x)}{PrRe_L} = \frac{\xi_L/8}{k + 12,7\sqrt{\xi_L/8}\left(Pr^{2/3} - 1\right)}$$

[14-131]

with

$$\xi_L = \frac{1}{\left(1,82\log_{10} Re_L - 1,64\right)^2}$$

[14-132]

and

$$k = 1,07 + \frac{900}{Re_L} - \frac{0,63}{1+10Pr} \qquad\qquad [14\text{-}133]$$

for the range of numbers $4 \times 10^3 \leq Re_L < 6 \times 10^5$ and $0,7 \leq Pr \leq 5 \times 10^5$.

Different curves of the liquid-alone Nusselt number, Nu_{SG}, given by the above correlations are shown as functions of Re_L for typical values of Pr and ρ_L/ρ_G and, when required, of $(1 - \alpha)/(1 - w)^{0,8}$ in Figure 14-20.
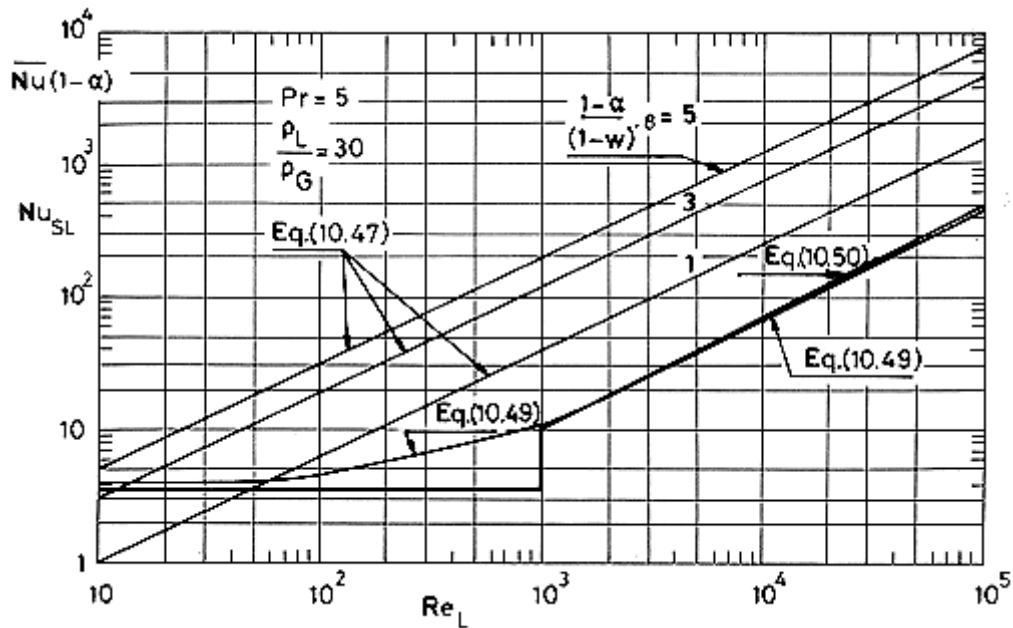
Figure 14-20: Liquid-alone Nusselt number, Nu_{SL}, vs.liquid Reynolds number, Re_L, as given by different correlations in typical cases. Calculated by the compiler.

It can be seen in the figure that Eqs. [14-129] and [14-131] give almost identical results except in a region of intermediate liquid Reynolds numbers, where Kosky & Staub's correlation (Eq. [14-129] furnishes a smoother transition than correlation [14-131]. Thus, Eq. [14-129] will be used in the computations which follow.

14.4.5   Variation of the vapor quality along the duct in the annular model

Proceeding as in clause 14.4.2 we reach a first order differential equation which relates α to w. This equation should be integrated with the boundary condition $w = 1$, $\alpha = 1$ to yield the curves of Figure 14-21.
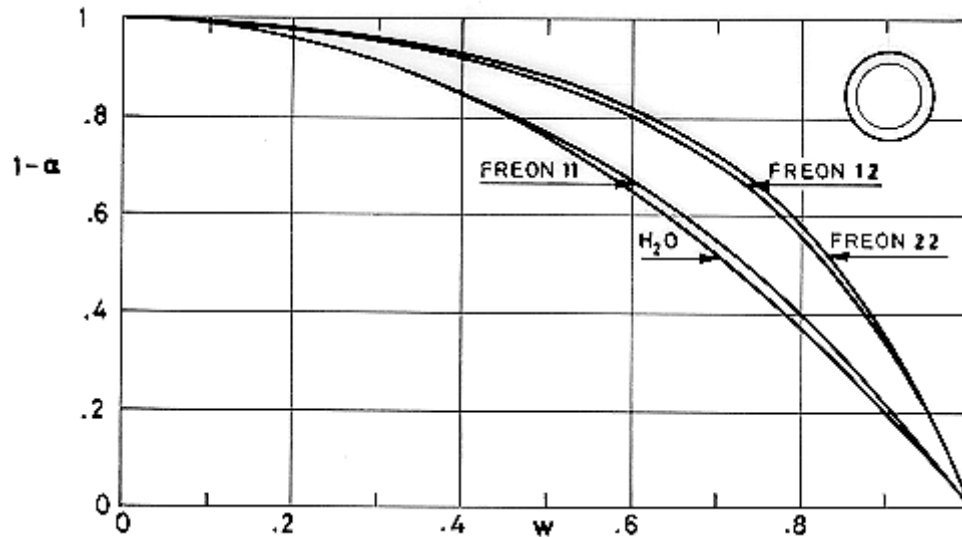
Figure 14-21: Liquid fraction, 1-α, as a function of vapor quality, w, for annular flow of several liquid along ducts. Calculated by the compiler.

A difficulty appears, however, near the origin ($w = \alpha = 1$), where the liquid is still absent and the vapour wets the walls of the duct. It is clear that both liquid and vapour friction terms, which appear in the right hand side of Eq. [14-119], should be taken into account. Since the onset of condensation is not included in the model, the problems associated with the transition of Π_G/Π from 1 to 0 are eluded starting the numerical integration with $\Pi_G/\Pi = 1$, $\Pi_L/\Pi = 0$ and then switching to $\Pi_G/\Pi = 0$, $\Pi_L/\Pi = 1$ with continuous $d\alpha/dw$ derivative.

Once a relation between α and w has been obtained, integration of Eq. [14-119] with $x = 0$, $w = 1$, and the same sharp transition between only-vapour and only-liquid wetting the wall, gives the evolution of the vapour quality, w, along the duct.

Typical results are given in Figure 14-22. A comparison of the results in Figure 14-18 and Figure 14-22 clearly indicates the large enhancing effect of gravity on condensation. This effect results to be considerably larger than that previously predicted (Keshock & Sadeghipour (1983) [104]).
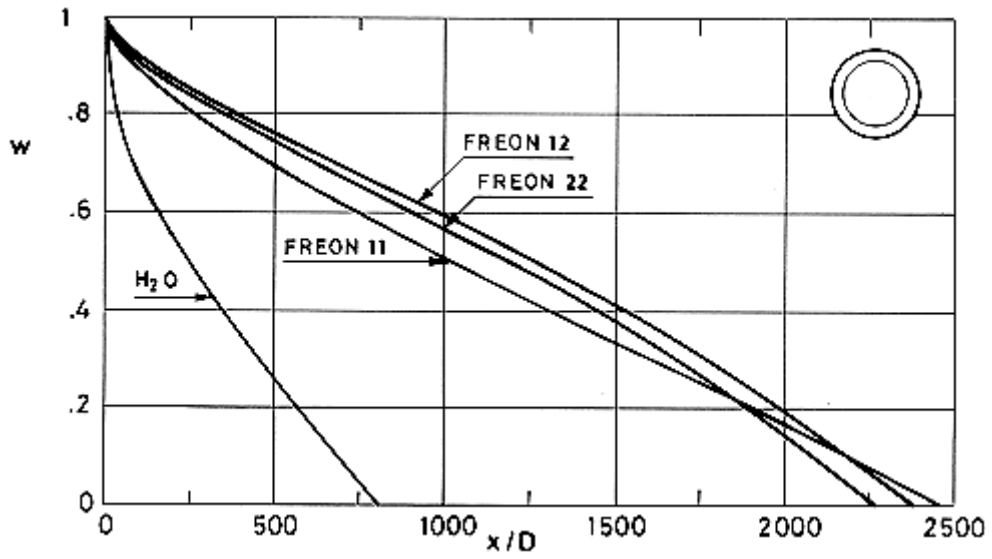
Figure 14-22: Vapor quality, *w*, as a function of dimensionless distance along the duct, *x/D*, for annular flow of several liquids along ducts. Calculated by the compiler.

15
Two-phase thermal transport systems

15.1 General

This clause is devoted to the description of two-phase thermal transport systems which could be typical of a Thermal Management System (TMS) for the Space Station. Single-phase loops are also considered, but only as current state systems for comparison purposes.

15.1.1 Evolution of thermal transport systems

Compared with present state-of-the-art technology, represented by the Space Transportation System (STS), advanced TMSs should reject 10 times more heat to space (up to 100 kW) , transport heat 10 times farther (up to 50 m) maintaining isothermal heat load interfaces, should require low electrical power, have a larger system flexibility and multiyear mission duration (up to 10 years with maintenance).

Two-phase heat transport systems are well suited to meet these requirements. One is tempted, however, to start this clause by exploring to which extent and at which expense in mass and pumping power the TMS design requirements can be achieved using available STS technology before dealing with more advanced configurations based on pumped two-phase flow systems, heat pipe networks or mechanically augmented heat pipe systems.

Changing trend during the last 10 years can be seen in Table 15-1 where the SPACELAB Active Thermal Control System (ATCS) requirements are compared to those of a typical laboratory of a space station.

Table 15-1: Evolution of Requirements

	Spacelab ATCS [a]	Space Station Laboratory [b]
Heat Rejection in Orbit [kW]	8,5 (Average) 12. (Peak)	30
Growth Capability [percent]	--	25
Isothermality [K]	288 ± 5	239 ± 2,5
Crew	3	8 (for more than 30 d)
Mission Time	7 d	10 yr (with maintenance)

[a]   From Owen, Sessions & Walker (1976) [139], Valerani, Degli Esposti & Sessions (1978) [181].

[b]   From Sadunas, Lehtinen & Parish (1985) [153].

The ATCS was devised to transfer the heat loads generated within the Module and on the Pallet by SPACELAB subsystems, experiments and metabolic to the Orbiter heat rejection system. A sketch of the ATCS loop is given in Figure 15-1.
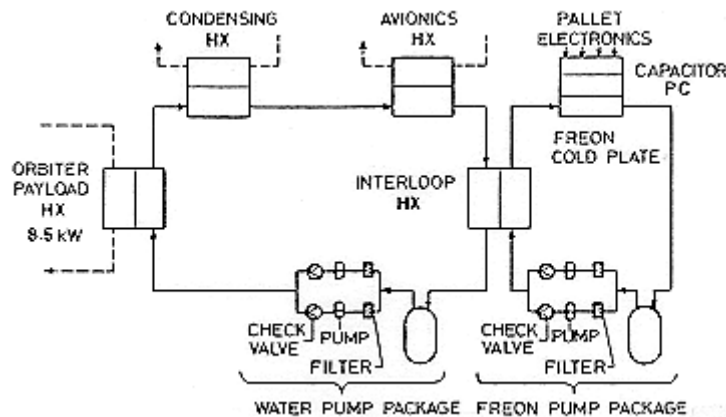
Figure 15-1: Schematic of ATCS fluid loop in the Module-Pallet mode. From Owen, Sessions & Walker (1976) [139].

The TMS representative loop used in this comparison is described with some detail in clause 15.2.

15.1.2 Two-phase loop general layout

The general layout of a single-phase loop has been presented in clause 13.2. Here we intend to introduce the main components of a two-phase loop thermal control system.

A two-phase loop basically consists of fluid-carrying ducts connecting heat sources to sinks, and a pump to overcome the pressure losses. The heat sources interface the loop through cold plates (evaporators) and the heat sinks through condensers (heat exchangers or radiators).

The fluid lines could carry liquid only, vapour only of liquid-vapour two-phase mixtures.

The loop also comprises accumulators for accommodating changes of fluid volume due to temperature changes.

Fluid temperature can be controlled via a reservoir where fluid is kept under saturated pressure-temperature conditions. Either the pressure can be increased by connection to a pressure tank or the temperature changed by thermostatically controlled heaters or by radiation to space. Additionally the pressure level can be changed by a pressure regulating valve placed downstream of the evaporators.

Controls (sensors, control logic, actuators, valves, diverters, phase separators, ...) are required to provide the appropriate mass flow rate at each moment with vapour qualities within a suitable range.

Three general types of loops are possible, namely: parallel circuit, series circuit and hybrid or series/parallel circuit, see Figure 15-2, each one with its own advantages and drawbacks as indicated in Table 15-2.
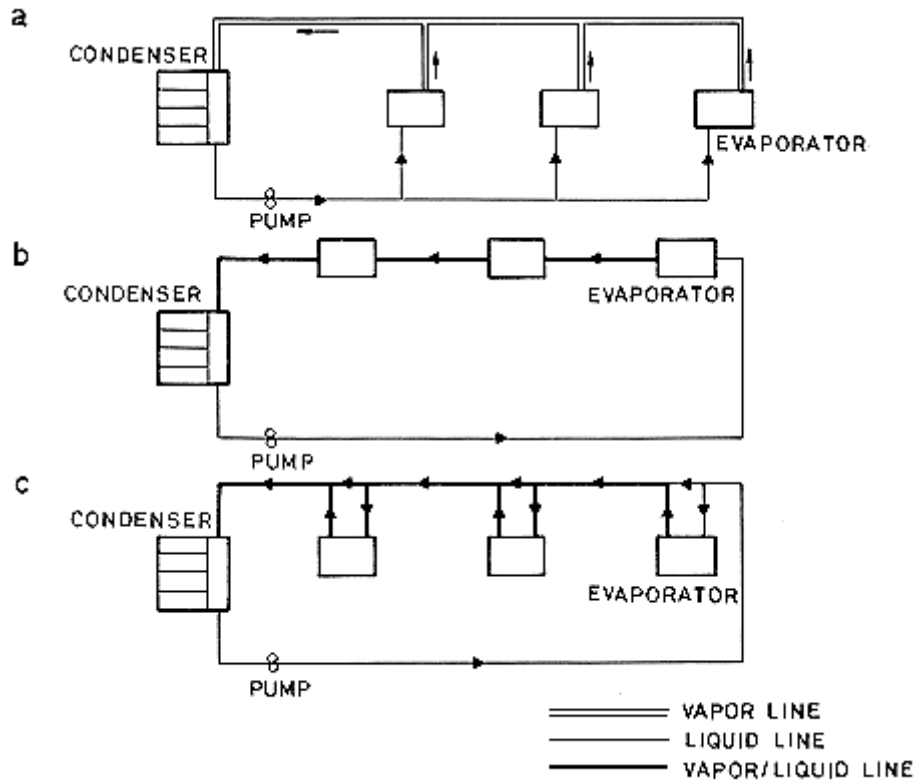
Figure 15-2: Schematic of three different types of two-phase flow loops. a) Parallel circuit. b) Series circuit. c) Series/parallel circuit.

Table 15-2: Two-Phase Loop Line Patterns

Circuit	Description	Advantages	Drawbacks
Parallel (Figure 15-2a)	• Separated liquid-only and vapor-only filled lines. • Liquid flow rate to the evaporator is controlled so that it completely evaporates there	• Complete separation between the liquid and vapor flows. • No g-dependent flow through the duct provided that the right flow rate is simulated. • Moderate impact of one evaporator on the operation of another. • Extendable and modular.	• A liquid flow control device must be provided at each evaporator. • Modules cannot work both as heat sources or heat sinks unless a return liquid line is added. • Liquid flow control can be achieved by capillary pumping. See clause 15.6
Series (Figure 15-2b)	• Saturated two-phase fluid flows through in-series-evaporators.	• No flow control devices are required. • Extreme simplicity.	• The pressure drop depends on the flow pattern and thus on gravity.

Circuit	Description	Advantages	Drawbacks
	• Heat exchange within the modules involves evaporation or condensation and thus changes in vapor quality.	• All modules can be used for either heating or cooling, with the exception of the first module when fed with liquid only.	• Optimal flow patterns should be sought. • Questionable Earth simulation. • Strong mutual influence between consecutive modules. • Reduced growth capability.
Hybrid (Figure 15-2c)	• Module by-pass provided to decrease the mass flow rate through the evaporators of the series circuit. • A phase separator increases the liquid concentration of the fluid entering the evaporator	• Same as above at the cost of greater complexity. • Reduced pressure drop in the evaporators.	• Temperature operated flow valves are required to adjust the fluid flow rate to the heat load on each evaporator. This adds complexity to the system.

NOTE   Prepared by the compiler after van Oost & Mathieu (1983).

Figure 15-3 shows a break-away view of a 25 kW technology demonstrator thermal bus.
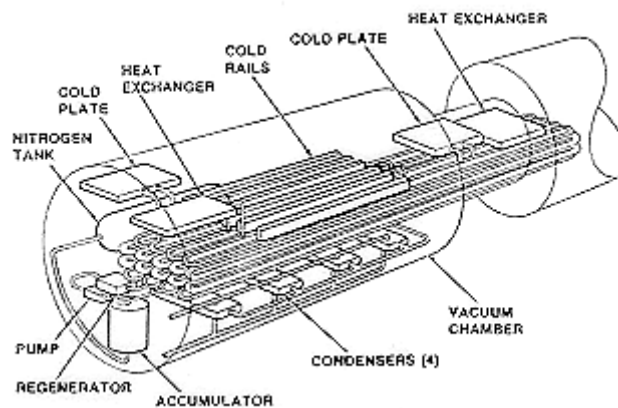
Figure 15-3: Physical layout of 25 kW technology demonstrator (thermal bus). From Carlisle / Nolan (1987) [18].

15.1.3 About the nomenclature of this clause

The following nomenclature is used:

1. Thermal Management System. It is the whole active thermal control system of the Space Station. It consists of 1) Interfacing devices; 2) Heat transport subsystem; and 3) Heat rejection subsystem. Very often (not in this clause) it is known as Thermal Utility.

2. Single-phase system. It refers to a pumped liquid loop the temperature gradient of which (between cold plate and heat rejector) is zero or negative.

3. Two-phase system. This heat transport system is often known as thermal bus. It can accept heat loads of various magnitudes and locations without affecting the whole system.

15.2 Tms trade-off study

The study baseline Space Platform Configuration is presented in Figure 15-4. It consists of the unpressurised experiment truss and resource (power) module and five pressurised (and manned) modules: Habitat, Logistics, Multiple Berthing Adaptor (MBA) and Laboratories No. 1 and 2. Solar arrays generate the electrical power, with regenerative fuel cells providing power on the dark side of the orbit. The current fully-equipped platform has 75 kW electrical power at the bus. The module heat rejection loads are given in Table 15-3, and the TMS design requirements in Table 11-14.
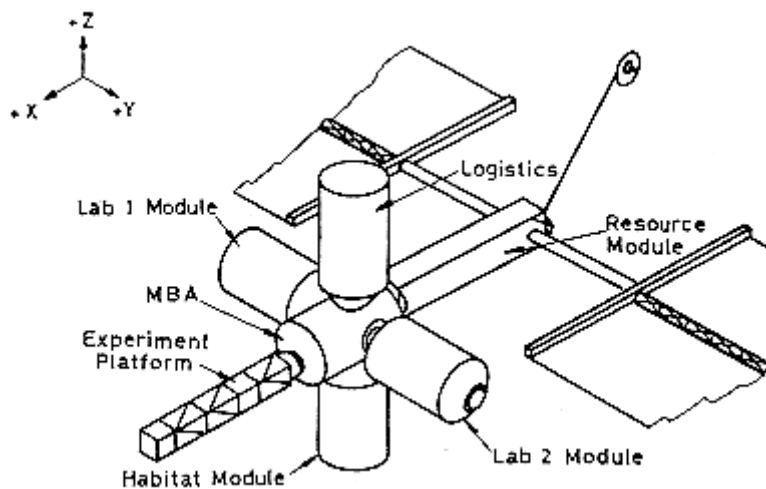
Figure 15-4: Space platform configuration. From Sadunas, Lehtinen & Parish (1985) [153].

Table 15-3: Power Dissipation by Module

Module	Heat Source	Sunside (kW)	Darkside (kW)	Orbital Average (kW)
Resource	Equipment Fuel Cell	13,41 0,0	11,46 46,96	12,68 15,65
MBA	Equipment Metabolic [a]	6,0 0,295	6,0 0,295	6,0 0,295
Logistics	Equipment Metabolic [a]	1,0 0,295	1,0 0,295	1,0 0,295
Habitat	Equipment Metabolic [a]	5,0 0,59	5,0 0,59	5,0 0,59
Laboratory 1	Equipment Metabolic [a]	10,0 0,59	10,0 0,59	10,0 0,59
Laboratory 2	Equipment Metabolic [a]	30,0 0,59	30,0 0,59	30,0 0,59
Experiment Truss	Equipment	21,0	21,0	21,0
Subtotal	Equipment Fuel Cell Metabolic [a]	86,41 0,0 2,36	84,46 46,96 2,36	85,68 15,65 2,36
TOTAL		88,77	133,78	103,69

[a] Represent typical distribution to meet safe-haven requirement. Each pressurized module is sized for 2,36 kW.

NOTE   From Sadunas, Lehtinen & Parish (1985) [153].

Table 15-4: TMS Design Requirements

Parameter	Requirement		
Heat Rejection	100-150 kW		
Growth Capability	25%		
	Metabolic	Equipment	Fuel Cell
Heat Source Temperature [K]	277	293	343
Cold Plate Temperature Range [K]	277-288	290,5-295,5	≤ 343
Meteoroid protection NASA TMX-82478	1% probability of penetration		
Safety, pressurized modules	No toxic or flammable fluids		
Safe-haven requirement	Crew of eight for minimum of 30 days		
Load Sharing Capability	20%		
TMS power requirement (Target)	1% of heat rejection load		
System life	10 years with maintenance		
Single-point failure	Design to preclude single-point failure; nominal level heat rejection with any component failed or subsystem inactivated for maintenance		

NOTE   From Sadunas, Lehtinen & Parish (1985) [153].

The following assumptions are considered in this study:

Orbital Environment Loads: Orbital average environment loads are used to size the radiators.

Centralised Radiator Orientation: The fixed radiators are assumed to be oriented in the Y-Z plane (Figure 15-4), which corresponds to the minimum orbital average environment load.

Thermal Storage: PC capacitors (see ECSS-E-HB-31-01 Part 10) are included in the thermal transport systems. Orbital average loads are used for radiator sizing. The benefits and characteristics of PC capacitors thermal storage as applied to TMS designs are examined in clause 15.3.1.

Thermal Coating Degradation: A 10 year end-of-life (EOL) α_s of 0,3 is assumed, based on α_s = 0,1 at beginning-of-life (BOL) and a degradation rate of 0,02 per year. Also, a constant emittance, ε = 0,78 over the 10-year design life period is assumed.

Space Temperature: The radiating surfaces are assumed to radiate to 0 K space.

Metabolic Heat Load: A metabolic heat load of 295 W per crew man is used. This corresponds to an active state.

Pump Power Efficiency: An overall efficiency for electrical to mechanical pumping power of 20 % is used.

The objective now is to perform an analysis of different thermal management options. The approach taken is to define a study baseline TMS which represents the current state-of-the-art technology, and

to analyze and compare this baseline with alternate concepts which reflect incremental improvements to the baseline system.

15.2.1   TMS study baseline

The study baseline schematic is presented in Figure 15-5. The system consists of a centralized pumped liquid (Freon 21) loop transport with a centralized two-stage radiator. The radiator provides 277 K coolant flow to the metabolic heat exchangers and 290,5 K coolant flow to the equipment heat exchangers. Part of the fluid, before returning to the main radiator, passes through the fuel cell heat exchanger raising the fluid temperature of that flow branch to 343 K.
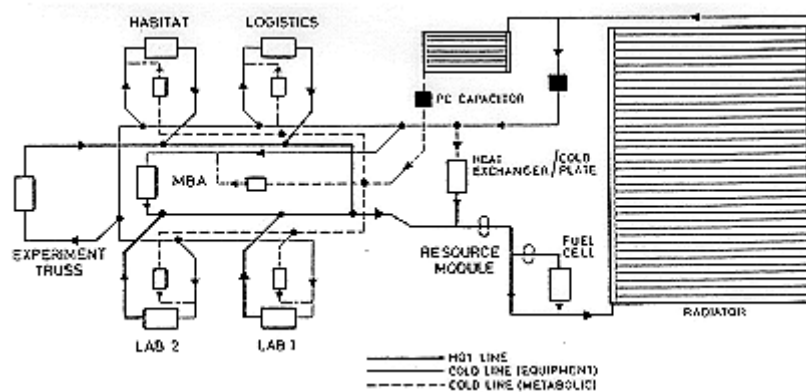
Figure 15-5: Study baseline centralized liquid loop external bus. From Sadunas, Lehtinen & Parish (1985) [153].

Due to the pressurised module safety requirement, all of the Freon lines and heat exchangers are located outside the pressure vessel. The intermodule fluid transfer is affected through fluid line connections in the docking ports. The external bus thermal transport system interfaces with the internal water loops through heat exchangers.

The external thermal bus is driven by a single redundant. pump package located in the resource module. A small auxiliary pump is included in the fuel cell branch to minimize total pumping power.

15.2.2   TMS design concepts

The design options considered are listed in Table 15-5 where the global characteristics of the different design concepts are included (Concept I is the baseline system).

Table 15-5: TMS Design Concepts

	Design Option		**Design Concept**				
			I	**II**	**III**	**IV**	**V**
Heat Acquisition	Interface Heat Exchanger		x	x	x	x	x
Heat Transport	Centralized		x	x			
	Decentralized (3 loops)				x	x	x
	Pumped Liquid Thermal Transport	Freon 21	x				
		Ammonia		x	x		
	Two-phase Fluid (Ammonia) Thermal Transport					x	x
Heat Rejection	Radiator	Heat Pipe		x	x	x	x
		Pumped Liquid Loop	x				
		Fixed	x	x	x	x	
		Steerable					x
	Thermal Storage		x	x	x	x	

NOTE   Prepared by the compiler after Sadunas, Lehtinen & parish (1985) [153].

The changes from one concept to the next are aimed at improving the overall performance. The design goals of each concept are presented in Table 15-6.

Table 15-6: TMS Design Goals

DESIGN CONCEPT	**DESIGN GOALS**
I	Current state-of-the-art technology
II	To reduce pumping power and overall system mass
III	To enhance module thermal autonomy, safe-haven provision capability and compatibility with the phased space platforms build-up in space
IV	To reduce pumping power and overall system weight, and to enhance isothermality capability
V	To reduce overall system mass and to eliminate the need for thermal storage

NOTE   Prepared by the compiler after Sadunas, Lehtinen & Parish (1985) [153].

Concept II is identical to the baseline system except that the liquid loop radiators are replaced by heat pipe radiators, and the working fluid is Ammonia instead of Freon 21.

Concept II consists of a decentralised pumped liquid loop system. The schematic of this system is presented in Figure 15-6. This concept has the following features: pressurised modules (except the Multiple Berthing Adaptor (MBA)) utilising body mounted radiators for metabolic heat rejection; MBA module metabolic heat rejection affected through a resource module deployed radiator; centralised external liquid loop with deployed radiator; and autonomous fuel cell pumped liquid loop and heat pipe radiator.
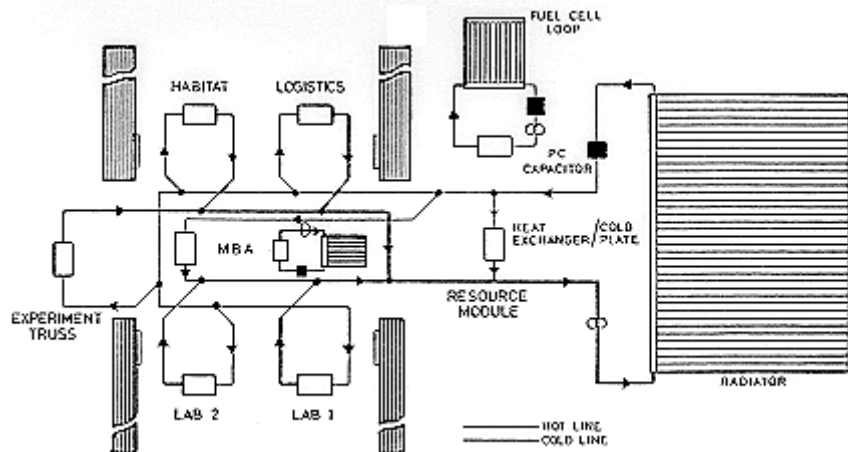
Figure 15-6: Concept III. Decentralized liquid loop. From Sadunas, Lehtinen & Parish (1985) [153].

Concept IV is identical to Concept III except that the pumped liquid Ammonia transport is replaced with a two-phase Ammonia transport. The schematic of this system is presented in Figure 15-7, where it can be seen that the thermal storage is now integral with the internal and external bus heat exchangers and central bus cold plates.
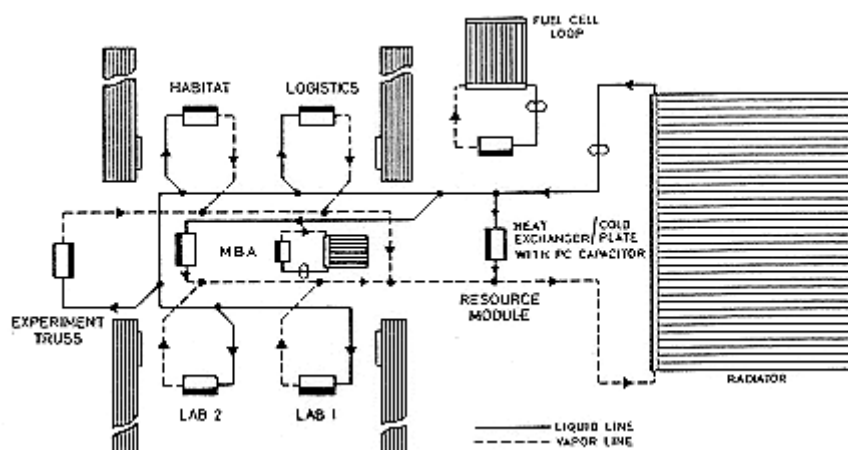
Figure 15-7: Concept IV. Decentralized two-phase transport. From Sadunas, Lehtinen & Parish (1985) [153].

Concept V is identical to Concept IV except that the fixed equipment radiator has been replaced by a steerable radiator. Because of the added complexity of steerable radiators (see clause 15.5.3), the benefits are considered insufficient to replace the fixed fuel celland MBA module's metabolic radiators.

The internal water loop is common to all the TMS concepts investigated.

15.2.3 Evaluation of tms concepts

The relative merits and performance of each TMS design concept are assessed on the following criteria: 1) system mass; 2) power requirement; 3) reliability; 4) modularity; 5) growth capability; 6) isothermality penalty; 7) safe-haven provision.

Table 15-7 presents the evaluation of the five TMS design concepts defined above. A pictorial mass summary of these concepts is presented in Figure 15-8.

Table 15-7: Evaluation of Concepts

CRITERION	CONCEPT I	CONCEPT II	CONCEPT III	CONCEPT IV	CONCEPT V
System mass, M	M = 10900 kg Radiator Mass: 6000 kg Thermal Storage Mass: 990 kg Freon mass: 940 kg	M = 6900 kg Radiator mass: 2500 kg Radiator Heat Exchanger mass: 770 kg Thermal Storage Mass: 1060 kg Ammonia mass: 210 kg	M = 8440 kg Decentralized systems weigh more. Radiator mass: 3310 kg Radiator Heat Exchanger mass: 920 kg Thermal Storage Mass: 1720 kg Ammonia mass: 210 kg	M = 7830 kg Ammonia mass: 18 kg Reduction of 91,6 %	M = 5690 kg Central bus radiator mass reduction of 1110 kg from Concept IV Thermal Storage reduction of 1040 kg from Concept IV
Power Requirement, P	P = 4,2 kW ≈ 0,04 Q 3% above design goal	P = 1,7 kW ≈ 0,016 Q 60% reduction from Concept I	P = 1,7 kW ≈ 0,016 Q Same power requirement as in centralized systems	P = 0,01 kW ≈ 10^{-4} Q Great pumping power reduction	
Reliability	Moderate. The most probable failure cause could be the intermodule and radiator fluid connectors. Leak detection and flow by-passes are required at each connector.	High. Heat pipe radiators are much less sensitive than pumped liquid loop radiators to meteoroid penetration.	High. Enhanced as compared to Concept II. Intermodule fluid connections are valves are eliminated. Probability of leakage is diminished (lower bus pressure).		Lower than in IV. The steerable radiator adds complexity to the system. Steering mechanism and sensors, leak detectors, valves and controls to by-pass are required.
Modularity	Feasible. Modularity requirements dictated the provision of additional fluid flow paths and connectors at the modules, and redundant pumping capacity.		Feasible. Enhanced as compared to Concept II. Decentralized systems enhance module thermal autonomy.		

CRITERION	CONCEPT I	CONCEPT II	CONCEPT III	CONCEPT IV	CONCEPT V
Growth Capability	Feasible. Provisions for growth capability require oversized fluid lines and redundant pumping capacity.		Metabolic subsystem: Limited: Limited to 1,75 kW by the Body Mounted radiator area. Equipment subsystem: Feasible: System growth can be accommodated in the design by increasing flow rates and pumping power, or by oversizing the fluid lines.		
Isothermality Penalty	540 kg ≈ 0,05 M. The 5 K Isothermality requirement affects transport system mass. Mass of radiator heat exchanger and cold plate remains unchanged.	227 kg ≈ 0,033 M. 58 % reduction from Concept I	227 kg ≈ 0,027 M.	Nil. Isothemal system.	
Safe-haven Provision	Crew of Eight. The safe-haven provision is met through redundant distributed metabolic heat rejection capability between modules and redundant intermodule fluid connections.		Crew of Eight. Enhanced as compared to Concept II, due to the autonomous nature of the metabolic loop of each module. However, the 1,75 kW capacity is probably adequate only for short-term safe-haven use.		

NOTE   Prepared by the compiler after Sadunas, Lehtinen & Parish (1985) [153].
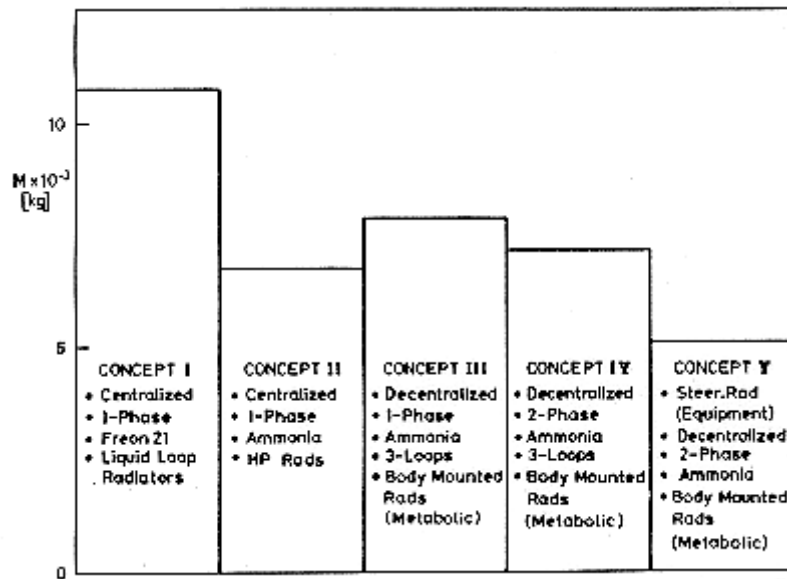
Figure 15-8: Trade study mass summary. From Sadunas, Lehtinen & Parish (1985) [153].

15.3 Design for orbital average load

The TMS design is complicated by a 10-year minimum life requirement, minimum on-orbit maintenance, mass constraints, and the fact that the system will operate in low earth orbit which reduces the effectiveness of the radiators. In order to optimise the overall system design, with respect to mass and power requirements, the TMS is sized for orbital average heat rejection loads and orbital average environments. This generates the requirement for incorporation of thermal storage (TS) within the TMS.

The benefits of TS in the context of TMS optimisation and as a means of compensating for radiator optical coating degradation (an idea already discussed in ECSS-E-HB-31-01 Part 10 clause 8.5) were analysed by Lehtinen & Sadunas (1985) [114]; their results will be summarized in clause 11.3.1.)

TS is implemented in the TMS by means of phase change capacitors (see ECSS-E-HB-31-01 Part 10), usually in series in the loop. The particular configuration of in series PC cells has not been disclosed, but for the time being they could be envisaged as a shell-and-tube heat exchanger, Figure 11-4, where the shell fluid is the PC material and the tube fluid that flowing through the loop.

In the following clause the characteristics of PC capacitors for both single and two-phase transport systems will be discussed.

15.3.1 Phase change capacitor performance

Two different systems were considered for the analysis of the characteristics and specifications of the required PC capacitors.

- System 1. Decentralised pumped liquid loop system. This system corresponds to Concept III (clause 15.2.2). Figure 15-9a shows a schematic of an idealised pumped liquid loop system with TS.

- System 2. Decentralised two-phase transport system. This system corresponds to Concept IV (clause 15.2.2). The schematic of an idealised two-phase system with TS is shown in Figure 15-9b The phase change capacitor is integral with the heat source, thus, for this arrangement the heat source continuously dumps heat into the capacitor. The system will have a varying flow rate which is controlled by the radiator heat rejection capacity; this, in turn, is a function of the radiator environmental heat flux history shown in Figure 15-10.
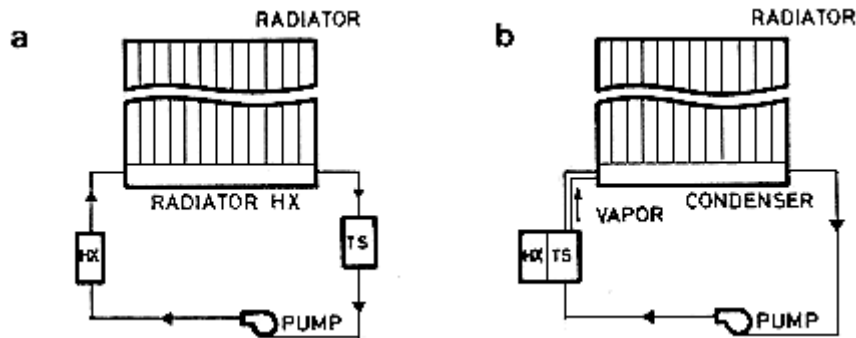
Figure 15-9: Decentralized systems with TS. a) Pumped liquid loop. b) Two-phase transport. From Lehtinen & Sadunas (1985) [114].
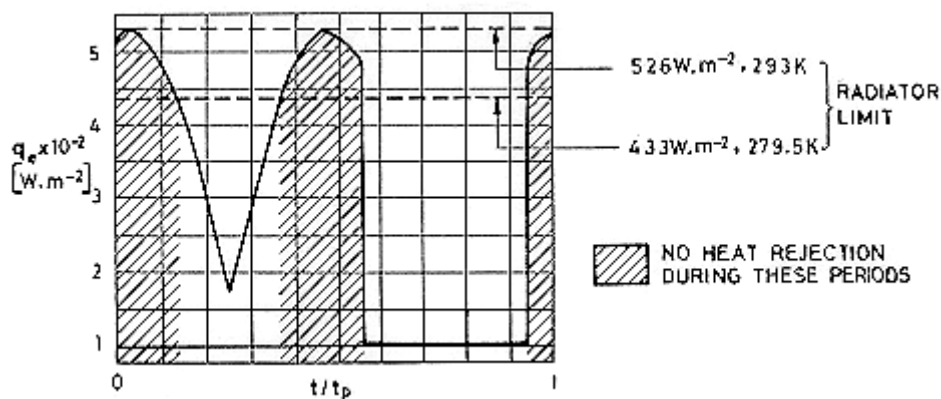
Figure 15-10: Radiator absorbed environmental heat flux, q_e, vs. dimensionless time, t/t_p. Orbital period, t_p = 90 min. Radiator limit: Black body emissive power. From Lehtinen & Sadunas (1985) [114].

The characteristics of single- and two-phase TMSs with TS are given in Table 15-8.

Table 15-8: Characteristics of Single-Phase and Two-Phase TMSs with PC Capacitor.

Characteristic	Single-Phase System	Two-Phase System
Mode of operation	Controls HX flow inlet temperature to prescribed value with varying radiator outlet temperatures. Capacitor adds or removes thermal energy from the fluid stream with varying loads.	Capacitor acts as an intermediate storage for source heat rejection with heat being continuously removed from the capacitor by evaporation of the fluid at the capacitor HX.
Capacitor Location	Downstream of radiator.	Integral with heat source.
Mass Flow Through HX	Constant, determined by the specified heat exchanger inlet and outlet temperatures and by the maximum heat rejection load.	Varying with and controlled by the net instantaneous heat rejection capacity of the radiator.
System Temperature	Constant at capacitor HX outlet, varying at capacitor HX inlet (radiator outlet).	Essentially constant temperature throughout the system and radiator with varying load and environment.[a]
PC Temperature	PC material with phase change temperature equal to desired HX inlet temperature.	PC material with phase change temperature equal to the nominal selected system temperature.

[a]   When operating at the design heat rejection load and environment condition.

NOTE   From Lehtinen & Sadunas (1985) [114].

In order to determine the TS characteristics, transient analyses were performed. The principal areas of interest are:

1.   Thermal capacitor energy storage rate, and

2.   Thermal capacitor stored energy history.

The equations used by Lehtinen & Sadunas (1985) [114] are summarised in Table 15-9. Figure 15-11 shows the performance of the PC capacitor in three different subsystems, namely: Metabolic Equipment and Fuel Cell. These results show no substantial differences between single- and two-phase systems.

Table 15-9: PC Capacitor Performance

	Single-Phase System	**Two-Phase System**
Radiator Area, A_R [m²]	$A_R = \dfrac{Q}{E_R - \overline{q}_e}$ Q: Heat Rejection Rate [W]	$A_R = \dfrac{\overline{Q}}{E_R - \overline{q}_e}$ $\overline{Q}$: Average Heat Rejection Rate [W]
	$\overline{q}_e$: Average Environmental Heat Flux [W.m⁻²] E_R: Radiator Emissive Power [W.m⁻²] $E_R = 2\sigma\varepsilon\eta T_R^4$ σ: Stefan-Boltzmann Constant [W.m⁻².K⁻⁴] ε: Radiator Emittance η: Radiating Effectiveness of the radiator T_R: Radiator Temperature [K]	
	$T_R^4 = \dfrac{T_o^5 - T_i^5}{5(T_o - T_i)}$ T_o: Average Radiator Outlet Temperature [K] T_i: Radiator Inlet Temperature [K]	$T_R = T_M$ T_M: Capacitor Phase Change Temperature [K]
Mass Flow Rate, m [kg.s⁻¹]	$m = \dfrac{Q_{max}}{c_p(T_i - T_M)}$ Q_{max}: Maximum Heat Rejection Load [W] c_p: Specific Heat of the Working Fluid [J.kg⁻¹.K⁻¹]	$m(t) = \dfrac{A_R\{E_R - q_{e(t)}\}}{h_{fg}}$ $q_e(t)$: Environmental Heat Flux [W.m⁻²] h_{fg}: Heat of Vaporization [J.kg⁻¹]
Thermal Capacitor Energy Storage Rate $Q_c(t)$ [W]	$Q_c(t)$: $mc_p\{T_o(t) - T_M\}$ $T_o(t)$: Radiator Outlet Temperature [K]	$Q_c(t) = Q(t) - m(t)h_{fg}$ Q(t): Heat Rejection Load [W]
Thermal Capacitor Stored Energy $J_c(t)$ [J]	$J_c(t) = \displaystyle\int_o^t Q_c(t)dt$	

NOTE   Prepared by the Compiler after Lehtinen & Sadunas (1985) [114]
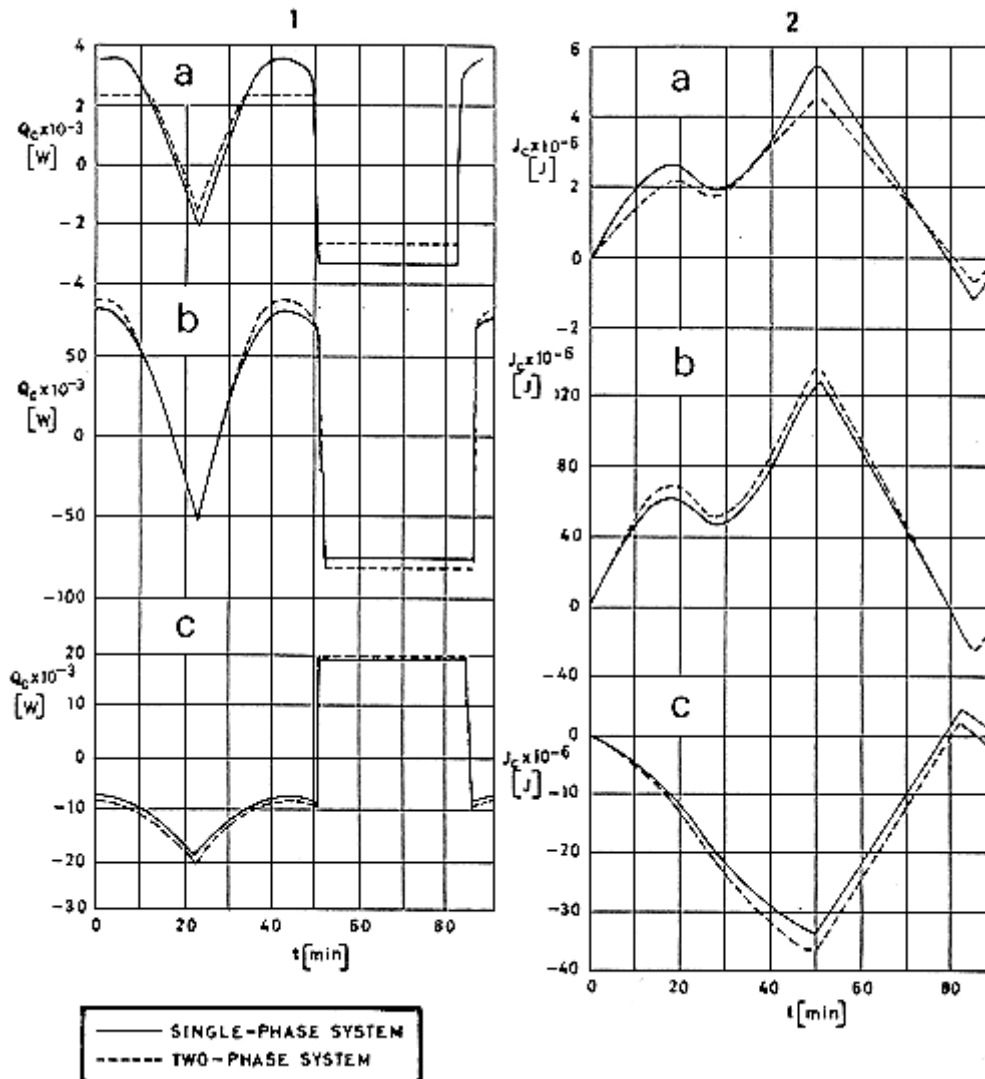
Figure 15-11: Thermal performance of PC capacitors in different subsystems. a) Metabolic. b) Equipment. c) Fuel cell. Thermal performance is given in terms of: 1) energy storage rate, Q_c; and 2) net stored energy, J_c. From Lehtinen & Sadunas (1985) [114].

The specifications of TMS with PC capacitors are summarised in Table 15-10.

Table 15-10: Single-Phase and Two-Phase TMS Capacitor Specifications

Parameter	Single-Phase				Two-Phase			
	Metabolic	Equipment	Fuel Cell	Total	Metabolic	Equipment	Fuel Cell	Total
Average Heat Load $\overline{Q}$ x 10³ [W]	2,36	88,24	21,92	112,52	2,36	88,24	21,92	112,52
Average Environment $\overline{q}_e$ [W.m⁻²]	306,7	306,7	306,7	---	306,7	306,7	306,7	---
Inlet Temperature T_i [K]	277	290,5	340,5	---	279,5	293	343	---
Outlet Temperature T_o [K]	282	295,5	345,5	---	279,5	293	343	---
Phase-Change Temperature T_M [K]	277	290,5	340,5	---	279,5	293	343	---
Radiator Area A_R [m²]	18,8	410,0	33,3	462,1	15,3	409,4	32,6	457,3
Flow rate m x 10³ [kg.s⁻¹]	103,6	3869,7	2083,6	6056,9	1,9	74,7	20,8	97,4
Energy Storage Rate Q_c x 10⁻³ [W]	3,71	84,08	17,88	105,67	2,36	88,24	18,89	109,49
Stored Energy [a] J_c x 10⁻⁶ [J]	7,16	161,93	36,86	205,95	5,69	174,85	38,95	219,49

[a]   Tabulated results are larger than those given in Figure 15-11.

NOTE   From Lehtinen & Sadunas (1985) [114].

A comparison of specific storage capacity, J_c/Q_c, for single- and two-phase transport systems is shown in Figure 15-12. It can be seen that the single-phase system has slightly higher storage requirement at low temperatures. The reason for this behaviour, which is model-dependent, can be understood as follows: when the system operating temperature is low, the heat rejection to space ceases for a while (see shadowed zones in Figure 15-10). For the two-phase system, once the liquid is fully vaporised, and provided that the sensible heat of thevapour is neglected, the heat transfer to the thermal capacitor will reach a top plateau, Figure 15-11a. For the single-phase system, on the contrary, the amount of heat to be transferred to the capacitor is controlled by the sensible heat of the liquid in the loop (Table 15-9) and exceeds that corresponding to the two-phase system.
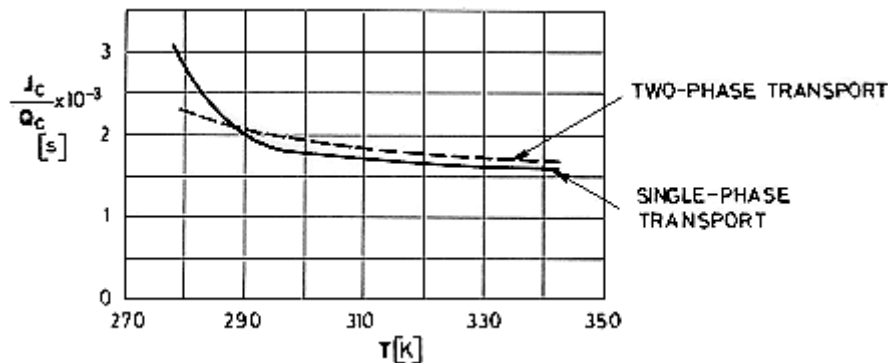
Figure 15-12: Required specific storage capacity. J_c/Q_c, of typical TMSs vs. temperature, T. From Lehtinen & Sadunas (1985) [114].

15.4 Off-design operation

In the study of Thermal Management Systems, sizing is usually made for maximum heat rejection and worst case radiator environment, which occurs near the end of design life because of radiator optical coating degradation. The TMS, then, will be required to operate for a considerable length of time with reduced heat rejection loads, that is, at off-design conditions. In this clause, the temperature control during off-Design operation is analysed.

One of the three subsystems studied in clause 15.3.1, namely the fuel cell loop, is selected here. As in that clause, two different thermal transport systems are considered:

- System 1. Pumped-liquid loop (Concept III of clause 15.2.2).
- System 2. Two-phase transport systems (Concept IV of clause 15.2.2).

The sketches of these two systems are shown in Figure 15-13.
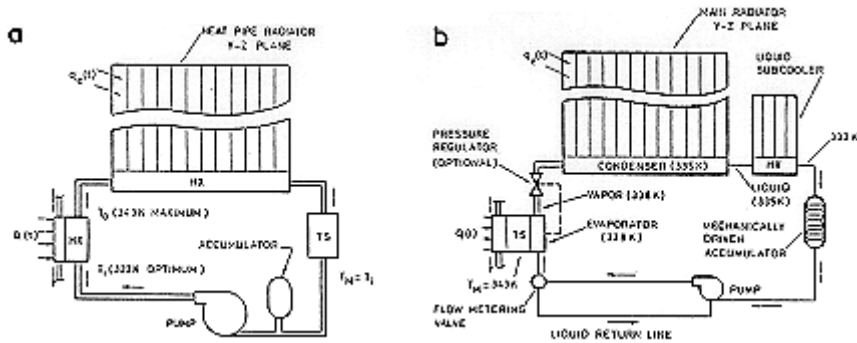
Figure 15-13: Schematic of the fuel cell loop TMS. a) Pumped liquid loop. b) Two-phase transport. From Sadunas, Lehtinen & Parish (1986) [153].

The selected fuel cell thermal control loop has a peak waste heat rejection load of 47 kW. Since the allowable fuel cell inlet temperature range is quite broad, an optimum fuel cell heat exchanger inlet temperature is determined by minimising radiator, pumping and wet plumbing weight. This optimum HX inlet temperature (322 K) also represents the thermal capacitor phase change temperature in the single-phase system. In the two-phase system the phase change temperature is the maximum HX outlet temperature (343 K).

As mentioned in the previous clause, a Phase-Change capacitor has been incorporated in order to size the radiator for orbital average heat rejection and external environment (instead of using peak values). In the two-phase transport system the PC capacitor (integral with the heat source) is in thermal contact with the fluid through an evaporator. Subcooled liquid is vaporised in the evaporator and recondensed in the radiator condenser. The liquid is subcooled to prevent boiling in the accumulator and cavitation in the pump (see Figure 15-13b) The liquid flow rate to the evaporator is controlled by a flow metering valve. Vapour pressure(and boiling temperature) in the evaporator can be controlled either by means of a mechanically driven accumulator, or by a pressure regulating valve downstream of the evaporator (this solution reduces, or eliminates, the cycling of the accumulator).

A summary of functional requirements of the fuel cell loop and radiator environments is presented in Table 15-11.

Table 15-11: Fuel Cell Loop Design Requirements

Parameter		Value
Orbital characteristics		β range ± 52° [a] Period 94,2 min
Fuel Cell Cycle (Darkside)		35,6 min at β = 0° 27,5 min at β = 52°
Fuel Cell Heat Rejection		47 kW peak 17,7 kW average at β = 0 [b] 12,5 kW average at β = 52°
Radiator Solar Absorptance		α_s = 0,1 BOL α_s = 0,3 EOL
Radiator Environment	Design Case	301 W.m^{-2} average at β = 0° with α_s = 0,3 [b]
	Coldest Off-Design Case	144 W.m^{-2} average at β = 52° with α_s = 0,1

[a] Here β is 90° minus the angle between the line to the sun and the normal to orbit plane (see the list of symbols of ECSS-E-HB-31-01 Part 15)

[b] These values slightly differ from 21,9 kW and 306,7 W.m^{-2} given in Table 15-10, clause 15.3.1.

NOTE   From Sadunas, Lehtinen, Nguyen & Parish (1986) [154].

15.4.1 Temperature control

Under off-design conditions an excess radiator area will exist and, in the absence of control, the PC material will solidify and subcool causing the heat exchange inlet temperature to fall below the minimum design (322 K). Schemes for system temperature control will be analysed in the following.

15.4.1.1 Pumped liquid loop system

The control scheme should maintain the fuel cell heat exchanger inlet temperature as close as possible to 322 K. Two optional schemes are available.

1.   Respond-to-demand scheme. This scheme is shown in Figure 15-14. The fuel cell heat exchanger inlet temperature, T_1, is controlled by mixing part of the fluid exiting the fuel cell heat exchanger at temperature T_2 with the fluid exiting the TS heat exchanger at temperature T_3. Because of the excess cooling capacity, the PC material remains solid and the temperature T_3 below the phase-change temperature.
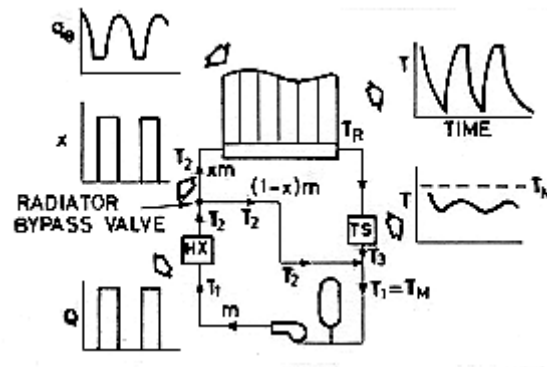
Figure 15-14: Respond-to-demand temperature control scheme From Sadunas, Lehtinen, Nguyen & Parish (1986) [154].

If *xm* is the mass flow rate through the radiator and PC capacitor, T_1 will be given by the following equation

$$T_1 = (1-x)T_2 + xT_3 \qquad\qquad [15\text{-}1]$$

which gives *x* once T_1, T_2 and T_3 are known.

The main drawbacks of this scheme are:

o   By-pass valve is continuously operating.

o   Radiator temperature experiments sharp time changes.

o   PC capacitor is inoperative.

2.   Orbital average scheme. The mass flow rate through the radiator heat exchanger is set to the orbital average conditions. See Figure 15-15 for a schematic of this system. The heat exchanger inlet temperature is now constant, equal to the constant TS temperature (the PC material is now in a two-phase state).
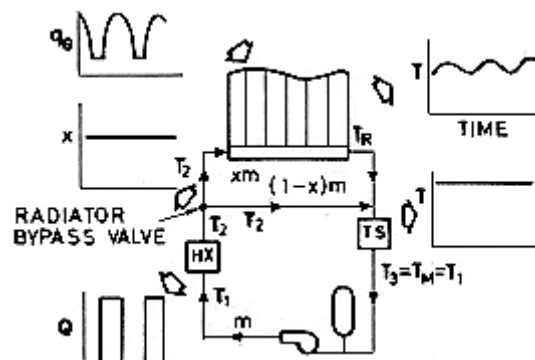
Figure 15-15: Orbital-average temperature control scheme. From Sadunas, Lehtinen, Nguyen & Parish (1986) [154].

The required radiator flow fraction, *x*, would be given by

$$(1-x)\overline{T}_2 + x\overline{T}_R = T_M \qquad\qquad [15\text{-}2]$$

where T_M is the phase-change temperature. The fuel cell heat exchanger average outlet temperature, $\overline{T}_2$, and the radiator average temperature, $\overline{T}_R$, can be obtained by expressing that both subsystems are able to manage the average heat rejection load.

In this scheme the fluid flow rate through both radiator and PC capacitor heat exchanger are kept constant, and the temperature excursions of the radiator are small provided that the fuel cell operating conditions change slowly with time.

Table 15-12 presents computed values of x for a range of off-design operating conditions. Also given in this table are the orbital average radiator temperatures, $\overline{T}_R$.

Table 15-12: Orbital-Average Schema. Values of *x* for Off-Design Operation

β [deg]	α_s	$\overline{q}_e$ [W.m-2]	$\overline{Q}$ x 10-3 [W]	x	$\overline{T}_R$ [K]
0	0,1	162	17,7	0,36	308
0	0,3	301	17,7	1,00	322
52	0,1	144	12,5	0,14	287
52	0,3	247	12,5	0,21	301

NOTE   From Sadunas, Lehtinen, Nguyen & Parish (1986) [154].

It should be noted that for the coldest operating case (β = 52°, α_s = 0,1) only 14 % of the flow passes through the radiator heat exchanger.

15.4.1.2   Two-phase transport system

The mode of operation during predictable off-design conditions of a two-phase transport system (see Figure 15-13b) is the same as during operation at the design point, except that, in the present case, T_R is set to a lower value based on orbital average heat rejection load, $\overline{Q}$, and environmental heat flux, $\overline{q}_e$.

The radiator operating temperatures for a range of off-design operating conditions are presented in Table 15-13. For the coldest operating case the radiator temperature results to be 299 K compared to 335 K when operating at the design point conditions.

Table 15-13: Two-Phase System. Radiator Temperatures for Off-Design Operation

β [deg]	α_s	$\overline{q}_e$ [W.m-2]	$\overline{Q}$ x 10-3 [W]	$\overline{T}_R$ [K]
0	0,1	162	17,7	322
0	0,3	301	17,7	335
52	0,1	144	12,5	299
52	0,3	247	12,5	311

NOTE   Assumed Radiator Area, A_R = 27,3 m².

From Sadunas, Lehtinen, Nguyen & Parish (1986) [154].

15.4.2   Instrumentation requirements

Three schemes for system temperature control under off-design conditions have been considered in clause 15.4.1. The respond-to-demand and the orbital-average schemes are used for pumped liquid loop systems(clause 15.4.1.1), and a variant of the orbital-average scheme for two-phase transport systems (clause 15.4.1.2).

The instrumentation requirements for these three control schemes are summarised in Figure 15-16.
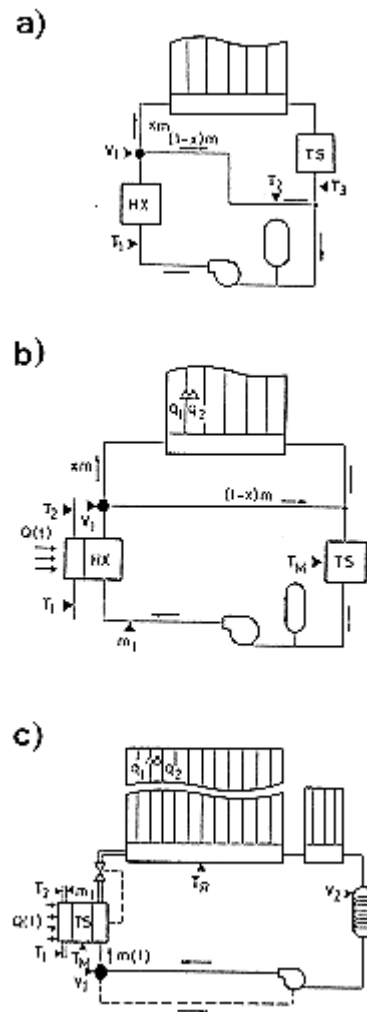
Figure 15-16: Instrumentation of the different control schemes. a) "Respond-to-demand" pumped-liquid-loop scheme. b) "Orbital-average" pumped-liquid-loop scheme. c) Two-phase transport loop scheme. From Sadunas, Lehtinen, Nguyen & Parish (1986) [154].

The "orbital-average" and the two-phase system control schemes are rather complicated, and since they operate on an orbital average basis, they will be sensitive to cumulative measurement errors, requiring provision for periodic corrections.

For the "respond-to-demand" control scheme, on the other hand, instrumentation requirements are much simpler. In addition, since this system operates on an instantaneous-response approach it is insensitive to cumulative measurement errors.

The "orbital-average" control scheme is the preferred approach from the thermal point of view (lower temperature excursions and full use of the PC capacitor), despite the necessity for a larger number of measurements and more complicated control algorithms. The "respond-to-demand" scheme could be incorporated as a backup of the orbital-average control scheme because of its simplicity.

15.5 Radiator-loop interaction

The radiator is the most massive component of a TMS. It is also the most exposed portion of the space station.

Table 15-14 gives the component mass of a typical pumped liquid loop system for different values of the heat rejection rate, Q. The ratio M_R/M, of radiator to system mass is shown in the last column. This ratio increases as Q increases.

Table 15-14: Component Mass of a Typical Pumped Loop TMS

$Q \times 10^{-3}$	Mass, M [kg]					M_R/M
	Power System	**Radiator**	**Pump**	**Other** [a]	**Total**	
1	5,9	42	0,91	7,2	56	0,75
2	9,1	84	1,80	13,1	108	0,78
5	15	210	3,60	31	260	0,81
10	22	420	6,30	62	510	0,82
20	32	840	10,4	128	1010	0,83
50	54	2100	21	320	2500	0,84
100	80	4210	35	630	4960	0,85

[a]   Includes cold plate and wet lines.

NOTE   From Dexter & Haskin (1984) [34].

Minimising the size of the radiators would save mass and cost, and would simplify design, vehicle attitude control and stability, maintenance, payload space sensor viewing, resupply vehicle docking and micrometeoroid protection.

Although radiators have been dealt with in ECSS-E-HB-31-01 Part 9, we will discuss in the following p

clauses several waysfor decreasing radiator area and mass, since these ways will affect the overall configuration of the TMS.)

15.5.1 Boosting radiator temperature with a heat pump

The range of applicability of pumped liquid loops and active heat pumps for long term TMSs has been studied by Dexter & Haskin (1984) [34]. Their main idea is summarised in Figure 15-17.
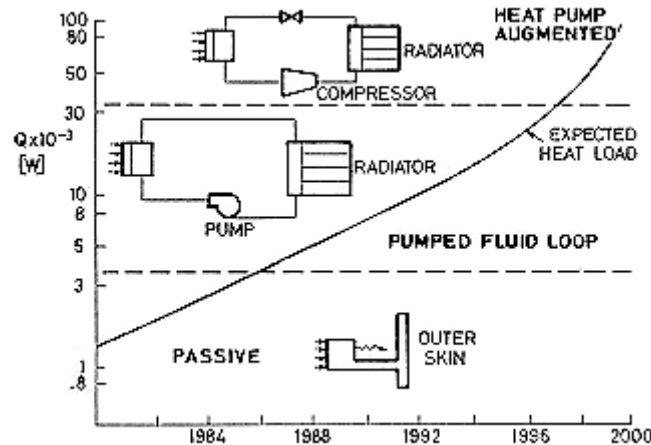
Figure 15-17: Evolution of the heat rejection rate and configuration of spacecraft thermal control systems. From Dexter & Haskin (1984) [34].

Pumped liquid active thermal control systems are useful in the 3×10^3 W to 30×10^3 W heat rejection rate range, above which heat pump augmented systems could be employed.

The heat pump raises the temperature of a circulating fluid through compression of the evaporated working fluid. The working principle is the same as for a refrigerator, Figure 15-18.
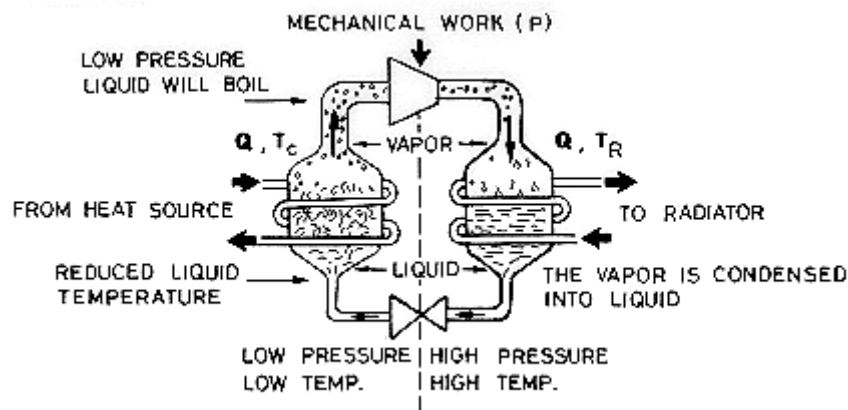
Figure 15-18: Schematic of the heat pump working principle. Adapted by the compiler after Rye & Steen (1986) [152].

The fluid circulates through a close system. When heat from the source is transferred to the fluid, in liquid phase and at low temperature and pressure, the liquid is evaporated. Then, vapour pressure and temperature are raised at the compressor. The vapour passes to a condenser where heat is rejected. The resulting liquid passes through a throttle valve where it regains the initial temperature and pressure before initiating the cycle.

The idea is not new. It is being increasingly used for industrial and domestic heating. See Heap (1979) [81] for a recent account of heat pump performance and applications. A heat pump for Spacelab

application in the 15 W - 20 W heat rejection rate range has been considered (Berner & Savage (1981) [11]).

In the present instance the heat pump aims at boosting radiator temperature, thence reducing radiator area and mass.

The relevant steps in the trade-off performed by Dexter & Haskin (1984) [34] are summarised in Table 15-15. Representative results are given in Figure 15-19 to Figure 15-22. These results are less striking than those presented by the mentioned authors because of one main reason: they assume a fairly large equivalent temperature of the surrounding space, T_e = 283 K, which apparently would be representative of unfavourable low altitude orbits. This means that a very modest increase in the radiator equilibrium temperature, T_R, will sharply increase the factor T_R^4-T_e^4 of the radiative term in the radiator thermal balance equation. In the present case it is assumed that T_e = 0.

Table 15-15: Heat Pump Augmented vs. Classical Fluid Loop Trade-Off

	Heat Pump Augmented Fluid Loop	Classical Fluid Loop
Basic Assumptions	Loop Temperature, T_c = 277 K Radiator Equilibrium Temperature, T_R	Loop Temperature, T_c = 277 K Working fluid: Freon 21, See clauses 15.5 and 15.5.1. ΔT = 11 K across the interface HX Δp = 1,4 x 10^5 Pa. Pressure loss through the loop
Radiator Mass, M_R [kg]	$$M_R = \frac{\Gamma}{\sigma s \eta T_R^4}\left(1+\frac{P}{Q}\right)Q$$ Γ: Radiator Area Density. Γ = 5 kg.m^{-2} σ: 5,6697 x 10^{-8} W.m^{-2}K^{-4}. Stefan-Boltzmann Constant ε: 0,82. Radiator Emittance η: 0,80. Radiating Effectiveness of the Radiator P: Power supplied to the heat pump or to the pump [W] Q: Heat load [W]	
	$$\frac{P}{Q} = \frac{T_R - T_c}{\eta_c T_c}$$ $$\frac{T_c}{T_R - T_c}$$ Carnot Coefficient of Performance η_c = 9,948[1,8(T_R-273)+32]$^{-0,612}$ Fraction of Carnot Efficiency	$$T_R = T_C$$ $$\frac{P}{Q} = \frac{1}{\eta_p}\Delta p \frac{1}{\rho c_p \Delta T}$$ See clause 15.3 η_P = 0,25. Overall Efficiency of the pump. c_P and ρ are respectively the specific heat and density of the working fluid.
Solar Panel Mass, M_{SP} [kg] (chargeable to the fluid driver)	$$M_{SP} = 4,67 Q^{0,562}\left\{\left(1+\frac{P}{Q}\right)^{0,562} - 1\right\}$$ This expression corresponds to a "conservative" estimate of the overall efficiency of a photovoltaic system.	

	Heat Pump Augmented Fluid Loop	Classical Fluid Loop
Fluid Driver Mass, M_P [kg]	$M_P = 2 \times 0{,}68\{2+9{,}4\text{x}10^{-3}P^{5/6} \times \times (n\text{x}10^{-4})^{-1,25}$	$M_P = 2 \times 0{,}80 \times 10^3 \left(\dfrac{Q}{\rho c_p \Delta T} \right)^{0,75}$
	Factor 2 has been introduced to account for redundancy.	
Cold Plate Mass, M_{CP} [kg]	$M_{CP} = 1{,}87 \times 10^{-3}\, Q$	
(Wet) Plumbing Mass, M_{WL} [kg]	$M_{WL} = (1/10)(M_R + M_P + M_{CP})$	
Total System Mass, M [kg]	$M = M_R + M_{SP} + M_P + M_{CP} + M_{WL}$	

NOTE   Prepared by the Compiler after Dexter & Haskin (1984) [34].
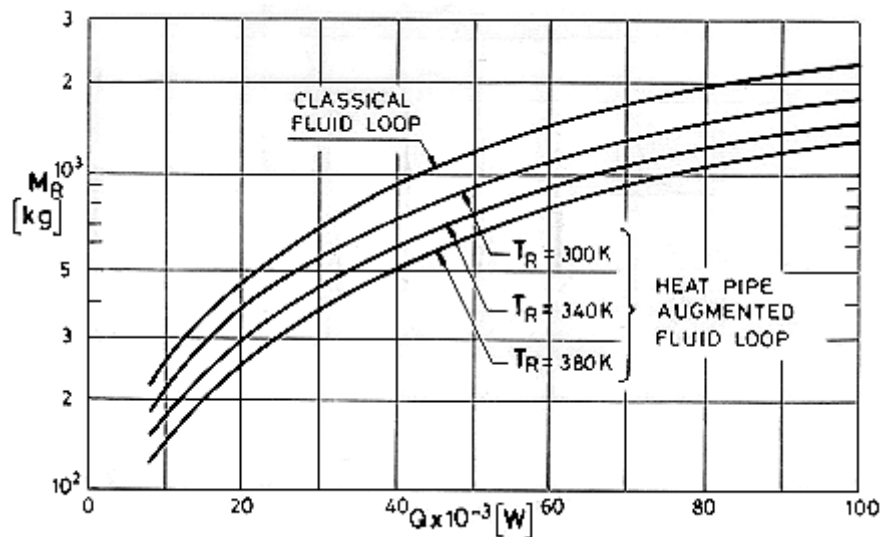
Figure 15-19: Radiator mass, M_R, of four typical systems (see text above) for different values of the heat rejection rate, Q. Calculated by the compiler.
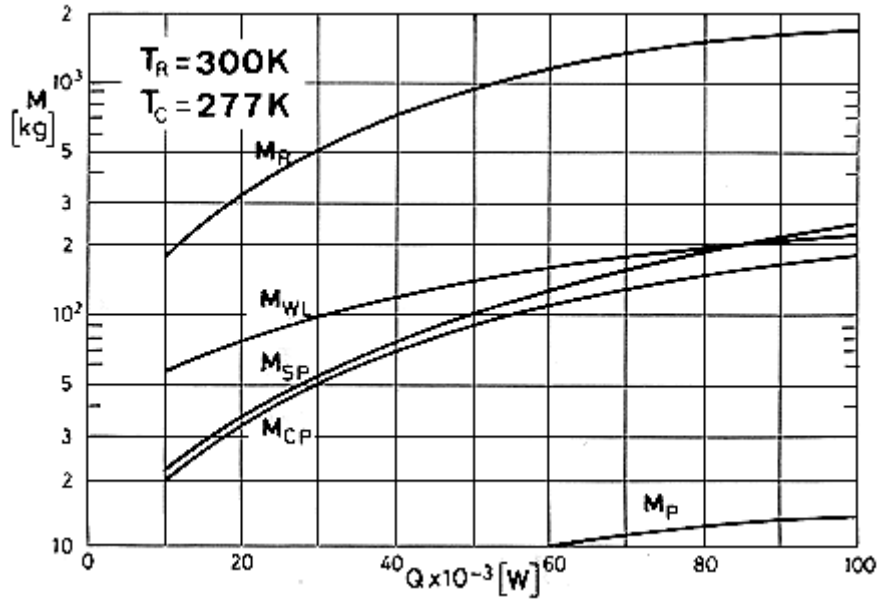
Figure 15-20: Mass breakdown of a heat pump augmented system for different values of the heat rejection rate, Q. T_R = 300 K. Calculated by the compiler.
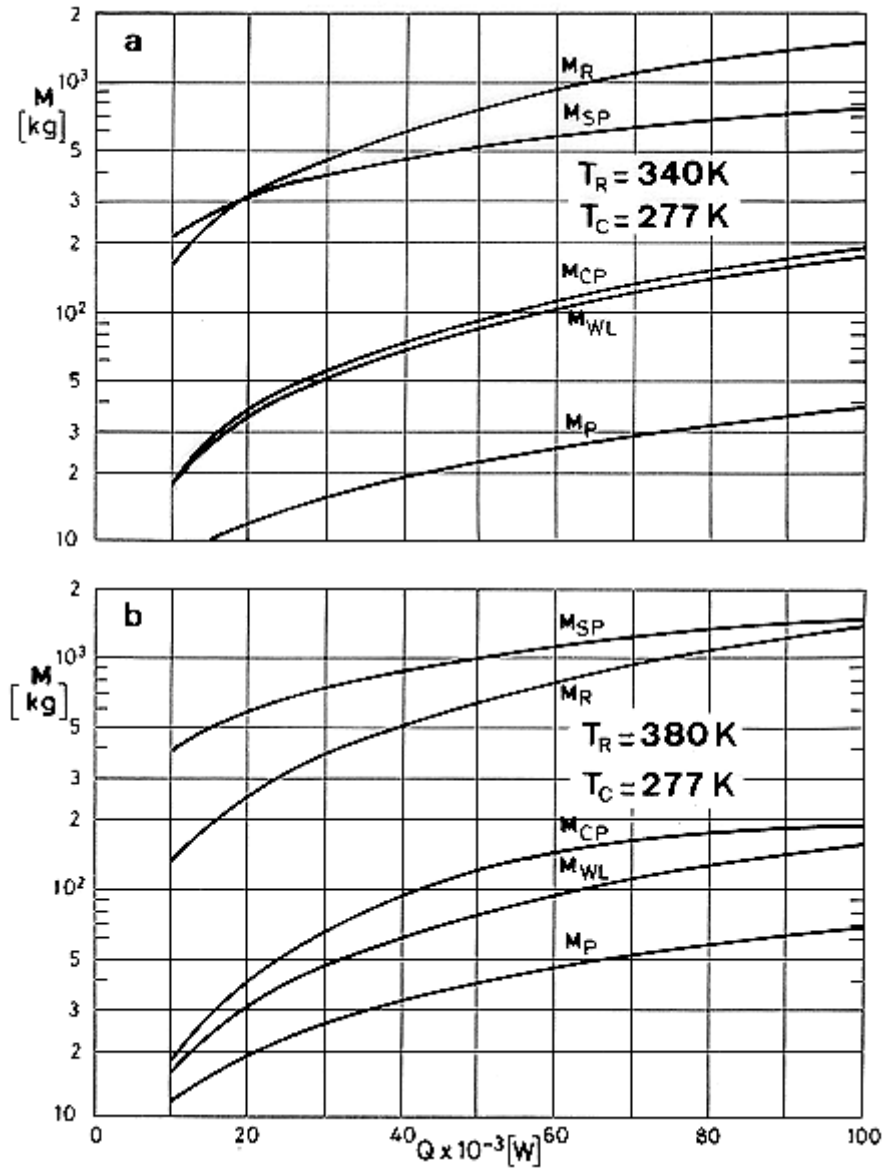
Figure 15-21: Mass breakdown of a heat pump augmented system for different values of the heat rejection rate, *Q*. a) *T*$_R$ = 340 K. b) *T*$_R$ = 380 K. Calculated by the compiler.
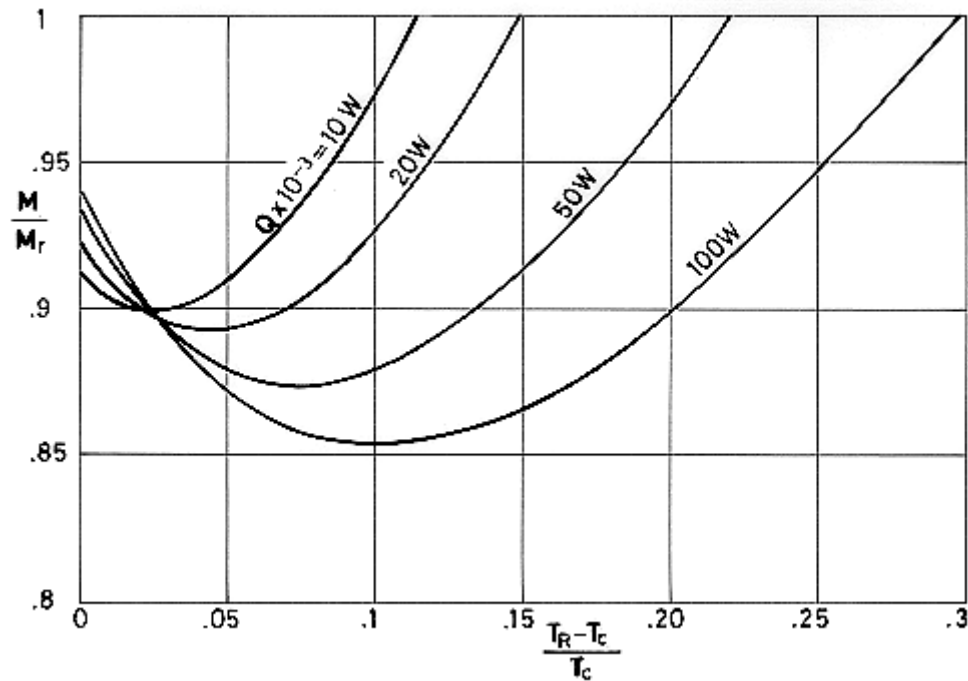
Figure 15-22: Ratio of total mass, *M*, of the heat pump augmented system to the total mass, *M*r, of the reference classical pumped-liquid loop vs. the inverse Carnot coefficient of performance [*T*R–*T*c]/*T*c for different values of the heat rejection rate, *Q*. Calculated by the compiler.

Systems considered in Figure 15-19 to Figure 15-22 are:

1. 1. Baseline system. A classical pumped liquid loop with a mean temperature close to T_c = 277 K.

2. 2. A heat pump augmented loop with a low temperature section at 277 K and a radiator at temperature T_R. Three different values of T_R have been assumed in Figure 15-19 to Figure 15-21, namely: T_R = 300 K, 340 K and 380 K.

Resulting mass savings are small (or nil). Only for a fairly reduced T_R range, near $T_R \approx T_c$, where the pump efficiency is large, a mass reduction can be achieved (Figure 15-22). In the high TR side the energy required to operate the rather insufficient heat pump is, at present, too costly in terms of added solar panel mass (see the increasing trend of the solar panel mass, M_{SP}, in Figure 15-20 and Figure 15-21).

15.5.2   Thermal-storage assisted radiator

It has been already shown in clause 15.3 that two basic TMS design options exist. 1) Design without thermal storage (TS) and size the radiator for peak heat rejection loads and peak environments or 2) include TS and size the radiator for orbital average heat rejection and external environment. In any case radiator sizing has to account for α_s degradation over the design mission file.

The radiator specific area, A_R/Q, is related to the incident solar, q_s, Earth infrared, q_{ir}, and Earth albedo, q_a, fluxes, to the radiator emissive power E_R, and to the optical properties α_s and ε by

$$\frac{A_R}{Q} = \frac{1}{E_R - \alpha_s(q_s + q_a) - sq_{ir}}$$

[15-3]

For the TMS design without TS, the (q_s+q_a) term represents the peak orbital value. For the design with TS, it represents the orbital average value. In both cases, the radiator is sized for EOL α_s. Note that the q_{ir} term can be assumed to be constant because the radiator plane remains normal to the orbital plane. The effect of the α_s/ε ratio on radiator specific area, for three different radiator temperatures is presented in Figure 15-23. These temperatures correspond to the metabolic radiator (279,5 K), equipment radiator (293 K) and fuel cell radiator (343 K) which were considered in clause 15.3.1.
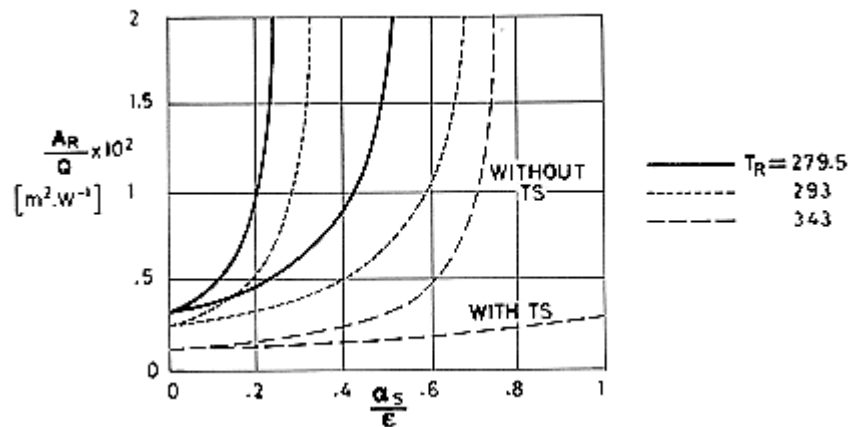
Figure 15-23: Effect of α_s/ε on radiator specific area, A_R/Q. From Lehtinen & Sadunas (1985).

The data shown in Figure 15-23 indicate that:

- Substantial radiator area savings can be achieved by incorporating TS in the TMS design.

- The radiator are growth requirement with α_s degradation is substantially decreased for design with TS.

- A limiting α_s/ε value exist for each radiator temperature.

In general, radiator area will be sized to meet EOL requirements, that is allowance is made for α_s degradation. In this study BOL and EOL α_s/ε values are 0,12 and 0,38 respectively. The data in Figure 15-23 show that for the 279,5 K metabolic radiator, the EOL requirement cannot be met since the limiting value of α_s/ε is 0,3. This is also true for the 293 K equipment radiator, which has a limiting α_s/ε value of 0,38 (this corresponds to an infinitely large radiator). Therefore, for these two cases, the designer has two options, design for shorter life (lower EOL α_s) with provision for coating refurbishment, or design with TS. The 343 K fuel cell radiator data show that, at this higher temperature, the radiator area reduction resulting from TS is very small for α_s/ε ratios up to 0,5. Because the fuel cell loop has a cyclic heat rejection load, with the maximum occurring on the darkside of the orbit, a third option exists for this subsystem, namely, size the radiator on the peak darkside heat rejection load without TS. The results above are summarised in Table 15-16.

Table 15-16: EOL Radiator Area for 10-year Life

Subsystem	Radiator	Radiator Area, A_R [m²]	
	Temperature [K]	Without TS	With TS
Metabolic	279,5	*	18,8
Equipment	293	*	410,0
Fuel Cell	343	56,7**	33,3

NOTE   * Radiator temperature will exceed design allowable at EOL.

              ** Sized for peak heat rejection load on the orbit darkside.

              From Lehtinen & Sadunas (1985). [114]

15.5.2.1   Coating degradation and radiator life

The preceding discussion showed that for low temperature radiator subsystems, EOL α_s values dictated the incorporation of TS into the TMS system. Conversely, designs without TS and hence lower EOL α_s values, require provision for periodic refurbishment of the radiator coatings. Figure 15-24 presents the estimated radiator life/refurbishment frequency for TMS designs with and without TS. Using these data, radiator area for 5-year and 10-year design life (or refurbishment frequency) are computed for the baseline configuration and are summarised in Table 15-17. These data show that the metabolic subsystem TMS design without TS can be achieved if the design/refurbishment frequency is reduced to 5 years. Even so, the radiator are penalty is substantial. Then TS is included in the design, 10-year life (or refurbishment frequency) is achieved at a modest radiator area penalty of 6,7 m². For all refurbishment frequencies, considerable radiator area savings are achieved with TS.
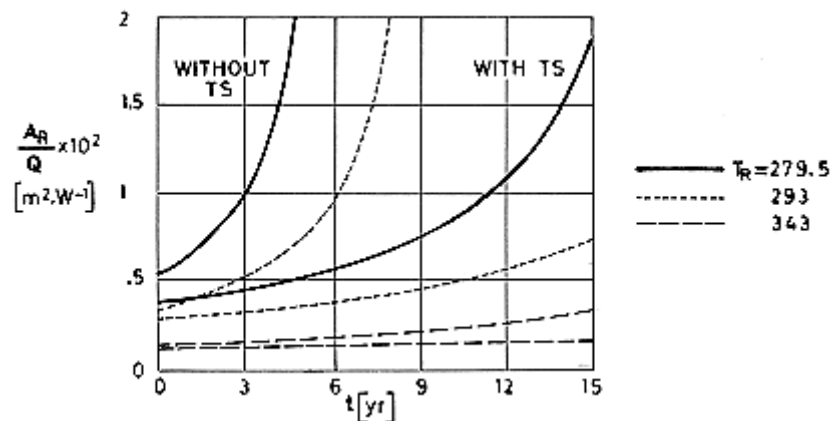
Figure 15-24: Radiator specific area, A_R/Q, vs. refurbishment frequency, t. From Lehtinen & Sadunas (1985) [114].

Table 15-17: Radiator Area vs. Design Life

Subsystem	Radiator Area, A_R [m²]			
	5-year life		10-year life	
	Without TS	With TS	Without TS	With TS
Metabolic	41,7	12,1	*	18,8
Equipment	615,6	297,7	*	410,0
Fuel Cell	53,0	28,8	53,0	33,3
Total	710,3	338,6	--	462,1

NOTE   *Design temperature exceeded.

From Lehtinen & Sadunas (1985) [114].

Similar conclusions are drawn for the equipment radiator with the exception that radiator area-refurbishment frequency penalties are lower than those for the metabolic radiator.

The fuel cell radiator data show that the radiator area increases very gradually with refurbishment frequency for the design with TS, which is sized for the orbital average load and environment. That is, the refurbishment frequency can be extended at a small cost of additional radiator area. On the other hand, the design without TS is independent of refurbishment frequency, since it is based on the orbital darkside heat rejection load and environment (i.e., independent of α_s degradation).

In summary, these results demonstrate that TS is essential for long life, low temperature design when α_s has to be considered. For all cases, radiator area is reduced and coating refurbishment frequency extended by including TS.

15.5.3   Steerable radiators

Considerable savings in radiator area can be achieved by steering the radiator to minimise incident solar flux, earth albedo and earth IR flux. Also steerable radiators partially prevent coating degradation by avoiding solar radiation impingement. This reduced surface degradation rate reduces the required radiator area projected for EOL performance and may significantly extend the useful life of the radiator elements. Typical variation of steerable to fixed radiator specific heat rejection ratios is presented in Figure 15-25.
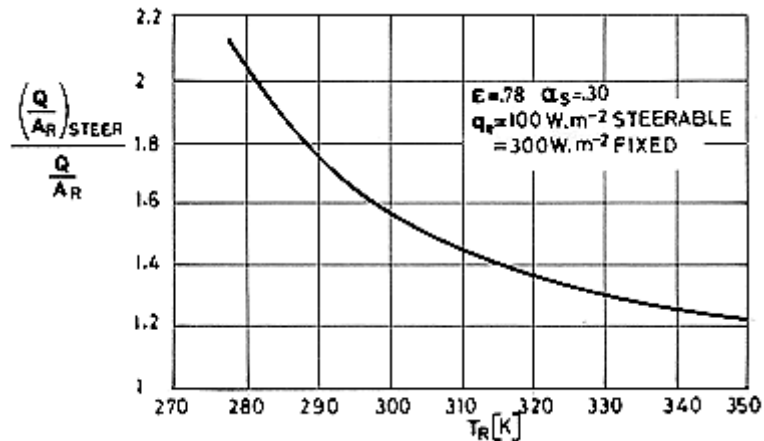
Figure 15-25: Steerable to fixed radiator specific heat-rejection ration, $(Q/A_R)_{steer}/(Q/A_R)$, vs. radiator temperature, T_R. From Sadunas, Lehtinen & Parish (1985) [154].

A comparison of fixed and steerable radiator areas for the TMS under study (see Concepts IV and V of clause 15.2.2) is shown in Table 15-18. Also shown in the table are radiator areas corresponding to peak and orbital average loads along with the amount of TS needed in the latter case. The 277 K metabolic radiator shows the largest relative reduction when steered, but because of its small area, the added complexity of steering would probably not be justified. In practical terms, only the 293 K equipment radiator should be steered resulting in a net savings of about 180 m² of radiator area compared to the fixed radiator. Since the difference between the peak and orbital average design areas is small (27,1 m² for the 293 K radiator) and the orbital average design requires TS (61,2 kg for the 293 K radiator), the trade is 27,1 m² of radiator area versus 61,2 kg of thermal storage. Thus, steering considerable reduces the radiator area and practically eliminates the need for thermal storage.

Table 15-18: Comparison of Fixed and Steerable Radiator Areas

Radiator Temperature T_R [K]	Heat Rejection Q [kW]	Radiator Area, A_R [m²]			TS [kg]
		Fixed [a]	Steerable [b]		
			With TS	Without TS	
277	2,36	21,4	8,0	10,5	2,3
293	88,24	409,9	222,1	249,2	61,2
348 [c]	15,65	30,3	24,2	25,4	6,1

[a]   Y-Z plane radiator.

[b]   Z-axis steering.

[c]   This value differs from 343 K given in Table 15-14, clause 15.2.

NOTE   From Sadunas, Lehtinen & Parish (1985) [153].

Finally, during operation at low heat rejection rates, external heating of the radiation system could be beneficial to avoid freezing or contraction of the working fluid within the radiator elements. In such situations it would be convenient to steer the radiators toward a warmer thermal environment to maintain an acceptable operating temperature.

The main subsystem of a steerable radiator to be discussed here is the rotary thermal coupling to achieve the heat transfer across the radiator interface.

15.5.3.1   Rotary thermal couplings

Several concepts can be imagined. The selection of the best one is based on many different considerations regarding temperature gradients, operational sensitivity or radiator configuration (fluid loop or heat pipe). The two main requirements to be fulfilled are: high thermal conductance and small steering torque. Rotary thermal coupling concepts could be classified into three main categories:

1.   Rotary contact coupling. Heat transfer is achieved through the joint thermal conductance of movable solid parts.

2.   Rewind mechanisms with flexible hoses connecting the inboard and outboard fluid lines.

3.   Continuously rotatable fluid transfer mechanisms using dynamical seals.

The requirements of a Category 3 thermal coupling being developed for the Space Station are listed in Table 15-19.

Table 15-19: Requirements for a Rotary Coupling Onboard. Space Station.

Operational Requirements
360-degree continuous rotation One axis of rotation per coupling Reversible, variable speed rotation Low maintenance
Physical Requirements
Ammonia compatible Thermal/Vacuum compatible Zero leakage to space Accommodate two fluid loops at different temperatures Redundancy capability On-orbit replaceable Minimum updating required with Space Station growth
Life and Reliability Requirements
10-year life without replacement Indefinite life with replacement 99% Reliability

NOTE   From Heizer, Goo, Rhodes, Thoreson & Parish (1986) [83].

Table 15-20 presents a preliminary evaluation of joint concepts with focus on near-term (Columbus) applications. Heat rejection load is 1,1 kW peak, operating temperature range from 278 K to 298 K and lifetime of at least 4 years. Most of the concepts are suited to deployment purposes only. The state-of-the-art looks far from satisfactory.

Table 15-20: Joints for Steerable Radiators

Concept	Fig.	Description	Advantages	Drawbacks	Evaluation (1987)
Rotatable Radial Heat Pipe	Figure 15-26 Figure 15-27	Radial flow heat pipe. The evaporator consists of a fine gauze wich attached to the inner tube. The condenser is placed radially outwards and separated from the outer tube wall by a small clearance.	Good thermal performance: $h_c \approx 500$ W.K^{-1}.m^{-1}. Low rotation torque.	Appropriate leak-tight end caps required.	In conceptual stage. No near term application.
Oscillating Hydrody-namic Thermal Joint	Figure 15-28	Two reservoirs at different temperatures connected via a (flexible) capillary bundle. Very large axial heat fluxes achieved when the fluid oscillates axially at high frequency and very large amplitudes.	Conductance can be controlled by the fluid oscillation. $h_{cmax} \approx 10^4$ W.K^{-1}.m^{-1}.	Power required. Fatigue limits lifetime. Poor state of the art.	No near term application. For deployment only.
Articulated Heat Pipe	Figure 15-29 Figure 15-30 Figure 15-31	A splitted heat pipe with a spherical or cylindrical joint and a flexible arterial wick. Sealing is particularly difficult in the hemispherical configuration. In the cylindrical configuration this problem is minimized, but only axial rotation is possible.	Minimum temperature drop. $\Delta T = 5$ K.	Sealing problems limit the operating pressure and temperature, and require careful manufacture. High torques.	Unmature state of the art.
Flexible Heat Pipe	Figure 15-32 Figure 15-33	Rigid evaporator and condenser connected with a flexible hose which incorporates a flexible wick. Several models developed with working fluids such as ammonia, acetone or liquid metals and lengths up to 1 m.	Minimum temperature drop. Available technology. $Q.l_{eff} \leq 2 \times 10^3$ W.m. Heat pipe extends to the radiator.	Temperature drop increases with increased bend angle. Large radii required. Very high torque. Fatigue limits lifetime.	Limited steerability. Mainly for deployment.
HP to HP with Vacuum Interstice	Figure 15-34	A finned heat exchanger thermally couples two coaxial, independently sealed heat pipes. The interstice is open to space.	Minimum torque.	Inadequate thermal performance.	Unfeasible.
HP to HP with Low	Figure 15-34	As above but the interstice is filled with low pressure	$h_c \approx 100$ W.K^{-1}.m^{-1}.	High manufacturing	Promising.

Concept	Fig.	Description	Advantages	Drawbacks	Evaluation (1987)
Pressure He Filled Interstice		(< 7 x 103 Pa) helium gas sealed within a joint.	Acceptable performance. Low torque.	cost. Sealing problems.	
HP to HP with Low-Melting Point Alloy Interstice	Figure 15-34	As above but the intersetice is filled with a low melting point metallic material (typically NaK). Extra heating is required to melt the interstitial material.	Moderately high thermal transport. $h_c \approx 190$ W.K^{-1}.m^{-1}.	Material compatibility. Freezing. Torque uncertain. Long term material migration.	Possible fall back concept.
HP to HP with Grease Filled Interstice	Figure 15-34 Figure 15-35	As above but the interstice is filled with a grease (typically Ecotherm). Extra heating required.	$h_c \approx 120$ W.K^{-1}.m^{-1}. Acceptable torque from 0,8 to 2 N.m in the 250 K-294 K temperature range.	Outgassing. Freezing.	Promising.
Braided Solid Conductor	Figure 15-36	Flexible arrangement of foils or interwoven strands of thermal conducting materials. It thermally couples moving and fixed interfaces allowing a certain degree of rotation.	$h_c \approx 50$ W.K^{-1}.m^{-1}. Simple, inexpensive, predictable performance.	Limited rotation. High torque. Fatigue limits lifetime. Massive.	For deployment only.
Clamped Joint Contact Conductor	Figure 15-37	Thermal contact between a heat pipe and a concentric heat exchanger is enhanced by gas or hydraulic pressure against a diaphragm. Contact conductance is pressure-dependent.	Good thermal contact. $h_c \approx 4 \times 10^3$ W.K^{-1}.m^{-1} at 2 x 10^6 Pa pressure.	Complexity introduced by the gas or hydraulic pressurization system. Needs extra retracting mechanism.	No near term application. Non-steerabe. Originally developed for on orbit assembly.
Rollable Membrane Radiator	Figure 15-38	Flat array of joined flexible heat pipes that can be deployed either passively by the internal pressure or actively by springs or cords. Limited steerability can be achieved in the latter case.	Small mass. Low sensibility to meteoroid damage.	Poor state-of-the-art. Fatigue limits lifetime.	No near term application. Mainly for deployment.

NOTE   Prepared by the compiler after Delil (1987a) [31].
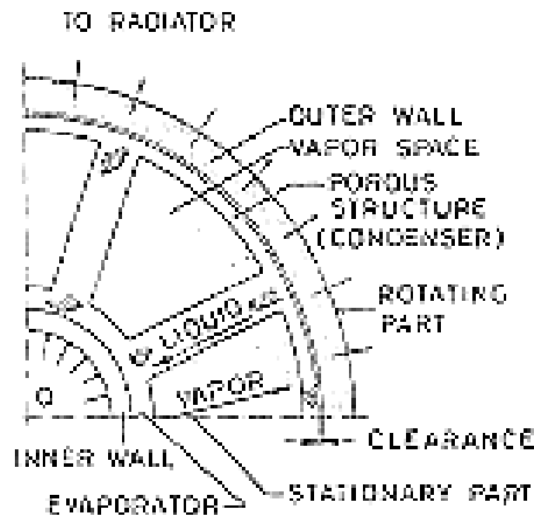
Figure 15-26: Rotatable radial flow heat pipe. From Delil (1986a) [33].
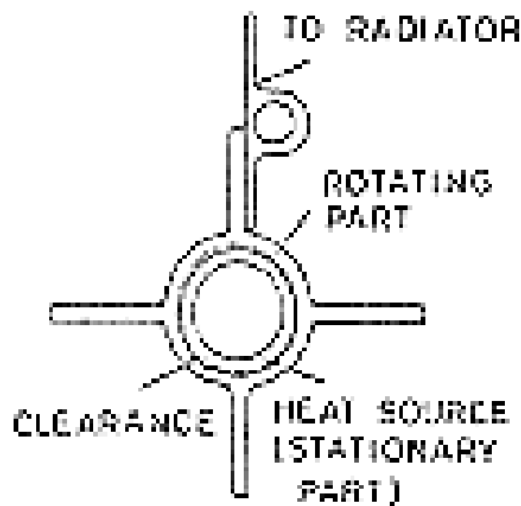
Figure 15-27: Thermal joint based on a radial flow heat pipe. From Hinderer & Savage (1978) [88].
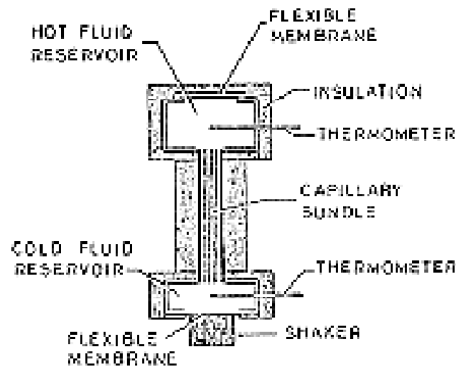
Figure 15-28: Heat transfer enhancement by flow oscillation demonstrator. From Kurzweg & Zhao (1984) [113].
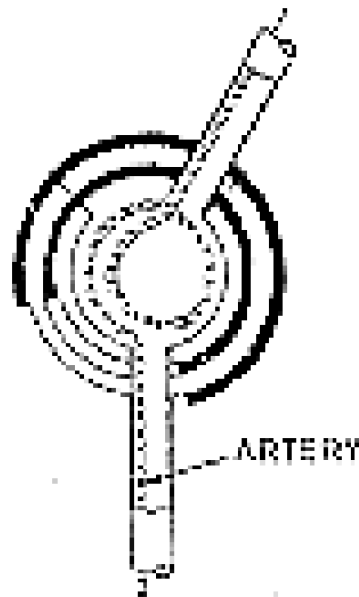
Figure 15-29: Hemispherical heat pipe junction. From Delil (1986a) [33].
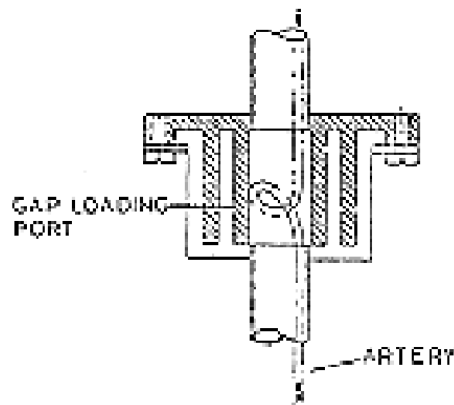
Figure 15-30: Cylindrical heat pipe junction. From Delil (1986a) [33].
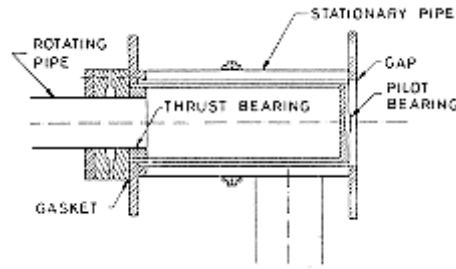
Figure 15-31: Heat pipe in heat pipe joint. This concept is an off-spring of the cylindrical heat pipe joint. From Shaubach (1985) [165].
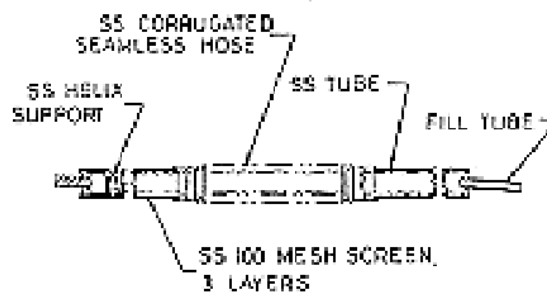
Figure 15-32: Felxible heat pipe consisting of a 0,15 m long rigid evaporator and a 0,20 m long rigid condenser. From Delil (1986)a [33].

Figure 15-33: Flexible cooper/acetone heat pipe. It features a 0,381 m long adiabatic section between an evaporator and a condenser both 0,178 m long. Inside diameter is 0,016 m. From Delil (1986a) [33].
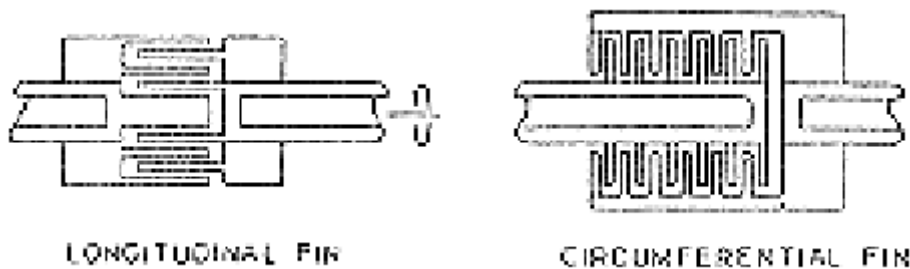
Figure 15-34: Finned heat exchangers. Interstice either vacuum-filled or filled with a gas, a low melting point or a grease. From French (1985) [68].
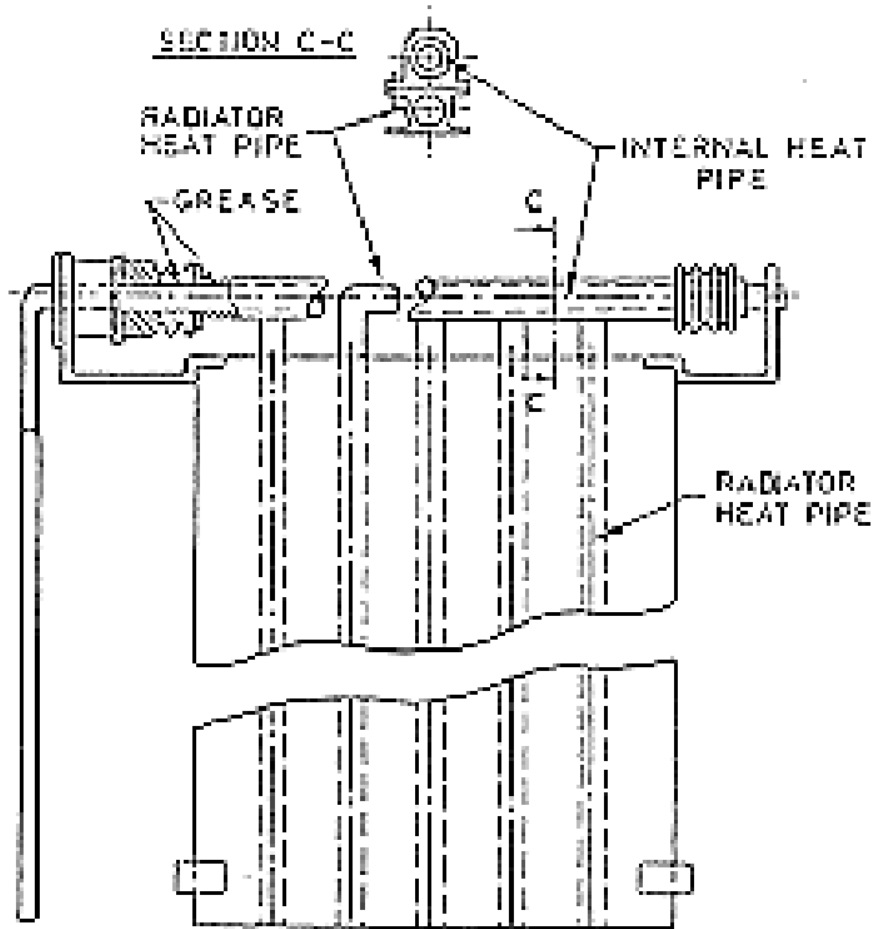
Figure 15-35: Grease-filled heat pipe-heat pipe joint. Hinge joint-coaxial with the internal heat pipe and parallel to the plane of the radiator heat pipe. From Delil (1986a) [33].
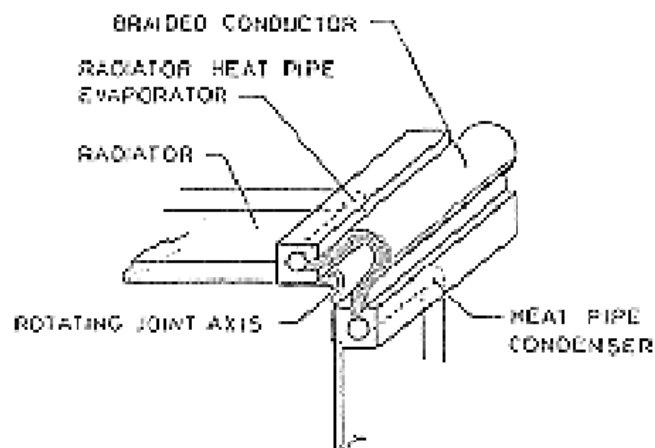
Figure 15-36: Braided conductor flexible thermal joint. From Delil (1987a) [31].
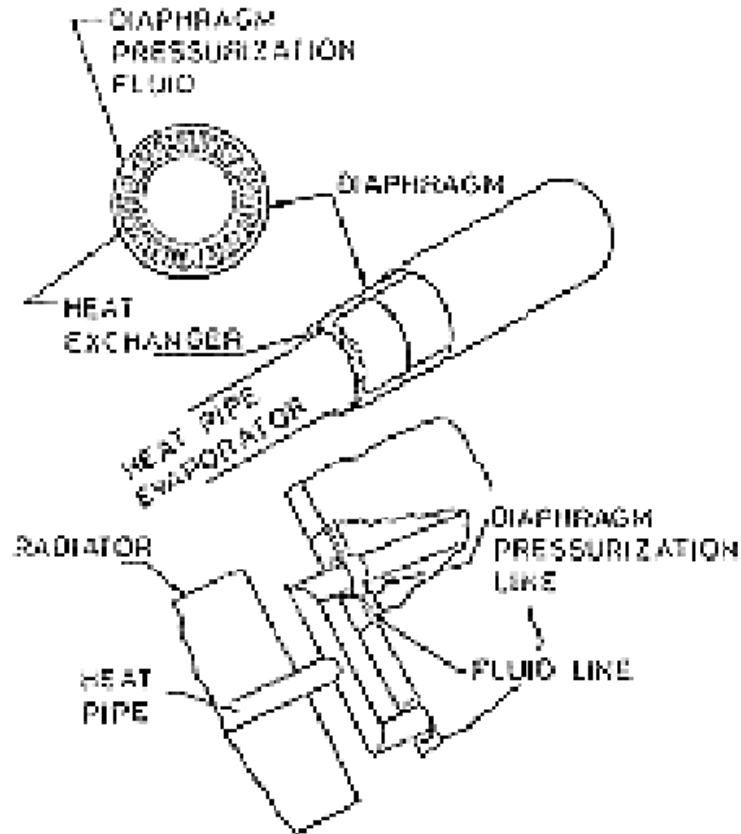
Figure 15-37: Clamped joint contact conductor. Heat pipe penetrates heat exchanger. Fluid pressure-enhanced thermal contact. From Ellis & Rankin (1983) [42].
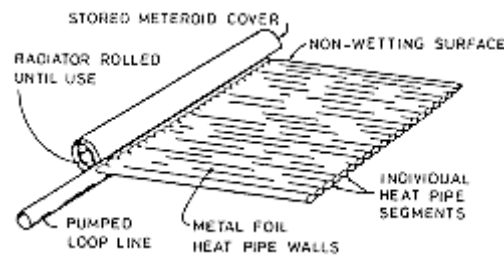
Figure 15-38: Self deployed membrane heat pipe radiator. Both deployed and undeployed configurations shown in the figure. From Delil (1986a) [33].

15.5.3.2   Rotatable fluid transfer coupling

A continuously rotatable fluid transfer mechanism to be used on board Space Station has been developed (Heizer et al. (1986) [83]). Operational, physical and life requirements for this type of rotary coupling have been summarised in Table 15-19.

The rotatable fluid transfer coupling consists, Figure 15-39, of a housing 0,56 m long and 0,20 m in diameter, made of 304 stainless steel (AISI designation: Fe-low C-0,19 Cr-0,10 Ni) and modular in construction.
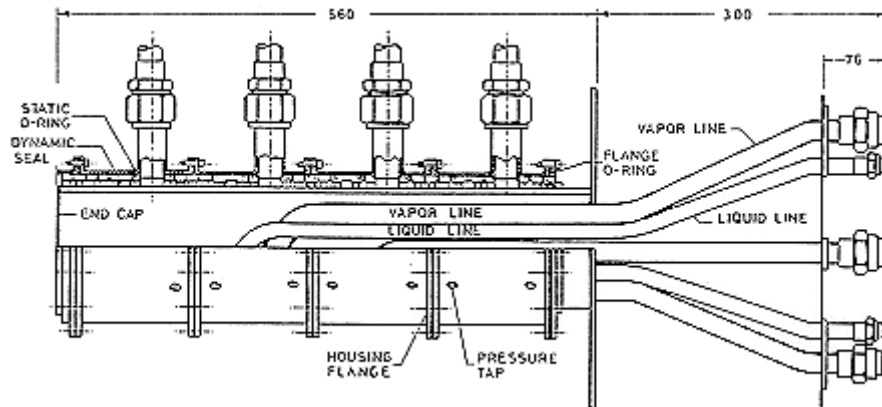
Figure 15-39: Internal details of the rotatable fluid transfer coupling. Dimensions are in mm. From Heizer, Goo, Rhodes, Thoreson & Parish (1986) [83].

Four modules, each with a fluid inlet and outlet port, are bolted together. Two modules will accommodate two refrigerant loops (at 275 K and 294 K respectively) from the main TMS, leaving the remaining two modules as backup. When one module fails the fluid is diverted to an unused module and the failed system shut down.

The aft end of the rotary coupling is sealed with an end cap to allow only one possible path to space. To prevent leakage at this point a ferrofluid low pressure (10^5 Pa) magnetic seal is used. For a description of typical ferrofluids seals see Perry (1978) [141].

The shaft is constructed in one piece of 17-4 PH stainless steel (commercial designation: Fe-0,17 Cr-0,04 Ni-0,04 Cu) with a 1-2 x 10^{-4} mm rms finish.

The overall size of the coupling is 0,86 m in length and 0,36 m in diameter. Overall mass is 50 kg.

The estimated required torque is 270 N.m.

The housing is mounted on the stationary portion of the spacecraft structure. The rotating shaft has mounting provisions that allow attachment to the rotating portion of the radiator boom.

The vapour from the heat source will enter the larger of the two radial ports (Figure 15-40a) of one active module and will flow around an annulus (Figure 15-40b) up to the inlet port of the rotating shaft. The vapour will then pass through an axial tube (Figure 15-39) out to the radiator heat exchanger.
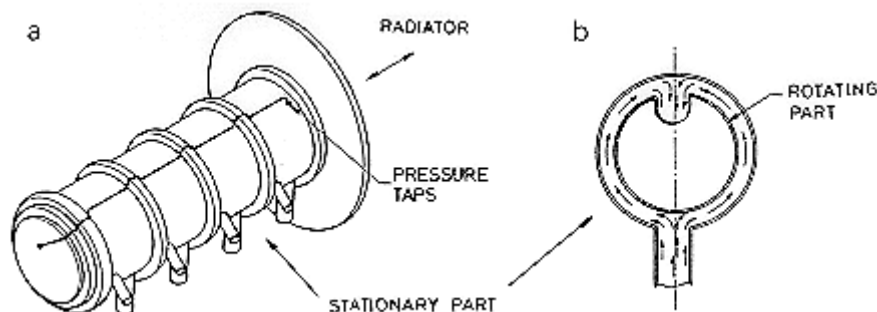
Figure 15-40: Rotatable fluid transfer coupling. a) General view showing the liquid and vapour radial ports. b) Channel geometry. From Heizer, Goo, Rhodes, Thoreson & Parish (1986) [83].

The condensate from the radiator will flow through the smaller diameter axial tube of the second active module toward the smaller port of the rotating shaft, and will flow around the annulus until it encounters the smaller diameter outer port. It then returns to the main loop. Fluid duct cross-sectional diameters are 0.016 m for the liquid line and 0.032 m for the vapour lines. These duct sizes are Space Station compatible.

Pressures losses through the ducts have been predicted at one position of the coupling shaft for a range of heat rejection rates, Q (Figure 15-41).
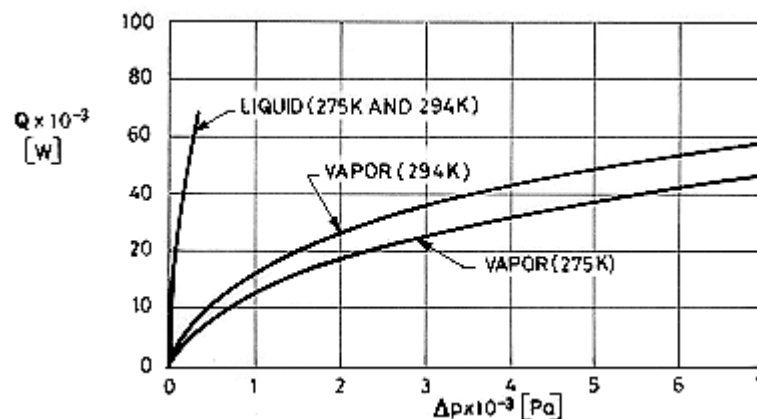
Figure 15-41: Pressure drop, Δp, along the duct at one position of the rotary coupling for different values of the heat rejection rate, Q. From Heizer, Goo, Rhodes, Thoreson & Parish (1986) [83].

This pressure drop will affect the performance of both the vapour and liquid legs of the fluid loops. In addition, assuming that the vapour is supplied to the coupling in saturated condition, the pressure loss will result in a lower saturation temperature, which will affect the required radiator area. This is not the case in the present instance where the values quoted in the reference $\Delta T \approx 0,2$ K) are really small.

A seal leakage management subsystem (SLMS) is designed to maintain the interstitial seal space at 10^5 Pa, the level of pressure the ferrofluid seal contains.

The SLMS is designed to monitor and measure seal leakage, remove leakage fluid from the interstitial seal space and store that leakage in a reservoir. It consists of (1) pressure taps to monitor the seal status; (2) a valve system to check each interstitial space and (3) a reservoir to contain the leakage.

15.5.4 Radiators coupling

East and west radiator panels of a three-axis stabilised geostationary communications satellite can be coupled, via passively controlled variable conductance heat pipes (VCHPs, see ECSS-E-HB-31-01 Part 8, clause 8.1), with the aim of sharing the heat load being radiated to space. This can be illustrated with reference to Figure 15-42a The spacecraft experiences a relative 360° diurnal rotation of the solar vector in the east/earth/west/anti-earth plane. When the solar vector is at 0° the earth facing side is directly illuminated, while the east and west sides are in shadow. As the solar vector starts rotating to the east the equivalent temperature of the space surrounding that radiator increases and that in the west radiator simultaneously decreases.
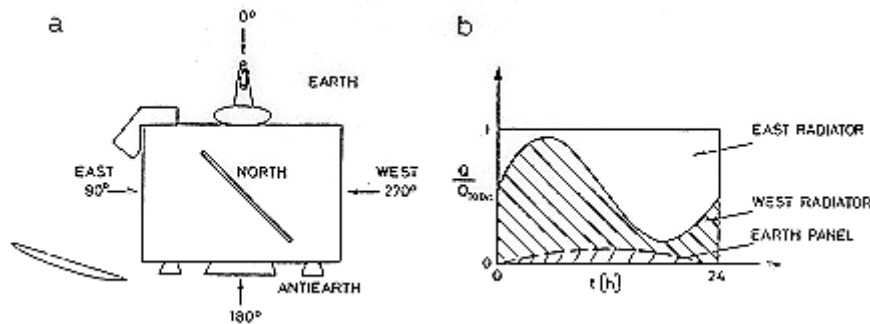
Figure 15-42: a) Schematic of a three-axis stabilized spacecraft in geosynchronous orbit. From Chalmers & Pustay (1986). b) Typical thermal load sharing of east-west faces. From Wise (1986) [192].

Both radiators are thermally coupled to the payload platform but the total heat radiated is differently shared among them (Figure 15-42b) because the VCHPs adjust to the changing environment. When the heat rejection capability of the east radiator is reduced, the source temperature increases and the heat transfer capability of west VCHPs also increases.

The limiting design case (within an orbital period) occurs when the east side is directly illuminated (at 90°) and most of the heat is rejected through the west radiator.

The remainder of the diurnal cycle produces a gradual reduction in the east radiator surrounding temperature (between 90° and 180°) as the solar vector moves towards the anti-earth spacecraft side, at which time (180°) the heat rejection rate of both east and west radiators is equalised.

The half cycle is then repeated (between 180° and 360°), this time with the west side illuminated and the east side in shadow.

The hot case corresponds to EOL winter solstice. Sufficient design margin (typically 25% in radiator area)should be allowed to accommodate this conditions.

Design optimisation of the VCHP involves:

1. Calculation of the volume ratio, i.e. reservoir volume under maximum operating conditions over inactive condenser volume in the minimum operating conditions.

2. Determination of reservoir and system mass for a specified heat pipe.

3. Assessment of the diode response of the VCHP when the sink temperature rises above the source temperature.

Detailed thermal and system-level trade analyses based on a RCA's series 4000 communication satellite with a generic payload indicate (Chalmers & Pustay (1986) [22]) that, compared with a conventional Series 4000 satellite, the variable east/west concept allows a 43% increased heat rejection rate with a 70% increase in radiator area within a cost increase of 100%.

A schematic of a spacecraft incorporating eat/west radiators coupled with VCHPs is shown in Figure 15-43 a. A second option based on Capillary Pumped Loop (CPL) systems (see clause 15.6) is introduced in Figure 15-43b
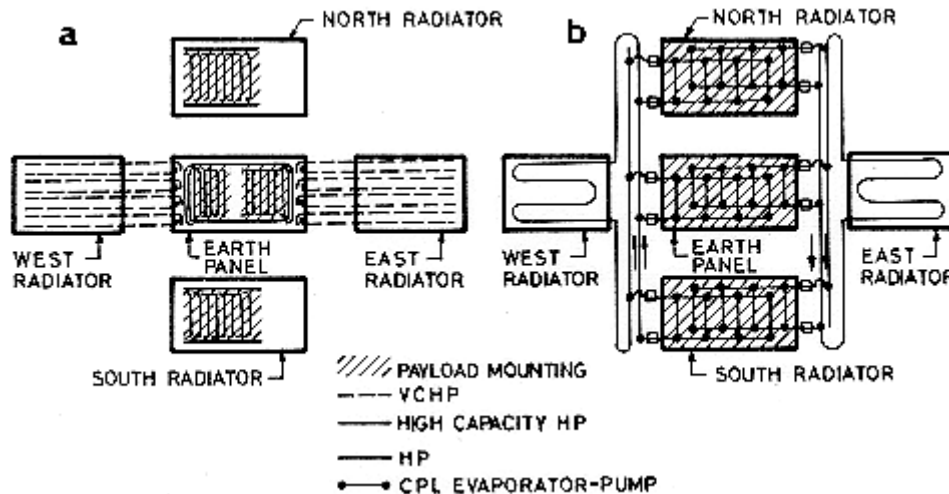
Figure 15-43: East-west radiator coupling. a) Based on HP technology. From Chalmers & Pustay (1986). b) Based on CPL technology. From Chalmers, Pustay, Moy & Kroliczek (1986) [23].

Two independent loops are used in the second concept of Figure 15-43. One loop transports payload heat to the east radiator while the second loop transports component waste heat to the west radiator. The temperature of each loop is controlled by reservoirs where fluid is kept in saturated pressure-temperature conditions (see clause 15.6.3.4). Because both loops operate independently, a Sun-illuminated radiator can be effectively shut down while the opposite radiator, viewing deep space, opens up.

Compared with HPs, CPL technology is particularly well suited to this application because of the following two reasons:

4. CPL evaporator pumps can handle much higher radial heat fluxed than conventional HPs (see clause 15.6.3.1). When component thermal dissipation increases, massive heat spreaders are required if HPs are used, and a heat flux is achieved above which the CPL is more mass-effective than the HP.

5. Heat exchangers between payload panels and radiator panels are required with HP systems. The resulting temperature drop greatly reduces the effectiveness of the radiator.

Several important design issued need to be evaluated in detail before a CPL system can be incorporated into a three-axis stabilised satellite, namely, reservoir location, start-up characteristics and one-g thermal testing.

For near term spacecraft applications, smaller CPL pumps than those being developed for the Space Station (see Figure 15-46) will be very mass-effective.

15.6 Capillary pumped loop (cpl) technology

CPL systems can be used to transfer, passively, heat loads below 10 kW over distances of the order of 10 m.

The CPL operating principle can be understood on the basis of Figure 15-44 where the same schematic loop is represented in two different situations: at low operating heat load, Figure 15-44a, and at high operating heat load, Figure 15-44b.
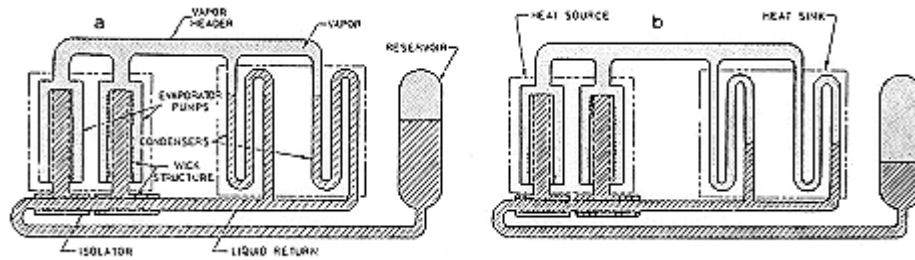
Figure 15-44: Schematic of CPL engineering model. In a) the liquid fills most of the loop, whereas in b) part of this liquid has been evaporated. From Chalmers, Pustay, Moy & Kroliczek (1986) [23].

When the evaporator-pumps are heated, the liquid from the saturated wick evaporates and flows toward the condenser where heat is removed. The condensed fluid flows again toward the evaporator-pump through a subcooled liquid return line. The wick structure in the evaporator-pump provides the required pumping, by capillary action for concurrent flow of vapour and liquid.

Wicked isolators, also sketched in Figure 15-14, isolate local failures in individual pumps preventing the deprime of a single pump from spreading to the other pumps. They also restrict the movement of any non-condensable gas into the pumps.

NASA in house, NASA sponsored and privately sponsored efforts in the field are summarised in Table 15-21.

Table 15-21: NASA development efforts in CPL technology

EXPERIMENT OR PROGRAM	MATERIALS	FEATURES	HEAT LOAD $Q \times 10^{-3}$ [W]	TRANSPORT DISTANCE L [m]	COMPLETION DATE
NASA/Lewis	Stainless steel/water	Feasibility demonstration.			1966
NASA/Goddard Ground Demonstration Eng. Model	Aluminium/Freon	Two 0,3 m pumps. Two 1,8 m conds. Eight pumps. Six condensers. Isolators.	0,35	10	Sept. 1981
CPL I Prototype	Aluminium/Ammonia[a]	As above. Welded. Thermal	6,3	10	March 1984
CPL II Prototype	Aluminium/Ammonia[a]	vacuum test.	7	10	July 1985
NASA/Goddard Flight Experiments CPL/GAS[b]	Aluminium/Ammonia	Two 0,15 m pumps.	0,2	1	June 1985
CPL/Hitchhiker[c]	Aluminium/Ammonia	Refurbished CPL/GAS	0,5	1	Jan. 1986
NASA/Goddard-Dynatherm CPL Evaporator		Two 0,3 m pumps.	3	10	1985
NASA/Goddard-RCA-OAO PCCP[d]	Aluminium/Ammonia	Four cold plates each 3×10^{-2} m². Six 0,3 m pumps. Figure 15-47.	3		July 1986
CAPL[e] Flight Experiment	Aluminium/Ammonia	Two cold plates each with 0,3 m pumps. Four condensers.	1,5	10	Late 1986
OAO Evaporator Pump		0,6 m pump.	4		Sept. 1985
HPSTM[f] - CPL		In design definition phase (1986).			Late 1986

CPL Scaling		Initiated (1986).			Late 1986
OAO IR & D[g] CPL Direct Condensation Radiator		Two 0,3 m pumps.	2 x 2,8	~ 7 m 1 x 3,6 m radiator	Jan. 1985

[a] 10^{-5} m Porex Wick Structure. Porous plastic wick (high density polyethylene).

[b]   GAS: Get Away Special. Experiment flown on Shuttle Flight STS-51G in June 1985.

[c]   Hitchhiker-G. Experiment flown on Shuttle Flight STS-61C in January 1986.

[d]   PCCP: Prototype Capillary Cold Plates.

[e]   CAPL: Capillary Pumped Heat Transport Loop. Shuttle mounted flight experiment.

[f]   HPSTM: High Power Spacecraft Thermal Management.

[g]   IR & D: Internal Research and Development.

NOTE   From Chalmers, Pustay, Moy & Kroliczek (1986) [23].

15.6.1 Advantages of cpl systems

CPL technology represents a potentially powerful tool for thermal control of high power spacecraft when high component reliability is required. The more quoted advantages of these systems are:

1. Passive operation.

2. Minimum power requirements. Electrical heating may be required for start-up by heating one of the evaporator-pump and for thermal control of the reservoir (saturated temperature-pressure controlled).

3. Heat is transferred directly to the vaporising surface.

4. Pumping action is self adjusted to the heat load.

5. Inherent two-phase liquid vapour separation.

6. Isolated evaporator wicks are insensitive to small non-condensable gas or vapour bubbles.

7. Heat loads can be shared among individual capillary pumps. Typically heat load sharing of up to 90% of applied load.

8. Easily expandable. Pumps can be added in parallel to reach large heat transport capabilities.

9. Readily configurable to other uses (see Figure 15-43b for CPL technology radiators).

10. Processing and testing can be based on available heat pipe technology standards.

15.6.2 CPL performance constraints

Performance constraints of CPL systems result from their capillary pumping action. Main limitations are listed below.

1. Heat transport capabilities limited to about 7 kW (at 300 K) for 10 m distances. Individual evaporator-pump capability near 2 kW.

2. Power densities limited to about 26×10^4 W.m^{-2}. This is, however, a fairly large value, compare for example with clause 11.7.

3. Capillary pumping limit of the order of $3,2 \times 10^3$ Pa (for 10^{-5} m Porex wicks and Ammonia at 293 K).

4. Precautions of pressure containment when Ammonia is used (Ammonia is appropriate at temperatures around 300 K).

5. CPLs are not as isothermal as mechanically pumped two-phase flow systems.

6. Reservoir size and performance under reduced gravity operation could be critical if upsizing is considered.

15.6.3 CPL basic system concept

On the basis of the experience derived from existing CPL breadboard and engineering models listed in Table 15-21, a typical CPL system is shown in Figure 15-45. It consists of four main subsystems namely: heat acquisition, heat transport, heat rejection and controls.
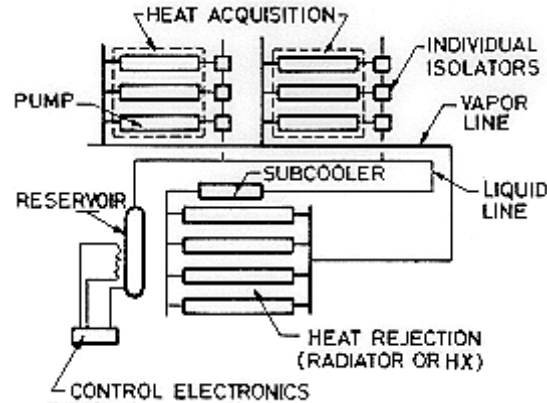
Figure 15-45: Schematic of a basic CPL system. From Chalmers, Pustary, Moy & Kroliczek (1986) [23].

15.6.3.1 Heat acquisition

Figure 15-46 shows a standard evaporator pump 3×10^{-2} m in diameter and 0,3 m long. Figure 15-46b indicates how the heat is transferred directly to the evaporating surface in contrast with other systems. This significant feature of the CPL systems, already mentioned in clause 15.6.2, is the reason why CPL evaporator pumps can handle much higher radial heat fluxes than, f.i., conventional heat pipes.
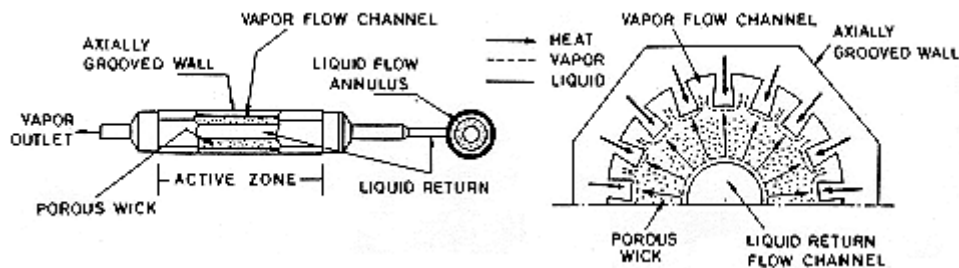
Figure 15-46: a) Standard CPL evaporator pump. From Chalmers et al. (1986) [23]. b) Heat flow in a cross section of a typical CPL evaporator. From Wise (1986) [192].

Heat transfer from the heat source to the evaporator takes place through a standard mounting plate to which a bunch of pumps in parallel are metallurgical bonded. Figure 15-47 shows the payload mounting plate developed in the PCCP program (Table 15-21) for the NASA Thermal Test Bed. More mass-optimised and system-compatible capillary cold plates are also under development. Two of them, which use capillary forces to distribute the liquid over the evaporating-condensing surface, are presented in clause 15.7.1.
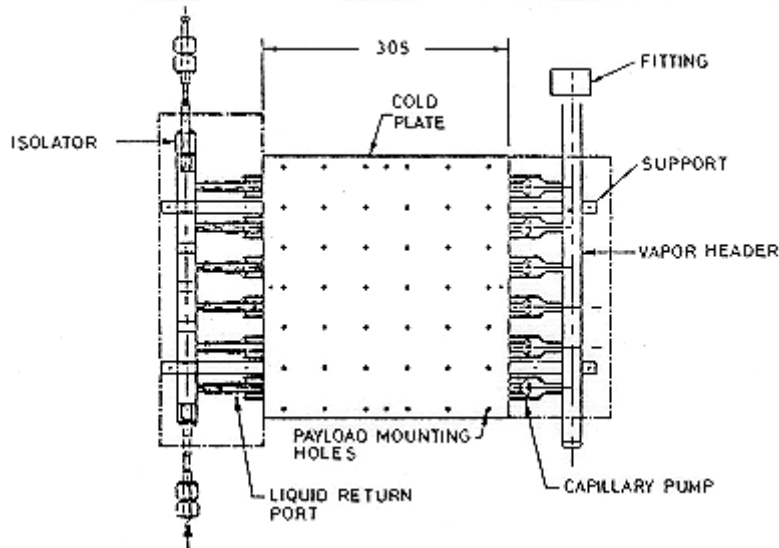
Figure 15-47: Prototype capillary cold plate (PCCP) design. Dimension in mm. From Chalmers, Pustay, Moy & Kroliczek (1986) [23].

15.6.3.2 Heat transport

The ducts connecting evaporator to condenser are smooth walled tubes selected on the basis of minimum pressure loss. As a general rule, lines are devised so that total pressure loss does not exceed 10% of the capillary pumping limit. This indicates that valves, fittings, flowmeters and pressure transducers in the lines should also be designed for minimum pressure loss.

Line diameters are chosen by means of a trade between minimum system mass and minimum pressure loss. Strategies to minimise the total mass of a two-phase fluid loop subject to a general loop pressure loss constraint have been formulated (Schember (1986) [156]).

15.6.3.3 Heat rejection

Condenser-Radiator. Several condenser designs should be used depending on the system application.

Figure 15-48 shows a Direct Condensation Radiator (DCR) where the condenser tubes are directly attached to a radiator. This in turn can be separated into different elements which can operate independently enabling modular addition or removal.
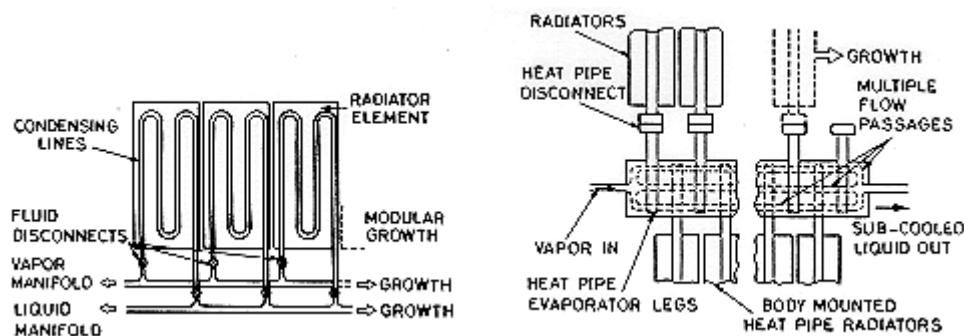
Figure 15-48: CPL technology radiators. a) Direct condensation radiator. b) Heat exchanger-heat pipe radiator. From Chalmers, Pustay, Moy & Kroliczek (1985) [23].

In the second type of radiator, heat from the system fluid is transferred through an interface heat exchanger to a number of independent heat pipes so that failure of one of them only influences a single section of the radiator. The interface heat exchanger results in a reduced radiator operating temperature and thence, in an increased radiator mass. Whether or not this added mass is balanced with the reduction in the required meteoroid protection depends on the mission.

15.6.3.4   Controls

Temperature control of the CPL systems is accomplished via a reservoir where fluid is kept in saturated pressure-temperature conditions. Temperature control of this reservoir is achieved by thermostatically controlled electrical heaters and by radiation to outer space.

Liquid acquisition baffles and a central wick structure in the reservoir serve as liquid flow conducts to the reservoir line, which is connected to the rest of the CPL system. Volume requirements are at present modest but could result in development needs for large volume systems.

Electrical heating could be also required for starting up the pumps. A minimum amount of power has to be supplied to an evaporator to ensure fluid flow in the system.

15.7   Components

This clause is intended to introduce the main components of a two-phase thermal transport system. The content of this clause is quite open at this writing.

15.7.1   Pumping systems

The pumping system furnishes the power required for fluid motion.

Power requirements have been discussed in Clause 7, regarding classical single-phase fluid loops and in Clause 10, for two-phase systems.

Different pumping systems have been or currently are being considered under various NASA contracts. A brief description of these systems follows, which is closed by a summary in Table 15-22, clause 15.7.1.6.

15.7.1.1   Monogroove heat pipe

This heat pipe (Alario, Haslett & Kosson (1981) [1]) consists of two parallel ducts, one for liquid and one for vapour, connected by a small monogroove slot, Figure 15-49. Since the two fluids flow independently, pressure losses are minimised. The small slot separating the channels creates a high capillary pressure difference which, coupled with the minimal flow resistance of the two separate channels, gives the high axial heat transport. The probability of liquid becoming entrained in the vapour is minimal.
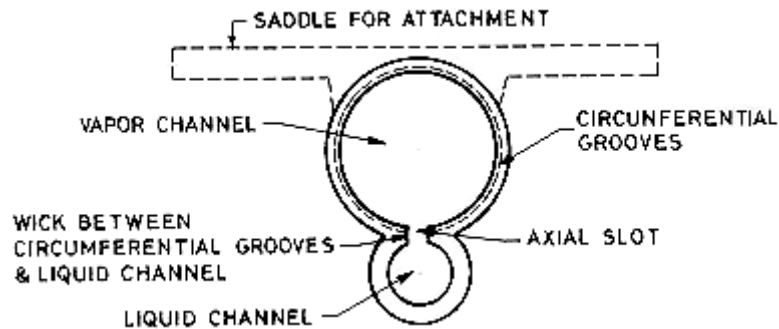
Figure 15-49: Monogroove heat pipe. From Alario, Haslett & Kosson (1981) [1].

Preliminary tests indicate that a heat transport factor (Ql_{eff}) of 25000 W.m can be achieved.

Initially the monogroove heat pipe was devised to provide both heat transport and pumping. This idea was dropped due to the wall wicking limitation of the heat pipe in the temperature range of interest, so that at present the monogroove heat pipe is considered as a purely pumping system.

15.7.1.2   Capillary pump

See clause 15.6.

15.7.1.3   Vapour compressor

See clause 15.5.1. This is the concept requiring the greatest amount of external power among the six pumping devices under consideration.

15.7.1.4   Mechanical pump

Usually the pump is placed in the liquid portion of the system (see Figure 15-2) and from this point of view it does not differ from the pumps introduced in Clause 8. The major difference is that now the power requirements are drastically reduced because the mass flow rate for a given heat load is much smaller when the heat is transferred by phase change than by sensible heat of the liquid (compare Concepts III and IV, in clause 15.2.2). Although this represents a significant advantage, the addition of a mechanical pump results in an overall reduction in system reliability and an increase in total system mass. The largest portion of this increase occurs as a result of the large surface area required for the radiator and is not associate to the pump itself. In addition, provisions for active control of the flow rate should be taken.

15.7.1.5   Osmotic pump

When two fluids, a solvent-solute mixture and a pure solvent are separated by a semi permeable membrane (impermeable to the solute), the solvent will flow through the membrane to attain equilibrium and this motion will persist as long as solute concentration gradients are high.

This osmotic effect can create pressure differences orders of magnitude greater than the capillary action in conventional heat pipe wicks.

The solvent is the working (heat transfer) fluid which will be evaporated at the cold plate, leaving behind the solute. From the evaporator the vapour solvent flows toward the condenser, reaching again the membrane as a liquid, Figure 15-50.
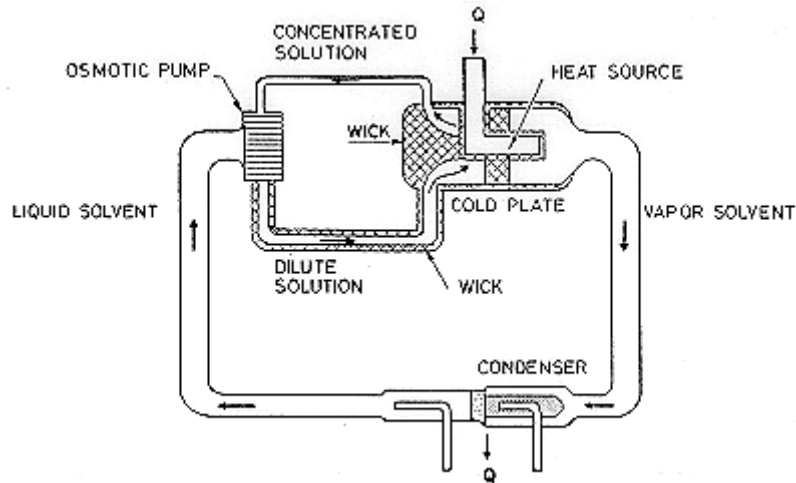
Figure 15-50: Osmotically pumped heat transfer system. From Tanzer, Fleischman & Stalmach (1982) [175].

A wick structure is employed in the cold plate to prevent solute from being carried over with the solvent vapour, which would contaminate the system.

Under normal gravity conditions the concentrated solution will flow toward the membrane by gravity action in order to increase the solute concentration in its vicinity, with the aim of promoting enhanced osmotic pressure. Some solution circulation method should be devised to perform the same operation under reduced gravity (Peterson (1987) [142]).

Osmotic pumping presents several major drawbacks. On one side, the pumping rate does not depend on the heat load and, thence, an additional control is required as in mechanical pumps. On the other side, water, which is the solvent used for testing, does not fit the temperature range of interest. Finally, available membranes are incapable of sustained operation at temperatures above 350 K.

15.7.1.6 Biomorph pump

It is a deformable-wall (peristaltic) pump. The wall consists of two layers of ferroelectric crystals or ceramic materials which have been bonded together, Figure 15-51.
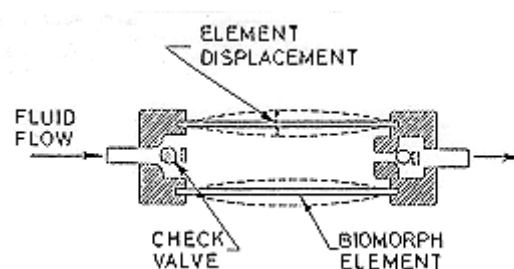
Figure 15-51: Biomorph (Biomorph) pump. From Peterson (1987) [142].

The two deformable elements are attached to separate electrical leads. When an AC potential is applied across the leads, the internal stresses (piezoelectric effect) results in repeated flexing of the walls, which combined with appropriate valve motion produce a pumping action.

Control of the mass flow rate is also required in this case but it can be easily achieved through a variation in either voltage or frequency.

This type of pump is still in its development stage. Its reliability has not yet been assessed.

Table 15-22 below presents a summary of the Pumping Systems which have been described above.

Table 15-22: Comparative Summary of Pumping Systems

Criteria	Monogroove Heat Pipe	Capillary Pump	Vapor Compressor	Mechanical Pump	Osmotic Pump	Biomorph Pump
External Power Required	None	None	Large	Small	Small	Small
Priming Limitations	Severe	Severe	None	None	Minimal	Minimal
Control Necessary	Unknown	Minimal	Considerable	Considerable [a] Moderate [b]	Unknown	Unknown
Accept and Reject Heat	No	No	Yes	Yes	Yes	Yes
Life Expectancy	Unknown	Excellent	Fair	Good [c]	Poor [c]	Poor [c]
Technology Level	Unknown	Adequate	Good	Excellent	Poor [c]	Poor [c]
System Complexity	Not feasible	Minimal	Complex	Fair	Complex [c]	Complex [c]

[a] Pump assisted.

[b] Pumped two-phase.

[c] At current state-of-the-art.

NOTE   From Peterson (1987) [142].

15.7.2   Mounting plates

The interface between a dedicated instrument or payload component and the TMS could be: a) A cold plate mounting surface in thermal contact with the TMS fluid. b) A fluid diversion of the TMS which internally or externally contacts the instrument to be cooled. c) A shroud or container enclosing one or more instruments and in thermal contact with the TMS. And d) an independent thermal control system in thermal contact with a local or remote cold plate. See sketches in Figure 15-52.
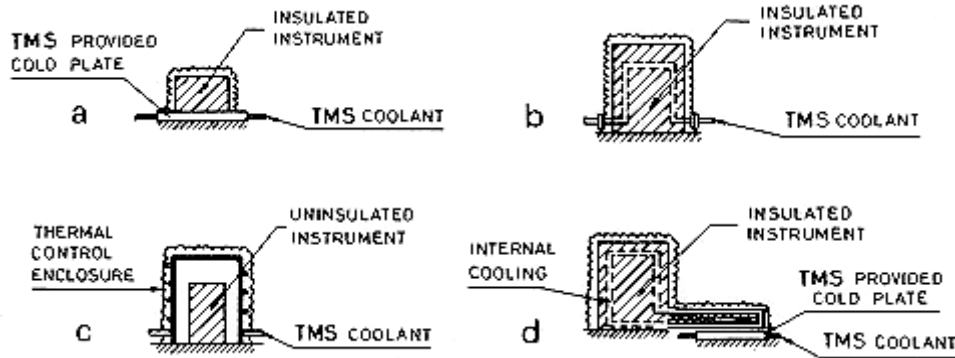
Figure 15-52: Instrument-TMS interfaces. From Almgren et al. (1981) [2].

A significant design parameter of the TMS is the thermal resistance between the instrument for which operating temperature limits have been set and the TMS fluid. If this resistance is large, the temperature difference will be large and this could force lowering the fluid loop temperature level of the TMS for a fixed level in the instrument.

A standard mounting plate based on CPL technology has been introduced in Figure 15-47, clause 15.6.3.1. Two different capillary plates, which are being investigated, are described in the following.

The model in Figure 15-53, which is purely conceptual, exhibits a grooved cold plate/hot plate which can operate as an evaporator or as a condenser. This model has been used in an analytical study aiming at the optimisation of the evaporator groove geometry. In the evaporator (cold plate) mode of operation the condensate flows by capillary action from a liquid reservoir through a communication (bridging) wick. The resulting vapour flows out of the cold plate to a separate condenser where the heat is rejected. The reservoir is replenished at intervals from a valved external liquid supply line.
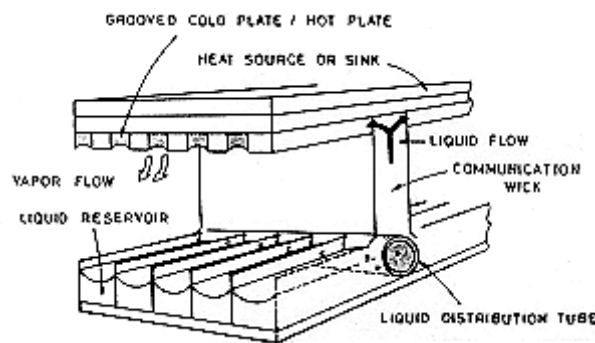
Figure 15-53: Schematic of a grooved cold plate/hot plate in the cold plate mode. From Hwangbo & McEver (1985) [94].

In the condenser (hot plate) mode of operation, heat is delivered to the heat sink by condensation of vapours from the vapour line. As liquid builds up in the capillary grooves it is carried to the reservoir where it is periodically removed by a condensate return line.

Results of an analytical study performed by Hwangbo & McEver (1985) [94] anticipate heat fluxes as large as 9×10^4 W.m^{-2}.

The mounting plate sketched in Figure 15-54 is being developed by McDonnell Douglas under NASA contract. Again it can operate either in the evaporator mode or in the condenser mode. In the evaporator mode liquid is pumped through a system of six feed tubes. Each tube has an interface wick inserted into a slot and kept in contact with the grooved face of the heated surface. The liquid in the

feed tube is drawn by the capillary action of the grooved surface. Only the amount of flow needed to transfer the heat load is pulled through the wick. The excess liquid flows out the end of the exit tube where it mixes with the vapour and exits the mounting plate. Because of this flow-through design, the plate can operate within a wide range of flow rates and flow qualities.
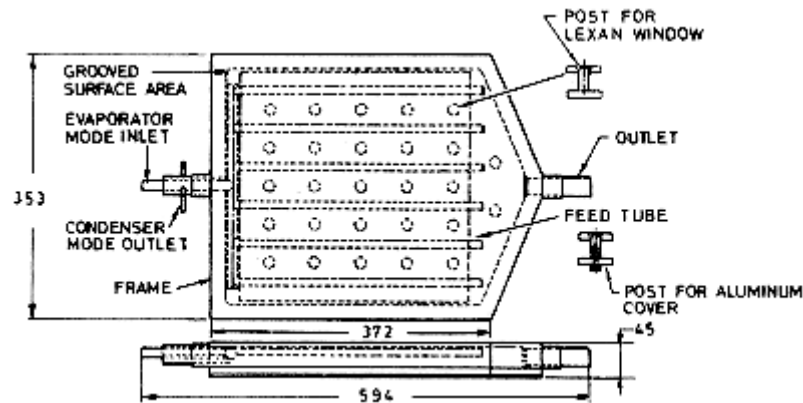
Figure 15-54: Two-Phase Mounting Plate (TPMP) development unit. The Lexan window has been incorporated to observe the flow during testing. All dimensions are in mm. From Grote & Swanson (1985) [77].

In the condenser mode of operation the feed tube inlet manifold is closed and the two-phase fluid enters through the evaporator mode exit. The vapour condensed and the condensate flows into the annular region of the evaporator mode inlet fittings, and exits through one of the two tubes that are at right angles to the fittings.

The unit was designed to operate either with Freon-11 or Ammonia, but testing was conducted with Freon-11.

The mounting plate was tested in the evaporator mode for total heat loads over 3×10^3 W and local heat fluxes over 4×10^4 W.m^{-2}. In the condenser mode the heat loads were in the 60 W - 400 W range.

15.7.3   Vapour quality sensors

Sensors, control logic and actuators are incorporated at different locations on the TMS to adjust pumping speed, working fluid reservoir content, throughput of valves, ... These sensors could be: flowmeters, pressure and temperature gages and, within the present context, vapour quality sensors.

Vapour quality sensors can be implemented, f.i., at the cold plate exit for monitoring the liquid flow rate and, thus preventing evaporator dry-out and controlling the flooding.

The vapour quality, w, is deduced from the void fraction, α, once the pressure, temperature, and liquid and vapour flow regimes (v or t) are known, see clause 14.2.1, Eqs. [14-8] and [14-11]. This requires temperature monitoring plus flow patterns identification(possibly through flow calibration). Pressure, on the other hand, varies slowly.

A wide variety of techniques are available for two-phase flow diagnosis. However, several among the proven techniques and certain on-the-shelf instrumentation cannot be applied on board orbital platforms; either they do not meet the strict safety requirements for manned platforms, they are very massive or depend on gravity for their performance. For a complete review of the subject see Hewitt (1982b) [87], where a chart for the selection of the most appropriate technique is given.

Similar negative conclusions were reached by Delil (1986b) [30] after confronting fourteen candidate methods for measuring the void fraction against the following requirements:

1. Simple, flexible and low system impact.

2. Small mass, size and power consumptions.

3. Safe and non-hazardous to man.

4. Fast response.

5. Accurate within a wide quality range up to vapour quality values exceeding w = 0,8.

6. Highly sensitive to quality variations.

7. Suited to the working fluid (Freon, Ammonia, ...)

8. Non contaminating the loop and long-term reliable.

9. Slightly disturbing the flow.

10. Testable under both normal and reduced gravity.

11. Low cost.

12. Low development risk.

Electrical impedance methods are apparently worth of further consideration although they are not very sensitive to the fluid flow pattern.

The electrical impedance of a two-phase flow depends on the concentration and distribution of the phases, and the use of impedance measurement is attractive because it gives a virtually instantaneous response. Depending on the frequency of the system the impedance will be governed by the conductance (low frequency), capacitance (high frequency) or both. Although conductance methods are easier to use (see f.i. Gao, Zhou & Chen (1985) [70]), capacitance methods are often preferred because the liquid dielectric permittivity varies less with temperature than does the liquid electrical conductivity.

15.7.3.2 Capacitance methods

Capacitance methods are based on the difference in relative permittivity, $\varepsilon/\varepsilon_0$, between a liquid and a gas. ε_0 is the vacuum permittivity and ε that of the (dielectric) material under consideration.

The electrical capacitance, C, of a parallel plate capacitor, plate area, A, distance, d, between plates and permittivity, ε, of the interstitial material is:

$$c = \frac{sA}{d} \qquad\qquad [15\text{-}4]$$

Slightly different expressions should be used for different capacitor geometries, but the above equation suffices for illustrative purposes.

Estimating the electrical capacitance of a two-phase fluid dielectric between suitable plates is not simple. For a given steady, two-phase configuration and assuming that dynamic currents are absent, Electrostatics allows the calculation of the electric field intensity from which the internal energy, u, of the capacitor can be expressed (Sommerfeld (1952))

$$u = \frac{1}{2}\int_V sE^2 dv = \frac{1}{2}C\left[\int_V \psi ds\right]^2 \qquad\qquad [15\text{-}5]$$

where the first integral is extended over the dielectric volume and the second over its surface. ψ is the electric potential and $E = -\nabla \psi$. The assumption is usually made that free and polar charges are absent from the fluid in which case $\nabla \cdot E = 0$, and since $\nabla \wedge E = 0$, the resulting differential equation is of Laplace type for the electric potential ψ, $\Delta \psi = 0$, but this equation must be solved with the appropriate boundary conditions at the duct walls and/or capacitor plates, plus jump conditions at the (supposedly known) liquid-vapour interfaces. This extraordinarily difficult the calculation of the capacitance, C, of a two-phase medium, which will only furnish an unequivocal result when the geometry of the flow pattern can be defined by one single characteristic length, as in the annular flow case.

In many instances the problem is circumvented by use of an in-parallel-type expression for the effective permittivity, ε_{TP}, of the fluid (Delil (1986b) [30])

$$s_{TP} = \frac{1}{\dfrac{\alpha}{s_G} + \dfrac{1-\alpha}{s_L}} \qquad\qquad [15\text{-}6]$$

Other expressions for homogeneous dispersions of gas bubbles in the liquid, and for liquid droplets dispersed in a gas, again characterised by a single length, can be found in Hewitt (1982b) [87].

Four types of capacitors have been sketched in Figure 15-55, three radial electric field capacitors (single coaxial capacitor, concave plate capacitor and double helix capacitor) plus an axial field capacitor (film thickness gage).
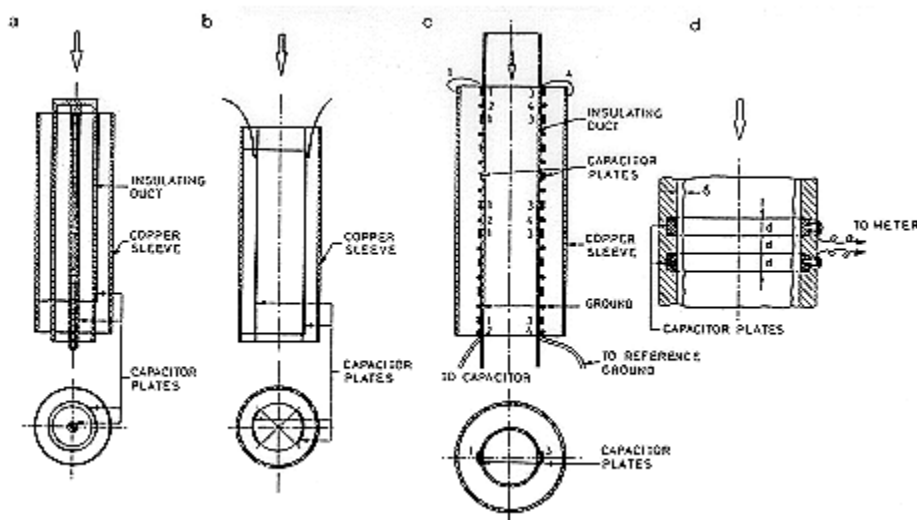
Figure 15-55: Void fraction sensors of the capacitance type. a) Single coaxial capacitor. b) Concave plate capacitor. c) Double helix capacitor. d) Film thickness gage. From Delil (1986b) [30].

The first three types are intrusive and then will result in a pressure loss in the duct. Although the concave plate and double helix type capacitors could be incorporated in the duct wall, the duct diameter will then determine the "interplate distance", d, presumably reducing the sensitivity. Only the film thickness gage can be easily mounted flush with the wall duct without compromising the optimum distance, d.

The coaxial and concave plate capacitors can be used only in axisymmetrical flow (either homogeneous or annular). The double helix capacitor is sensitive to any steady flow because of the averaging effect of the helix electrodes. The film thickness gage can be used only with annular flows.

Information on the sensitivities of the different systems has been collected in Figure 15-56 and Figure 15-57, which show some dimensionless functions of the measured capacitance, C, versus the void fraction, α, or the dimensionless film thickness, δ/d.
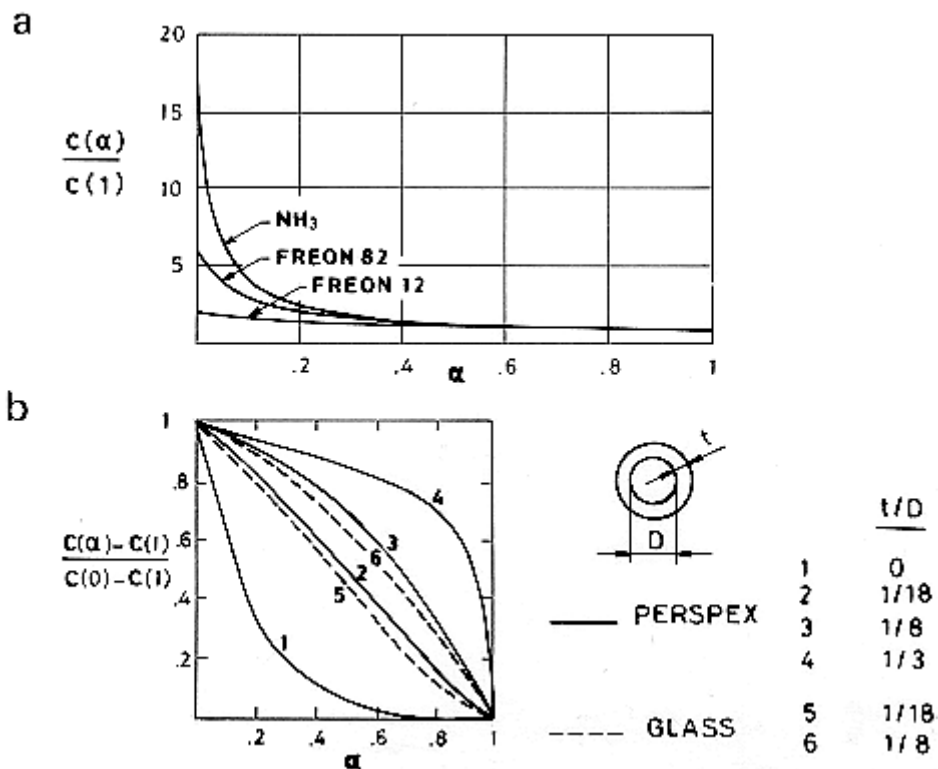
Figure 15-56: Dimensionless capacitance as a function of void fraction, α. a) Annular flow, single coaxial capacitor. b) Annular flow, concave plate capacitor. From Delil (1986b) [30].
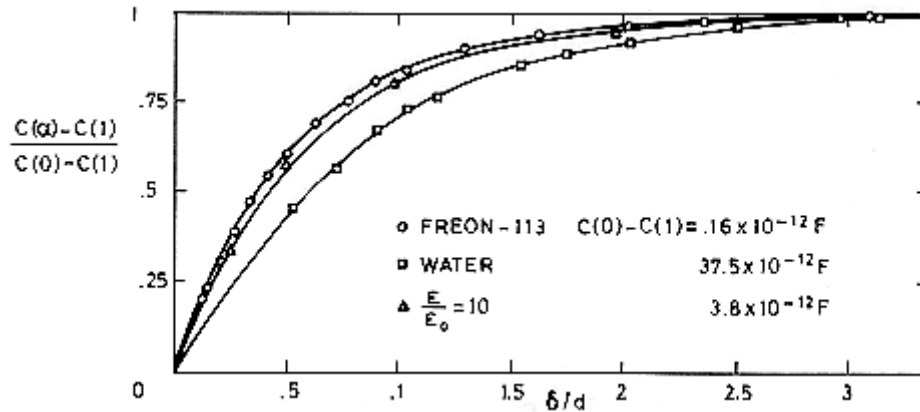
Figure 15-57: Dimensionless capacitance as a function of dimensionless film thickness, δ/d. Flat wall, film thickness gage. From Delil (1986b) [30].

This information can be summarised as follows:

1. No reliable fast response method exists for measuring the void fraction in slug flow (Figure 14-1, Figure 14-2, in clause 14.1) because of its unsteadiness. This does not represent a major difficulty here since this type of flow will not appear in TMSs, which are characterised by high vapour quality flows ($\alpha \approx 1$) and reduced gravity operation.

2. The sensitivity of the single coaxial capacitor to α changes in the high void fraction side is poor, Figure 15-56a

3. The concave plate (and also the double helix) capacitor exhibits good performance figures for annular flow, Figure 15-56b Unfortunately, the absolute capacitance level and the sensitivity are too poor for the high void fractions foreseen in the TMS.

4. the film thickness gage is well suited to annular, high-α flow because of its sensitivity, Figure 15-57. The signal could be enhanced by optimising the geometry.

The feasibility of a film thickness gage has been demonstrated (Delil (1987b) [32]). The breadboard model is based on a two-strip planar configuration. The distance, d, between strips is approximately equal to the anticipated liquid film thickness, δ. Plastic sheets were used to represent the liquid. The implementation of more realistic tests does not face insurmountable difficulties.

15.7.4 Fluid disconnects

A fluid disconnect is an important component of a TMS and has been incorporated in many systems where maintenance or reconfiguration must be quickly effected without the accompanying necessity for depressurization.

The requirements of these devices should be minimal pressure drop when fully engaged and minimal spillage during disengagement, low mass, reliability and ease of employment (one-hand or remote arm manipulation under reduced gravity).

Of the several available designs, the Rotary Shutoff (RSO) Disconnect, manufactured by MOOG Inc. East Aurora, New York, seems to meet the above requirements.

The RSO disconnect utilises, instead of traditional poppets, spherical valving elements to open and close the flow orifice. The design can incorporate a wide variety of materials. While stainless steel and aluminium have been used to date, titanium, plastics and composites could be employed without altering the design and degrading its characteristics.

Once the disconnect is engaged, the flow path is unobstructed, which allows the placement in series of several of these devices without affecting the pressure loss. During disengagement the spillage is less than 10^{-6} m³ and an optional ability to purge the device can reduce spillage to virtually zero.

The engagement sequence of the RSO disconnect is summarised in Figure 15-58.
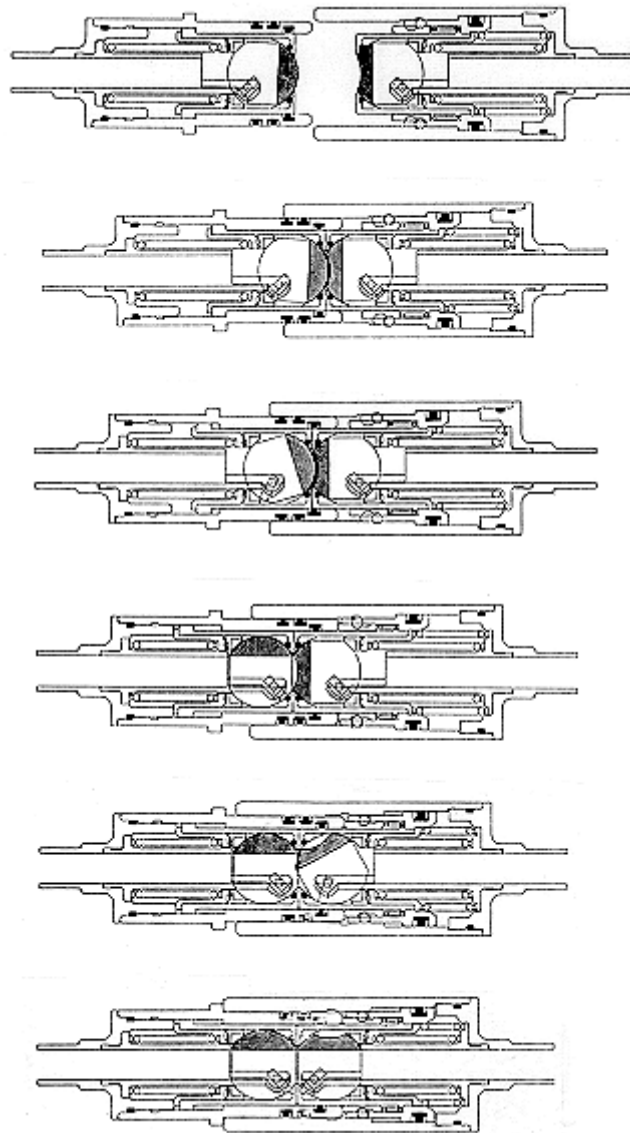
Figure 15-58: Engagement sequence of the RSO disconnect. Disengagement is achieved through the reverse sequence. From MOOG [127].

16
Control technology

16.1 Basic definitions

In this clause, terminology commonly used in this clause about control systems is defined.

Actuating signal: A signal used to influence in the plant in feedback control systems.

Analog signal: A signal defined over a continuous range of time whose amplitude can assume a continuous range of values.

Analog–to–Digital Converter (A/D): A device (also called an encoder) which converts an analog signal into a digital signal.

Analog transducer: A transducer in which the input and output signals are continuous functions of time.

Automatic regulation system: A feedback–controlled system in which the reference input and the desired output are constant or change slowly in time. The main task is to maintain the output at a desired level, independently of existing disturbances.

Continuous–time signal: A signal defined over a continuous range of time.

Control system of process: An automatic regulation system where the output is a variable as temperature, pressure flow, liquid level or pH.

Decoder: See Digital–to–Analog Converter.

Digital control system: A control system in which a digital computer is encharged of the signal processing.

Digital signal: A discrete-time signal with quantized amplitude.

Digital–to–Analog Converter (D/A): A device (also called a decoder) which converts a digital signal into an analog signal.

Digital transducer: A transducer in which the input and output signals occur only at discrete instants of time and the signal magnitudes are quantized.

Discrete–time signal: A signal defined only at discrete instants of time.

Encoder: See Analog–to–DiGgital Converter

Error: Signal resulting from the difference between the actual output and the desired state.

Feedback control: An operation which, in the presence of disturbances, tends to reduce the difference existing between the output and the reference input of a system (or a desired state, randomly varied) and it does it based on that difference.

Gain: The gain of a system is the output-input ratio of it.

Perturbation: An irregularity which affects a signal, and deteriorates the system output. Perturbations generated inside the system are known as internal perturbations. Those proceeding from outside can be considered as inputs for the system.

Plant: In control systems, plant means the apparatus or equipment for a certain physical operation that has to be controlled.

Process: A continuing development involving many changes, which is going to be controlled. A process can be chemical, physical, mechanical, economical, biological, ...

Sample–and–Hold (S/H): "Sample–and–hold" is a general term used for a sample–and–hold amplifier. It describes a circuit that receives an analog input signal and holds this signal at a constant value for a specified period of time.

Sampled–data transducer: A transducer in which the input and output signals occur only at discrete instants of time (usually periodic), and the magnitudes of the signals, as in the case of the analog transducer, are unquantized.

Servomechanism: A feedback–controlled system in which the output is a mechanical variable, as position, velocity or acceleration.

Stability: The notion that describes whether the system will be able to follow the input command. In a nonrigurous manner, a system is said to be unstable if its output is out of control or increases without bound.

System: A set or arrangement of components related or connected as to form a unit performing a specific task. A system is not constrained to achieve physical objectives. This concept can be applied to abstract and dynamic phenomena, as in economy. Therefore, the term system has to be understood regarding physical, biological, economical, ...

System with feedback control: A system which tends to maintain a preset ratio between the output and the reference input, by comparing both signals and using the difference between them as the control parameter.

Transducer: A device which converts an input signal into an output signal of another form, such as a device that converts a pressure signal into a voltage output.

16.2 General description of control systems

16.2.1 Introduction

The purpose of this clause is to introduce the different types of control systems. A typical classification is:

- Closed-loop control systems.

- Open-loop control systems.

- Adaptive control systems.

- Learning control systems.

First, these types of control systems are described and after that the most used types, closed-loop and open-loop, are compared.

16.2.2 Closed-loop control systems

A closed-loop control system is that in which the output signal affects directly the control action.

Thus, a closed-loop control system is a feedback-controlled system. The actuating signal, u, is a function of the feedback signal (which is a function of the output signal or variable to be controlled) and of the reference input.

The block diagram of a closed-loop control system is shown in Figure 16-1.
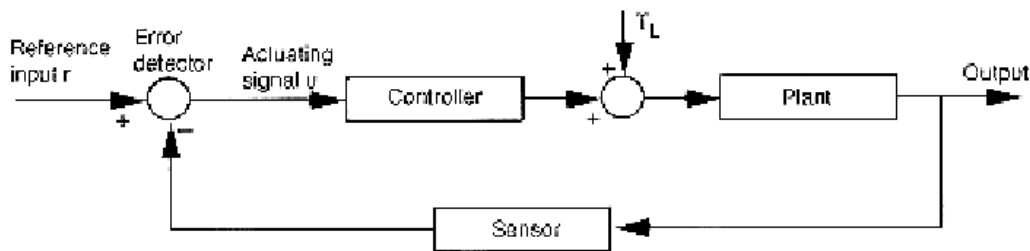
Figure 16-1: Closed-loop control system block diagram.

The actual output is measured, and a signal corresponding to this measurement is fed back to the input station, where it is compared with the input (desired output).

This comparison is performed in some device which produces a signal related to the difference between the two signals fed into it. This signal may be called the "error" if the two signals compared are the true input and output signals. Frequently, the signal fed back from the output is modified in some way before comparison with the input, and in such cases the result is not the error. The signal thus determined is used to drive the system and may always be called "actuating signal".

16.2.3 Open-loop control system

In open-loop control systems the output signal does not affect in any way the control action. In such systems, the output signal is not compared with the reference input, as it is sketched in Figure 16-2. Thus, each point of work corresponds to a different reference input. The expected output, and its accuracy, depends upon the calibration, and, thus, the actual output may vary from the expected one.
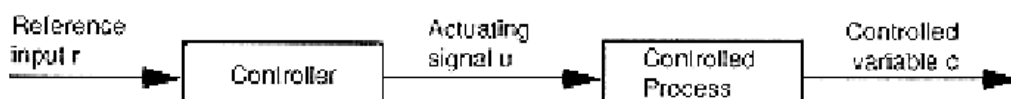
Figure 16-2: Open-loop control system block diagram.

The elements of an open-loop control system can usually be divided into two parts: the controller and the controlled process as shown by the block diagram. An input signal, or command, is applied to the controller, whose output acts as the actuating signal u; this signal then controls the process, so that the controlled variable c will perform according to some prescribed standards.

In simple cases, the controller can be an amplifier, mechanical linkage, filter, ..., depending upon the nature of the system. In more sophisticated cases, the controller can be a computer such as a microprocessor, and more recently a microcontroller.

Because of the simplicity and economy of these systems, open-loop control systems are found in many non-critical applications.

16.2.4   Adaptative control systems

This type of control systems are presently under research and they are not commonly used in spacecraft technology.

The dynamic characteristics of most systems are not constant (components deterioration and wasting during their operative life, modification in parameters or in the environment as atmospheric behaviour or solar radiation, ...). Although feedback control systems attenuate the effects of small changes in dynamic characteristics, when modifications in the parameters of the system or in the environment are large enough, a system has to be able to adapt to have a satisfactory response and behaviour. Adaptation means to have capacity of automodification and autoadjusting according to the nonforeseen modifications of the environment and the plant.

Control systems with any capacity of adapting are known as adaptive control systems.

The main interest of this type of control system is its capacity of adapting not only to changes in the system (plant and environment) but also to moderate defects in the design of the system, uncertainties and minor component failures. Therefore, the system reliability is highly increased.

An adaptive control system may consist in three functions as follows:

1.   To identify the dynamic characteristics of the plant.

2.   To adopt decisions based on the plant identification.

3.   Modification or action based on the adopted decision.

The plant identification is a process that must be performed according to the plant modification velocity. Systems high accurately known and very constant in their characteristics can be characterised with an initial identification at the beginning of their operative life and an initial modification of the decision process to minimise the behaviour index.

When the characteristics of the system change continuously, procedures must be revised continuously.

Figure 16-3 is a typical block diagram of adaptive control systems.
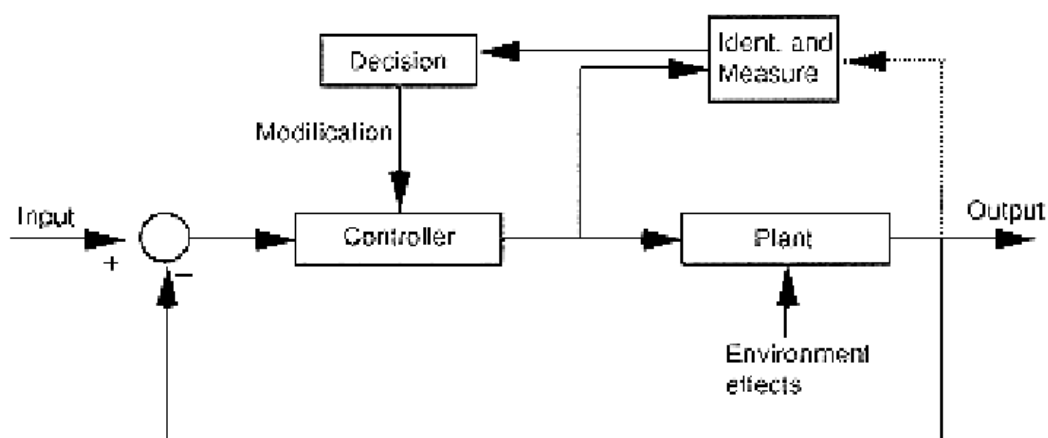
Figure 16-3: Typical block diagram of adaptative control systems.

16.2.5   Learning control system

Control systems apparently being open-loop are, in fact, closed-loop control systems due to the action of a human control, who compares input and output signals and executes the corrective actions, based on his appreciation of the error or difference.

It is difficult to mathematically represent the human behaviour. The most important characteristic is the human capacity of learning. At the beginning, the human control may seem inaccurate or even mistaken, but, as he is becoming an expert, his decision becomes optimal, and this must be taken into account in the analysis.

Recently, computers are becoming with learning capacity and are being implemented in control systems, and, therefore, control systems which are able to learn are known as learning control systems. This is a very new concept and has not been explored deeply yet.

16.2.6   Trade-off of open- and closed-loop control systems

It is important to point out that, when inputs are previously known and disturbances do not exist, an open-loop control system is preferable. Close-loop control systems present advantages when nonforeseen disturbances and/or variation of components performances exists. It is noted that the servomechanism output power influences, partially, its cost, weight and size. To reduce the required output power of a system, it is preferable to implement an open-loop control, when applicable; but generally for a satisfactory working of the system an adequate combination of open and closed-loop control system is the optimal solution.

Commonly, the use of feedback is applicated with the purpose of reducing the error between the reference input and the system output. However, the significance of the effects of feedback in control systems is more complex and has a wider effect. In fact, the reduction of system error is merely one of the many important effects that closing the loop may have on (upon) a system. The following paragraphs analyse the effects of feedback on such system performance characteristics as overall gain, stability, sensitivity and noise.

Let us consider the simple feedback system configuration shown in Figure 16-4, where r is the input signal, c the output signal, e the error, and b the feedback signal. The parameters G and H may be considered as constant gains. By simple algebraic manipulations, it is easy to show that the output-input ratio of the system is
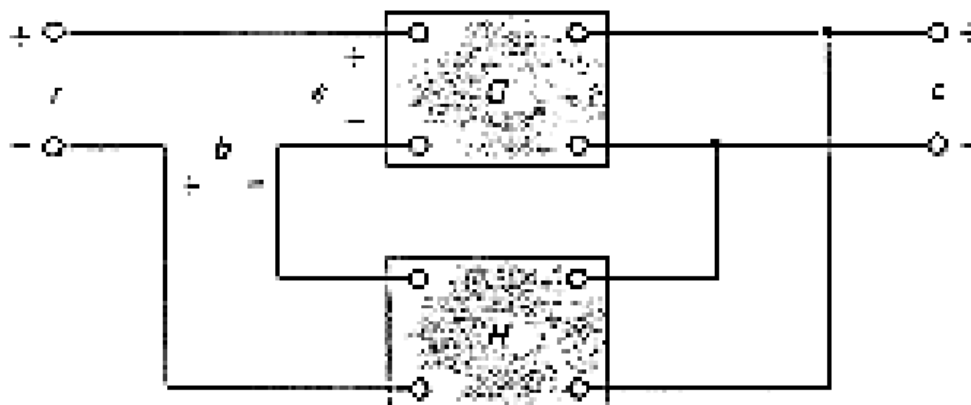
Figure 16-4: Feedback system

$$M = \frac{c}{r} = \frac{G}{1+GH} \qquad \text{[16-1]}$$

Using this basic relationship of the feedback system structure, some of the significant effects of the feedback can be uncovered .

16.2.6.1   Effect of feedback on overall gain

As it can be seen from Eq. [16-1], feedback affects the gain G of a nonfeedback system by a factor $1+GH$. The system of Figure 16-4 is said to have negative feedback, since a minus sign is assigned to the feedback signal. The quantity GH may itself include a minus sign, so the general effect of feedback is that it may increase or decrease the gain G. In a practical control system, G and H are functions of frequency, so the magnitude $1+GH$ may be greater than unity in one frequency range but less than unity in another. Therefore, feedback could increase the gain of the system in one frequency range but decrease it in another. This is sketched in Figure 16-5.
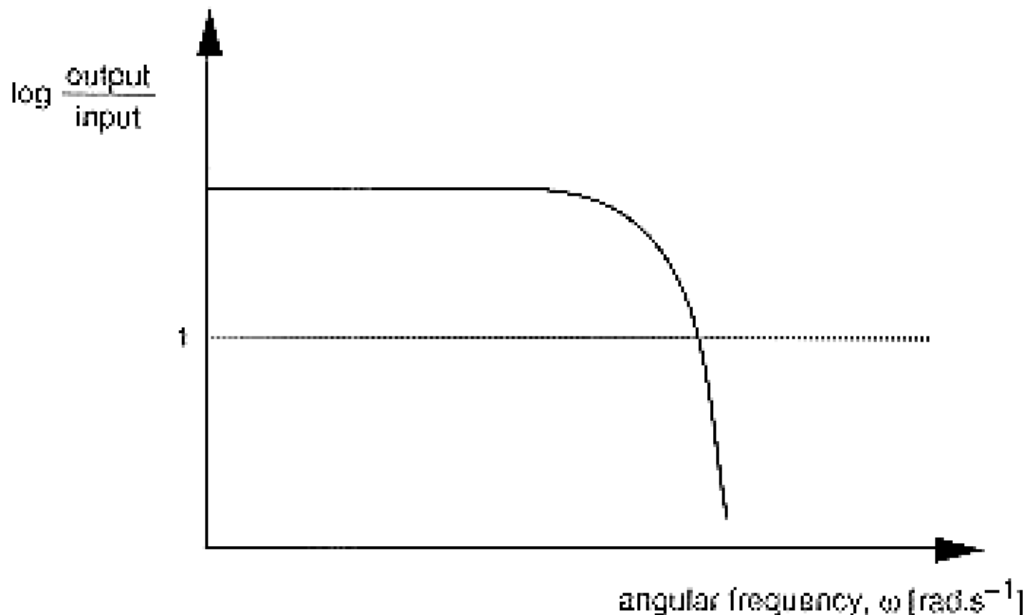
Figure 16-5: Sketch of the gain of a system as a function of frequency.

16.2.6.2   Effect of feedback on stability

To investigate the effect of feedback on stability, we can again refer to Eq. [16-1]). If $GH = -1$, the output of the system is infinite for any finite input, and the system is said to be unstable. Therefore, we may state that feedback can cause a system that is originally stable to become unstable. Certainly, feedback is a two-edged sword; when it is improperly used, it can be harmful. It should be pointed out, however, that only the static case is being considered here, and, in general, $GH = -1$ is not the only condition for instability.

It can be demonstrated that one of the advantages of incorporating feedback is that it can stabilise an unstable system. Let us assume that the feedback system in Figure 16-4 is unstable because $GH = -1$. If

we introduce another feedback loop through a negative feedbackgain *F*, as shown in Figure 16-6, the output-input ratio of the overall system is
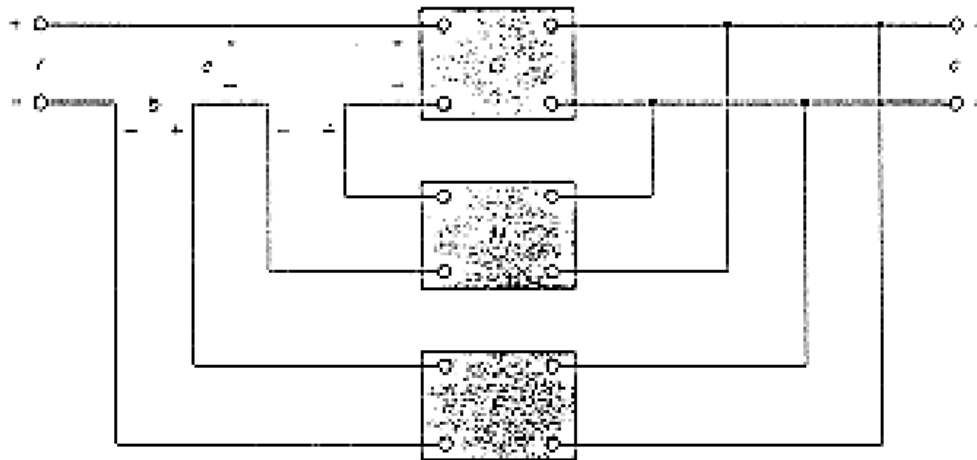
Figure 16-6: Feedback system with two feedback loops.

$$\frac{c}{r} = \frac{G}{1 + GH + GF}$$ [16-2]

It is apparent that although the properties of *G* and *H* are such that the inner-loop feedback system is unstable, because *GH* = -1, the overall system can be stable by properly selecting the outer-loop feedback gain *F*.

In practice, *GH* is a function of frequency, and the stability condition of the closed-loop system depends on the magnitude and phase of *GH*. The bottom line is that feedback can improve stability or be harmful to stability if it is not properly applied.

16.2.6.3   Effect of feedback on sensitivity

Sensitivity considerations often are important in the design of control systems. Since all physical elements have properties that change with environment and age, the parameters of a control system cannot always be considered as completely stationary over the entire operating life of the system. For instance, the winding resistance of an electric motor changes as the temperature of the motor rises during operation. In general, a good control system should be very insensitive to parameter variations but sensitive to the input commands. Now the effect that feedback has on the sensitivity to parameter variations will be investigated.

Referring to the system in Figure 16-8, *G* is considered as a gain parameter that may vary. The sensitivity of the gain of the overall system, *M*, to the variation in *G* is defined as

$$S_G^M = \frac{\partial M / M}{\partial G / G} = \frac{percentage\ change\ in\ M}{percentage\ change\ in\ G}$$ [16-3]

where δM denotes the incremental change in M due to the incremental change in G, δG. By using Eq. [16-1], the sensitivity function is written

$$S_G^M = \frac{\partial M / M}{\partial G / G} = \frac{1}{1 + GH} \qquad [16\text{-}4]$$

This relation shows that, if GH is a positive constant, the magnitude of the sensitivity function can be made arbitrarily small by increasing GH, provided that the system remains stable. It is apparent that in an open-loop system, the gain of the system will respond in a one-to-one fashion to the variation in G; i.e., S_G^M. It should again be reminded that, in practice, GH is a function of frequency; the magnitude of $1 + GH$ may be less than unity over some frequency ranges, so that feedback could be harmful to the sensitivity to parameter variation in certain cases.

In general, the sensitivity of the system gain of a feedback system to parameter variations depends on where the parameter is located.

16.2.6.4   Effect of feedback on external disturbance or noise

All physical systems are subject to some types of extraneous signals or noise during operation. Examples of these signals are thermal-noise voltage in electronic circuits and brush or commutator noise in electric motors. Therefore, in the design of a control system, consideration should be given to ensure that the system is insensitive to noise and disturbances and sensitive to input commands.

The effect of feedback on noise and disturbance depends greatly on where these extraneous signals occur in the system. No general conclusions can be made; but in many situations, feedback reduces the effect of noise and disturbance on system performance.

Referring to the system shown in Figure 16-7, in which r denotes the command signal and n is the noise signal, in the absence of feedback, $H = 0$, the output c is
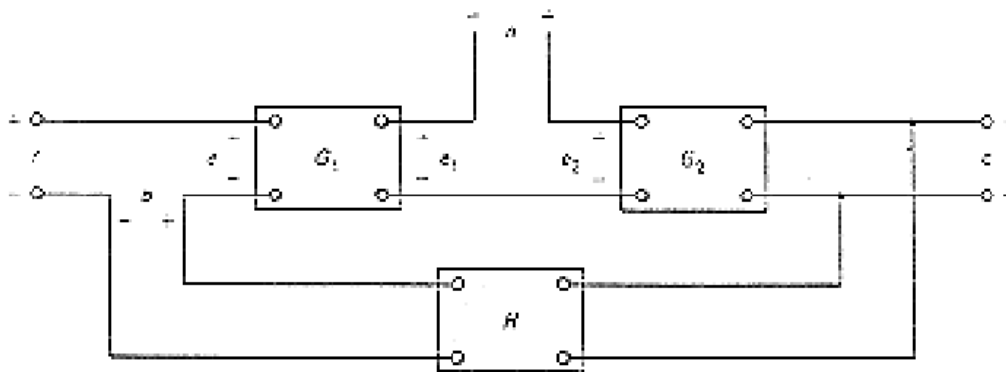
Figure 16-7: Feedback system with a noise signal.

$$c = G_1 G_2 e + G_2 n \qquad [16\text{-}5]$$

where $e = r$. The signal-to-noise ratio of the output is defined as

$$\frac{Output\ due\ to\ signal}{Output\ due\ to\ noise} = \frac{G_1 G_2 e}{G_2 n} = G_1 \frac{e}{n} \qquad \text{[16-6]}$$

To increase the signal-to-noise ratio one should increase the magnitude of either G_1 or e relative to n. Varying the magnitude of G_2 would have no effect whatsoever on the ratio.

With the presence of feedback, the system output due to r and n acting simultaneously is

$$c = \frac{G_1 G_2}{1 + G_1 G_2 H} r + \frac{G_2}{1 + G_1 G_2 H} n \qquad \text{[16-7]}$$

Comparison of Eq. [16-7] with Eq. [16-5] shows that the noise component in the output of Eq. [16-7] is reduced by the factor $1+G_1 G_2 H$ if the latter is greater than unity, but the signal component is also changed by the same amount. The signal-to-noise ratio is

$$\frac{Output\ due\ to\ signal}{Output\ due\ to\ noise} = \frac{G_1 G_2 r /\left(1 + G_1 G_2 H\right)}{G_2 n /\left(1 + G_1 G_2 H\right)} = G_1 \frac{r}{n} \qquad \text{[16-8]}$$

and it is the same as that without feedback. In this case, feedback is shown to have no direct effect on the output signal-to-noise ratio of the system. However, the application of feedback suggests the possibility of improving the signal-to-noise ratio under certain conditions. If it is assumed that, in the system of Figure 16-7, the magnitude of G_1 is increased to G'_1 and that of the input r to r', with all other parameters unchanged, the output due to the input signal acting alone is at the same level as that when feedback is absent. In other words,

$$\frac{c}{r} = \frac{G}{1 + GH + GF} \qquad \text{[16-9]}$$

with G_1 increased to G'_1, the output due to noise acting alone becomes

$$c\Big|_{r=0} = \frac{G_2}{1 + G'_1 G_2 H} n \qquad \text{[16-10]}$$

which is smaller than the output due to n when G_1 is not increased. The signal-to-noise ratio is now

$$\frac{G_1 G_2 r}{G_2 n /\left(1 + G'_1 G_2 H\right)} = \frac{G_1 r}{n}\left(1 + G'_1 G_2 H\right) \qquad \text{[16-11]}$$

which is greater than that of the system without feedback in a factor of $(1+G'_1 G_2 H)$.

16.3 Basic control actions

16.3.1 Introduction

An automatic controller compares the actual value of the plant output with the reference input (desired value), determines the deviation, and produces a control signal that will reduce the deviation to zero or to a small value. The manner in which the automatic controller produces the control signal is called the control action. In this clause the basic control actions used in control systems are discussed.

The central element of typical feedback control systems is the "controller." This device has as its input a low-power-level signal, which is a measure of a process variable, and as its output a high-power-level signal, which is related to the input signal by some specified, but usually adjustable, input-output relation. Note that ideally, the controller is a strictly unilateral device (the conditions at the output end of the controller should in no way have any effect "backward" through the controller on the process). The output signal itself is used to manipulate the process in some way through an "actuator". Because a high-power-gain device by itself can be very difficult to regulate, a common technique in building controllers is to use a passive feedback element around the high-gain device. This reduces the overall gain considerably, but the end result is an instrument that has sufficient power gain and is capable of precise regulation. This method is shown schematically in Figure 16-8. The power unit has an external power supply (not shown) to provide the power gain, and the input-output relation is controlled completely by the passive feedback.
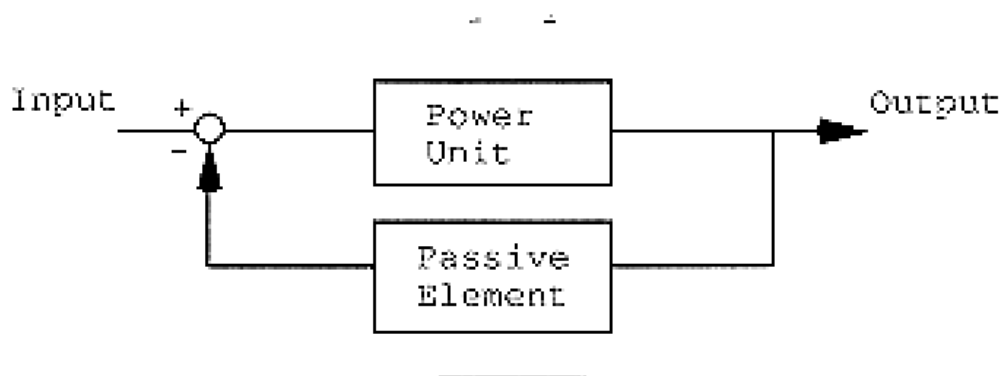
Figure 16-8: Feedback structure of instruments and regulators. From Ogata (1990) [137].

Controllers can be classified in six groups:

1. Two-position or on-off controllers.

2. Proportional controllers (P).

3. Integral controllers (I).

4. Proportional-integral controllers (PI).

5. Proportional-derivative controllers (PD).

6. Proportional-integral-derivative controllers (PID).

Most controllers use electricity or pressurised fluid as power sources. Controllers may also be classified according to the kind of power employed in the operation, such as pneumatic, hydraulic, or electronic controllers, as will be shown in clause 16.4.

Figure 16-9 presents a block diagram of a typical control system, which consists of an automatic controller, an actuator, a plant, and a sensor (measuring element). The controller detects the actuating error signal and amplifies it to a sufficiently high level. (Thus the automatic controller comprises an error detector and amplifier. Quite often a suitable feedback circuit, together with an amplifier, is used to alter the actuating error signal by amplifying, and sometimes by differentiating and/or integrating it to produce a better control signal). The actuator is a power device that produces the input to the plant according to the control signal so that the feedback signal will correspond to the reference input signal.
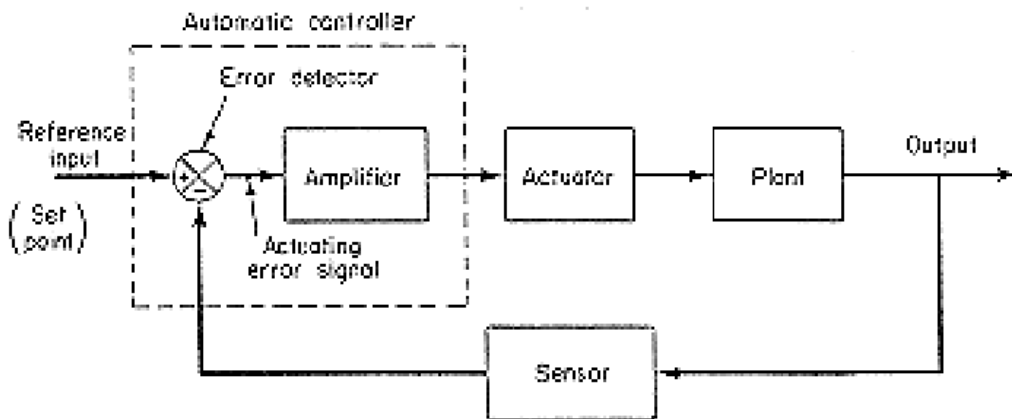
Figure 16-9: Block diagram of an industrial control system, which consists of an automatic controller, an actuator, a plant, and a sensor (measuring element). From Ogata (1990) [137].

The sensor, or measuring element, is a device that converts the output variable into another suitable variable, such as a displacement, pressure, or voltage, that can be used to compare the output to the reference input signal. This element is in the feedback path of the closed loop system.

16.3.2　Two-position or on-off control action

In a two-position control system, the actuating element has only two fixed positions, which are, in many cases, simply on and off. Two-position or on-off control is relatively simple, reliable and inexpensive.

Let the output signal from the controller be $u(t)$ and the actuating error signal be $e(t)$. In two-position control, the signal $u(t)$ remains at either a maximum or minimum value, depending on whether the actuating error signal is positive or negative, so that

$$On-off\ control\ law \begin{cases} u(t)=U_1 & , \quad if\ e(t)>0 \\ u(t)=U_2 & , \quad if\ e(t)\leq 0 \end{cases}$$

[16-12]

where U_1 and U_2 are constants. The minimum value U_2 is usually either zero or $-U_1$. Two-position controllers are generally electrical devices, and an electric solenoid-operated valve is widely used in such controllers (see clause 16.4.3.1.1). Pneumatic proportional controllers with very high gains act as two-position controllers and are sometimes called pneumatic two-position controllers .

Figure 16-10 shows two block diagrams of two-position controllers. The range through which the actuating error signal moves before the switching occurs is called the differential gap (as it is indicated in Figure 16-10(b)). Such a differential gap causes the controller output $u(t)$ to maintain its present value until the actuating error signal has moved slightly beyond the zero value (see Figure 16-10(c)). In some cases, the differential gap is a result of unintentional friction and lost motion; however, quite often it is intentionally provided in order to prevent too frequent operation of the on-off mechanism.
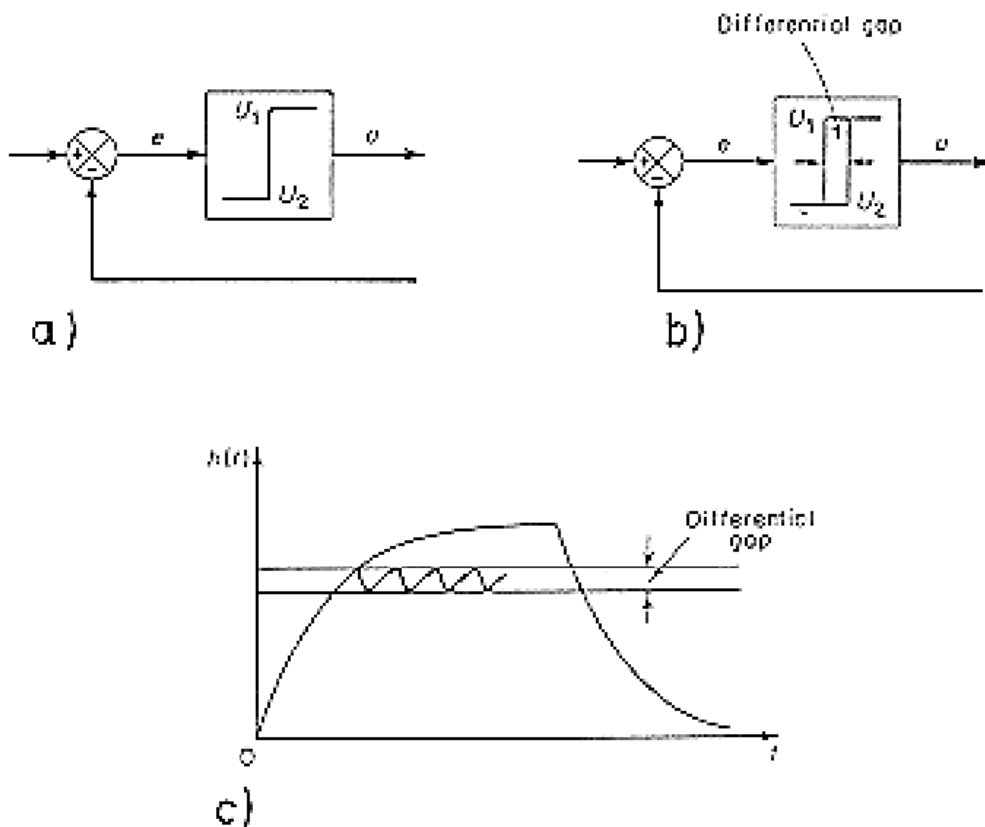
Figure 16-10: a) Block diagram of an on-off controller; b) block diagram of an on-off controller with differential gap; c) output versus time curve. From Ogata (1990) [137].

16.3.3 Proportional control action (p controller)

For a controller with proportional control action, the relationship between the output of the controller $u(t)$ and the actuating error signal $e(t)$ is

$$u(t) = K_p e(t)$$

[16-13]

or, in Laplace-transformed quantities,

$$\frac{U(s)}{E(s)} = K_p \qquad [16\text{-}14]$$

where K_p is called the proportional gain.

In fact, a proportional controller is an amplifier with adjustable gain. A block diagram of such a controller is shown in Figure 16-11.
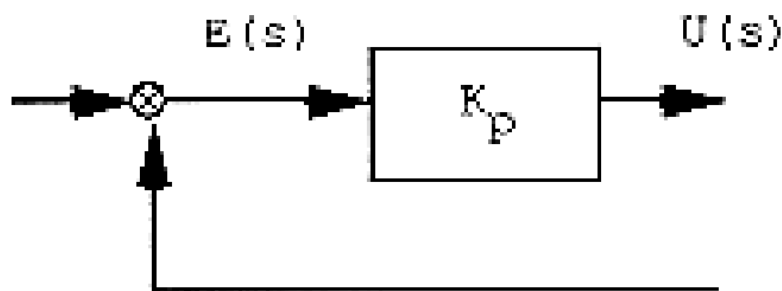
Figure 16-11: Block diagram of a proportional controller. From Ogata (1990) [137].

16.3.4   Integral control action (i controller).

In a controller with integral control action, the value of the controller output $u(t)$ is changed at a rate proportional to the actuating signal $e(t)$. That is,

$$\frac{du(t)}{dt} = K_i e(t) \qquad [16\text{-}15]$$

or

$$u(t) = K_i \int_0^t e(t)dt \qquad [16\text{-}16]$$

where K_i is an adjustable constant. In Laplace´s domain, the transfer function of the integral controller is

$$\frac{U(s)}{E(s)} = \frac{K_i}{s} \qquad [16\text{-}17]$$

It is important to point out that when the value of $e(t)$ is doubled, then, the value of $u(t)$ varies twice as fast. For zero actuating error, the value of $u(t)$ remains stationary. The integral control action is sometimes called reset control. Figure 16-12 shows a block diagram of such a controller.
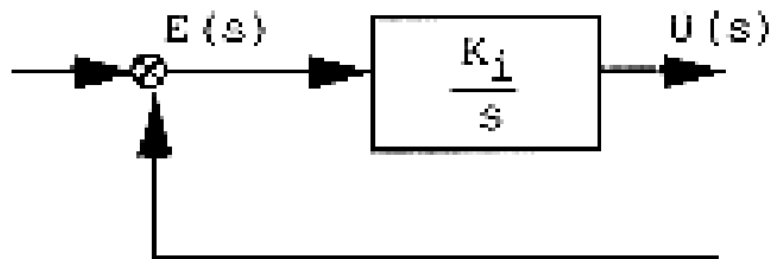
Figure 16-12: Block diagram of an integral controller. From Ogata (1990) [137].

16.3.5 Proportional-integral control action (pi controller)

The control action of a proportional-integral controller is defined by the following equation:

$$u(t) = K_p e(t) + \frac{K_p}{T_i} \int_0^t e(t) dt \qquad [16\text{-}18]$$

thus, the transfer function of the controller is

$$\frac{U(s)}{E(s)} = K_p \left(1 + \frac{1}{T_i s} \right) \qquad [16\text{-}19]$$

where K_p is the proportional gain, and T_i is called the integral time. The inverse of the integral time T_i is called the reset rate. The reset rate is the number of times per minute that the proportional part of the control action is duplicated. Figure 16-13(a) shows a block diagram of a proportional-integral controller. If the actuating signal $e(t)$ is a unit-step function, as shown in Figure 16-13(b), the controller output $u(t)$ becomes as shown in Figure 16-13(c).
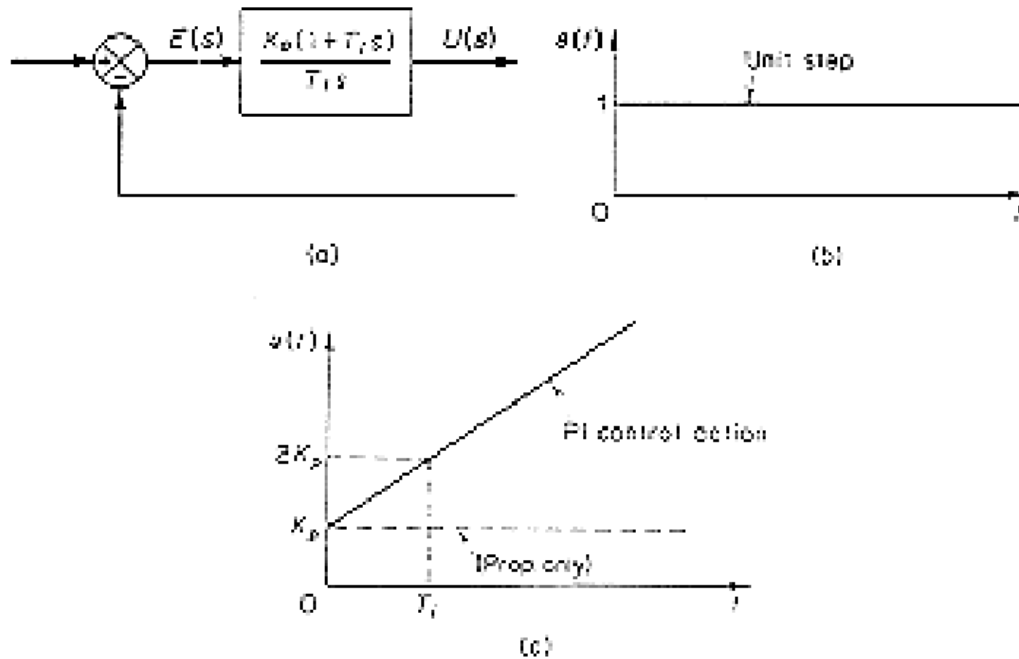
Figure 16-13: a) Block diagram of a proportional-integral controller; b) and c) diagrams depict a unit-step input and the controller output. From Ogata (1990) [137].

16.3.6 Proportional-derivative control action (pd controller)

The control action of a proportional-derivative controller is defined by the following equation:

$$u(t) = K_p e(t) + K_p T_d \frac{de(t)}{dt}$$ [16-20]

and its transfer function is

$$\frac{U(s)}{E(s)} = K_p(1 + T_d s)$$ [16-21]

where K_p is the proportional gain and T_d is a constant called the derivative time. The derivative control action, sometimes called rate control, is where the magnitude of the controller output is proportional to the rate of change of the actuating error signal. The derivative time T_d is the time interval by which the rate action advances the effect of the proportional control action. Figure 16-14(a) shows a block diagram of a proportional-derivative controller. If the actuating error signal $e(t)$ is a unit-ramp function as shown in Figure 16-14(b), then the controller output $u(t)$ becomes as shown in Figure 16-14(c). As may be seen from Figure 16-14(c), the derivative control action has an anticipatory character.
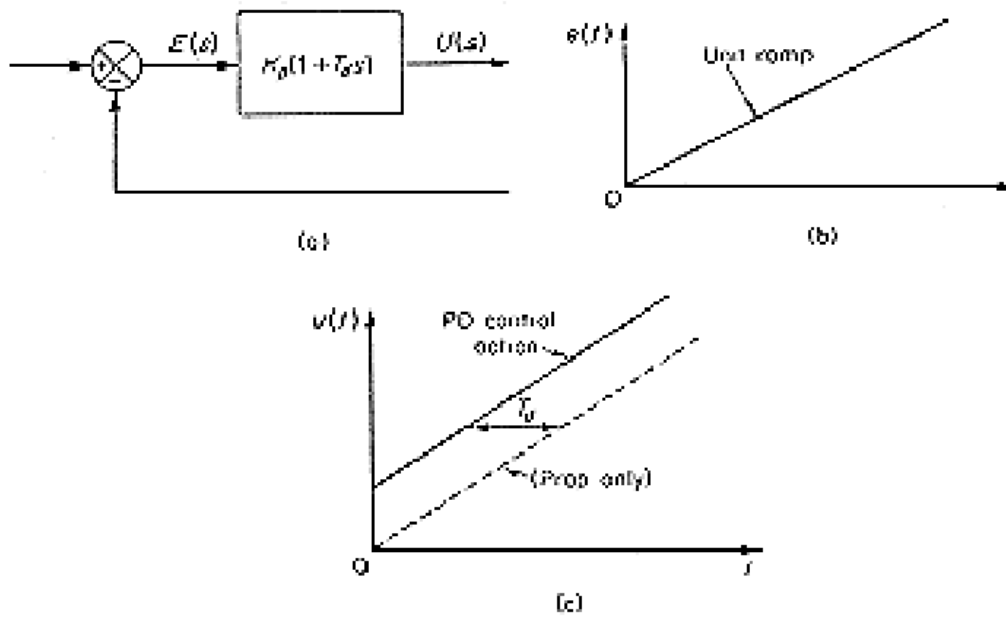
Figure 16-14: a) Block diagram of a proportional-derivative controller; b) and c) diagrams depict a unit-ramp input and the controller output. From Ogata (1990) [137].

While derivative control action has the advantage of being anticipatory, it has the disadvantages of amplifying noise signals (thereby causing a saturation effect in the actuator) and of being effective only during transient periods.

16.3.7 Proportional-integral-derivative control action (pid controller)

The combination of proportional control action, integral control action, and derivative control is termed proportional-integral-derivative control action. This combined action has the advantages of each of the three individual control actions. The equation of a controller with this action is:

$$u(t) = K_p e(t) + \frac{K_p}{T_i} \int_0^t e(t) dt + K_p T_d \frac{de(t)}{dt} \qquad [16\text{-}22]$$

thus, the corresponding transfer function is

$$\frac{U(s)}{E(s)} = K_p \left(1 + \frac{1}{T_i s} + T_d s \right) \qquad [16\text{-}23]$$

where K_p is the proportional gain, T_i is the integral time, and T_d is the derivative time. The block diagram of a proportional-integral-derivative controller is shown in Figure 7-8(a). If $e(t)$ is a unit-ramp function, as shown in Figure 16-15(b), the controller output $u(t)$ becomes as shown in Figure 16-15(c).
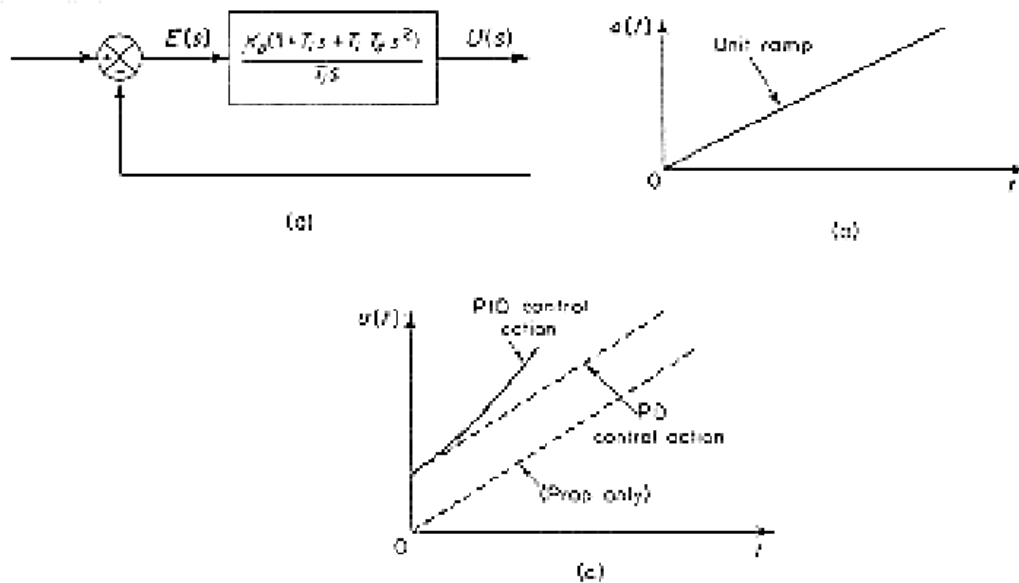
Figure 16-15: a) Block diagram of a proportional-integral-derivative controller; b) and c) diagrams depict a unit-ramp and the controller output. From Ogata (1990) [137].

16.3.8 Summary

In this clause the six basic control actions have been presented, and modeled as block diagrams. Also, their advantages and disadvantages have been mentioned.

Table 16-1 summarises the previous data, in particular the equation of its output, $u(t)$, as function of the actuating signal, $e(t)$, in the time domain, and the transfer function in the Laplace´s plane.

Table 16-1: Summary of basic control actions

Control Law	Equation	Transfer function	Block diagram	Parameters
ON/OFF	$u(t) = U_1$, if $e(t) > 0$ $u(t) = U_2$, if $e(t) \le 0$	NA	Figure 16-10	U_1, U_2
P	$u(t) = K_p e(t)$	$\dfrac{U(s)}{E(s)} = K_p$	Figure 16-11	K_p
I	$u(t) = K_i \displaystyle\int_0^t e(t)dt$	$\dfrac{U(s)}{E(s)} = \dfrac{K_i}{s}$	Figure 16-12	K_i
PI	$u(t) = K_p e(t) + \dfrac{K_p}{T_i} \displaystyle\int_0^t e(t)dt$	$\dfrac{U(s)}{E(s)} = K_p\left(1 + \dfrac{1}{T_i s}\right)$	Figure 16-13a	K_p, T_i

Control Law	Equation	Transfer function	Block diagram	Parameters
PD	$u(t) = K_p e(t) + K_p T_d \dfrac{de(t)}{dt}$	$\dfrac{U(s)}{E(s)} = K_p \left(1 + T_d s\right)$	Figure 16-14a	K_p, T_d
PID	$u(t) = K_p \left[e(t) + T_d \dfrac{d}{dt} e(t) + \dfrac{1}{T_i} \displaystyle\int_0^t e(t) dt \right]$	$\dfrac{U(s)}{E(s)} = K_p \left(1 + \dfrac{1}{T_i s} + T_d s\right)$	Figure 16-15a	K_p, T_i, T_d

16.4 Implementation techniques of control laws

16.4.1 Introduction

This clause will be focused on the controller block of a control system (see Figure 7-2 (clause 16.3.1) for a typical block diagram). Different techniques of implementing the control actions (P–action, PD–action, PI–action and PID–action) will be presented.

The recent evolution of microprocessors and microcomputers which can be used for various control functions has established a new trend toward the inclusion of digital computers to implement the control actions by signal processing and calculations. Before this situation, the control action was commonly implemented by a combination of devices as nozzles, relays, valves, ..., which act continuously in time, and are known as analog controllers.

The current trend toward digital rather than analog control of dynamic systems is mainly due to the availability of low–cost digital computers and the advantages found in working with digital signals rather than continuous–time signals. Also, the decision–making capability and flexibility in the control program are an additional major advantage of digital control systems.

This clause will be focused on analog devices for implementing control actions, although a brief description of digital control systems will be included. (In clause 16.5 computers commonly used in space system to implement digital control laws will be listed and discussed).

16.4.1.1 Digital control systems

A control scheme in which a digital computer is included in a control loop to perform signal processing in a desired fashion is called digital control.

Direct digital control of a process or plant has the following advantages over the corresponding analog control:

1. Data processing in the digital controller is straightforward; complex control calculations can be performed easily.

2. Control programs (controller characteristics) can be changed easily if such changes are needed.

3. Digital controllers are far superior to the corresponding analog controllers from the viewpoint of internal noise and drift effects.

The main disadvantages of digital control are:

1. The sampling and quantizing processes tend to result in more errors, which degrade system performance.

2. Designing digital controllers to compensate for such degradation is more complex than designing analog controllers at an equivalent level of performance.

Figure 16-16 depicts a block diagram of a digital control system showing a configuration of the basic control scheme.
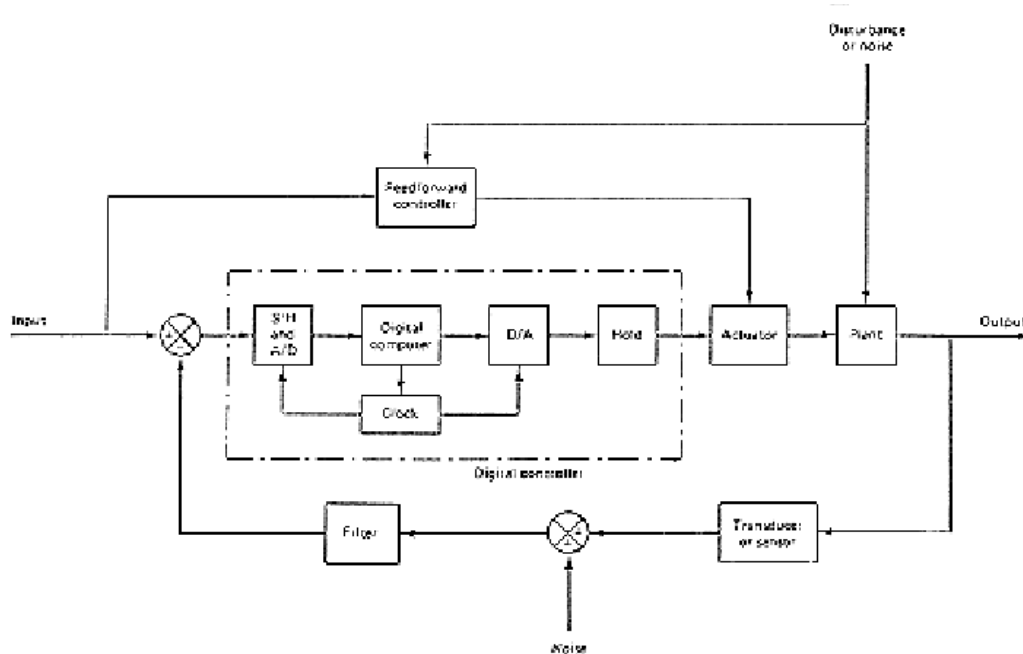
Figure 16-16: Block diagram of a digital control system. From Ogata (1987) [135].

Figure 16-17 shows a block diagram of a simplified digital control system. The controller operation is controlled by the clock. In such a digital control system, some points of the system pass signals of varying amplitude in either continuous time or discrete time, while other points pass signals in numerical code.
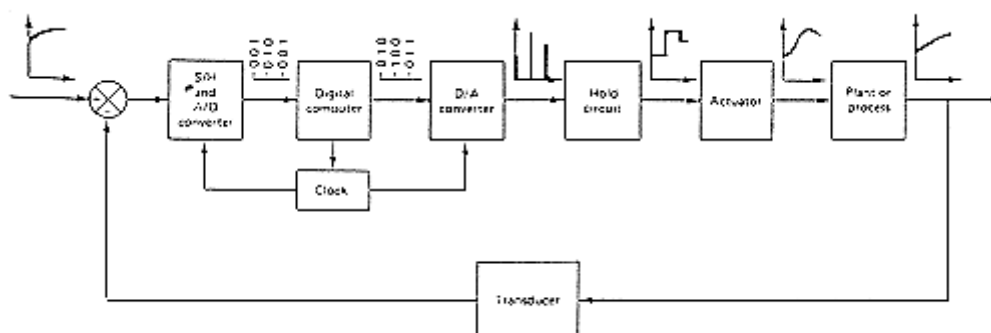
Figure 16-17: Block diagram of a digital control system showing signals in binary or graphic from. From Ogata (1987) [135].

The output of the plant is a continuous–time signal. The error signal is converted into digital form by the sample–and–hold circuit and the analog–to–digital converter. The conversion is done at the sampling time. The digital computer processes the sequences of numbers by means of an algorithm and produces new sequences of numbers. At every sampling instant a coded number (usually a

binary number consisting of eight or more binary digits) must be converted to a physical control signal, which is usually a continuous–time, or analog, signal. The digital–to–analog converter and the hold circuit convert the sequence of numbers in numerical code into a piecewise continuous–time signal. The real–time clock in the computer synchronises the events. The output of the hold circuit, a continuous–time signal, is fed to the plant, either directly or through the actuator, to control its dynamics.

16.4.1.2 Analog controllers

Most analog controllers use electricity or pressurised fluid as the power source. Analog controllers may be classified according to the kind of power employed in the operation as follows:

- Pneumatic controllers

- Hydraulic controllers

- Electronic controllers.

The type of controller to use should be decided based on the nature of the plant and the operating conditions, including such considerations as safety, cost, availability, reliability, accuracy, weight and size.

Before describing how control actions are implemented, a brief description of devices is presented and their way of operation analysed.

16.4.2 Devices characterization

16.4.2.1 Pressure systems

Consider the pressure system shown in Figure 16-18. The gas flow through the restriction is a function of the gas pressure difference p_i-p_o. Such a pressure system may be characterised in terms of a resistance and a capacitance.
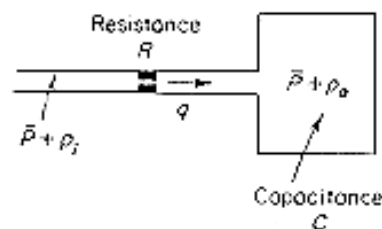
Figure 16-18: Schematic diagram of a pressure system. From Ogata (1990) [137].

The gas flow resistance, R, is defined as:

$$R = \frac{change\ in\ pressure\ difference}{change\ in\ gas\ flow\ rate} = \frac{d(\Delta p)}{dq}$$

[16-24]

and the capacitance of the pressure vessel, C, is defined as:

$$C = \frac{change\ in\ gas\ stored}{change\ in\ gas\ pressure} = \frac{dm}{dp} \qquad [16\text{-}25]$$

where

m = mass of gas inside the vessel,

p = gas pressure,

q = gas flow rate, being $q = dm/dt$

With respect to the system shown in Figure 16-18, only small deviations in the variables from their respective steady–state values are permitted. Thus, let define the following variables:

p_i = small change in flow gas pressure.

p_o = small change in gas pressure in the vessel.

For small values of p_i and p_o, the resistance R becomes constant and may be written as

$$R = \frac{p_i - p_o}{q} \qquad [16\text{-}26]$$

and for capacitance C one has

$$C\frac{dp_o}{dt} = \frac{p_i - p_o}{R} \qquad [16\text{-}27]$$

which can be written as

$$RC\frac{dp_o}{dt} + p_o = p_i \qquad [16\text{-}28]$$

If p_i and p_o are considered the input and output, respectively, then the transfer function of the system is

$$\frac{P_o(s)}{P_i(s)} = \frac{1}{RCs + 1} \qquad [16\text{-}29]$$

where RC has the dimension of time and is the time constant of the system (Ogata (1990) [137].

16.4.2.2 Valves

Consider the schematic diagram of a pneumatic actuating valve shown in Figure 16-19. In the following analysis, only small variations in the variables are considered, so that the model of the pneumatic actuating valve can be linearized.
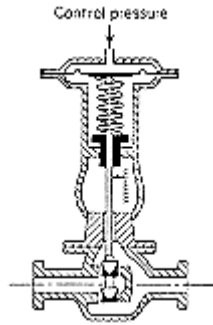
Figure 16-19: Schematic diagram of a pneumatic actuating valve. From Ogata (1990) [137].

Let p_c and x be the small variation in the control pressure and the corresponding valve displacement, respectively. If the force due to the mass and viscous friction in Figure 16-19 are negligibly small, the restoring force due to changes in pressure is

$$Ap_c = kx \qquad \text{[16-30]}$$

where A is the area of the diaphragm and k plays the role of a spring constant.

In Laplace's domain, the transfer function between x and p_c thus becomes

$$\frac{X(s)}{P_c(s)} = \frac{A}{k} = K_c \qquad \text{[16-31]}$$

where $X(s) = L[x]$ and $P_c(s) = L[p_c]$, L being the Laplace transform. If q_i, the change in flow through the pneumatic actuating valve, is proportional to x, the change in the valve-stem displacement, then

$$\frac{Q_i(s)}{X(s)} = K_q \qquad \text{[16-32]}$$

where $Q_i(s) = L[q_i]$ and K_q is a constant. The transfer function between q_i and p_c is then

$$\frac{Q_i(s)}{P_c(s)} = K_c K_q = K_v \qquad \text{[16-33]}$$

where K_v is a constant.

16.4.2.3   Dashpots

The dashpot shown in Figure 16-20(a) acts as a differentiating element. Suppose a step displacement to the piston position x. Then the displacement y becomes equal to x momentarily because of the

spring force. However, the fluid will flow through the resistance R and the cylinder will come back to the original position. The curves x versus t and y versus t are shown in Figure 16-20(b).
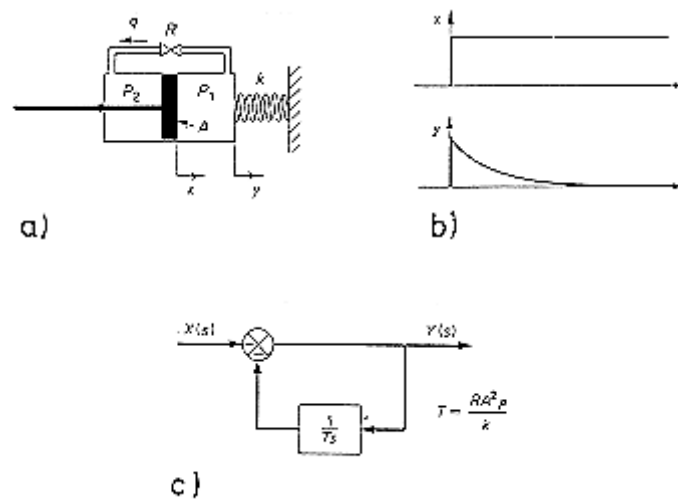
Figure 16-20: a) Dashpot; b) step change in x and the corresponding change in y plotted versus t, c) block diagram of the dashpot. From Ogata (1990) [137].

Define the pressures existing on the right and left sides of the piston as p_1 and p_2 respectively. Suppose that the inertia force involved is negligible. Then the force acting on the piston must balance the spring force. Thus

$$A(p_1 - p_2) = ky \qquad [16\text{-}34]$$

where

A = piston area,

k = spring constant.

The flow rate q is given by

$$q = \frac{p_1 - p_2}{R} \qquad [16\text{-}35]$$

where

q = flow rate through the restriction,

R = resistance to flow at the restriction.

Since the flow through the restriction during dt seconds must equal the change in the mass of fluid to the left of the piston during the same dt seconds, one obtains

$$qdt = A\rho(dx - dy) \qquad [16\text{-}36]$$

where ρ is the density (it has been assumed that the fluid is incompressible). This last equation can be rewritten as

$$\frac{dx}{dt} - \frac{dy}{dt} = \frac{q}{A\rho} = \frac{p_1 - p_2}{RA\rho} = \frac{ky}{RA^2\rho} \qquad [16\text{-}37]$$

or

$$\frac{dx}{dt} = \frac{dy}{dt} + \frac{ky}{RA^2\rho} \qquad [16\text{-}38]$$

Taking the Laplace transforms of both sides of this last equation, assuming zero initial conditions, then

$$sX(s) = sY(s) + \frac{ky}{RA^2\rho} Y(s) \qquad [16\text{-}39]$$

The transfer function of this system thus becomes

$$\frac{Y(s)}{X(s)} = \frac{s}{s + \dfrac{k}{RA^2\rho}} \qquad [16\text{-}40]$$

Let us define $T = RA^2\rho/k$ then

$$\frac{Y(s)}{X(s)} = \frac{Ts}{Ts+1} = \frac{1}{1 + \dfrac{1}{Ts}} \qquad [16\text{-}41]$$

Figure 16-20(c) shows a block diagram representation for this system.

Writing the inverse of the relation (16.4-18a)

$$\frac{X(s)}{Y(s)} = \frac{Ts+1}{Ts} = 1 + \frac{1}{Ts} \qquad [16\text{-}42]$$

which, in fact, is the transfer function corresponding to a proportional-integral control action

16.4.3   Analog-controller implementation techniques

This clause describes different techniques of implementing the control laws through physical devices (analog control).

16.4.3.1 Proportional control actions

16.4.3.1.1 Pneumatic force-distance p controller

Figure 16-21(a) shows a schematic diagram of such a proportional controller. The nozzle flapper amplifier constitutes the first-stage amplifier, and the nozzle back pressure is controlled by the nozzle–flapper distance. The relay-type amplifier constitutes the second–stage amplifier. The nozzle back pressure determines the position of the diaphragm valve for the second-stage amplifier, which is capable of handling a large quantity of fluid flow.
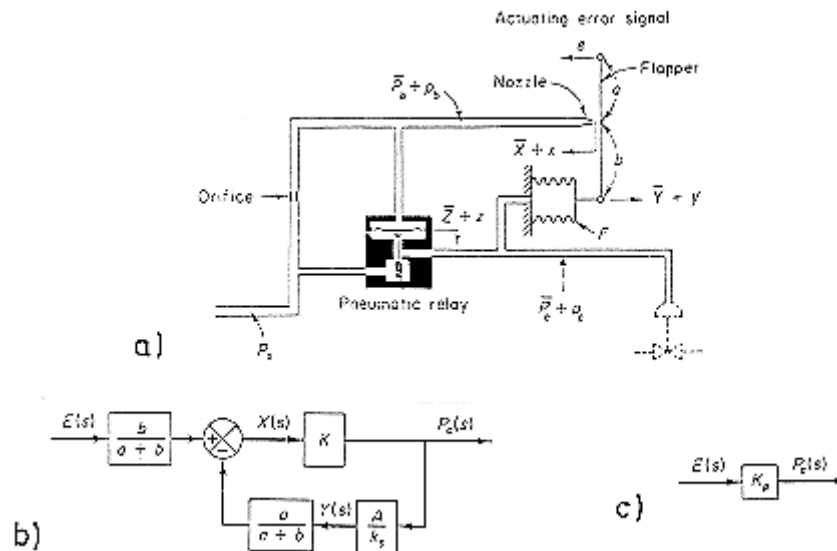
Figure 16-21: a) Schematic diagram of a force-distance type pneumatic proportional controller; b) block diagram; c) simplified block diagram. From Ogata (1990) [137].

In most pneumatic controllers, some type of pneumatic feedback is employed. Feedback of the pneumatic output reduces the amount of actual movement of the flapper. Instead of mounting the flapper on a fixed point, it is often pivoted on the feedback bellows, as shown in Figure 16-21(a). The amount of feedback can be regulated by introducing a variable linkage between the feedback bellows and the flapper connecting point. The flapper then becomes a floating link. It can be moved by both the error signal and the feedback signal.

The operation of the controller shown in Figure 16-21(a) is as follows. The input signal to the two-stage pneumatic amplifier is the actuating error signal. Increasing the actuating error signal moves the flapper to the left. This move will, in turn, increase the nozzle back pressure, and the diaphragm valve moves downward. This results in an increase of the control pressure. This increase will cause the bellows F to expand and move the flapper to the right, thus opening the nozzle. Because of this feedback, the nozzle-flapper displacement is very small, but the change in the control pressure can be large.

Assuming that all variations in the variables are within a linear range, a block diagram for the system is shown in Figure 16-21(b). The transfer function between $p_c(t)$ and $e(t)$ is given by

$$\frac{P_c(s)}{E(s)} = \frac{\dfrac{a}{a+b}K}{1+K\dfrac{a}{a+b}\dfrac{A}{K_s}} = K_p \qquad [16\text{-}43]$$

being $P_c(s)$ and $E(s)$ the Laplace transforms of $p_c(t)$ and $e(t)$. Equation [16-43] can be simplified as shown in Figure 16-21(c).

16.4.3.1.2   Pneumatic force-balance p controller

Figure 16-22 represents a force-balance pneumatic proportional controller. The basic principle of operation does not differ from that of the force-distance controller. The main advantage of the force-balance controller is that it eliminates many mechanical linkages and pivot joints, thereby reducing the effects of friction.
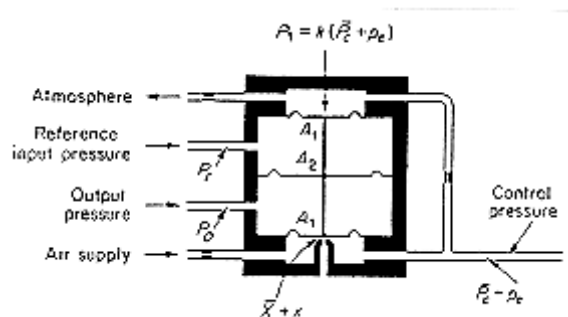
Figure 16-22: Schematic diagram of a force-balance pneumatic proportional controller. From Ogata (1990) [137].

In the controller shown in Figure 16-22, the reference input pressure P_r and the output pressure P_o are fed to large diaphragm chambers. Note that a force-balance pneumatic controller operates only on pressure signals. Therefore, it is necessary to convert the reference input and system output to corresponding pressure signals.

The transfer function between P_c and $P_e = P_r - P_o$ is

$$\frac{P_c(s)}{P_e(s)} = \frac{A_2 - A_1}{A_1} = K_p \qquad [16\text{-}44]$$

16.4.3.1.3   Hydraulic p controller

Consider the hydraulic controller in Figure 16-23.
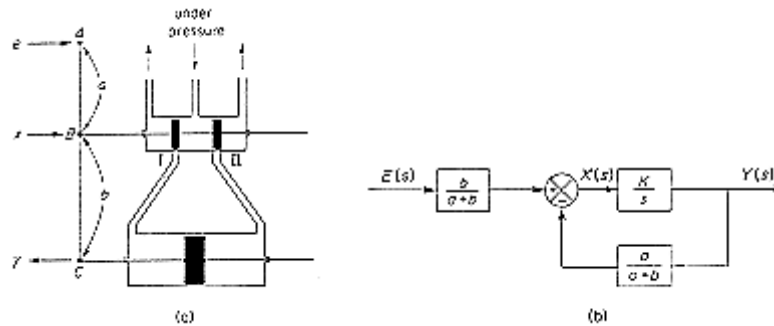
Figure 16-23: a) Servomoter that acts as a proportional controller; b) block diagram of the servomotor. From Ogata (1990) [137].

The left side of the pilot valve is joined to the left side of the power piston by a link ABC. This link is a floating link rather than one moving about a fixed pivot.

The controller operates in the following way. If input x moves the pilot valve to the right, port II will be uncovered and high-pressure fluid will flow through it into the right side of the power piston and force this piston to the left. The power piston, in moving to the left, will carry the feedback link ABC with it, thereby moving the pilot valve to the left. This action continues until the pilot piston again covers ports I and II. A block diagram of the system is shown in Figure 16-23(b). The transfer function between $Y(s)$ and $E(s)$ is given by

$$\frac{dm_G}{dx} = \frac{dm_L}{dx} = 0 \qquad\qquad \text{[16-45]}$$

Notice that under normal operating conditions the relation $|Ka/[s(a+b)]| > 1$ holds, so that the last equation can be simplified to

$$\frac{Y(s)}{E(s)} \approx \frac{b}{a} = K_p \qquad\qquad \text{[16-46]}$$

The transfer function between y and x becomes a constant. Thus, the hydraulic controller shown in Figure 16-23(a) acts as a proportional controller, the gain of which is K_p. This gain can be adjusted by effectively changing the lever ratio b/a.

16.4.3.2   Proportional-derivative control actions

16.4.3.2.1   Pneumatic pd controller

Consider the pneumatic controller shown in Figure 16-24(a). Assuming small changes in the actuating error, nozzle-flapper distance, and control pressure, the operation of this controller can be described as follows: Let first assume a small step change in e. Then the change in the control pressure p_c will be instantaneous. The restriction R will momentarily prevent the feedback bellows from sensing the pressure change p_c. Thus the feedback bellows will not respond momentarily, and the pneumatic actuating valve will feel the full effect of the movement of the flapper. As time goes on, the feedback bellows will expand or contract. The change in the nozzle-flapper distance x and the change in the control pressure p_c, can be plotted against time t, as shown in Figure 16-24(b). At steady state, the

feedback bellows acts like an ordinary feedback mechanism. The curve p_c versus t clearly shows that this controller is of the proportional-derivative type.
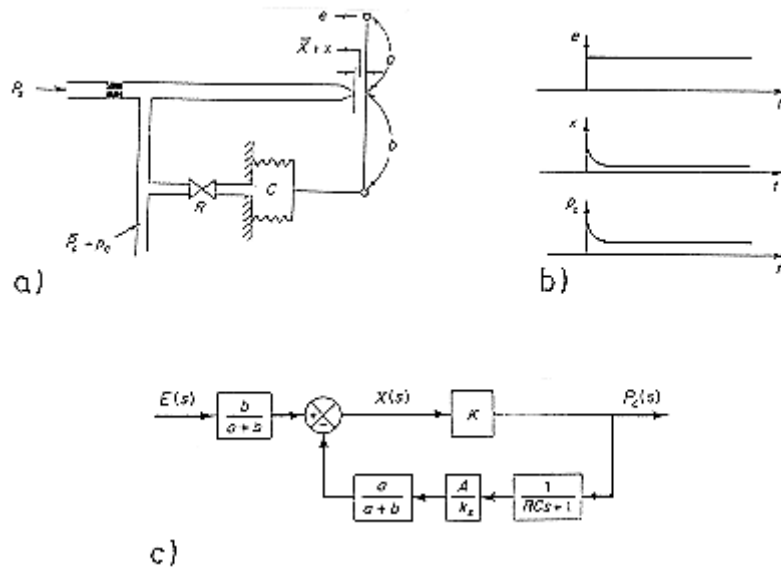
Figure 16-24: a) Pneumatic proportional-derivative controller; b) step change in *e* and the corresponding changes in *x* and *p_c* plotted versus *t*; c) block diagram. From Ogata (1990) [137].

A block diagram corresponding to this pneumatic controller is shown in Figure 16-24(c). In the block diagram, K is a constant, A is the area of the bellows, and k_s is the equivalent spring constant of the bellows. The transfer function between p_c and e can be obtained from the block diagram as follows:

$$\frac{P_c(s)}{E(s)} = \frac{\dfrac{b}{a+b}K}{1+\dfrac{Ka}{a+b}\dfrac{A}{K_s}\dfrac{1}{RCs+1}}$$

[16-47]

In such a controller the loop gain $KaA/[(a+b)k_s(RCs+1)]$ is normally very much greater than unity, thus the transfer function $P_c(s)/E(s)$ can be simplified to give

$$\frac{P_c(s)}{E(s)} = K_p(1+T_d s)$$

[16-48]

where

$$K_p = \frac{bk_s}{aA} \quad , \quad T_d = RC$$

[16-49]

Thus, delayed negative feedback, or the transfer function $1/(RCs+1)$ in the feedback path, modifies the proportional controller to a proportional-derivative controller.

16.4.3.2.2   Hydraulic pd controller

Figure 16-25(a) depicts a schematic diagram of a hydraulic proportional-derivative controller. The cylinders are fixed and the pistons are able to move. For this system, a block diagram is shown in Figure 16-25(b).
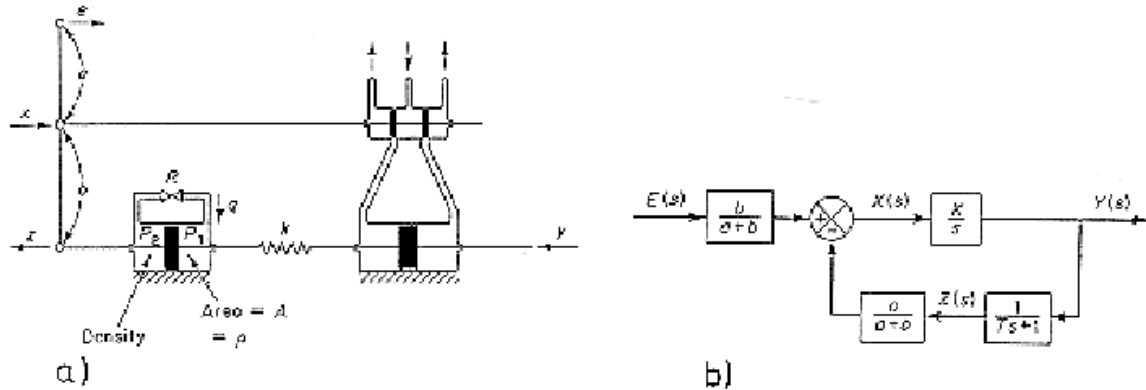
Figure 16-25: a) Sketch of a hydraulic proportional-derivative controller; b) block diagram. From Ogata (1990) [137].

By analysing the mechanism can be stated that

$$k(y-z) = A(p_2 - p_1) \tag{16-50}$$

and, the pressure loss through the resistance R is

$$q = \frac{p_2 - p_1}{R} \tag{16-51}$$

being the flow mass rate, q,

$$q = \rho A \frac{dz}{dt} \tag{16-52}$$

Hence,

$$y = z + \frac{RA^2 \rho}{k} \frac{dz}{dt} \tag{16-53}$$

and, defining the time constant T as

$$T = \frac{RA^2 \rho}{k} \tag{16-54}$$

so

$$y = z + T\frac{dz}{dt} \qquad \text{[16-55]}$$

which implies that in Laplace domain the transfer function is

$$\frac{Z(s)}{Y(s)} = \frac{1}{Ts+1} \qquad \text{[16-56]}$$

Taken into account the feedback branch, and the block diagram in Figure 16-25(b), the transfer function $Y(s)/E(s)$ is:

$$\frac{Y(s)}{E(s)} = \frac{\dfrac{b}{a+b}\dfrac{K}{s}}{1 + \dfrac{a}{a+b}\dfrac{K}{s}\dfrac{1}{Ts+1}} \qquad \text{[16-57]}$$

and, because usually $|aK/[(a+b)s(Ts+1)]| \gg 1$, then

$$\frac{Y(s)}{E(s)} = K_p(1+Ts) \qquad \text{[16-58]}$$

being $K_p = b/a$.

Thus, the controller in Figure 16-25(a) acts as a proportional-derivative controller.

16.4.3.3 Integral control actions

16.4.3.3.1   Hydraulic i controller

The hydraulic servomotor shown in Figure 16-26 is essentially a pilot-valve hydraulic power amplifier and actuator. The pilot valve is a balanced valve in the sense that the pressure forces acting on it are all balanced.
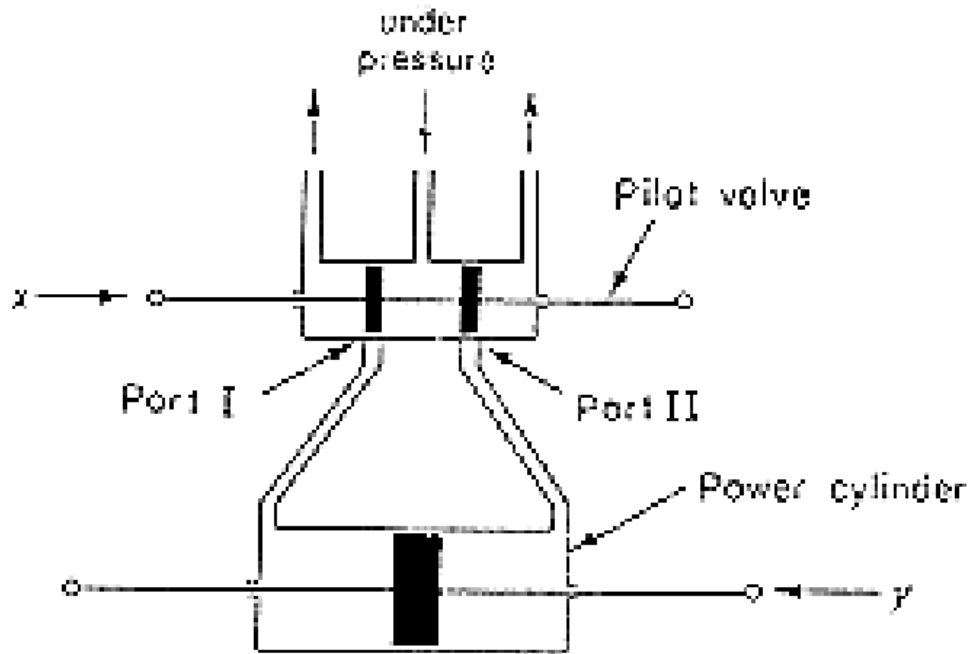
Figure 16-26: Hydraulic integral controller. From Ogata (1990) [137].

The operation procedure is as follows. If input x moves the pilot valve to the right, port II is uncovered, and so high-pressure fluid enters the right side of the power piston. Since port I is connected to the drain port, the fluid in the left side of the power piston is returned to the drain. The fluid flowing into the power cylinder is at high pressure; the fluid flowing out from the power cylinder into the drain is at low pressure. The resulting difference in pressure on both sides of the power piston will cause it to move to the left.

By analysing the system performance, the transfer function is

$$\frac{Y(s)}{X(s)} = \frac{K_1}{A\rho s} = \frac{K}{s} \qquad \text{[16-59]}$$

where $K = K_1/(A\rho)$, being A the piston area, ρ, the fluid (incompressible) density, and K_1 the proportionality constant between the fluid flow rate, q, and the pilot valve displacement, x

$$q = K_1 x \qquad \text{[16-60]}$$

Thus, the simple hydraulic servomotor shown in Figure 16-25(a) acts as an integral controller.

16.4.3.4 Proportional-integral control actions

16.4.3.4.1 Pneumatic pi controller

Consider the pneumatic controller shown in Figure 16-27(a). The operation of this controller is as follows: The bellows denoted by I is connected to the control pressure source without any restriction. The bellows denoted by II is connected to the control pressure source through a restriction R. Assume

a small step change in the actuating error. This will cause the back pressure in the nozzle to change instantaneously. Thus a change in the control pressure p_c also occurs instantaneously. Due to the restriction of the valve in the path to bellows II, there will be a pressure drop across the valve. As time goes on, air will flow across the valve in such a way that the change in pressure in bellows II attains the value p_c. Thus bellows II will expand or contract as time elapses in such a way as to move the flapper an additional amount in the direction of the original displacement e. This will cause the back pressure p_c in the nozzle to change continuously, as shown in Figure 16-27(b).
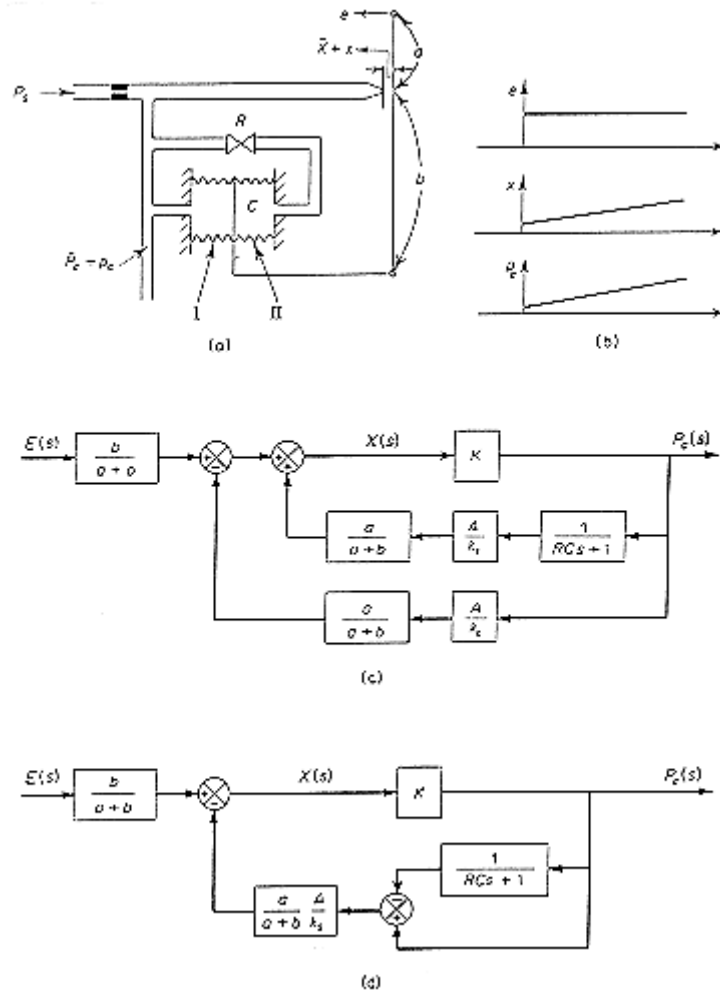
Figure 16-27: a) Pneumatic proportional-integral controller; b) step change in *e* and the corresponding changes in *x* and *p_c* plotted versus *t*; c) block diagram on the controller; simplified block diagram. From Ogata (1990) [137].

A block diagram of this controller under the assumption of small variations in the variables is shown in Figure 16-27(c). A simplification of this block diagram yields Figure 16-27(d). The transfer function of this controller is

$$\frac{P_c(s)}{E(s)} = \frac{\dfrac{a}{a+b}K}{1 + K\dfrac{a}{a+b}\dfrac{A}{k_s}\left(1 - \dfrac{1}{RCs+1}\right)}$$

[16-61]

where K is a constant, A is the area of the bellows, and k_s is the equivalent spring constant of the combined bellows. If $|KaARCs/[(a+b)k_s(RCs+1)]| > 1$ which is usually the case, the transfer function can be simplified to

$$\frac{P_c(s)}{E(s)} = K_p\left(1 + \frac{1}{T_i s}\right) \tag{16-62}$$

where

$$C\frac{dp_o}{dt} = \frac{p_i - p_o}{R} \tag{16-63}$$

Transfer function [16-62] represents a proportional-integral control action.

16.4.3.4.2   Hydraulic pi controller

Figure 16-28(a) shows a schematic diagram or a hydraulic proportional-integral controller. A block diagram of this controller is shown in Figure 16-28(b).
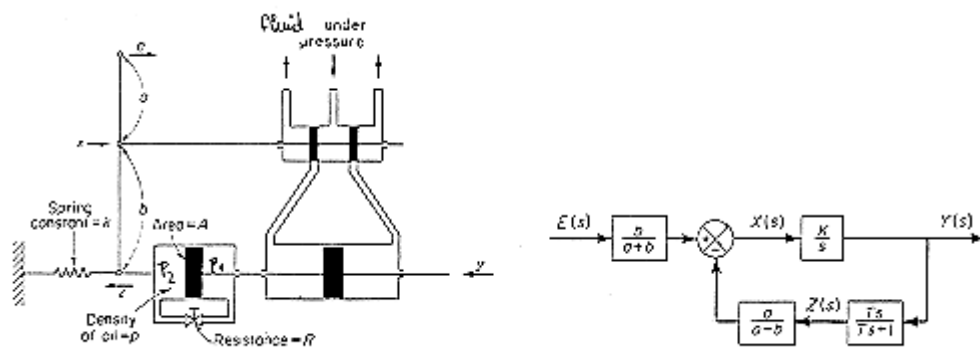
Figure 16-28: a) Schematic diagram of hydraulic proportional-integral controller; b) block diagram. From Ogata (1990) [137].

The transfer function $Y(3s)/E(s)$ is given by

$$\frac{Y(s)}{E(s)} = \frac{\dfrac{b}{a+b}\dfrac{K}{s}}{1 + \dfrac{ka}{a+b}\dfrac{T}{Ts+1}} \tag{16-64}$$

In such a controller, under normal operation $|KaT/[(a+b)(Ts+1)]| > 1$ with the result that

$$\frac{Y(s)}{E(s)} = K_p\left(1 + \frac{1}{T_i s}\right) \tag{16-65}$$

where

$$K_p = \frac{b}{a} \quad , \quad T_i = T = \frac{RA^2\rho}{k} \qquad [16\text{-}66]$$

Thus the controller shown in Figure 16-28(a) is a PI controller.

16.4.3.5 Proportional-integral-derivative control actions

16.4.3.5.1 Pneumatic pid controller

A combination of controllers shown in Figure 16-24(a) and Figure 16-25(a) yields the PID-controller shown schematically in Figure 16-29(a), whose corresponding block diagram is depicted in Figure 16-29(b).
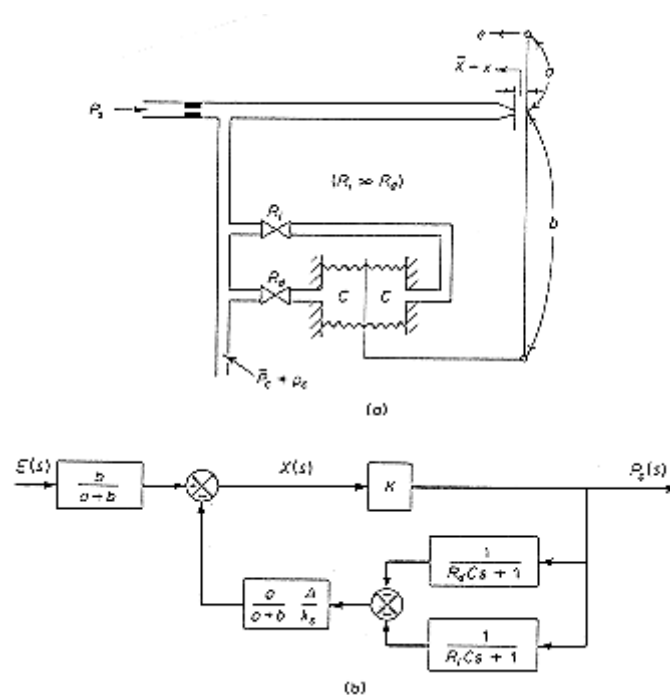
Figure 16-29: a) Pneumatic proportional-integral-derivative controller; b) block diagram of the controller. From Ogata (1990) [137].

Under the assumption of small perturbations, the transfer function is

$$\frac{P_c(s)}{E(s)} = \frac{\dfrac{bK}{a+b}}{1 + K\dfrac{a}{a+b}\dfrac{A}{k_s}\dfrac{(R_iC - R_dC)s}{(R_dC_s + 1)(R_iC_s + 1)}} \qquad [16\text{-}67]$$

By defining

$$T_i = R_iC \quad , \quad T_d = R_dC \qquad [16\text{-}68]$$

and noting that under normal operation

$$\left|KaA(T_i - T_d)s/\left[(a+b)k_s(T_d s + 1)(T_i s + 1)\right]\right| \gg 1 \ and \ T_i \gg T_d \qquad [16\text{-}69]$$

and $T_i \gg T_d$, equation [16-62] reduces to

$$\frac{P_c(s)}{E(s)} = K_p\left(1 + \frac{1}{T_i s} + T_d s\right) \qquad [16\text{-}70]$$

with

$$K_p = \frac{bk_s}{aA} \qquad [16\text{-}71]$$

Equation [16-70] indicates that the system in Figure 16-29(a) is a PID controller.

16.4.4   Summary

Table 16-2 summarises the theory presented in previous clauses. It also includes the main physical parameters and how the parameters in the transfer function can be calculated based on its physical characteristics.

Table 16-2: Summary of Implementation Techniques

Control Action	Analog Device	Clause	Parameters	Functional Scheme	Block Diagram
P	Force-Distance, Pneumatic	12.4.3.1.1	$K_p = \dfrac{b/(a+ab)}{1 + K\dfrac{a}{a+b}}\dfrac{A}{k_s}$ a,b: lever geometry A: bellows area K: ratio between control pressure and nozzle-flapper distance k_s: bellows equivalent spring constant	Figure 16-21a	Figure 16-21b
	Force-Balance, Pneumatic	12.4.3.1.2	$K_p = \dfrac{A_2 - A_1}{A_1}$ A_2: area of the middle diaphragm A_1: area of the upper and lower diaphragms	Figure 16-22	
	Hydraulic	12.4.3.1.3	$K_p = \dfrac{b}{a}$ b,a: lever geometry	Figure 16-23a	Figure 16-23b

Control Action	Analog Device	Clause	Parameters	Functional Scheme	Block Diagram
PD	Pneumatic	12.4.3.2.1	$K_p = \dfrac{bk_s}{aA}$, $T_d = RC$ b,a: lever geometry R: valve resistance C: bellow capacitance k_s: bellow equivalent spring constant A: bellow area	Figure 16-24a	Figure 16-24c
	Hydraulic	12.4.3.2.4	$K_p = \dfrac{b}{a}$, $T_d = \dfrac{RA^2\rho}{k}$ ρ: fluid density A: piston area R: valve resistance k: spring constant b,a: lever geometry	Figure 16-25a	Figure 16-25b
I	Hydraulic	12.4.3.2.3	$K_p = \dfrac{b}{a}$, $T_i = \dfrac{RA^2\rho}{k}$ b,a: lever geometry k: spring constant A: piston area ρ: fluid density R: valve resistance	Figure 16-26	
PI	Pneumatic	12.4.3.2.2	$K_p = \dfrac{bk_s}{aA}$, $T_i = RC$ b,a: lever geometry R: valve resistance C: bellow capacitance k_s: bellow equivalent spring constant A: bellow area	Figure 16-27a	Figure 16-27c
	Hydraulic	12.4.3.2.4	$K_p = \dfrac{b}{a}$, $T_i = \dfrac{RA^2\rho}{k}$ b,a: lever geometry k: spring constant A: piston area ρ: fluid density R: valve resistance	Figure 16-28a	Figure 16-28b
PID	Pneumatic	12.4.3.3.1	$K_p = \dfrac{bk_s}{aA}$, $T_d = R_d C$, $T_i = R_i C$ b,a: lever geometry $R_i \gg R_d$ R_i: circuit 2 valve resistance R_d: circuit 2 valve resistance	Figure 16-29a	Figure 16-29b

Control Action	Analog Device	Clause	Parameters	Functional Scheme	Block Diagram
			C: bellow capacitance k_s: bellow equivalent spring constant A: bellow area		

16.5 Hardware description

16.5.1 Introduction

This clause covers a description of the hardware generally used in fluid loops existing in spacecraft control systems. Hardware to be described is classified from the point of view of its function in the control loop. Figure 16-30 depicts a typical block diagram of a fluid loop modelled as a control system.
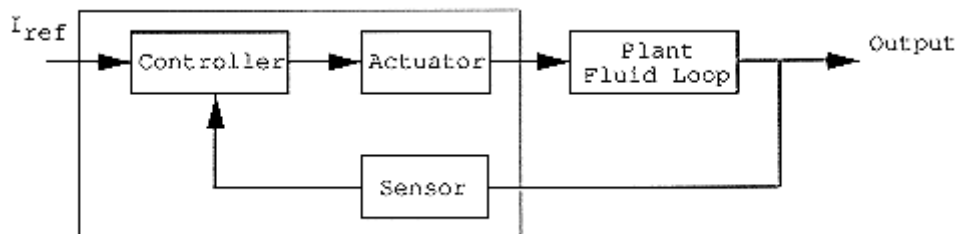
Figure 16-30: Fluidloop modelled as a control system.

The aim of this clause is to enumerate the elements inside the dashed square in Figure 16-30, which are the elements capable of being adapted once the plant design has been closed.

A sensor is a device which converts an input signal into an output signal in a format adequate to be understood by the controller; for example, a device which measures temperature, converting it into a voltage output.

The actuator responds to the controller's demand and gives an output which is a mechanical variable as position, velocity, acceleration, ...

As it has already been mentioned, the low-cost of digital computers and the advantages of handling digital signals are the main reasons for the use of computers as the controller kernel.

Fluid loops are usually designed and sized for operating under specific environmental conditions and component properties (coatings emittance, absorptance, ...). During operative life environmental conditions change and degradation of components occurs; thence, off-design subsystem operation is an important task to be taken into account (Sadunas et al. (1986). In a digital computer the control law can be programmed with parameters that can adapt to the actual working conditions in order to optimise the subsystem performance. Figure 9-3 depicts the control unit block diagram for the fluid loop used for cooling Spacelab Experiments (Microtecnia (1977) [126]) in which the controller is a computer, with interfaces to adapt the signals to those required by the actuators.
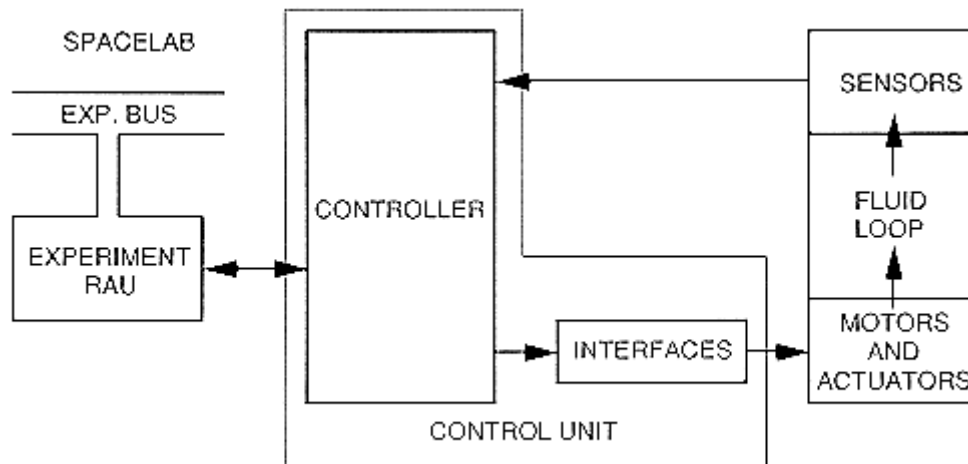
Figure 16-31: Control block diagram of the fluid loop for cooling Spacelab experiments. From Microtecnia (1977) [126].

Due to the new trend toward the inclusion of digital computers as controllers, and since analog controllers have been studied in clause 16.4, clause 16.5.2 focuses on digital computers which can be used as controllers.

Regarding sensors and actuators, a wide variety of combinations can be chosen. They will be analysed in clause 0 and clause 16.5.4 respectively. Figure 16-32 shows two typical fluid loop configurations (already presented in clause 14); in a first approach, only the devices here used will be analysed.
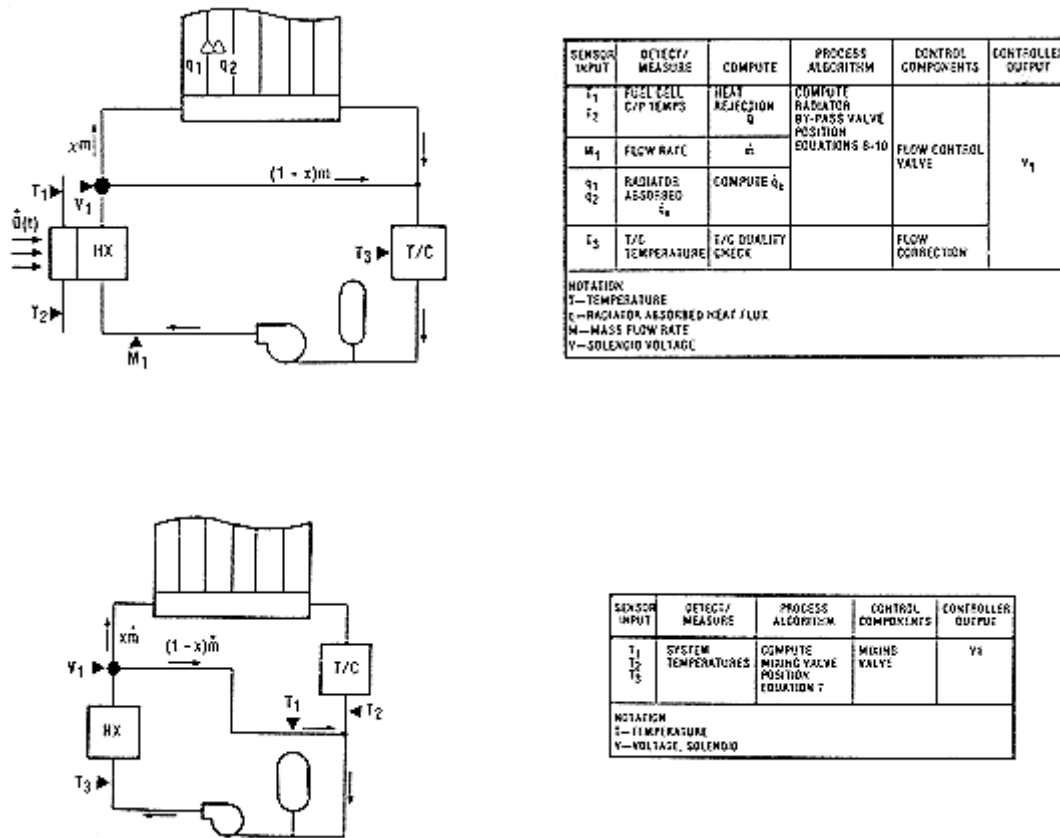
Figure 16-32: Instrumentation and control system schematics. From Sadunas et al. (1986) [154].

16.5.2 Controllers

16.5.2.1 Digital/analog controllers trade/off

The general requirements for the fluid loop control unit (see Figure 16-32) can be described as follows:

(a) To receive electrical signals, corresponding to sensed physical quantities from fluid loop sensors.

(b) To receive commands from a remote processor or from the Ground operation center.

(c) To process both commands and signals and generate actuating commands, to be used by the fluid loop regulating elements in keeping the controlled variables within the specified band.

(d) To provide adequate flexibility for mission to mission and dynamic variations.

The analog controller may be pneumatic/hydraulic (see clause 16.4) or electronic. An electronic analog controller is made up of analog circuitry and modules such as amplifiers, integrators, compensating networks, analog functional modules and similar, which perform, alone or as a whole, the required control functions and laws. A minimum of digital circuitry is also included in order to fulfil the requirement of configuration selection.

A digital controller is built around a central processing unit (CPU) or microprocessor (MPU) which can process both numerical and logical functions, according to a preselected program. Auxiliary hardware consists of memories, input/output devices, timing circuits, ...

The comparison of the main features offered by either solution is shown in Table 16-3. Eleven evaluation criteria are used in order to assess the merit figure of each solution.

Table 16-3: Control unit philosophy trade-off. From Microtecnia (1977) [126].

EVALUATION ITEM	ANALOG CONTROLLER	DIGITAL CONTROLLER
1. Flexibility 1.1. Mission configuration changes	Extensive hardware modification required provided	Dedicated memory cards can be easily
1.2. Payload configuration changes within the same session	Extensive hardware duplication required	Duplication is limited to dedicated memory cards
1.3. Equipment flexibility during development	Very poor. Hardware rework required	Very good [1]. Only software needs to be changed
1.4. Possibility of multimodal operation	Very limited, unless complex hardware arrangement provided	Very good. Instruction by software required
2. Growth capability	Poor	Poor
3. Capability of additional signals processing	Poor. Additional circuitry required	Very good [2]
4. Self-monitoring capability	Limited	Very good
5. Ease of interface with CMDs	Fair. Requires commands D/A conversion. Signal transmission is analog	Good. No conversion required. Digital signal transmission is possible
6. Ease of interface with ECL sensors	Goor for analog signals. Fair for discretes signals	Requires A/D conversion for analog signals. Discrete signals can be readily accepted
7. Ease of interface with actuating elements	Fair [3]	Fair [3]
8. Resistance to the environment	Good	Very good
9. Usage of critical components	Several critical components are foreseen	Very few critical components are foreseen
10. Possibility of introducing redundancies	Fair	Good
11. Need for auxiliary circuitry	Auxiliary circuitry required	No auxiliary circuitry required

NOTE [1] During the development phase, erasable memory may be used.

[2] Provided that the computing time and addressable memory size limitations are not exceeded.

[3] Depends upon actuator requirements.

16.5.2.2 Digital controllers

As the result of this trade-off analysis, it seems that the digital controller offers, generally, advantages over the analog solution in the areas which are more important for the fluid loop applications (Microtecnia (1977) [126]). For this reason, this clause is concentrated on the existing digital option for the controller.

The availability of suitable, qualified hardware has been assessed by means of a literature survey, and looking for the selection adopted in existing satellites. These computers are described in Table 16-4 in terms of CPU, memory I/O system, technology, dimensions, weight, resistance to vibrations and temperature. And Table 9-3 shows other space qualified CPU's.

Table 16-4: Space computers

Name	CPU	Memory [bits]	Power [W]	Temp. [K]	Envir.	Weight [kg]	Size x 10³ [m]	Manufacturer Supplier
DACS	8086 (8087) 5 MHz	RAM: 64 K UVROM: 256 K to 1 M	35 to 80	220 to 340	vib: 14g rms	10,4	217,4x168,3x266,7	SCI Technology INC
SC-1E	80c86 8087 5 MHz	RAM: 1,5 M EEPROM: 1 M UVROM: 1 M	(15) 45	240 to 330	vib: 15g rms	(5.3) 10,7	(454,7x250,0x76,2) 454,7x250,0x193,0	SwRI South-western Research Institute
SC-2	80c86 8087 8 MHz	RAM: 1 M or EEPROM: 1 M or EEPROM + UVROM: 0,5 M Bubble me.: 4 M	30	250 to 350	vib: NA	10,8	355,6x266,7x139,7	SwRI South-western Research Institute
GSVC	Honey-well 1750A	Up to 24 M	15	NA	vib: NA	5,4	203,2x177,8x114,3	Honeywell

Table 16-5: Available microprocessor options

CPU	Supplier	Technology	Bit No.	Remarks
8080A	INTEL	NMOS	8	Extended temperature range. Manufactured according to MIL-M 38510. Screening per MIL—STD 883, level B
PPS4-8 μp16	ROCKWELL ROCKWELL	PMOS PMOS	4-16	Extended temperature range. Screening per MIL-STD 883, level B
Z 80	ZYLOG	NMOS	8	Extended temperature range. Screening per MIL-STD 883, level B
SP B9900	TEXAS INST.	I²L	16	Extended temperature range. Needs only one supply voltage; wide tolerance to voltage variation. Low power consumption
IM6100	INTERSIL/ HARRIS	CMOS	12	Extended temperature range
F100	FERRANTI	BIPOLAR	16	Extended temperature range. Qualification per BS9000
80c31	MATRA/ HARRIS	CMOS	8	Low power consumption. Velocity 12 MHz
80386	INTEL	CHMOS	32	High velocity. High performance. Low cost

16.5.3   Sensors

16.5.3.1   Effects of the sensor on system performance

Since the dynamic and static characteristics of the sensor, or measuring element, affect the indication of the actual value of the output variable, the sensor plays an important role in determining the overall performance of the control system. The sensor usually determines the transfer function in the feedback path. If the time constants of a sensor are negligibly small compared with other time constants of the control system, the transfer function of the sensor simply becomes a constant. Figure 16-33 shows block diagrams of automatic controllers having a first-order sensor, an overdamped second-order sensor, and an underdamped second-order sensor. The response of a thermal sensor is often of the overdamped second-order type.
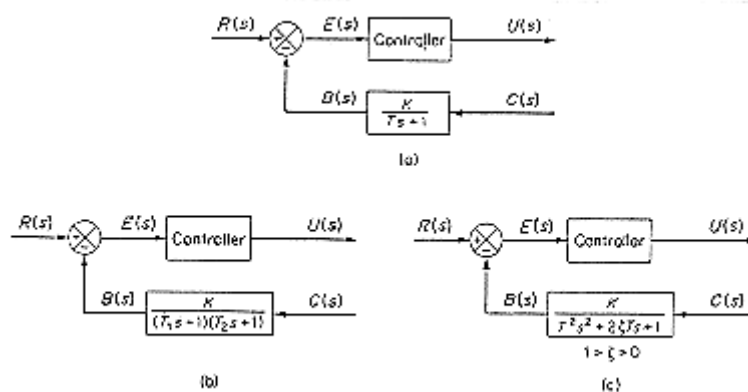
Figure 16-33: Block diagrams of automatic controllers with a) first-order sensor; b) overdamped second-order sensor; c) underdamped second-order sensor. From Ogata (1990) [137].

A block diagram of a simple automatic control system may be obtained by connecting the plant to the automatic controller, as shown in Figure 16-34. Feedback of the output signal is accomplished by the sensor. Then, equation relating the output variable $C(s)$ to the reference input $R(s)$ and disturbance variable $N(s)$ is given by
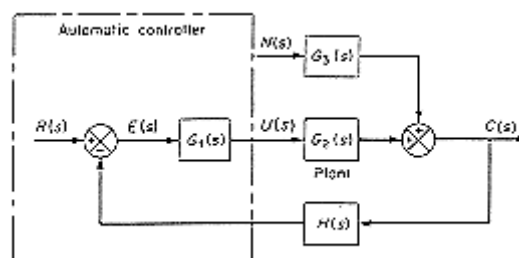
Figure 16-34: Block diagram of a control system.

$$C(s) = \frac{G_1(s)G_2(s)}{1+G_1(s)G_2(s)H(s)}R(s) +$$

$$+ \frac{G_3(s)}{1+G_1(s)G_2(s)H(s)}N(s)$$

[16-72]

16.5.3.2 Temperature sensors

The temperature sensor must be more than just something which responds to a temperature change. Its output must be capable of interpretation and measurement as simply as possible. Table 16-6 presents characteristics of several temperatures sensors.

Table 16-6: Characteristics of several temperature sensors.

Type	Temperature range [K]	Accuracy [K]	Linearity	Repeatability	Response Time	Partial List of Suppliers
Glass Steam Thermometer	145 to 590	0,05 to 1	Linear	Excellent	Good	Brannon Thermometers Ltd. Palmer Instrument Inc. Taylor Instrument Companies Wesksler Instrument Corp.
Bimetallic Thermometer	210 to 700	0,5 to 10	Linear over most of range	Fair	Good	W.M. Chose Co. Cooper Thomas Co. Engelhard Industries Inc.
Resistance Thermometer Ni, Pt	15 to 1250	0,05	Ni- Non linear Pt- linear	Excellent	Good	Honeywell Industrial Div. Fischer & Porter Co. Taylor Instrument Co.
Thermistor	170 to 590	0,05	Non linear	Good	Good	Atkins Technical Inc. Carborundum Co. Thermistor Instruments Co.
Thermocouple T, J, K, R & S	10 to 3030	0,1	K- most linear J-nearly linear	Good	Excellent	Foster Instrument Co. Honeywell Industrial Div.

Type	Temperature range [K]	Accuracy [K]	Linearity	Repeatability	Response Time	Partial List of Suppliers
						Omega Engineering Inc.
Integrated circuit temperature transducer	215 to 420	0,3	Linear	Excellent	Excellent	Analog Devicer Inc.

16.5.3.3   Pressure sensor

There are three basic methods for pressure measurement. The simplest method consists in balancing the unknown pressure against the pressure produced by a column of liquid of known density (Manometers). In the second method the unknown pressure is allowed to act on a known area and the resultant force is measured either directly or indirectly (Dead-weight testers). And the third method, the great majority of pressure sensors, allows the known pressure to act on a flexible member as a Bourbon tube, a stacked diaphragm, or a bellows to sense the pressure; the applied pressure causes a change in the shape of the sensor that is used to move a pointer with respect to a scale.

The application of electronic techniques to measure the deflection of a diaphragm and hence to infer the pressure has resulted in major improvements in both sensitivity and resolution as well as providing means for compensating for nonlinear effects. One of the devices in which these techniques have been applied is the Capacitance manometer. The Piezo-resistive pressure sensors utilise the piezo–resistive effect in order to measure the pressure. The characteristics of most pressure transducers used in fluid loops are presented in Table 16-7.

Table 16-7: Characteristics of pressure sensors.

Name	Type	Pressure range $\times 10^{-3}$ [Pa]	Linearity	Operation Temperature Range [K]	Response time $\times 10^{3}$ [s] (10% to 90%)	Supplier
OEM 1431	Piezo-resistive	0-2000	±0,25%	230 to 400	1,0	IC Sensors
Kavlico	Capacitive	10-3500	±0,3%	260 to 330	--	Dresser Industries
Setra	Capacitive	0,01-70000	< ±0,1%	270 to 350	--	Dresser Industries
PS	Quartz resonant	0-5500	--	330 to 390	--	Paroscientific Inc.

16.5.3.4   Flow sensors

Flow measurement is a technique used in any process requiring the transport of a fluid from one point to another. Depending on the nature of the process streams involved, several types of flow sensors can be considered: displacement flowmeters, magnetic flowmeters, turbine-type flowmeters and metering pumps are generally utilised. Some characteristic of these sensors are shown in Table 16-8.

Table 16-8: Characteristics of flow sensors.

Type	Design pressure x 10^{-3} [Pa]	Flow range x 10^3 [m².s^{-1}]	Accuracy	Partial Suppliers
Magnetic flowmeters	up to 2000	0,001 to 6000	±0,5%	Books Instrument Div. Taylor Instrument Companies Fisher & Porter Co.
Turbine flowmeter	up to 20000	0,0001 to 2500	±0,25%	Books Instrument Div. Cox Instrument Div. Daniel Industries Inc.
Liquid positive displacement meter	up to 2000	0,001 to 1250	±2%	Neptune Meter Co. Books Instrument Div. Dresses Industries
Metering pumps (Diaphragm)	up to 10000	5 to 150	1%	Lapp Insulator Co. Mecomatic Inc. Yarway Corp.

16.5.4 Actuators. Control valves

A control valve is a valve designed to modify the fluid flow in pipes and used for control purposes via an actuator responding to an external signal.

Control valves are used with an external controller having the flexibility of various control modes and with remote manual operation; they are compatible with any measuring system.

The purpose of this clause is to provide a summary of the more important characteristics of valves used in fluid loops, see Table 16-9.

Table 16-9: Characteristics of control valves. From Liptak (1969) [115].

Valve body Features	Conventional Ball Valve and Cage Valve	Pinch Valve	Plug Valve V-ported Type	Plug Valve Adjustable Cylinder Type	Plug Valve Expanding Seat Plate Type	Tube or Diaphragm Type Valve
$\dfrac{Capacity}{d^2} \times 10^6$ [1] [m.s^{-1}]	800	3750	1000	800	1000	750
Max/min Operating Pressure x 10^{-3} [Pa]	17000/ vacuum	1000/ vacuum	5000/ vacuum	800	5000	10000
Max/Min Operating Temperature [K]	1250/20	450	500	475	475	330/250
Available [2] Rangeability	Over 50:1	15:1	20:1	10:1	20:1	20:1

Valve body Features	Conventional Ball Valve and Cage Valve	Pinch Valve	Plug Valve V-ported Type	Plug Valve Adjustable Cylinder Type	Plug Valve Expanding Seat Plate Type	Tube or Diaphragm Type Valve
Flow Characteristics	Good	Poor	Good	Fair	Fair	--
Available Size Range x 10^3 [m]	6-350	3-600	12-600	10-150	50-400	25-300
Cost	Medium-High	Low	Low	Medium	Low	Low-Medium
Low Maintenance	Average	No	Yes	Average	Yes	Average

NOTE   [1] Capacity: is the number of [$m^2.s^{-1}$] of 288 K water that will pass through the valve with a pressure drop of 6,89 KPa.

d: is the valve size.

[2] Rangeability: the ratio of maximum to minimum controllable flows. It establishes the point at which the flow-lift characteristic starts to deviate from the expected.

16.6 Control software

The main objective of this clause is to provide an overview on commonly available software products for analysing control system performances. After a brief historical note on computer-aided control systems design (CACSD), various techniques and tools will be reviewed.

Long before computers were used to design control systems, they were being used to simulate them. Each simulation program consists of two primary segments: one is written to represent the mathematical model of the system, while the other is written to do the experiment itself. One of the earliest simulation programs is CSMP (Continuous Systems Modelling Program) which was a popular simulation environment in the 1960s on various IBM main frame machines. The basic experiment performed in most simulation runs has been the determination of the behaviour of the systems trajectory under the influence of known signals such as "step", "sinusoidal", ... This experiment still constitutes the main feature of many simulation packages of today.

Improper data structure offered with early CAD (Computer-Aided-Design) packages was the main defect. This trend was broken by Moler (1980) introducing a matrix manipulation laboratory software program called MATLAB. It provides a convenient environment for linear algebra and matrix analysis. MATLAB has a rich collection of functions immediately useful to the control engineer or system theorist. Control systems can be modelled as transfer functions or in state-space form, allowing both "classical" and "modern" techniques to be used. Both continuous-time and discrete-time systems are handled.

From MATLAB, several CACSD (Computer-Aided Control Systems Design) package and languages were derived. Table 16-10 shows a list of six CACSD software programs which have been based on the original MATLAB.

Table 16-10: Some MATLAB-Driven CACSD Software .From Cellier and Rimvall (1988) [21]

Software Name	Location Developed, Year	Principle Developer(s)
MATRIXx	Integrated Systems, Inc., USA, 1984	S. Shah, et al.
CRTL-C	Systems Control, Inc., USA, 1984	J.N. Little, et al.
IMPACT	SWISS Federal Institute of Technology, Switzerland, 1983	M. Rimvall, et al.
CONTROL.lab	University of New Mexico, USA, 1985	M. Jamshidi, et al.
PRO-MATLAB	Math Works, Inc., USA, 1985	J.N. Little, et al.
MATLAB-SC	Philips Research Laboratories, Germany, 1985	M. Vanbegin and P. van Dooren

Parallel to, and even before the discovery of MATLAB by control systems engineering community, a number of non-MATLAB software programs were created both in North America and Western Europe. A list of eight non-MATLAB CACSD programs are summarised in Table 16-11.

Table 16-11: Some non-MATLAB CACSD Software Packages. From Cellier and Rimvall (1988) [21]

Software Name	Location Developed, Year	Principle Developer(s)
KEDDC (CADACS)	University of Bochum, Germany, 1979	H. Unbehauen and Chr. Schmid
LUND	Lund Ints. Technology, Sweden, 1978	K.J. Aström and H. Elmqvist
L-A-S	University of Illinois, USA, 1980	S. Bingulac, et al.
TIMDOM	University of New Mexico, USA, 1983	M. Jamshidi, et al.
CC	California Inst. of Technology, USA, 1984	P.M. Thompson
TRIP	Delft University of Technology, The Netherlands, 1985	P.P.J. van den Bosch
WCDS	University of Waterloo, Canada, 1986	J.P. Aplevich
CATPAC	Philips Laboratories, Germany, 1986	D. Buenz

It is estimated that over 50 different packages of different degrees of development exist in the world today. Table 16-12 shows a brief survey of 22 CACSD packages. This table is an abbreviated version of a more extensive one of Cellier and Rimvall (1988) [21] with new additions from Jamshidi et et al. [100]; 14 aspects of CACSD packages have been highlighted. The first six are considered as basic attributes which should be available in all packages, the next five attributes are considered as more advanced ones which may not be available in all programs; the final three attributes are a matter of choice on the part of the developers and purchasers of the particular program.

Table 16-12: A Brief Survey of 22 CACSD Packages. From Jamshidi et al. (1992) [100]

GLOBAL CLASSIFICATION	1 MATLAB	2 CTRL-C	3 MATRIXx	4 PC-MATLAB	5 CATPAC	6 CONTROL-lab	7 IMPACT	8 MATLAB-SC	9 CADACS (KEDDC)	10 LUND	11 LAS	12 TIMDOM	13 CC	14 TRIP	15 WCD-DSC	16 ICARE	17 MADPAC	18 PAAS	19 SANCAD	20 SSPAK	21 SUBOPT	22 SUNS
Continuous Systems	0	2	2	2	1	2	2	1	2	2	1	2	2	2	2	2	0	1	1	0	2	2
Discrete Systems	0	2	2	2	1	2	2	1	2	2	1	2	2	2	2	0	2	0	1	2	0	2
Time Domain	0	2	2	2	1	2	2	1	2	2	1	2	2	2	2	2	0	0	0	2	2	0
Frequency Domain	0	2	2	2	1	1	2	0	2	2	1	0	2	2	2	2	2	2	1	0	0	2
SISO*	0	2	2	2	1	2	2	1	2	2	1	2	2	2	2	2	2	2	1	2	2	2
Multivariable	0	1	1	1	1	2	2	0	2	1	1	1	2	0	2	2	0	0	1	0	2	2
Nonlinear Systems	0	2	2	0	1	1	1	0	1	1	1	0	0	1	0	0	0	0	2	1	0	2
Adaptive Control	0	0	1	1	0	0	0	0	2	2	0	0	0	0	0	0	2	0	0	0	0	0
Identification	0	1	1	1	1	0	1	0	2	2	1	0	0	1	0	0	2	0	0	2	1	0
Real-Time Interface	0	0	2	0	0	0	0	0	2	2	0	0	0	0	0	0	0	0	0	0	0	0
Extendability	2	2	2	2	2	1	2	1	1	1	2	0	0	1	0	1	0	1	1	0	0	0
Source Code Availability	2	0	0	1	0	2	0	0	1	1	0	2	0	2	0	0	2	1	1	0	2	0
Maintenance	0	2	2	2	1	0	0	1	1	1	1	1	2	1	1	1	1	1	1	1	1	1
Cost	2	0	0	1	1	2	2	1	1	1	2	2	2	1	1	1	1	1	1	1	0	0
Total No. of Points	6	18	21	19	12	17	18	7	23	22	13	14	14	17	14	13	13	9	11	10	12	13

NOTE   * Single Input Single Output

Among the MATLAB-based programs, this particular survey reveals that MATRIXx is the most complete CACSD package.

Among the non-MATLAB packages the CADACS(KEDDC) and LUND score very high. It is noted that among all packages in Table 16-3, CADACS of Schmid (1985) ranks on the top CACSD programs availabletoday.

16.7 Existing systems

16.7.1 Space radiator system

16.7.1.1 General description

This example has been extracted from a paper by Baker et. al (1967) [3]. The study focuses on the design of the radiator system for the vehicle control/life support system. The vehicle considered is a large manned orbital research laboratory. The system illustrates the proportional control, along with concepts as saturations and a differential gap

Figure 16-35 depicts the system, and its main characteristics are summarised in Table 16-13.
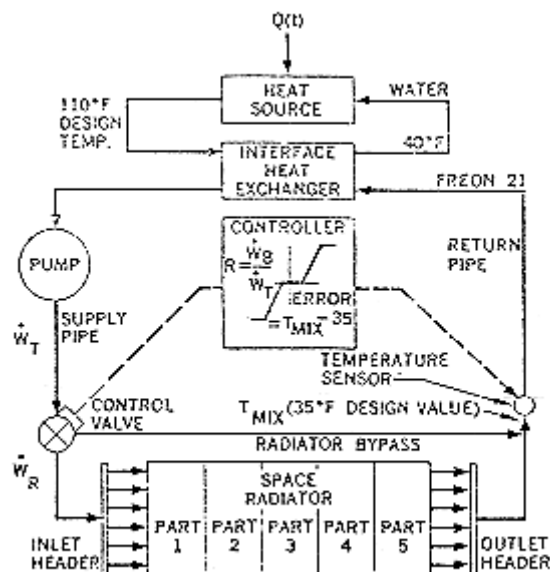
Figure 16-35: Space radiator system. From Baker et al. (1967) [3].

Table 16-13: System characteristic. From Backer et al. (1967) [3]

Radiator system
1.   Coolant: Freon 21 at 2000 kPa.
2.   Fluid in interfacing loop: water. Water inlet temperature to heat exchanger = 316 K Water outlet temperature from heat exchanger = 277 K.
3.   Design point circumferential average sink temperature = 500 K.
4.   Freon 21 minimum permissible temperature = 165 K.
Interface heat exchanger
1.   Counterflow type
2.   Plate and fin construction
3.   AISI 301 stainless steel ρ_m = 7800 kg.m^{-3} K = 14,4 W.m^{-1}.K^{-1} c = 460 J.kg^{-1}.K^{-1}
4.   Heat exchanger headers and shell weight accounted for by the ratio 1,3 between total heat exchanger weight and core weight.
Radiator
1.   Circumferential length for 1 pass = 20,7 m.
2.   Classical tube and fin construction
3.   Tube wall thickness = 2,54 x 10-3 m.
4.   Freon 21.
5.   6061-T6 aluminium alloy
Pump
1.   Overall efficiency, η = 30%
Supply and Return Plumbing
1.   Supply and return plumbing effective lengths = 18,3 m each.
2.   Ten bends in each branch. Pressure loss coefficient for bends = 0,7
3.   Pressure loss based on length and bends multiplied by 2 to account for fittings, valves, manifolds, and so on.
4.   6061-T6 aluminium alloy.
Sensor
1.   Temperature sensor. Time constant 30 s
Actuator
1.   By-pass valve.
Controller
1.   Controls Freon mix temperature in return plumbing to 275 K nominal.
2.   Proportional speed controller: Dead band = ± 0,5 K.
3.   Gain = 1,8 (sK)$^{-1}$ (control valve position rate of change per Freon mix temperature error).

The 316,5 K water inlet temperature is indicative of acceptable electronic cold plate temperatures and the 280 K outlet temperature is indicative of required cabin condenser fluid inlet temperatures. The 15 kW transferred to the Freon stream at the heat exchanger is indicative of expected environmental control/life support system heat loads and it is considered as the design point. The system includes a by-pass valve upstream of the radiator and a controller which adjusts the valve by-pass flow such that the mixed fluid temperature downstream of the radiator is maintained at a nominal 275 K. The system was designed for no by-pass flow with steady-state conditions at the above design heat load (15 kW). For reduced thermal environmental conditions, the radiator outlet temperature is reduced due to the increased cooling effect of this environment. Initially the mixed radiator outlet temperature is also reduced. The controller then increases the by-pass flow until the mixed outlet temperature approaches 275 K. The reduced flow in the radiator results in even lower radiator outlet temperatures since the heat rejection rate is proportional to the product of radiator flow rate and radiator temperature drop.

From the point of view of control theory the system is comprised of the following elements:

1. Plant. It consists in:

    o - Interface heat exchanger

    o - Coolant pump

    o - Radiator supply plumbing

    o - Radiator return plumbing

    o - Bypass plumbing

2. Controller

3. Sensor: Temperature sensor

4. Actuator: By-pass valve.

Figure 16-36 depicts a block diagram of the system.
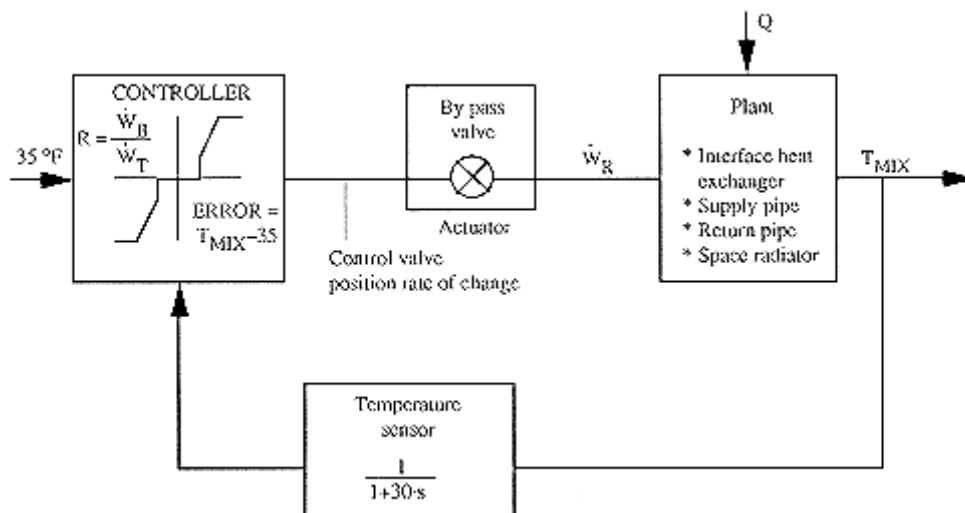
Figure 16-36: Space radiator block diagram. From Baker et al. (1967) [3].

The temperature sensor measures the mixed radiator outlet temperature and the controller is required to maintain it a 35 F despite variations in the system heat load, Q, and variation in the thermal environment. The system is designed for zero position of the by-pass valve (no flow through the by-pass pipe) at the nominal heat load.

The error signal is calculated inside the controller and then, a signal is generated which determines the position rate of change. Therefore, the controller input is an error in temperature ($e(t) = T_{MIX} - T_{ref}$) and its output is the speed of the valve anchor, $u(t)$, as follows:

$u(t) = G.e(t)$, G being the gain; in this case, $G = 1,8$ [s.K]$^{-1}$

The real control law is a proportional action with slight modifications: to prevent for an excessive power consumption a dead band of ±0,5 K has been included, so that when the temperature error is less than 0,5 K no output is generated.

Also, the output must not be greater than the maximum speed which the actuator is able to produce, and constraints have been added in this sense.

The control law implemented in the controller is summarised in Table 16-14.

Table 16-14: Control law for the block diagram in Figure 16-36

Input	Output	Remarks
$\|e(t)\| < 1$	$u(t) = 0$	Dead band. Avoid excessive power consumption.
$\|G.e(t)\| < U_{MAX}$	$u(t) = G.e(t)$	Proportional law
$\|G.e(t)\| > U_{MAX}$	$u(t) = U_{MAX}$	Physical contract one to maximum speed at valve actuator.
$\|G.e(t)\| < -U_{MAX}$	$u(t) = -U_{MAX}$	Physical constraint due to minimum speed of valve actuator.

Bibliography

[1]   Alario, J., Haslett, R., Kosson, R., "The Monogroove High Performance Heat Pipe", AIAA Paper No. 81-1156, AIAA 16th Thermophysics Conference, Palo Alto, Calif., June 23-25, 1981. Also published in "Spacecraft Radiative Transfer and Temperature Control", Progress in Astronautics and Aeronautics, Vol. 83, M. Summerfield, Ed., AIAA, New York, 1982, pp. 305-324.

[2]   Almgren, D.W., Fowle, A.A., Bartoszek, J.T., Ollendorf, S., McIntosh, R., "The Use of a Thermal Utility with Space Platform Mounted Instruments", AIAA Paper No. 81-1114, AIAA 16th Thermophysics Conference, Palo Alto, Calif., June 23-25, 1981.

[3]   Barker, R.S., Stephens, H.M., Taylor, B.N., "Design and Transient Performance of a Liquid Coolant System", SAE Paper No. 670838, SAE Aeronautics & Space Engineering Meeting, Los Angeles, California, October 2-8, 1967.

[4]   Barker, R.S., Stephens, M.M., Taylor, B.N., "Design and Transient Performance of a Liquid Coolant System", SAE Paper No. 670838, SAE Aeronautics & Space Engineering Meeting, Los Angeles, California, October 2-8, 1967.

[5]   Baum, J.R., "Thermal - Design Considerations for Packaging Electronic Equipment", in "Handbook of Electronic Packaging", 1st ed., C.A. Harper, Ed., McGraw-Hill Book Company, New York, 1969, Chap. 11, pp. 1-43.

[6]   Bellomo, M., "Performance of the Interloop Heat Exchanger for the Spacelab T.C.L.", Microtecnica S.p.A., Torino, Italy, TR No. 352, June 1975.

[7]   Bergles, A.E., "Recent Developments in Convective Heat-Transfer Augmentation", Appl. Mech. Rev., Vol. 26, No. 6, June 1973, pp. 675-682.

[8]   Bergles, A.E., "Survey and Evaluation of Techniques to Augment Convective Heat and Mass Transfer", in "Progress in Heat and Mass Transfer", 1st ed., Vol. 1, U. Grigull and E. Hahne, Eds., Pergamon Press, Oxford, 1969, pp. 331-424.

[9]   Bergles, A.E., Lee, R.A., Mikic, B.B., "Heat Transfer in Rough Tubes with Tape - Generated Swirl Flow", Transactions of the ASME, Journal of Heat Transfer, Vol. 91, Series C, No. 3, August 1969, pp. 443-445.

[10]   Berner, F., Oesch, M., Goetz, K., "Development of an Engineering Model Dynamics Cooler", F+W Document No. 5275/82/NL/PB(SL), 1987.

[11]   Berner, F., Savage, C.J., "Development of a Vapor Compression Heat Pump for Space Use", AIAA Paper No. 81-1113, AIAA 16th Thermophysics Conference, Palo Alto, Calif., June 23-25, 1981.

[12]   Berner, F., Scheider, M., "Study of Fluid Systems for Use in Spacecraft Thermal Control", F-W Document No FO-1332, 1976.

[13]   Berner, F., Schleicher, M., "Study of Fluid Loop Systems for Use in Spacecraft Thermal Control", Eidgenossisches Flugzeugwerk-Emmen, Switzerland, F+W Document No. FO-1332, prepared under Contract No. 2447/75 for ESA/ESTEC, October, 1976.

[14]   Berner, F., Schleicher, M., Oesch, H., Nyfeler, H., Steinhauser, H., "Design Study of an Experiment Cooling System with Liquid/Air Heat Exchanger for Spacelab Payloads", Eidgenossisches Flugzeugwerk-Emmen, Switzerland, F+W Document No. FO-1378, prepared under Contract No. 2886/76 for ESA/ESTEC, August, 1977.

[15]   Bolla, G., De Giorgio, G., Pedrocchi, E., "Heat Transfer and Pressure Drop Comparison in Tubes with Transverse Ribs and with Twisted Tape", Energia Nucleare, Vol. 20, No. 11, November 1973, pp. 604-613.

[16]   Boyko, L.D., Kruzhilin, G.N., "Heat Transfer and Hydraulic Resistance During Condensation of Steam in a Horizontal Tube and in a Bundle of Tubes", Int. J. Heat Mass Transfer, Vol. 10, 1967, pp. 361-373.

[17]   Butterworth, D., "Condensers: Basic Heat Transfer and Fluid Flow", in "Heat Exchangers", 1st ed., S. Kakac, A.E. Bergles, F. Mayinger, Eds., Hemisphere Publishing Corporation, Washington, 1981, pp. 289-313.

[18]   Carlisle, R.F., Nolan, M., "Application of Advanced Technology to a Permanently Manned Space Station", Space Technology, Vol. 7, No. 4, 1987, pp. 327-336.

[19]   Carnavos, T.C., "Some Recent Developments in Augmented Heat Exchangers: Design and Theory Sourcebook", 1st ed., N. Afgan and E.U. Schlunder, Eds., McGraw-Hill Book Company, New York, 1974, Clause 21, pp. 441-489.

[20]   Carson, M.A., "Liquid Pump for Astronaut Cooling", in NASA TM-X-58106, pp. 181-185, November 1972, presented at the 7th Aerospace Mechanisms Symposium. Houston, Texas, September 7-8, 1972.

[21]   Cellier, F.E., Rimvall, C.M., "Computer-Aided Control Systems Design: Techniques and Tools", in Systems Modeling and Computer Simulation, N.A. Kheir (ed.), Appendix A, New York, Marcel and Dekker, 1988.

[22]   Chalmers, D.R., Pustay, J.J., "Advanced Communications Satellite Thermal Design Using East/West Radiators", AIAA Paper No. 86-0065, AIAA 24rd Aerospace Sciences Meeting, Reno, Nevada, Jan. 6-9, 1986.

[23]   Chalmers, D.R., Pustay, J.J., Moy, C.B., Kroliczek, E.J., "Application for Capillary Pumped Loop Heat Transport Systems to Large Spacecraft", AIAA Paper No. 86-1295, AIAA/ASME 4th Joint Thermophysics and Heat Transfer Conference, Boston, Mass, June 2-4, 1986.

[24]   Chapter, J.J., Johnsen, G.W., "Thermoelectric Device Application to Spacecraft Thermal Control", AIAA Paper No. 73-722, AIAA 8th Thermophysics Conference, Palm Springs, California, July 16-18, 1973.

[25]   Chisholm, D., "A Theoretical Basis for the Lockhart-Martinelli Correlation for Two-Phase Flow", Int. J. Heat Mass Transfer, Vol. 10, 1967, pp. 1767-1778.

[26]   Cichelly, M.T., Boucher, D.F., "Design of Heat Exchanger Heads for Low Holdup", Chem. Engng. Progr., Vol. 52, No. 5, May 1956, pp. 213-218.

[27]   Colburn, A.P., King, W.J., "Heat Transfer and Pressure Drop in Empty, Baffled, and Packed Tubes. III-Relationship between Heat Transfer and Pressure Drop", Ind. Engng. Chem., Vol. 23, No. 8, August 1931, pp. 919-923.

[28] Cowans, K.W., "A Countercurrent Heat Exchanger that Compensates Automatically for Maldistribution of Flow in Parallel Channels", in "Advances in Cryogenic Engineering", 1st ed., Vol. 19, K.D. Timmerhaus, Ed., Plenum Press, New York, 1974, pp. 437-444.

[29] Csanady, G.T., "Theory of Turbomachines", 1st ed., McGraw-Hill Book Company, New York, 1964, Chap. 1, pp. 1-42.

[30] Delil, A.A.M., "Considerations Concerning a Thermal Joint for a Deployable or Steerable Battery Radiator for the Columbus Polar Platform", NLR TR 86055 U, 1986.

[31] Delil, A.A.M., "Feasibility Demonstration of a Sensor for High-Quality Two-Phase Flow", NLR TR 87009 U, Amsterdam, Jan. 1987.

[32] Delil, A.A.M., "Moveable Thermal Joints for Deployable or Steerable Spacecraft Radiator Systems", NLR MP 87016 U, Amsterdam, Feb. 1987.

[33] Delil, A.A.M., "Sensors for a System to Control the Liquid Flow into an Evaporative Cold Plate of a Two-Phase Heat Transport System for Large Spacecraft", NLR TR 86001 U, 1986.

[34] Dexter, P.F., Haskin, W.L., "Analysis of Heat Pump Augmented Systems for Spacecraft Thermal Control", AIAA Paper No. 84-1757, AIAA 19th Thermophysics Conference, Snowmass, Colorado, June 25-28, 1984.

[35] Dipprey, D.F., Sabersky, R.H., "Heat and Momentum Transfer in Smooth and Rough Tubes at Various Prandth Numbers", Int. J. Heat Mass Transfer, Vol. 6, No. 5, May 1963, pp. 329-353.

[36] Domingos, J.D., "Analysis of Complex Assemblies of Heat Exchangers", Int. J. Heat Mass Transfer, Vol. 12, No. 5, May 1969, pp. 537-548.

[37] DOW CORNING, "Information about Silicone Fluid Products from Dow Corning", Dow Corning, Chemical Products Division, Midland, Michigan 48641, Bulletin 05-061, November 1963.

[38] DOW CORNING, "Information about Silicone Fluids", Dow Corning International LTD, Chaussée de la Hulpe 177, B-1170, Brussels, Belgium, Bulletin 22-039a-01 June 1972.

[39] Dukler, A.E., Wicks III, M., Cleveland, R.G., "Frictional Pressure Drop in Two-Phase Flow: An Approach through Similarity Analysis", A.I.Ch.E. Journal, Vol. 10, No. 1, January 1964, pp. 44-51.

[40] Dunn, P., Reay, D.A., "Heat Pipes", 1st ed., Pergamon Press, Oxford, 1976, Appendix 1, pp. 263-269.

[41] Ebersole, R., "Biosatellite Environmental Control Coolant Loop System Design", in "Proceedings of the Symposium in Thermodynamics and Thermophysics of Space Flight", Palo Alto, California, March 21, 1970, pp. 133-149.

[42] Ellis, W.E., Rankin, J.G., "Heat Buses Will Operate Like a Public Utility", Astronautics & Aeronautics, Vol. 21, No. 3, March 19983, pp. 56-61.

[43] Engel, J., Walter, H., "Design of a Small Centrifugal Pump for Subcooled and Boiling Liquids ($77 < T < 300$ K)", Fifth International Cryogenic Engineering Conference, Kyoto, Japan, May 7-10, 1974, Paper No. 11.

[44] ESA, "Environmental and Thermal Control Systems for Space Vehicles", ESA SP-200, Toulouse, Session III, 1983.

[45] ESA-NASA, "Spacelab Payload Accomodation Handbook", SLP 2104, Iss. 2, Rev. 14/Appendix C, Rev. 5, 1988.

[46]   ESDU 66027, "Friction Losses for Fully - Developed Flow in Straight Pipes", Engineering Sciences Data Unit, 4 Hamilton Place, London, WI, September 1966.

[47]   ESDU 67040, "Pressure Losses for Incompressible Flow in Single Bends", Engineering Sciences Data Unit, 4 Hamilton Place, London WI, November 1967.

[48]   ESDU 68006, "Forced Convection Heat Transfer in Circular Tubes. Part II: Data for Laminar and Transitional Flows Including Free Convection Effects", Engineering Sciences Data Unit, 251-259 Regent Street, London WI, February 1968.

[49]   ESDU 68035, "Interaction Factors for Calculating Pressure Losses for Incompressible Flow in Some Combinations of Two Bends in Series", Engineering Sciences Data Unit, 251-259 Regent Street, London W1R 7AD, July 1968.

[50]   ESDU 69004, "Convective Heat Transfer During Forced Crossflow of Fluid over a Circular Cylinder Including Free Convection Effects", Engineering Sciences Data Unit, 251-259 Regent Street, London, W1R 7AD, May 1969.

[51]   ESDU 69022, "Pressure Losses in Valves", Engineering Sciences Data Unit, 251-259 Regent Street, London, W1R 7AD, October 1969.

[52]   ESDU 72009, "Pressure Drop in Ducts across Round-Wire Gauzes Normal to the Flow", Engineering Sciences Data Unit, 251-259 Regent Street, London W1R 7AD, June 1972.

[53]   ESDU 72010, "Pressure Losses across Perforated Plates, Orifice Plates and Cylindrical Tube Orifices in Ducts", Engineering Sciences Data Unit, 251-259 Regent Street, London W1R 7AD, June 1972.

[54]   ESDU 72011, "Flow through a Sudden Enlargement of Area in a Duct", Engineering Sciences Data Unit, 251-259 Regent Street, London W1R 7AD, June 1972.

[55]   ESDU 73022, "Pressure Losses in Three-Leg Pipe Junctions: Dividing Flows", Engineering Sciences Data Unit, 251-259 Regent Street, London W1R 7AD, October 1973.

[56]   ESDU 73023, "Pressure Losses in Three-Pipe Junctions: Combining Flows", Engineering Sciences Data Unit, 251-259 Regent Street, London W1R 7AD, October 1973.

[57]   ESDU 73031, "Convective Heat Transfer During Crossflow of Fluids over Plain Tube Banks", Engineering Sciences Data Unit, 251-259 Regent Street, London W1R 7AD, November 1973.

[58]   ESDU 77008, "Pressure Losses in Curved Ducts: Single Bends", Engineering Sciences Data Unit, 251-259 Regent Street, London W1R 7AD, May 1977.

[59]   ESDU 77009, "Pressure Losses in Curved Ducts: Interaction Factors for Two Bends in Series", Engineering Sciences Data Unit, 251-259 Regent Street, London W1R 7AD, May 1977.

[60]   EURAMO-POMPES SALMSON, "Euramo XA15-R", 102/7//06/77-ed.1. "Euramo MX", 102/8/09/77-ed.1. Division Electro-Hydraulique LMT, 46-47, Quai A. Le Gallo, Boulogne-Billancourt, France, 1977.

[61]   Evans, L.B., Churchill, S.W., "The Effect of Axial Promoters on Heat Transfer and Pressure Drop Inside a Tube", Chem. Engng. Progr. Symposium Ser., Vol. 59, No. 41, 1963, pp. 36-46.

[62]   Evans, S.I., Sarjant, R.J., "Heat Transfer and Turbulence in Gases Flowing Inside Tubes", J. Inst. Fuel, Vol. 24, No. 5, September 1951, pp. 216-227.

[63] Filippi, F., Arcidiacono, A., "Design Study of a Liquid Heat Transfer Loop for Thermal Conditioning of Spacelab Experiment Payloads", MICROTECMICA Document No. RT-598, 1977.

[64] Filippi, F., Guerra, L., "Screening and Selection of Coolant Fluids for E.C.L.", Microtecnica, Turin, Italy, TR No 584, prepared under ESTEC Contract 2995/76/NL/PP(SC), 15 December 1977.

[65] Fleming, R.B., "The Effect of Flow Distribution in Parallel Channels of Counterflow Heat Exchangers", in "Advances in Cryogenic Engineering", 1st ed., Vol. 12, K.D. Timmerhaus, Ed., Plenum Press, New York, 1967, pp. 352-362.

[66] Fortescue, P., Stark, J., "Spacecraft Systems Engineering", John Wiley & Sons, Baffing Lane, Chichester, 1991.

[67] Fraas, A.P., Ozisik, M.N., "Heat Exchanger Design", 1st ed., John Wiley & Sons, Inc., New York, 1965, Chap. 6, p. 98.

[68] French, E., "Thermal Design of Rotatable Cryogenic Heat Pipe Joints", AIAA Paper No. 85-0068, AIAA 23rd Aerospace Sciences Meeting, Reno, Nevada, Jan. 14-17, 1985.

[69] Gambill, W.R., Bundy, R.D., Wansbrough, R.W., "Heat Transfer, Burnout and Pressure Drop for Water in Swirl Flow through Tubes with Internal Twisted Tapes", Chem. Engng. Progr. Symposium Ser., Vol. 57, No. 32, 1961, pp. 127-137.

[70] Gao, H.H., Zhou, F.D., Chen, X.J., "Void Fraction Measurement Using the Conductance-Probe Technique in Air-Water Two-Phase Flow", in "Two-Phase Flow and Heat Transfer", X.J. Chen & T. Nejat Veziroglu, Eds., Hemisphere Publishing Corporation, Washington, 1985, pp. 57-61.

[71] GELBER, "Gelber Pumps 77-78", Gelber Pump Co., 5806 North Lincoln Avenue, Chicago, Illinois 60659, 1976.

[72] Gilmour, C.H., "No Fooling - No Fouling", Chem. Engng. Prog., Vol. 61, No. 7, July 1965, pp. 49-54.

[73] Goldstein, S., " Modern Developments in Fluid Dynamics", 3rd ed., Vol. II, Oxford at the Clarendon Press, 1950, Chap. XV, pp. 646-660.

[74] Gomelauri, V.I., "Methods and Results of an Experimental Investigation into Processes of Intensification of Convective Heat Transfer", Thermal Engineering (Teploenergetika), Vol. 211, No. 9, Sept. 1974, pp. 1-5.

[75] Govier, G.W., Aziz, K., "The Flow of Complex Mixtures in Pipes", 1st ed., Van Nostrand Reinhold Company, New York, 1972.

[76] Greene, N.D., "Convair Aircraft, private communication to W.R. Gambill", quoted by Bergles (1969), May 1960.

[77] Grote, M.G., Swanson, T.D., "Design and Test of a Pumped Two-Phase Mounting Plate", AIAA Paper No. 85-0919, AIAA 20th Thermophysics Conference, Williamsburg, Virginia, June 19-21, 1985.

[78] Hall, W.B., "Heat Transfer in Channels Having Tough and Smooth Surfaces", J. Mech. Engng. Sci., Vol. 4, No. 3, March 1962, pp. 287-291.

[79] HAMILTON STANDARD, "GSE Heat Exchanger Package", CEI No. MC 250-0001-0025 Item No. 7.5. "Freon-to-Water Interchanger Package", CEI No. MC 250-0001-0040 Item No. 7.7. "Avionics Cooling Assembly", CEI No. MC 621-0008-0002 Item No. 3.70.

Hamilton Standard, Division of UAC Electronic System, Bradley Field Road, Windsor Locks, Connecticut 06096.

[80] Hanjalic, K., Launder, B.E., "Fully Developed Asymmetric Flow in a Plane Channel", J. Fluid Mech., Vol. 51, Part 2, 25 January 1972, pp. 301-335.

[81] Heap, R.D., "Heat Pumps", 1st ed., E & F.N. Spon Ltd., London, 1979.

[82] Heaton, H.S., Reynolds, W.C., Kays, W.M., "Heat Transfer in Annular Passages. Simultaneous Development of Velocity and Temperature Fields in Laminar Flow", Int. J. Heat Mass Transfer, Vol. 7, No. 7, July 1964, pp. 763-781.

[83] Heizer, B.L., Goo, S.D., Rhodes, G.D., Thoreson, D.W., Parish, R.C., "A Steerable Radiator for Spacecraft Application", AIAA Paper No. 86-1298, AIAA/ASME 4th Joint Thermophysics and Heat Transfer Conference, Boston, Mass, June 2-4, 1986.

[84] Helenbrook, R.G., Antony, F.M., Fisher, R.M., "Selection of Space Shuttle Thermal Protection Systems", AIAA Paper No. 71-443, AIAA 6th Thermophysics Conference, Tullahoma, Tennessee, April 26-28, 1971.

[85] Hetsroni, G., "Handbook of Multiphase Systems", 1st ed., Hemisphere Publishing Corporation, Washington, 1982.

[86] Hewitt, G.F., "Liquid-Gas Systems - Flow Regimes", in "Handbook of Multiphase Systems", 1st ed., G. Hetsroni, Ed., Hemisphere Publishing Corporation, Washington, 1982, Chap. 22, pp. 2-3 to 2-43.

[87] Hewitt, G.F., "Measurement of Void Fraction", in "Handbook of Multiphase Systems", 1st ed., G. Hetsroni, Ed., Hemisphere Pub. Co., Washington, 1982, Chap. 10, pp. 10-21 to 10-33.

[88] Hinderer, B., Savage, C.J., "Development of a Movable, Thermally Conducting Joint for Application to Deployable Radiators", in "Spacecraft Thermal and Environmental Control Systems", ESA SP-139, Paris, Nov. 1978, pp. 449-452.

[89] Hinze, J.O., "Turbulence", 1st ed., McGraw-Hill Book Company, Inc., New York, 1959, Chap. 7, pp. 537-553.

[90] Holmberg, R.B., "Heat Transfer in Liquid-Coupled Indirect Heat Exchanger Systems", Transactions of the ASME, Journal of Heat Transfer, Vol. 97, Series C, No. 4, November 1975, pp. 499-503.

[91] Hong, S.W., Bergles, A.E., "Augmentation of Laminar Flow Heat Transfer in Tubes by Means of Twisted-Tape Inserts", Transactions of the ASME, Journal of Heat Transfer, Vol. 98, Series C, No. 2, May 1976, pp. 251-256.

[92] Hu, M., Chang, Y.P., "Optimization of Finned Tubes for Heat Transfer in Laminar Flow", Transactions of the ASME, Journal of Heat Transfer, Vol. 95, Series C, No. 3, August 1973, pp. 332-338.

[93] Hutchinson, P., Whalley, P.B., "A Possible Characterization of Entrainment in Annular Flow", Chem. Engng. Sci., Vol. 28, 1973, pp. 974-975.

[94] Hwangbo, H., McEver, W.S., "High Thermal Capacity Cold Plate/Hot Plate", AIAA Paper No. 85-0921, AIAA 20th Thermophysics Conference, Williamsburg, Virginia, June 19-21, 1985.

[95] HYDRAULIC INSTITUTE, "Hydraulic Institute Standards for Centrifugal, Rotary & Reciprocating Pumps", 13th ed., Hydraulic Institute, 1230 Keith Building, Cleveland, Ohio 44115, 1975, pp. 11, 133-134, 173-174.

[96] Ibragimov, M.H., Nomofelov, E.V., Subbotin, V.I., "Heat Transfer and Hydraulic Resistance with the Swirl-Type Motion of Liquid in Pipes", (in Russian), Teploenergetika, Vol. 8, No. 7, July 1961, pp. 57-60.

[97] Idel'cik, I.E., "Memento des Pertes de Charge", Translated from the Russian by M. Meury, 1st ed., Eyrolles Editeur, Pairs, 1969, Chap. II, pp. 55-80, Chap. III, pp. 95-96. Chap. VII, pp. 233-287, Chap. VIII, pp. 312-314.

[98] Ignationis, A.J., Mitchell, K.L., "MSFC Sortie Laboratory Environmental Control Systems (ECS). Phase B Design Study Results", NASA-TM-X-64832, March 1974.

[99] Jakob, M., "Heat Transfer", 6th ed., Vol. 1, John Wiley & Sons, Inc., New York, 1958, Chap. 11, pp. 207-243.

[100] Jamshidi, M., Tarakh, M., Shafai, B., "Computer-Aided Analysis and Design of Linear Control Systems", Prentice-Hall, Inc., Englewood Cliffs, New Jersey, pp. 360-364, 1992.

[101] Kays, W.M., "Convective Heat and mass Transfer", 1st ed., McGraw-Hill Book Company, New York, 1966, Chap. 8, pp. 118-133. Chap. 9, pp. 169-194.

[102] Kays, W.M., London, A.L., "Compact Heat Exchangers", 2nd ed., McGraw-Hill Book Company, New York, 1964, Chap. 1, p. 3, Chap. 2, pp. 10-63, Chap. 4, pp. 86-91. Chap. 6, pp. 103-119. Chap. 9, pp. 137-159. Chap 10, pp. 161-230. Appendix A, p. 232.

[103] Kemeny, G.A., Cyphers, J.A., "Heat Transfer and Pressure Drop in an Annular Gap with Surface Spoilers", Transactions of the ASME, Journal of Heat Transfer, Vol. 83, Series C, No. 2, May 1961, pp. 189-198.

[104] Keshock, E.G., Sadeghipour, M.S., "Analytical Comparison of Condensing Flows Inside Tubes under Earth-Gravity and Space Environments", Acta Astronautica, Vol. 10, No. 7, July 1983, pp. 505-511.

[105] Kissner, G., "Comparison of Heat Transport Fluids for Space Lab Active Thermal Control Systems", DORNIER SYSTEM, SL-B DS- 0076, Friedrichshafen, Germany, 1973.

[106] Klaczak, A., "Heat Transfer in Tubes with Spiral and Helical Turbulators", Transactions of the ASME, Journal of Heat Transfer, Vol. 95, Series C, No. 4, November 1973, pp. 557-559.

[107] Knudsen, J.G., Katz, D.L., "Fluid Dynamics and Heat Transfer", 1st ed., McGraw-Hill Book Company, Inc., New York, 1958, Chap. 15, pp. 407-455.

[108] Kosky, P.G., Staub, F.W., "Local Condensing Heat Transfer Coefficients in the Annular Flow Regime", AIChE Journal, Vol. 17, No. 5, September 1971, pp. 1037-1043.

[109] Kreith, F., Margolis, D., "Heat Transfer and Friction in Swirling Turbulent Flow", 1958 Heat Transfer and Fluid Mechanics Institute, Held at University of California, Berkeley, California, June 19-21, 1958, pp. 126-142.

[110] Kroeger, P.G., "Performance Deterioration in High Effectiveness Heat Exchangers Due to Axial Heat Conduction Effects", in "Advances in Cryogenic Engineering", 1st ed., Vol. 12, K.D. Timmerhaus, Ed., Plenum Press, New York, 1967, pp. 363-372.

[111] Kubair, V., Kuloor, N.R., "Heat Transfer to Newtonian Fluids in Coiled Pipes in Laminar Flow", Int. J. Heat Mass Transfer, Vol. 9, No. 1, January 1966, pp. 63-75.

[112] Kuo, B.C., "Automatic Control Systems", Prentice-hall International, Inc., 1991.

[113] Kurzweg, U.H., Zhao, L.d., "Heat Transfer by High-Frequency Oscillations: A New Hydrodynamic Technique for Achieving large Effective Thermal Conductivities", Phys. Fluids, Vol. 27, No. 11, Nov. 1984, pp. 2624-2627.

[114] Lehtinen, A., Sadunas, J., "Thermal Storage Analysis for Large Manned Space Platforms", AIAA Paper No. 85-0066, AIAA 23rd Aerospace Sciences Meeting, Reno, Nevada, Jan. 14-17, 1985.

[115] Liptak, B.G., "Instrument Engineers Handbook", Chilton Bock Company, 1969.

[116] Lockhart, R.W., Martinelli, R.C., "Proposed Correlation of Data for Isothermal Two-Phase, Two-Components Flow in Pipes", Chem. Engng. Progr., Vol. 45, No. 1, January 1949, pp. 39-48.

[117] London, A., "Thermal Control of the NIMBUS Satellite System", General Electric MSD, AIAA Unmanned Space Meeting, 1965.

[118] London, A.L., "Laminar Flow Gas Turbine Regenerators-The Influence of Manufacturing Tolerances", Transactions of the ASME, Journal of Heat Transfer, Vol. 92, Series A, No. 1, January 1970, pp. 46-56.

[119] London, A.V., "Factors in the Selection of Pumps for Process and Chemical Duties", Pumps-Pompes-Pumpen, No. 88, January 1974, pp. 25-31.

[120] Lopina, R.F., Bergles, A.E., "heat Transfer and Pressure Drop in Tape - Generated Swirl Flow of Single-Phase Water", Transactions of the ASME, Journal of Heat Transfer, Vol. 91, Series C, No. 3, August 1969, pp. 434-442.

[121] Lundgren, T.S., Sparrow, E.M., Starr, J.B., "Pressure Drop Due to the pp. 620-626.

[122] Martinelli, R.C., Nelson, D.B., "Prediction of Pressure Drop During Forced-Circulation Boiling of Water", Transactions of the ASME, Vol. 7, No. 6, August 1948, pp. 695-702.

[123] Masliyah, J.H., Nandakumar, K., "Heat Transfer in Internally Finned Tubes", Transactions of the ASME, Journal of Heat Transfer, Vol. 98, Series C, No. 2, May 1976, pp. 257-261.

[124] Mason, J.L., "Heat Transfer in Crossflow", Proc. Appl. Mechanics, 2nd US National Congress, 1954, pp. 801-803.

[125] McAdams, W.H., "Heat Transmission", 3rd. Ed., McGraw-Hill Book Company, Inc., New York, 1954, Chap. 7, p. 180.

[126] MICROTECNICA, "Heat Exchangers from MICROTECNICA", Microtecnica, Torino, Italy, private Communication by G. Lapidari, February 1977.

[127] MOOG, "Rotary Shutoff (RSO) Disconnect", CAT585-1087 2M. MOOG Space Products Division, Moog Inc., East Aurora, New York, 14052-0018.

[128] Mori, Y., Nakayama, W., "Study on Forced Convective Heat Transfer in Curved Pipes", Int. J. Heat Mass Transfer, Vol. 8, No. 1, January 1965, pp. 67-82.

[129] Nachtigl, C.L., "Instrumentation and Control. Fundamentals and Applications", John Wiley & Sons, 1990.

[130] NASA, "Space and Planetary Environment Criteria Guidelines for Use in Space Vehicle Development (1982 Revision)", NASA TM 82478, Vol. 1, 1983.

[131] Nast, T.C., Barnes, C.B., Wedel, R.K., "Development and Orbital Operation of a Two-Stage Solid Cryogen Cooler for Infrared Detector Cooling", AIAA Paper No. 76-475, AIAA 11th Thermophysics Conference, San Diego, California, July 14-16, 1976.

[132] Nekrasov, B., "Hydraulics for Aeronautical Engineers", Translated from the Russian by V. Talmy. 1st ed., MIR Publishers, Moscow, 1969, Chapter VI, pp. 80-87, Chapter XII, pp. 182-221.

[133] Noltingk, B.E., "Jones Instrument Technology Mechanical Measurements", Butterworths, 1985.

[134] Nunner, W., "Wärmeübergang und Druckabfall in Rahuen Rohren", VDI - Forschungsheft 455, Ausgabe B, Band 22, 1956, pp. 1-39.

[135] Ogata, K., "Discrete-time Control Systems", Prentice-hall International, S.A., Inc., 1987.

[136] Ogata, K., "Ingeniería de Control Moderna", Prentice-hall Hispanoamericana, S.A., Mexico, 1988.

[137] Ogata, K., "Modern Control Engineering", Prentice-hall International, Inc. 2nd Edition, 1990.

[138] Owen, P.R., Thomson, W.R., "Heat Transfer across Rough Surfaces", J. Fluid Mech., Vol. 15, Part 3, March 1963, pp. 321-334.

[139] Owen, R.H., Sessions, B.W., Walker, D.L., "Spacelab Environmental Control System Thermal Studies", Teledyne Brown Engineering, Huntsville, Alabama, Interim Report ESD-EPO1-1993, May 1976.

[140] Palen, J.W., "Principles of Gas-Liquid Two-Phase Flow Calculations", Report TPG-1, Heat Transfer Research, Inc., Alhambra, California, June 1976.

[141] Perry, M.P., "A Survey of Ferromagnetic Liquid Applications", in "Thermomechanics of Magnetic Fluids", B. Berkovsky, Ed., Hemisphere Publishing Corporation, Washington, 1978, pp. 219-230.

[142] Peterson, G.P., "Thermal Control Systems for Spacecraft Instrumentation", J. Spacecraft, Vol. 24, No. 1, Jan-Feb 1987, pp. 7-13.

[143] Petukhov, B.S., Roizen, L.I., "Generalized Dependences for Heat Transfer 3, May-June 1974, pp. 565-569.

[144] Pollak, F., Cruger, C.O., "Comparison of Applications and Characteristics of Positive Displacement and Centrifugal Pumps", Pumps-Pompes-Pumpen, No. 96, September 1974, pp. 400-407.

[145] Pucci, P.F., Howard, C.P., Piersall Jr., C.H., "The Single-Blow Transient Testing Technique for Compact Heat Exchanger Surfaces", Transactions of the ASME, Journal of Engineering for Power, Series A, Vol. 89, No. 1, January 1967, pp. 29-40.

[146] Rabald, E., "Corrosion Guide", 2nd ed., Elsevier Publishing Company, Amsterdam, 1968, pp. 153-156.

[147] Raznjevic, K., "Tables et Diagrammes Termodynamiques", Translated from Serbo-Croatian by R. Podhorsky. 1st ed., Editions Eyrolles, Paris, 1970.

[148] Rehme, K., "Turbulence Measurements in Smooth Concentric Annuli with Small Radius Ratio", J. Fluid Mech., Vol. 72, part 1, 11 November 1975, pp. 189-206.

[149] Reynolds, A.J., "Turbulent Flows in Engineering", 1st ed., John Wiley & Sons, Inc., London, 1974, Chap. 4, pp. 181-240. Chap. 5, pp. 241-285.

[150] Rittenhouse, J.B., Singletary, J.B., "Space Materials Handbook", 3rd ed., NASA SP-3051, 1969, pp. 655-658.

[151] Rufer, C.E., Kezios, S.P., "Analysis of Two-Phase, One-Component Stratified Flow with Condensation", Transactions of the ASME, Journal of Heat Transfer, Vol. 88, Series C, No. 3, August 1966, pp. 265-275.

[152] Rye, H., Steen, J-E., "Seawater as an Energy Resource for Heat Pumps in Norway", in "Water for Energy", J. Standbury, Ed., BHRA, Cranfield, Bedford, England, 1986, pp. 203-216.

[153] Sadunas, J.A., Lehtinen, A., Parish, R., "Thermal Management System Options for High Power Space Platforms", AIAA Paper No. 85-1047, AIAA 20th Thermophysics Conference, Williamsburg, Virginia, June 19-21, 1985.

[154] Sadunas, J.A., Lehtinen, A.M., Nguyen, H.T., Parish, R., "Spacecraft Active Thermal Control Subsystem Design and Operation Considerations", AIAA Paper No. 86-1267, AIAA/ASME 4th Joint Thermophysics and Heat Transfer Conference, Boston, Mass, June 2-4, 1986.

[155] Sadunas, J.A., Lehtinen, A.M., Nguyen, M.T., Parish, R., "Spacecraft Active Thermal Control Subsystem Design and Operation Considerations", AIAA Paper No. 86-1267, AIAA/ASME Conference, Boston, Mass, June 2-4, 1986.

[156] Schember, H.R., "Network Optimization of Line Diameters for Two-Phase Management Systems", AIAA Paper No. 86-1247, AIAA/ASME 4th Joint Thermophysics and Heat Transfer Conference, Boston, Mass, June 2-4, 1986.

[157] Schlichting, H., "Boundary Layer Theory", Translated from the German by J. Kestin. 4th ed., McGraw-Hill Book Company, Inc., New York, 1960, Chap. XX, pp. 502-531.

[158] Schmid, C., "KEDDC - A Computer-Aided Analysis and Design Package for Control Systems", in Computer-Aided Control Systems Engineering M. Jamshidi and C.J. Herget, (eds.), North-Holland, Amsterdam, pp. 159-180, 1985.

[159] Schmidt, F.W., Zeldin, B., "Laminar Heat Transfer in the Entrance Region of Ducts", Appl. Sci. Res., Vol. 23, No. 1-2, October 1970, pp. 73-94.

[160] Scobie, G., "Select the Pump that Meets Your Needs", Chart. Mech. Eng., Vol. 21, No. 5, May 1974, pp. 59-63.

[161] Scott, A.W., "Cooling of Electronic Equipment", 1st ed., John Wiley & Sons, Inc., New York, 1974, Chap. 5, p. 126. Chap. 8, pp. 215-226.

[162] Seban, R.A., McLaughlin, E.F., "Heat Transfer in Tube Coils with Laminar and Turbulent Flow", Int. J. Heat Mass Transfer, Vol. 6, pp. 387-395, 1963.

[163] Settles, G.S., Hamrick, J.T., Barr, W.J., Summerfield, M., Gunn, M., "Energy-Efficient Pump Utilization", J. Energy, Vol. 1, No. 1, January 1977, pp. 65-72.

[164] Shah, R.K., London, A.L., "The Influence of Brazing on Very Compact Heat Exchanger Surfaces", Department of Mechanical Engineering, Stanford University, Stanford, California, TR No. 73, November 1970.

[165] Shaubach, R.M., "Heat Transfer across Structural Boundaries", AIAA Paper No. 85-0977, AIAA 20th Thermophysics Conference, Williamsburg, Virginia, June 19-21, 1985.

[166] Sheriff, N., Gumley, P., "Heat-Transfer and Friction Properties of Surfaces with Discrete Roughnesses", Int. J. Heat Mass Transfer, Vol. 9, No. 12, December 1966, pp. 1297-1320.

[167] Sleicher, C.A., Tribus, M., "Heat Transfer in a Pipe with Turbulent Flow and Arbitrary Wall-Temperature Distribution", Transactions of the ASME, Vol. 79, No. 2, May 1957, pp. 789-797, reprinted in "Recent Advances in Heat and Mass Transfer", 1st ed., J.P. Hartnett, Ed., McGraw-Hill Book Company, Inc.,, New York, 1961, pp. 281-301.

[168] Smithberg, E., Landis, F., "Friction and Forced Convection Heat Transfer Characteristics in Tubes with Twisted Tape Swirl Generators", Transactions of the ASME, Journal of Heat Transfer, Vol. 86, Series C, No. 1, February 1964, pp. 39-49.

[169] Sparrow, E.M., Haji-Sheikh, A., "Flow and Heat Transfer in Ducts of Arbitrary Shape with Arbitrary Conditions", Transactions of the ASME, Journal of Heat Transfer, Vol. 88, Series C, No. 4, November 1966, pp. 351-358.

[170] Stevens, R.A., Fernandez, J., Woolf, J.R., "Mean-Temperature Difference in One, Two, and Three-Pass Crossflow Heat Exchangers", Transactions of the ASME, Vol. 79, No. 1, February 1957, pp. 287-297.

[171] Taborek, J., "Design Methods for Heat Transfer Equipment - A Critical Survey of the State-of-the-Art", in "Heat Exchangers: Design and Theory Sourcebook", 1st ed., N.H. Afgan and E.U. Schlunder, Eds., McGraw-Hill Book Company, New York, 1974, Clause 7, pp. 45-74.

[172] Taborek, J., Aoki, T., Ritter, R.B., Palen, J.W., Knudsen, J.G., "Fouling: The Major Unresolved Problem in Heat Transfer", Chem. Engng. Progr., Vol. 68, No. 2, February 1972, pp. 59-78.

[173] Taborek, J., Aoki, T., Ritter, R.B., Palen, J.W., Knudsen, J.G., "Predictive Methods for Fouling Behavior", Chem. Engng. Progr., Vol. 68, No. 7, July 1972, pp. 69-78.

[174] Taitel, Y., Dukler, A.E., "A Model for Predicting Flow Regime Transitions in Horizontal and Near Horizontal Gas-Liquid Flow", A.I.Ch.E. Journal, Vol. 22, No. 1, January 1976, pp. 47-55.

[175] Tanzer, H.J., Fleischman, G.L., Stalmach, D.D., "Osmotic Pumped Heat Pipes for Large Space Platforms", AIAA Paper No. 82-0902, AIAA-ASME 3rd Joint Thermophysics, Fluids, Plasma and Heat Transfer Conference, St. Louis, Missouri, June 7-11, 1982.

[176] TEMA, "Standards of Tubular Exchanger Manufacturers Association, Inc., 331 Madison Avenue, New York, 1968, Section 9, pp. 123-127.

[177] Thaller, G.J., Brown, R.G., "Analysis and Design of Feedback Control Systems", McGraw-Hill, 1960.

[178] Thorsen, R., Landis, F., "Friction and Heat Transfer Characteristics in Turbulent Swirl Flow Subjected to Large Transverse Temperature Gradients", Transactions of the ASME, Journal of Heat Transfer, Vol. 90, Series C, No. 1, February 1968, pp. 87-97.

[179] Trusch, R.B., "Shuttle Orbiter Atmospheric Revitalization System and Freon Coolant Loop System Trade Studies", SAE Paper No. 740921, Intersociety Conference on Environmental Systems, Seattle, Washington, July 29 - August 1, 1974.

[180] Trusch, R.B., Nason, J., "Compact Heat Exchangers for the Space Shuttle", ASME Paper 75-ENAs-54, Intersociety Conference on Environmental Systems, San Francisco, California, July 211-24, 1975.

[181] Vallerani, E., Degli Esposti, P.L., Sessions, B., "Present Capabilities and Extension Possibilities of the Spacelab Thermal Control Systems", AIAA Paper No. 78-1676, AIAA Conference on Large Space Platforms: Future Needs and Capabilities, Los Angeles, Calif., Sept. 27-29, 1978.

[182] Van Oost, S., Mathieu, J.P., "Two-Phase Heat Transport System Conceptual Studies", ESA CR(P)1873, Sabca, Chaussée de Haecht, B. 1130, Bruxelles, Belgium, Aug. 1983.

[183] Vargaftik, N.B., "Tables on the Thermophysical Properties of Liquid and Gases", 2nd ed., Hemisphere Publishing Corporation, Washington-London, 1975.

[184] Wallis, G.B., "One-Dimensional Two-Phase Flow", 1st ed., McGraw-Hill Book Company, Inc., New York, 1969.

[185] Weast, R.C., "Handbook of Chemistry and Physics", 47th ed., The Chemical Rubber Co., Cleveland, Ohio, 1966, pp. E24 and F56.

[186] Webb, R.L., Eckert, E.R.G., Goldstein, R.J., "Heat Transfer and Friction in Tubes with Repeated - Rib Roughness", Int. J. Heat Mass Transfer, Vol. 14, No. 4, April 1971, pp. 601-617.

[187] Weimer, R.F., Hartzog, D.G., "Effect of Maldistribution on the Performance of Multistream, Multipassage Heat Exchangers, in "Advances in Cryogenic Engineering", 1st ed., Vol. 18, K.D. Timmerhaus, Ed., Plenum Press, New York, 1973, pp. 52-64.

[188] Welty, J.R., Wicks, C.E., Wilson, R.E., "Fundamentals of Momentum, Heat and Mass Transfer, 1st ed., John Wiley & Sons, Inc., New York, 1969, Chap. 22, pp. 380-383.

[189] Werth, G.R., Vernon, R.M., Moudy, W.D., Hansen, W., Reed, R.D., Hawkins, R.S., Waller, C., Warner, B.W., "Study of Thermal Isolation Techniques", Lockheed Missiles & Space Company, Sunnyvale, California, M-92-66-1, NASA CR-71743, prepared under Contract No. JPL 950950, March 1966.

[190] Wicks III, M., Dukler, A.E., "Entrainment and Pressure Drop in Concurrent gas-Liquid Flow. 1. Air-Water in Horizontal Flow", A.I.Ch.E. Journal, Vol. 6, No. 3, September 1960, pp. 463-468.

[191] Wiebelt, J.A., "Design Considerations for Thermostatic Fin Spacecraft Temperature Control", NASA CR-500, 1966.

[192] Wise, P.C., "Spacecraft Thermal Control Technology: Design Challenges into the 1990's", Acta Astronautica, Vol. 14, 1986, pp. 489-502.

[193] Wyn-Roberts, D., "Environmental Control System Hardware for Spacelab. A Survey of Some European Aircraft Equipment Manufacturers", ESTEC, Noordwijk, The Netherlands, Internal Working Paper No. 811, February 1974.

[194] Wyn-Roberts, D., "Pumps for Manned Spacecraft. A Short Survey of Some Possible European Manufacturers", ESTEC, Noordwijk, The Netherlands, Internal Working Paper No. 788, November 1973.

[195] Yang, C.C., Palen, J.W., "Two-Phase Pressure Drop in Tubeside Condensation", Report CT-4, Heat Transfer Research, Inc., Alhambra, California, January 1977.